Diagnostic potential of extracellular vesicles (EVs) and single-cell photonics (scPH) in subclinical atherosclerotic disease

A dissertation for the degree of Ph.D

by

Denise Burtenshaw,

BSc. Genetics and Cell Biology

Under the supervision of

Prof. Paul A. Cahill

School of Biotechnology

Dublin City University

January 2022

Declaration

I hereby certify that this material, which I now submit for assessment on the programme of study leading to the award of PhD, is entirely my work and that I have exercised reasonable care to ensure that the work is original and does not to the best of my knowledge breach any law of copyright, and has not been taken from the work of others save and to the extent that such work has been cited and acknowledged within the text of my work.

Signed: Denise Burlenshaw ID No.:11370211 Date: 23/12/2021

Dedication

This thesis is dedicated to my granny, May Cooley, who taught me from a young age that your education is your wealth and the key to independence.

Publications

Di Luca, M., Fitzpatrick, E., **Burtenshaw, D**., Liu, W., Helt, J. C., Hakimjavadi, R., … Cahill, P. A. (2021). The calcium binding protein S100β marks hedgehog-responsive resident vascular stem cells within vascular lesions. Npj Regenerative Medicine, 6(1), 1–15.

Burtenshaw, D., Kitching, M., Redmond, E. M., Megson, I. L., & Cahill, P. A. (2019). Reactive Oxygen Species (ROS), Intimal Thickening, and Subclinical Atherosclerotic Disease. *Frontiers in Cardiovascular Medicine*.

Burtenshaw, D., Emma Fitzpatrick, Weimin Liu, David Morrow, Eileen M Redmond, Paul A Cahill. 5 Resident S100β/SCA1+ multipotent vascular stem cells undergo myogenic and vasculogenic differentiation *in vitro*. *Heart* **104**, A6–A6 (2018).

Burtenshaw, D., Hakimjavadi, R., Redmond, E. & Cahill, P. Nox, Reactive Oxygen Species and Regulation of Vascular Cell Fate. *Antioxidants* **6**, 90 (2017).

Di Luca M, Hakimjavadi R, **Burtenshaw D**, Fitzpatrick E, Mathiue P, Lally C, Redmond EM. Cahill PA, 2018. The Dichotomy of Vascular Smooth Muscle Differentiation/De-differentiation in Health and Disease, in K. Sakuma (ed) *Muscle Cell and Tissue Current Status of Research Field.* IntechOpen.

Acknowledgments

First and foremost, I would like to thank my supervisor Prof. Paul Cahill. From our first encounter during my undergraduate studies, to the pursuit of this PhD you have never doubted my abilities and have provided me with great encouragement, support and most importantly, self-belief. You have always been there to address any issues or frustrations I've had along the way, going above and beyond the role of any supervisor, which I will be forever grateful for.

Next, I would like to acknowledge the members of my lab group along with others that I have met throughout my PhD in DCU. To Roya, Mariana, Abi & Claire, not only did you provide a welcoming and friendly environment to work in, you went out of your way to teach me everything I know today, all your tips and tricks saved me hours of experimental optimisation. To all the technical staff at DCU, in particular, Graham, Monica, Deirdre, David, Janice, Teresa, Kasia, Allison and Carmen from daily chats in the corridors to your helping hand when experiments weren't going too well. I cannot thank you enough for your generosity, guidance and help throughout my five years. Although there were many stressful days had over the past 5 years there was just as many laughs along the way. A big thanks to past and present members of the Biological Research Society in particular, Kim, Niamh, Gill, Ray and Donal from the hours spent ranting about our PhDs to the nights out and trips away, they will always be my fondest memories.

A PhD is often considered a lonely experience, this was not the case for me as I was lucky enough to have shared the journey with two of my closest friends Eoin & Susan. From our daily de-briefing meetings that could be anything from tinder tales to experiment frustrations, to the endless hours spent working together in a Covid-PCR laboratory during the pandemic, I truly believe I wouldn't have gotten through this without you both. There aren't many people who can tell exactly what I'm thinking through my facial expressions but Eoin seemed to have this innate ability to do so! There's only one person who will be happier than me to see the end of my PhD and that's my boyfriend, Tomás. Your endless support and patience over the past five years hasn't gone unnoticed. You've been my number one supporter through the darkest days of the PhD providing me with endless laughter and most importantly endless amounts of caffeine to get through the last few months.

Lastly, I would like to thank my family my brothers David and Gary for keeping me grounded by reminding me I will not be a “real” doctor but most importantly my mam, Linda. Thank you for your continued support over the years in particular for talking my 17 year-old self out of pursuing a career in hairdressing. I think it’s safe to say your persistent guidance and advice worked out for the best! I will be forever grateful for the opportunities you have given me.

Table of Contents

List of Figures

List of Tables

Abbreviations

ACS	Acute Coronary Syndrome
AF	Autofluorescence
AIT	Adaptive Intimal Thickening
AMI	Acute Myocardial Infarction
BM-SCs	Bone Marrow-derived Stem Cells
BNP	B-type Natriuretic Peptides
CA	Coronary Angiography
CAD	Coronary Artery Disease
CDM	Chemically Defined Media
cIMT	Carotid Intimal-Medial Thickness
CLSM	Confocal Laser Scanning Microscope
CNN1	Calponin 1
CRP	C-reactive Protein
cTn1	Cardiac Troponin I
CVD	Cardiovascular Disease
DAPT	N-[N-(3,5-Difluorophenacetyl)-L-alanyl]-S-phenylglycine t- butyl ester
DHE	Dihydroethidium
DHh	Desert Hedgehog
DIT	Diffuse Intimal Thickening
DLS	Dynamic Light Scattering
DMEM	Dulbecco's Modified Essential Medium
DUOX	Dual Oxidase

E8	Essential Eight Medium
ECG	Electrocardiogram
ECs	Endothelial Cells
EDFR	Endothelial-Derived Relaxing Factor
EndoMT	Endothelial-Mesenchymal Transition
eNOS	Nitric Oxide Synthase
ER	Endoplasmic Reticulum
ESCRT	Endosomal Sorting Complex Required for Transport
EVs	Extracellular Vesicles
FeSEM	Field Emission Scanning Electron Microscopy
FLDA	Multiclass Fisher's Linear Discriminant Analysis
FTIR	Fourier Transform Intra Red
GWAS	Genome-wide Association Studies
H_2O_2	Hydrogen Peroxide
H3K27me3	Tri-methylation of lysine 27 on histone H3 H3K4me2
H3K4me2	Di-methylation of lysine four on histone H3
HAEC	Human Primary Aortic Endothelial Cells
HDL	High-Density Lipoprotein
HG	High Glucose
HG-EVs	EVs from High Glucose
Hh	Hedgehog
HHIP	Hedgehog Interacting Protein
HiPSC	Human induced Pluripotent Cells

hPSCs	Human Pluripotent Stem Cells
ICC	ICC
IHh	Indian Hedgehog
ILVs	Intraluminal Vesicles
IMT	Intimal-medial Thickening
iPSCs	Induced Pluripotent Stem Cells
LDA	Linear Discriminant Analysis
LDL	Low-Density Lipoproteins
LM	Lateral Plate Mesoderm
LM-SMCs	LM-derived VSMCs
LMs	HiPSC-derived Lateral Mesoderm Progenitor Stem Cells
LoaD	Lab-on-a-Disc
LPS	Lipopolysaccharide
miRNAs	microRNAs
MLP	Multiplayer Perception
MM1	Maintenance Media one
MRI	Magnetic Resonance Imaging
mRNA	Messenger RNA
MT	Mannitol
MVBs	Multivesicular Bodies
MVSCs	Multipotent Vascular Stem Cells
MYH11	Smooth Muscle Myosin Heavy Chain 11
NADPH	Nicotinamide Adenine Dinucleotide Phosphate-Oxidase

NBT	Nitroblue Tetrazolium
NE	Neuroectoderm
NEP-SMCs	NEP-derived VSMCs
NEPs	HiPSC-derived NE Progenitor Stem Cells
NG	Normal Glucose
NG-EVs	EVs from Normal Glucose
NO	Nitric Oxide
NOS	NO Synthase
NOS3	Endothelial NO Synthase
NOX	NADPH Oxidase
NPCs	Human iPSC Derived Neural Progenitor Stem Cells
NSTEMI	Non-ST-segment Elevation Myocardial Infarction
NTA	Nanoparticle Tracking Analysis
O_2^-	Superoxide
PBS	Phosphate-Buffered Saline
PC	Principal Component
PCA	Principal Components Analysis
PDGF	Platelet-derived Growth Factor
PIT	Pathologic Intimal Thickening
PM	Paraxial Mesoderm
PM-SMCs	PM-derived VSMCs
PMs	HiPSC-derived Paraxial Mesoderm Progenitor Stem Cells
POC	Point of Care

POCT	Point of Care Testing
Ptch	Patched
RAB GTPase	Rab Guanosine Triphosphatases
RAEC	Rat Primary Aortic Endothelial Cells
Redox	Reduction and Oxidation
rMVSC	Resident Multipotent Vascular Stem Cells
ROS	Reactive Oxygen Species
RT	Reverse Transcriptase
RT-qPCR	Real-Time quantitative polymerase chain reaction
Sca1	Stem cell antigen-1
scPH	Single-cell Photonics
scRNA-seq	Single-cell RNA sequence analysis
SEM	Standard Error of the Mean
SHh	Sonic Hedgehog
SM α-actin	Smooth Muscle α-actin
Smo	Smoothened
SNAREs	Soluble N-ethylmaleimide-sensitive factor Attachment Protein Receptors
SNEP-SMCs	SNEP-derived VSMCs
SNEPs	HiPSC-derived Spontaneous NE Progenitor Stem Cells
STEMI	ST-segment Elevation Myocardial Infarction
Sufu	Suppressor of fu
T1D	Type 1 Diabetes
T2D	Type 2 Diabetes

TGF-β1	Transforming Growth Factor β1
VEGFs	Vascular Endothelial Growth Factors
VSMC	Vascular Smooth Muscle Cells
VVOs	Vesiculo-Vacuolar Organelle

Units of measurement

^{o}C	Degrees Celsius
cm	centimetre
g	grams
hr	hour
L	litre
M	molar
mg	milligram
min	minute
mL	millilitre
mM	millimolar
nm	nanometre
nM	nanomolar
rpm	revolutions per minute
sec	second
µL	microlitre
µg	microgram
µm	micrometre
µM	micromolar
x g	G force

Abstract

Diagnostic potential of extracellular vesicles (EVs) and single-cell photonics (scPH) in subclinical atherosclerotic disease.

Denise Burtenshaw

Arteriosclerosis is an important age-dependent disease encompassing atherosclerosis, in-stent restenosis, pulmonary hypertension, and autologous bypass grafting. The accumulation of neointimal vascular smooth muscle (VSMC)-like cells is a critical event in the pathology of vascular disease leading to intimal-medial thickening (IMT) and vessel remodelling, and is considered an essential marker of subclinical arteriosclerotic disease. Their origin remains controversial, with several cell fate-mapping studies in mice indicating that they are derived from medial VSMCs, resident Nestin/S100β $^{+}$ vascular stem cells, and/or endothelial cells (ECs) following endothelial-mesenchymal transition (EndoMT). It is widely accepted that exposure to pathologic reactive oxygen species (ROS) generating risk factors is central to this pathology. The effective pathophysiological response within the vessel wall following vascular injury is endothelial cell apoptosis rendering the vascular endothelium dysfunctional. In the past few years, compelling evidence now suggests a role for the generation of endothelial-derived extracellular vehicles (EVs) as crucial regulators in transferring biological information, either locally or remotely, to initiate the proliferation, migration, and accumulation of VSMC-like cells within subclinical arteriosclerotic lesions. Early detection of these lesions represents an important diagnostic objective.

In this context, the main focus of this study was to develop novel strategies that interrogate and discriminate these discrete cell populations and detect the key signalling molecules within endothelial-derived EVs that dictate their fate. Specifically, single-cell photonic analysis using broadband light (autofluorescence), Raman and Fourier Transform Intra Red (FTIR) spectral datasets from normal VSMCs and lesional cells derived from human vessels *ex vivo,* in addition to human-induced pluripotent stem cell (HiPSC) progenitors and their myogenic progeny *in vitro,* were analysed using supervised machine learning as a novel diagnostic platform for early detection of vascular phenotypes within lesions. Moreover, the characteristics and effects of endothelial-derived EVs on resident vascular stem cell fate following hyperglycaemic-induced endothelial dysfunction were assessed using rat and HiPSC models *in vitro* as a potential surrogate marker for early lesion formation. The data clearly demonstrates that single cell photonic analysis can successfully discriminate and predict vascular phenotypes within lesions. Furthermore, endothelial derived EVs following hyperglycaemic-induced endothelial dysfunction promote resident vascular stem cell myogenic differentiation, growth and migration *in vitro.* These characteristics may represent important surrogate biomarkers for detection of early subclinical arteriosclerosis.

Chapter 1:

Introduction

1.1 The vasculature, an efficient transport system.

The cardiovascular system is comprised of a hollow muscular organ, the heart, connected to a network of arteries and veins of varying sizes. There are essentially two components of the cardiovascular system, the systemic circuit servicing blood flow from the heart to the body, and the pulmonary circuit, servicing blood flow from the heart to the lungs. The presence of an extensive network of arteries and arterioles pumps oxygenated blood away from the heart to various organs and tissues throughout the body, facilitating day-to-day cellular activities such as growth, development, and absorption of nutrients. In contrast, the presence of an extensive network of veins and venules ensures the return of deoxygenated blood and the removal of cellular waste products from the body back to the heart, where the process begins again. The function of these vessels dictates, in part, their structural composition. Although the general three-layered structure, the adventitia, media, and intima, are common to both arteries and veins, each layer's size and compositional makeup differ (Figure 1.1). The rapid admission and expulsion of blood from the heart to the body by both elastic and muscular arteries, respectively, require a muscular predominance. This is represented by an increase in the medial layer and a narrow lumen to maintain substantial blood pressure (Holford, 2009). These structural characteristics are not present in veins and venules due to reduced blood flow pressure needed to facilitate the transport of deoxygenated blood back to the heart (Pugsley and Tabrizchi, 2000).

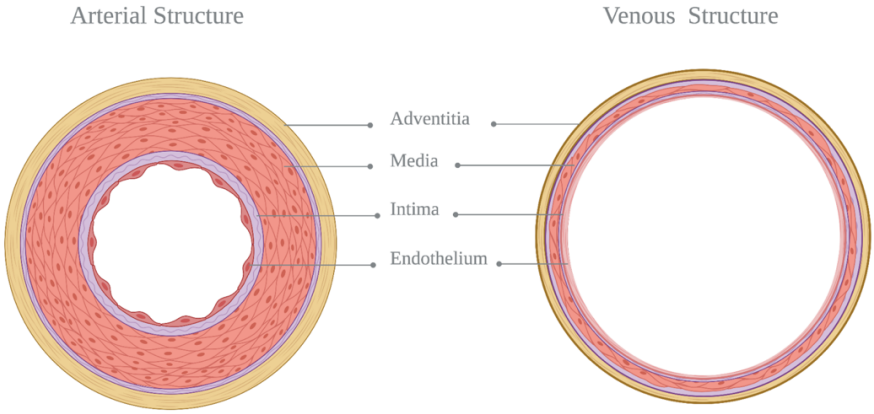

Figure 1.1 Comparison of arterial and venous structure. The structure of a healthy artery and vein composed of three main layers, the adventitia, the media, and the intima. (Created with BioRender.com).

1.2 Cardiovascular disease, a global killer.

Premature death from non-communicable diseases such as cardiovascular disease (CVD), cancer and respiratory diseases are responsible for 71% of all deaths worldwide. According to latest data from the World Health Organisation (World Health Organization, 2018). CVDs alone represent a staggering 43% of all deaths and remain the major cause of death globally. The CVD umbrella includes coronary artery disease, stroke, hypertension, cardiomyopathy and in-stent restenosis (Timmis *et al.*, 2018). Although it is natural for many of these diseases to prevail in the later years of life, we are now witnessing an increase in the incidence of these chronic diseases much earlier in life, leading to premature deaths in both male and female populations (Ediriweera *et al.*, 2018). CVD affects the morbidity and mortality rates of the global population and puts a significant financial burden on healthcare systems and government budgets. CVD was estimated to cost healthcare systems of the EU approximately €169 billion in 2006 (Townsend *et al.*, 2012) rising to €210 billion by 2015 (Wilkins E, Wilson L, Wickramasinghe K, Bhatnagar P, Leal J, Luengo-Fernandez R, Burns R, Rayner M, 2018). This empirical evidence supports the immediate clinical unmet need to address the current strategies used to detect, prevent, and manage CVD.

1.2.1 Atherosclerosis, the silent killer.

CVD includes a wide variety of diseases. However, the most common pathologic condition affecting today's generation is atherosclerosis. Atherosclerosis is classed as a chronic, progressive, inflammatory disease characterised by lesions in the arterial wall. Unlike other non-communicable diseases, atherosclerosis has a long asymptomatic silent phase, with the first clinical manifestation arising in the late stages of well-advanced atherosclerosis. Interventions required for the prevention and reversibility of atherosclerosis require sub-clinical detection to prescribe primordial and primary treatments. A crucial hallmark of sub-clinical atherosclerosis is pathologic intimal thickening (PIT). PIT is defined as the initial progressive plaque responsible for the rise of advanced lesions.

PIT can be divided into two categories of vascular lesion morphologies (i) diffuse intimal thickening (DIT) consisting of VSMC-like cells and extracellular matrix with little or no accumulation of lipid, generally associated with the natural aging of the arterial vessel, and (ii) adaptive intimal thickening (AIT) primarily composed of infiltrating macrophage cells and intimal VSMC-like cells defined as an important transitional non-atherosclerotic plaque that likely represents the earliest phase of lesion progression (Figure 1.2) (Kolodgie *et al.*, 2007; Sakamoto *et al.*, 2018).

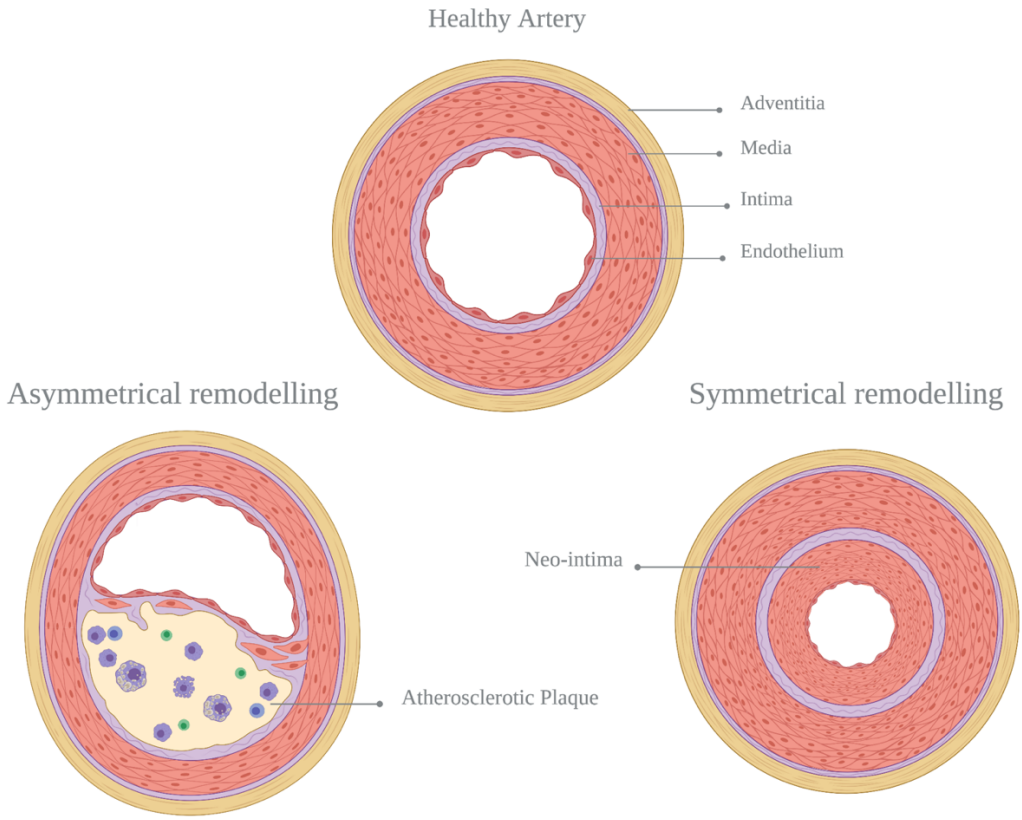

Figure 1.2 Models of arterial disease. Schematic representation of cross-sections of healthy vessels, arteriosclerotic vessels and atherosclerotic vascular lesions. Asymmetrical remodelling of the vessel is represented by the formation of a lipid-dependent plaque protected by a fibrous cap resulting in blood flow restriction, possible plaque rupture, and vessel occlusion. In contrast, symmetrical remodelling, typical or arteriosclerotic vessels is represented by formation of a neointima due to the accumulation of VSMCs like cells, resulting in a decrease in luminal size and blood flow restriction. (Created with BioRender.com).

Pathological studies from human vessels have shown that early adaptive 'transitional' lesions enriched with VSMC-like cells are present in atherosclerotic-prone regions of the vessel (Ikari *et al.*, 1999). A multitude of factors contributes to the development of PIT at these athero-prone areas, including; (i) disturbed blood flow resulting in endothelial dysfunction, (ii) exposure to various blood-borne components and circulating CVD risk factors, and more recently, (iii) the effect of embryological origin of neointimal cells (Debakey and Glaeser, 2000; Cheung *et al.*, 2012; Bennett, Sinha and Owens, 2016). Adaptive lesions have been identified in human vessels prior to the retention of lipid representing an important therapeutic target for sub-clinical detection and implementation of primary preventative measures that may treat or delay the pathogenesis of CVD (Sakamoto *et al.*, 2018). It is widely recognised that VSMC-like cells are primarily responsible for most neointimal cells found in arteriosclerotic lesions following vessel injury. This process has proven to be true for many murine arterial injury models, including balloon angioplasty, coronary artery bypass grafting (CABG), transplant arteriosclerosis, pulmonary hypertension, and ISR (Bennett, Sinha and Owens, 2016). Early lesions have also been identified on routine disease modelling in mouse carotid arteries following flow restriction caused by ligation.

Furthermore, these ligation-induced lesions can develop into advanced atherosclerotic plaques in *ApoE* knockout mice on western diets (Korshunov and Berk, 2003; Nam *et al.*, 2009; W. Liu *et al.*, 2011). Characteristics associated with IMT include a reduced lumen diameter, inhibition of matrix degradation, and the accumulation of neointimal cells (Lan, Huang and Tan, 2013). The origin of these neo-intimal cells has driven much debate and controversy within the vascular biology research community.

1.3 The neointima, the key to subclinical atherosclerosis detection.

There are three main locations within the layers of the arterial wall that may harbour the source of neointimal cells; namely the intima composed of endothelial cells, the media composed primarily of vSMCs with a small population of resident vascular stem cell , and the adventitia composed of mainly fibroblasts with a small population of resident vascular stem cells (Figure1.3). Most cells found in the neointima are primarily VSMC-like cells (Schiele, 2005); however, the origin of these cells is widely debated. Initially, it was proposed that neointimal VSMC-like cells originated from differentiated medial VSMCs that undergo phenotypic switching, becoming de-differentiated and proliferate

and migrate to the site of injury. Subsequent lineage tracing studies have provided compelling evidence for the involvement of a population of (i) de-differentiated resident medial VSMCs (Laura S. Shankman *et al.*, 2015; Chappell *et al.*, 2016; Cherepanova *et al.*, 2016) (ii) circulating bone-marrow cells (Sata, 2003) (iii) resident vascular stem cells (Tang, Wang, Yuan, *et al.*, 2012; Tsai *et al.*, 2012; Shikatani *et al.*, 2016; Di Luca *et al.*, 2021; Molony *et al.*, 2021) and (iv) ECs, through a process known as EndoMT (Cooley et al., 2014; Gang et al., 2015). As varying theories surround this topic, an in-depth knowledge of arterial wall structure and the cellular microenvironments they reside within is required to decipher a possible source (Figure 1.4).

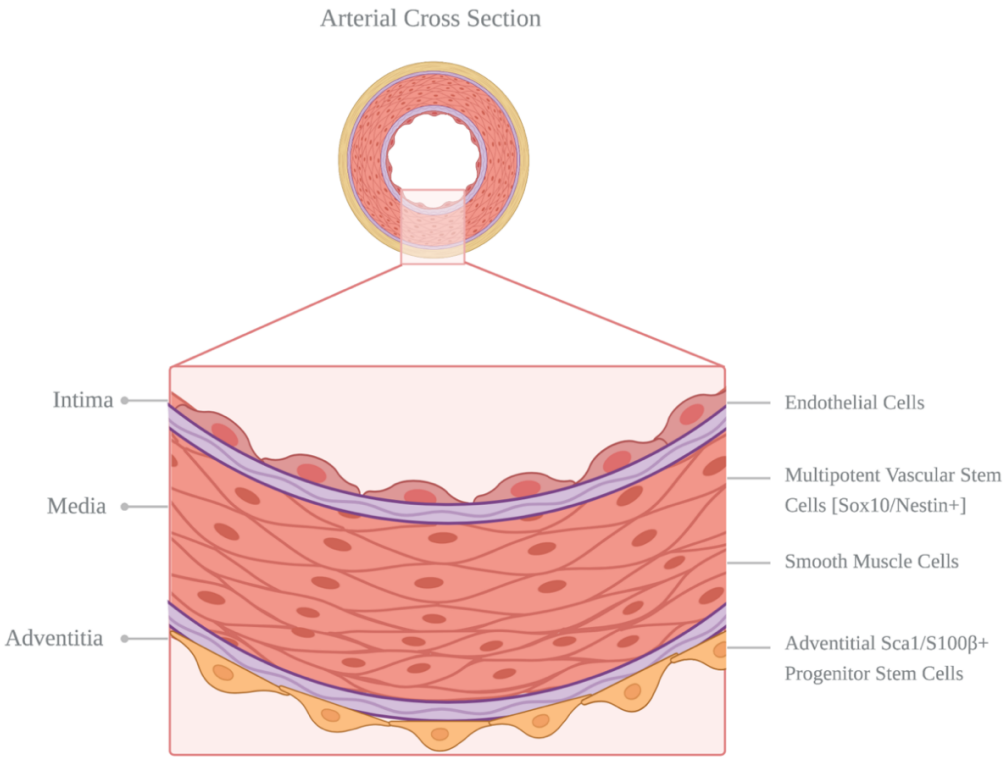

Figure 1.3 Structural composition of a healthy arterial wall. The structural composition of a healthy arterial wall and its distinct resident cell populations. The innermost layer, the intima, is home to a single layer of ECs known as the endothelium. The middle layer, the intima, is home to differentiated vascular muscle cells giving the artery structural function due to their contractile abilities. The outermost layer, the adventitia, is home to multiple cell populations, including fibroblasts, immune cells, and an adventitial progenitor stem cell population. (Created with BioRender.com).

1.3.1 The intima

The intima, also known as the vascular endothelium, is a single layer of vascular ECs that line the luminal surface of the entire circulatory system from tiny capillaries to large arteries. The intimal layer is the initial layer of the vessel formed during embryogenesis. Vascular ECs reside in the intimal layer of the vessel and originate from a mesoderm-derived progenitor cells, the hemangioblast, through a process known as hematopoiesis (Palis, McGrath and Kingsley, 1995; Choi *et al.*, 1998). Following this process, ECs expressing markers such as platelet endothelial cell adhesion molecule (PECAM-1) also known as cluster of differentiation 31 (CD31), leukosialin also known as sialophorin or cluster of differentiation 43 (CD43), and vascular endothelium cadherin organise to form the endothelium. Recruitment of VSMCs is then initiated to form a complex vascular system (During, 2000; Jain, 2003). ECs are the interface cell, as they come in direct contact with blood flow through the lumen of the blood vessel. Although small, approx. 20 – 40 μM long, 10 – 15 μM wide, these cells act as an endocrine organ playing a vital role in vascular homeostasis (Pearson, 1996), regulation of cell growth, modulation of vascular tone (Sandoo *et al.*, 2010), and act as a permeable barrier against the entry of macromolecules and fluid exchange between circulating blood and underlying tissues. While the general three-layered structure is common in both murine and human arteries, there are stark differences in the compositional make-up of the intimal layer. The intimal layer in rodents is made up exclusively of the endothelium throughout their lifespan, however in humans, an intimal VSMC layer builds up from birth and can be established in adulthood, this can be further enlarged in subclinical atherosclerosis (Schwartz, DeBlois and O'Brien, 1995).

1.3.1.1 Endothelial cells (ECs)

ECs retain the potential to contribute to vascular remodelling and neointimal hyperplasia through a process known as an endothelial-mesenchymal-transition (EndoMT). This transforming growth factor β1 (TGF-β1) mediated process allows an EC to express its plasticity properties, undergoing a transition to a mesenchymal stem-like cell and further to a smooth muscle-like progenitor cell. During this process, the EC loses endothelial-specific markers such as CD31 while acquiring mesenchymal markers such as fibroblast-specific protein 1, SMαA, and N-cadherin (Potts and Runyan, 1989; Nakajima *et al.*,

2000). Elevated levels of TGF-β1 and altered downstream signalling have been implicated in the aetiology of atherosclerosis, vessel restenosis, and the development of the neointima (Bobik, 2006; Pang *et al.*, 2014; Chen *et al.*, 2019). Recent research has demonstrated the role of EndoMT and VSMC differentiation in neointimal formation following early activation of TGF-β1 /Smad signalling in response to vascular injury (Cooley *et al.*, 2014; G. Wang *et al.*, 2015). This evidence, along with similar studies, suggest a potential role for vascular ECs as a possible source of neointimal cells following EndoMT to VSMC transition, proliferation, and migration.

1.3.2 The media

The media, the middle layer of the artery, accounts for 90% of the vessel structure and is composed of differentiated VSMC, known as the contractile cell of the vessel, and a small population of resident multipotent vascular stem cells (rMVSC) (Tang, Wang, Yuan, *et al.*, 2012). The majority of VSMC populations are derived from various mesodermal lineages, including lateral plate, paraxial and somatic mesoderm. However, a small subset of VSMC originates from the neural crest (Jiang *et al.*, 2000; Wasteson *et al.*, 2008). Classically, medial VSMCs are thought not to be terminally differentiated and can undergo phenotypic modulation or de-differentiation in response to their environment (Owens, 1995). In a healthy vessel wall, the proliferation of VSMCs is a slow process as there is little need for regeneration. These proliferating VSMCs express a unique repertoire of contractile proteins indicative of VSMC differentiation, some of which include smooth muscle myosin heavy chain 11 (MYH11), smooth muscle a-actin (SMA), and calponin 1 (CNN1) (Churchman and Siow, 2009). In contrast, when VSMCs are exposed to a change in local environmental cues, such as vascular injury, they are purported to undergo a phenotype switch resulting in the downregulation of previously expressed contractile proteins and a rapid increase in proliferation capability. In addition, a small population of resident multipotent vascular stem cells have been identified in the medial layer; however, the function of these cells is debatable (Tang, Wang, Yuan, *et al.*, 2012; G. Wang *et al.*, 2015).

1.3.2.1 De-differentiated VSMCs

There are two major possible candidates responsible for the origin of VSMC-like cells in a neointimal lesion that reside in the medial layer. The first of which was historically proposed by many research groups and includes the possibility of de-differentiation of medial differentiated VSMC following phenotypic modulation or switching and proliferation/migration to the site of injury (Ross and Glomset, 1973). This process refers to the ability of SMCs to not only de-differentiate but also to take on a new phenotype with contractile SMCs spontaneously switching to a synthetic SMC phenotype with higher levels of proliferation and inflammatory cell recruitment (Rensen, Doevendans and Van Eys, 2007). Subsequent studies have supported this theory, reporting the downregulation of VSMC markers in neointimal cells post injury (Chamley-Campbell, Campbell and Ross, 1979). Not only do VSMCs retain the ability to de-differentiate but they also have the potential to take on a new phenotype. This process termed phenotypic modulation of VSMCs may occur following vessel injury with contractile VSMCs spontaneously switching to a synthetic VSMC phenotype with higher proliferation and inflammatory cell recruitment (Brandes, Takac and Schröder, 2011). Numerous research groups have since supported this theory using lineage tracing analysis with tamoxifen-induced Myh11-CreER transgenic reporter mice to mark Myh11 differentiated VSMCs prior to injury (Nemenoff et al., 2011; Herring et al., 2014).

Subsequent studies carried out by Chappell and colleagues expanded upon this theory, reporting that not all marked medial differentiated VSMCs are responsible for neointimal formation but rather a rare discrete subpopulation of plastic medial $Myh11^{+}$ VSMC (Chappell *et al.*, 2016) that are also stem cell antigen-1 positive ($Sca1^{+}$) using single-cell RNA-sequencing (scRNA-seq) (Dobnikar *et al.*, 2018). However, concerns have persisted regarding the lack of relevant negative controls and the possibility that the time allowed for tamoxifen depletion before vessel ligation is performed. Tamoxifen induction has been regularly used in lineage tracing studies to and initiate fluorescent tag expression and indelibly mark cells with an active target promoter. However, issues have arisen regarding its use due to the remnants of tamoxifen in tissues for up a month after the last injection has taken place leading to induction of fluorescently tagged expression in off-target cells that acquire an active promoter (Reinert *et al.*, 2012). Longer washout periods must be introduced to overcome this issue prior to vessel injury to ensure tamoxifen

depletion. Several studies have challenged this hypothesis of VSMC phenotypic switching and re-programming, with a number of other cell types reported to be involved in the development of the neointima, such as vascular ECs, bone-marrow-derived mesenchymal stem cells, and resident vascular stem cells (Sata, 2003; Torsney, Hu and Xu, 2005; Cooley *et al.*, 2014; Tang *et al.*, 2020; Di Luca *et al.*, 2021; Molony *et al.*, 2021).

1.3.2.2 Resident vascular stem cells

In the past decade, numerous studies have supported the role of resident vascular stem cells that undergo myogenic differentiation during neo-intimal formation following vascular injury. Although vascular stem cells are most abundant in the adventitia, populations of multipotent cells have also been identified in the tunica media (Tintut *et al.*, 2003). In 2012 Tang et al. challenged the VSMC de-differentiation model, reporting the presence a new population of Sca1- cells in the tunica media of rat carotid arteries, termed multipotent vascular stem cells (Tang et al., 2012). Furthermore, this small niche of neuroectoderm (NE) derived rMVSCs that reside in the medial and adventitial layer of various animal and human vessels and express neural crest stem cell markers Sox10, Sox17, S100β, and Nestin and have the ability to differentiate down a myogenic lineage following vessel injury. These controversial studies suggested that VSMC-like cells found in neointimal lesions are derived from a resident multipotent vascular stem cell (MVSC) niche (Tang et al., 2012).

These studies were subsequently questioned by Nguyen *et al*. in 2013 as issues arose regarding the design and use of the constitutive Cre lineage tracing model chosen (Nguyen *et al.*, 2013). In addition to this, as the isolation of these rMVSCs required complete removal of the adventitial layer prior to explant and cell culture, the possibility arose that a residual adventitial stem cell remained at the medial adventitial boundary on the medial explants only to expand in culture. Follow-up lineage tracing studies were subsequently performed to validate and confirm the 'stem cell' hypothesis using Sox10-Cre/Rosa-loxP-LacZ mice to trace the $Sox10^{+}$ cohort of medial cells present in the neointima following vascular injury. The results supported their original hypothesis confirming the presence of a resident $Sox10^{+}$ MVSC that plays a significant contributory

role in VSMC-like proliferation and migration following vascular injury (Yuan *et al.*, 2017). At the same time, cell fate mapping and scRNA-seq studies also implicated a rare medial Myh11^{+}/Sca1^{+} population and a Myh11^{-} non-VSMC adventitial Sca1^{+} cell as both these populations expand more rapidly than pre-existing VSMCs within severe lesions (Dobnikar *et al.*, 2018; Tang *et al.*, 2020).

Due to the complexity of these findings further research has focused on the role of resident vascular stem cell during the progression of lesion formation. Recent studies from our group, using transgenic eGFP mice and genetic lineage tracing of S100β^{+} vascular stem cell *in vivo*, have identified S100β/Sca1 cells derived from a S100β non-SMC parent population within lesions that co-localise with smooth muscle α-actin cells following iatrogenic flow restriction (Di Luca *et al.*, 2021). This evidence supports the theory that MVSCs may contribute, at least to some degree, in the formation of a neointimal lesion following vessel injury.

1.3.3 The Adventitia

Lastly, the tunica adventitia is the outmost layer of the artery composed of connective tissue, mainly collagen. It is supported by an external elastic lamina that functions to anchor vessels to its surrounding external tissues. The primary cell types habitant in this layer include; fibroblasts, macrophages, T-cells, B-cells, and dendritic cells carrying out routine surveillance and innate immune functions (Tieu *et al.*, no date; Galkina *et al.*, 2006). Studies have shown the presence of a Sca1^{+} resident stem cell population in the periphery of the adventitial layer, mainly localised around the aortic root, that retains the ability to differentiate into VSMCs in response to injury (Hu *et al.*, 2004). In addition to this, these cells also retain the ability to differentiate into other types of cells present in vascular lesions such as macrophages and osteocytes (Psaltis *et al.*, 2012; Cho *et al.*, 2013). This population of Sca1^{+} cells in the adventitia could be stimulated to differentiate through a myofibroblast intermediate into a VSMC population. These Sca1^{+} cells migrate through the media *in vivo* and contribute to neointimal formation (Sartore *et al.*, 2001; Torsney, Hu and Xu, 2005). Cell fate mapping data suggests that adventitial stem cells may indeed play a role in lesion formation, but only in cases of severe vessel injury (Roostalu *et al.*, 2018).

1.3.3.1 Bone marrow-derived stem cells

In contrast to the above findings, various studies have suggested that the origin of neointimal cells lies not within the vasculature but rather in circulation in the form of circulating bone marrow-derived stem cells (BM-SCs) and hematopoietic progenitor cells. To demonstrate the role of circulating BM-SCs in the neointima, bone marrow transplant from ROSA26 mice expressing β-galactosidase (LacZ) to control mice were performed and revealed that 63% of the neointimal cells were LacZ positive, indicating their bone marrow origin (Shimizu *et al.*, 2001; Sata, 2003). Double staining further showed that the $LacZ^{+}$ cells in the neointima were also either α-actin or CD31 positive, which would suggest that the BM-SCs differentiated to VSMCs or ECs following injury. Human studies of coronary atherosclerosis have also been carried out using X, Y linkage during bone marrow transplants and suggest that cells within an atherosclerotic lesion may be derived from donor bone-marrow stem cells (Caplice *et al.*, 2003). However, it has since been suggested that although these cells are recruited to the injury site, they do not undergo myogenic differentiation to neointimal cells (Hoofnagle *et al.*, 2006). While the contribution of bone-marrow-derived stem cells has since been clarified, the origin of neointimal VSMC-like cells remains contentious and incompletely understood.

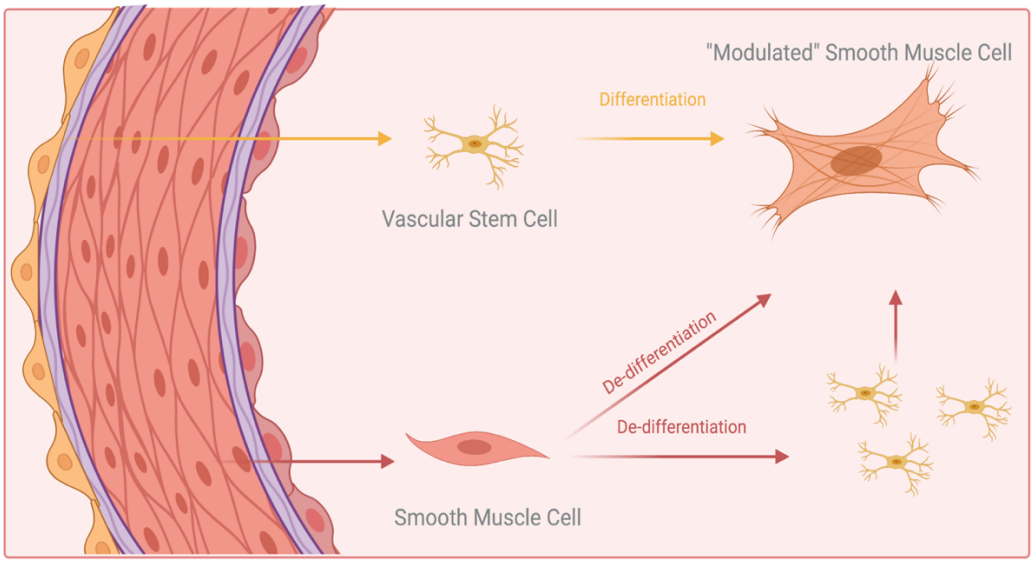

Figure 1.4 Origin of neointimal VSMCs. There are two main possible sources of neointimal VSMCs (i) Partial differentiation of resident vascular stem cells (ii) De-differentiation of vascular VSMCs to a more plastic phenotype capable of undergoing proliferation, migration, and differentiation. (Created with BioRender.com).

1.4 Atherosclerosis diagnostics, do or die?

Irrespective of the source of VSMC-like cells found in the neointima, measurement of the resulting increase in arterial IMT, referred to as carotid intima-media thickness (cIMT) in carotid arteries, is currently used as the cornerstone for sub-clinical atherosclerotic detection. There are four critical levels associated with CVD prevention, detection, and management (i) primordial prevention; actively avoiding the development of CVD risk factors through the promotion of population-based healthy lifestyle choices, (ii) primary prevention; early detection, and treatment of circulating risk factors in susceptible individuals to subclinical disease and mitigation through lifestyle changes, (iii) secondary prevention; detection and treatment of individuals with subclinical forms of disease generally associated with prescription of medications or surgical interventions, (iv) tertiary prevention; treatment of individuals having had CVD, improving their ability to function, quality of life and life expectancy through rehabilitation programs and support groups (Hobbs, 2004; Singh *et al.*, 2018). To truly tackle rising CVD prevalence in the population, a paradigm shift from secondary and tertiary treatment of atherosclerosis to primordial and primary treatments of subclinical atherosclerosis is of utmost importance.

Atherosclerosis is a complex disease in which vascular remodelling events lead to the activation of a cascade of inflammatory and fibrosis pathways (Ross, 1999). The detection of changes in vessel structure through the use of imaging platforms and monitoring the release of circulating pathological biomolecules are two attractive diagnostic approaches for routine detection of CVD. A biomarker is defined as a biological compound that is easily accessible and measurable in the body. Although often associated with circulating biological molecules such as proteins, nucleic acids, metabolites, and extracellular vesicles (EVs), biomarkers can also be classified using imaging platforms. Imaging platforms provide insights into structural and functional abnormalities of the vasculature.

1.4.1 Imaging biomarkers for detection of CVD

In recent years a variety of techniques have been deployed to measure sub-clinical atherosclerosis, including coronary angiography (CA), intravascular ultrasound, magnetic resonance imaging (MRI), and electrocardiogram (ECG). Although the techniques mentioned above all play an essential role in sub-clinical detection, the sonographic measurement of cIMT is arguably the most widely used, non-invasive technique currently employed by clinicians to stratify patient cohorts. cIMT refers to the distance between the luminal border of the intima and the outer border of the media, which is used as a surrogate marker of detection in symptomatic and, more importantly, asymptomatic individuals (Papageorgiou *et al.*, 2016). Clinical evaluation of cIMT has dual functionality, quantifying the extent of subclinical disease and monitoring changes over time, acting as a tool to assess the efficacy of CVD treatments (Lorenz *et al.*, 2007). cIMT is not only an important surrogate marker for disease synonymous with subclinical atherosclerosis but can also result from non-atherosclerotic processes such as vascular aging, whereby an increase in IMT is observed even in populations with a low incidence of lipid-driven atherosclerosis (Al Rifai *et al.*, 2018). IMT increases threefold between ages 20–90 years and may at any given age predict future outcomes that can be accelerated in the presence of known CVD risk factors. Hence, IMT, typical of adaptive lesions in early subclinical atherosclerosis, provides an essential substrate for lipoprotein retention leading to accelerated atherosclerotic plaque formation and acute coronary syndrome (ACS) (Nakashima, Wight and Sueishi, 2008). When combined with elevated fasting remnant cholesterol levels, cIMT has also recently been successfully deployed in stratifying patients with ischemic stroke and optimal LDL cholesterol levels (Qian *et al.*, 2021). Thus, ultrasound detection and evaluation of atherosclerosis, mainly through carotid plaque assessment, and more recently, femoral plaque assessment, are increasingly utilised in clinical decision-making for at-risk and prevalent CVD patients.

Although clinicians routinely use the sonographic measure of cIMT, there are limitations to its application in detecting sub-clinical atherosclerosis. Chronic coronary artery disease (CAD), typical of AMI, is usually associated with a rupture of atherosclerotic plaque, thrombus formation, and obstruction of blood flow leading to necrosis of the myocardium. However, in some patients with AMI, there are no significant lesions present in coronary arteries interrogated by angiography, thus confounding early

identification of atherosclerosis. Acute coronary syndrome, which can be divided into subgroups of ST-segment elevation myocardial infarction (STEMI), non-ST-segment elevation myocardial infarction (NSTEMI), unstable angina, and stable CAD, carries significant morbidity and mortality. As a result, prompt diagnosis and appropriate treatment are essential in preventing adverse outcomes. ECG analysis and morphological features suggest STEMI has smaller lumen areas, more significant plaque burden, and more plaque rupture or virtual histology thin-cap fibroatheroma compared with lesions causing NSTEMI/unstable angina or stable CAD. In lesions with plaque rupture, only plaque burden predicted STEMI, and in lesions without plaque rupture, only minimum lumen cross-sectional area predicted STEMI (Dong *et al.*, 2015). The limitation of techniques discussed above is the inability to detect plaques before their formation. In most cases, to detect the presence of CVD, a plaque or obstruction to the vessel must already be present, which at this point reduces the chance of disease reversal. Early detection of cIMT due to the migration of VSMCs irrespective of their source through a novel photonic interrogation system is highly desirable.

1.4.1.2 Photonics for CVD detection

Amongst the various imaging platforms deployed to interrogate IMT, label-free techniques such as vibrational spectroscopy have proven promising (Cheng and Xie, 2015). Considerable advancements in vibrational spectroscopy with the focus on morphological measurements and the relationship between biochemical content and functionality have opened up discussion surrounding their role in the early detection of disease (Pence and Mahadevan-Jansen, 2016). One such technique with diagnostic potential for early detection of de-differentiating VSMC and/or differentiation of stem cell-derived VSMC progeny *in vivo* is Raman spectroscopy. Raman spectroscopy is a form of vibrational spectroscopy that analyses vibrations within a molecule that indicate the molecular structure giving rise to a unique spectroscopic signature of that molecule. The unique spectroscopic signature often referred to as a 'fingerprint,' is generally between 400-2000cm^{-1} wavenumbers (Butler *et al.*, 2016; Kiselev *et al.*, 2016). Although much work has been done to establish the use of Raman for the characterisation of atherosclerotic plaque to date, there is little research focusing on its use to detect AIT before lipid retention. However, some work has been initiated in this field with Raman studies of VSMC and associated extracellular matrix proteins serving as possible spectral

early biomarkers for AIT detection (Narayanan *et al.*, 1976; Bank *et al.*, 1996; Wanjare, Agarwal and Gerecht, 2015; Molony *et al.*, 2018).

A second vibrational spectroscopy method used in the diagnostic field to date is Fourier Transform Infra-Red (FTIR). In contrast to Raman, FTIR relies on the absorption of infrared radiation rather than the scattering of light. For biological samples, the 'fingerprint' region lies between 600-1450cm^{-1} wavenumbers. Similar to Raman, the use of FTIR for the detection of atherosclerotic plaques has been well established (Wrobel *et al.*, 2015). Furthermore, FTIR analysis of human atherosclerotic carotid arteries has been performed to determine biochemical markers of mechanical stiffness associated with the pathogenesis of atherosclerosis (Barrett *et al.*, 2015).

A third spectroscopy diagnostic tool based on light scattering has recently emerged as a potential addition to the repertoire of label-free diagnostics. LiPhos, living photonics, is a diagnostic and prognostic tool that incorporates microfluidics and auto-fluorescent signalling to enable real-time measurement of autofluorescence emissions from cells and analytes in small sample volumes (Burger *et al.*, 2012). The combination of microfluidics and light detection enables single-cell capture in a microfluidic system before exposure to broadband light, resulting in auto-fluorescent single-cell signatures. The autofluorescence emissions are closely associated with metabolism and/or structural changes under normal or pathological conditions (Monici, 2005; Burger *et al.*, 2012; Croce *et al.*, 2018). Interpretation of these distinct differences can be analysed using various mathematical models.

Using, LiPhos, recent murine *in vitro* models, reveal specific alterations in the cellular profile of nucleic acid, protein, lipid content and extracellular matrix of bone marrow mesenchymal stem cells and their myogenic progeny can be detected. Furthermore, this technology was used to discriminate normal differentiated medial VSMCs from arteriosclerotic VSMC-like cells *ex vivo* following vascular injury (Molony *et al.*, 2021). Recent studies show promising attributes for applying vibrational spectroscopy to detect discrete changes in cellular components in the arterial wall (Molony *et al.*, 2021) (Figure 1.5); however, further research needs to be conducted to determine their application in human atherosclerotic models.

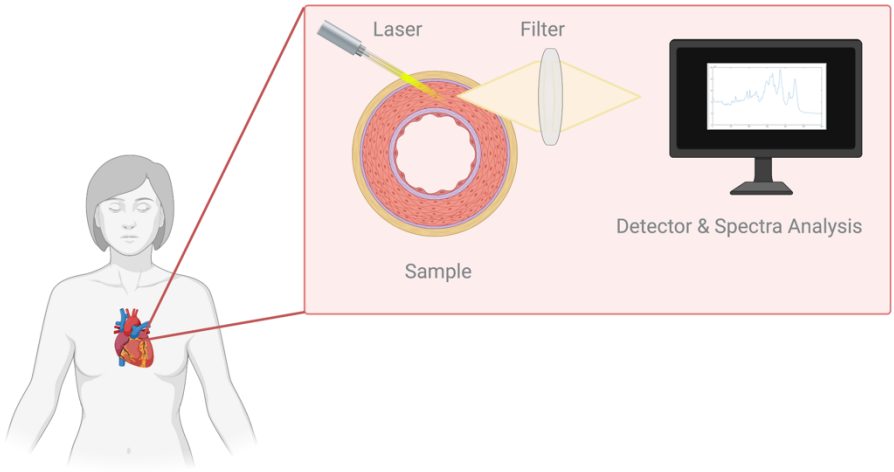

Figure 1.5 Vibrational spectroscopy for sub-clinical detection of CVD. The use of vibrational spectroscopy techniques including Raman, LiPhos, and FTIR for sub-clinical diagnosis of CVD through changes in cellular spectroscopy signatures. (Created with BioRender.com).

1.4.2 Biological biomarkers for detection of subclinical CVD

Due to the complex nature of CVD detection, continuous efforts are being made to find other, non-classical biomarkers of sub-clinical atherosclerosis. Currently, the most frequently studied are circulating biomarkers indicative of arterial wall alteration. The use of circulating biomarkers for subclinical disease detection is favourable due to their abundance in bodily fluids such as blood, saliva, and urine and their prognostic and diagnostic value. Characteristics of ideal biomarkers include high sensitivity, high specificity, easily accessible and low cost (Vasan, 2006). Due to the multifactorial nature of CVD, a panel of biomarkers used for diagnostic purposes includes proteins, miRNAs, and molecules, has recently been reviewed (Ghantous *et al.*, 2020).

Clinical biomarkers used for the detection of various CVDs include C-reactive protein (CRP) for the detection of inflammatory conditions (Landry *et al.*, 2017; Ries *et al.*, 2021), cardiac troponin I and T (cTn1, cTnT) for the detection of acute myocardial infarction (AMI) and ACS (Apple and Collinson, 2012), B-type natriuretic peptides (BNP AND NT-proBNP) for detection of AMI (Di Angelantonio *et al.*, 2009) and D-dimer for detection of thrombosis, ischemic heart disease and cardiovascular mortality (Tokita *et al.*, 2009). Although these biomarkers are routinely used in clinical practice, they are considered late-stage biomarkers proving beneficial for detecting a cardiovascular event after it has already occurred. With the advent of precision medicine,

focus has shifted to the discovery of early-stage biomarkers in predicting subclinical disease. A panel of early-stage biomarkers has been discovered, some of which include myeloperoxidase elevated in early stages of CAD and stroke (Meuwese *et al.*, 2007; Ndrepepa *et al.*, 2008), secreted frizzed related proteins for early detection of MI (Askevold *et al.*, 2014) and junctional adhesion molecule elevated in acute endothelial activation and dysfunction (Curaj *et al.*, 2018). Although several promising biomarkers have been identified, it is unlikely that a single biomarker will unambiguously aid early detection of sub-clinical atherosclerosis in all patient cohorts; therefore, a multi-marker panel approaches are the most likely way forward.

In recent years extracellular vesicles (EVs) have attracted huge research interest due to their promising medical diagnostic and prognostic attributes and applications. EVs possess many favourable traits that shape them to be the perfect biomarker contender to serve as early diagnostic tools for CVD and other diseases such as cancers (Soung *et al.*, 2017) and neurodegenerative diseases (Yoo *et al.*, 2018). EVs are unique candidates for disease detection and therapeutic delivery as they are non-immunogenic, non-tumorigenic, circulate the entire body and cross the blood-brain barrier. (Ha, Yang and Nadithe, 2016; Zhu *et al.*, 2017; Matsumoto *et al.*, 2018). Recent progress in EV discovery has identified a potential application of EVs as tools for diagnosis, prognosis, and therapy in CVD. The ubiquitous nature of EVs in biological fluids is advantageous compared to current diagnostic tools. Secreted by virtually all cell types in the body, EVs play a unique role in intercellular communication, suggesting their pathophysiological role in CVD progression. The cellular origin, composition, and functional property of circulating EVs can be exploited as a sub-clinical non-invasive biomarker to detect pathological diseases represented by various proteins, lipids, and nucleic acids encapsulated in the vesicular membrane. It has been reported that the role of EVs in the pathogenesis of CVD may be due to the transfer of molecules such as inflammatory cytokines, proteins, and miRNAs from injured cells to neighbouring resident vascular cells resulting in the initiation of an inflammatory response and angiogenesis (Boulanger *et al.*, 2017; Ribeiro-Rodrigues *et al.*, 2017; Loyer *et al.*, 2018; Sluijter *et al.*, 2018).

1.5 Extracellular vesicles, the dark horse of diagnostics

In both physiological and pathological conditions, EVs are continuously secreted by most cell types within the body. Upon secretion, their stable structure allows them to protect their cargo from destruction as they travel through the body, enabling their detection in bodily fluids, including; blood (Abdel-Haq, 2019), saliva (Machida *et al.*, 2015) urine (Street *et al.*, 2017), breast milk (Qin *et al.*, 2016), cerebrospinal fluid (Yagi *et al.*, 2017), semen (Madison, Jones and Okeoma, 2015) and amniotic fluid (Keller *et al.*, 2007). Although EVs can travel around the body, it is suggested that certain biological fluids will be enriched with EVs representing the cells they are derived form and in contact with. Circulating EVs have a specific makeup of miRNAs, proteins, and lipids which mirror their cellular origin and physiological state. Under pathological conditions, this 'signature' changes; therefore, vesicular content may be useful as a biomarker for the early diagnosis of disease. Several studies have shown an association between elevated EVs and prediction and development in the past decade. Elevation of circulating EVs have been shown in the following; development of atherosclerotic plaques (Aikawa, 2016; Kapustin and Shanahan, 2016), peripheral arterial disease (Mallat *et al.*, 1999; Badimon *et al.*, 2016), and the Framingham risk score, a risk assessment tool to determine patients 10-year risk of developing CVD (Chironi *et al.*, 2006; Nozaki *et al.*, 2009; Ueba *et al.*, 2010).

Specifically, microRNAs (miRNAs) are the most studied element of vesicular cargo for their role in CVD. A study by Kuwabara *et al.* reported the importance of two cardiac-specific miRNAs, miR-1 and miR-133a, which are upregulated in serum from patients presenting with an acute coronary event (Kuwabara *et al.*, 2011). In 2013 Li *et al.* expanded further on this study, reporting that miR-1, mi-R133a, mi-R208b, and miR-499 are significantly increased in patients after an acute coronary event relative to the levels of healthy volunteers. However, compared to cardiac troponin 1, none of the four miRNAs were superior for early detection of CVD (Li *et al.*, 2013). In contrast, a study carried out by Wang *et al.* detected a particular circulating miRNA, miR-208a, which was undetectable in healthy patients but was elevated in 100% of patients presenting with myocardial infarction. Not only did it become elevated, but it was detected within 4 hours from the onset of chest pain, reaching its peak earlier than that of troponin (Wang *et al.*, 2010). Although many miRNAs markers have been discovered as possible diagnostic

markers, Matsumoto and colleagues found a particular trio of has-miRNAs, has-mi-R-192, has-miR034a, that may potentially be used as an early prognosis of CVD. They reported that all three miRNAs were upregulated in serum samples of CVD patients that experienced CVD events within a year of their detection. This suggests a putative role for EV encapsulated miRNA as a biomarker in CVD diagnosis and prognosis (Matsumoto *et al.*, 2013). Although EV miRNAs have attracted huge interest as potential biomarkers in disease, few studies have analysed their pathologic proteomic profile. Of particular interest to this study is the identification of a potential novel diagnostic biomarker that acts as a putative regulator of stem cell myogenic differentiation *in vitro*, contributing to stem cell myogenic differentiation, proliferation, and migration during arterial remuddling *in vivo*. Although classically secreted ligands can reach their destiny by cellular diffusion, there is a growing realisation that secreted EVs may contribute and or mediate the release and spread of key ligands from one cell to another (McGough and Vincent, 2016).

1.6 Extracellular vesicles, the cellular postmen!

Initially thought of as merely a disposal mechanism of cellular waste, EVs have recently become a focal point in research due to their multifunctional role in many biological processes such as cell-cell communication (Bang and Thum, 2012), protein clearance (Johnstone *et al.*, 1987) regulation of immune response (Bobrie *et al.*, 2011), cancer (Muralidharan-Chari *et al.*, 2010) and CVD (Jansen, Nickenig and Werner, 2017). Various mechanisms constitutively release this heterogeneous population of phospholipid bi-layer-enclosed vesicles from many cell types, including immune cells, tumour cells, neurons, and ECs. Upon formation, these EVs are packed with informative goodies from their host cells such as proteins, DNA, and miRNA and released into the extracellular environment to be captured and internalized by neighbouring cells or travel through the systemic circulation system to neighbouring tissues.

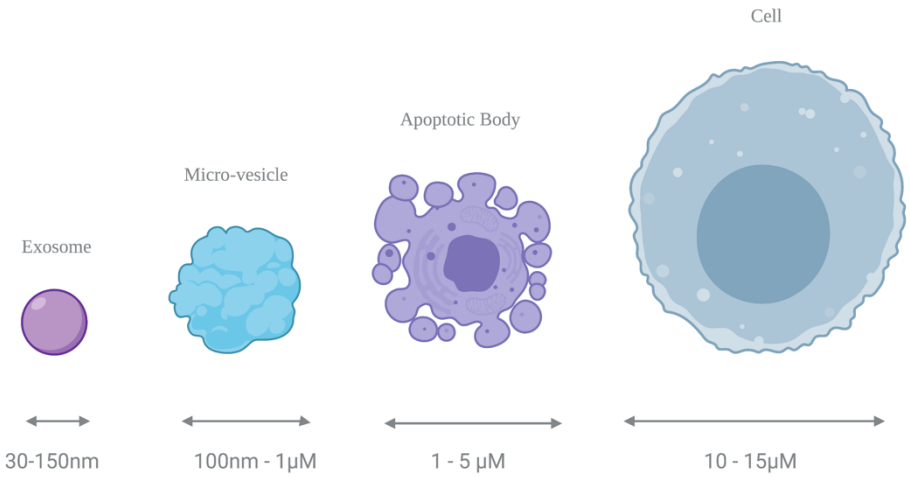

Figure 1.6 Comparison of size ranges of extracellular vesicles. The smallest characterised extracellular vesicle is the EVs ranging between 30-150nm. Microvesicles are slightly larger ranging from 100nm to 1μM in diameter. Apoptotic bodies are the largest of the extracellular population, are the most heterogeneous, ranging anywhere between 1 – 5μM. (Created with BioRender.com).

1.6.1 Characterisation of Extracellular Vesicles

1.61.1 Apoptotic Bodies

EVs are released in various shapes and forms by mammalian and non-mammalian cells. Due to their small nature, classification of EVs can prove challenging; however, they can be somewhat characterised by their size, content, and sub-cellular origin (Figure 1.6) (Colombo, Raposo and Théry, 2014). There are three main mechanisms by which EVs may arise, resulting in three distinct subpopulations of vesicles (Figure 1.7) (van der Pol *et al.*, 2012). The first and most studied involves cell fragmentation during a programmed cell death process known as apoptosis. During this process, the cell undergoes several morphological changes in response to an internal breakdown of intracellular proteins resulting in membrane blebbing, thin membrane protrusion formation, and release of apoptotic bodies. Apoptotic bodies are the largest sub-population of EVs and range between 1-5 μM in diameter (Kerr, Wyllie and Currie, 1972), consisting of membrane-bound cytoplasm with tightly packed organelle and nuclear debris from the host cell. Once secreted into the extracellular space, these vesicles undergo phagocytosis by neighbouring immune cells (Arandjelovic and Ravichandran, 2015).

1.6.1.2 Microvesicles

The second method of EV generation involves the shedding of membrane-bound sacs, known as microvesicles, from various cell types. Small cytoplasmic vesicles protrude from the host cell membrane during this process, detaching through a blebbing process. The mechanism that drives this process is not fully understood; however, the rate of the shedding process has been dramatically increased upon stimulation of cytosolic concentrations of calcium ions. The increase of calcium ions activates scramblase and calpain, resulting in a loss of membrane phospholipid asymmetry and degradation of various proteins facilitating outward budding of microvesicles from the cellular membrane (Zwaal and Schroit, 1997; Yuana, Sturk and Nieuwland, 2013). Microvesicles can vary in size but generally fall between 100nm to 1 μm in diameter. The cargo packaged within these cells includes proteins, DNA, and miRNAs; however, not all microvesicles will carry the same messages. The proteins carried within indicate the host cell in which they have fled (Del Conde *et al.*, 2005; Pluskota *et al.*, 2008; Flaumenhaft *et al.*, 2009).

1.6.1.3 Exosomes

Exosomes are the smallest subset of EVs ranging between 30-150nm in size. These endosomal derived microvesicles first came to light in the 1980s when researchers Pan, Stahl, and Johnstone reported their existence in the extracellular space while studying the maturation of reticulocytes to erythrocytes via exosomal secretion of transferrin receptors in the bloodstream (Harding and Stahl, 1983; Pan and Johnstone, 1983; Kowal, Tkach and Théry, 2014). These vesicles are double-layered, with the lipid bilayer corresponding to the cells from which they are released. The secretion of exosomes from cells was initially considered produce of cellular waste, secreted during the maintenance of cellular homeostasis, bearing no significant impact on neighbouring cells and tissues.

Interestingly, in the past decade, it has been widely accepted that these vesicles are functional vehicles carrying a variety of membranous bound complex cargo of lipids (Vidal *et al.*, 1989), proteins (Simpson *et al.*, 2009), DNA (Waldenström *et al.*, 2012), mRNA and microRNA (Valadi *et al.*, 2007). This unique process enables the delivery of these cargos to proximal and distal cells and tissues, initiating a response, representing a

mode of intracellular communication. Although initial discoveries proved the release of exosomes from blood cells, it has since been confirmed for almost all eukaryotic cells within the body, including, but not limited to, various immune cells (dendritic cells, T-cells, B-cells, astrocytes)) (Peters *et al.*, 1989; Zitvogel *et al.*, 1998) tumour cells (Wolfers *et al.*, 2001; Verma *et al.*, 2015), epithelial and resident vascular cells (cardiomyocytes, VSMCs, vascular progenitor cells, ECs) (Hergenreider *et al.*, 2012; Zhao *et al.*, 2017). However, it is well established that the cargos secreted by these cell types may differ significantly from each other. With this in mind, exosomes and the cargo within may offer potential insight into cell-cell communication as well as prognostic information in various diseases such as cancers (Soung *et al.*, 2017), neurodegenerative diseases (Howitt and Hill, 2016), chronic inflammation (Lässer *et al.*, 2016) renal and CVD (Gonzalez-Calero, Martin-Lorenzo and Alvarez-Llamas, 2014; Kishore, Garikipati and Gumpert, 2016).

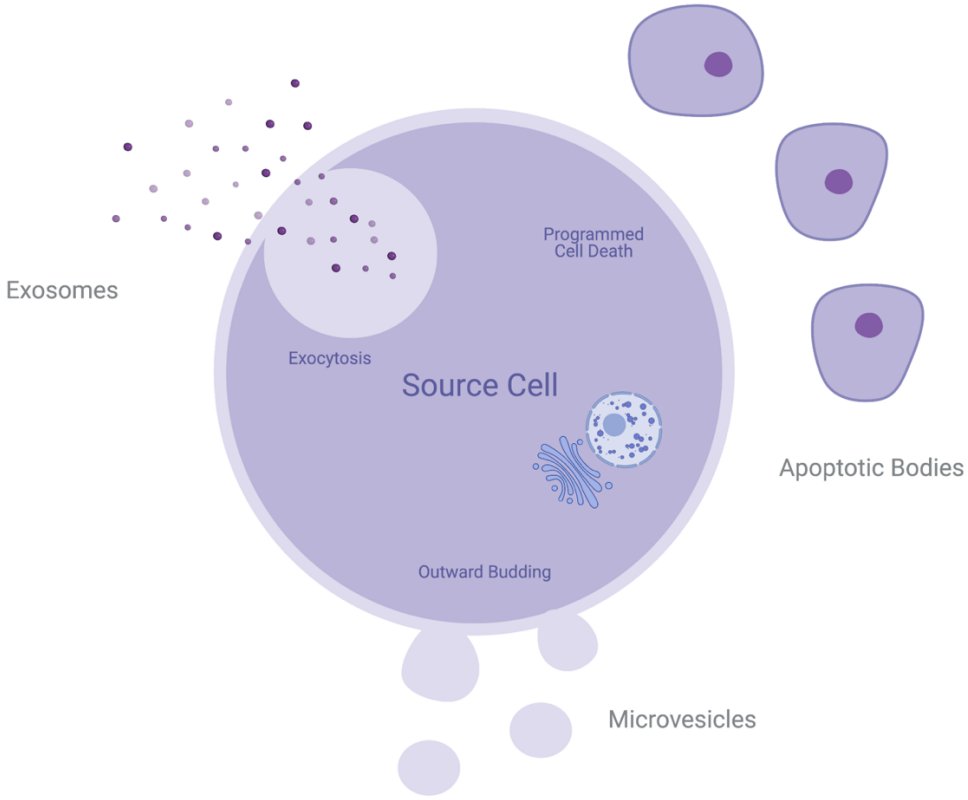

Figure 1.7 Subtypes of EVs and mode of formation. There are three subtypes of EVs that can be classified based on their mode of biogenesis. EVs are released from the cell through a process called exocytosis. In contrast, microvesicles are secreted by the outward budding of the plasma membrane. Apoptotic bodies are released by dying cells through a controlled programmed cell death known as apoptosis. (Created with BioRender.com).

1.6.2 Exosome biogenesis

Upon their discovery in the 1980s, the production of exosomes was reported to be via an intracellular process in the endosomal compartment of the cell. This process is initiated by an inward membrane budding of an early endosome into the luminal department, leading to multivesicular bodies (MVBs). Following this, invagination of late endosomal membranes results in intraluminal vesicles (ILVs) within large MVB's. In 1987 Johnstone *et al*. later coined these ILVs' exosomes (Pan *et al.*, 1985; Johnstone *et al.*, 1987). At this stage, various proteins along with cytosolic compounds from the host cell are incorporated into the invaginating membrane-bound ILVs. There are two distinct pathways in which MVB's are fated, the first of which involves fusion to the plasma membrane and subsequent release of exosomes into the extracellular space, or fusion with lysosomes, leading to the degradation and recycling of their nucleotide, lipid, and protein contents (Figure 1.8) (Babst, 2011).

1.6.2.1 ESCRT-dependent

Several proposed models are currently associated with the mechanism by which exosomes are formed. However, the most robust system for eukaryotic cells is the utilization of the established endosomal sorting complex required for transport (ESCRT) system and possibly additional ESCRT-independent pathways (Raiborg and Stenmark, 2009; Wollert *et al.*, 2009; Colombo *et al.*, 2013). ILV formation requires two distinct pathways. The first involves endosomal enrichment for tetraspanin CD9 and CD63, along with membrane reorganization (Pols and Klumperman, 2009). Secondly, the recruitment of the ESCRT complex to the site of ILV formation. The ESCRT pathway consists of approximately 20 proteins sorted into four soluble multi-protein complexes ESCRTs, -0,-I -II, and -III that work cooperatively to facilitate MVB formation, vesicle budding, and protein cargo sorting (Pocognoni, Berberián and Mayorga, 2015; Christ *et al.*, 2017). ESCRT complexes contain ubiquitin-binding subunits. Initiation of the pathway begins by recognition and sequential binding of ESCRT -0 to ubiquitylated proteins in the endosomal membrane (Meister *et al.*, 2017).

ESCRT -I complex then recruited to the cytosolic side of the early endosomes via various stimuli including tsg101, phosphatidylinositol 3-phosphate, and hepatocyte growth factor-regulated tyrosine kinase substrate forming a sophisticated binding ubiquitinated cargo proteins and activating the ESCRT-II (Fernandez-Borja *et al.*, 1999; Katzmann, Babst and Emr, 2001; Bache *et al.*, 2003; Razi, 2006; Shields *et al.*, 2009; Tamai *et al.*, 2010). Activation of the ESCRT -11 initiates the oligomerization and the formation of the ESCRT-III complex. This whole protein complex is involved in promoting the budding processes. Following budding formation and successful cleavage, the ESCRT -111 complex separates from the MVB membrane via the sorting protein Vps4 and is dissembled by AAA-ATPase suppressor-of-potassium-transport-growth-defect-1 protein (Bishop and Woodman, 2001; Benedetto *et al.*, 2006). In summary, following endosomal membrane reorganization, ESCRT- I and -II initiate and drive intraluminal budding of the MVB while ESCRT -III completes the budding and cleavage process resulting in the formation of ILVs ready for secretion.

1.6.2.2 ESCRT-independent

Exosomes can also be formed in an ESCRT-independent manner. Several ESCRT-independent mechanisms have resulted in the successful generation of ILVs in MVBs following complete disruption of ESCRT function (Stuffers *et al*., 2009). Although ESCRT-independent biogenesis of exosomes does not disrupt the general formation of ILVs, the formation of specific ILV populations may be hindered (Colombo, Raposo and Théry, 2014; Edgar, Eden and Futter, 2014). The discovery of a ceramide-based mechanism of ILV biogenesis initiated the hypothesis that exosome formation was not ESCRT dependent. Studies carried out by Trajkovic *et al.* have shown that exosome biogenesis requires the generation of ceramide, a cone-shaped lipid produced during the hydrolyses of sphingomyelin by the enzyme sphingomyelinase. Production of ceremide may then facilitate the generation of membrane domains by membrane invagination due to its cone-like structure and further induce ILV curvature (Trajkovic *et al*., 2008; Kajimoto *et al*., 2013). Further studies have shown that MVBs loaded with CD63 positive ILVs were formed following depletion of components essential for ESCRT complexes (Stuffers *et al*., 2009). In addition to this, several other ESCRT-independent generations of ILVs have been reported, including the role of the tetraspanin-mediated organization

of particular proteins, such as the amyloidogenic protein premelanosome in endosomal sorting and release (Escola *et al*., 1998; Fast *et al*., 2017).

Interestingly, different pathways may act together or even in parallel to promote ILV formation and release. This theory was brought to light by Baietti *et al*. during the discovery of an alternative ESCRT pathway, the syndecansyntenin-ALIX pathway. The leading players facilitating vesicle formation, loading of proteins, and exosome biogenesis include heparinase, syndecan heparan sulfate proteoglycans, phospholipase D2, ADP ribosylation factor 6, and syntenin. The formation of ILVs is dictated by the interaction of syntenin with ALIX and relies on the bioavailability of heparan sulfate, syndecans, ALIX, and ESCRTSs (Baietti *et al.*, 2012). A further study carried out by Hoshiono *et al.* in cancer cells reported that ESCRTs and ceramide function in unison to facilitate the formation of ILVs (Hoshino *et al.*, 2013). To date, proteomic analysis of exosomes suggests that a cell type can release mixed vesicles populations at any given time (Bobrie *et al.*, 2012; Chen *et al.*, 2016; Kowal *et al.*, 2016). Therefore, it is not surprising that exosomal biogenesis may involve both ESCRT-dependent and ESCRT-independent pathways. Although the ESCRT pathway is generally considered the primary driver of exosome biogenesis, a major challenge for the future is to understand how different regulators of exosome biogenesis interact with one another the effect of each mediator on the production of diverse exosome populations.

1.6.3 Exosome secretion and release

Exosomes are secreted by many cell types during physiological and pathological conditions. There are two main pathways by which exosomes are released and secreted from their host MVB; the constitutive release pathway, associated with general physiological secretion of exosomes (Record *et al.*, 2011; Record, 2013) and the inducible release pathway initiated by stimuli such as heat shock, hypoxia (Sluijter *et al.*, 2014), DNA damage (Yu, Harris and Levine, 2006), increased intracellular calcium release and LPS (Théry *et al.*, 1999). The initiation of exosome release begins with the transport of MVBs to the plasma membrane; this process is dependent on their interaction with actin and the microtubule cytoskeleton (Villarroya-Beltri *et al.*, 2014; Sinha *et al.*, 2016). Many mediators are involved during membrane trafficking of ILVs, including vesicle budding, membrane fusion, and transport along actin and tubulin (Ostrowski *et*

al., 2010). The most important of which are Rab guanosine triphosphatases (RAB GTPase), the most prominent family of small GTPases composed of approximately 70 distinct proteins that facilitate different purposes (Pfeffer, 2001; Stenmark, 2009; Blanc and Vidal, 2018). Among these proteins are Rab11 and Rab35, known for their role in trafficking membrane cargo to and from recycling endosomes on the way to the plasma membrane (Sato *et al.*, 2008; Takahashi *et al.*, 2012; Klinkert and Echard, 2016), Rab27A, known to promote the docking of MVBs and fusion to the plasma membrane and Rab27B facilitating vesicle transfer from the Golgi to MVBs (Ostrowski *et al.*, 2010). In 2002 Savina *et al*. were the first to show the role of Rab GTPase, Rab11, in exosome secretion in human leukemic K562 cells. They reported that overexpression of a dominant-negative Rab11 mutant inhibited exosome release (Savina, Vidal and Colombo, 2002). Similarly, Koles et al. reported that depletion of Rab11 in drosophila S2 cells reduced the levels of exosome secretion (Koles *et al.*, 2012). Further to this, a study by Ostrowski *et al*. reported the role of Rab2b, Rab5a, Rab9a, Rab27a, and Rab27b in exosome secretion in an shRNA screening targeting 59 Rab GTPases in HeLa cells. Interestingly they showed that depletion of Rab27a and Rab27b reduced the ability of MVBs to dock onto the plasma membrane (Ostrowski *et al.*, 2010). Similarly, Hsu *et al*. reported the role of Rab35 localisation onto an oligodendrocyte in a GTP-dependent manner during MVB docking and membrane fusion. Inhibition of Rab35 resulted in intracellular accumulation of vesicles and impaired exosome secretion (Hsu *et al.*, 2010). In contrast, there are several methods of GTPase independent methods of exosome release during the inducible secretion of exosomes. In 2012 King *et al*. demonstrated that the release of exosomes from breast cancer cells under hypoxic conditions could be mediated through a hypoxia-inducible factor 1a (Michael, Gleadle and King, 2012). Inducible release of exosomes was reported in rat microglial cells upon culture with cysteine-rich glycoprotein, Wnt3a, exosome secretion was mediated through a glycan synthase kinase 3-independent mechanism (Hooper *et al.*, 2012). During cellular stress, this enhanced exosome secretion depends on activation of p53, a regulator of the transcription of the tumour suppression-activated pathway 6 TSAP6 gene (Yu, Harris and Levine, 2006; Lespagnol *et al.*, 2008).

Once transported to the plasma membrane, MVBs undergo a fusion event followed by exosome secretion into the extracellular space. To allow this several coordinated multilevel changes in cytoskeletal plasma, membrane interactions have to be overcome. The first of which involves energy reduction of the membrane via several protein-protein, protein-lipid interactions followed by local enzymatic degradation and activation of membrane fusion machinery. MVBs fuse with the plasma membrane via soluble N-ethylmaleimide-sensitive factor attachment protein receptors (SNAREs), tethering factors, Rabs, and other Ras GTPases (Pfeffer, 2007). To date, the exact molecular necessities for MVB membrane fusion are not well established; however, many studies have reported the crucial role of SNARE proteins and synaptotagmin family members (Jahn and Scheller, 2006). The primary function of SNARE proteins and their associated complexes is to facilitate vesicle fusion to the plasma membrane while providing specificity for membrane trafficking via the formation of a SNARE complex (Bonifacino and Glick, 2004). Members of this family of proteins are classified into two categories, R or Q SNAREs. The formation of the SNARE complex involved in membrane fusion includes one R-SNARE, vesicle-associated membrane protein 7, and three Q-SNAREs forming four coiled-coil helices (Pfeffer, 2007). RSNARE proteins VAMP7 and YKT6 have been reported to be necessary during exosome fusion of leukemic K562 cell lines and HEK293 cells, respectively (Fader *et al.*, 2009; Gross *et al.*, 2012).

During membrane fusion, vesicle SNAREs localized on MVBs interact directly with the target SNAREs localised on the intracellular side of the plasma membrane to form a SNARE complex. Once formed, the MVB successfully fuses with the plasma membrane, ready for exosome secretion into the extracellular space. Importantly, it has been shown that exosome secretion can be initiated independent of Rab GTPases through increases in intracellular calcium levels. Increased intracellular calcium levels following monensin or calcium ionophore A23187 have been shown to increase exosome secretion in human erythroleukemia K562 cells (Savina *et al.*, 2003). Similarly, Fauré *et al*. reported that following potassium-induced depolarisation of critical neurons, the subsequent influx of intracellular calcium led to increased exosome secretion (Fauré *et al.*, 2006). Similar findings have since been valid for oligodendrocytes (Krämer-Albers *et al.*, 2007) and breast carcinoma cell lines (Messenger *et al.*, 2018).Interestingly it has been shown that some proteins such as the synaptotagmin family function as calcium sensors controlling exosome secretion. Knockdown of synaptotagmin-7 has been shown to reduce the rate of

exosome secretion in head and neck squamous cells and measured by nano-tracking analysis (Hoshino *et al.*, 2013). Regardless of the mechanism by which they are released from MVBs, exosomes are released into the extracellular space remaining close to their host cell, interacting with neighbouring cells, or travel through various bodily fluids.

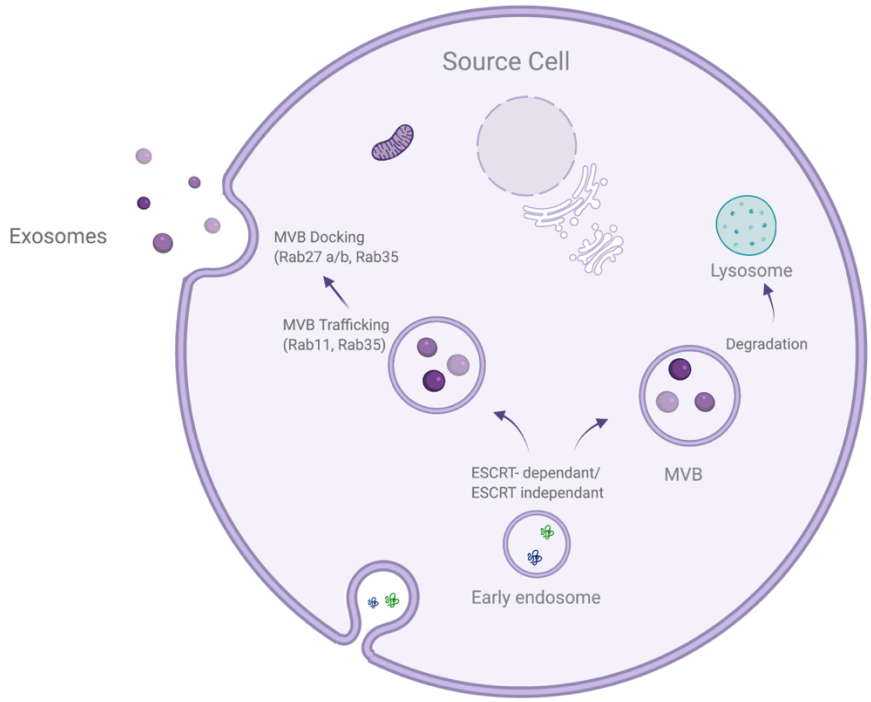

Figure 1.8 Exosome biogenesis. Exosome biogenesis is a complex process and can be conducted in an ESCRT dependent/independent manner. The internalisation of the plasma membrane initiates the formation of exosomes by endocytosis. The fusion of early endosomes results in the production of multivesicular bodies. Upon maturation, MVBs are directed to the plasma membrane via a tightly Rab GTPase-dependent multistep process. They undergo a SNARE-mediated plasma membrane fusion event followed by secretion into the extracellular space. (Created with BioRender.com).

1.6.4 Exosome Uptake and Function

Once released into the extracellular space, exosomes can reach their target cell and delivering their contents to initiate functional responses and/or promote phenotypic changes affecting their physiological or pathological status. Current research suggests successful delivery of exosomal cargo can occur via two main mechanisms; endocytosis or direct fusion with the target cell (Figure 1.9). Exosomal endocytosis is a multi-step process; the first step involves exosome docking onto the plasma membrane of the recipient cell via receptor-ligand binding. Although the cellular and molecular basis for

specific targeting of recipient cells are not clearly defined, several mediators are known, including specific lipids, lectins, tetraspanin, various extracellular matrix components, and heparan sulfate proteoglycans. For example, uptake of tumour and non-tumour-derived exosomes is substantially reduced following the block of heparan sulfate proteoglycans (Atai *et al.*, 2013; Christianson *et al.*, 2013). Similarly, the presentation of integrins on exosomes interacts with cell adhesion molecules at the surface of recipient cells, facilitating stable docking and attachment.

Irrespective of the mechanism by which exosomes dock to the recipient cell, once bound, they either remain attached to the plasma membrane (Denzer *et al.*, 2000; Buschow *et al.*, 2009) or become internalised. The method by which the exosome becomes internalised differs depending on the cell type. Multiple mechanisms of endocytosis have been shown, for example, phagocytosis and clatherin-mediated endocytosis in neurons, micropinocytosis by microglia, caveolin-mediated endocytosis in epithelial cells, and lastly lipid-raft endocytosis in tumour cells (Morelli *et al.*, 2004; Barrès *et al.*, 2010; Feng *et al.*, 2010; Fitzner *et al.*, 2011; Frühbeis, Fröhlich and Krämer-Albers, 2012; Montecalvo *et al.*, 2012; Nanbo *et al.*, 2013; Svensson *et al.*, 2013). Alternatively, exosomal uptake can occur via a direct membrane fusion event. However, this requires the insertion of fusogenic proteins into the plasma membrane, followed by lipid reorganisation, protein reconstruction, and membrane dimpling (Bonifacino and Glick, 2004; Podbilewicz, 2014). Following interaction and uptake by recipient cells through the mechanisms discussed above, exosomes may fuse with internal cytoplasmic endosomes resulting in the transfer of bioactive materials or possible degradation. However, it is currently unclear exactly how the cargo transfer occurs (Abels and Breakefield, 2016). Once internalised by the receipt, cell exosomes can initiate a diverse array of biological functions in both physiological conditions such as; intercellular communication (Meldolesi, 2018), immune modulation (Raposo *et al.*, 1996), coagulation, and thrombosis (Kapustin *et al.*, 2017) and protection against cellular stress and death, and pathological conditions such as; development and progression of neurodegenerative disease (Vella *et al.*, 2008), liver disease (Masyuk, Masyuk and Larusso, 2013), cancers (Hannafon and Ding, 2013) and CVD (Lawson *et al.*, 2016).

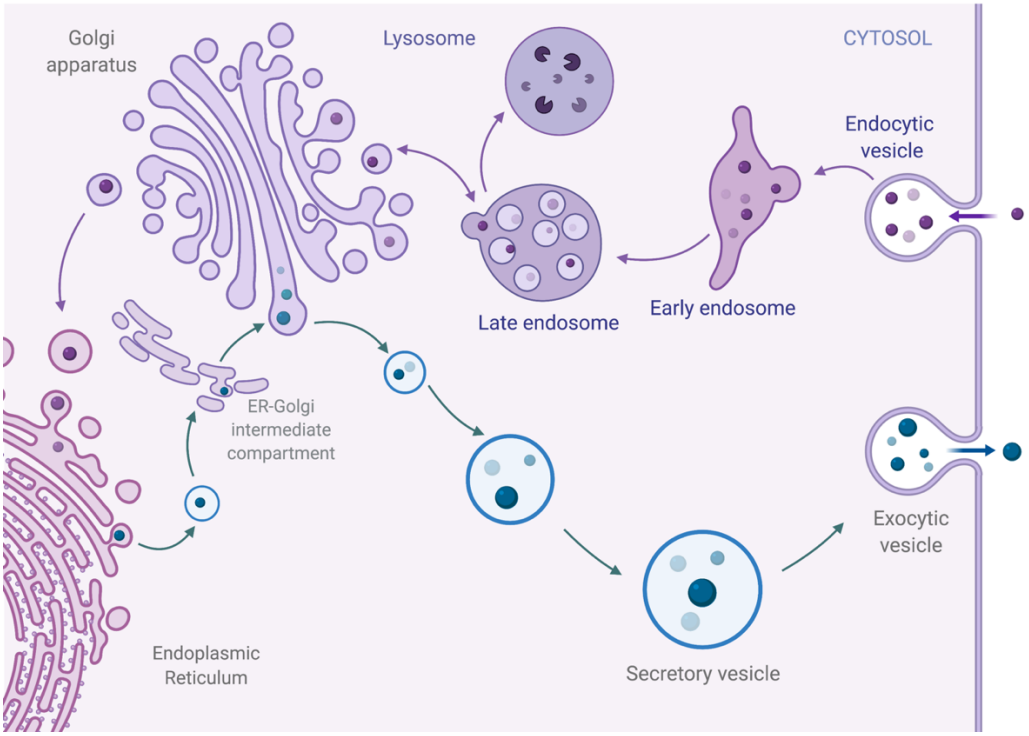

Figure 1.9 Exosome uptake by neighbouring cells. Schematic representation of exosome uptake by neighbouring cells. Once secreted into the extracellular space, exosomes can be taken up by neighbouring cells via two main processes (i) exosomes are engulfed into the target cell via endocytosis. Once endocytosed, exosomes fuse with the endocytic compartment delivering various cargo (ii) exosomes dock onto the target cell's plasma membrane and directly deliver their cargo into the cytoplasm of the target cell. (Created with BioRender.com).

1.6.5 Exosome Structure and the Cargo Within

Since their discovery in the 1980's exosomes have somewhat been regarded as a miniature version of the host cell in which they originate. This theory is predominantly due to the complex nature of exosomes in terms of structure and content mirroring that of the parent cell. In general, exosomes are heavily loaded with a diverse range of bioactive materials such as proteins, lipids, and nucleic acids (Figure 1.10) (Colombo, Raposo and Théry, 2014). In recent years extensive research has been carried out in a bid to identify and characterise exosomal content. This has led to the establishment of three main publicly accessible databases: EVpedia, Vesiclepedia, and Exocarta, which include helpful information such as protein, lipid, and nucleic acid content and isolation and purification procedures (Mathivanan and Simpson, 2009; Kalra *et al.*, 2012; Kim *et al.*, 2013).

Although exosomes contain a comprehensive and heterozygous range of molecules, some aspects of exosome structure are generally conserved across many populations. Scattered amongst their lipid bilayer is a cohort of proteins with various functions. Amongst these proteins are the tetraspanin family, typically CD9, CD37, CD63, CD81. Moreover, CD82 assisting in multiple functions such as cell penetration, invasion, and fusion (Escola *et al.*, 1998; Théry, Zitvogel and Amigorena, 2002; Yakimchuk, 2015). Although CD9 was the first of the family discovered in dendritic cells, several studies have reported an abundance of CD63 and CD81 expressed across a broad range of exosomes and are therefore are considered a robust marker for exosome detection (Escola *et al.*, 1998; Théry *et al.*, 1999; Raposo and Stoorvogel, 2013). Also present within exosomes are small heat shock proteins, mainly HSP27, HSP60, HSP70, and HSP90, involved in cellular response and antigen presentation during cellular stress, assisting protein folding and trafficking (Srivastava, 2002) as well as MVB formation proteins involved in exosomes formation and release, Alix, TSG101, Rab GTPases such as RAB11B, RAB27A, and ARF6. Interestingly, proteins associated with the endoplasmic reticulum, Golgi, and nucleus have not been detected in exosomal fractions (Théry *et al.*, 2001); however, numerous studies have shown the presence of EV membrane bound ligands involved in gene activation in target cells via receptor binding and internalisation (Kalra *et al.*, 2012; McGough and Vincent, 2016). Although the above proteins are commonly encapsulated in exosomes, it has been suggested that they are not uniformly distributed in all subpopulations highlighting that even the same cell can release structurally homogenous vesicles containing heterogeneous contents (Tauro *et al.*, 2013).

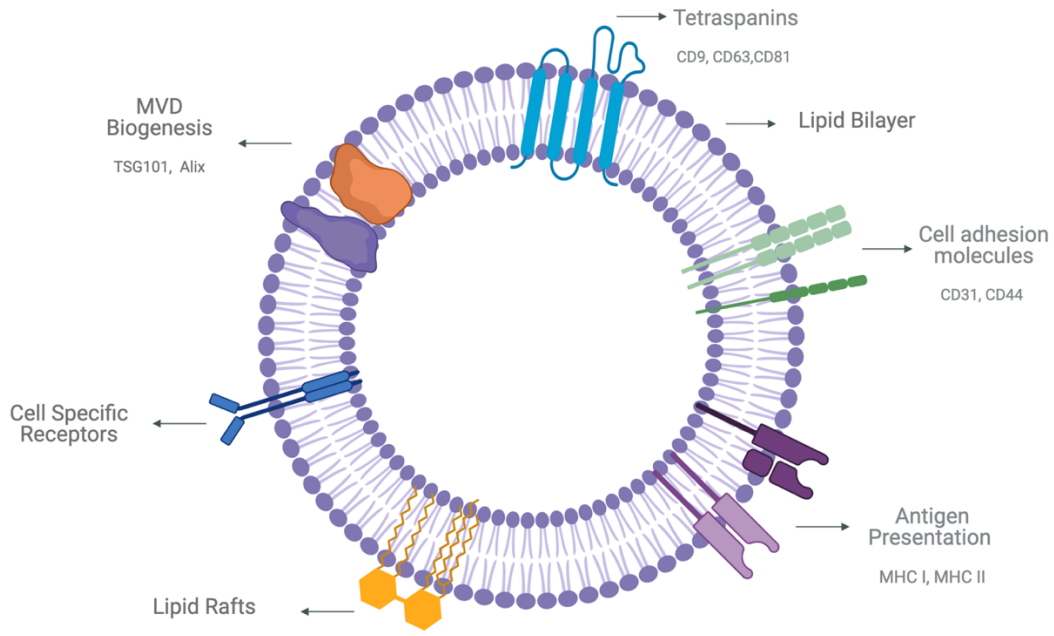

Figure 1.10 Structure and molecular components of exosomes. Exosomes are composed of a plasma membrane-derived phospholipid bilayer containing cytosol components from the cell of origin. The exosomes' composition depends on the cell type of origin, the state of health of the source cell, and extracellular stimuli. There are various proteins, lipids, and miRNAs common to most exosomes, including depicted above. (Created with BioRender.com).

1.7 Endothelial EVs

Like most cells in the body, vascular ECs retain the ability to release EVs into the extracellular space in response to cellular activation or apoptosis. Characterised by their expression of various EC specific surface markers (CD31, CD55, CD144, and von Willebrand factor), vascular endothelial EVs have been proven to play a putative role in physiological processes maintaining vascular homeostasis (Ridger *et al*., 2017), vascular development (Sheldon *et al*., 2010), endothelial regeneration and vascular cell protection (Abid Hussein *et al*., 2005), as well as the pathological progression of vascular disease (Abid Hussein *et al*., 2005; Bellin *et al*., 2019). Under basal conditions, the endothelium functions to maintain vascular homeostasis. A unique feature enabling this is the capacity to respond to various intrinsic physical stimuli. However, this trait is a double-edged sword as the endothelium actively responds to circulating CVD risk factors, including LDL, nicotine, and elevated glucose levels. Basic mechanisms involved in sub-clinical atherosclerosis indicate that deleterious alterations of the endothelium, referred to as

endothelial dysfunction (ED), represent a critical early step in the development of atherosclerosis (Anderson *et al.*, 1995; Kinlay and Ganz, 1997). Endothelial dysfunction is characterised by reducing the bioavailability of vasodilators, in particular NO, and/or an increase in endothelium-derived contracting factors. In addition to this, ED leads to endothelial activation characterised by a procoagulant, proinflammatory, and proliferative state that aids the development of sub-clinical atherosclerosis (Anderson, 1999). To truly understand the role of endothelial-derived EVs as a driving force during the pathogenesis of CVD, an understanding of the pivotal role of the vascular endothelium as the primary responder to physiological and pathological stimuli is required.

1.7.1 The endothelium, protector of the frontline.

1.7.1.1 Vascular barrier

The primary, most basic function of the endothelium is to act as a physical, semipermeable barrier. This physical barrier is formed by the close alignment of a single layer of ECs supported by the development of multiple cell-cell junctions, including adherens junctions, tight junctions, and gap junctions (Figure 1.11) (Yuan and Rigor, 2011). The central role of the formation of adherens and tight junctions is to establish and maintain cell-to-cell adhesion along the endothelium. The initiation of adherens junctions requires VE-cadherin recruitment, a calcium-dependent transmembrane endothelial-specific member of the cadherin family of adhesion proteins. VE-cadherin is linked through its cytoplasmic domain to catenin binding proteins p120, β-catenin, and α-catenin resulting in a reorganisation of the cytoskeleton actin filaments forming a tight cell-cell barrier (Meng and Takeichi, 2009). Similarly, the formation of tight junctions further enhances the endothelial barrier. Unlike adherens junctions, they have a complex protein composition consisting of a network of 40 different proteins (Schneeberger and Lynch, 2004), some of which include occludin, tetraspanin, and claudin protein family members, as well as many junctional adhesion molecules (Aijaz, Balda and Matter, 2006).

This network of proteins works together to form two distinct pathways across the tight junction referred to as a pore pathway, allowing passage of small ions and other various uncharged molecules, and a leak pathway, allowing the passage of larger macromolecules (Shen *et al.*, 2011). Junctions act as a physical barrier and play a vital role in the

permeability of the endothelium. In contrast, the primary function of gap junctions is cell-cell communication. This communication pathway is facilitated by forming inter-cellular hemichannels formed by members of the connexion transmembrane protein family (Goodenough, 1996). These inter-cellular channels allow for the bidirectional flow of ions and signalling molecules acting as a crucial intercellular communication channel involved in multiple cellular processes such as transport of metabolites, apoptosis, differentiation, and homeostasis in the vasculature (Laird, 2010).

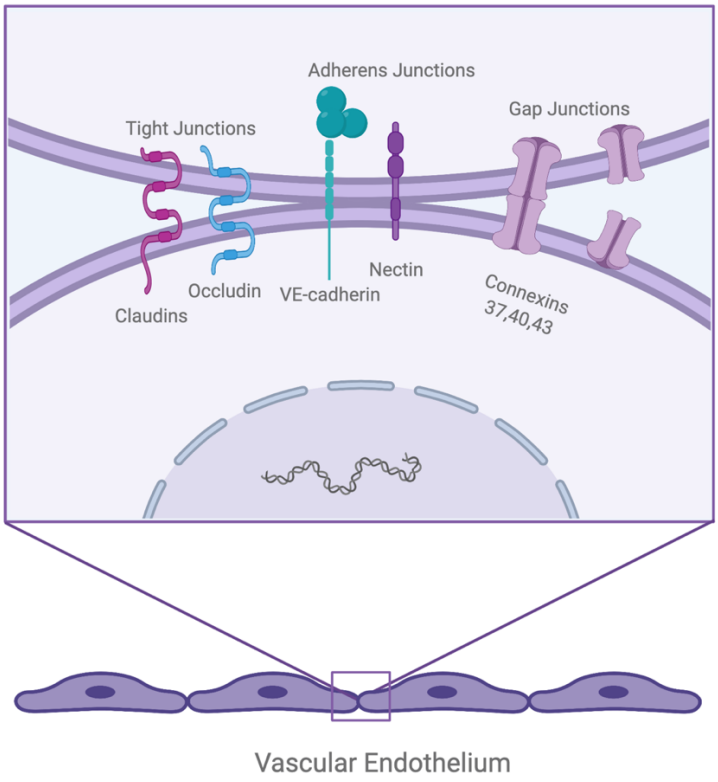

Figure 1.11 Compositional make up of inter-endothelial junctions. Schematic representation of the three inter-endothelial junctions; tight junctions composed of adhesion proteins such as claudins and occludin connected to actin present in the cytoskeleton of adjacent ECs, adherens junctions composed of vascular endothelial-cadherin connected to adjacent cells via α-catenin, β-catenin, and p-120-catenin connected to the actin cytoskeleton and finally gap junctions composed of connexin hexamers forming hemichannels. (Created with BioRender.com).

1.7.1.2 Oxidative Stress

One of the major targets of oxidative stress is the endothelium, playing a crucial role in the pathophysiology of several vascular diseases and disorders. Specifically, oxidative stress increases the permeability of the endothelium promoting infiltration of immune

cells, alterations in endothelial signalling, and redox-regulated transcription factors (Higashi *et al.*, 2009; Förstermann, 2010). Reactive oxygen species (ROS) is a term used to describe chemically reactive molecules and free radicals containing oxygen, some of which include primary ROS O2-, hydrogen peroxide (H_2O_2), nitric oxide (NO), and hydroxyl radicals (Finkel, 2011). ROS production under controlled conditions activates the intracellular reduction and oxidation (redox) signalling pathways mediating many physiological processes. However, overproduction of ROS leads to oxidative stress. The delicate balance between the beneficial and detrimental roles of ROS production is controlled by the presence of an internal antioxidant defence system comprising of endogenous pro-oxidative enzymes such as nicotinamide adenine dinucleotide phosphate-oxidase (NADPH) oxidase and xanthine oxidase, and anti-oxidative enzymes such as glutathione reductase, superoxide dismutase and peroxidase (Tiwari, 2014).

1.7.1.3 NADPH production of ROS

Initially, the overproduction of ROS metabolites within a cellular system was considered to be random. However, the advent discovery of NADPH oxidase (NOX) and dual oxidase (DUOX) enzymes have clarified that the generation and regulation of ROS is a controlled signalling system driven by two main enzymes; NOX and DUOX (Lambeth, Kawahara and Diebold, 2007). The NOX family of proteins are classified as hetero-protein transmembrane proteins (except for NOX5) and function as gateways to transfer electrons, specifically molecular oxygen, across biological membranes. There are seven classified NOX proteins present in the plasma membrane in mammals, NOX1 to 5 and DUOX 1/2 and the endoplasmic reticulum, NOX 2,4 and 5 the mitochondrial membrane NOX4 and the nuclear membrane, NOX4 and 5 (Skonieczna *et al.*, 2017). Although all isoforms are structurally similar to each member of the NOX family, enzymes have specific regulatory mechanisms, tissue specificity, and unique downstream targets (Drummond and Sobey, 2014).

1.7.1.4 Diabetes and NOX activation

Low levels of NOX isoforms are expressed under physiological conditions. However, upregulation of these isoforms is associated with vascular pathologies in response to endothelial injury. Among the seven isoforms of NOX enzymes, ECs express four NOX

isoforms, including the O2--generating enzymes NOX1, 2, and 5 and the hydrogen peroxide-generating enzyme NOX4 (Figure 1.12) (Drummond and Sobey, 2014). Under physiological conditions, these enzymes are expressed at relatively low levels on membranes of the endoplasmic reticulum (ER) and nucleus, contributing to intracellular redox signalling processes.

One of the main risk factors associated with the development of CVD is a condition known as diabetes mellitus, often referred to as diabetes. Diabetes is a metabolic disorder that is classically characterised by chronically elevated blood glucose clinically referred to as hyperglycaemia. Endothelial exposure to hyperglycaemic conditions results in an array of adverse effects triggering endothelial dysfunction due to attenuation of endothelium vasodilation, the release of inflammatory proteins, and insulin secretion (Williams *et al.*, 1998; Lin *et al.*, 2001; Toschi *et al.*, 2002; Simsek *et al.*, 2010). Insulin is an essential hormone produced in the pancreas that facilitates glucose entry into the body's cells, subsequently converted to energy. The absence of insulin in the body leads to high circulating glucose levels in the bloodstream, often clinically referred to as hyperglycemia. There are two sub-groups of diabetes (i) type 1 diabetes (T1D), an autoimmune reaction in which the body's immune system attacks insulin-producing beta cells of the pancreas resulting in daily dependence on insulin, and (ii) type 2 diabetes (T2D), the inability of the body's cells to respond to insulin resulting in resistance and subsequent inadequate production (World Health Organization, 2006; International Diabetes Federation, 2019). Many of the systemic changes in diabetes are known activators of NOX (Zhang *et al.*, 2013). Although the role of individual NOX isoform is not fully cemented, there is evidence of excess NOX-derived ROS using various *in vitro* models of hyperglycemia. The role of various NOX isoforms activated under hyperglycaemic conditions varies depending on the species with NOX1 and NOX2 elevation reported in murine models after induction of hyperglycemia (Youn, Gao and Cai, 2012; Sukumar *et al.*, 2013; Rezende *et al.*, 2018), while NOX2 and NOX4 associated with human *in vitro* induction of hyperglycemia (Taye *et al.*, 2010; Williams *et al.*, 2012). Interestingly although originally positively associated with regulation of vascular endothelial function, upregulation of NOX4 has been linked to ED. Studies in cultured human ECs under normal (5.5mol/L) or high glucose (30 mmol/L) concentrations showed an increase in both NOX2 and NOX4 protein expression (Taye *et al.*, 2010). Further studies have identified NOX4 as the primary source of ROS generation

following NF-κB activation, a strong inflammation, and metabolic malfunction. Induction of hyperglycemia enhanced interactions between NF-κB/p65 and the NOX4 promoter, indicating a strong association with NOX4-derived ROS via NF-κB/p65 transcription (Williams *et al.*, 2012).

The clinical relevance of NOX4 in human studies has not been explored. *In vivo* animal models have given insight into possible roles for NOX4 in hyperglycaemic environments. NOX4 has been identified as a curtail regulator of glucose homeostasis, as shown by Li and colleagues. Wild-type mice fed a 12-week high fat diet gained significant body weight as expected; however, NOX4 KO exacerbated the development of obesity within two weeks. Weight gain also continued through the administration of interventions suggesting NOX4 may be somewhat responsible for elevations in blood glucose during the development of insulin resistance (Li *et al.*, 2012). Previous studies support this finding with enhanced NOX4 protein levels report in streptozotocin-induced diabetic rats with unchanged levels of NOX1 and NOX2 (Maalouf *et al.*, 2012).

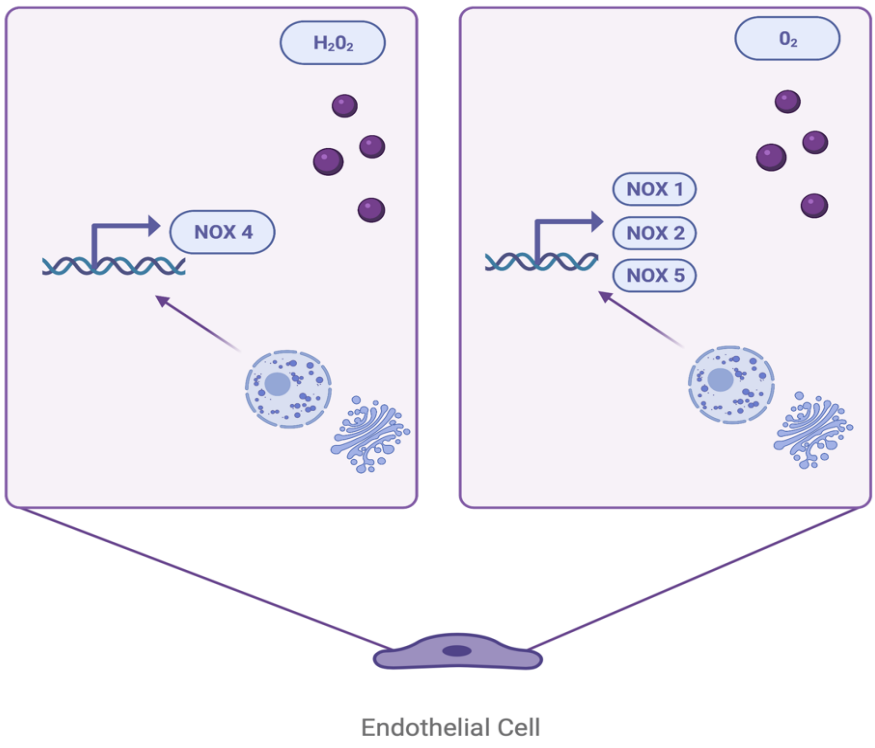

Figure 1.12 NOX isoforms present in the endothelium. Schematic representation of the NOX isoforms present in the ER of ECs. (Created with BioRender.com).

1.7.2 Endothelial EVs in CVD

Under physiological conditions, vascular ECs secrete low concentrations of EVs into the bloodstream. However, upon induction of ED, the concentration of EVs significantly increases (Vicencio *et al*., 2015; Dougherty *et al*., 2020; Zhang *et al*., 2021). It is widely accepted that when exposed to cellular stress or damage, ECs release growth factors and cytokines, which render change amongst neighbouring vascular cells. Whether this bioactive material is packaged into an exosome and secreted to other cardiac compartments remains clarified. Many studies have shown an increase in exosome content during the onset of CVDs such as diabetes mellitus, atherosclerosis, and myocardial infarction (Mallat *et al*., 2000; Bernal-Mizrachi *et al*., 2003). Although multiple studies have shown a direct role for the endothelial release of circulating microparticles and CVD, the study and consequence of EVs secretion and cargo content are less know. Quantitative proteomic studies have shown that EVs derived from ECs under different culture conditions have unique cargo content. When cultured in hypoxic conditions, EC-EVs present a high content of proteins involved in extracellular matrix remodelling. In contrast, when treated with TNF-a mimicking inflammation, EC EVs enriched for several factors associated with immune response and protection suggesting a vital role for EC release of EVs composed of a unique repertoire of proteins, lipids, and miRNAs in the development and progression of vascular disease (de Jong *et al*., 2012).

EV-mediated cell-cell communication is thought to drive vascular pathology. Studies have suggested that upon induction of ED, the consequential release of EVs into the subendothelial space facilitates communication with neighbouring cells such as VSMCs, vascular progenitor cells, and circulating immune cells. The uptake of EC-derived EVs containing various miRNAs and transcription factors initiates a functional response in neighbouring cells. *In-vitro* co-culture studies have shown KLF4-induced secretion of EVs from HUVECs harboured miR-143 and miR-145 enriched cargo. Upon co-culture with VSMCs, uptake of these EVs regulates VSMC phenotype depicted by a change in vascular de-differentiation genes such as ELK1, KLF4, CAMK2d, and SHH2. Furthermore, they established that EVs derived from ECs expressing KLF4 also induced the formation of atherosclerotic lesions (Hergenreider *et al*., 2012).

A similar cross-talk mechanism exists between vascular ECs and circulating monocyte macrophages, promoting atherosclerotic plaque formation. Studies by Tang and colleagues reported that EVs secreted by LPS/INFα activated monocytes are endocytosed by human ECs, resulting in the expression of ICAM-1 and pro-inflammatory cytokines. This process results in ED via the TLR4 and NF-κB pathways contributing to the development of heart disease and potentially other chronic immune activation diseases (Tang *et al*., 2016). Further studies have shown exosome-dependent monocyte to endothelial crosstalk exists between monocytes and ECs and visa-versa in response to hyperglycaemic conditions. Similar to previous studies, they reported that EVs derived from both monocytes and ECs modulate the expression of surface proteins such as ICAM-1 in response to high glucose (Sáez *et al*., 2019). This study is in line with previous data showing that circulating EVs from newly diagnosed diabetes type 2 patients are enriched with proteins responsible for cell activation, i.e., ICAM-1 (Xu *et al*., 2016).

In summary, a large body of research provides substantial evidence in favour of the active involvement of endothelial-derived EVs in the development and progression of associated vascular diseases. Endothelial EVs can efficiently deliver their cargo into recipient vascular cells driving pathological processes. Isolation and interrogation of endothelial EVs have the potential to serve as a snapshot of vascular health at any given stage of life. This favourable trait marks them as new contenders for use in early detection and prevention of disease. Although extensive research has focused on the role of EV miRNA as potential diagnostic biomarkers for disease due to their involvement in post-transcriptional regulation of gene expression, the role of EV proteomic profiles is recently becoming evident. Differences in EV protein content occurs in response to a variety of physiological or pathologic stimuli. The protein profile of circulating endothelial EVs may stand as a sub-clinical diagnostic biomarker for CVD. Studies of EV proteomic profiles have suggested a link between EV proteins and atherosclerosis which showed that hypercholesterolemic patients with subclinical lipid-rich atherosclerotic plaques have a higher abundance of CD45/CD3-derived ECs than those in patients with fibrous plaques (M. A. Rogers *et al*., 2020). Interestingly current research has focused on the cargo encapsulated within EVs as diagnostic biomarkers. Research carried out by our group along with others have shown the role of Hh signalling during vascular pathogenesis (Di Luca *et al*., 2021). Local inhibition of the Hh receptor, pathched-1, attenuates subclinical atherosclerotic disease in murine models (Redmond *et al*., 2013). Furthermore HHIP-

LIGWAS studies have shown an association of Hh SNPs with coronary artery disease (Schunkert *et al*., 2011). Therefore, taking these findings on board further research is needed to identify the possible role of EVs during the transport of Hh morphogens as initiators of this pathologic cascade.

1.8 Sonic hedgehog protein

Paracrine signalling refers to the release of a ligand from its site of production into the extracellular environment, where it travels until binding to its targeted receptor. Under physiological and pathological conditions, cell-fate decisions and tissue homeostasis require precise information input from the extracellular space. First discovered for their role in embryogenesis, secreted morphogens act in a paracrine manner aiding essential processes within the body. Failures in the secretion of these morphogenic signals lead to severe developmental disorders and disease pathogenesis (Briscoe and Thérond, 2013). The hedgehog (Hh) signalling pathway is a critical mediator of many cellular and developmental processes. The Hh protein family consists of morphogenic molecules crucial in embryogenesis, postnatal morphogenesis, and general tissue homeostasis. Hh proteins are post-translationally modified by cholesterol at the C-terminus and palmitate at the N-terminus; these lipid modifications act as an anchor to the cell (Porter *et al.*, 1996; Pepinsky *et al.*, 1998). Hh proteins can act in a dose-dependent manner or induce factors to control cell fate, proliferation, patterning, and survival. Three Hh proteins have been described in vertebrates, Sonic Hh (SHh), Indian Hh (IHh), and Desert Hh (DHh), of which SHh is the most studied (Echelard *et al.*, 1993). These proteins have some redundant properties. However, each has been shown to almost exclusively mediate particular developmental processes, such as neural tube patterning, endochondral skeletal development, and spermatogenesis, respectively, through the regulation of stem cell populations.

In vertebrates, the SHh signalling pathway is mediated by transcription factors Gli1, Gli2, and Gli3, transmembrane proteins Ptch 1, and smoothened (Smo). In the absence of Hh proteins, transcription factors Gli 1,2, and 3 are bound to suppressor of fu (sufu) kinase family members seven and cos-2, forming a repressor complex. The Hh-dependent signalling cascade is initiated when the Hh ligand binds to the integral-membrane protein

Ptch receptors via interaction of the Ptch sterol-sensing domain and Hh cholesterol motif. Once bound, the Ptch-Smo receptor complex dissociates, resulting in the phosphorylation and activation of Smo. This phosphorylation process leads to the disassembly of the Gli-sufu repressor complex allowing translocation of Gli transcription factors to the nucleus to initiate transcription of Hh target genes (Figure 1.13) (Hooper and Scott, 2005; Choudhry *et al.*, 2014; Mooney *et al.*, 2015). Gli activators induce the transcription of Hh target genes primarily involved in cell proliferation, cell survival, and cell fate specification, including PTCH and GLI (Marigo and Tabin, 1996). HHIP (Hh interacting protein) modulates Hh signalling activity by binding and inhibiting the action of Hh proteins (Chuang and McMahon, 1999).

Genome-wide association studies (GWAS) in patients presenting with CAD have identified variants at the 14q332 HHIPL1 that encode a paralog hedgehog interacting protein (HHIP) to increase Hh signalling activity, by binding and inhibiting the action of hedgehog proteins, resulting in VSMC proliferation and migration *in vitro* (Schunkert *et al.*, 2011). Hh has been identified through increased lipid uptake by macrophages in murine atherosclerotic models, while HHIP1 deletion reduces atherosclerotic plaque formation (Beckers *et al.*, 2007; Aravani *et al.*, 2019). Furthermore, SHh signalling and EGF-like domain-containing two and signal peptide CUB domains are overexpressed in injured arteries (Morrow *et al.*, 2009; Ali *et al.*, 2013; Dutzmann, Koch, Weisheit, Sonnenschein, Korte, Haertlé, Thum, Bauersachs, Sedding and J. M. Daniel, 2017). The role of stem cell differentiation during VSMC migration in response to vessel injury remains a possible source of neointimal cells during vessel remodelling. Adventitial $Sca1^{+}$ cells that co-localise with SHh and Ptch1 significantly contribute to intimal thickening *in vivo* (Tsai *et al.*, 2012; Shikatani *et al.*, 2016; Dutzmann, Koch, Weisheit, Sonnenschein, Korte, Haertlé, Thum, Bauersachs, Sedding and J. M. Daniel, 2017) while Hh inhibition with cyclopamine or local perivascular depletion of Ptch1 attenuates intimal thickening following iatrogenic flow restriction *in vivo* (Redmond *et al.*, 2013; Fitzpatrick *et al.*, 2017). Recent findings have highlighted the role of an alternative $S100\beta^{+}$ resident vascular stem cells as a source of neointimal VSMCs through lineage tracing analysis of transgenic S100β-Egfp-cREert2-Rosa26-tdTomato reporter mice. Morphometric analysis of S100β-Egfp-CREer2-Rosa26tdT confirmed a significant increase in the number of S100β-tdT marked cells within the intimal and medial layers of the injured vessel. Interesting, parallel studies determined that inhibition of Hh signalling, through the

administration of Hh inhibitor cyclopamine, controls neointimal thickening following flow restriction by attenuating the volume and accumulation of Sca1 cells within lesions. Furthermore, Hh signalling directly promotes Sca1/S100β cells from mouse and S100β neuroectoderm (NE) stem cells derived from HiPSC to undergo growth and myogenic differentiation to VSMC-like cells *in vitro* (Di Luca *et al.*, 2021).

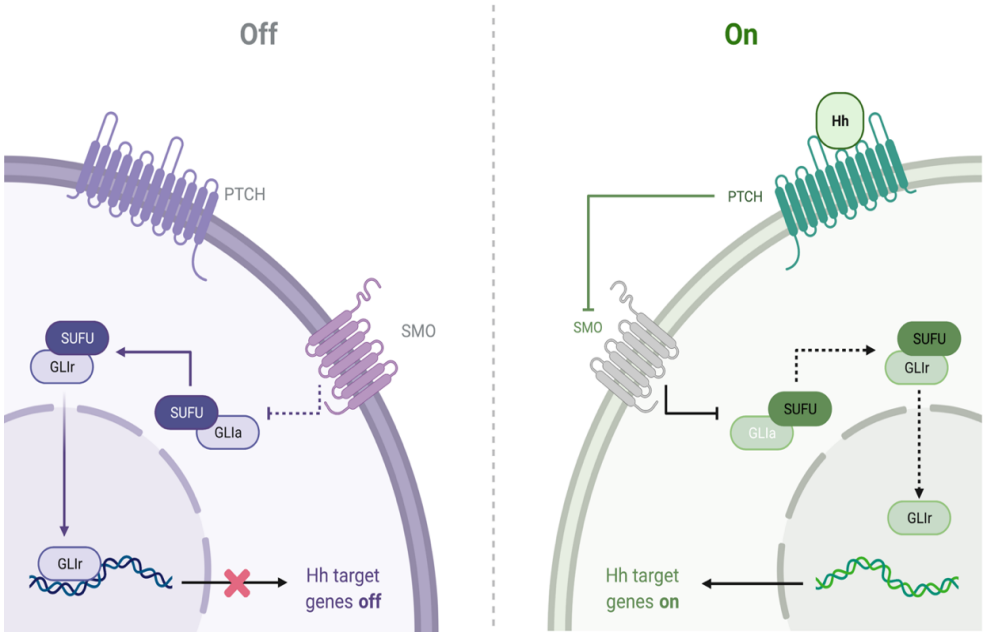

Figure 1.13 Hh signalling pathway. In the absence of Hh, membrane-bound Ptch receptor inhibits Smo, resulting in the repression of Gli genes by forming a Gli repressor complex composed of Gli full-length proteins, suppressor of Fu, kinesin family member seven and costal-2. In contrast, the Hh signalling pathway is activated when the Hh ligand binds to Ptch receptor resulting in phosphorylation of Smo, promoting disassembly of the Gli repressor complex. This complex then localises in the nucleus activating target gene expression of Hh genes (Mooney *et al.*, 2015).

1.8.1 EVs and Hh Signalling

Although several mechanistic models are proposed for the extracellular transport of Hh, recent studies have identified the role of EVs as means of transport exerting their long-range signalling function. Overexpression of GFP/CFP tagged Hh in Drosophila wing discs showed Hh trafficking was localised in the plasma membrane of producing cells where it forms nanoclusters, tagged Hh is then re-internalised by producing cells (Callejo *et al.*, 2011; D'Angelo *et al.*, 2015). Proteomic analysis of vesicles isolated from conditioned media of insect cells has identified Hh morphogen and known regulators of EV formation, including ESCRT machinery, small GTPase, and Rab proteins. Interestingly depletion of these proteins in culture leads to decreased morphogen

secretion on EVs (Matusek *et al.*, 2014; Vyas *et al.*, 2014; Parchure *et al.*, 2015). How Hh-EVs interact with their receptors is not known. Two possible pathways for interaction include endocytosis by neighbouring cells or direct binding to its receptor Ptch at the surface of receiving cells (Matusek *et al.*, 2014).

The secretion of Hh has been extensively investigated in Drosophila. Little is known about the secretion of Hh invertebrates. As discussed above, SHh plays a vital role during embryogenesis and recapitulates in adulthood during various human pathologies. With this in mind, SHh-containing EVs have been intensively studied. EVs carrying SHh are released into the extracellular space. An increase in circulating SHh-EVs has been shown following apoptosis and or T-cell stimulation (Carmen Martínez *et al.*, 2006), following endothelial injury (AgouTii *et al.*, 2007) during angiogenesis (Soleti *et al.*, 2009) and following myocardial infarction (Bueno-Betí *et al.*, 2019). Murine studies have identified the release of HHIP-EVs from damaged ECs when released into circulation; HHIP-EVs bind to SHh-EVs, blocking the activation of the Hh signalling pathway in recipient cells (Nie *et al.*, 2016). These studies highlight the importance of EVs as viable cell-cell communicators during the onset of disease.

1.8.2 EVs and Notch Signalling

Similar to the hedgehog signalling pathway, notch signalling in an evolutionarily conserved pathway which plays a significant role during the regulation of embryonic development, stem cell fate and maintenance of tissue homeostasis (Guruharsha, Kankel and Artavanis-Tsakonas, 2012). The Notch receptor is a transmembrane protein that requires ligand-receptor binding of Notch to the adjacent cell. In mammals, there are four Notch receptors, Notch 1-4, which can be activated by five different types of ligands Jagged-1, Jagged-2, and Delta-like ligands 1 – 4. Initiation of the Notch signalling pathway is through a transactivation process whereby a Notch receptor binds to 1 of 5 ligands at the ligand-binding region, EGF 12, resulting in a small conformational change (Bray, 2006). This process is controlled by the enzymatic activity of furin convertase, which aids ligand-receptor binding. The second proteolytic event involves the cleavage of the notch receptor at site two by the ADAM family of metalloproteases, mainly ADAM 10/ADAM1 followed by a γ-secretase cleavage at S3 in the transmembrane domain (TMD) (van Tetering and Vooijs, 2011) (Gordon, Arnett and Blacklow, 2008).

Subsequently, the Notch intracellular domain (NICD) is released from the membrane to facilitate translocation to the nucleus where it binds to numerous transcription factors at the RAM domain. Interaction with the DNA-binding protein RBPJ initiates the recruitment of the co-activator Mastermind which subsequently activates the MED88 mediator transcription activation complex resulting in the activation of Notch target genes including the hairy enhancer of split (HES), HES-related repressor protein (HERP -1 to -3) and the hairy enhancer of split related with YRPW motif protein Hey-1, -2 and Hey L in humans (Iso, Kedes and Hamamori, 2003) (Gridley, 2010). While HES genes are generally associated with neural and endocrine functions, Hey genes play a vital role during vascular development and more recently vascular disease (Wiese, Heisig and Gessler, 2010; Louvi and Artavanis-Tsakonas, 2012).

EVs can act as delivery vehicles facilitating Notch signalling via vesicular membrane-tethered Notch receptor-ligand binding on adjacent cells. Accumulation of Delta-like ligands in intracellular vesicles have been studied in Drosophila and zebrafish models; this has led to the hypothesis that these ligands may be incorporated into exosomes for transport (Le Borgne and Schweisguth, 2003). Although extensive research has been published about Notch signalling after cleavage, the mechanism by which the Delta-like ligands are cleaved is less known. Previous studies have suggested the Delta-like ligands require endocytosis in order to become functional (Le Borgne, 2006). In 2010 Sheldon et at., demonstrated the role for endothelial exosome incorporation of Delta-like 4 Notch ligand in vascular pathologies and cancer. During this study, they demonstrated that upon induction of Delta-like-4 in HUVECs, the protein is incorporated into an exosome. They also proved via coincubation that endothelial exosomes containing Delta-like-4 ligands are transferred to neighbouring cells resulting in inhibition of Notch signalling and loss of notch reporter activity (Sheldon *et al.*, 2010).

1.9 Current models used to study CVD

There are several challenges to understanding the complex pathophysiology of CVD. The most obvious of which is the inaccessibility to human tissues with the majority of tissue usually obtained post-mortem, representing end stage disease. However, despite this several *in vivo* and *in vitro* models have been developed to determine the potential power

of diagnostic biomarkers further advancing our knowledge of CVD progression and detection.

The use of *in vivo* animal models to study sub-clinical atherosclerosis has proven an essential tool toward our current understanding of the molecular mechanisms driving the development of atherosclerosis (Conn, 2013; Konstantinov and Jankovic, 2013) . An ideal animal model resembles human anatomy and pathophysiology, are easy to acquire, and can be maintained at a reasonable cost. In order to successfully model human subclinical atherosclerosis as best possible, the choice of animal and choice of injury inflicted are paramount. For this reason, animals such as mice and rats are often best suited for disease modelling for research purposes due to their fast reproduction rates, basic maintenance requirements and suitability for genetic manipulation (Chorro, Such-Belenguer and López-Merino, 2009; Santos *et al.*, 2015).

To date, several *in vivo* animal models have been used to study subclinical atherosclerosis including; (i) diet and genetic manipulation using low-density lipoprotein receptor-deficient mice ($LDLR^{-/-}$) resembling human hypercholesterolemia caused by high levels of LDL and decreased levels of HDL molecules in plasma with lesion formation induced through feeding of a high fat/cholesterol diet (Ishibashi *et al.*, 1993; Farese *et al.*, 1996; Sanan *et al.*, 1998), (ii) genetic manipulation using animals deficient in Apolipoprotein E (ApoE-/-) resulting in atherosclerotic plaque formation distributed throughout the aorta proportional to age and diet of the animal resembling the process of atherosclerosis in humans (Farese *et al.*, 1996; Egido *et al.*, 2011; Fuster *et al.*, 2012), (iii) complete carotid artery ligation, typically used to study vascular remodelling, and intima-media thickening, whereby blood flow in the carotid artery is completely disrupted by knotting the vessel at the distal bifurcation resulting in a decrease (approximately 80%) in luminal area, medial cell death, reduction in vessel circumference and increased thickness of the medial and intimal layers (Kumar and Lindner, 1997; Wang *et al.*, 2006), (iii) partial carotid artery ligation, represented by partial distribution of blood flow by knotting the left internal and external carotid leaving the occipital free flow of blood, resulting in significant reduction in lumen diameter accompanied by an increase in the media and intima thickening, typically used to study genetic and molecular mechanisms involved in vascular remodelling and intima-media thickening owing to changes in shear stress (Korshunov and Berk, 2003; Wang *et al.*, 2006), and lastly, (iv) wire induced injury of

the carotid or femoral artery resulting in complete denudation of the endothelium through the introduction of a small incision into the respected artery followed by the insertion of a wire that is passed along the vessel in a rotational motion. The wire is then removed from the vessel and the implication of the resulting damage to the endothelium assessed to determine the effect proliferation and migration of resident vascular cells in response to endothelial injury (Lindner, Fingerle and Reidy, 1993; Kumar and Lindner, 1997; Sata *et al.*, 2000; Wang *et al.*, 2006; Takayama *et al.*, 2015).

Although *in vivo* mechanisms of atherosclerosis have advanced our knowledge of the development and progression of atherosclerosis there are several disadvantages to their use including; the need for ethical approval for use, differences in vessel size and make-up, species-specific metabolic and biochemical activities, and most importantly, various chromosomal and genomic differences (Barré-Sinoussi and Montagutelli, 2015).

The use of *in vitro* cell culture models is an alternative platform used to study many aspects of the pathogenesis of atherosclerosis including the response of isolated vascular cells to various pathological stimuli, evaluation of new treatments in addition to delivery methods for plasmid DNA and nanoparticles for specific therapeutic targets (Korin *et al.*, 2012; Gupta *et al.*, 2015; Sada *et al.*, 2016). The most common type of *in vitro* cell culture model is the use of primary human cells derived from living tissues, representing cell behaviour *in vivo*. Various primary human aortic cells are commercially available for *in vitro* disease modelling including ECs, VSMCs, and SCs (Thormodsson and Olafsson, 2005; Sainz *et al.*, 2006; Tang, Wang, Yuan, *et al.*, 2012; Poursaleh *et al.*, 2019). In addition to standard *in vitro* cell culture models, co-culture-based models including direct co-culture, and in-direct co-culture, have been utilised to evaluate cellular responses between various resident vascular cells. The use of in-direct co-culture enables the creation of cellular environments specific to each cell type to determine cell-cell interaction during the development of sub-clinical atherosclerosis through the secretion of EVs, cytokines and other secretory products. The use of in-direct co-culture to study cell-cell communication can be achieved through conditioned media culturing. This process involves the following steps: (i) independent growth of cell lines (ii) removal of cell culture media (iii) introduction of conditioned cell culture media from one cell culture to another to elicit cell-cell interaction via soluble mediators produced and secreted by cells. The advantages of using CM co-culture methods include ease of use as cell medias

do not have to be optimised for co-culture and experimental flexibility as CM supernatants can be frozen and analysed after the experiment is terminated. The use of CM models has been used to study the development of atherosclerotic plaques with an overwhelming focus on the role of CM-mediated crosstalk between VSMC and macrophage/monocyte communication (Vijayagopal and Luke Glancy, 1996; Fillinger *et al.*, 1997; Halloran *et al.*, 1997; Zhang *et al.*, 1999; Shioi *et al.*, 2002; Srivastava, 2002; Tintut *et al.*, 2002).

Although the use of primary cells *in vitro* has been used to mimic VSMCs *in vivo* many limitations have been associated with the isolation and growth of VSMCs in culture. It has been reported that upon isolation, primary VSMCs undergo a phenotypic shift from a quiescent contractile phenotype to a proliferative dedifferentiated phenotype with a significant decrease in the expression of VSMC markers (Owens, Kumar and Wamhoff, 2004). Extensive characterisation of three commonly used, commercially available, vSMC lines from various species in culture reported that following sub-culture, VSMCs *in vitro* exhibit a decrease in SMC marker MYH11 and increase in MVSC markers Sox10, Sox17 and S100β suggesting that VSMCs in culture revert to a more multipotent state suggesting these VSMC lines clearly acquire MVSC markers either by de-differentiation to $Sox10^+$ cells during culture or are outgrown by a small percentage of $Sox10^+$ MVSCs over time or both (Kennedy, Mooney, *et al.*, 2014). The complexity of cellular components in the vascular wall adds to the challenge during isolation of VSMCs with an increased risk of isolating contaminant cells such as ECs, resident vascular stem cells, and fibroblasts. Although cell sorting has been utilised to isolate vascular cells, such as isolation of ECs using endothelial surface markers, there is a lack of definitive VSMC markers to facilitate purification with varying expression levels and poor specificity of known VSMC markers, smooth muscle α-actin, CNN1, and MYH11. This limitation further applies to the isolation of VSMCs from distinct embryological origins due to the lack of markers discovered to date to distinguish VSMC subtypes. The multiple limitations of primary VSMC cultures highlight the imminent need to develop novel sources of VSMCs from defined embryological origins.

The isolation of human embryonic stem cell (hESCs) in 1981 followed by the discovery of HiPSCs in 2006 captured the interest of many researchers as a platform for disease modelling due to their favourable characteristics such as the ability to proliferate indefinitely and differentiate into almost every cell type (Evans and Kaufman, 1981;

Takahashi and Yamanaka, 2006). The identification of four essential transcription factors, (Oct3-4, Sox2, c-Myc, and Krüppel-like factor 4), for pluripotency maintenance allowed for reprograming of human fibroblast cells to HiPSCs with the capability of self-renewal, indefinite growth and ability to differentiate in the three germ layers. This model proved advantageous over the use of hESC as they were easily available, were not of ethical concern and most importantly have the advantage of being patient and pathology specific (Takahashi and Yamanaka, 2006; Takahashi *et al.*, 2007; Yamanaka, 2007). The use of iPSCs has been extensively used to model the role of vSMCs in the development of vascular diseases, for example the neointimal hyperplasia and atherosclerosis associated with Hutchison-Gilford Progeria Syndrome (HGPS) (G. H. Liu *et al.*, 2011). Such modelling resulted in the identification of premature senescence markers associated with the vascular ageing of the disease. Similarly, iPSC-derived VSMC models have too been used to investigate the pathogenesis of aortic aneurysms that occurs in Marfan syndrome patients and providing an insight for novel therapeutic targets (Granata *et al.*, 2017). Finally, iPSCs are emerging as a useful tool for modelling the cardiovascular of arteriosclerosis. These models can be used to investigate the influence of embryonic origin on disease susceptibility and the source of SMC-like cells found in arterial thickening (Liang and Du, 2014; Bargehr *et al.*, 2016).

Generation of iPSC-derived mesodermal models, which account for the majority of SMC throughout the vascular tree, can be performed using two approaches. A monolayer method can initiate mesodermal differentiation through glycogen synthase kinase (GSK) inhibition and treatment with bone morphogenetic protein 4 (BMP4) (Yang *et al.*, 2016). These progenitors can be subsequently differentiated into contractile VSMCs when cultured with PDGF-BB, TGF-β1, FGF and VEGF (vascular endothelial growth factor) in several steps, or into 'synthetic' VSMCs using an altered protocol of growth factor treatment (Yang *et al.*, 2016). Neuroectoderm derived VSMCs have too been generated via initial differentiation to an neural crest stem cell intermediate before further directed progression through the mesenchymal lineage (Wang *et al.*, 2011). Furthermore, Sanjay Sinha's group at Cambridge, UK generated origin-specific vSMCs through separate and distinct paraxial mesoderm, lateral plate mesoderm and neuroectoderm lineages (Bargehr *et al.*, 2016). Interestingly, the data suggests that each lineage produces an origin-specific subtype of vSMCs based on the differential upregulation of particular genes associated with each origin, despite appearing phenotypically and functionally identical. The

resulting cells must be extensively characterised to confirm the true existence of a functional vSMC population. Routinely, confirmation by analysis of gene and protein expression is executed using microarray, qRT-PCR, immunofluorescent staining and western blot of key VSMC markers including transgelin (SM22α), h1-calponin (CNN1), α-smooth muscle actin (α-SMA) and most specifically, myosin heavy chain 11 (MHY11) and smoothelin (SMTN) (Sinha, Iyer and Granata, 2014). However, *in vitro* confirmation of vSMCs is made difficult by the fact that several other cell types transiently express such markers during development or disease. Therefore, cells should be functionally tested for their ability to modulate calcium transients and contract accordingly in response to a variety of agonists including carbachol and KCl (Sinha, Iyer and Granata, 2014). Additionally, telomerase activity assays can be used throughout the differentiation protocol to monitor the stemness of cells and somatic cell progression through loss of telomerase activity and telomere length (Zhou *et al.*, 2014).

In summary, rat and human cell culture models *in vitro* are invaluable tools to address the diagnostic value of EVs released from dysfunctional ECs to control the differentiation state of S100β^{+} stem cells responsible in part for the accumulation of SMC-like cells in the neointima, a hallmark of subclinical atherosclerosis. Moreover, if EC-derived EVs contribute to the differentiation and migration of resident S100β^{+} stem cells during the accumulation of SMC-like cells in the neointima, can the photonic signatures of these human stem cells and their myogenic progeny *in vitro* and *ex vivo* be used as a diagnostic discriminator to detect S100β^{+} stem cell derived SMC-like cells in vascular lesions indicative of sub-clinical atherosclerotic disease.

1.10 Aims and Objectives

The primary aim of this study was to develop a murine and human *in vitro* cell model to investigate the role of endothelial-derived EVs in dictating the fate of resident vascular stem cells following ED due to hyperglycaemia.

To achieve this goal, the following objectives were addressed:

- To characterise rat aortic endothelial (RAEC) and human aortic endothelial (HAEC) cells in culture before isolation and characterisation of secreted EVs from endothelial cell conditioned media following exposure of cells to normal glucose (NG-EVs) and high glucose (HG-EVs), respectively, based on size, morphology, expression of EV-associated proteins and tracking following endogenous and exogenous labelling.
- To isolate and characterise rat and human multipotent Nestin/S100β^+ vascular stem cells from medial explants *ex vivo* and human induced pluripotent stem cells (HiPSC) *in vitro,* respectively, before examining the effects of secreted EVs from endothelial cells on vascular stem cell growth and myogenic differentiation following exposure of ECs to normal glucose (NG-EVs) and high glucose (HG-EVs)
- To determine the putative role of SHh in dictating the myogenic response of vascular stem cells in response to secreted EVs from endothelial cells following exposure of ECs to normal glucose (NG-EVs) and high glucose (HG-EVs).

The secondary aim of this study was to develop a human *in vitro* model to facilitate the interrogation and discrimination of undifferentiated stem cells and their myogenic progeny from distinct embryological origins indicative of sub-clinical atherosclerosis using single cell photonics from RAMAN, FTIR and LiPhos spectral datasets before these spectra (RAMAN and LiPhos) were deployed using supervised machine learning to interrogate spectra from human arteriosclerotic and atherosclerotic lesions to truly evaluate their clinical application for early detection of sub-clinical atherosclerosis.

In order to achieve this goal, the following objectives were addressed:

- To generate and characterise HiPSC-derived NE, paraxial mesoderm (PM), and lateral mesoderm progenitor (LM) stem cells and their myogenic progeny (NE-SMC, PM-SMC and LM-SMC) *in vitro*, and isolate single cells from human cadaveric atherosclerotic and arteriosclerotic aortic tissue *ex vivo.*
- To generate Raman, FTIR and LiPhos spectral datasets from HiPSC-derived NE, PM, and LM progenitor stem cells and their myogenic progeny (NE-SMC, PM-SMC and LM-SMC) and discriminate these cells *in vitro* using multivariate analysis (PCA: Principal Component Analysis, LDA: Linear Discriminant Analysis) and supervised machine learning with multilayer perceptron neural network analysis (MLP).
- To employ Raman and LiPhos single cell spectral datasets from HiPSC-derived NE, and PM progenitor stem cells and their myogenic progeny (NE-SMC and PM-SMC) to interrogate Raman and LiPhos spectra from human arteriosclerotic and atherosclerotic lesions using supervised machine learning and evaluate the contribution of undifferentiated stem cells and their myogenic progeny to human lesions.

Chapter 2:

Materials & Methods

2.1 Biological Materials

All materials used during these experiments were of the highest purity commercially available and were of cell culture standard where applicable.

2.1.1 Commercial cell lines & tissue-derived cells

Table 2.1. Commercial cells used during the study

Cells	Morphology	Cell Origin	Description	Supplier
Rat Primary Aortic Endothelial (RAEC)	Cobblestone	Adult rat aorta	Rat aortic ECs (R304-05a) Isolated from adult rat aorta	Cell Applications
Human Primary Aortic Endothelial (HAEC)	Cobblestone	Primary Aortic	Primary Human Aortic ECs are isolated from the human ascending (thoracic) and descending (abdominal) aorta.	PromoCell
HiPSCs	Embryoid Body	Skin Tissue	White British Male 65-69, Disease Status: Normal, Source material Skin tissue	HipSci
HiPSC-Derived Neural Progenitor Stem Cells (NPCs)	Spindle	HiPSC	Human neural progenitor cells (NPCs) are derived from induced pluripotent stem cells (iPSCs).	Merck Millipore

Table 2.2. Tissue-derived cells used during the study

Cells	Morphology	Cell Origin	Description
Rat MVCSs	Spindle	NE	MVSCs derived from the thoracic aortic medial layer of a female Sprague- Dawley at the age of 6-8 weeks by explanting.
Rat VSMC (rMVSC)	Cobblestone and Spindle Cells	Not Clarified	MVSCs derived from the thoracic aortic medial layer of a female Sprague- Dawley at the age of 10 weeks by enzymatic dispersion.

Table 2.3 HiPSC-Derived Cells used during the study

Cells	Morphology	Cell Origin	Description
NEPs	Spindle	HiPSC	HiPSC-derived NE progenitor cells (NEPs) are derived from induced pluripotent stem cells generated using a chemically defined stimulus.
SNEPs	Spindle	HiPSC	HiPSC-derived spontaneous NE progenitor cells (SNEPs) are derived from induced pluripotent stem cells generated using a non-chemical stimulus.
PMs	Spindle	HiPSC	HiPSC-derived Progenitor cells (PMs) are derived from induced pluripotent stem cells generated using chemically defined media.
LMs	Spindle	HiPSC	HiPSC-derived lateral mesoderm progenitor cells (LMs) are derived from

			induced pluripotent stem cells generated using chemically defined media.
NEP-VSMCs	Filamentous	NEPs	NEP-derived VSMCs (NEP-SMCs) are derived from HiPSC-derived NEPs.
SNEP-VSMCs	Filamentous	SNEPs	SNEP-derived VSMCs (SNEP-SMCs) are derived from HiPSC-derived SNEPs.
PM - VSMCs	Filamentous	PMs	PM-derived VSMCs (PM-SMCs) are derived from HiPSC-derived PMs.
LM - VSMCs	Filamentous	LMs	LM-derived VSMCs (LM-SMCs) are derived from an HiPSC-derived LMs.

2.1.2 Antibodies

Table 2.3 Antibodies used during the study

Antibody/Product	Description	Application	Supplier/Product Number
Anti-Calponin-1 [EP798Y]	Rabbit monoclonal IgG to Nestin, EP798Y.	ICC	Abcam (ab46794)
Anti–CD31 [EPR17260-263]	Rabbit monoclonal to CD31. Recombinant fragment within Mouse CD31 aa 400-600.	ICC, FACS	Abcam (ab222783)

Anti- eNOS [M221]	Mouse monoclonal to eNOS. Recombinant fragment of mouse eNOS protein that included amino acid residues in the C terminal region.	ICC	Abcam (ab76198)
Anti- Myosin Heavy Chain 11 [1G12]	Mouse monoclonal to smooth muscle Myosin heavy chain 11 antibody	ICC	Abcam (ab683)
Anti-Nestin [Rat-401]	Mouse monoclonal to Nestin.	ICC	Abcam (ab11306)
Anti-Nestin [196908]	Mouse monoclonal to Nestin. Nestin-transfected NS0 cells transfected with a human Nestin fragment aa residues 618-1618.	ICC, FACS	Abcam (ab6320)
Anti- S100β [EP1576Y]	Rabbit monoclonal to S100ß, Synthetic peptide within Human S100 beta aa 50 to the C-terminus	ICC, FACS	Abcam (ab52642)
Anti-Oct4	Rabbit polyclonal to Oct4 reacts with 45 kDa Oct4	ICC	Abcam (ab18976)
Anti-SOX10 [EPR4007]	Rabbit monoclonal to Sox10 Synthetic peptide	ICC	Abcam (ab155279)
Alexa Flour 488 donkey anti-goat IgG	Donkey polyclonal IgG (whole antibody) conjugated with Alexa Flour® 488 fluorochrome to goat IgG.	IF	Bioscience (A-11055)

Alexa Flour 546 goat anti-mouse IgG	Goat polyclonal IgG (whole antibody) conjugated with Alexa Flour® 546 fluorochrome to mouse IgG.	IF	Bioscience (A-11030)
Alexa Flour 488 Anti-Rabbit	Goat polyclonal IgG (whole antibody) conjugated with Alexa Flour® 488 fluorochrome to rabbit IgG.	IF	Bioscience (A-11008)

2.1.3 Primers used in this study

Table 2.4 QIAGEN QuantiTech Primers used in this study

Primer	Product Name	Reference Sequence
Human CNN1	Hs_CNN1_1_SG_	NM_001299
Human Gli1	Hs_GLI1_1_SG	NM_001160045
Human Gli2	Hs_GLI2_1_SG	NM_005270
Human Hey1	Hs_HEY1_1_SG	NM_001040708
Human HeyL	Hs_HEYL_1_SG	NM_014571

Human HPRT1_1	Hs_HPRT1_1_SG	NM_000194
Human KDR	Hs_KDR_1_SG	NM_002253
Human Myh11	Hs_MYH11_1_SG	NM_001040113
Human NES_1	Hs_NES_1_SG	NM_006617
Human NKX2-5	Hs_NKX2-5_1_SG	NM_001166175
Human PAX1	Hs_PAX1_1_SG	NM_006192
Human PAX6	Hs_PAX6_1_SG	NM_000280
Human S100B	Hs_S100B_1_SG	NM 006272
Human TBX6	Hs_TBX6_1_SG	NM_004608
Human rSHh	Hs_SHH_1_SG	NM_000193
Human Ptch-1	Hs_PTCHD1_1_SG	NM_173495
Human Smo	Hs_SMO_1_SG	NM_005631
Human NOX 4	Hs_NOX4_1_SG	NM_001143836

Rat CNN1	Rn_Cnn1_1_SG	NM_031747
Rat Gapd_1	Rn_Gapd1_1_SG	NM_017008
Rat Gli1	Rn_Gli1_1_SG	NM_001191910
Rat Gli2	Rn_Gli2_1_SG	NM_001107169
Rat HeyL	Rn_Heyl_2_SG	NM_001107977
Rat HPRT	Rn_Hprt1_1_SG	NM_012583
Rat Myh11	Rn_Myh11_1_SG	NM_001170600
Rat Nos3	Rn_Nos3_1_SG	NM_021838
Rat Pecam1	Rn_Pecam1_1_SG	NM_031591

2.1.4 Chemical and biological agents used in this study

Table 2.5 Chemical and biological agents used in this study

Supplier	Product and Catalogue No.
ATCC	Fetal Bovine Serum ESC Qualified (Lot number #62207060)
Bio-Rad	Bio-Rad Protein Assay (Product #23235, Lot #C148587)
Bioscience	B-27™ Supplement (50X), serum-free, (17504001), Pierce Protein G Agarose beads (20398)
BD	FITC Annexin V Apoptosis Detection Kit (Catalog No.556547, Lot #8029889)
Cell Applications	Attachment Factor Solution (123-100, Lot #428), Rat Endothelial Growth Medium (R211-500, Lot #263),
Cell Biologics	Antibiotic – Antimycotic Solution (M1168, Lot #0317), EC growth supplement (M1168, Lot #0417), Epidermal growth factor (M1168, Lot #0317), Fetal Bovine Serum (M1168, Lot #0317), Heparin (MII68, Lot #0417), Hydrocortisone (M1168, Lot #0317), L-Glutamine (M1168, Lot #0317),
ExBio	Anti-Hu CD9 PE (1P-208-T025), Anti-Hu CD81 (1P-558-T025), Anti-Hu CD63 (1P-343-T025), Mouse IgG1 Isotype control PE (1P-632-CO25).
Gibco	VEGF (M1168, Lot #0317).

	2-Mercaptoethanol (50Mm) (31350010, Lot #1176783), Advanced DMEM/F12 (12634-010, Lot #1836495), B-27® Supplement (50X) serum free (17504044, Lot #), CD lipid concentration (11905-031, Lot # 1815262), CTS™ N-2 Supplement (A1370701, Lot #44577), TrypLE™ Select Enzyme 10X no phenol red (12563029, Lot # 1911606)
R&D Systems	Recombinant Human FGF basic 146 aa (223-FB-025, Lot # HKW12916061), Recombinant human, mouse, rat Activin A (338-AC-010, Lot # BNV3715111), Recombinant human jagged 1 Fc Chimera Protein (1277-JG-050), Recombinant human IgG1 (110-HG-100), Recombinant Rat Jagged-1 Fc (599-JG-100), 599-JG-100 (7666-MB-005).
RCSI	Nir-Aza exosome stain
SBI	ExoQuick-TC, 50 ml (EXOTC50A-1-SBI, Lot #180326-001), EXOCET Exosome Quantitation Kit (EXOCET96A-1-SBI-96react), Lysis Buffer (EXOCET96A-1, Lot #170110-026), PBS-B Buffer (EXOCET96A-1, Lot#180309-001), Buffer A (EXOCET96A-1, Lot #180313-003), EXOCET Standard (Lot #180313-002), Buffer B (Lot #180313-001). ExoGlow-Membrane EV Labelling Kit (EXOGM600A-1-SBI). Exo-Check Exosome Antibody Array (EXORAY210A-8)
Seralab	Chick Embryo Extract (CE-650-J, Lot #CHK1785)
Sigma-Aldrich	

	(+/-)-A-Tocopherol (T3251-5G, Lot #MKCG1370) , (+)-A-Tocopherol acetate (T3001-10G, Lot #MKBV1182V), 1-Thioglycerol (M6145, Lot # MKBZ1849V), 2-mercaptoethanol (M-7154, Lot #117683), 3,3",5-Triiodo-L-thyronine Sodium*cell (T6397-100MG#BCBS7501), Bovine Serum Albumin (A4503, Lot # SLBR5258V), Catalase from bovine liver (C40-100MG, Lot#SLBT7844), Corticosterone crystalline (C2505-500MG, Lot #SLBT2966), Collagenase from Clostridium histolyticum (C9891, Lot #075M4006V), Dulbecco's Modified Eagle's Medium (D6046, Lot # RNBD9755), D-(+)-Galactose (G0625-100G, Lot#SLBR6074V), D-Mannitol (m4125-100MG. Lot#WXBC3441V) Elastase from porcine pancreastype III (E0127) Flouromount™ Aqueous Mounting Medium (F4680, Lot # SLBD6805), Glycine (G8898, Lot # SZBE3310V), Gelatin solution (G1393,Lot #SLBG9890V)Ham's Nutrient Mixture F12 (51651C, Lot #SLBF8068), Holo-transferrin from human bioreagent (T0665-100MG, Lot#SLBT9543), Hanks balanced salt solution (H6648, Lot #RNBG1246) Insulin human (11376497001, Lot #15898200), Insulin human recombinant (91077C-250MG, Lot #17N329), L-glutathione Reduced (G6013-5G, Lot #SLBV2396), Linoleic acid (L1012-100MG, Lot #SLBV9486), Linolenic Acid (L2376-500MG. Lot #SLBT8488), L-carnitine hydrochloride, synthetic (C0283, Lot#SLBP4786V), Minimum Essential Medium (56416C, Lot #66K2411),Penicillin-Streptomycin (P4333, Lot #025M4818V), Putrescine hydrochloride (P5780, Lot#BCBV6583), Poly-vinyl alcohol (P8136, Lot #SLBM1859V), Protease Inhibitor (P8340),

	Retinoic Acid (100Mm) (R2656, Lot #), RIPA (R0278, Lot #SLBK387OV), RPMI-1640 Medium (R8758, Lot # RNBC2874), O2-dismutase from bovine erythro (S5395-75KU, Lot #SLBW5001), Sodium selenite g-irradiated, bioxtra, l (S9133-1MG, Lot #SLBR3105V), Retinyl acetate (R7882-1G, Lot#SLBW3919), Transferrin (10652202001, Lot # 16170600), Triton X-100 (T8787, Lot #110012) Trypan Blue (T8154, Lot #RNBC9030), Trypsin-EDTA solution (T4174, Lot #SLBL1977V), TWEEN®20 (P1379), Progesterone (P8783-1G, Lot#SLBS7040), Oleic acid bioreagent, suitable for cell (O1383-1G, Lot#SLBQ9717V), L-Pipecolic Acid (P2519-100MG, Lot#MKCF0248), Biotin, powder, bioreagent, suitable (B4639-100MG, Lot# SLBV3617)
StemCell	VitronectinXF™ (07180, Lot #15A60726-3), Y-27632 (ROCK Inhibitor 73202, Lot #17J00261)
Thermo-Scientific	RNASE AWAY SPRAY 475ML bottle (10666421, Lot #15051819).
QIAGEN	Rotor-Gene®SYBR® Green RT-PCR Kit (204174, Lot #1570129665)

2.1.5 Plastic wear used during this study

Table 2.6 Chemical and biological agents used in this study

Supplier	Catalogue Number
Lennox	15mL conical centrifuge Tubes (ACF450/10X), 50mL centrifuge tubes (ACF450.30X), 5mL pre-sterilized serological pipet (APP260.30,), 10mL

	pre-sterilized serological pipet (APP260.40), 25ml pre-sterilized serological pipet (APP260.60,), Minisart® NML 0.2µm filter (2020-5,), Minisart® NML 0.45µm filter (2020-11,)
Thermo Scientific	Cover Glass (1244OS), Nunc™EasYFlask™ 75cm2 Nunclon™Delta Surface (156499,), Nunc™EasYFlask™ 25cm2 Nunclon™Delta Surface (156367)

2.2 Methods

2.2.1 Animal stem cell culture

2.2.1.1 Animal stem cell culture and maintenance

All stem cell culture techniques were carried out aseptically in a Bioscience Air 2000 M.AC. Laminar flow cabinet. Cells were maintained in a Hera cell water jacket cell incubator at 37℃ in an atmosphere humidified with 5% CO_2. Cells were visualised and imaged using an Olympus CK30 phase-contrast microscope

2.2.1.2 Primary rat multipotent vascular stem cell isolation and culture

Rat MVSCs were isolated from the aortas of female Sprague-Dawley rats, grown and maintained in maintenance media one (MM1) which consisted of DMEM basal media supplemented with chick embryo extract (2%), B27 (2%), N2 (1%), FBS (1%) Penicillin Streptomycin (PS) (1%), rFGF (20ng/ml), Retinoic Acid (100nM) and 50nM 2-mercaptoethanol. Sprague-Dawley rats were sacrificed by anaesthetisation overdoes of pentobarbital sodium, death was confirmed by exsanguination. The aorta was then removed and placed in PBS. The aorta was then carefully cleaned of surrounding fatty tissue. Aortic tissue was incubated in DMEM solution containing collagenase type 1A (0.7mg/ml), soybean trypsin inhibitor (0.4mg/ml), and BSA (1mg/ml) for 20 min at 37°C to loosen the adventitia before complete removal using a fine-forceps under a dissecting

microscope. The resulting aortic tissue was then cut into sections using a sterile blade and placed into a 6-well tissue culture plate pre-coated with CELLstart™ for 48 hours to allow migration of the MVSC population. Following this, the explants were removed and the resulting cells were subcultured by washing three times with Hanks Balanced Salt Solution, incubated with TrypLE (0.5X) for 5 minutes, and visualised post-incubation, ensuring all cells were detached. The TrypLE was neutralised with a serum-containing medium (MM1), and the cells were centrifuged at 1500 x rpm for 5 mins. The resulting pellet was then re-suspended in a fresh MM1 complete medium and seeded at a density determined by experimental requirements. Cells were frozen down in a complete MM1 medium with 10% DMSO, 10% FBS. All procedures were ap- proved by the University Animal Care Committee and were carried out in accordance with EU guidelines for the Protection of Animals used for Scientific Purposes, (Amendment) Regulations 2013 (S.I. No 434 of 2013).

2.2.2 Primary cell culture and maintenance

All primary cell culture techniques were carried out aseptically in a Bioscience M.D.H X117A laminar flow cabinet. Cells were maintained in an MSC Galaxy B cell incubator at 37℃ in an atmosphere humidified with 5% CO_2. Cells were visualised and imaged using an Olympus CK30 phase-contrast microscope at varying magnifications.

2.2.2.1 Rat aortic EC culture

RAECs (Cell Applications, R304-05a) were cultured in complete rat aortic endothelial media, composed of a basal media supplemented with 10% growth supplement (ingredients proprietary to manufactures formulation) as per manufacture instructions. Before seeding cells, the surface of the culture wear was pre-coated using Attachment Factor Solution and incubated at 37°C for 30 minutes. After the incubation time had elapsed, the attachment factor solution was removed, and complete rat aortic endothelial media, was added to the culture wear. Cells were grown and maintained complete rat aortic endothelial media. Cells were frozen down complete rat aortic endothelial media with 10% DMSO. The cells were used between passages 3-15.

2.2.2.2 Primary rat smooth muscle cell culture

Primary rat VSMCs (rVSMCs) were previously isolated from the thoracic aorta of Sprague-Dawley rats as described in section 2.2.1.2 by members of the Vascular Biology & Therapeutics lab group. rVSMCs were maintained in RPMI high glucose basal media supplemented with FBS (Sigma) (10%), and PS (1%). In order to subculture, cells were washed X3 with HBSS followed by incubation in 1X Trypsin for 5 minutes at 37°C for 5 minutes. Following trypsin incubation, trypsin was inactivated by the addition of RPMI 10% FBS collected in a 15ml tube and centrifuged at 1500rpm for 5mins. The cell pellet was re-suspended in the appropriate volume of fresh media (RPMI 10% FBS) and seeded in tissue culture treated flasks. Cells were frozen down in RPMI, FBS (10%), DMSO (10%). The cells were used between passages 5-8.

2.2.2.3 Primary human aortic EC culture

Human aortic ECs (HAEC) (PromoCell, C12271) were cultured as per the manufacturer's instructions. Cells were grown and maintained in complete medium (C22020) which contained a basal media supplemented with fetal calf serum (0.05ml/ml), endothelial cell growth supplement (0.004ml/ml), recombinant human epidermal growth factor (10ng/ml), heparin (90µg/ml) and hydrocortisone (1µg/ml). In order to subculture, cells were washed X3 with HBSS followed by incubation in 1X Trypsin for 5 minutes at 37°C for 5 minutes. Following Trypsin incubation cells were collected in a 15ml tube and centrifuged at 1500rpm for 5mins. The cell pellet was re-suspended in the appropriate volume of fresh media and seeded in 6/well plates or tissue culture treated flasks depending on requirements for experiments. Cells were frozen down in complete human endothelial growth medium supplemented with 10% DMSO.

2.2.3 HiPSC culture

All HiPSC culture techniques were carried out aseptically in a Bioscience Air 2000 M.AC. laminar flow cabinet. Cells were seeded in Corning® Costar® TC-Treated 6-Well Plates and maintained in a Nuaire™ DH Autoflow CO_2 Air-Jacketed incubator at 37℃ in an atmosphere humidified 5% CO_2. Cells were visualised and imaged using an Olympus CK30 phase-contrast microscope at varying magnifications.

2.2.3.1 HiPSC

HiPSCs were cultured as per the manufacturer's instructions. Before seeding cells, the surface of the culture wear was pre-coated using Vitronectin (10µg/ml) and incubated at room temperature for 1 hour. Cells were grown and maintained in feeder-free conditions in xeno-free, serum-free, complete Essential 8™ medium (E8) media (ingredients proprietary to manufactures formulation), replacing 95% of the medium daily. Cells were sub-cultured by washing once with sterile PBS, incubated with EDTA (0.5mM) for 4-8 at room temperature while being observed under phase-contrast microscopy until colonies displayed bright halos around the edges and small holes appeared throughout. The EDTA was aspirated, and the recommended volume of E8 was added to the well. The dislodged cell colonies were then gently washed from the culture-wear by pipetting the medium around the well using a 5ml/10 stripette until the desired cell aggregates were achieved. The resulting cell solution was then seeded into as many wells as were required. ROCK inhibitor (10mM) was added to optimise colony growth after subculturing. The culture wear was then agitated gently within the tissue culture incubator, ensuring even distribution of cells across the culture wear was achieved. Cells were frozen down in knock-out serum solution with 10% DMSO.

2.2.3.2 Generation of HiPSC-derived NE progenitor stem cells (NEP)

HiPSCs were cultured as described in Section 2.2.3.1 until reaching 70% confluency. Cells were then split at a splitting ratio of 1:10 and left at 37°C, five %CO_2 for 24 hours. Following 24-hour incubation, cells were incubated in a chemically defined media (CDM) consisting of 250 ml of IMDM, 250 ml of Ham's F12 nutrient mix, 5 ml of chemically defined lipid concentrate, 250 µL of transferrin (30mg/ml), 350 µL of insulin (10mg/ml) (added after filtration) and 20 µL of monothioglycerol and 1% PS supplemented with FGF2 (12ng/ml) and SB431542 (10µM/ml) to induce NE differentiation. Cells were monitored daily under the phase-contrast microscope. Half of the complete medium was changed every second day until reaching day 7. Cells were sub-cultured by washing once with sterile PBS, incubated with EDTA (0.5mM) for 4-6 minutes. Following incubation, the EDTA solution was aspirated, and the recommended volume of CDM was added to the well. The resulting NE progenitor cells were

maintained in CDM and used between passages 1-10. Cells were frozen down in knock-out serum solution with 10% DMSO (Figure 2.1).

2.2.3.3 Generation of HiPSC-derived NE progenitors (SNEP)

HiPSCs were cultured as described in Section 2.2.3.1 until reaching 70% confluency. Cells were then split at a ratio of 1:10 and left at 37°C, 5 %CO_2 for 24 hours. Following 24-hour incubation, cells were incubated in E8 and left for 4-5 days. After this time period HiPSC colonies began to lose their typical defined boarders followed by cell migration from the colonies. In order to promote proliferation of the migrated cells dense HiPSC colonies were manually removed using a sterile glass picker. The remaining cells were sub-cultured at 60% confluency using EDTA solution (1:1000) for 4-8 minutes at room temperature while observed under phase-contrast microscopy until cells displayed bright halos. When this was achieved the EDTA solution was aspirated, and the recommended volume of E8 medium was added to the well. The dislodged cell colonies were then gently washed from the culture-wear by pipetting the medium around the well three times until a single cell suspension was obtained. Cells were then centrifuged at 300 x g for four 3mins; the supernatant was removed, and the required amount of E8 media was added. Cells were then titrated into single cells using a 1ml syringe and 0.22μm gauge needle. Cells were frozen down in knock-out serum solution with 10% DMSO. The cells were used between passages 2-15 (Figure 2.1).

2.2.3.4 Generation of HiPSC-derived mesoderm progenitors (PM)

HiPSCs were cultured as described in Section 2.2.3.1 until reaching 70% confluency. Cells were then split at a splitting ratio of 1:10 and left at 37°C, five %CO_2 for 24 hours. Following 24-hour incubation, cells were incubated in a CDM consisting of 250 ml of IMDM, 250 ml of Ham's F12 nutrient mix, 5 ml of chemically defined lipid concentrate, 250 μL of transferrin (30mg/ml), 350 μL of insulin (10mg/ml) (added after filtration) and 20 μL of monothioglycerol and 1% PS supplemented with FGF2 (20ng/ml) and LY294002 (10μM) to induce paraxial mesoderm and FGF2 (20ng/ml) and BMP4 (50ng/ml) to induce lateral mesoderm differentiation. PM progenitors required culturing in CDM supplemented with FGF2 and LY294002 for a subsequent 3.5 days. Lateral plate

mesoderm progenitors required culturing in CDM supplemented with FGF2 and BMP4 for 3.5 days. The respective media were replenished after two days of treatment. Progenitors were immediately induced into VSMC differentiation as they have not yet been shown as stable in culture (Figure 2.1).

2.2.3.5 Human induced pluripotent progenitor derived VSMC

Human-induced pluripotent derived progenitor stem cell populations were generated as outlined in sections 2.2.3.2 – 2.2.3.4. Following progenitor differentiation, cells were treated with 1X TrypLE for 3–5 min at 37 °C in a 5% CO_2 incubator. Cell culture plates were gently taped and checked periodically under a phase-contrast microscope to ensure that all cells had been dissociated into single cells. TrypLE was terminated by the addition of 10 volumes of DMEM to dilute one volume of TrypLE used. Cells were then collected and centrifuged he cell for 3 minutes at 200g at room temperature. The supernatant was aspirated and discarded. The remaining cells were re-suspended in DMEM supplemented 10% FBS (Sigma) 1% PS, PDGF-BB (10ng/ml) and TGF-β1 (2ng/ml). Cells were then plated onto gelatin-coated (0.1% wt/vol) plates at a seeding density of 20,000 cells per cm^2. Cells were maintained at 37°C in a 5% CO_2 incubator. After one day of PDGF-BB and TGF-β1 treatment, 50–70% of the cells attached to the plate. The media was discarded to remove floating cells and replaced with a fresh medium. After day 12 of PDGF-BB and TGF-β1 treatment, all cells appeared spindle-shaped. Complete medium was then changed to DMEM 10% FBS, 1% PS for expansion. Cells were frozen down using 90% (volume/volume) FBS + 10% (vol/vol) DMSO (Figure 2.1).

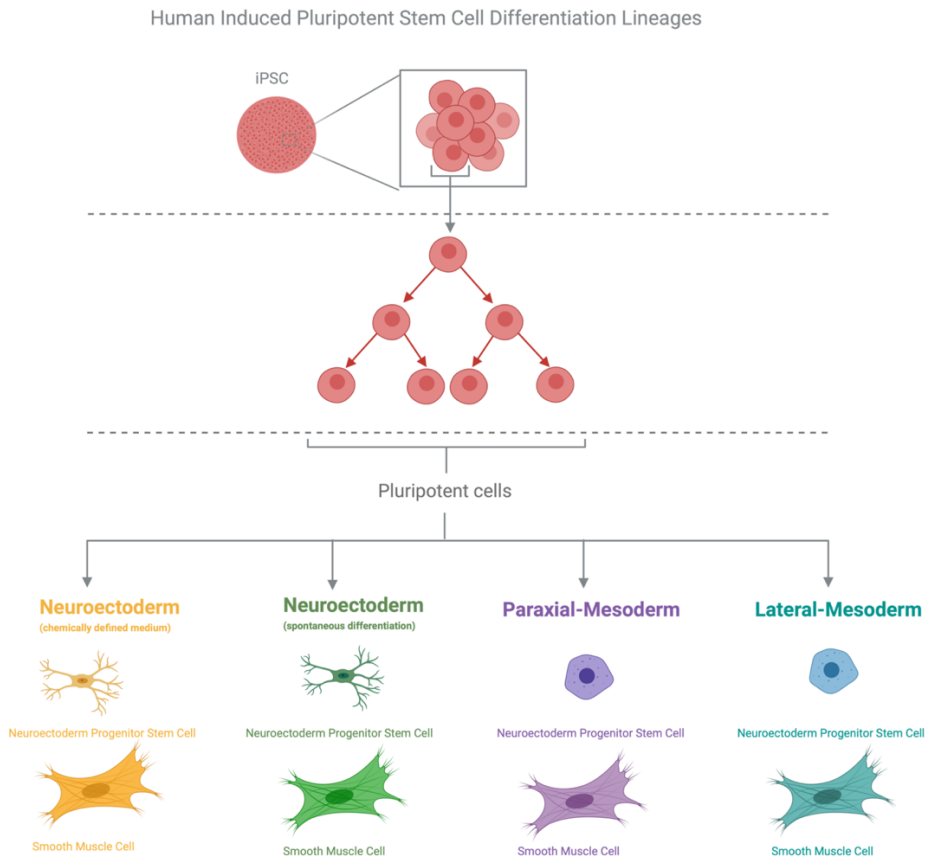

Figure 2.1 Schematic representation of HiPSC-derived progeny. Development of human *in vitro* cell line model using defined differentiation protocols to generate NE and mesodermal progenitor stem cells and further VSMC progeny generation.

2.2.4 Isolation of single cells from human atherosclerotic cadaveric tissue samples

Human fixed cadaveric atherosclerotic and arteriosclerotic tissue sections from the right carotid artery were collected from the Royal College of Surgeons, Dublin Ireland. All cadaver tissue was sanctioned for research use by The Royal College of Surgeons in Ireland Museum Committee. Tissues 3cm thick from 3 patients (both left and right carotids) were rehydrated at room temperature by immersing the slides gradients of ethanol for 5 minutes, respectively: 100 %, 90 %, 70 %, and 50 % ethanol. Afterward, the slides were rinsed in distilled H_2O, and incubated once in 1x PBS for 10 minutes. Under sterile conditions, vascular tissue was rinsed three times with phosphate-buffered saline (PBS), the intima was removed manually by gently rubbing the lumen with a

scalpel 2-3 times in each direction. Following this, the adventitial layer was carefully removed by incubating tissue sections in DMEM medium supplemented with PS (1%), BSA (1mg/ml), soybean trypsin inhibitor (0.4mg/ml), and type I collagenase (0.1%). The reaming tissue composed of the medial layer only was finely cut into 2-3 mm pieces. 4-5 ml of 0.1% type I collagenase (Gibco, Invitrogen Corp) was added to the culture dish. This was incubated for 1.5 to 2 hours at 37°C. Digestion media were collected and filtrated with BD Falcon™ Cell Strainer to remove the undigested explants, then centrifuged (1000 rpm, 5 minutes, four °C). The above procedures were repeated three times to acquire more cells. Acquired cells were fixed in 4% formaldehyde for single-cell photonic processing.

2.2.5 Differentiation treatments *in vitro*

2.2.5.1 Vasculogenic Differentiation

Rat MVSCs were seeded onto 6-well plates with coverslips at a density of 10,000 cells/well and allowed to grow for 24 hours in MM1 (as described in section 2.2.1.2). After recovery, cells were washed three times using Hank's balanced salt solution. Following this, cells were treated with 2ml/well of complete rat endothelial media (Cell Applications, ingredients propriety to manufacture formulations) for 14 days at 37℃ 5% $C0_2$.

2.2.5.2 Myogenic Differentiation

2.2.5.2.1 TGF-β1 mediated VSMC differentiation

Rat MVSCs were seeded onto 6-well plates with coverslips at a density of 10,000 cells/well and allowed to grow for 24 hours in MM1 (as described in section 2.2.1.2). After recovery, cells were washed three times using Hank's balanced salt solution. Following this, cells were treated with DMEM basal media supplemented with 10% FBS (Sigma Aldrich), PS (1%), TGF-β1 (R&D 7666-MB-05) (2ng/ml) or Jagged1-1Fc (2µg/ml) (R&D, 599-JG-100) for 12 days.

2.2.5.2.2 Hh-mediated VSMC differentiation

Rat MVSCs were seeded onto 6-well plates with coverslips at a density of 10,000 cells/well and allowed to grow for 24 hours in MM1 (as described in section 2.2.1.2).

After recovery, cells were washed three times using Hank's balanced salt solution. Following this, cells were treated with rSHh (1.0µg/ml) for 7 days in DMEM basal media supplemented with 10% FBS (Sigma Aldrich), 1% PS. To ensure VSMC differentiation is mediated by activating the Hh signalling pathway, cells were pre-treated with Hh inhibitor cyclopamine (15mM) for 1 hour before rSHh treatments.

2.2.5.2.3 Notch Dependent myogenic differentiation (Jagged-1)

To immobilise Jag-1 to a cell culture plate, each well was first treated with protein G (20 µg/ml) overnight at 4℃. Following the overnight incubation, Protein G was discarded and wells were washed 3 times with sterile PBS. 1ml of blocking buffer (1% BSA in PBS) was added to each well. Plate was incubated at room temperature for 2 hours. Blocking buffer was discarded and wells were washed 3 times with PBS. 1ml of either Recombinant Rat Jagged-1-Fc or Recombinant Human IgG1-Fc (negative control) was added to each well. Plate was incubated at room temperature for 2 hours. Jag-1 and IgG1 were discarded and wells were washed once with PBS. Cells were seeded into wells with an appropriate volume of maintenance media.

2.2.6 Cell characterisation

2.2.6.1 Immunocytochemistry (ICC)

Cells seeded onto UV sterilized coverslips were fixed with 3.7% formaldehyde for 15 mins at room temperature. If cells required permeabilization to detect intracellular antigens, cells were incubated in 0.025% Triton X-100 PBS at room temperature for 15mis. All coverslips were blocked using BSA (5%), Glycine (0.3M), Tween (1%) PBS solution for 1 hour at RT. Cells were incubated with primary antibodies overnight at 4°C, then washed twice with PBS to remove any unbound primary antibody before being incubated (1h,RT) with the recommended concentration of fluorochrome-conjugated secondary antibodies diluted in blocking buffer. Following 2X wash in PBS, cell nuclei were stained using DAPI: PBS (dilution 1:1000) for 15mins at RT. Secondary control and an IgG isotype control were performed for each primary and secondary antibody used to assess nonspecific binding. An Olympus CK30 microscope and FCell™ software were used to capture images. Images were analysed using ImageJ software as described above.

Settings were fixed at the beginning of both acquisition and analysis steps and were unchanged. Brightness and contrast were lightly adjusted after merging (Figure 2.2).

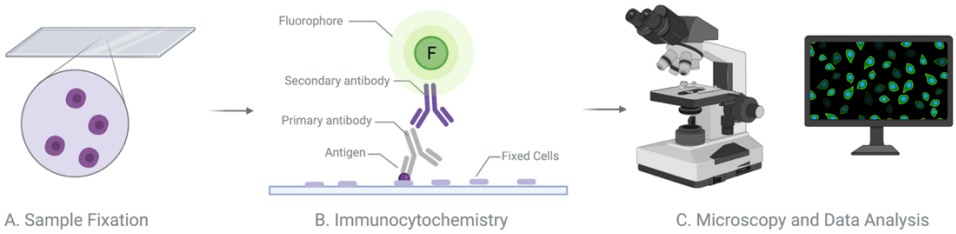

Figure 2.2 Schematic of ICC protocol. Visualisation of the presence/ localisation of a specific protein or antigen using ICC. (A) The cell of interest is fixed to a glass surface for interrogation. To reduce non-specific binding, the cells are then blocked using bovine serum albumin (BSA). (B) Fixed cells are then incubated with a primary antibody specific to the antigen of interest. Following overnight incubation, the cells are then exposed to a secondary antibody that has a conjugated fluorophore. (C) The fluorophore is exposed to light leading to a detectable level of excitation. The excitation of the fluorophore is visualised using a fluorescent microscope.

2.2.6.2 Quantitative PCR

Total RNA was isolated from cultured cells using the ReliaPrep^{TM} RNA Cell Miniprep System by Promega according to manufactures instructions. The concentration of purified nucleic acid samples was determined spectrophotometrically using the NanoDrop. 2-10 micrograms of RNA were used for reverse transcription with Rotor-Gene SYBR Green RT-PCR (QIAGEN) protocols for Real-Time One-Step RT-PCR using the Real-Time Rotor-GeneRG-3000 TM light cycler from Corbett Research using primers listed in section 2.1.3. Total RNA (2-10 ng) was then reverse transcribed and PCR amplified in a one-step reaction containing RT mix, SYBR green mix, and RNase free water at 55°C for 10 mins, 95°C for 5 mins, followed by 40 cycles of 95°C for 5 seconds, 60°C for 10 seconds (Figure 2.3 A) and subsequent melt curve analysis (Figure 2.3 B). Samples were run in triplicate with a no reverse transcriptase (-RT) control. Gene expression was normalised to that of the housekeeping gene, GAPDH or HPRT (for terminally differentiated cells or HPRT for stem cells). Ratio of gene expression was calculated using the efficiency corrected delta Ct method. The ratio of sample:control was calculated therefore the control when compared to itself will always have a value of 1 as the ratio is 1:1. Results were plotted using PRISM software (Figure 2.3 C). Melt curve analysis was performed on all runs to confirm that amplification of a single transcript product per primer occurred at the validated melt temperature.

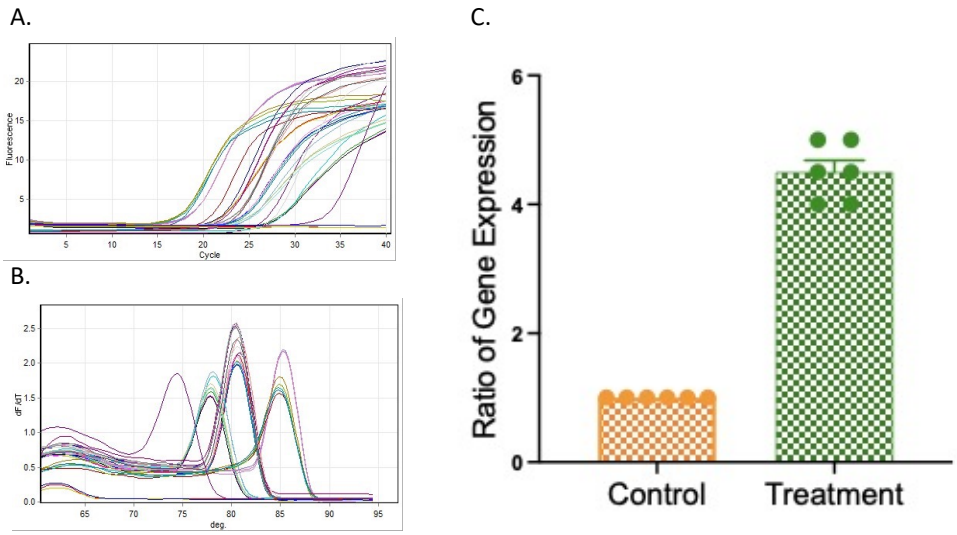

Figure 2.3 qRT-PCR. (A) Amplification of target genes using QuantiTech QC primers presented as fluorescence vs. number of cycles (40 cycles). Threshold baseline values were set at the point of exponential growth on the amplification curve to determine Ct values. (B) Melt curve analysis was performed for each run as an in-house validation to ensure amplification of single transcript product per gene. (C) Gene expression was normalised using housekeeping gene GAPDH or HPRT. Ratio of gene expression was calculated using the efficiency corrected delta Ct method. Results were plotted using PRISM software.

2.2.6.3 Flow cytometry

Cells were re-suspended in media, counted, and fixed using BD Cytofix/Cytoperm solution for 20 minutes at 4°C. Following incubation, cells were then washed in 1X BD Perm/Wash solution by centrifugation at 500g for 3 minutes X3. The remaining pelleted cells were then re-suspended in (i) fluorochrome-conjugated antibodies and control IgG's or (ii) the appropriate primary antibody with fluorochrome-conjugated secondary antibodies at a final concentration of 1 µg per sample and incubated at four °C for 30 min. Fluorescence labelled cells analysis was performed using a BD FACS Aria flow cytometry system (BD Biosciences) or the Amnis™ CellStream ™ flow cytometer. Cells were selected from debris based on their forward and side scatter properties. Single cells were defined as having an aspect ratio of approximately 1 (Figure 2.4 A,B). Antibody expression was displayed on a bivariant plot e.g. FITC vs SSC (Figure 2.4 C). Multiple histogram overlays were created using the analysis software tool to demonstrate the difference between control vs treated samples (Figure 2.4 D). For identification of potential EVs, the Cell Stream™ flow cytometer was set to small particle detection. A

gate was set up using an SSC vs FSC plot to identify “potential EVs” (Figure 2.5 A). Using this “potential EVs” gated population antibody + EVs e.g. PE+ events were gated (Figure 2.5 B). Antibody expression was displayed on a bivariant plot using Frequency vs Intensity (Figure 2.5 C). To verify the detection of EV particles a panel of control samples were ran simultaneously as listed in Table 2.8.

Table 2.7 FACs controls for detection of cellular antibody expression

Control Name	Purpose
Unstained Cells	Gating
PBS only (filtered)	Determine background signal from PBS
PBS + Antibody	Fluorescence compensation
PBS + IgG	Fluorescence compensation
Cells + IgG	Fluorescence compensation
Cells + Antibody	Determine antibody + cells

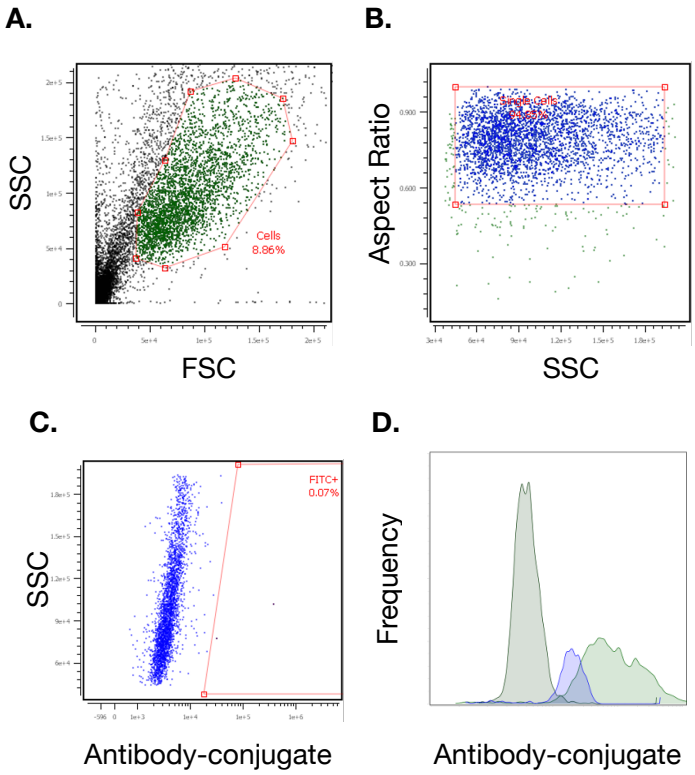

Figure 2.4 Gating strategy for FACs. Cells were selected from debris based on their forward and side scatter properties and a gate was appropriately drawn (A). Single cells were defined as having an aspect ratio of approximately 1 (B). Antibody expression was displayed on a bivariant plot e.g. FITC vs SSC. (C) Multiple histogram overlays were created using the analysis software tool to demonstrate the difference between control vs treated samples (D).

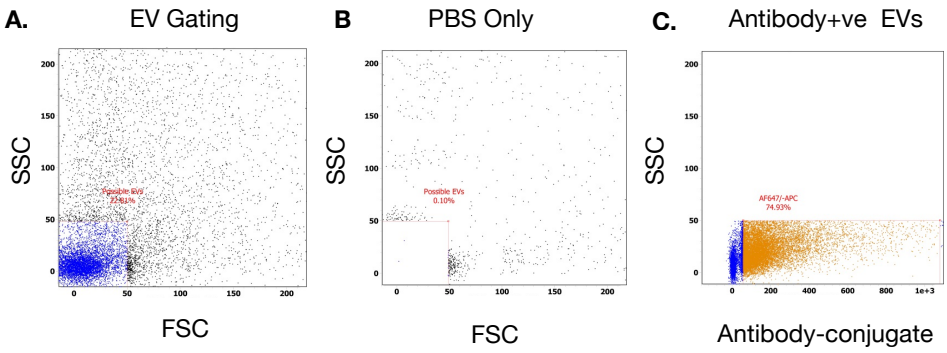

Figure 2.5 Gating strategy for EV detection. A gate was set up using an SSC vs FSC plot to identify "potential EVs" (A). Using this "potential EVs" gated population antibody + EVs e.g. PE+ events were gated (B). Antibody expression was displayed on a bivariant plot using Frequency vs Intensity (C).

Table 2.8 nanoFACs controls for detection of EV antibody expression

Control Name	Purpose
Unstained EVs	Gating
PBS only (filtered)	Determine background signal from PBS
PBS + Antibody	Fluorescence compensation
PBS + IgG	Fluorescence compensation
EVs + IgG	Fluorescence compensation
EVs + Antibody	Determine antibody + EVs
EVs + Antibody + Triton X-100	Determine signals are coming from lipid-based particles

2.2.6.3.1 Imaging Flow cytometry

Cells were re-suspended in media, counted, and fixed using BD Cytofix/Cytoperm solution for 20 minutes at 4°C. Following incubation, cells were then washed in 1X BD Perm/Wash solution by centrifugation at 500g for 3 minutes X3. The remaining pelleted cells were then re-suspended in (i) fluorochrome-conjugated antibodies and control IgG's or (ii) the appropriate primary antibody with fluorochrome-conjugated secondary antibodies at a final concentration of 1µg per sample and incubated at four °C for 30 min. Fluorescence labelled cells analysis was performed using the ImageStream™ imaging flow cytometer. Cells were selected from debris based on their forward and side scatter properties. Single cells were defined as having an aspect ratio of approximately 1. Morphometric analysis of single cells including size and shape was carried out by plotting Area vs. Aspect Ratio (width divided by length) (Figure 2.6).

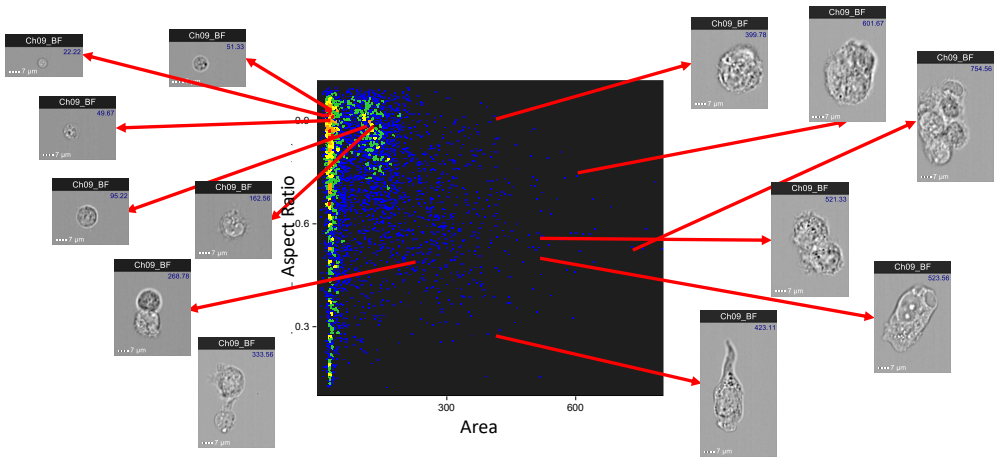

Figure 2.6 Gating strategy for morphometric analysis of cells using ImageStream™ . Morphometric analysis of single cells including size and shape was carried out by plotting Area vs. Aspect Ratio. Individual cells were analysed by selecting a blue point on the graph with smaller cells gathered close to the Y axis and larger cells further on the X axis.

Antibody expression was displayed on a bivariant plot, Intensity vs. Area. Multiple histogram overlays were created by plotting Normalized frequency vs. Antibody Intensity using the analysis software tool to demonstrate the difference between control vs treated samples.

2.2.6.4 Confocal microscopy

Cells were analysed with a Zeiss LSM 510 Confocal Laser Scanning microscope (CLSM). Prior to CLSM imaging, cells were seeded on pre-coated glass-bottom dishes (50 mm, MatTek Corporation, USA). After the solidification of matrices, the suspensions of cells in the medium were seeded onto the glass surface at specific densities. The samples were then incubated at 37°C and 5% of CO_2 for 24 hours before fixation. Images were taken using a Zeiss LSM 510 Confocal Laser Scanning microscope with a white-light 100x objective.

2.2.6.5 Celigo imaging cytometer

2.2.6.5.1 Proliferation assay

Cells were seeded onto a 48 well plate at a density of 100 cells/well in maintenance media. Following overnight, cells media was removed and replaced with various cell treatments. Cell proliferation was monitored over a period of time (0, 24, 48 and 72 hours). Using the Celigo Application software, a confluence channel was selected for brightfield imaging. Cells were autofocused, and the entirety of each well was imaged at each time point. Using the confluence application, all cells are outlined by the use of a texture algorithm. A graphic overlay is then applied to each well. A heat map of cell confluence is then provided for analysis stating the % confluency of each well at a defined time point.

2.2.7 Detection of cellular oxidative stress

2.2.7.1 Determination of intracellular ROS production via DHE

A qualitative DHE stain was used to determine intracellular O2- anion production in HAECs following a 48-hour incubation in NG and HG conditions. Cells were seeded onto a 48-well plate at a density of 1,000 cells/well. Following HG and NG treatment, cells were washed with HBSS, and cell media was replaced. DHE stain was added at a concentration of 5uM and incubated for 15 mins avoiding exposure to light. Fluorescent images were taken immediately using the Celigo.

2.2.7.2 Determination of intracellular ROS production via NBT

A quantitative nitroblue tetrazolium (NBT) assay was used to determine intracellular O2- anion production in HAECs following a 48-hour incubation in NG and HG conditions. Cells were washed once with PBS and incubated with NBT (0.36 ml at 0.33 mg/ml) for 2 hours. Following NBT incubation, cells were washed with PBS, and the NBT crystals were solubilised in 0.6 ml DMSO:ethanol:0.9 N NaOH (1/1/1, v/v/v). Absorbance measured at 680nm.

2.2.8 Analysis of EVs

2.2.8.1 Conditioned media harvesting

ECs were optimised for short-term growth in 0% serum conditions. This was achieved by lowering serum concentrations by 0.5% over a period of time (every 24 hours until growth in 0% serum was achieved). Once optimised, a T75cm^2 of 80% confluent ECs were treated with normal glucose (NG) (5mmol/l, NG) and high glucose media (HG) (30mmol/l, HG). The conditioned media from both groups were harvested every 48 hours. A batch of NG and HG conditioned media was collected and spun down at 2000rpm for 5 minutes to remove cellular material. Following this CM was pooled for downstream experiments to avoid batch to batch variability. Condition media was stored at -80°C.

2.2.8.2 Isolation of EVs from conditioned media

EV isolation was achieved using ExoQuick-TC reagent. EVs were isolated as per the manufacturer's protocol. All centrifugation steps were done at 4°C. Briefly, NG and HG conditioned media was centrifuged at 3,000g for 15 minutes removing cells and cellular debris (Figure 2.7, B). The supernatants were then transferred to a sterile 50ml tube, appropriate amounts of ExoQuick-TC reagent were added to of conditioned media. Samples were mixed by inverting, followed by overnight incubation at 4°C for 24 hours (Figure 2.7, C). After 24 hours, samples were then centrifuged for 1,500 x g for 30 minutes. The resulting supernatants were removed, and a further centrifugation step was carried out at 1,500 x g for 5 mins (Figure 2.7, D). The supernatant was then aspirated, and the resulting pellet was re-suspended in NaCl solution, ddH_20 or cell culture media depending on downstream application. Note: Functional experiments which included the treatment of both rat and human stem cells with EVs from endothelial cell conditioned media were carried out immediately after EV isolation. EVs were stained using a CFSE, Nir-Aza, and ExoGlow and analysed using the Amnis™ CellStream ™ flow cytometer. In the case of EV treatments. EVs isolated from 10mls of conditioned media was treated with 9cm^2 of adherent cells.

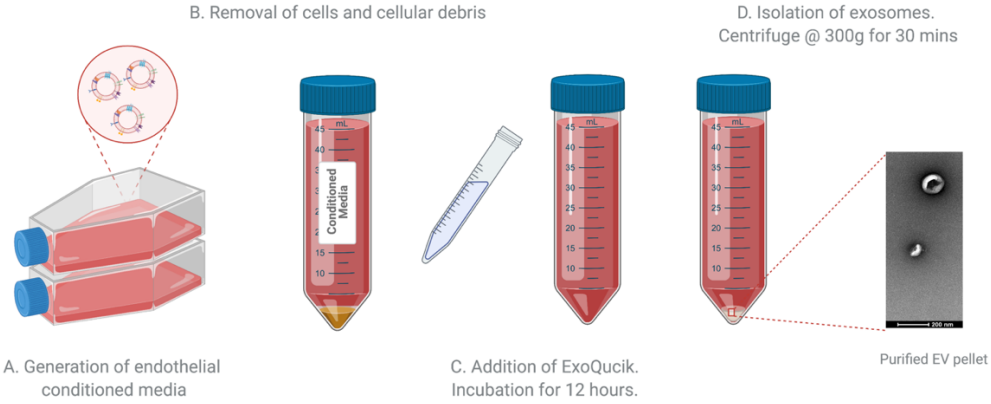

Figure 2.7 Schematic representation of EV isolation. Schematic representation of EV isolation. EC were grown in 0% serum RAEC media in normal glucose and high glucose conditions. Cell culture media was harvested for EV isolation. EVs were isolated using ExoQuickTC™ reagent.

2.2.8.3 Dynamic light scattering

Dynamic light scattering (DLS) measurements were performed to determine the size of the isolated EVs using the Malvern Zetasizer Nano. This technique is laser-based, sending a beam through a polarised sample whilst measuring the scatter light to determine the size of particles in the EV solution. Samples were diluted 100ul of isolated EVs were diluted in 900 ul of ultrapure water and filtered through a 0.45µM filter into a disposable plastic cuvette and covered with parafilm to prevent the entry of dust particles. 12 reads at 30 seconds each were performed using standard settings Refractive Index = 1.331, viscosity = 0.89, temperature = 25°C.

2.2.8.4 Nanoparticle tracking analysis

Nanoparticle tracking analysis (NTA) was performed by Particular Sciences Ltd. using the NanoSight NS300 nanoparticle analyser (NanoSight, Malvern NTA Version: NTA 3.2 Dev Build 3.2.16.) as per the manufacturer's instructions. EVs purified from conditioned cell media were diluted (1:1000) in PBS and filtered using a 0.45µM filter and subjected to size and concentration measurements. Analysis settings were set up as follows; Detection threshold 3, blur size auto, max jump size auto. The video was then analysed with NTA 2.3 software to obtain the size and concentration information of the EVs, including the mean, mode, standard deviation.

2.2.8.5 Exogenous EV labelling using ExoGlow-Membrane™ EV labelling kit

EVs were labelled using ExoGlow-Membrane™ EV Labelling Kit as (EXOGP100A-1, SBI) per manufacturer's instructions. Briefly, total EV protein concentration was measured using Pierce™ BCA Protein Assay Kit. 100µg of EVs was mixed with labelling dye and incubated at 30 minutes at room temperature (Figure 2.8 A,B). Free dye removal was carried out using PD SpinTrap G-25 columns. Labelled EVs were resuspended in essential eight media and incubated with SNEPs for periods 2hrs-24 hrs. Cells were fixed with 4% paraformaldehyde for 20 min (Figure 2.8, C). After washing with PBS, nuclei were stained with DAPI (1:1000). The signals were analysed using the Leica TCS SP8 Confocal microscope (Figure 2.8, D).

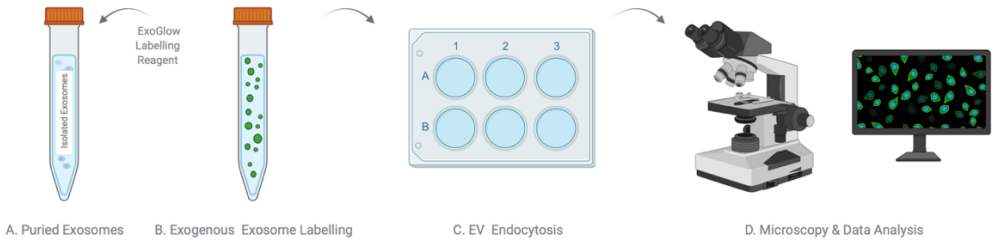

Figure 2.8 Schematic representation of exogenous HG-EV labelling using ExoGlow EV-labelling dye. EVs were isolated using ExoQuickTC™ reagent. Purified EV pellets from conditioned media were labelled using ExoGlow labelling kit. ExoGlow-labelled EVs were cultured with reporter cell line to determine EV uptake. Following 24 hour incubation reporter cell lines were fixed and visualised to determine uptake of EC-derived EVs.

2.2.8.6 Endogenous EV labelling using an amphiphilic NIR-fluorescent probe

Endothelial EVs were labelled using an amphiphilic NIR-fluorescent probe to favour chemical and photo-stability and effective internalisation by cells. HAECs were grown in 0% serum maintenance media. Once they reached 80% confluence, NIR-AZA was added to a concentration of 5 mM, and a 37°C incubation was maintained for two h – 24 hours (Figure 2.9 A). Fluorescence imaging of live cells at this time point showed a high degree

of the plasma membrane and cytoplasmic staining. Following removal of the media from the cells, EVs were isolated as per section 2.2.8.2 (Figure 2.9 B). Non-labelled controls were produced via an identical procedure but by omitting the addition of probe NIR-AZA. Biochemical analyses were performed on both labelled and unlabelled EVs using flow cytometry and fluorescent microscopy (Figure 2.9 C,D).

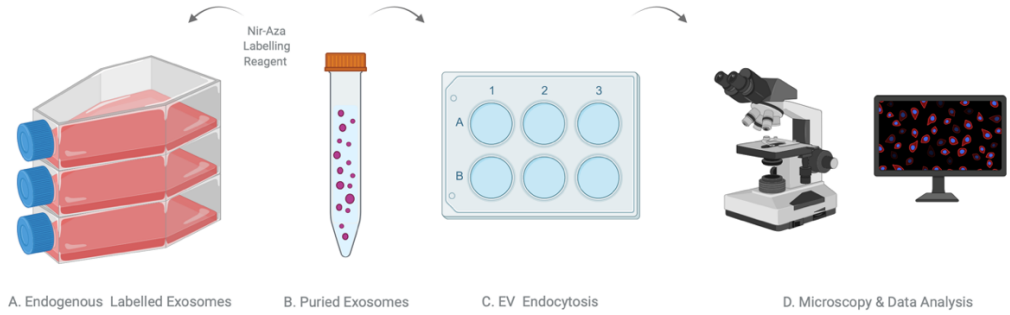

Figure 2.9 Schematic representation of endogenous HG-EV labelling using NirAza EV-labelling dye. EC EV labelling using NirAza dye *in vitro*. EVs were labelled from point of EC secretion. EVs were isolated using ExoQuickTC™ reagent. Purified EV pellets from conditioned media were cultured with reporter cell line to determine EV uptake. Following 24 hour incubation reporter cell lines were fixed and visualised to determine uptake of EC-derived EVs.

2.2.8.7 EV tracking using fluorescent imaging cytometer

Fluorescent microscopy using the Celigo Imaging Cytometer was used to (i) monitor EV staining during HAEC-EV production using Nir-Aza stain and (ii) tracking of EV uptake by SNEPs. Cells were treated with an EV-stain and imaged over various timepoints to increase fluorescent intensity. The Celigo Imaging software was set up using a fluorescent mask depending on the excitation and emission of stains for visualisation. Before imaging, cells were autofocused using the BF channel. The level of exposure was then auto-defined for each well. Simultaneous BF and fluorescent images were taken at each time point. Levels of fluorescent intensity were recorded and analysed at each time point.

2.2.8.8 Antibody Array

Surface proteins of isolated EVs were confirmed using the Exo-Check™ Antibody Array (EXORAY210A-8). A BCA protein array was used to determine vesicular protein

concentration, with 100ug/ml of protein being used for the arrays. The manufacturer's protocol was followed to determine EV protein cargo including GM130, FL0T-1, ICAM, ALIX, CD81, CD63, EpCAM, ANXA5 and TSG101. Protein blots were developed with TMB solution (Sigma Aldrich) 5-10 minutes.

2.2.8.9 Field Emission Scanning Electron Microscopy (FeSEM)

A 1mL of isolated EVs solution was resuspended in dH_2O. FeSEM of EVs was carried out by trained staff in the NRF DCU using the Hitachi S5500 Field Emission SEM.

2.2.9 FTIR and Raman spectroscopy

For both FTIR and Raman spectroscopic analyses, cells were seeded on calcium fluoride slides in 6 well plates at approximately 10,000 cells/well and incubated for a period of 24 hours. After fixation, the slides were washed with PBS and placed briefly in distilled water. The slides were left to air dry before recording spectra. Colleagues recorded Raman spectra at the Facility for Optical Characterisation and Spectroscopy, Technology University Dublin (TuDublin). Using a custom-built Raman micro-spectroscopy system. Briefly, this system employed a 150 mW laser with a wavelength of 532 nm (Laser Quantum, Torus), spectrograph (Andor, Shamrock 500) operating with 600 lines/mm grating, and a CCD camera (Andor; DU420A-BR-DD) cooled to −80 °C. A 50× microscope objective, with a numerical aperture of 0.8 (Olympus, UMPlanFl), was used to image the spectral irradiance to a 100μm confocal aperture, which isolates the signal from the cell nucleus, and minimises background noise from the sample substrate, as well as from optical elements in the system.

IR absorption measurements were carried out using a Perkin Elmer Spotlight 400 N FTIR imaging system. The system was equipped with an Auto Image microscope system operating with a ×40 Cassegrain objective and operated in transmission or reflection mode. FTIR images were acquired in transmission mode with ten scans of a 150 × 150 μm area of the slide for each cell population. All experiments were carried out in triplicate (576 spectra per scan were recorded, 30 scans per sample, ~15,000 spectra per cell population). Individual spectra were acquired with liquid nitrogen-cooled mercury cadmium telluride line detector of pixel size 6.25 μm × 6.25 μm at a spectral resolution

of 4 cm^{-1}, interferometer speed of 1.0 cm/s, and the useable spectral range is restricted to 900–4000 cm^{-1}. Background measurements were acquired on a region with no cells with 120 scans- s per pixel, whereas 32 scans per pixel were recorded from the sample.

2.2.9.1 FTIR/ Raman data processing

FTIR and Raman data processing was carried out as previously published (Molony *et al.*, 2018). The different data pre-processing and analysis steps were performed using MatLab (Mathworks, USA). For FTIR data, the resonant Mie scattering correction algorithm (RMieS-EMSC) was employed to re-move scattering effects from FTIR spectra (Bassan *et al.*, 2009), as has been successfully demonstrated in a number of studies (Hughes *et al.*, 2010). Due to differences in spectral resolution of the instrumentation used to acquire Raman signatures of cells versus tissues interpolation of the tissue data set was carried out. Linear interpolation is an imputation technique that assumes a linear relationship between data points and utilises non-missing values from adjacent data points to compute a value for a missing data point. Using Python, The Pandas data frame interpolate function was applied to all tissue data sets before the application of cosmic ray removal of an extended multiplicative signal correction algorithm as described in detail previously (Bassan *et al.*, 2009). After pre-processing, Principal Components Analysis (PCA) and Linear Discriminate Analysis (LDA) using Past 4 and WEKA software tools respectively was employed as an unsupervised multivariate analysis tool to differentiate the data recorded from different cell phenotypes.

2.2.10 Living photonics of individual cells

2.2.10.1 Biochip Device

The biochip device for single-cell capture was prepared by colleagues in the Cell Handling Group, Fraunhofer Project Centre for Embedded Bioanalytical Systems at DCU (Figure 2.10). Briefly, the biochip design was based on cell sedimentation under stagnant flow conditions due to the application of centrifugal force into an array of V-shaped capturing elements. Briefly, the sedimentation takes place with the liquid bulk at rest to provide high capture efficiency. V-cups (13 μm diameter) staggered in an array of 47 ×

24 cups which can thus trap up to 1128 individual cells. Additional trap and pillar-based locations are also on the biochip to facilitate a subpopulation of cells to be selected and further single-cell assays. Finally, a disc for holding three biochips and for mounting onto the centrifugal test stand was manufactured using 3D printing. The centrifugal test setup comprised a motor for spinning the microfluidic chips (4490H024B, Faulhaber micromotor SA, Switzerland), a synchronized camera for image acquisition during rotation (TXG14c, Baumer AG, Germany) coupled to a motorized 12x zoom lens (Navitar, USA) and a strobe light unit (Drelloscop 3244, Drello, Germany). The system integration between the microfluidic and optical systems for SCA was performed using an in-built optical detection and imaging system on the centrifugal test stand.

Excitation was performed by a 250-W halogen lamp (KL 2500 LCD, Schott, Germany) with an enclosed filter wheel to allow both broadband light (λ = 360–800 nm) and selected fluorescent excitation (filtered at excitation wavelengths of 403 ± 32 nm, 492 ± 15 nm, 515 ± 25 nm, 572 ± 15 nm and 610 ± 32 nm) and emission wavelengths (emission filters are 465 ± 20 nm, 530 ± 20 nm, λ565 ± 20 nm and 630 ± 20 nm and 670 ± 20 nm). The module was mounted on a computer-controlled X-Y stage (Qioptiq, Germany). Measurement of background photons assessed the contribution of the chip PDMS material and the surrounding liquid (cell media) on a fully primed empty chip. The images are acquired post-capture when the cells settle into the capture V-cup region. The method of travel through the chip was sedimentation-based and did not impact the fluorescence emissions as the cells experience minimum shear force as they travel through the chip. Spin speed for the cells travelling through the chip is fixed at 10 Hz for all experiments to reduce any instrumentation variations. Excitation (lamp power etc.) and image acquisition settings (exposure time, min and max values, etc.) were fixed and uniform across all experiments. The effect of the width of the excitation (15–32 nm) using commercial filters fitted into the imaging system revealed that changing an excitation filter bandwidth by a small increment had little impact on fluorescence excitation. The entire cell was selected as the region of interest (ROI) in all studies, and the mean value across the entire cell is presented. The experimental volume fraction of the cell probed and the standard deviation across each cell, in each wavelength, was low.

The device was placed in a vacuum before introducing the liquids for a minimum of 30 min ensure complete and bubble-free filling. The biochip was primed with the appropriate

cell culture media formulation for the cell type under test via the loading chamber on the top right section of the biochip. After priming, cells were introduced via the loading chamber on the top left section of the biochip. All pumping was performed the centrifugal test stand and a 3D-printed chip holder, which allows three biochips to be tested in parallel, thus significantly increasing the cell capture efficiency of the V-cup array system compared to common, flow-driven systems. Initial cell capture tests were performed using 20-µm polystyrene beads to emulate cell behaviour before being repeated using cells. In all cases, the sedimentation in the absence of flow led to significantly increased occupancy of the V-cups (≥ 95%) compared to common, flow-driven methods (data not shown).

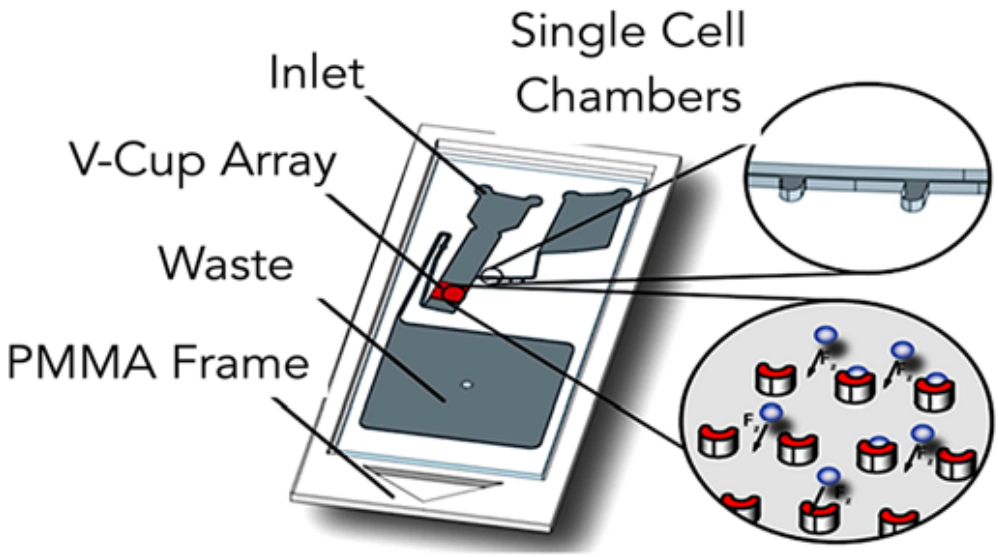

Figure 2.10 Biochip device. Schematic of the capture of individual cells using the LoaD platform (Molony *et al.*, 2021).

2.2.11 Supervised machine learning (ML)

Supervised ML is a technique in which a model is trained on a range of inputs (or features) that are associated with a known outcome. Once the algorithm is successfully trained, it will be capable of making outcome predictions when applied to new data. Spectra from FTIR, Raman and single cell AF were first classified to create ground truth for each sample before the data were normalized. Dimensionality reduction was achieved through Multiclass Fisher's Linear Discriminant Analysis (FLDA), as previously described before MLP artificial neural network analysis was performed on each dataset using the WEKA machine learning tool kit (Frank *et al.*, 2004). Once the dataset was loaded and pre-processed using the FLDA filter, it was processed using the "Classify" panel to implement MLP artificial neural network (ANN) analysis. ANNs are algorithms that are loosely modelled on the neuronal structure observed in the mammalian cortex and are arranged with a number of input neurons, which represent the information taken from each of the features in the dataset, which are then fed into any number of hidden layers before passing to an output layer in which the final decision is presented. The algorithm was iteratively improved using an optimization technique by changing the number of hidden layers (1,2.3., etc.) and the momentum (0.1–0.5) and rate of learning (0.1–0.5) to reduce the error of prediction and then evaluated using cross-validation. The risk of over-fitting was mitigated when our dataset was split into two segments, a training segment, and a testing segment, to ensure that the training model can generalize to predictions beyond the training sample. Each segment contained a randomly selected proportion of the features and their related outcomes, which allowed the algorithm to associate certain features, or characteristics, with a specific outcome and is known as training the algorithm. Once training was completed, the algorithm was then applied to the features in the testing dataset without their associated outcomes. The predictions made by the algorithm were then compared to the known outcomes of the testing dataset to establish model performance.

For single cell AF analysis PCA and LDA multivariate analysis, the cells were first classified to create ground truth for each sample before the spectral data were normalized to one by dividing the fluorescence intensity at each wavelength by the average background intensity at that wavelength. Dimensionality reduction was for FTIR, Raman and single-cell AF achieved through an FLDA pre-processing filter, as previously

described using WEKA machine learning tool kit, version 3.8.4, and further analysed by PCA and LDA using the multivariate statistical package PAST4. A scatter plot of specimens along the first two canonical axes produces maximal and second to maximal separation between all groups. The axes are linear combinations of the original variables as in PCA, and eigenvalues indicate the amount of variation explained by these axes. When only two groups are analysed, a histogram is plotted. The data are classified by assigning each point to the group that gives minimal Mahala Nobis distance to the group mean. The Mahala Nobis distance is calculated from the pooled within-group covariance matrix, giving a linear discriminant classifier. The given and estimated group assignments are listed for each point. In addition, group assignment is cross validated by a leave one outcross validation (jack-knifing) procedure. To interrogate the photonic profiles from unknown 'mystery' groups, i.e., data not included in the discriminant analysis itself but classified. In this way, it is possible to classify new datasets that are not part of the training set.

2.2.12 Quantification and Statistical Analysis

All data were determined from multiple individual biological samples and presented as mean values ± standard error of the mean (SEM). All *in vitro* experiments were performed in triplicate and repeated three times unless otherwise stated. All data were checked for normal Gaussian distribution for statistical comparisons before parametric and non-parametric tests were performed. An unpaired two-sided Student's t-test was performed to compare differences between two groups, and significance was accepted when $p \leq 0.05$. A one-sample t Wilcoxon test was performed on fold changes, and significance was accepted when $p \leq 0.05$. An ANOVA test was performed for multiple comparisons with Tukey's multiple comparisons test using GraphPad Prism software v8. Significance was accepted when $p \leq 0.05$.

Chapter 3:

Endothelial cell-derived EVs induce Hh-signalling in resident murine S100β^{+} vascular stem/progenitor cells in response to hyperglycaemic conditions *in vitro*

3.1 Introduction

Diabetes mellitus is a chronic metabolic disorder characterised by an inability to produce or effectively utilise insulin in the body. Notably, the leading cause of mortality and morbidity among subjects with diabetes is CVD (Grundy *et al.*, 1999; Zimmet, Alberti and Shaw, 2001). Patients with diabetes are at a two to three-fold higher risk of developing many CVDs, including coronary heart disease, stroke, peripheral arterial disease, and cardiomyopathy. Of interest in this study is the relationship between diabetes and the development of atherosclerosis.

Atherosclerosis is a widespread chronic inflammatory disorder of the arterial wall characterised by the accumulation of VSMC-like neointimal cells from various possible sources including medical VSMCs, resident stem cells, ECs or a combination of all three, lipid retention and infiltration of immune cells. The relationship between diabetes and atherosclerosis is multifactorial and includes a complex interaction of dyslipidaemia, hyperglycemia, increased oxidative stress, and inflammation (Grundy *et al.*, 1999; Bornfeldt, 2016; Hagensen *et al.*, 2019). It is widely accepted that the predominant response within the vessel wall following vascular injury is the essential pathophysiological process of endothelial dysfunction before the accumulation of neointimal VSMC-like cells. In the past decade, compelling evidence now suggests that endothelial dysfunction has harmful effects during the development of CVD.

Hyperglycaemia, a hallmark of diabetes, is an essential initiator of endothelial dysfunction, with many of the earliest pathological responses to hyperglycemia manifested in vascular ECs. Hyperglycemic-induced endothelial dysfunction is driven by constant EC exposure to elevated circulating glucose levels resulting in an imbalance of endothelial-derived factors and subsequent malfunction in vasodilation (Shi and Vanhoutte, 2017). A hallmark of atherosclerosis is pathological arterial re-modelling due to the accumulation of VSMC-like neointimal cells, either derived from medial VSMC, resident vascular stem cells, endothelial cells, or a combination of all three thereby resulting in the formation of a neointima, reduced blood flow, and vessel occlusion. The origin of neointimal cells has been extensively studied for many years. Initially, it was widely accepted that the origin of cells in the neointima involved the de-differentiation and migration of VSMC in the medial layer of the artery (Owens, Kumar and Wamhoff,

2004; Rensen, Doevendans and Van Eys, 2007). Initial studies of this process describe the downregulation of VSMC markers such as smooth muscle α-actin (SM α-actin) and Myh11 in neointimal cells post vessel ligation, which led to these cells being termed VSMC-like rather than VSMC (Ross and Glomset, 1973; Chamley-Campbell, Campbell and Ross, 1979). Numerous studies have since reported the ability of VSMCs to de-differentiate and take on a new phenotype, switching from contractile VSMCs to a synthetic VSMC displaying higher levels of proliferation and inflammatory cell recruitment following vascular injury (Rensen, Doevendans and Van Eys, 2007). In recent years, this assumption has been challenged. Several other cell types have been reported to be involved in the development of the VSMC-like cells of the neointima. Lineage tracing and scRNA-seq have provided compelling evidence for the involvement of a discrete population of (i) differentiated $Myh11^{+}$ medial SMCs that are $Sca1^{+}$ (Chappell *et al.*, 2016; Dobnikar *et al.*, 2018) and (ii) various medial and adventitial progenitors in progressing intimal thickening (Tang, Wang, Yuan, *et al.*, 2012; KRamann *et al.*, 2016; Yuan *et al.*, 2017; Tang *et al.*, 2020).

Given the multiple origins of cells within lesions and their cellular heterogeneity, a greater understanding of cell-cell communication and the subsequent initiating factors underlying the vascular pathology is needed. Activation of pathological inflammatory processes through paracrine and endocrine signalling has long been considered the driving source of cellular communication during the development of CVD. However, the advent of EVs as key intercellular communicators raises the possibility of EVs serving as an important nexus for signalling between the EC and the underlying vessel wall during vascular disease progression. EC-derived EVs are small membrane-derived vesicles shed by ECs into the extracellular space. Upon secretion, these lipid-bilayer protected EVs travel to neighbouring cells within the vasculature to be phagocytosed or dock to recipient cells eliciting a functional response. Since their discovery, extensive research has focused on the putative changes in EV cargo in response to various stimulants of vascular injury as early indicators for diagnosing sub-clinical atherosclerosis (Bank *et al.*, 2015; Yin, Loyer and Boulanger, 2015; Kowal *et al.*, 2016).

Of particular interest is EV-dependent transport of the secreted morphogen, SHh a known driver of myogenic differentiation recapitulated during vascular pathogenesis (Beckers *et al.*, 2007; Aravani *et al.*, 2019) and Notch receptor, a key signalling pathway involved in

mammalian cardiogenesis, including cell fate decisions, differentiation and proliferation, and angiogenesis (Gridley, 2010; Del Monte *et al.*, 2011; MacGrogan, Luxán and de la Pompa, 2014).Hh activates signalling in recipient cells by binding to its receptor Patched (Ptch). The binding of Hh to Ptch abrogates its inhibition on Smo and activates signalling via Gli transcription factors. Although mammals possess three distinct forms of the Hh morphogen, SHh has been the most widely implicated vascular disease. Recent studies have shown that Hh morphogen can be released through EV-mediated pathways (Liégeois *et al.*, 2006; Callejo *et al.*, 2011). Furthermore, it was demonstrated that SHh morphogen is secreted by two types of EVs (Vyas *et al.*, 2014). Similarly, activation of Notch signalling requires binding to its receptors Jagged-1, Jagged-2, and Delta-like ligands 1 – 4 activating the transcription of Notch target genes *Hey1 Hey 2* and *HeyL.* Various studies have investigated the role of EV-mediated transport of Notch and associated ligands, through overexpression of Notch1 in MSCs promoting angiogenesis (Xuan, Khan and Ashraf, 2020), detection of Jagged-1-EVs regulating EC behaviour and function (Tan, Asada and Ge, 2018) and transport of Dll4-EVs from ECs to neighbouring cells resulting in inhibition of Notch signalling and loss of Notch receptor (Sheldon *et al.*, 2010).

This chapter investigated the functional role of hyperglycaemic-induced secretion of EC-derived EVs from RAEC in controlling activation of SHh and/or Notch signalling in resident S100β/Sca1^{+} vascular stem cells *in vitro* as a potential early diagnostic biomarker for subclinical atherosclerosis.

3.2 Objectives

The main aims of this chapter were.

(i) To develop an *in vitro* murine model of RAEC in culture and characterise EC-derived EVs under normal and hyperglycaemic conditions that mirror diabetic conditions of the vasculature *in vivo*.

(ii) To determine whether EC-derived EVs under normal and hyperglycaemic conditions impact hedgehog and Notch signalling in S100β/Sca1^{+} resident vascular stem cells *in vitro.*

3.3 Strategy

The main objective was to develop an *in vitro* murine cell culture model to test our hypothesis that EC-derived EVs harbouring SHh, and Notch are involved in the communication between ECs and resident vascular stem cells to promote the activation of Hh and/or Notch signalling of S100β/Sca1^{+} resident vascular stem cells *in vitro.* Two murine cell models were developed (i) diabetic endothelial model for EV production, (ii) vascular reporter stem cell model to determine EV functionality (Figure 3.1).

Primary RAECs were purchased from Cell Applications (R304-05) and cultured in normal glucose (NG:5mM) until reaching 70% confluency (Section 2.2.2.1). ICC was carried out to characterise the cell population by probing for membrane-bound protein CD31 and cytoplasmic protein eNOS (Section 2.2.5.1). ICC was also used to ensure these cells were not enriched for Cnn1, a VSMC differentiation cell marker. Confirmatory qRT-PCR analysis was used to determine mRNA levels of *CD31*, *eNOS*, and *Cnn1* and compared to rat smooth muscle cells (Section 2.2.5.2). To mimic vascular diabetic conditions found *in vivo*, RAECs were treated with high glucose (HG:30mM)) for 48 hours. Prior to cell treatments, RAECs were treated with decreasing percentages of serum until reaching 0% serum with minimal cellular apoptosis to achieve (i) cell quiescence and synchronisation and (ii) to remove contaminating serum containing EVs from the EC conditioned media. Having reached 80%, confluency RAEC media was replenished with normal glucose, high glucose, or mannitol (MT) (30mM), serving as an osmotic control.

Cell culture media was harvested and stored at -80°C for EV isolation and characterisation following each cellular treatment. EC-derived EVs following exposure to normal and hyperglycemic conditions were isolated from stored conditioned media using ExoQuick-TC™, a proprietary polymer for gentle precipitation of EVs (Section 2.2.7.1). To characterise the resulting purified EVs, two methods were deployed (i) NTA to measure the Brownian motion of nanoparticles where the speed of motion, or diffusion coefficient, is related to particle size through the Stokes-Einstein equation (2.2.7.4) and (ii) nanoFACs analysis using the Amnis™ Cell Stream FACS analyser (Section 2.2.5.3) following CFSE staining of EVs.

To investigate whether EVs derived from hypoglycaemic RAECs activate SHh and/or Notch signalling in S100β$^+$ Sca-1$^+$ resident vascular stem cell *in vitro,* S100β$^+$ multipotent stem cells from the medial layer of rat aortic explants were isolated (Section 2.2.1.2) and characterised. Medial VSMCs within the aortic arch develop from a NE embryological origin and are associated with the high-risk site for vascular re-modelling events, especially in aging populations (Redheuil *et al.*, 2010; Bacakova *et al.*, 2018). Therefore, following dissection and harvest of the rat aortic vessel, rMVSCs were isolated from the arch region of a female Sprague-Dawley rat and expanded in MM1. ICC was then carried out to characterize the cell population by probing for the calcium-binding protein S100β and the neural stem cell marker Nestin. ICC was also used to investigate if these cells, isolated from an area rich in smooth muscle cells (VSMCs), expressed VSMC markers, such as Cnn1 and Myh11.

The multipotency of the rMVSCs was evaluated using vasculogenic (endothelial) and myogenic (smooth muscle) inductive media. Rat MVSCs were cultured for 14 days in inductive differentiation media to obtain endothelial (Section 2.2.5.1) and myogenic differentiation, respectively (Section 2.2.5.2.1). Phase-contrast images were taken during the differentiation process to interrogate for changes in cell morphology. ICC was performed to detect the endothelial marker, CD31, and the loss of a discrete subpopulation of Cnn1$^+$ partially differentiated rMVSCs. Myogenic differentiation of rMVSCs was achieved via activation of the Notch signalling pathway using immobilised Jagged-1 (Section 2.2.5.2.3). The ɣ-secretase inhibitor, N-[N-(3,5-Difluorophenacetyl)-L-alanyl]-S-phenyl glycine t-butyl ester (DAPT) was used to confirm that the myogenic differentiation process was Notch-dependent. After 14 days, the transcript and protein expression of myogenic genes *Cnn1* and *Myh11* were measured by qRT-PCR and ICC, respectively. Lastly, to determine the role of RAEC-EV-mediated activation of Hh and Notch signalling in rMVSCs, cells were treated with EVs derived from normal and hyperglycemic RAECs for 48 h before Notch, and SHh target gene expression was evaluated by qRT-PCR (Section 2.2.5.2).

For statistical comparisons, all data were checked for normal Gaussian distribution using the Kolmogorov-Smirnov normality test before parametric and non-parametric tests were performed. In the case of data containing only two samples, an unpaired t-test with Welch's correction was performed on normally distributed data. For non-parametric

(skewed) data, the Wilcoxon test was carried out to calculate statistical significance. ANOVA testing was used to perform multiple comparisons between all samples for data containing more than two samples. This could be carried out using an ordinary one-way (one parameter to compare) or two-way (two parameters to compare) ANOVA for normalised data or the Kruskal-Wallis test for non-parametric data. Further post hoc test, Tukeys method, was carried out to identify the group comparisons that are significantly different while limiting the family error rate to the significance level. Significance was accepted when $p \leq 0.05$.

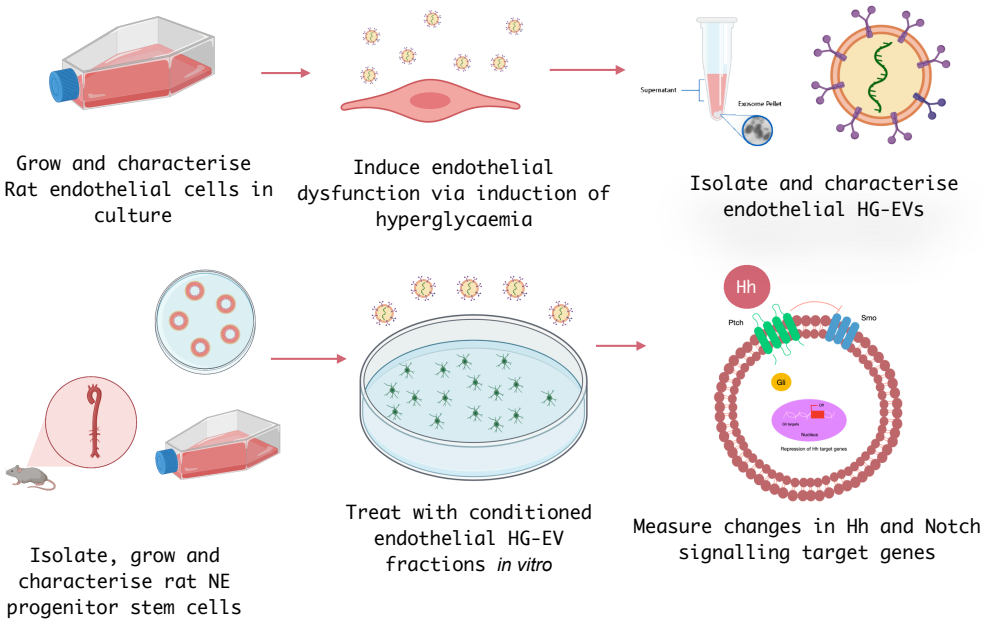

Figure 3.1 Graphic summary of experimental strategy. Graphic summary of the experimental strategy to determine the role of RAEC-derived-EVs under normal and hyperglycaemic conditions in activating the Hh and Notch signalling pathway in murine resident S100β^{+} stem/progenitor cells *in vitro*.

3.4 Results

3.3.1 Primary RAECs express distinct endothelial markers CD31, vWF, and eNOS under NG conditions.

To develop an *in vitro* murine cell culture model for EV secretion, RAECs were grown in culture and characterised for their expression of endothelial markers, including CD31 and eNOS, before RAEC were exposed to normal and hyperglycaemic conditions. RAECs displayed typical EC characteristics when grown as a single adherent monolayer. A distinct cobblestone morphology was observed by phase-contrast microscopy at 4X and 10X magnification (Figure 3.2 A, B). The cells were significantly enriched for *Cd31* and *eNOS* mRNA levels compared to rat VSMCs in culture (Figure 3.2 C, D).

The expression of eNOS, Cd31, and Cnn1 proteins was determined by immunocytofluorescence staining (ICC). Cells were seeded onto sterile coverslips in a 6-well plate at a low density (4,000 cells/well) and incubated at 37°C for 48 h. Cells were fixed with 3.7% formaldehyde and stained with primary antibodies for Cd31 (1:100), eNOS (1:50), or Cnn1 (1:200). To generate a fluorescent signal for staining, fluorophore-Alexa Fluor 488-conjugated secondary antibodies were added, and nuclei were stained with DAPI. Using a fluorescent microscope, these stains were visualised, imaged, and analysed to determine the expression of each protein. An IgG control (secondary antibody probing without primary antibody staining) was included to account for background fluorescence or off-target binding of secondary IgGs. The expression of endothelial markers eNOS and Cd31 were abundant in RAECs (Figure 3.3 A-B). Although both proteins were abundantly expressed, the localisation of protein expression differed. The expression of Cd31 was localised around the membrane of the cell. In contrast, the expression of eNOS was localised in the cytoplasm of the cell. In order to ensure RAEC did not contain a contaminant VSMC cell in culture, the expression of early myogenic differentiation Cnn1 protein was determined (Figure 3.3 C). As expected, RAECs did not express Cnn1 protein. Positive cells were counted and compared against the total cell DAPI stain cell count for quantitative analysis and are presented as the fraction of positive cells compared to a negative cell control (Figure 3.3 D-F).

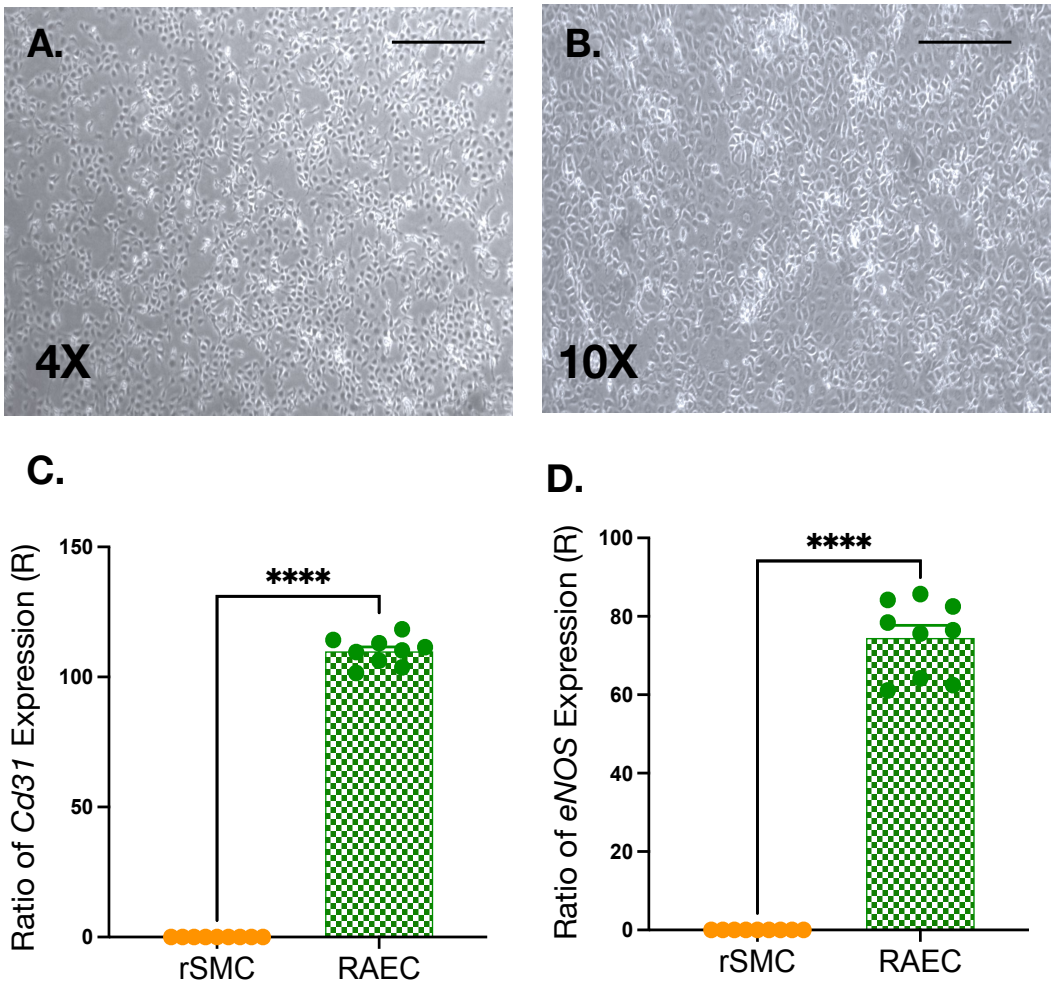

Figure 3.2 Characterisation of primary RAECs. (A) Phase-contrast images of RAEC in culture at 4X and 10X magnification. Scale bar representative of 20µm and 50µm respectively. (B) Relative mRNA levels of endothelial markers *Cd31* and *eNOS* in RAECs. Data are expressed as the ratio of mRNA expression relative to *Gapdh* and are the mean ± SEM, n = 9, * $p \leq 0.05$ versus rVSMCs.

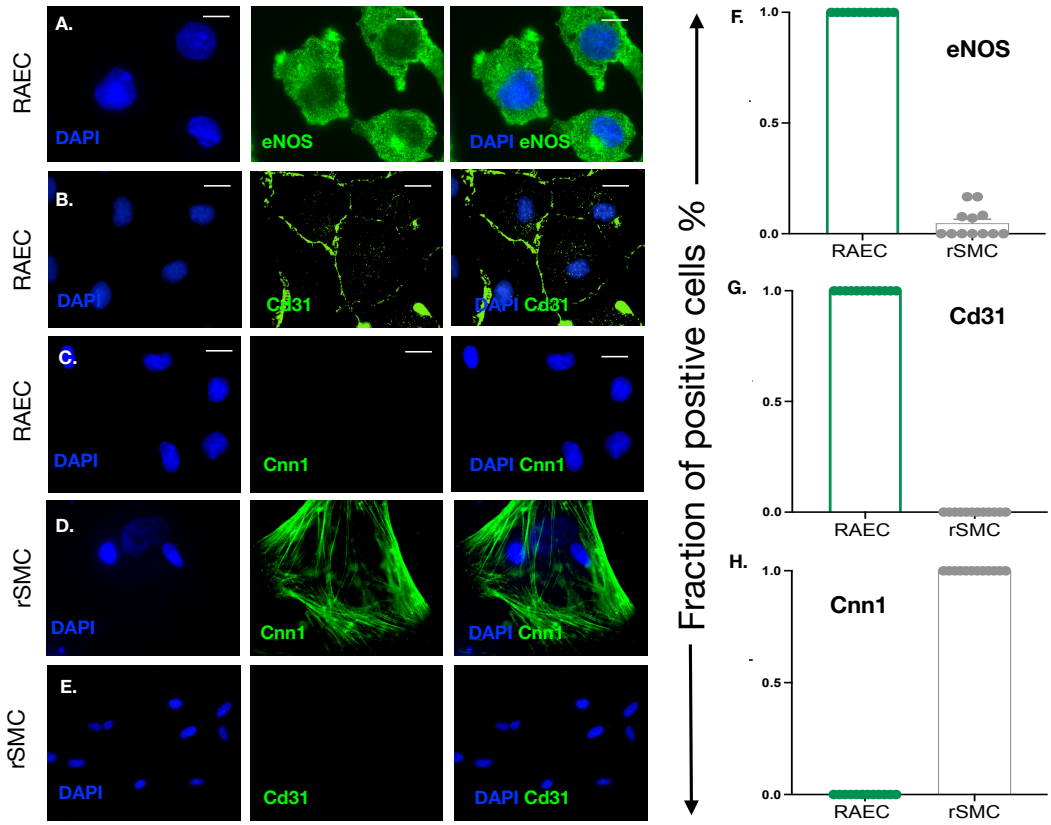

Figure 3.3 Characterisation of primary RAECs by ICC. (A-C) Representative images of fluorescence staining of DAPI nuclei and immunocytochemical analysis of the expression of endothelial markers eNOS, Cd31, and myogenic marker Cnn1 in RAECs. (D-F) Fraction of $eNOS^+$, $Cd31^+$ and $Cnn1^+$ cells. All images were taken using Olympus DP-50 fluorescent microscope. Alexa Fluor 488 secondary antibody used for visualisation of primary antibody binding. All images are representative of $n \geq 6$ images per experimental group from three independent cultures—scale bar representative of 10µm.

3.3.2 Labelling of RAEC-derived EVs following exposure of cells to normal and hyperglycaemic conditions *in vitro*

Secreted by virtually all cell types in the body, EVs are small, membranous particles that have recently emerged as an important mediator of intracellular communication, suggesting their pathophysiological role in CVD progression. The cellular origin, composition, and functional property of circulating EVs can be exploited as a sub-clinical non-invasive biomarker used to detect pathological diseases represented by various proteins, lipids, and nucleic acids encapsulated in the vesicular membrane. RAECs were cultured under normal and hyperglycemic conditions facilitating the release of EVs into conditioned cell culture media *in vitro*. After 48 h, cell culture media was harvested, followed by EV isolation using ExoQuick TC reagent as described in section 2.2.8.2. Once purified, EVs were resuspended in dH_20 for characterisation. Submicron particle detection and characterisation of EVs from normal and hyperglycemic conditions were carried out using the Amnis™ CellStream nanoFACs analyser that employs a time delay integration charge-coupled device (TDI CCD) camera technology for detection, offering exceptional sensitivity for studying small particles.

CFDA-SE was used as an intra-vesicular dye becoming converted to CFSE once hydrolysed by esterase within EVs, removing diacetate residues resulting in activation of the CFSE green fluorescence. RAEC-EVs derived from normal and hyperglycemic conditions positively expressed CFSE staining (Figure 3.4 C, Figure 3.5 C). In order to determine the true isolation of intact EVs, appropriate controls were performed in parallel to eliminate detection of false-positive CFSE staining of particles, including unstained EVs (Figure 3.4 A, Figure 3.5 A) and CFSE staining in the absence of EVs (Figure 3.4 B, Figure 3.5 B). In order to differentiate RAEC-derived EVs following exposure to normal and hyperglycemic conditions from protein aggregates, detergent treatment (0.1% Triton X-100) was used. CFSE stained RAEC-derived EVs from normal and hyperglycemic conditions showed a decrease in CFSE+ events following TritonX-100 treatment (Figure 3.4 D, Figure 3.5 D).

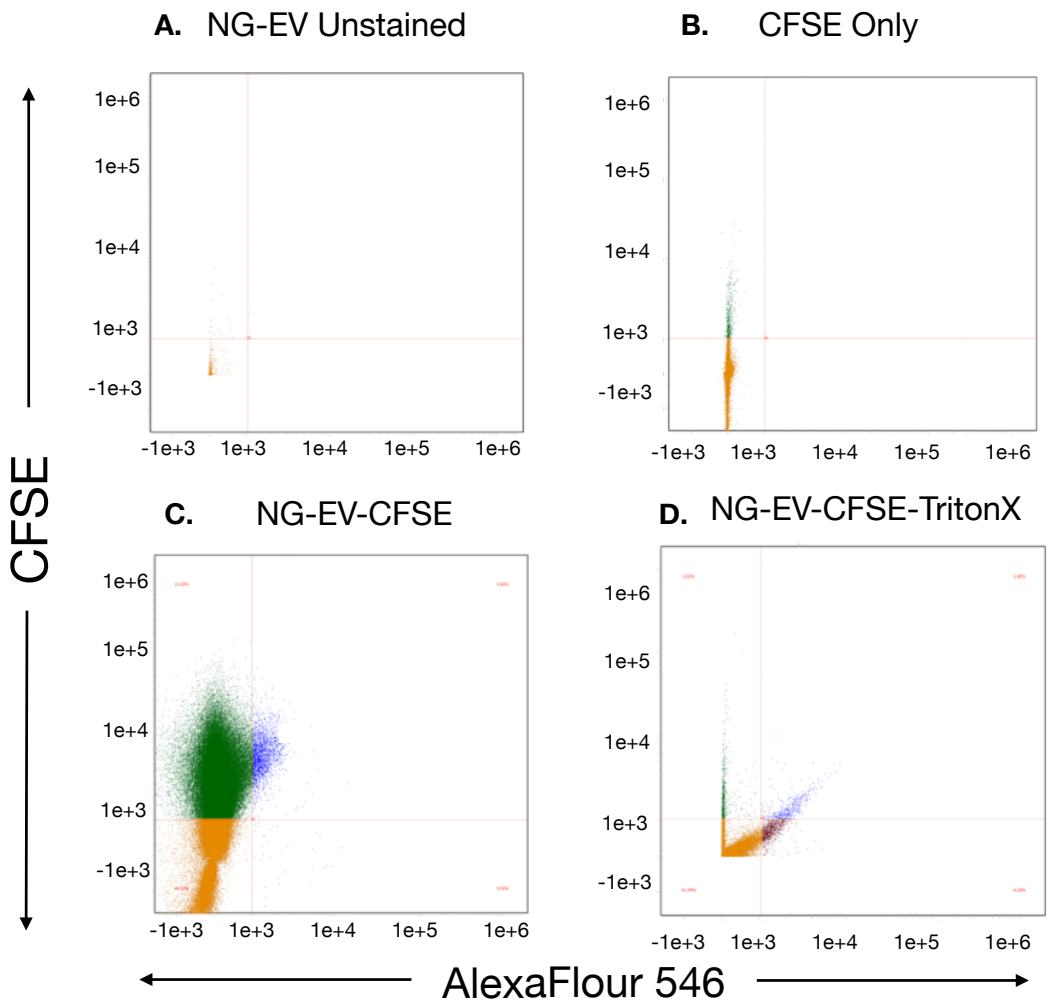

Figure 3.4 CFSE labelling of RAEC-derived NG-EVs. Submicron particle detection by nanoFACs of CFSE stained NG-EVs from RAECs (A) CFSE+ events of unstained NG-EVs (B) CFSE+ events of CFSE stain without NG-EVs (C) CFSE+ events of NG-EVs stained with CFSE (D) CFSE+ event of CFSE-NG-EVs treated with TritonX-100. Data is representative of n=3.

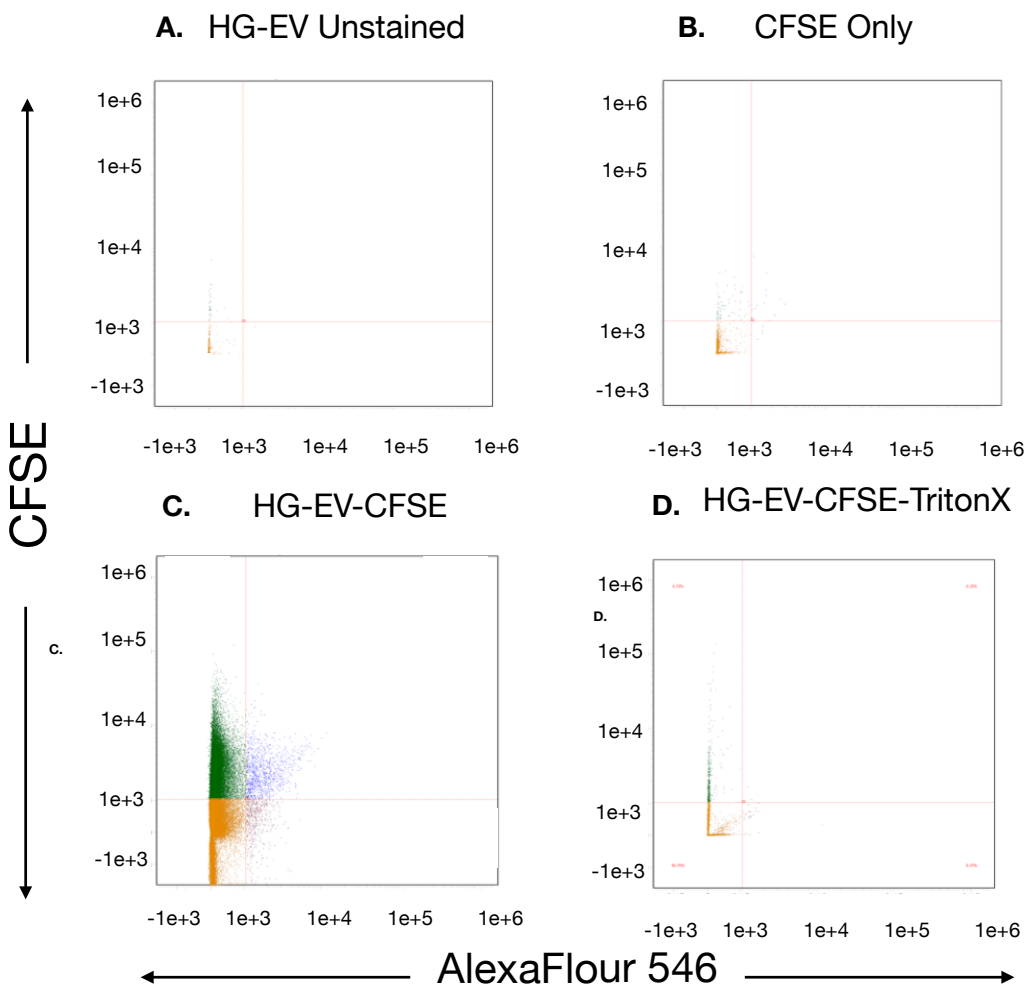

Figure 3.5 CFSE labelling of RAEC-derived HG-EVs. Submicron particle detection by nanoFACs of CFSE stained HG-EVs from RAECs (A) CFSE+ events of unstained HG-EVs (B) CFSE+ events of CFSE stain without HG-EVs (C) CFSE+ events of HG-EVs stained with CFSE (D) CFSE+ event of CFSE-HG-EVs treated with TritonX-100. Data is representative of n=3.

3.3.3 Characterisation of RAEC-derived EVs following exposure of cells to normal (NG) and hyperglycaemic conditions (HG) *in vitro* using Nanoparticle Tracking Analysis (NTA)

NTA was performed using a NanoSight NS300 instrument (Malvern Ltd) equipped with NTA 3.2 analytical software to determine particle size and concentration. Samples were first thawed on ice and diluted in dH_20. Each sample was then loaded in the sample chamber, and the camera focus was adjusted. Using Brownian motion and light scattering properties, particle size distribution was determined for RAEC-derived EVs from normal and hyperglycemic conditions. The camera operating at 30fps captures a video of particles moving in Brownian motion (Figure 3.6 A). A camera level of 12 (RAEC-derived EVs from normal conditions) and 9 (RAEC-derived EVs from hyperglycemic conditions) was used for the recordings, and the detection threshold was fixed at 3. All comparisons were made at consistent camera levels. Five 30 or 60 s videos were recorded for each sample. Statistical analysis of merged data was performed using NTA 3.2 Dev Build 3.2.16. The mean mode and standard deviation for RAEC-derived EVs from normal conditions were 183.2nm, 160.6nm, and 69.6nm, respectively. The mean, mode, and standard deviation of HG-EVs were 183.2nm, 160.6nm and 69.6nm, respectively. Furthermore, a distinct peak at 161nm was obtained for RAEC-derived EVs from normal conditions, whereas multiple peaks at various sizes, mainly at 137nm, 202nm, and 296nm was obtained for RAEC-derived EVs from hyperglycemic conditions (Figure 3.6 B and C).

An increase in EV particle secretion has been reported in response to EC exposure to hyperglycemic conditions (Li *et al.*, 2016). In order to investigate particle concentration of RAEC-derived EVs from normal conditions (NG) versus hyperglycemic conditions (HG), analysis of particle concentration was determined using the NTA platform. 10mls of conditioned media from normal and hyperglycemic RAECs following 24 h treatment was collected. RAEC-derived EVs from normal and hyperglycemic conditions were isolated characterised using NTA under the same conditions as mentioned above. An increase in the secretion of EVs was observed in EVs isolated from hyperglycemic RAECs in comparison to EVs isolated from normal RAECs. The concentration of particles for RAEC-derived EVs from normal conditions and RAEC-derived EV from hyperglycemic conditions was 2.67×10^8 and 1.42×10^9 particles/ml, respectively.

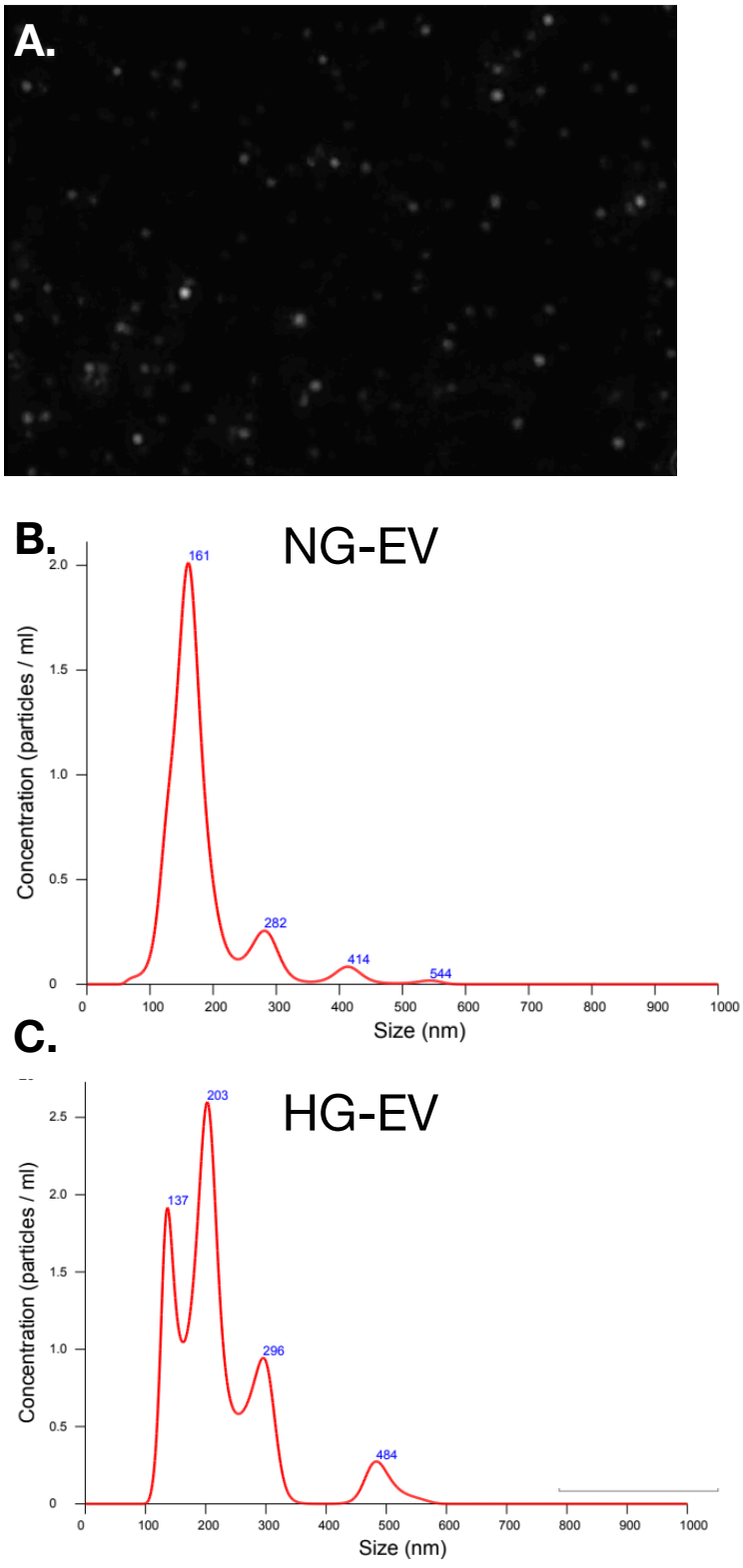

Figure 3.6 NTA of RAEC derived NG and HG-EVs. (A) Representative video screenshot of EV particles moving in Brownian motion for NTA. (B) A representative particle size distribution profile from NTA of NG-EV rich fractions. (C) A representative particle size distribution profile from NTA of NG-EV rich fractions.

3.3.4 Resident vascular stem cells isolated from the medial explants of rat aortic tissue express stem-associated markers

To determine the functional effect of RAEC-derived EVs from hyperglycemic cells on the response of resident vascular stem cells, a reporter *in vitro* murine cell culture model was developed. S100β^{+} stem cells have been shown to contribute to the development of ligation-induced neointima through migration and differentiation (Di Luca *et al.*, 2021; Molony *et al.*, 2021). Therefore, cultured rMVSCs from rat aortic medial explants were isolated and characterised for specific stem cell makers. The expression of Sox17, Sca1, Sox10 and S100β stem cell markers and VSMC myogenic marker Cnn1 was determined by ICC staining. Cells were seeded onto sterile coverslips in a 6-well plate at a low density (7,000 cells/well) and incubated at 37°C for 48 h. Cells were fixed with 3.7% formaldehyde and stained with primary antibodies Sox17 (1:200), Sca1 (1:150), Sox10 (1:100), S100β (1:50) and Cnn1 (1:200). To generate a fluorescent signal for staining, fluorophore-Alexa Fluor 488-conjugated secondary antibodies were added, and nuclei were stained with DAPI. Using a fluorescent microscope, these stains were visualised, imaged, and analysed to determine the expression of each protein. IgG controls (secondary antibody probing without primary antibody staining) were used to account for background fluorescence or off-target binding of secondary IgGs. Cultured rVSMCs were used as a comparative myogenic cell. Stem cell markers Sox17, Sca1, Sox10, and S100β, were detected in isolated rMVSCs (Figure 3.7 A-D). Although all proteins were abundantly expressed, the localisation of protein expression differed. The expression of Sox17 and Sox10 was localised in the nucleus of rMVSCs. In contrast, the expression of Sca1 and S100β was localised in the cytoplasm of the cell. No expression of stem cell proteins was detected in the comparator rVSMC cell, as expected (Figure 3.7 E-H). Positive cells were counted and compared against the total cell DAPI stain cell count for quantitative analysis and are presented as the fraction of positive cells compared to a negative cell control (Figure 3.7 E-H).

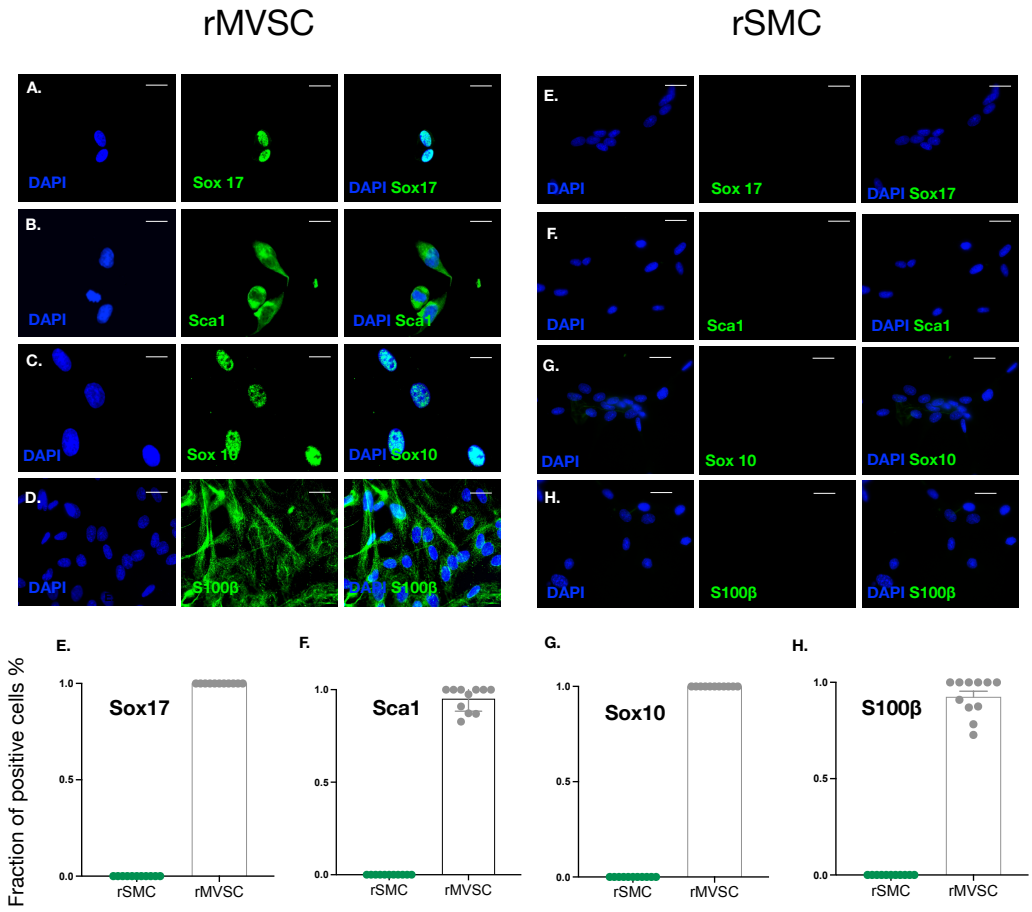

Figure 3.7 Characterisation of rMVSCs from rat aortic explants. (A-D) Representative images of fluorescence staining of DAPI nuclei and immunocytochemical analysis of the expression of stem markers Sox17 (Green) (A), Sca1 (B), Sox10 (C), and S100β (D) in rMVSCs. E-H) Fraction of Sox17, Sca1, Sox10, and S100 positive cells. (E-H) Fraction of $Sox17^{+}$, $Sca1^{+}$, $Sox10^{+}$, and S100β cells. All images were taken using Olympus DP-50 fluorescent microscope. Alexa Fluor 488 secondary antibody used for visualisation of primary antibody binding. All images are representative of $n \geq 6$ images per experimental group from three independent cultures—scale bar representative of 10μm.

3.3.5 Vasculogenic differentiation of rMVSCs

As a measure of the multipotency of isolated rMVSCs, vasculogenic differentiation stimuli were used to demonstrate stem cell plasticity. Cultured rMVSCs were seeded in wells of a 6-well plate at 5000 cells/well and incubated at 37°C for 24 h. Media was then replaced with a 1:1 dilution of MM1 (stem cell maintenance media) and complete EC media (RAEC + MM), and RAEC complete media (RAEC) composed of a basal media and 10% vasculogenic growth supplement. Cells were incubated at 37°C for 14 d with media replacement every 3-4 days. Following 7 d incubation, phase-contrast images of rMVSCs pre- and post-treatment were analysed and revealed distinct morphological changes from stem-like neural elongated cells to endothelial-like cobblestone morphology following treatments (Figure 3.8 A). Cells were harvested, and RNA was isolated. RNA samples were analysed by qRT-PCR to measure the expression of EC markers *eNOS* and *Cd31* in treated samples relative to the MM1 control. In all RAEC media-treated samples (1:1 dilution and neat), a significant increase was detected in the expression of both *eNOS* and *Cd31* compared to the MM1 control (Figure 3.8 B, C).

Parallel ICC analysis was carried out to determine the expression of EC protein eNOS. Cells were seeded onto sterile coverslips in a 6-well plate at a low density (5,000 cells/well) and incubated at 37°C for 24 h. Media was removed and replaced with RAEC media for 14 d. Cells were fixed with 3.7% formaldehyde and stained with a primary eNOS (1:50) antibody. To generate a fluorescent signal for staining, fluorophore-Alexa Fluor 488-conjugated secondary antibodies were added, and nuclei were stained with DAPI. Using a fluorescent microscope, these stains were visualised, imaged, and analysed to determine the expression of each protein. IgG controls (secondary antibody probing without primary antibody staining) were used to account for background fluorescence or off-target binding of secondary IgGs. Following RAEC treatment rMVSCs expressed a significant increase in eNOS protein expression in comparison to rMVSC in MM (Figure 3.9 A, B). Positive cells were counted and compared against the total cell DAPI stain cell count for quantitative analysis and are presented as the fraction of positive cells compared to a control (Figure 3.9 C).

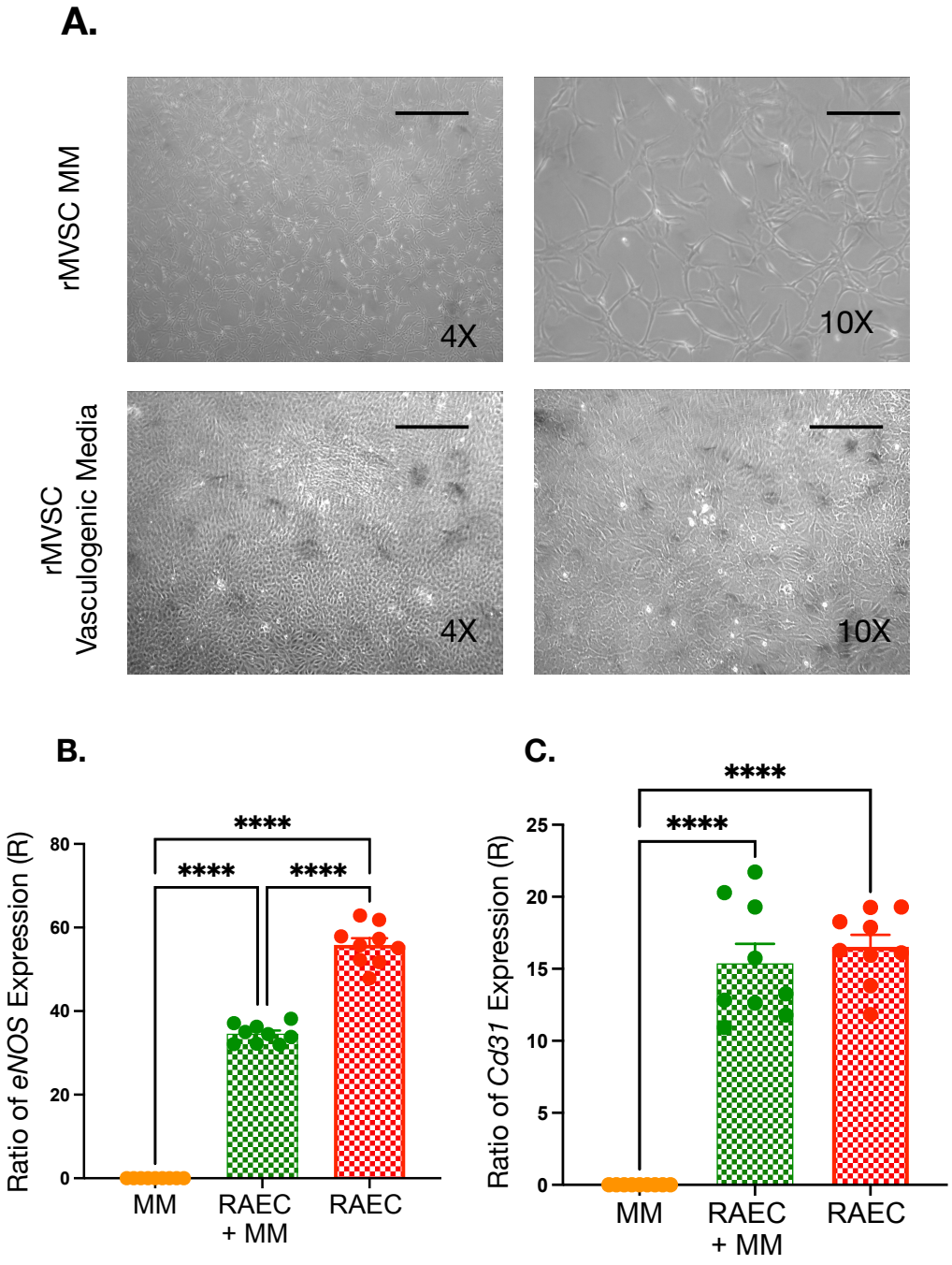

Figure 3.8 Vasculogenic differentiation of rMVSCs *in vitro*. (A) Phase-contrast images of morphological changes in rMVSC in culture pre-and post-treatment with vasculogenic differentiation media at 4X and 10X magnification. Scale bar representative of 20µm and 50µm respectively. (B, C) Relative mRNA levels of endothelial markers *Cd31* and *eNOS* in rMVSCs following vasculogenic treatments. Data are expressed as the ratio of mRNA expression relative to control and are the mean ± SEM, n = 9, * $p \leq 0.05$ versus RAEC + MM and RAEC.

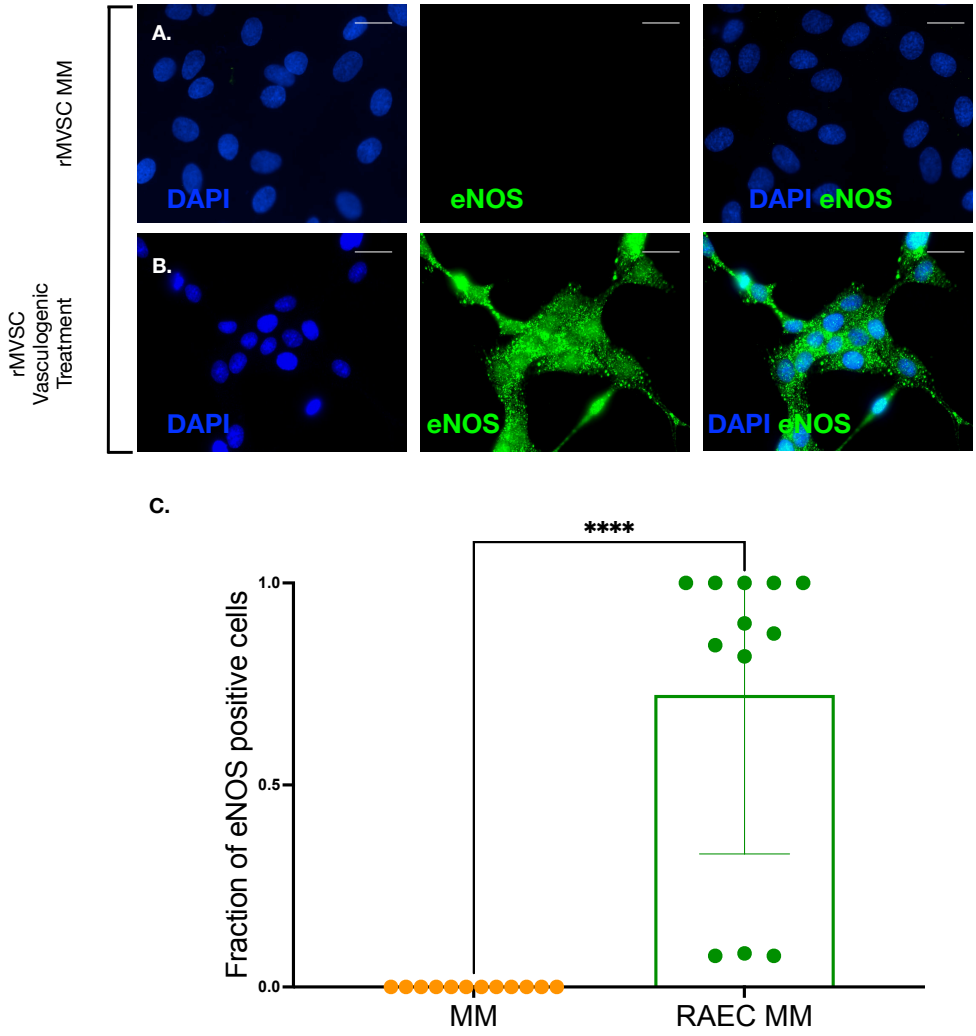

Figure 3.9 Vasculogenic differentiation of rMVSCs *in vitro*. (A, B) Representative images of fluorescence staining of DAPI nuclei and immunocytochemical analysis of the expression of endothelial marker eNOS in rMVSCs. (C) Fraction of $eNOS^{+}$ cells after treatment. All images were taken using Olympus DP-50 fluorescent microscope. Alexa Fluor 488 secondary antibody used for visualisation of primary antibody binding. All images were taken using Olympus DP-50 fluorescent microscope. Alexa Fluor 488 secondary antibody used for visualisation of primary antibody binding. All images are representative of $n \geq 6$ images per experimental group from three independent cultures—scale bar representative of 20µm.

3.3.6 Recombinant Jagged-1 and SHh activation of Hh and Notch signalling and subsequent myogenic differentiation in rMVSCs.

To investigate the role of EV facilitated activation of Hh and Notch signalling via transport of vesicular cargo, it was first imperative to confirm that direct treatment with Jagged-1 protein and recombinant SHh in the absence of EVs activates Hh and Notch signalling and subsequent myogenic differentiation of rMVSCs. In order to activate the Notch signalling pathway, rMVSCs were cultured in plates pre-coated with 1µg/mL immobilised IgG-Fc, Jagged-1-Fc, and Jagged1-Fc plus the ɣ-secretase inhibitor, DAPT (80µM) for 14 d. Cell viability was analysed after 14d. DAPT treatment showed no effect on cell viability.

Following treatments, cells were fixed before ICC was performed. Expression of the early myogenic differentiation protein, Cnn1 and the late differentiation protein , Myh11 protein was evaluated. Cells were incubated with primary Cnn1 (1:200) and Myh11 (1:250) antibodies overnight. After overnight incubation, cells were incubated with secondary antibody Alexa Fluor 488 (1:1000) and stained using DAPI stain for nuclear visualisation. Treatment of rMVSCs with Jagged-1 significantly increased the fraction of Cnn1 (Figure 3.10 A, B) and Myh11 (Figure 3.11 A, B) positive cells after 14 d in culture. The levels of *Cnn1* and *Myh11* mRNA mirrored the changes in protein, where rMVSCs treated with Jagged-1 became significantly enriched for Cnn1 and Myh11, an effect attenuated by theγ-secretase inhibitor, DAPT (Figure 3.11 C).

In order to activate the Hh signalling pathway, rMVSCs were cultured with recombinant SHh (1.0µg/ml) protein and recombinant SHh plus the smoothened inhibitor, cyclopamine (15mM) for 7 d. Following treatments, cells were fixed before ICC was performed. Expression of the early myogenic differentiation protein, Cnn1 was determined as described in section 2.2.6.1. Cells were incubated with primary Cnn1 (1:200) antibody overnight. After overnight incubation, cells were incubated with secondary antibody Alexa Fluor 488 (1:1000) and stained using DAPI stain for nuclear visualisation. Treatment of rMVSCs with rSHh (1.0µg/ml) significantly increased the fraction of Cnn1 positive cells after 7 d in culture (Figure 3.12 A, B). The levels of *Cnn1* mRNA mirrored the changes in protein, where rMVSCs treated with rSHh became

significantly enriched for *Cnn1*, an effect attenuated following Hh inhibition with cyclopamine (15mM) (Figure 3.12 C).

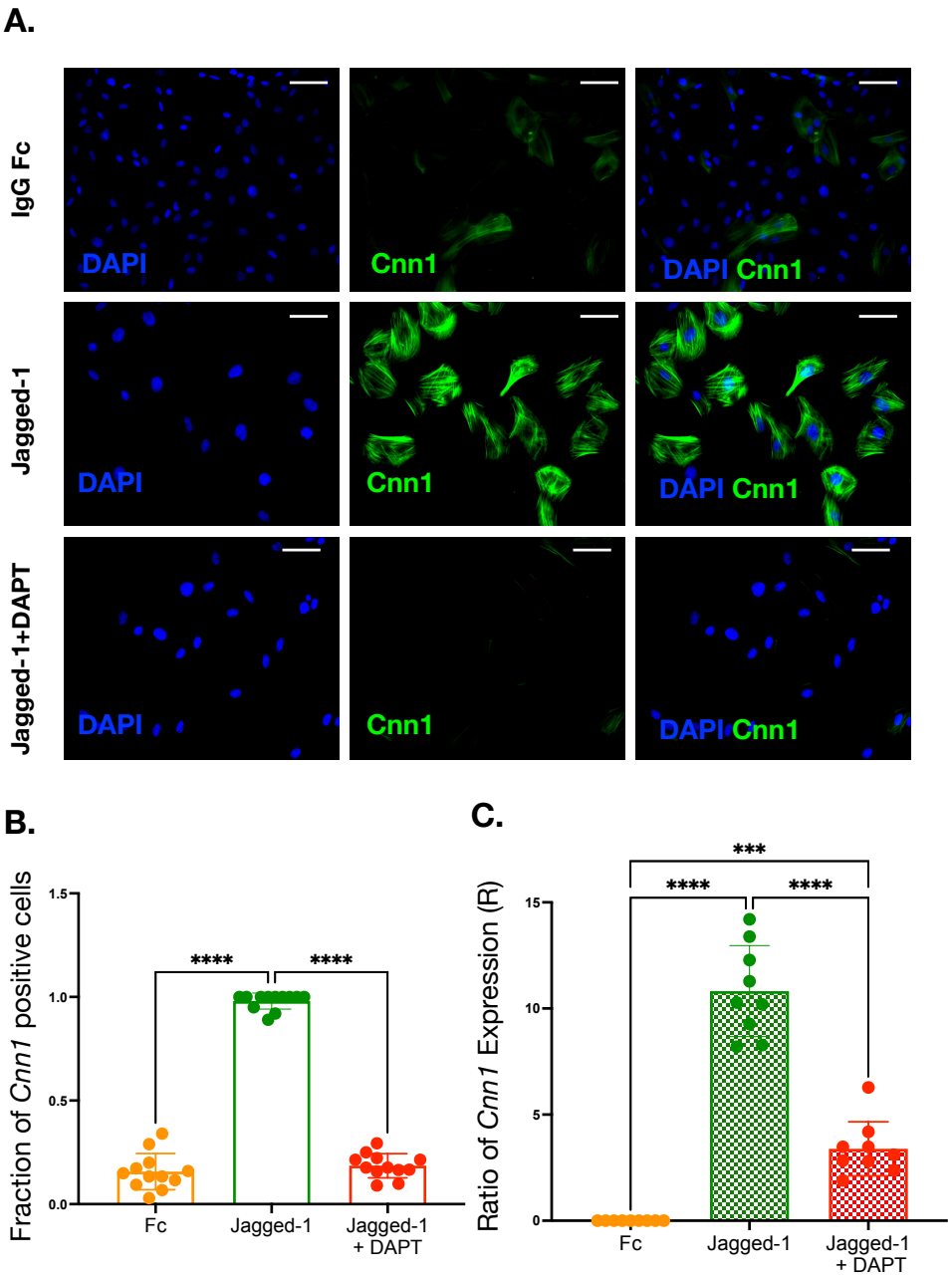

Figure 3.10 Jagged-1 stimulation of Notch-mediated myogenic (VSMC) differentiation of rMVSCs. (A) Representative images of fluorescence staining of DAPI nuclei and immunocytochemical analysis of endothelial marker Cnn1 expression in rMVSCs. (B) Fraction of $Cnn1^{+}$ cells after treatment. All images were taken using Olympus DP-50 fluorescent microscope. Alexa Fluor 488 secondary antibody used for visualisation of primary antibody binding. All images were taken using Olympus DP-50 fluorescent microscope. Alexa Fluor 488 secondary antibody used for visualisation of primary antibody binding. All images are representative of $n > 6$ images per experimental group from three independent cultures—scale bar representative of 50µm. (C) Relative levels of Cnn1 mRNA expression in rMVSCs following jagged-1 treatment. Data are expressed as the ratio of mRNA expression relative to control Fc and are the mean ± SEM, $n = 9$, * $p \leq 0.05$ versus Jagged-1 and * $p \leq 0.05$ Jagged-1 versus jagged-1 DAPT.

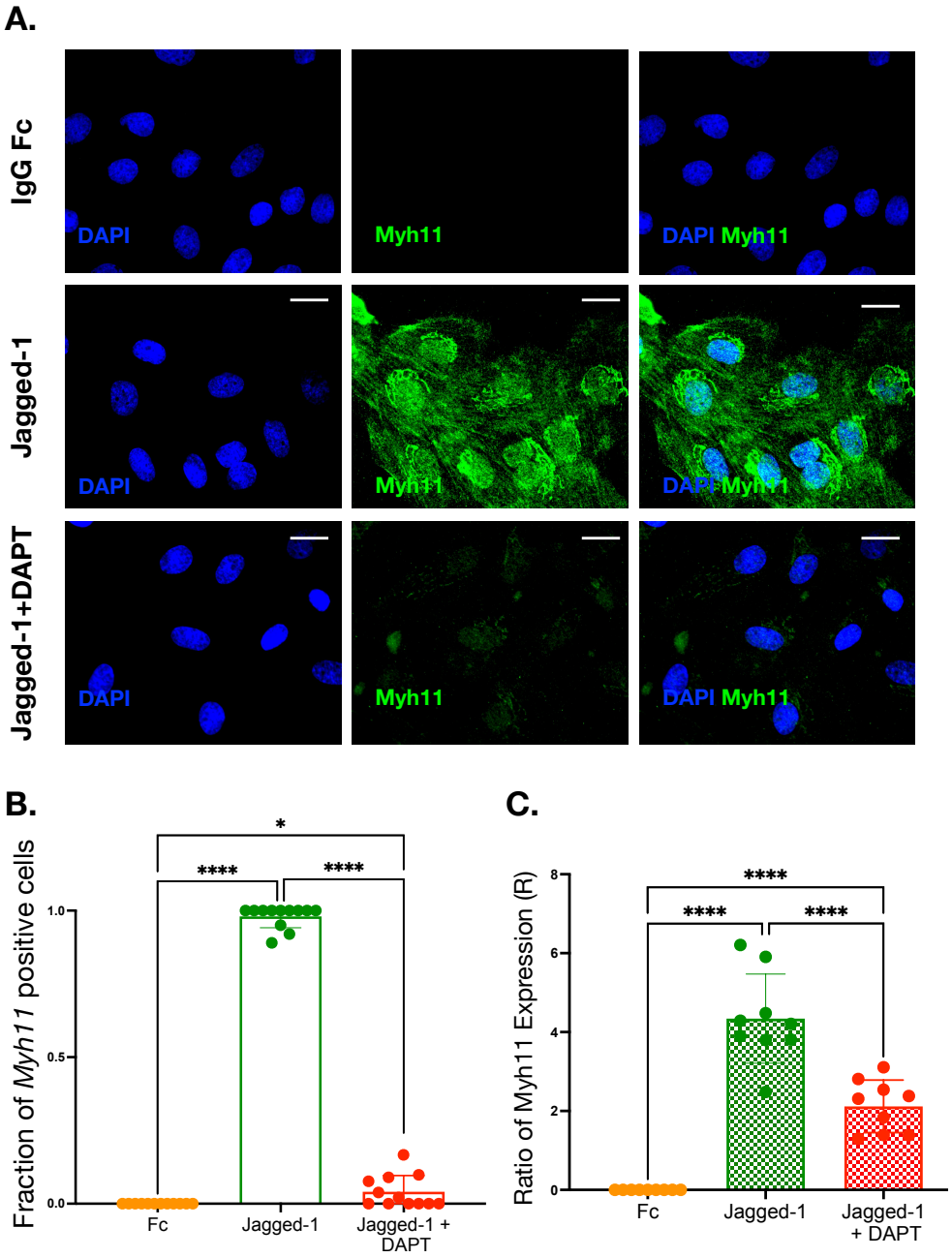

Figure 3.11 Jagged-1 stimulation of Notch-mediated myogenic (VSMC) differentiation of rMVSCs. (A) Representative images of fluorescence staining of DAPI nuclei and immunocytochemical analysis of the expression of endothelial marker Myh11 in rMVSCs. (B) Fraction of Cnn1^{+}cells after treatment. All images were taken using Olympus DP-50 fluorescent microscope. AlexaFluor 488 secondary antibody used for visualisation of primary antibody binding. All images were taken using Olympus DP-50 fluorescent microscope. AlexaFluor 488 secondary antibody used for visualisation of primary antibody binding. All images are representative of n ≥ 6 images per experimental group from three independent cultures—scale bar representative of 25µm. (C) Relative levels of *Myh11* mRNA expression in rMVSCs following jagged-1 treatment. Data are expressed as the ratio of mRNA expression relative to control Fc and are the mean ± SEM, n = 9, * $p \leq 0.05$ versus Jagged-1 and * $p \leq 0.05$ Jagged-1 versus jagged-1 DAPT.

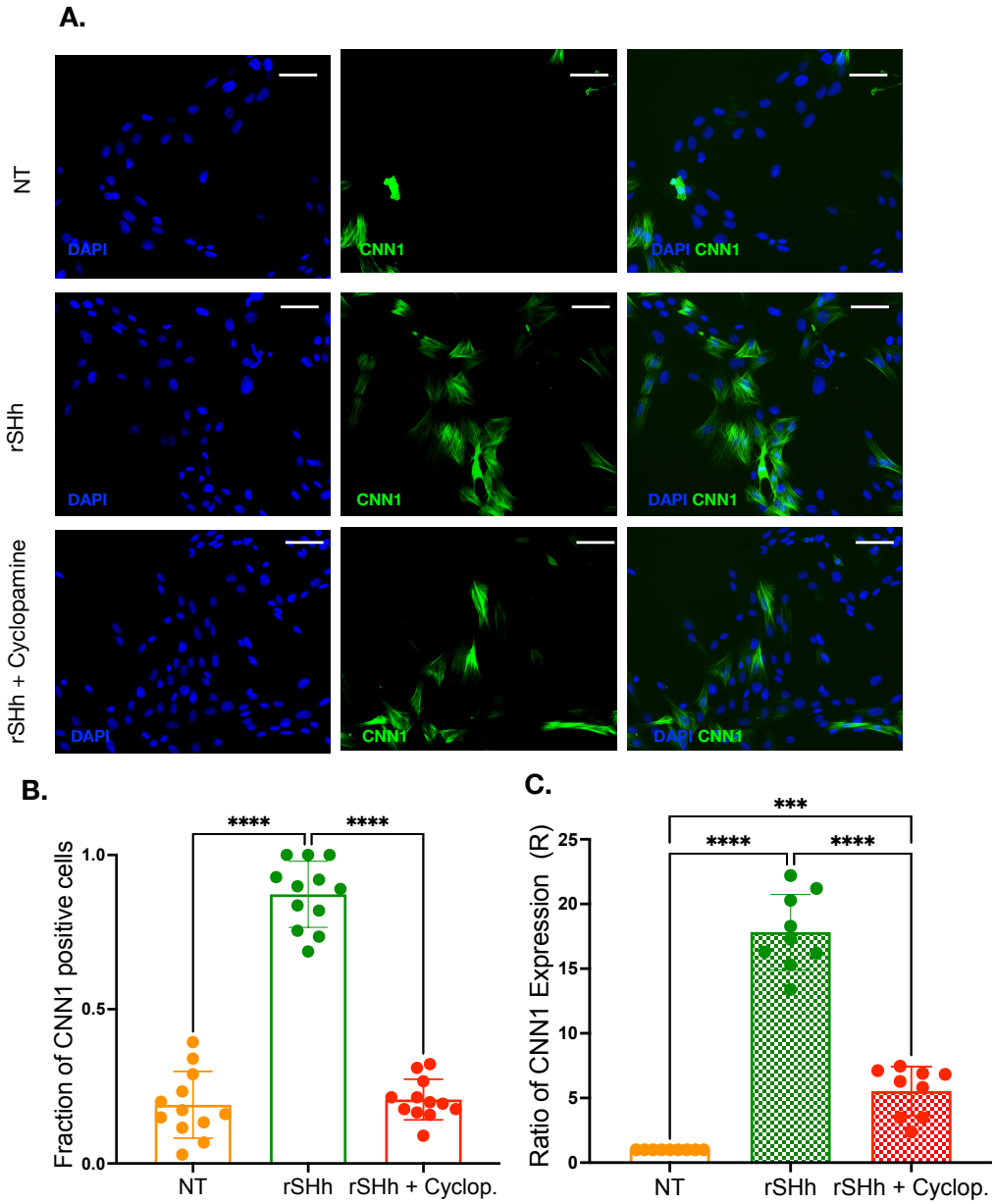

Figure 3.12 rSHh stimulation of Hh-mediated myogenic (VSMC) differentiation of rMVSCs. (A) Representative images of fluorescence staining of DAPI nuclei and immunocytochemical analysis of endothelial marker Cnn1 expression in rMVSCs. (B) Fraction of Cnn1^{+}cells after treatment. All images were taken using Olympus DP-50 fluorescent microscope. AlexaFluor 488 secondary antibody used for visualisation of primary antibody binding. All images were taken using Olympus DP-50 fluorescent microscope. AlexaFluor 488 secondary antibody used for visualisation of primary antibody binding. All images are representative of n ≥ 6 images per experimental group from three independent cultures—scale bar representative of 50µm. (C) Relative levels of *Cnn1* mRNA expression in rMVSCs following rSHh treatment. Data are expressed as the ratio of mRNA expression relative to control Fc and are the mean ± SEM, n = 9, * p ≤ 0.05 versus rSHh and * p ≤ 0.05 rSHh versus rSHh + cyclopamine.

3.3.7 EVs derived from hyperglycaemic RAECs do not activate Notch target genes

To determine a putative role for EVs harbouring Notch ligands in dictating the phenotypic changes in rMVSCs, the levels of Notch target genes were evaluated in rMVSC before and after treatment with EVs derived from normal and hyperglycemic RAECs for 48 h. In order to ensure the increase of Notch target genes is due to EVs derived for hyperglycemic conditions a panel of controls were ran in parallel which included; EVs derived from normal RAEC culture, EVs derived from mannitol treated RAEC culture as well as normal, glucose and mannitol conditioned media in the absence of cells.

Following RAEC culture, conditioned media was removed and EVs were isolated from normal mannitol and hyperglycemic RAECs and respected conditioned medias in the absence of cells. Isolated EVs were resuspended in rMVSC maintenance media (MM1) for further downstream applications. Cultured rMVSCs were seeded at a density of 200,000/well for 24 h at 37°C. Following removal of MM1 media, rMVSCs were treated with fresh MM1 media supplemented with EVs isolated from the three treatment groups. Changes in mRNA expression of the Notch target genes, *Hey1* and *Hey L* were evaluated using qRT-PCR after 48 hours. A significant increase in the ratio of *Hey1* was observed across all three EV treatment groups, NG-EV, HG-EV and MT-EVs in comparison to the their control groups. However, when comparing EV groups, a significant increase in *Hey1* expression was only observed when comparing NG-EVs and HG-EVs with no significant increase present in HG-EVs compared to MT-EVs (Figure 3.13 A). Similarly, a significant increase in the ratio of *HeyL* was observed across EV treatment groups, NG-EV, HG-EV in comparison the their control groups. However, there was a significant increase in *HeyL* expression in HG-EVs when compared to NG-EVs and the MT-EVs control (Figure 3.13 B).

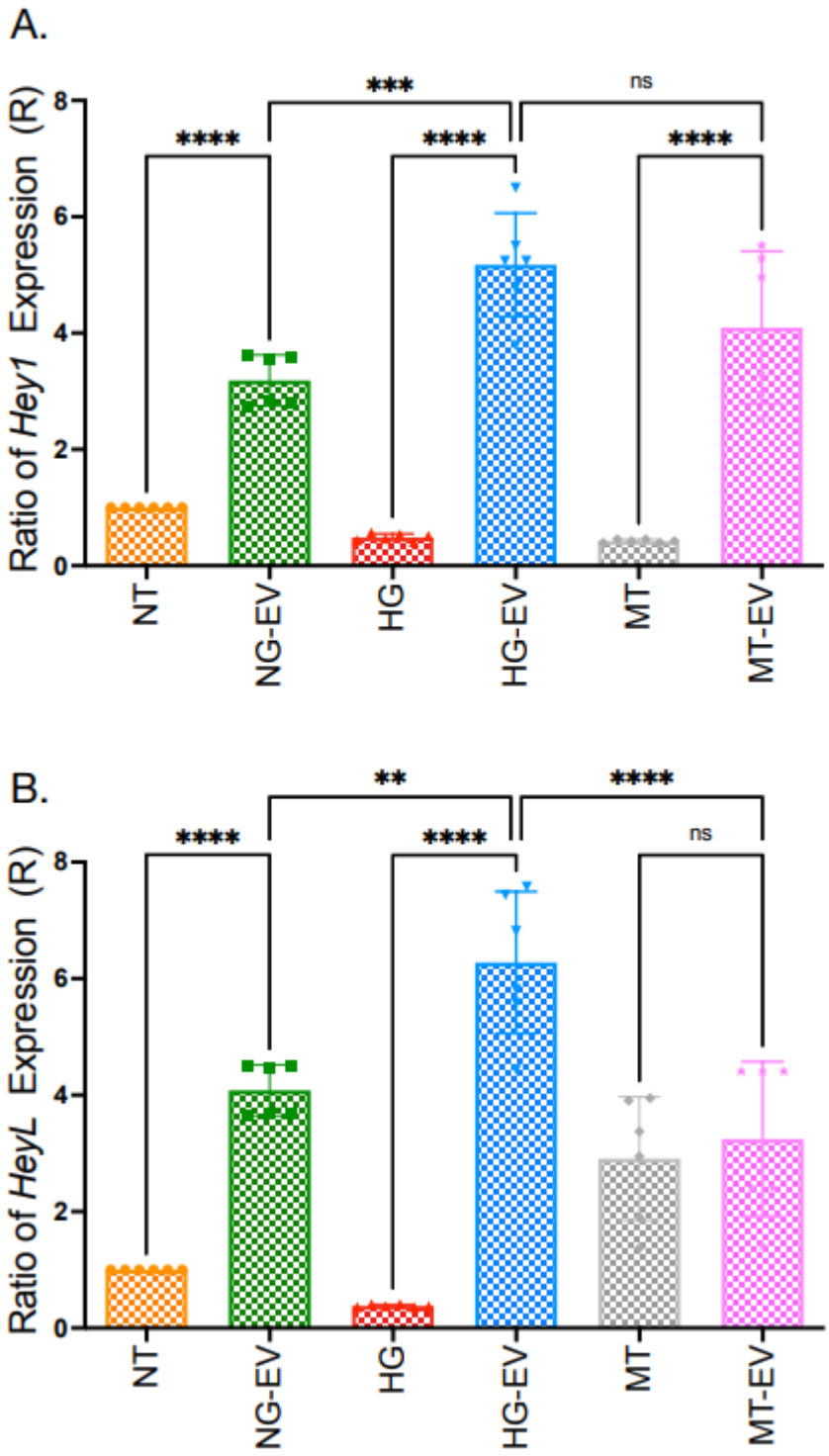

Figure 3.13 RAEC-derived HG-EVs do not activate Notch signalling in rMVSCs *in vitro*. Relative mRNA levels of Notch target genes *Hey1* (A) and *HeyL* (B) in rMVSCs. Data are expressed as the ratio of mRNA expression relative to control and are the mean ± SEM, n = 3,* $p \leq 0.05$ versus NG-EVs and * $p \leq 0.05$ versus MT-EVs.

3.3.8 EVs derived from hyperglycaemic RAECs activate Hh target genes

To determine a putative role for EVs harbouring Hh ligands in dictating the phenotypic changes in rMVSCs, the levels of Hh target genes were evaluated in rMVSC before and after treatment with EVs derived from normal and hyperglycemic RAECs for 48 h. In order to ensure the increase of Notch target genes is due to EVs derived for hyperglycemic conditions a panel of controls were ran in parallel which included; EVs derived from normal RAEC culture, EVs derived from mannitol treated RAEC culture as well as normal, glucose and mannitol conditioned media in the absence of cells.

Following RAEC culture, conditioned media was removed and EVs were isolated from normal mannitol and hyperglycemic RAECs and respected conditioned medias in the absence of cells. Isolated EVs were resuspended in rMVSC maintenance media (MM1) for further downstream applications. Cultured rMVSCs were seeded at a density of 200,000/well for 24 h at 37°C. Following removal of MM1 media, rMVSCs were treated with fresh MM1 media supplemented with EVs isolated from the three treatment groups. Changes in mRNA expression of the Hh target genes, *Gli1* and *Gli2* were evaluated using qRT-PCR after 48 hours. A significant increase in Hh target genes *Gli1* and *Gli2* was observed following rMVSC treatment with EVs derived from hyperglycemic RAEC cells in comparison to normal EV and mannitol EV controls (Figure 3.14 A,B).

In order to determine whether the activation of SHh signalling in rMVSCs is due to EVs-derived from hyperglycaemic cells, the expression of SHh was measured in RAEC exposed to hyperglycemic conditions in comparison to RAECs from normal and mannitol conditioning. A significant increase in SHh mRNA expression was observed in RAECs exposed to hyperglycemic conditions (Figure 3.15). Although RAECs exposed to hyperglycemic conditions have an increased expression of SHh, Hh signalling is activated in effector cells if the ligand is successfully bound to its receptor, Ptch1 resulting in phosphorylation and activation of Smo. For this reason, we measured the levels of SMO gene expression in RMVSCs following RAEC-derived EV treatments. A significant increase in *Smo* was observed in rMVSCs treated with EVs derived from RAECs exposed to hyperglycemic conditions (Figure 3.16

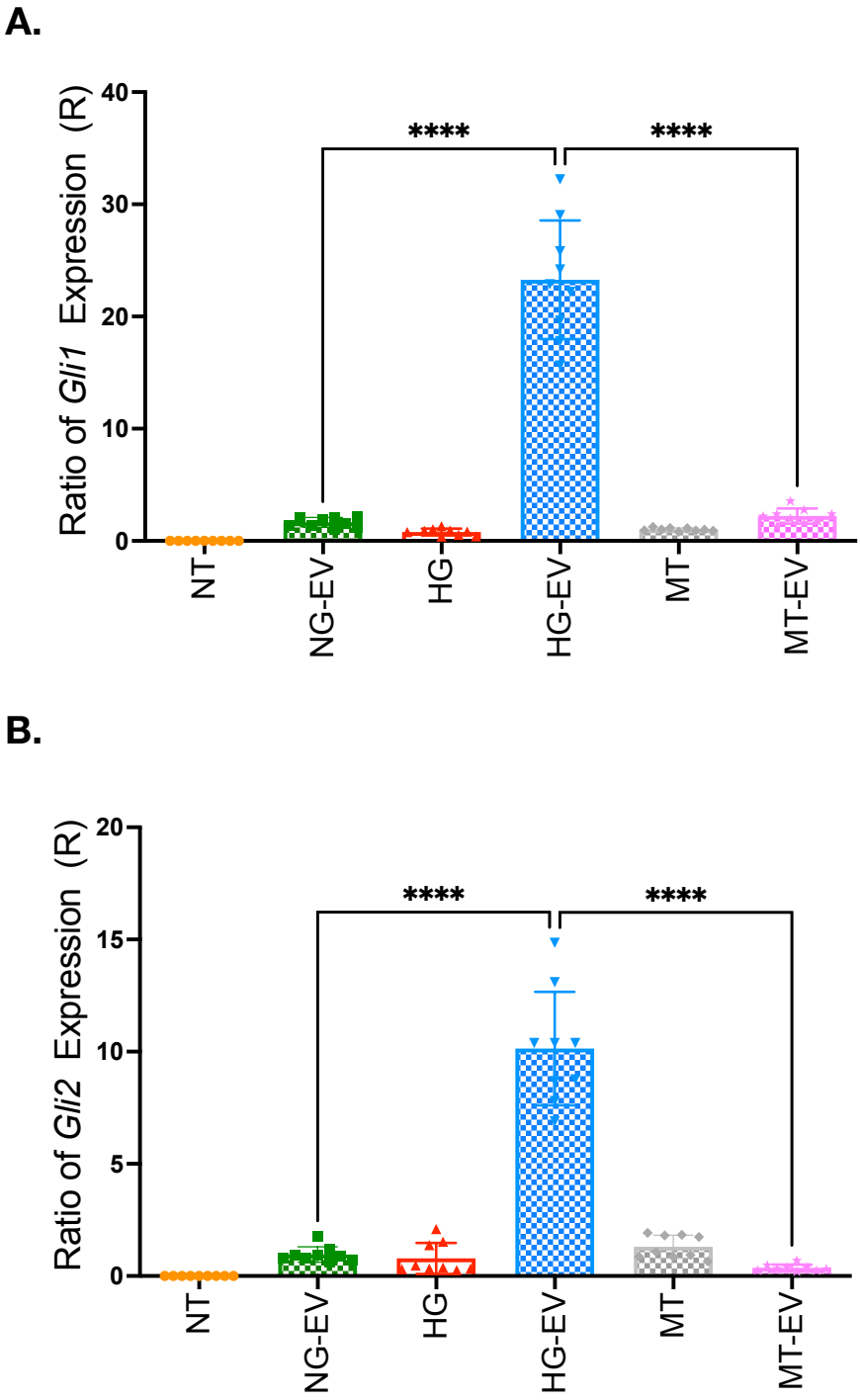

Figure 3.14 RAEC-derived HG-EVs activate Hedgehog signalling in rMVSCs *in vitro*. Relative mRNA levels of Hh target genes *Gli1* (A) and *Gli2* (B) in rMVSCs. Data are expressed as the ratio of mRNA expression relative to control and are the mean ± SEM, n = 3,* $p \leq 0.05$ versus NG-EVs and * $p \leq 0.05$ versus MT-EVs.

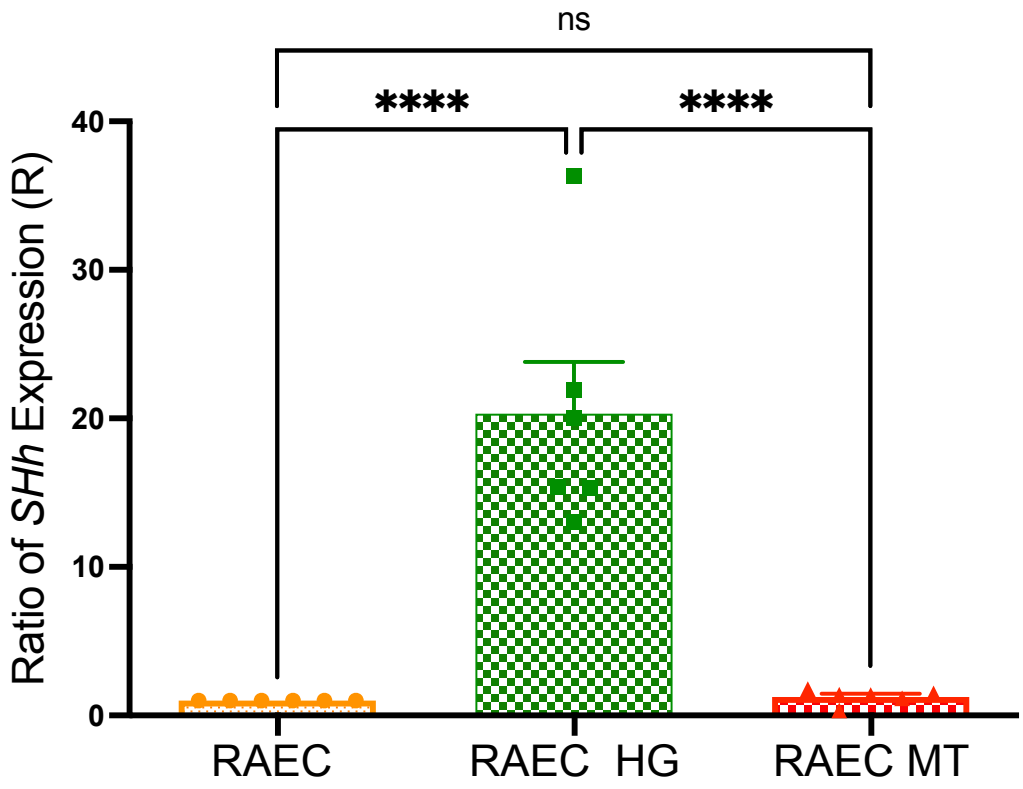

Figure 3.15. Effect of HG on *SHh* expression in RAECs. The relative expression of *SHh* mRNA levels by qRT-PCR in RAECs exposed to hyperglycemic conditions for 48 hours. Data are expressed as the ratio of mRNA expression relative to control and are the mean ± SEM, n = 6,* $p \leq 0.05$ versus RAEC and * $p \leq 0.05$ versus RAEC-MT.

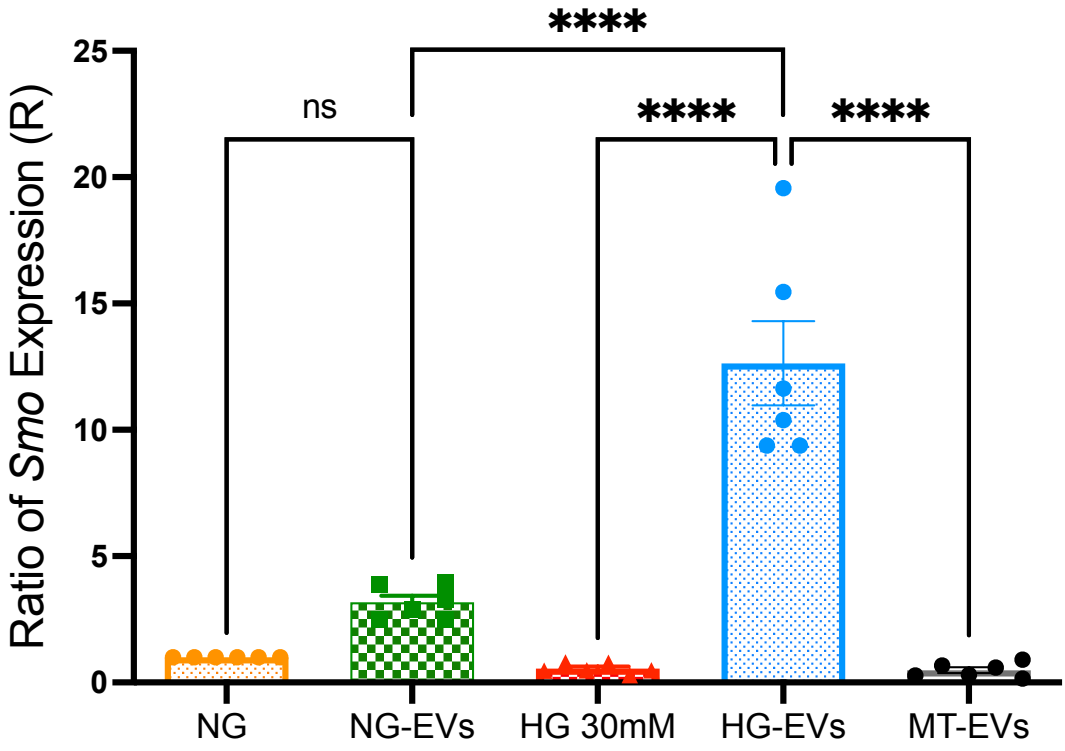

Figure 3.16. Effect of RAEC-derived NG, HG and MT-EVs on *Smo* expression in rMVSCs. The relative expression of *Smo* mRNA levels by qRT-PCR in rMVSCs exposed to RAEC-derived NG-EVs, HG-EVs and MT-EVs for 48 hours. Data are expressed as the ratio of mRNA expression relative to control and are the mean ± SEM, n = 6,* $p \leq 0.05$ versus HG, ,* $p \leq 0.05$ versus NG-EVs and * $p \leq 0.05$ versus MT-EVs.

3.5 Summary

- Cultured RAEC display distinct endothelial cobblestone morphology in culture. ICC and transcriptional analysis confirmed the expression of endothelial-associated markers/genes CD31 and eNOS.
- Healthy and dysfunctional hyperglycaemic RAECs secrete EVs *in vitro*. Nano FACS analysis using CFSE staining confirmed the presence of a discrete EV population following isolation using the ExoQuick TC commercial precipitant. NTA analysis revealed a distinct difference in the size and number of EV particles secreted from healthy and dysfunctional hyperglycaemic RAECs.
- Resident multipotent vascular stem cells (rMVSCs) isolated from rat aortic explants express NE stem cell markers - Sox10, Sox17, Sca1 and S100β.
- Rat MVSCs are multipotent capable of differentiating down a vasculogenic and myogenic lineage following exposure to vasculogenic (endothelial media) and myogenic stimuli (Jagged-1).
- RAEC exposure to hyperglycaemic conditions increased SHh expression in comparison to RAECs in normal and mannitol culture conditions.
- EVs derived from RAEC conditioned media under hyperglycaemic conditions (HG-EVs) promoted Hh target gene (*Gli1* and *2*) and *Smo* expression in resident rMVSCs when compared EVs from cells grown under normal glucose conditions (NG) or with mannitol (MT). Moreover, this effect was not mimicked by non-conditioned media supplemented with NG, HG or MT.

3.6 Discussion

Vascular complications resulting from diabetes account for a substantial proportion of morbidity and mortality in diabetic patients. Although diabetes is considered a driver of many complications' atherosclerosis is regarded as the leading cause of death amongst diabetic patients. A hallmark of atherosclerosis is the formation of fibrous neointima (Fishbein and Fishbein, 2009). The occurrence of intimal medial thickening (IMT) has become one of the significant challenges for CVD treatment as routine procedures such as stenting, balloon angioplasty and vein-graft bypass often lead to further vascular injury and emergence of arteriosclerotic lesions (Haery, Sachar and Ellis, 2004). Therefore, the discovery of early diagnostic biomarkers for the detection of sub-clinical atherosclerosis is clearly an unmet clinical need. To facilitate this, further research is required to greater understand the role of cell-cell communication as the primary orchestrator of neointimal VSMC-like cell accumulation leading to intimal thickening and neointima formation.

Initially considered as cellular waste, EVs have recently emerged as a critical player in cellular communication. The composition of EVs can play an important role in vascular homeostasis and pathological processes such as angiogenesis, inflammation, and senescence (Fujita *et al.*, 2015; Andrews and Rizzo, 2016; Takasugi, 2018). Recent studies have reported a notable increase in EC-EV secretion in response to circulating CVD risk factors (Heiss *et al.*, 2008; Gordon *et al.*, 2011; Liu *et al.*, 2014, 2017). One such risk factor of interest in this study is the role of EVs secreted from EC exposure to hyperglycemic conditions. Prolonged exposure to hyperglycemia is widely recognised as one of the main factors in the pathogenesis of diabetic complications (Grundy *et al.*, 1999; Laakso, 1999). Hyperglycaemia induces an increase in oxidative stress by producing intracellular ROS resulting in endothelial dysfunction and accelerated atherosclerosis. Various studies have reported deleterious effects of the endothelium in response to hyperglycaemic conditions, including reduced NO production (Ding *et al.*, 2000; Du *et al.*, 2001), enhanced NF-κB activation (Hamuro *et al.*, 2002), an increase in EC apoptosis (Sheu *et al.*, 2005; Su *et al.*, 2018). This response has also been shown for EVs secreted from ECs when exposed to hyperglycemic conditions. Using *in vitro* cell culture models' studies have shown that EC exposure to hyperglycemic conditions effectively enhances EC-EV generation and secretion (Burger *et al.*, 2017). Furthermore, differences in both protein and RNA content of EVs secreted from ECs in response to cellular stress stimuli

including hypoxic and hyperglycemic conditions (de Jong *et al.*, 2012). Proteomic analysis of EC-EVs derived from normal and hyperglycemic conditions have identified differential expression of proteins highlighting differences in vesicular cargo in response to pathologic stimuli. Similarly, EC-derived EVs cultured under high glucose conditions induced endothelial dysfunction, vascular inflammation and prompted atherosclerosis *in vivo* (Burger *et al.*, 2017). Although the aforementioned studies have reported differences in the profile of EVs derived from hyperglycemic conditioning the use of *in vitro* hyperglycemic modelling generally involves treatments of cells with supra-physiological doses of glucose (30mmol and above) which does not mimic hyperglycemic conditions *in vivo*. Therefore, changes in vesicular cargo harvested from *in vitro* hyperglycemic cell culture models may not be clinically relevant.

The first aim of this study was to develop a reliable *in vitro* cell culture murine model to evaluate the secretion of EC-derived EVs under normal and hyperglycaemic conditions and determine differences in their functionality. The use of cell culture conditioned media enables a controlled environment for EV secretion and isolation. RAECs in culture were characterised by their expression of associated endothelial markers CD31, and eNOS. In order to investigate changes in RAEC secretion of EVs, RAECs were exposed to normal, hyperglycemic and mannitol conditions for 48 h. Upon exposure to hyperglycemic conditioning RAECs become dysfunctional demonstrated by an increase in the expression of Annexin V (Appendix A). Although many EV isolation techniques exist, including ultracentrifugation, the use of density gradients, sequential filtration, size exclusion chromatography and immunoaffinity techniques (Brennan *et al.*, 2020), commercially available precipitation technique, ExoQuick TC™ was used to purify EVs utilizing a decrease in the solubility of compounds in the solutions of super hydrophilic polymers. ExoQuick TC™ EV isolation was chosen as it is less time consuming than alternative methods, with isolated EVs produced in less than 24 hours, requires less labour due to the use of proprietary polymer and overnight incubation as opposed to lengthily ultracentrifugation and chromatography methods and was appropriate for starting experimental volumes and downstream applications. Although many studies have reported isolation of functional EVs using ExoQuick TC™ (Kong *et al.*, 2018; Leszczynska *et al.*, 2018; Naseri *et al.*, 2018; Brenner, Su and Momen-Heravi, 2019; Ono *et al.*, 2019; Wang *et al.*, 2019; Youn *et al.*, 2019) several disadvantages have been

reported including contamination of isolated EV fractions with proteins, protein complexes and lipoproteins (Van Deun *et al.*, 2014; Lobb *et al.*, 2015). Therefore extensive verification and characterisation of EVs was carried out to validate the isolation of EVs from RAECs *in vitro*.

The concentration of isolated EV from hyperglycemic and normal RAEC culture was initially assessed using NTA, the most widely used quantitative method for EV analysis (Gardiner *et al.*, 2016). An increase in particle count was detected in RAEC-derived EVs exposed to hyperglycemic conditions in comparison to EVs derived from normal and mannitol conditioning. In addition to particle count NTA was used to determine the size of isolated EVs. The various methods of sizing EVs have been compared in recent studies and often report differences in average size values (Van Der Pol *et al.*, 2010; van der Pol *et al.*, 2014; Varga *et al.*, 2014). EVs derived from RAECs exposed to normal conditions were approx. 161nm in comparison to a more heterogenous population of EVs derived from hyperglycemia conditions with distinct peaks at 137nm and 203nm.

Labelling fluorescent techniques and FACs analysis have previously been used to detect EVs (Morales-Kastresana *et al.*, 2017; Monopoli *et al.*, 2018; Ender *et al.*, 2020). The use of standard FACs analysis for EV detection requires extensive EV sample preparation including initial NTA characterisation to determine the number of particles, antibody staining or EV-binding to appropriate beads that are large enough to be reliably resolved on the flow cytometer (Koga *et al.*, 2005). To overcome these challenges CFSE-stained RAEC EVs derived from normal and hyperglycemic conditions along with appropriate experimental controls including buffer only, CFSE-only, CFSE-EVs and CFSE-EVs-Triton X-100 were detected using the Amnis™ CellStream ® Flow Cytometer, which enables high-throughput flow cytometry with increased sensitivity for detecting small particles. EVs-derived from normal and hyperglycemic conditions demonstrated positive expression of CFSE, which was depleted following Triton X-100 treatment of EV-$CFSE^{+}$ samples confirming detection of EVs through lysis of the vesicular membrane (Osteikoetxea *et al.*, 2015).

The diagnostic and therapeutic value of EVs lies in their capacity to deliver their cargo to various target cells and tissues in the body (Revenfeld *et al.*, 2014). The effects of EVs in CVD are pathogenesis are complex and depend on many variables such as their origin,

intervascular content, and target cell. While the release of EC-derived EVs has been shown to be upregulated during pathogenesis of CVD the effect of their uptake in resident vascular cells is not well understood. Previous studies have shown a role EC-derived EVs in cell-cell communication between neighbouring ECs, pericytes and vSMCs (Buzas *et al.*, 2014; Robbins and Morelli, 2014; Yamamoto *et al.*, 2015; Robbins, Dorronsoro and Booker, 2016) however, little is known about the role of EC-derived EV and resident vSCs. Resident vascular stem cells have been repeatedly shown to migrate to the site of injury in the arterial wall and differentiate to become SMC-like cells (Tang, Wang, Yuan, *et al.*, 2012; KRamann *et al.*, 2016; Di Luca *et al.*, 2021). The presence of resident vascular stem cells within the arterial layers has been well established (Sartore *et al.*, 2001; Tintut *et al.*, 2003; Sainz *et al.*, 2006). Recent studies suggest that S100β cells are present in adaptive lesions following vascular injury in S100β-eGFP transgenic mice accompanied by a significant increase in intimal thickness (Di Luca *et al.*, 2021). Moreover, genetic lineage tracing analysis of marked perivascular S100β-tdTomato cells revealed that many neointimal cells originate from a resident S100β perivascular non-VSMC parent population following flow restriction (Luca *et al.*, 2018; Di Luca *et al.*, 2021). Cell fate mapping studies have been extensively utilized to address the origin of neointimal VSMCs. However, concerns have persisted regarding the lack of relevant negative controls and the possibility that the tamoxifen can remain in the tissue and still be labelling cells for at least four weeks post-treatment (Reinert *et al.*, 2012). Lineage tracing studies in vascular injury murine models set up within our research group have mitigated against this issue by introducing a 4 week washout period prior to injury. In these studies, $S100\beta^{+}$ cells were indelibly marked with tdTomato red fluorescence protein using S100β-Cre-LoxP- tdTomato red transgenic mice prior to the 4 week washout period and revealed a significant accumulation of $tdTomato^{+}$ cells in the neointimal following vessel injury (Di Luca *et al.*, 2021). This data provided justification for the use of $S100\beta^{+}$ resident vascular stem cells as a reporter cell line for examining the effects of RAEC-derived EVs following exposure to hyperglycemic conditions.

Using ICC, isolated rMVSCs showed an abundance of stem cell marker expression including S100β, Nestin, Sox10, Sox17, and Sca1 (Tang, Wang, Yuan, *et al.*, 2012; Kennedy, Hakimjavadi, *et al.*, 2014). The expression of Sca1 has previously been reported to be upregulated in SMC phenotypic switching (Dobnikar *et al.*, 2018) and a number of stem cell populations have also been reported to express Sca1 (Torsney, Hu

and Xu, 2005; Sainz *et al.*, 2006; Tang *et al.*, 2020). However, the media in which resident stem cells are maintained may have an effect on their expression of Sca1 as previous studies using isolated MVSCs reported that the cells were Sca1^{-} when grown in DMEM with 10% FBS as opposed to MM1 (Tang, Wang, Yuan, *et al.*, 2012). As the primary cell of the medial layer is a differentiated VSMC population, parallel immunocytochemical analysis of the expression of intermediate VSMC markers, Cnn1, and terminal differentiation marker Myh11 was performed by ICC. Isolated MVSCs showed no expression of either protein suggesting that these cells are unlikely to be VSMCs. This is further supported by previous studies in our lab that demonstrated the epigenetic profile of murine MVSCs is enriched for stem cell-specific tri-methylation of lysine 27 on histone H3 (H3K27me3) but not enriched for the VSMC-specific epigenetic signature of di-methylation of lysine 4 on histone H3 (H3K4me2) at the Myh11 locus. As epigenetic signatures are retained following phenotypic switching (Gomez, Swiatlowska and Owens, 2015), the lack of enrichment of H3K4me2 at the Myh11 locus suggests the MVSCs are not derived form a medial VSMC (Di Luca *et al.*, 2021).

Multipotency has been defined as a critical hallmark identified in medial vascular stem cells. Recent studies have reported the multipotent potential of MVSCs to differentiate down various lineages such as adipogenic and osteogenic (Tang, Wang, Yuan, *et al.*, 2012; Kennedy, Hakimjavadi, *et al.*, 2014; Di Luca *et al.*, 2021). To investigate the multipotent potential of isolated rMVSCs, cells were treated with vasculogenic inductive media to stimulate endothelial differentiation. Following a 14 day treatment, rMVSCs undergo vasculogenic differentiation characterised by increased expression of endothelial genes, *Cd31* and *eNOS.* Further interrogation of protein expression by immunocytochemical analysis revealed an increase in eNOS protein expression and decreased VSMC early differentiation marker Cnn1. Furthermore, activation of the Notch receptor by the Notch ligand, Jagged-1 and the patched receptor with SHh both promoted myogenic differentiation *in vitro* with increased levels of VSMC markers Cnn1 and Myh11 observed. The ability of isolated rMVSCs to respond to both vasculogenic and myogenic stimuli underscores their multipotency capacity. These data indicate that MVSCs pose high levels of multipotency to differentiate down vasculogenic, myogenic, adipogenic, and osteogenic pathways offering a potential explanation for the complexity of cellular phenotypes residing in disease vessels (Tang, Wang, Yuan, *et al.*, 2012; Kennedy, Hakimjavadi, *et al.*, 2014; Di Luca *et al.*, 2021)

The mechanisms by which resident vascular stem cells undergo differentiation into mature VSMC are not yet fully understood. Interestingly, a number of different signalling pathways have been reported to play a role in VSMC differentiation including; TGF-β/PDGF signalling (Hao, Gabbiani and Bochaton-Piallat, 2003; Xie *et al.*, 2011; Cheung *et al.*, 2014; G. Wang *et al.*, 2015), Wnt/β-catenin signalling (Ezan *et al.*, 2004; Hooper *et al.*, 2012) as well as and two pathways investigated in this study Hh and Notch signalling (Hooper and Scott, 2005; Morrow, Scheller, *et al.*, 2005; High *et al.*, 2007; Morrow *et al.*, 2009; Shin, Nagai and Sheng, 2009; Di Luca *et al.*, 2021). To date the role of the Notch receptor in regulation of both embryonic and adult stem cell fate has been extensively reported (Guruharsha, Kankel and Artavanis-Tsakonas, 2012). Of interest, the Notch signalling pathway has been report to promote proliferation of SCs in response to vascular injury as well as activation of myogenic differentiation (Morrow, Sweeney, *et al.*, 2005; Kurpinski *et al.*, 2010). Similarly Hh signalling has also been shown to play a pivotal role in maintenance of adult progenitor/stem cells, tissue repair and atherosclerosis (Dutzmann, Koch, Weisheit, Sonnenschein, Korte, Haertlé, Thum, Bauersachs, Sedding and J. M. Daniel, 2017; Aravani *et al.*, 2019; Di Luca *et al.*, 2021)

Previous studies have highlighted the role of SHh in atherosclerosis through increased lipid uptake by macrophages. Our research group, along with others, has shown a putative role for SHh signalling in the control of 'de-differentiation VSMC growth in cultured cells *in vitro* and neointimal formation *in vivo* (Morrow *et al.*, 2007; Polizio *et al.*, 2011; Redmond *et al.*, 2013). Therefore, having previously shown upregulation of Hh and Notch signalling using recombinant proteins in MVSCs the next objective of this study was to investigate if activation of the Notch and Hh signalling pathway in MVSCs could be facilitated by RAEC-derived EVs from hyperglycemic cells.

Canonical Notch signalling occurs through *trans* activation whereby a ligand, Jagged-1 or Delta-like ligand (DLL)-1,-3 and -4, located on neighbouring cell binds to the Notch receptor requiring direct cell-cell contact (Bray, 2006). Although non-canonical modes of Notch signalling have not been thoroughly researched (D'Souza, Meloty-Kapella and Weinmaster, 2010; Andersen *et al.*, 2012) the role of EV-mediated transport of Notch ligands has recently been highlighted enabling the activation of Notch signalling not only in cells in direct contact but also cells and tissues further afield (Simons and Raposo,

2009). To date the detection of EV bound Notch ligands Dll4 and Jagged-1 have been reported. In 2010, Sheldon et al. were the first to report that Dll4, a Notch ligand shown to play a role in pathogenesis of atherosclerosis, (Guruharsha, Kankel and Artavanis-Tsakonas, 2012), naturally secreted in EVs from human umbilical vein endothelial cells *in vitro*. Furthermore they demonstrate Dll4+ EVs can transfer Dll4 from one cell to another where it can be incorporated into the plasma membrane of recipient cells both *in vitro* and *in vivo* (Sheldon *et al.*, 2010). Subsequent studies have identified the presence of Jagged-1 in EVs from human cancer cell lines (Beckler *et al.*, 2013; Liang *et al.*, 2013; Lazar *et al.*, 2015; Tan, Asada and Ge, 2018). However, the detection of Notch signalling components in EVs or the role of EVs-mediated transport of Notch signalling components has not been addressed in resident vascular cells.

RAEC-derived EVs were isolated from normal, hyperglycemic and mannitol conditioned media followed by subsequent incubation with rMVSCs in culture for 48 hours to determine the effect of RAEC-derived EVs on Notch signalling. A significant increase in *Hey 1* and *Hey L* mRNA levels was shown in rMVSCs treated with RAEC-derived EVs from normal and hyperglycemic conditions in comparison to their relevant controls. Although the direct treatment of rMVSCs with RAEC-derived NG, HG and MT-EVs resulted in an increase in Notch target gene expression, the levels of *Hey 1* and *HeyL* mRNA in HG-EV treated rMVSCs were higher than their NG-EV counterparts. However since the level of *Hey1* expression following treatment of rMVSCs with HG-EVs was similar to the level with MT-EVs, the increased levels may be due to osmotic changes. Moreover, further analysis using the Notch signalling inhibitor DAPT should be included to ensure the increase in Notch target gene expression is ligand dependant. Alternatively, overexpression of Notch1 in RAECs or knockdown using siRNAs could be employed to control the levels of Notch transported by EVs to MVSCs. Additionally, proteomic analysis of RAEC-derived EVs would provide an insight into the expression profile of Notch ligands and/or receptors determining if differences exist in response to pathologic stimuli.

Paracrine signalling, in which a ligand is released from its site of production into the extracellular environment plays an instructive role in pathological conditions. Hh, a secreted morphogen acts in a paracrine manner activating signalling in recipient cells by binding to its receptor Ptch. The mechanism by which morphogens are secreted into the

extracellular space has been extensively investigated and a number of different processes have been described including the secretion of unmodified Hh and the release of Hh via lipoproteins (Panáková *et al.*, 2005; Eugster *et al.*, 2007; Dierker, Dreler, *et al.*, 2009; Palm *et al.*, 2013). Extensive research has been carried out to determine to role of EV-mediated Hh in Drosophila (Callejo *et al.*, 2011; Bischoff *et al.*, 2013; Sanders, Llagostera and Barna, 2013; Kornberg and Roy, 2014), however little is known about the secretion of Hh, particularly EV-mediated Hh in vertebrates.

In order to address this, RAEC-derived EVs exposed to hyperglycemic conditions were isolated from normal, hyperglycemic and mannitol conditioned media followed by subsequent incubation with rMVSCs in culture for 48 hours. The treatment of rMVSCs with RAEC-derived EVs was normalised based on conditioned media volumes. A significant increase in *Gli1* and *Gli2* was demonstrated between rMVSC treated with RAEC-derived EVs from normal conditions versus RAEC-derived EVs from hyperglycemic conditions suggesting that RAEC EVs secreted under hyperglycemic conditions may have a higher level of Hh morphogen tethered to their membrane. Although it is easy to surmise that the increase in Hh target gene expression is specifically due to the generation of SHh^{+} EVs upon exposure to hyperglycemic conditioning, one trivial reason for this increase may be the direct effect of a higher concentration of EVs in the HG-EV group as the experiments were normalised to volume of conditioned media as opposed to normalisation of EV particles. In order to prove the increase in Hh target genes is ligand specific, acute knockdown of Hh in RAECs using siRNA knockdown prior to RAEC-EV generation is required. Alternatively, prior treatment of rMVSCs with a Hh signalling inhibitor such as cyclopamine before the addition of RAEC-derived EVs would be favourable. Although an increase in Hh target gene expression was demonstrated in rMVSCs treated with RAEC-derived HG-EVs, it is important to note the possibility of the isolation of Hh independent of EVs as a contaminant during the isolation process. To rule out the possibility of Hh protein precipitation during isolation of EVs RAEC complete media spiked with recombinant Hh was collected and processed through the EV isolation protocol. Subsequent treatment of Hh spiked RAEC media with rMVSCs showed no increase in Hh target genes *Gli 1* and *Gli 2* (data not shown). Therefore the isolation of Hh aggregates as a contaminant during EV isolation is unlikely. It is however important to highlight the a further limitation regarding ExoQuick precipitation of growth factors and cytokines although the aforementioned experiment has shown precipitation

of SHh independently is unlikely cation needs to be taken when assigning activities specifically to EVs as the co-isolation of growth factors and cytokines may trigger activation of Hh signalling.

Although vertebrates express three Hh genes, SHh signalling has been reported to induce vSMC proliferation (Li *et al.*, 2010) and as well as myogenic differentiation of murine and HiPSC-derived SCs *in vitro* (Di Luca *et al.*, 2021). A significant increase in SHh gene expression in RAEC exposed to hyperglycemic conditions was demonstrated which most likely results in a greater percentage of EV-SHh^{+} secretion. Hh signalling is activated by binding to its receptor Ptch resulting in the phosphorylation of Smo and subsequent activation of Hh target gene (Mooney *et al.*, 2015). For this reason the expression of Smo was measured in rMVSCs following exposure to RAEC-derived normal, hyperglycemic and mannitol EVs and a significant increase in Smo was demonstrated. This along with previous data presented provides supportive evidence of EV-mediated activation of Hh signalling in resident vascular stem cells.

In conclusion, the development of a murine cell culture model *in vitro* was validated to investigate the role of RAEC-derived EVs on a population of resident vascular stem cells previously shown to play a role in lesion formation (Di Luca *et al.*, 2021). Using this model it was shown that (i) RAECs exposed to hyperglycemic conditions undergo endothelial dysfunction *in vitro* mimicking diabetic environments *in vivo* (ii) induction of RAEC dysfunction results in an increase in the secretion of EVs that differ in size compared to normal EC culture conditions (iii) the pathological repercussions of this change in RAEC EV properties when exposed to hyperglycaemia was shown by an increase in Hh signalling in resident vascular stem cells which highlights the role for EV secretion and transport of Hh morphogen and subsequent activation of Hh target genes during the onset of sub-clinical atherosclerosis.

Chapter 4:

Endothelial cell-derived EVs induce SHh-dependent myogenic differentiation of human iPSC-derived S100β^{+} stem/progenitor cells in response to hyperglycaemic conditions *in vitro*

4.1 Introduction

Recent advances in molecular biology and personalised medicine have significantly broadened our understanding of the biological components of various diseases such as cancers, immunological disorders, and CVD. Animal models remain vital to improve our understanding of fundamental mechanisms involved in the development and progression of CVD and facilitate improved methods for the detection and treatment of disease. However, these discoveries more often than not do not seamlessly translate from animal to human models due to various factors such as disparities in vessel size and make-up, species-specific metabolic and biochemical activities, and most importantly, various chromosomal and genomic differences (Barré-Sinoussi and Montagutelli, 2015).

The discovery of HiPSCs in 2007 by Prof. Yamanaka has enabled a new realm of ethics-free, patient-specific *in vitro* models of disease (Takahashi *et al.*, 2007). This discovery was the first of its kind, reverting a terminally differentiated cell into a pluripotent state without the need for a complex mechanism such as somatic cell nuclear transfer or cellular fusion. Since this, HiPSC-based systems generated by direct reprogramming of patient-derived somatic cells such a fibroblasts and skin cells have emerged as a critical model for investigating disease pathophysiology (Soldner and Jaenisch, 2012; Liang and Du, 2014; Kim, 2015).

Atherosclerosis is considered a chronic inflammatory disease of the arterial blood vessel wall and the most common pathophysiologic process underlying CVD (Bennett, Sinha and Owens, 2016). Like many such processes, atherosclerosis exists along a continuum from subclinical atherosclerosis to clinical atherosclerotic vascular disease. Subclinical atherosclerosis underlies most cardiovascular events, and its detection can greatly improve risk stratification (Singh *et al.*, 2018). The importance of the early neointima in subclinical atherosclerosis as fertile soil for plaque development cannot be overemphasized (Schwartz, DeBlois and O'Brien, 1995). A thickened intimal layer, observed in 30% of new-born children, is a fundamental structural difference that separates human arteries from other animals. The intima is primarily defined as a single layer of ECs separated from the underlying media by a relatively thin layer membrane. This earliest intimal layer is exposed to various blood borne components such as elevated

levels of glucose and positive hemodynamic forces, which strongly influence atherosclerosis development (Kolodgie *et al.*, 2007).

Based on numerous studies using animal models, migration and proliferation of VSMC-like cells derived from differentiated medial VSMCs and/or undifferentiated resident vascular stem cells and the deposition of lipids within macrophage foam cells are two key events during the pathogenesis of atherosclerosis. A critical role for medial VSMCs in the progression of atherosclerosis has become increasingly apparent due to the introduction of rigorous VSMC lineage tracing, scRNA-seq analysis, and conditional gene knockout studies in murine models (Gomez and Owens, 2012; Laura S Shankman *et al.*, 2015; Cherepanova *et al.*, 2016; Dobnikar *et al.*, 2018). Lesion formation due to the clonal expansion of a rare subset of mature $Myh11^{+}$, $Sca1^{+}$ medial VSMCs has been reported (Dobnikar *et al.*, 2018). These lesional cells lack characteristic VSMC markers but express markers for macrophages, mesenchymal stem cells, and myofibroblasts (Gomez *et al.*, 2013; Laura S Shankman *et al.*, 2015; Cherepanova *et al.*, 2016; Newman *et al.*, 2018). Moreover, VSMC-specific knockout studies have shown that VSMCs can have key beneficial or detrimental effects on lesion pathogenesis, depending on the nature of their phenotypic transitions (Laura S Shankman *et al.*, 2015; Cherepanova *et al.*, 2016; Durgin *et al.*, 2017). Recent discoveries using lineage tracing models have identified a sub-population of $S100\beta^{+}$ resident stem cells in the medial/adventitial layer of the vessel, termed MVSCs, which migrate and differentiate to become neointimal VSMC-like cells (Tang, Wang, Wang, *et al.*, 2012; Yuan *et al.*, 2017). Furthermore, studies from our research group have supported these finding using indelibly marked $S100\beta^{+}$ cells and demonstrated that a significant number of neointimal cells are derived from a small parent $S100\beta^{+}$ population of medial stem cells (Di Luca *et al.*, 2021; Molony *et al.*, 2021). Due to conflicting arguments surrounding the origin of VSMCs in the neointima, a model system of embryologically distinct VSMCs originating from the same genetic source is favourable to truly understand the intrinsic differences between various regions of the vasculature.

The atherosclerotic process in humans is more nuanced and develops in a different manner (Nakagawa and Nakashima, 2018). Vascular VSMCs are already abundantly present in the thickened intima before developing subclinical atherosclerosis in lesion-prone arteries. This non-atherosclerotic intima exhibits DIT or later AIT. The developing

intima is diverse in its structural composition and function (Potente and Mäkinen, 2017). There are striking regional differences in disease development that are thought to be governed by hemodynamic factors and vessel wall structure (Langille, 1996; Riha *et al.*, 2005). While hemodynamic forces are important factors driving adaptive lesion formation and the progression of atherosclerotic lesions (Otero-Cacho *et al.*, 2018), disease susceptibility may also be dictated by the embryonic origin of VSMCs and/or their progenitors within the vasculature, and the consequences of this heterogeneity on disease (Sinha, Iyer and Granata, 2014; Bargehr *et al.*, 2016). Lineage tracing studies have indicated that VSMCs arise from multiple origins during development and respond differently to risk factors such as changes in blood flow, shear stress, and hyperglycaemia (Majesky and W., 2007). The aorta offers a unique region to study the impact of embryonic origin on vascular phenotype and disease susceptibility as it consists of VSMC derived from the three lineages, the NE, the paraxial mesoderm (PM), and the lateral plate mesoderm (LM), across the ascending, descending and root of the aorta, respectively.

Many limitations have been associated with the isolation and growth of VSMCs in culture. Upon isolation, primary VSMCs undergo a phenotypic shift from a quiescent contractile phenotype to a proliferative dedifferentiated phenotype with a significant decrease in the expression of VSMC markers (Owens, Kumar and Wamhoff, 2004). The complexity of cellular components in the vascular wall adds to the challenge during isolation of VSMCs with an increased risk of isolating contaminant cells such as ECs, resident vascular stem cells, and fibroblasts. Although cell sorting has been utilised to isolate vascular cells, such as isolation of ECs using endothelial surface markers, there is a lack of definitive VSMC markers to facilitate this process as definitive markers for VSMCs such as MYH11 and Smoothelin B are intracellular proteins. Furthermore, the isolation of VSMCs from distinct embryological origins proves difficult due to the lack of markers discovered to date to distinguish VSMC subtypes. The multiple limitations of primary VSMC cultures highlight the unmet need to develop novel sources of VSMCs from defined embryological origins.

Studies have attempted to recapitulate the germ layer-specific developmental processes *in vitro* to model and characterise the influence of lineage-specific differentiation on the phenotype of vascular progenitors and VSMCs (Sinha, Iyer and Granata, 2014; Bargehr *et al.*, 2016). The discovery of human pluripotent stem cells (hPSCs) over the past three

decades, initially embryonic and now the increasing use of induced pluripotent stem cells (iPSCs), serves as a platform for generating unlimited amounts of isogenic VSMC subtypes. The directed differentiation of HiPSCs through distinct NE, PM, and LM lineages via progenitor intermediates generates origin-specific and functional VSMCs harbouring many of the phenotypic differences observed *ex vivo*, revealing inherent differences and thus allowing for the categorisation of origin-specific-VSMC subtypes (Bargehr *et al.*, 2016). Not only can this HiPSC-derived model be utilised to determine the effects of VSMC embryological origin on atherosclerotic pathogenesis, but it also represents lineage-specific multipotent progenitor stem cell population for use during the study of vascular cell-cell communication *in vitro.*

Initiation of subclinical atherosclerosis results from continued damage to the endothelium, activation of endothelial cell dysfunction, and subsequent lesion formation. Endothelial injury triggers a cascade of events, including an increase in the release of small membrane-bound intracellular communicators known as EVs (Libby, 2000; Koga *et al.*, 2005; Dignat-George and Boulanger, 2011). EVs have emerged as crucial vascular homeostasis and CVD progression regulators by transferring biological messages to target vascular stem cells. Once released, EVs may target neighbouring cells within the vascular wall, including resident vascular progenitor stem cells. Based on the data presented in Chapter 3, murine EVs derived from hyperglycaemic ECs promote Hh target gene expression in murine S100β resident vascular stem cells *in vitro.* These S100β resident vascular stem cells cells contribute to subclinical atherosclerosis and lesion formation in murine models and can undergo myogenic differentiation in response to recombinant Hh ligands (SHh*) in vitro* (Di Luca *et al.*, 2021). Attenuation of Hh signalling in murine models of arteriosclerotic disease attenuates IMT and lesion formation (Redmond *et al.*, 2013; Aravani *et al.*, 2019; Di Luca *et al.*, 2021). By using HiPSC derived progenitor stem cells *in vitro,* it is now possible to study the transfer of potential pathogenic biological messages from various cell types within the vascular wall, including but not limited to endothelial to stem cell, endothelial to VSMC, and stem cell to VSMC crosstalk. We therefore sought to determine whether these data could be recapitulated in a human iPSC model to further validate the importance of endothelial derived EVs harbouring Hh ligands in response to hyperglycaemic conditions to promote a change in S100β vascular stem *in vitro.*

4.2 Objectives

The main aims of this chapter were.

(i) To develop an *in vitro* human cell model of HAEC in culture and characterise EC-derived EVs released under normal and hyperglycaemic conditions

(ii) To develop and validate an *in vitro* human reporter cell model using HiPSC-derived progenitor stem cells from neuroectoderm (NE), paraxial mesoderm (PM), and lateral mesoderm (LM) embryological origins.

(iii) To determine whether HAEC-derived EVs under normal and hyperglycaemic conditions impact Hh signalling and myogenic differentiation of HiPSC derived S100β^{+} vascular stem cells *in vitro*

4.3 Strategy

The main aim of this Chapter is to characterise HAEC-derived EVs under normal (NG-EVs) and hyperglycaemic conditions (HG-EVs) and determine their uptake by HiPSC-derived NE S100β^{+} progenitor stems and subsequent Hh-induced myogenic differentiation *in vitro.* To investigate the potential role of HG-EV-dependant myogenic differentiation of HiPSC-derived NE S100β^{+} progenitor stem cells it was essential to develop two *in vitro* cell culture models (i) human primary aortic ECs exposed to HG conditions for secretion of HG-EVs and (ii) HiPSC-derived reporter NE S100β^{+} progenitor stem cell population for HG-EV uptake and subsequent activation of VSMC-associated signalling pathways (Figure 4.1).

Endothelial exposure to circulating HG levels *in vivo*, clinically referred to as hyperglycaemia, results in endothelial dysfunction, development of diabetes, and subsequent acceleration of CVD (Williams *et al.*, 1998; Debakey and Glaeser, 2000; Sheu *et al.*, 2005). Hallmarks associated with hyperglycaemia-induced ED are (i) an increase in cellular NOX-dependant ROS production, (ii) loss of NO bioavailability (iii) an increase in the secretion of HG-EVs (Simsek *et al.*, 2010; Dimassi *et al.*, 2016; Meza *et*

al., 2019). As part of this study, a human primary aortic endothelial cell model was developed *in vitro* to investigate the secretion of HG-EVs when exposed to HG conditions. Human primary aortic ECs were purchased commercially from PromoCell (C-12271) and cultured until reaching 70% confluency (Section 2.2.2.3). ICC was carried out to characterise the cell population by probing for membrane-bound protein CD31 (Section 2.2.6.1). Confirmatory qRT-PCR analysis was used to determine mRNA expression levels of endothelial markers *CD31, vWF,* and early myogenic VSMC differentiation marker *CNN1* (Section 2.2.6.2).

To mimic vascular diabetic conditions found *in vivo*, HAECs were grown in HG conditions (2.2.8.1). Several biochemical pathways have been associated with hyperglycaemia, including a glucose-mediated increase in ROS and O_2- and a decrease in NO availability. To investigate changes in the biochemical activity of HG-treated HAECs, a number of techniques were used to measure intracellular O2- and NO availability. A quantitative NBT assay was used to determine intracellular O_2^- production in NG and HG-treated ECs in culture (2.2.7.2). Cells were visualised under the microscope for the presence of NBT formazan deposits formed by the reduction of the membrane-permeable NBT by O_2^-. Following this, NBT formazan particles were quantified by solubilizing crystals using DMSO/ethanol solution, and absorbance was measured at 680nm. Confirmatory experiments were performed to assess the presence of O_2^- production in HG-ECs using an O_2^- indicator, dihydroethidium (DHE), whereby blue fluorescence in the cytosol is oxidised intercalating within the cell's DNA resulting in a bright fluorescent red nuclear stain (2.2.7.1). Furthermore, gene expression changes important to functional changes, including nitic oxide synthase enzyme NOS3 and NADPH enzyme NOX4 were measured by qRT-PCR.

In addition to changes in biochemical pathways in response to HG conditions, changes in EV secretion and cargo content have also been reported (Freeman *et al.*, 2018). To further investigate this, EVs from NG and HG cell culture conditions were isolated using ExoQuick-TC, a proprietary polymer for gentle precipitation of EVs (Section 2.2.8.2). A limitation to the use of commercially available EV isolation kits is the precipitation of contaminants, including cellular organelles, lipids, cholesterol, and other undesired microparticles (Morales-Kastresana *et al.*, 2017). Therefore, it was essential to verify the purity of isolated EV samples. HAEC-NG and HG-EVs were characterised using DLS

(Section 2.2.8.3), Fe-SEM imaging (Section 2.2.8.8), and nanoFACs technology (Section 2.2.6.3). DLS of isolated HG-EVs was carried out to determine the distribution profile of isolated EVs in solution providing an average value of EV particle size. Following this, Fe-SEM imaging which uses beams of electrons to produce a magnified image of a sample, was used to check the purity of the sample by providing a high-resolution image to distinguishing EVs from similarly sized non-EV particles.

Lastly, nanoFACs technology using the Amnis™ CellStream flow cytometer was used for the analysis of isolated EVs, combining measurements from high sensitivity multiparametric scattered light and fluorescence to analyse EVs individually (Morales-Kastresana *et al.*, 2017; Mastoridis *et al.*, 2018). Firstly, using specific endogenous and exogenous EV-labelling dyes NirAza and ExoGlow, respectively, HG-EV populations were characterised in isolated fractions to determine the true presence of intact EVs (Section 2.2.8.5, Section 2.2.8.6). Triton X-100 detergent was used to degrade the HG-EV membrane resulting in a decrease in intact EV detection. Secondly, the percentage of CD9, CD63, and CD81 positive HG-EVs were assessed using specific fluorescently labelled antibodies to stain EV surface proteins. Confirmatory experiments were carried out to confirm the expression of a panel of EV-associated proteins using an EV antibody array (Section 2.2.8.7).

Having developed a human endothelial cell model for EV secretion and confirmed the presence of isolated EVs from HG-conditioned cell culture media, HG-EV induced SHh-dependent myogenic differentiation of an S100β^+ vascular stem cell population *in vitro* was evaluated. HiPSCs were purchased from HipSci, cultured (Section 2.2.3), and characterised to ensure expression of specific embryological markers OCT4 and NANOG (Section 2.2.6.1). Once suitable starting HiPSC cells had been selected, differentiation protocols were used to drive myogenic differentiation using intermediate progenitor cells. The differentiation protocol comprised of three main steps (i) preparation of HiPSCs for differentiation, (ii) chemically and non-chemically driven differentiation of HiPSC to NE, PM, and LM progenitor stem cells, and finally (iii) differentiation of progenitor stem cells into VSMC subtypes.

Several stem cell populations have been identified in the vasculature by several different research groups. Of interest, many of these groups have reported that cells present in the

neointimal lesion during sub-clinical atherosclerosis may arise from a stem cell parent population (Wang *et al.*, 2018). A sub-population of adventitial/medial S100β+ stem cells contribute to the development of a ligated-induced neointima through migration and differentiation (Liu *et al.*, 2020; Di Luca *et al.*, 2021; Molony *et al.*, 2021) . In order to determine the functional effects of HG-EV cargo on resident vascular stem cells, a HiPSC-derived S100β+ NE stem cell reporter was developed through the use of defined chemically derived and non-chemically derived differentiation protocols (Section 2.2.3.2, Section 2.2.3.3). Following differentiation of HiPSCs to NE, both NEP and SNEP cells were characterised using ICC by probing for NE markers S100β and NESTIN. ICC was also used to ensure NE cells were not enriched for VSMCmarkers CNN1 (Section 2.2.6.1). Confirmatory qRT-PCR analysis was used to determine the mRNA expression levels of NE markers *S100β*, *NESTIN*, *PAX6,* and mesodermal markers *PAX1*, *TBX6,* and *KDR* (Section 2.2.6.2). As both chemically defined (NEPs) and non-chemically defined (SNEPs) protocols generated S100β$^+$, NESTIN$^+$ HiPSC-derived SCs, further analysis was undertaken to determine their myogenic capacities was carried out using both NEPs and SNEPs before and the selection of an applicable reporter cell line.

The ability of NE, PM, and LM-derived progenitor stem cells to undergo myogenic differentiation was evaluated through activation of TGF-β1-PDGF-dependent pathways (Section 2.2.3.5). Furthermore, the responsiveness of NE progenitor stem cells to recombinant SHh ligand was undertaken to confirm myogenic differentiation of S100β+ stem cells in the presence of SHh prior to EC treatment. Phase-contrast images were taken during differentiation to track changes in cell morphology. ICC and RT-qPCR were then carried out to detect transcript and protein expression of myogenic genes markers, *CNN1* and *MYH11*. Both NEP and SNEP HiPSC-derived NE stem cell populations displayed similar expression of S100β and NESTIN mRNA and protein levels following HiPSC differentiation. Furthermore, both NE populations displayed the capacity to differentiation toward a myogenic lineage. However non-chemically derived NE STEM CELL population SNEPs were chosen as a reporter cell line to determine HAEC-derived EV functionality due to advantages characteristics including; less time taken for generation and the use of a less complex maintenance media therefore providing a more cost effective model.

To determine the role of HAEC-EVs in regulating SHh-dependent myogenic differentiation of NE vascular stem cells, S100β+ HiPSC-derived SNEPs *in vitro* were

exposed to previously isolated and characterised HAEC-NG and HG-EVs. Fluorescent microscopy using labelled EVs was used to assess phagocytosis/receptor docking of isolated HG-EVs by SNEP populations using the Leica microscope. Z-stack images were taken to determine to localisation of HG-EVs in SNEP populations. The migratory and proliferative changes in HiPSC-derived SNEPs were monitored after HG-EV incubation using the Celigo imaging cytometer to determine the effect of HG-EV induced myogenic differentiation of HiPSC-derived *in vitro* via EV-dependent cell-cell communication (Section 2.2.6.5).

To determine the role of HAEC HG-EVs in regulating SHh-dependent myogenic differentiation of NE vascular stem cells, previously isolated and characterised HAEC-NG and HG-EVs were exposed to S100β+ HiPSC-derived SNEPs *in vitro*. Hedgehog target genes *GLI 1* and *GLI 2* were measured after 48 hours to determine activation of EV-mediated activation of Hh signalling. Followed by the measurement of early myogenic differentiation marker CNN1 after 7 days. To confirm that the changes in *GLI1* and *CNN1* gene expression was ligand dependent, S100β^{+} HiPSC-derived SNEPs were pre-treated with the SHh signalling inhibitor cyclopamine or the SHh neutralising antibody 5E1 (Section 2.2.5.2.2).

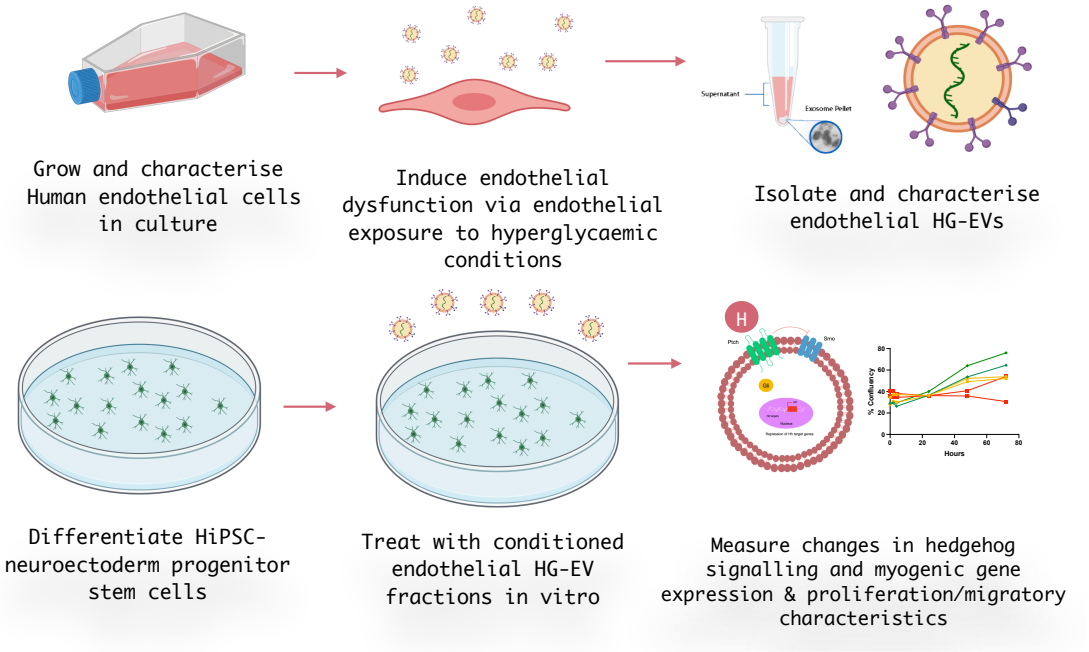

Figure 4.1 Graphic summary of experimental strategy. Graphic summary of the experimental strategy to determine the role of HG -EV induction of SHh-dependent myogenic differentiation of HiPSC-derived NE progenitor stem cells *in vitro.*

4.4 Results

4.4.1 Primary HAECs express distinct endothelial markers CD31 and eNOS

To develop a human *in vitro* cell model for EV secretion under hyperglycaemic conditions (HG-EVs), primary HAECs were grown in culture and interrogated for typical endothelial markers, including CD31 and eNOS, before EVs from normal (NG-EV) and hyperglycaemic (HG-EV) HAECs were generated. HAECs from passages 3-12 displayed typical EC characteristics when grown as a single adherent monolayer. A distinct cobblestone morphology was observed by phase-contrast microscopy at 10X magnification (Figure 4.2 A). The cells were significantly enriched for *CD31* and *ENOS* mRNA levels compared to HiPSCs in culture (Figure 4.2 B, C).

The expression of CD31 protein was determined by ICC. Cells were seeded onto sterile coverslips in a 6-well plate at a low density (4,000 cells/well) and incubated at 37°C for 48 h. Cells were fixed with 3.7% formaldehyde and stained with primary antibodies for CD31 (1:100). To generate a fluorescent signal for staining, fluorophore-Alexa Fluor 488-conjugated secondary antibodies were added, and nuclei were stained with DAPI. Using a fluorescent microscope, these stains were visualised, imaged, and analysed to determine the expression of each protein. IgG controls (secondary antibody probing without primary antibody staining) were used to account for background fluorescence or off-target binding of secondary IgGs. The expression of endothelial marker CD31 was abundant around the cell membrane of HAECs (Figure 4.2 D).

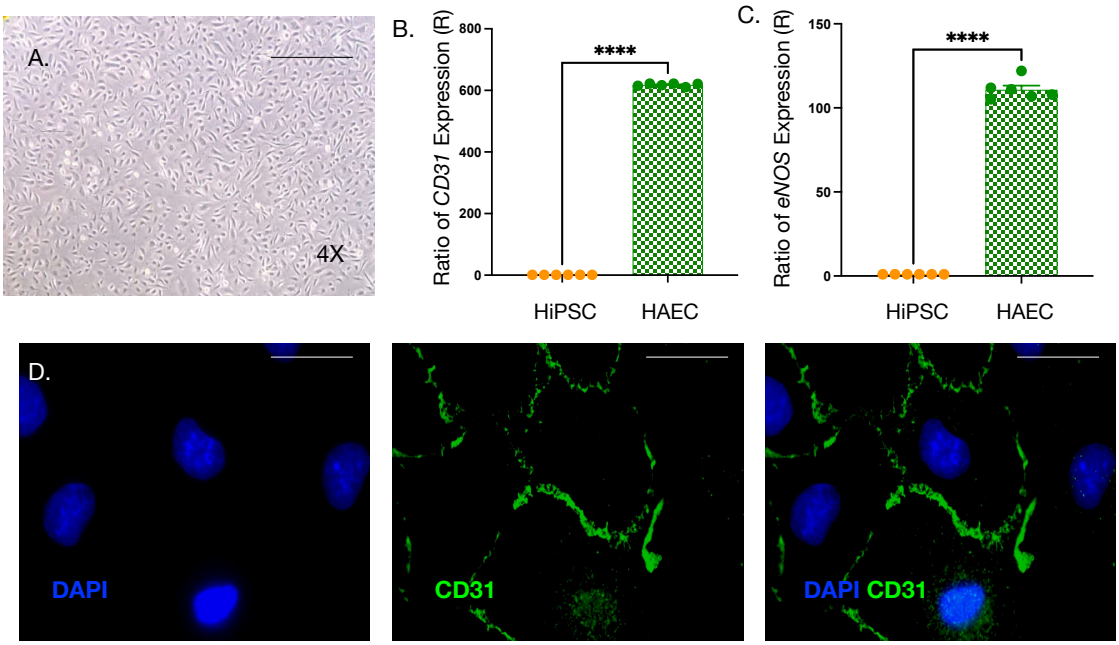

Figure 4.2 Characterisation of HAECs. (A) Phase-contrast images of HAEC in the culture at 10X magnification —scale bar representative of 50µm respectively. (B, C) Relative mRNA levels of endothelial markers CD31 and eNOS in HAECs. Data are expressed as the ratio of mRNA expression relative to *GAPDH* and are the mean ± SEM, n = 6, * $p \leq 0.05$ versus HiPSCs. (D) Representative images of fluorescence staining of DAPI nuclei and immunocytochemical analysis of the expression of an endothelial marker, CD31 in HAECs. All images were taken using Olympus DP-50 fluorescent microscope. AlexaFluor 488 secondary antibody used for visualisation of primary antibody binding. All images are representative of n > 6 images per experimental group from three independent cultures—scale bar representative of 25µm.

4.4.2 HG increases intracellular $O2^{-}$ production accompanied by elevated *NOX4* and *NOS3* gene expression levels

Diabetes is a complex metabolic syndrome associated with the acceleration of CVD. A hallmark of diabetes is endothelial exposure to hyperglycaemic conditions leading to dysregulation of endothelial function and initiation of vascular complications (Versari *et al.*, 2009). During exposure to HG, intracellular production of ROS is one of the main factors responsible for pathophysiological changes. EC generation of ROS includes O2-, H_2O_2, peroxynitrite, and NO radicals (Li and Shah, 2004). HAECs were grown in HG conditions. Increases in ROS generation in HG-HAEC treated cells were measured by an increase in O_2^{-}. A quantitative NBT assay was used to determine intracellular O_2^{-} production in NG and HG treated HAECs *in vitro*. An increase in NBT formazan deposits formed by reducing the membrane-permeable NBT by $O2^{-}$ was observed in HG-HAECs compared to NG-HAECs (Figure 4.3 A). NBT formazan particles were quantified by solubilizing crystals using DMSO/ethanol solution, and absorbance was measured at 680nm. An increase in NBT formazan particles was observed in HAECs treated with 30mM and 100mM glucose, respectively (Figure 4.3 B).

Confirmatory experiments were performed to assess the presence of O_2^{-} production in HG-HAECs using a O2- indicator, DHE, whereby blue fluorescence in the cytosol is oxidised intercalating within the cell's DNA resulting in a bright fluorescent red nuclear stain. An increase in fluorescent red nuclear stain was observed in HG-HAECs in comparison to NG-HAECs (Figure 4.3 C).

During exposure to HG conditions, intracellular $O2^{-}$ increases from various sources, which include the NOX family of enzymes (NOX)-dependant generation and uncoupled constitutive NO synthase (eNOS) (Zhou *et al.*, 2012; Jansen *et al.*, 2013). HAECs were treated in NG and HG conditions for 24 h. Following treatment, RNA samples were analysed by qRT-PCR to measure the expression of *NOS3 (eNOS)* and *NOX4*. A significant increase in *NOX4* and *NOS3* was observed in HG-HAECs in comparison to NG-HAECs (Figure 4.3 D).

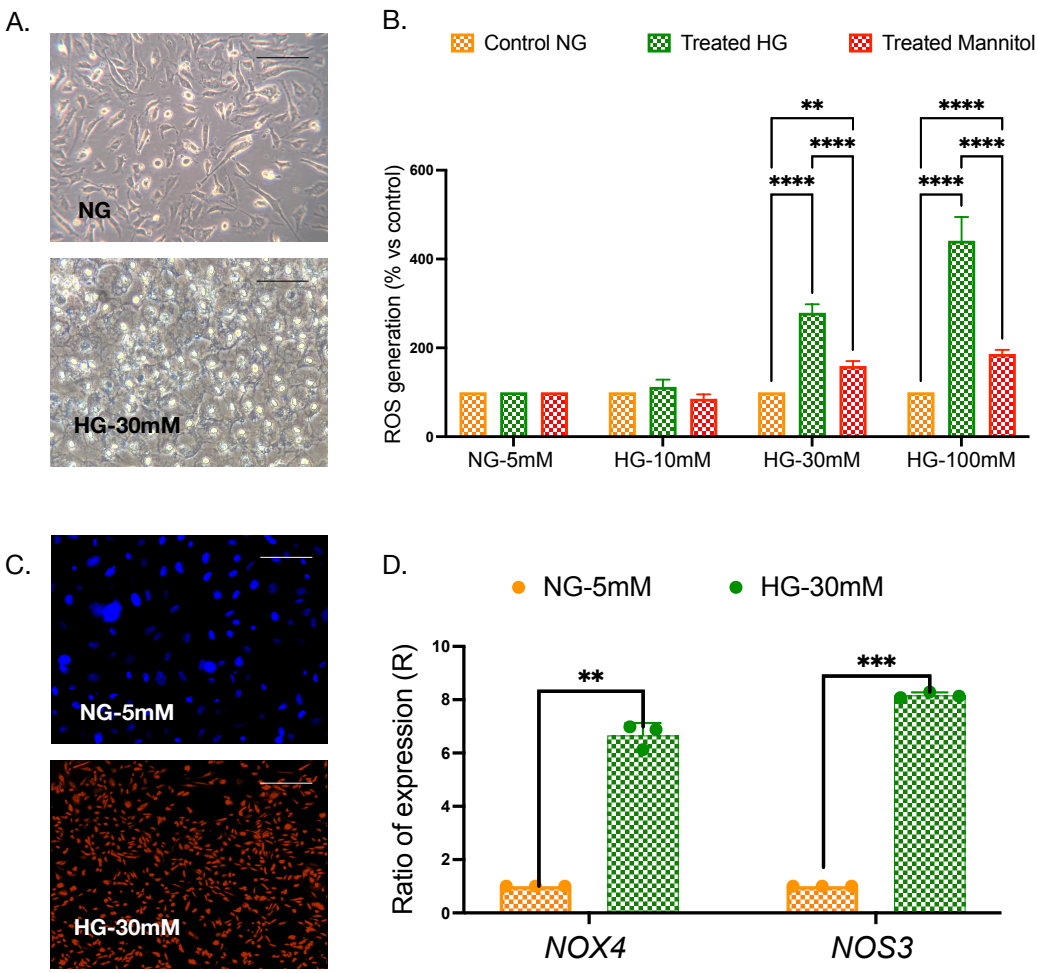

Figure 4.3 HG-HAEC induces an increase in endothelial ROS through increased levels of $O2^{-}$ production. (A) Phase-contrast images following NBT incubation of HG-HAECs (B) Quantification of $O2^{-}$ following 48 h HAEC-HG culture. Results presented as a percentage of HAEC-NG control treatment, n=3 (C) Representative fluorescence imaging capturing DHE fluorescence in NG and HG conditions after 48 h —scale bar representative of 10µm respectively. (D) Relative mRNA levels of endothelial markers *NOX4* and *NOS3* in NG and HG-HAECs. Data are expressed as the ratio of mRNA expression relative to control and are the mean ± SEM, n = 3, * $p \leq 0.05$ versus NG-5mM.

4.4.3 NG and HG treated HAECs secrete EVs *in vitro*

It is well established that ECs are the first responder to circulating risk factors associated with CVD *in vivo*. For this reason, EC-derived EV secretion provides a platform to study the health of the vasculature at any given time. HAEC derived NG- and HG-EVs were generated and characterised *in vitro*. HAECs were cultured in NG and HG for 48 h facilitating EV secretion. After 48 h, cell culture media was removed and EVs isolated, as before. Once purified, EVs were resuspended in dH_20 for characterisation. Cryo-electron microscopy SEM was performed on EVs purified by ExoQuick TC, revealing the presence of vesicular bodies. Morphometric analysis showed heterogeneity in EV sizes, with isolated populations falling between 80nm-120nm in size (Figure 4.4 A-D). Having confirmed the presence of intact EVs in isolated fractions, DLS technology was used to confirm the size of NG-EV and HG-EV particles. NG-EVs ranged between 25nm-60nm with a small sub-population at 86nm, where-as HG-EVs ranged between 30 – 80nm with a small sub-population at 122nm (Figure 4.4 E, F).

To further evaluate HG-EV content, the expression of EV-associated proteins was assessed using nanoFACs and dot-blot analyses. Amnis™ CellStream analysis of HG-EVs expressed endosomal protein markers CD81 (Figure 4.5 A) and CD63 (Figure 4.5 B) with minimal expression of CD9 (Figure 4.5 C) noted. Control samples were examined for antibody only and IgG, respectively.

Dot-blot analyses of NG and HG-EV protein expression identified differences in the expression of various endosomal and cytoplasmic protein markers (Figure 4.6 A, B). Densitometry was carried out on samples to measure the intensity of EV-associated protein expression and normalised to the positive control. The main differences in expression were identified for TSG101, ANXA5, ALIX, ICAM EV-proteins in NG and HG-EVs with elevated TSG101, ANXA5, and ALIX proteins and decrease in expression of ICAM in HG-EVs compared to NG-EVs (Figure 4.6 C, D).

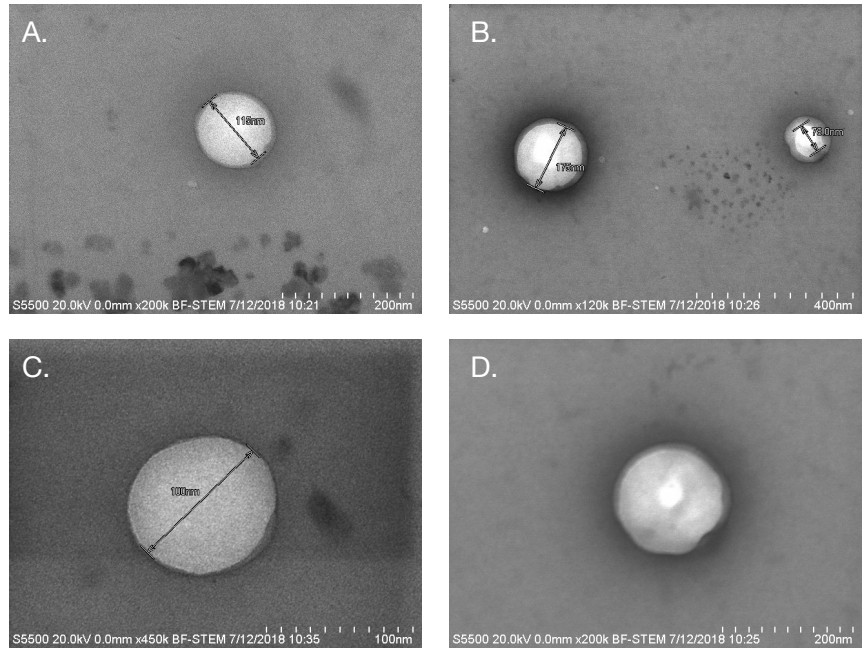

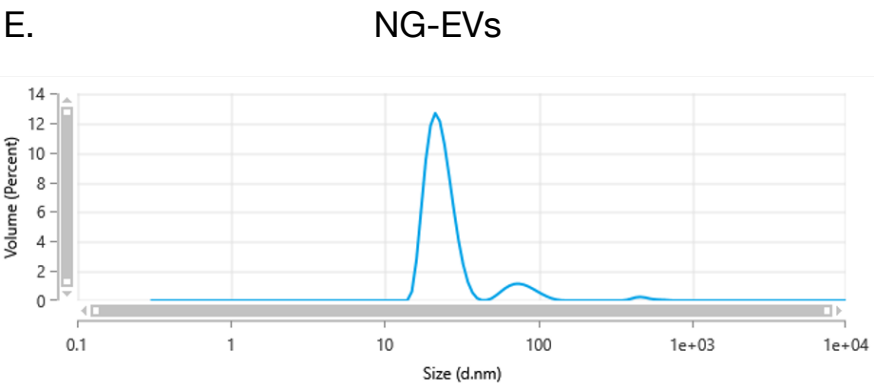

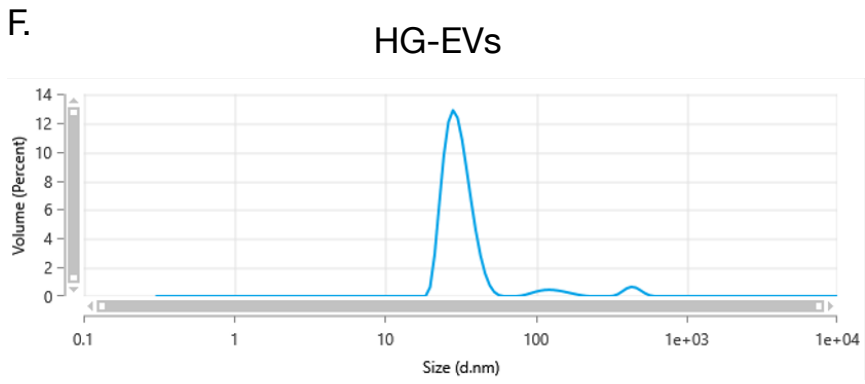

Figure 4.4 Characterisation of HAEC-derived EVs following ExoQuick TC isolation. (A-D) Scanning electron microscopy images representative of HG-EVs precipitated using ExoQuick TC —scale bar representative of 100, 200, and 400 µm. Size distribution profile of isolated NG-EVs (E) and HG-EVs (F) measured by DLS.

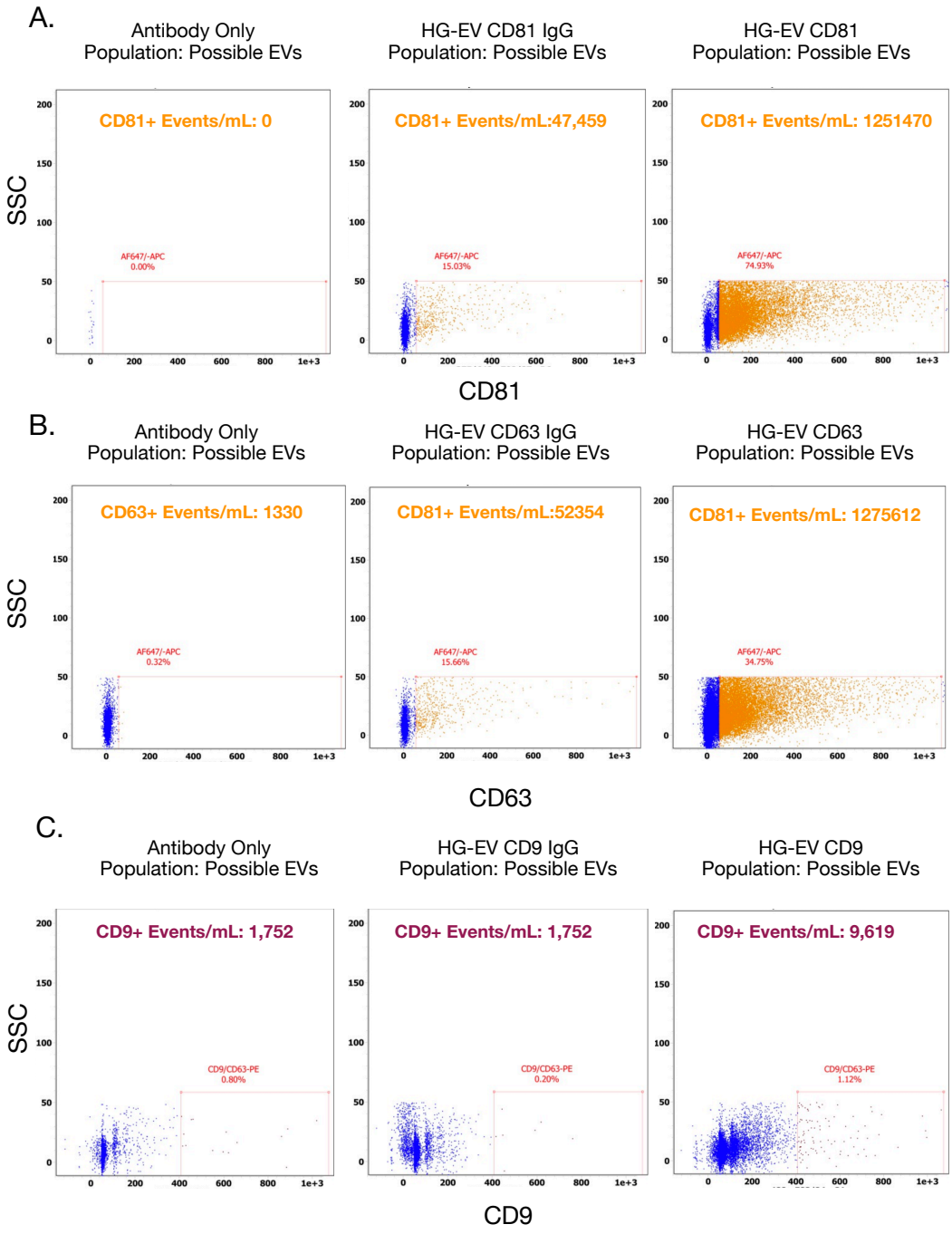

Figure 4.5 Amnis ™ CellStream characterisation of tetraspanin protein expression in HAEC HG-EVs. Representative scatter plot analysis of the expression of (A) CD81 positive HAEC HG-EVs, (B) CD63 positive HAEC HG-EVs, and (C) CD9 positive HAEC HG-EVs. Control comparisons include antibody only and IgG, n=4.

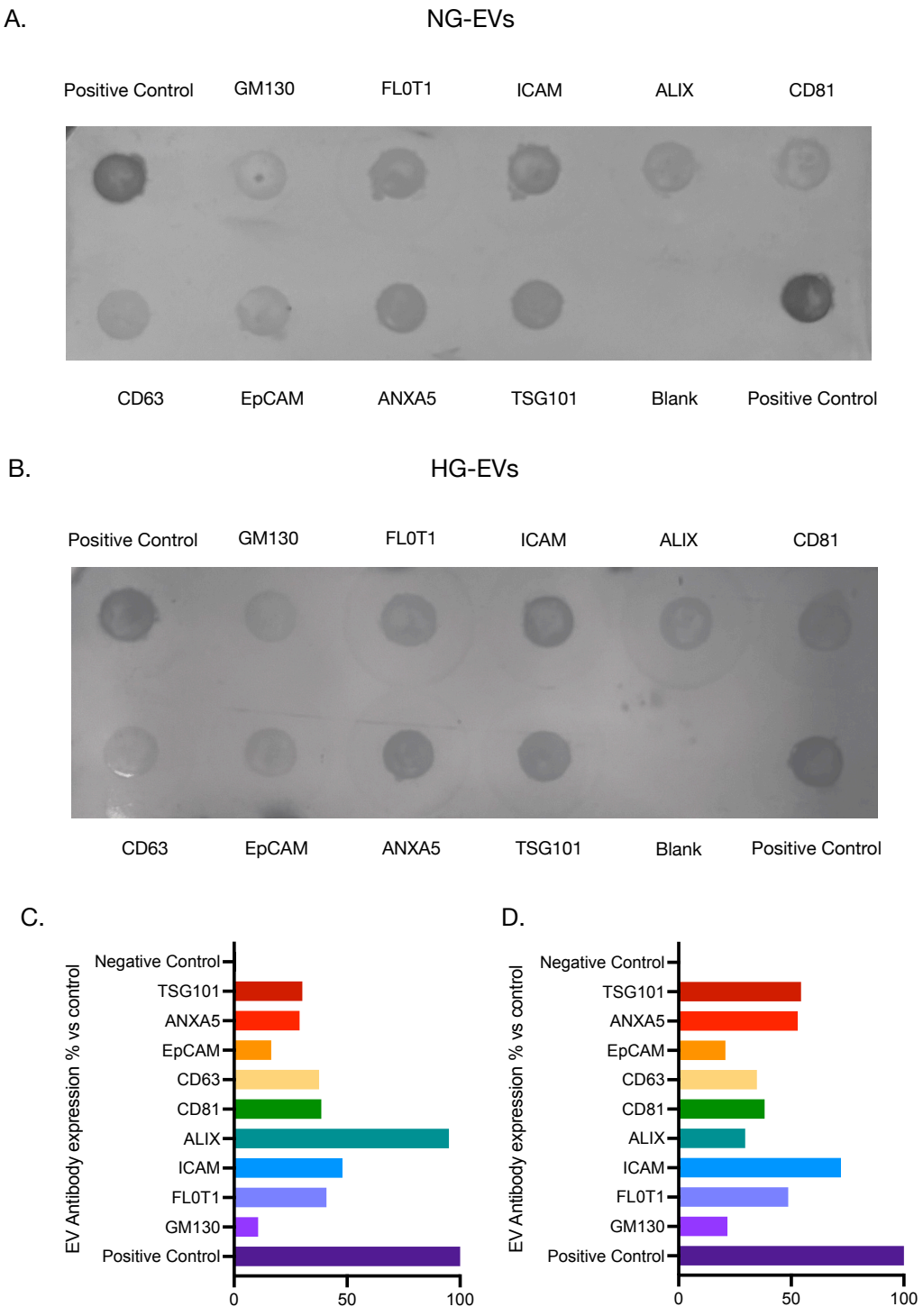

Figure 4.6 Characterisation of EV-protein profile in NG-EVs and HG-EVs. (A, B) Representative dot blot images for qualitative evaluation of endosomal and cytoplasmic EV-associated protein expression in NG and HG-EVs. (C, D) Densitometry analysis of the intensity of EV-associated protein expression in NG and HG-EVs. Data expressed as a percentage of the positive control.

4.4.4 Exogenous and endogenous labelling of HAEC-derived HG-EVs

Following characterisation of NG and HG-EVs, endogenous and exogenous labelling of HG-EVs was carried to enable subsequent tracking of EV uptake by reporter target resident vascular stem cells *in vitro*. Two labelling techniques were used, (i) NIR-Fluorescent probe (Nir-Aza) for endogenous HAEC HG-EV labelling and (ii) ExoGlow™ membrane EV labelling dye for exogenous HAEC-EV labelling. In order to optimise the concentration of Nir-Aza used to label the generation of EVs, HAECs were seeded at 500 cells/well onto a 48 well plate. Following 24 h culture in maintenance media varying concentrations from 1µM to 5µM of Nir-Aza was added to each well. Cells were imaged using the Celigo Imaging Cytometer at various time points from 0 hours – 24 h using bright field and far-red detection channels (Figure 4.7 A). A heat map was generated indicating fluorescent intensity levels at each time point (Figure 4.7 B). The percentage of Nir-Aza positive cells from 0-5 hours (Figure 4.7 C) and 0-24 hours (Figure 4.7 D) was graphed. The optimal concentration of Nir-Aza for endogenous labelling of HAEC-EVs in culture was 3µM.

Further analysis of HAEC Nir-Aza-EVs was carried out using the Amnis™ CellStream ™. HG-Nir-Aza-EVs were isolated from conditioned media. The isolated EVs were analysed using the Amnis™ CellStream ™. Data were acquired using the Amnis™ CellStream ™ flow cytometer for 3 minutes per sample. The 642nm was run at 100% laser power, and no thresholding was used. Control samples were collected for NirAza only and EV only (Figure 4.8 A, B). Detergent controls were collected for the NirAza-labelled EV samples, which were incubated in 0.1% Triton X-100 for 10 mins. To identify potential HG-NirAza-HG-EVs, a gate was set using an SSC vs. FSC plot. Using the "potential EVs" gated population, Nir-Aza positive events were gated. HG-NirAza-EVs positive events were 3,840,893,100 (Figure 4.8 C). When incubated with detergent, a reduction of 99.95% in positive events was detected, demonstrating labelling of intact HG-EVs (Figure 4.8 D).

Similarly, exogenous HG-EV labelling was carried out using ExoGlow. Labelled HG-EVs were analysed using the Amnis™ CellStream ™. Data were acquired using the Amnis™ CellStream ™ flow cytometer for 3 minutes per sample. The 488nm was run at 100% laser power, and no thresholding was used. Control samples were collected for ExoGlow only and HG-EV only (Figure 4.9 A, B). Detergent controls were collected for

the ExoGlow-labelled HG-EV samples, which were incubated in 0.1% Triton X-100 for 10 mins. A gate was set using an SSC vs. FSC plot (Figure 4. A). Using the "potential EVs" gated population, ExoGlow positive events were gated. HG-ExoGlow-EVs positive events detected were 1,456,401 (Figure 4.9 C). When incubated with detergent, a reduction of 86.72% in positive events was detected, demonstrating labelling of intact HG-EVs (Figure 4.9 D).

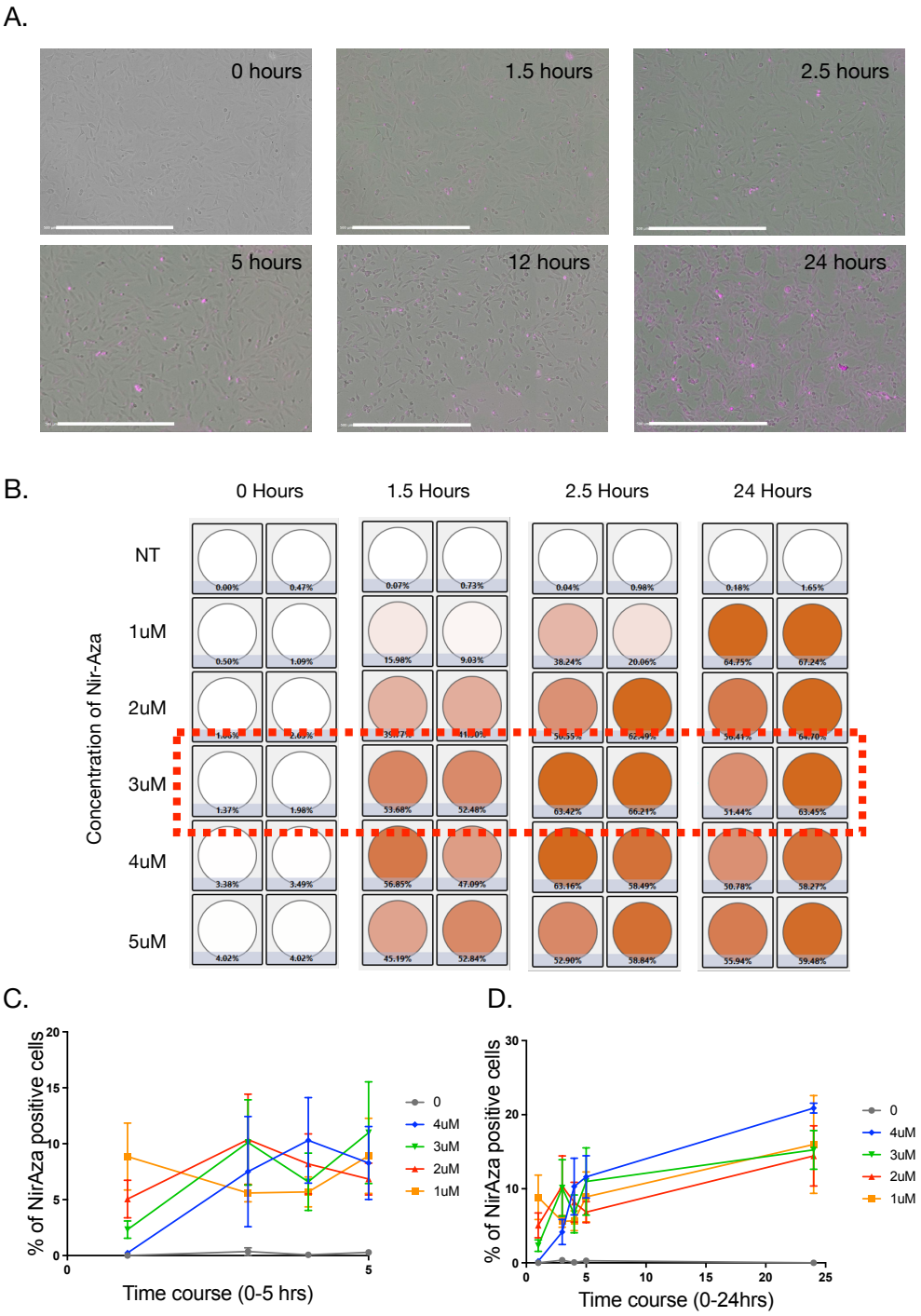

Figure 4.7 Endogenous labelling of HG-EVs using NirAza *in vitro*. (A) Representative phase-contrast and immunostaining overlay images of NirAza uptake by HAECs in culture from 0 -24 h. (B) Heatmap representation of the intensity of NirAza stain following incubation over a time course of 0-24 h. (C,D) Graphic representation of NirAza positive cells over time from 0-5 h (B) and 0-24 h.

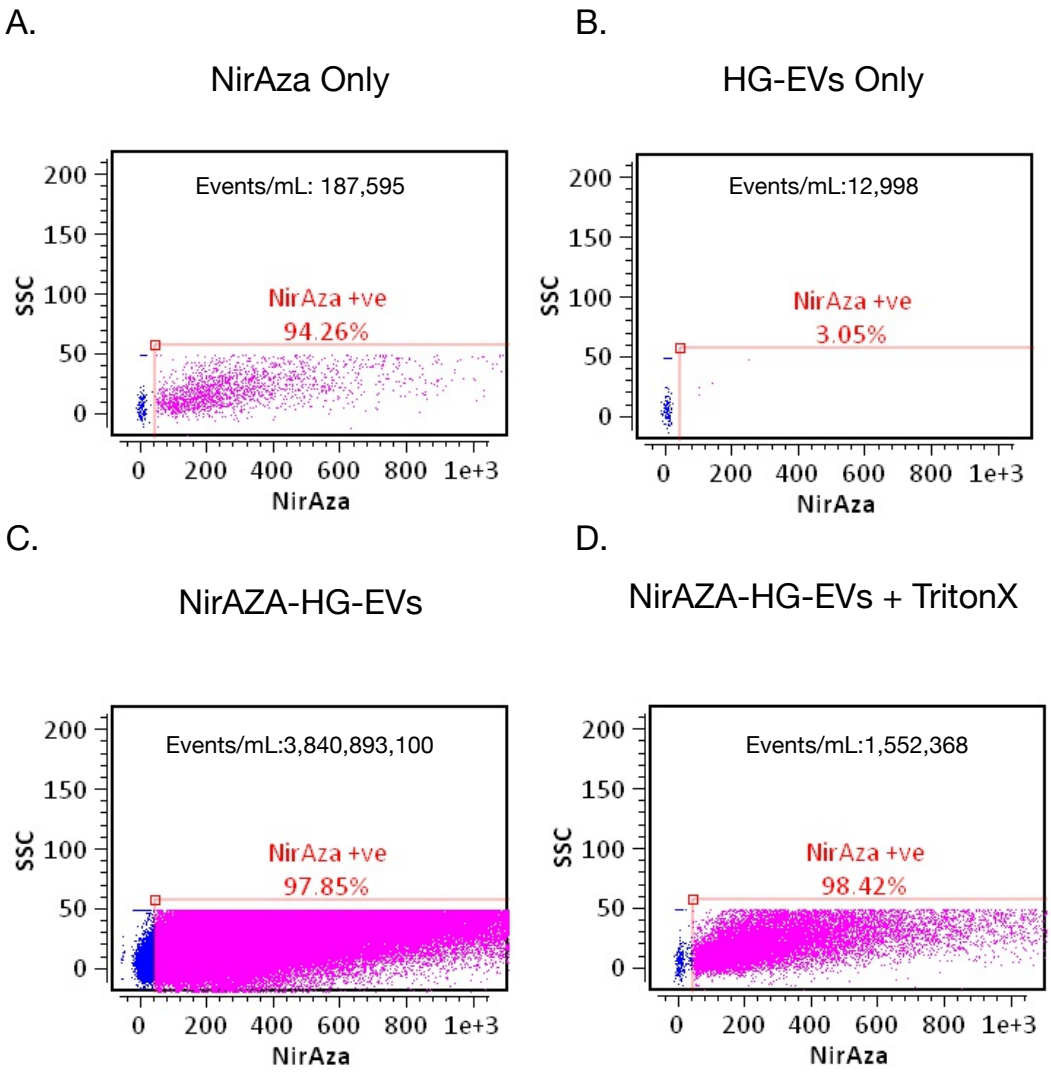

Figure 4.8 Detection of Nir-Aza positive HG-EVs following endogenous labelling. (A-D) Detection of NirAza positive HG-EVs following endogenous labelling in culture. Representative images of control samples (A) NirAza dye only, (B) HG-EVs only, and (D) NirAza-HG-EVs treated with Triton X detergent. Data representative of n=3.

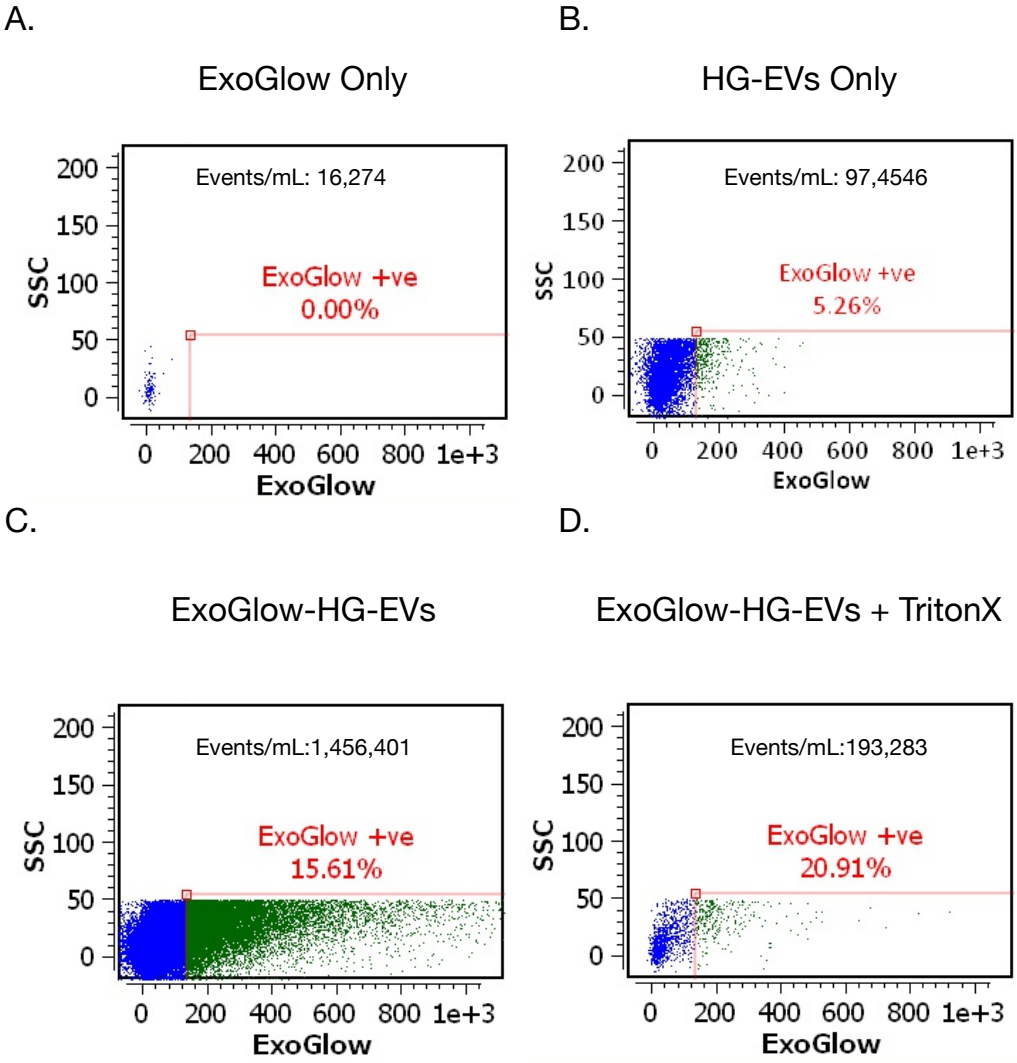

Figure 4.9 Detection of ExoGlow positive HG-EVs following exogenous labelling. (A-D) Detection of ExoGlow positive HG-EVs following endogenous labelling in culture. Representative images of control samples (A) ExoGlow dye only, (B) HG-EVs only, and (D) ExoGlow-HG-EVs treated with Triton X detergent. Data representative of n=3.

4.4.5 HiPSCs express distinct embryological markers NANOG and OCT4

To determine the functional effect of HAEC-HG-EVs uptake, an *in vitro* human cell model was developed. The reprogramming of autologous somatic cells into HiPSCs has provided a key translational technology to differentiate highly pure and functional pluripotent vascular stem cells from various embryological origins. HiPSCs were purchased from the Welcome Sanger Institute HiPSC Initiative. The source material of the HiPSC generation was skin tissue of a white British European male or normal disease status. Upon receipt, HiPSCs were cultured, phase-contrast images of HiPSC culture demonstrate typical iPSC morphology including a high nucleus: cytoplasm ratio, predominant nucleoli, and formation of compact colonies observed by phase-contrast microscopy at 4X and 10X magnification (Figure 4.10 A, B) HiPSCs were significantly enriched for *OCT4* and *NANOG* mRNA levels when compared to HAECs in culture (Figure 4.10 C, D).

The expression of embryological marker OCT4 and NE markers NESTIN and S100β were determined by ICC. Cells were fixed with 3.7% formaldehyde and stained with primary antibodies OCT4 (1:250), NESTIN (1:200), and S100β (1:100) overnight. To generate a fluorescent signal for staining, fluorophore-Alexa Fluor 488-conjugated secondary antibodies were added, and nuclei were stained with DAPI. Using a fluorescent microscope, these stains were visualised, imaged, and analysed to determine the expression of each protein. IgG controls (secondary antibody probing without primary antibody staining) were used to account for background fluorescence or off-target binding of secondary IgGs. The expression of embryological marker OCT4 and NE marker, NESTIN was detected in HiPSC colonies (Figure 4.11 A, B). However, HiPSCs were negative for the expression of NE marker S100β (Figure 4.11 C). Although both OCT4 and NESTIN were expressed in HiPSC colonies, OCT4 expression was abundant in all HiPSC cells within the colony. However, the expression of NESTIN was localised around the periphery of the colony. Positive cells were counted and compared against the total cell DAPI stain cell count for quantitative analysis and are presented as the fraction of positive cells compared to a negative cell control (Figure 4.11 D-F).

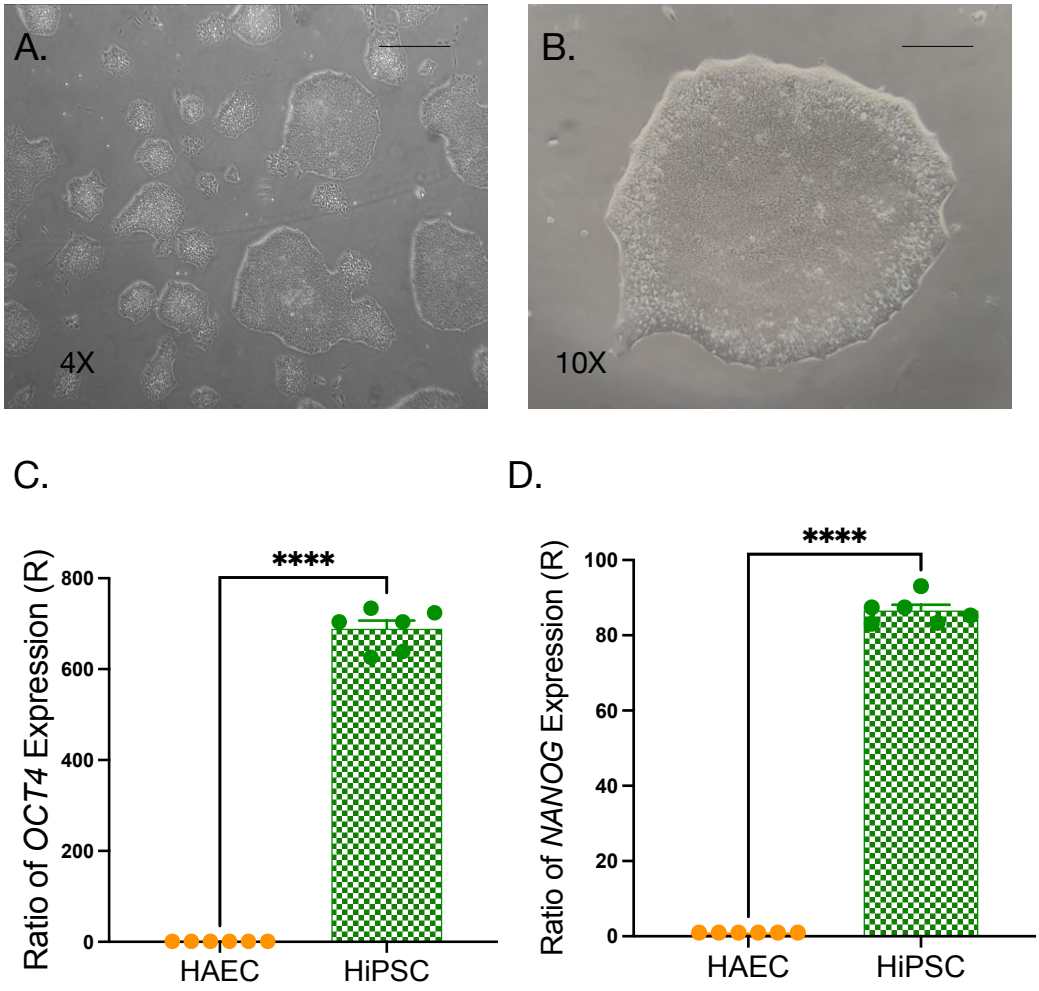

Figure 4.10 Characterisation of HiPSCs. (A) Phase-contrast images of HiPSCs in the culture at 4X and 10X magnification Scale bar representative of 20µm and 50µm respectively. (B) Relative mRNA levels of embryological markers *OCT4* and *NANOG* in HiPSCs. Data are expressed as the ratio of mRNA expression relative to *GAPDH* and are the mean ± SEM, n = 6, * $p \leq 0.05$ versus HAEC.

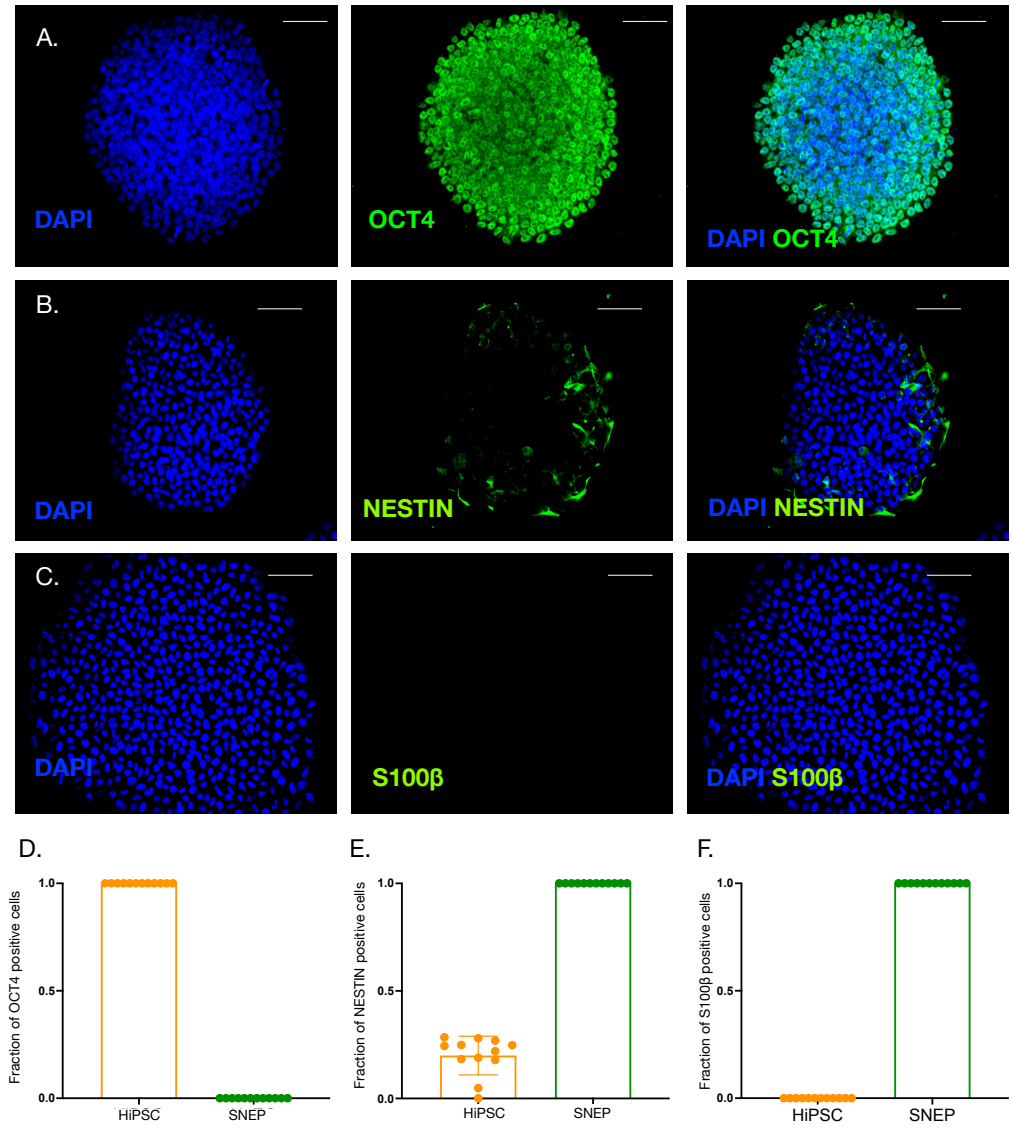

Figure 4.11 Characterisation of HiPSC by ICC. (A-C) Representative images of fluorescence staining of DAPI nuclei and immunocytochemical analysis of the expression embryological marker OCT4 and NE markers NESTIN (green), S100β in HiPSC colonies. (D-F) Fraction of OCT4+, NESTIN+ and S100β + cells. All images were taken using Olympus DP-50 fluorescent microscope. AlexaFluor 488 secondary antibody used for visualisation of primary antibody binding. All images are representative of n ≥ 12 images per experimental group from three independent cultures—scale bar representative of 50μm.

4.4.6 HiPSC differentiation to NE multipotent progenitor stem cells (NEP)

Several stem cell populations have been identified in the vasculature by several different research groups. The use of lineage tracing studies has confirmed that cells in a neointimal lesion may arise, at least in part, from a stem cell parent population (Wang *et al.*, 2018). $S100\beta^+$ stem cells have been shown to contribute to the development of a ligation-induced neointima through migration and differentiation (Di Luca *et al.*, 2021). As part of this study, HiPSCs were utilised to generate $S100\beta^+$ human NEPs to investigate the possible role of $S100\beta^+$ cells in vascular lesion formation. Prior to differentiation, HiPSC exhibited clear, distinct colony boundaries. Before differentiation, HiPSC colonies were first allowed to grow to approximately 20% confluency, keeping colony size relatively small (Figure 4.12 A). NE differentiation was carried out and phase-contrast microscopy was performed to monitor changes in cellular morphology during differentiation. Over three days, HiPSC began to lose defined colony borders (Figure 4.12 B, C). Colonies grew larger, giving rise to a NE morphology by day 7 (Figure 4.12 D). HiPSC-derived NEPs were maintained in culture using Essential 8™ Medium. Cells were harvested, and RNA was isolated from each sample. RNA samples were analysed by qRT-PCR to measure the expression of embryological marker *OCT4* and NE markers *NESTIN, S100β,* and *PAX6* compared to HiPSCs. Following NE differentiation, decreased *OCT4* and an increase in *NESTIN, S100β,* and *PAX6* mRNA levels were observed compared to HiPSC (Figure 4.13 A-D).

The expression of embryological marker OCT4 and NE markers NESTIN and S100β were determined by ICC staining as described in section 2.2.6.1. Cells were fixed with 3.7% formaldehyde and stained with primary antibodies OCT4 (1:250), NESTIN (1:200), and S100β (1:100) overnight. To generate a fluorescent signal for staining, fluorophore-Alexa Fluor 488-conjugated secondary antibodies were added, and nuclei were stained with DAPI. Using a fluorescent microscope, these stains were visualised, imaged, and analysed to determine the expression of each protein. IgG controls (secondary antibody probing without primary antibody staining) were used to account for background fluorescence or off-target binding of secondary IgGs. The expression of NE markers NESTIN and S100β was detected in NEPs (Figure 4.14 A, B). However, NEPs were negative for the expression of OCT4 (Figure 4.14 C). Although both NESTIN and S100β were expressed in NEPs, S100β was expressed in the cytoplasm. However, NESTIN expression was detected in the Golgi apparatus. Positive cells were counted and compared

against the total cell DAPI stain cell count for quantitative analysis and are presented as the fraction of positive cells compared to a negative cell control (Figure 4.14 D-F).

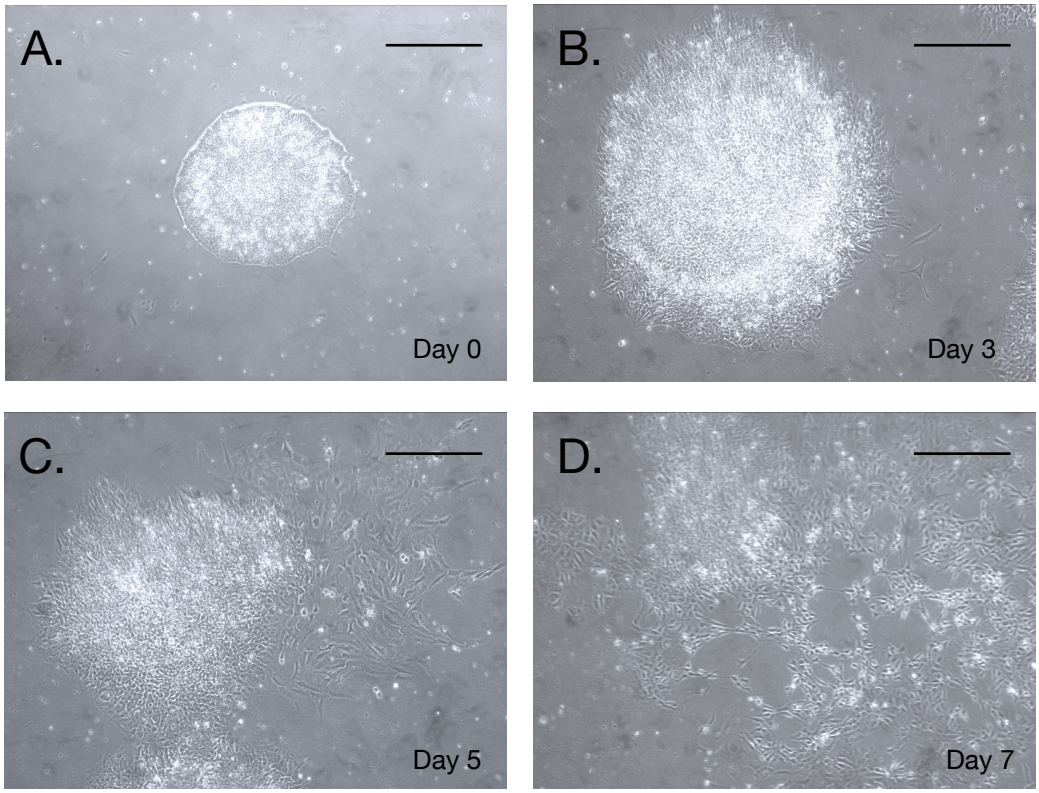

Figure 4.12 Timeline for induction of NEPs from HiPSC with chemically defined media. (A) Representative phase-contrast images of typical morphology of HiPSC colony in culture prior to differentiation. (B-D) Induction of NEP differentiation after 3,5 and 7 d following incubation in CDM supplemented with FGF2 (12 ng ml−1) and SB431542 (10 μM).Scale bar representative of 20μm respectively.

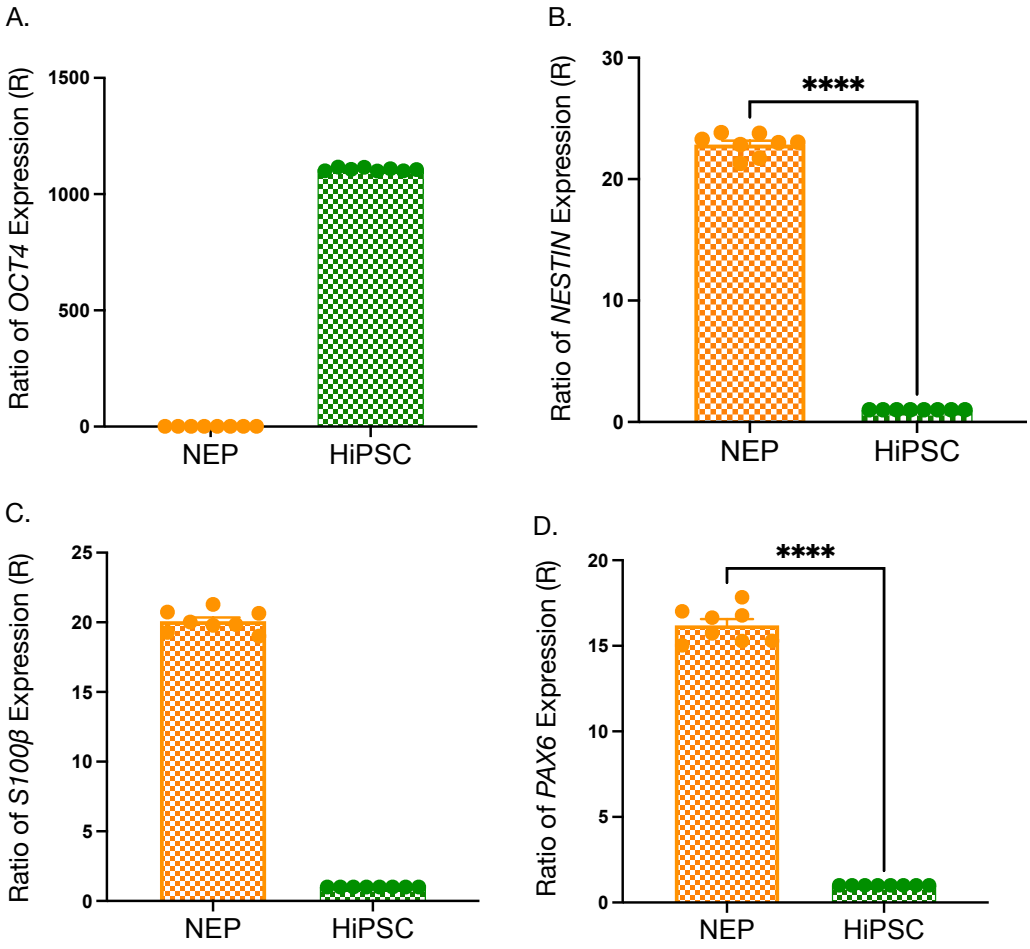

Figure 4.13 Characterisation of HiPSC-derived NEPs by qRT-PCR. (A) Relative levels of embryonic stem cell marker *OCT4* (A), *NESTIN* (B), *S100β* (C), and *PAX6* mRNA expression in NEPs (D) Data are expressed as the ratio of mRNA expression relative to *HPRT* and are the mean ± SEM, n = 8, * $p \leq 0.05$ versus NEP and * $p \leq 0.05$ versus HiPSC.

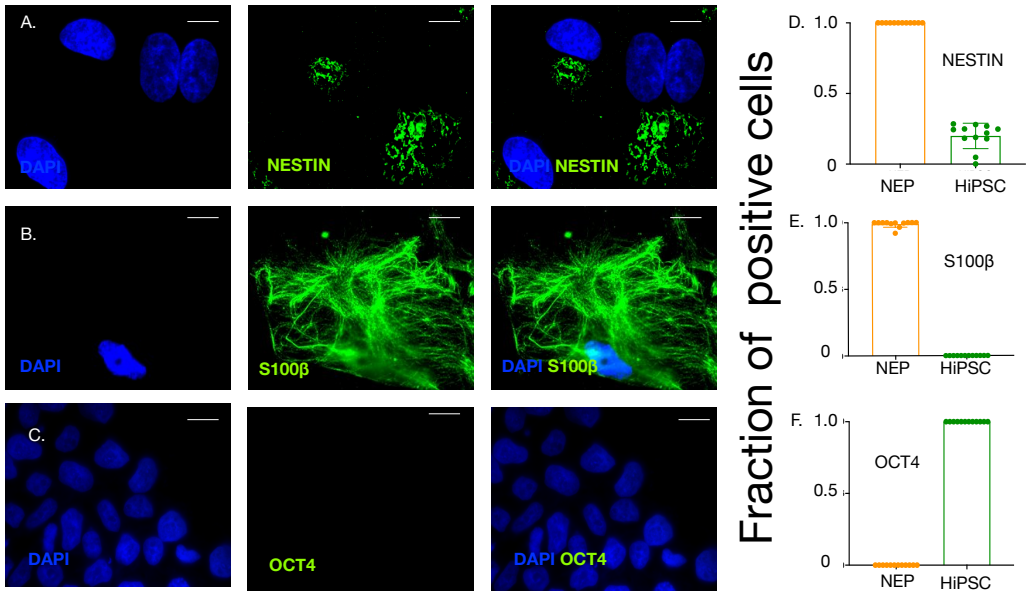

Figure 4.14 Characterisation of HiPSC-derived NEPs by ICC. (A-C) Representative images of fluorescence staining of DAPI nuclei and immunocytochemical analysis of NE markers NESTIN, S100β, and embryological marker OCT4 in HiPSC-derived NEP. (D-F) Fraction of $NESTIN^{+}$ $S100\beta^{+}$ and $OCT4^{+}$ cells. All images were taken using Olympus DP-50 fluorescent microscope. AlexaFluor 488 secondary antibody used for visualisation of primary antibody binding. All images are representative of n $\geq$ images per experimental group from three independent cultures—scale bar representative of 25µm.

4.4.7 TGF-β1/PDGF induces myogenic differentiation of HiPSC-NEP.

In order to generate embryologically defined myogenic (VSMC) subtypes, HiPSC-derived NEPs were cultured in DMEM supplemented with 10% FBS, 1% PS, TGFβ-1 (2ng/ml), and PDGF (10ng/ml) for 12 d. Following the myogenic differentiation protocol, phase-contrast analysis revealed a distinct change in cellular morphology from an appearance of small spindle neural-like cells (Figure 4.15 A) to large filamentous cells at day 12 (Figure 4.15 B). Cells were harvested, and RNA was isolated from each sample. RNA samples were analysed by qRT-PCR to measure the expression of NE markers *NESTIN* and *PAX6* and VSMC markers *CNN1* and *MYH11*. Following myogenic differentiation, a significant increase in CNN1 and MYH11 mRNA levels was observed (Figure 4.15 D, E) concomitant with a decrease in *NESTIN* and *PAX* levels (Figure 4.15 C, F).

The expression of NE markers NESTIN, S100β and VSMC markers CNN1 and MYH11 were determined by ICC as described in section 2.2.6.1. Cells were fixed with 3.7% formaldehyde and stained with primary antibodies NESTIN (1:200), S100β (1:100), CNN1 (1:200), and MYH11(1:50) overnight. To generate a fluorescent signal for staining, fluorophore-Alexa Fluor 488-conjugated secondary antibodies were added, and nuclei were stained with DAPI. Using a fluorescent microscope, these stains were visualised, imaged, and analysed to determine the expression of each protein. IgG controls (secondary antibody probing without primary antibody staining) were used to account for background fluorescence or off-target binding of secondary IgGs. The expression of CNN1 and MYH11 increased significantly in NEP-VSMC compared to NEPs (Figure 4.16 A-C). In contrast, NESTIN's expression decreased by ~60% in NEP-VSMC compared to NEPs (Figure 4.16 D). Positive cells were counted and compared against the total cell DAPI stain cell count for quantitative analysis and are presented as the fraction of positive cells compared to a negative cell control (Figure 4.16 E-G).

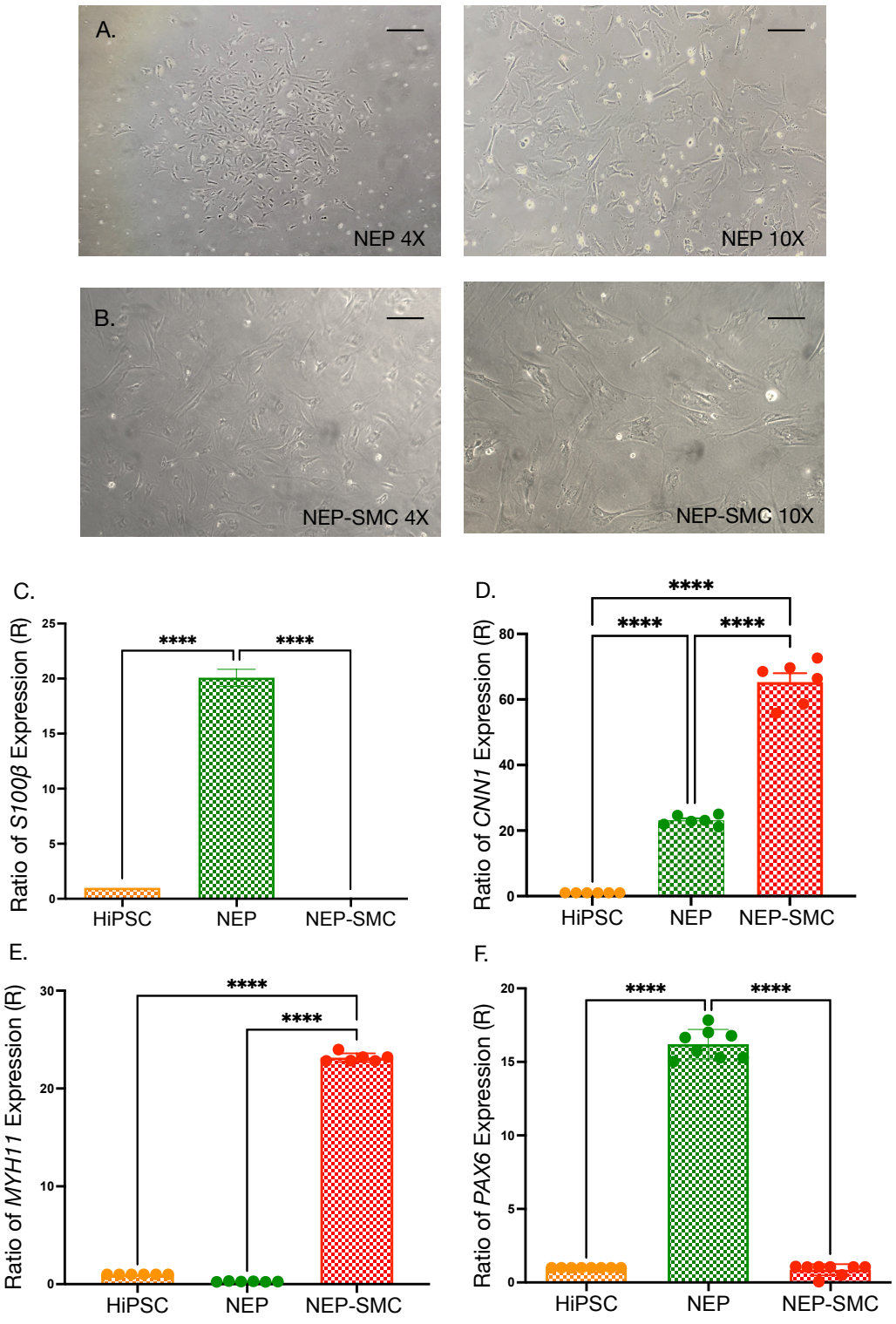

Figure 4.15 Characterisation of TGF-β1/PDGF-mediated myogenic differentiation of NEPs by qRT-PCR. (A) Phase-contrast images of morphological changes in NEP following VSMC myogenic differentiation at 4X and 10X magnification. Scale bar representative of 20µm and 50µm respectively. (B, C) Relative mRNA levels NE markers *S100β*, *PAX6,* and myogenic markers *CNN1*. Data are expressed as the ratio of mRNA expression relative to control and are the mean ± SEM, n = 6, * $p \leq 0.05$ versus HiPSC and * $p \leq 0.05$ versus NEP.

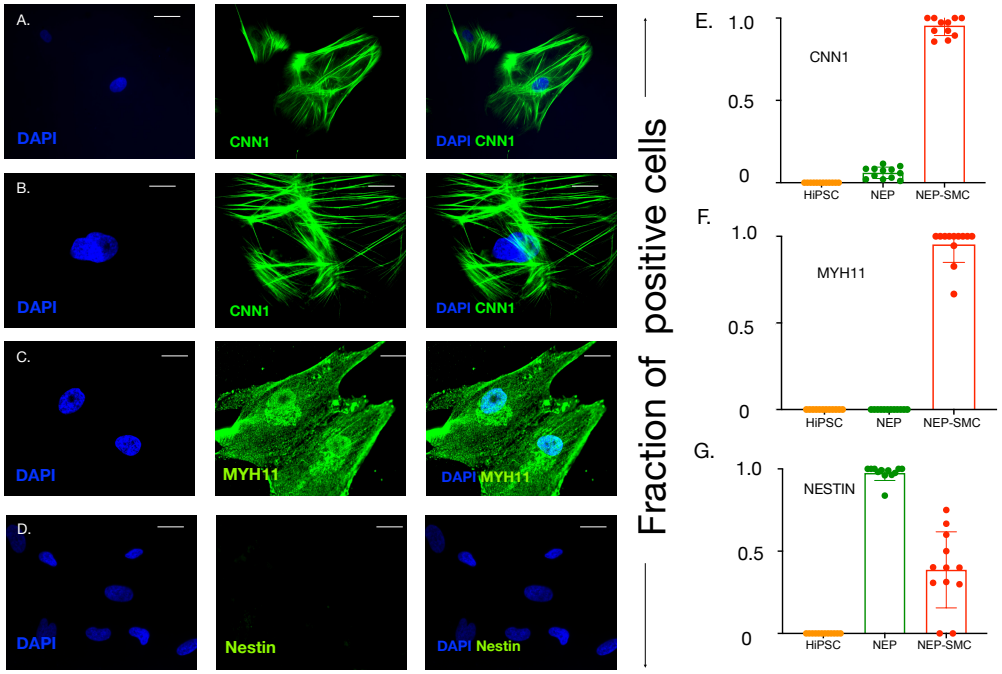

Figure 4.16 Characterisation of TGF-β1/PDGF-mediated myogenic differentiation of NEPs by ICC. (A-E) Representative images of fluorescence staining of DAPI nuclei and immunocytochemical analysis of the expression of myogenic markers CNN1, MYH11, NE markers S100β, and NESTIN. (F-1) Fraction of $CNN1^{+}$, MYH11+, and S100β+ cells after TGFβ-1/PDGF treatment. All images were taken using Olympus DP-50 fluorescent microscope. AlexaFluor 488 secondary antibody used for visualisation of primary antibody binding. All images are representative of $n \geq 12$ images per experimental group from three independent cultures—scale bar representative of 25µm.

4.4.8 Non-chemical spontaneous differentiation of HiPSC to NE progenitors (SNEP)

HiPSC differentiation to various progenitor lineages has been previously defined (Cheung *et al.*, 2014). Although chemically defined HiPSC differentiation protocols have advanced the generation of embryologically defined VSMCs, there are several limitations, including (i) the preparation of HiPSC colonies for differentiation to ensure correct colony sizes are obtained (ii) the cost of associated factors using to drive various progenitor stem cells in culture (iii) optimisation of maintenance media used to maintain progenitor stem cell lineages in culture. Lineage tracing studies carried out by our research group have shown the role of resident S100β+ progenitor stem cells during the progression of neointimal in atherosclerosis pathogenesis (Di Luca *et al.*, 2021). With this in mind, an alternative HiPSC-NEP differentiation method in the absence of chemically defined stimuli was developed, reducing the cost associated with CDM culture and the necessity to prepare HiPSC colonies of distinct size and colony formation.

HiPSC-derived SNEPs were generated before phase-contrast microscopy was performed to monitor the migration of peripheral HiPSC cells and the loss of distinct colony borders (Figure 4.17 A). Following the migration of peripheral cells, HiPSC colonies were removed from the culture as described in Section 2.2.3.3. Expansion of SNEPs was achieved by day 10 (Figure 4.17 B). HiPSC-derived SNEPs were maintained in culture using Essential 8™ complete medium. Although both HiPSC-derived NEPs and SNEPS were maintained in Essential 8™ complete medium their morphologies differed as SNEPs resembled a more neural like morphology with distinct elongated lamopodia.

Cells were harvested, and RNA was isolated from each sample. RNA samples were analysed by qRT-PCR to measure the expression of embryological marker *OCT4* and NE markers *NESTIN, S100β,* and *PAX6* compared to HiPSCs. Following SNEP differentiation, a significant decrease in *OCT4* and an increase in *NESTIN, S100β,* and *PAX6* mRNA levels were observed compared to HiPSC (Figure 4.17 C-F).

The expression of embryological marker OCT4 and NE markers NESTIN and S100β were determined by immunocytofluorescence staining as described in section 2.2.6.1. Cells were fixed with 3.7% formaldehyde and stained with primary antibodies OCT4 (1:250), NESTIN (1:200), and S100β (1:100) overnight. To generate a fluorescent signal

for staining, fluorophore-Alexa Fluor 488-conjugated secondary antibodies were added, and nuclei were stained with DAPI. Using a fluorescent microscope, these stains were visualised, imaged, and analysed to determine the expression of each protein. IgG controls (secondary antibody probing without primary antibody staining) were used to account for background fluorescence or off-target binding of secondary IgGs. The expression of NE markers NESTIN and S100β was detected in SNEPs (Figure 4.18 A-D). SNEPs were negative for the expression of OCT4 (Figure 4.18 E). Positive cells were counted and compared against the total cell DAPI stain cell count for quantitative analysis and are presented as the fraction of positive cells compared to a negative cell control (Figure 4.18 F-H).

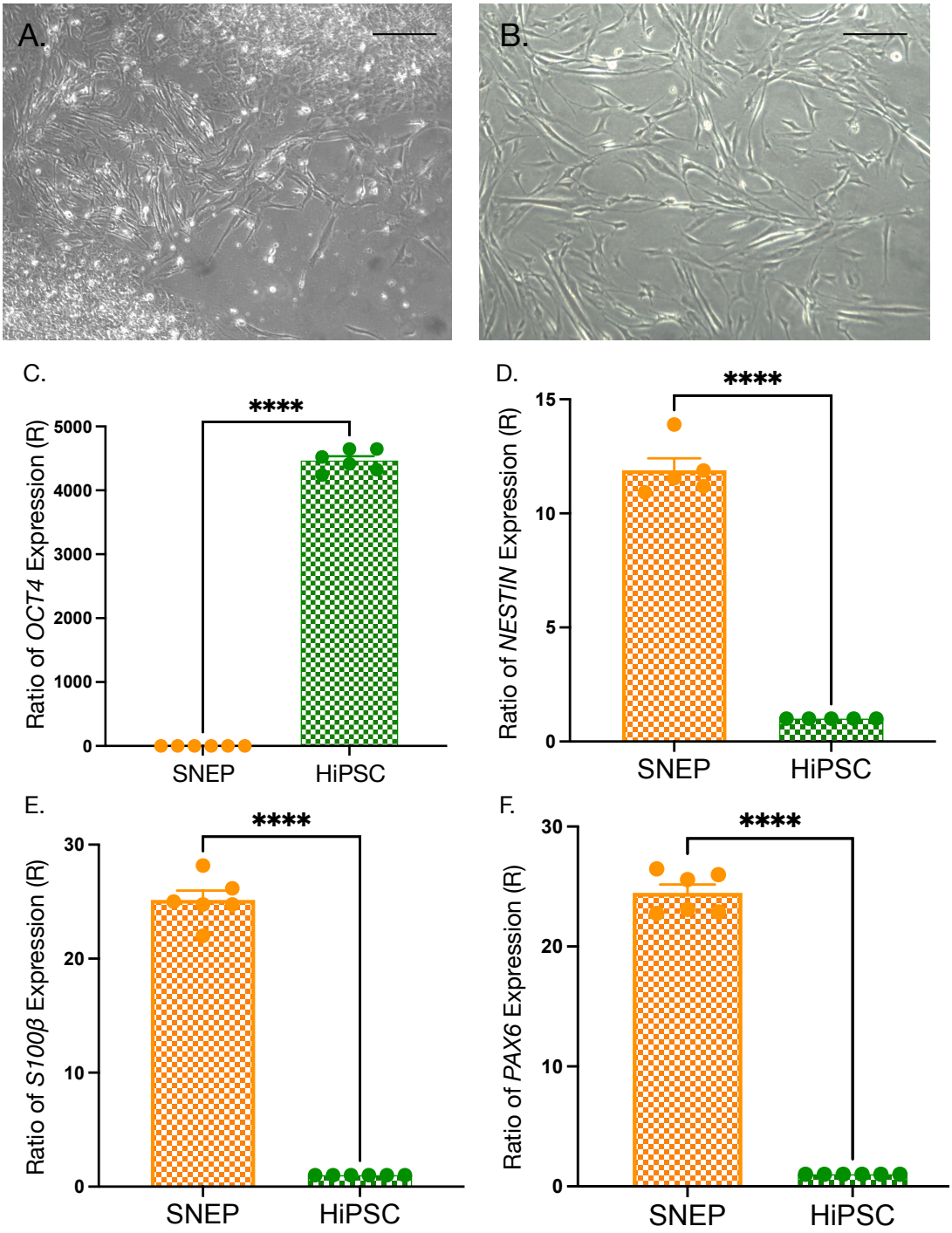

Figure 4.17 Characterisation of HiPSC-derived SNEPs by qRT-PCR. (A, B) Representative phase-contrast images following induction of NE differentiation after 7 d. Scale bar representative of 20µm and 50µm respectively. (C-F) Relative levels of embryological stem cell marker *OCT4* and NE markers, *NESTIN*, *S100β*, and *PAX6* mRNA expression in SNEPs (D) Data are expressed as the ratio of mRNA expression relative to *HPRT*. They are the mean ± SEM, n = 6, * $p \leq 0.05$ versus SNEP and * $p \leq 0.05$ versus HiPSC.

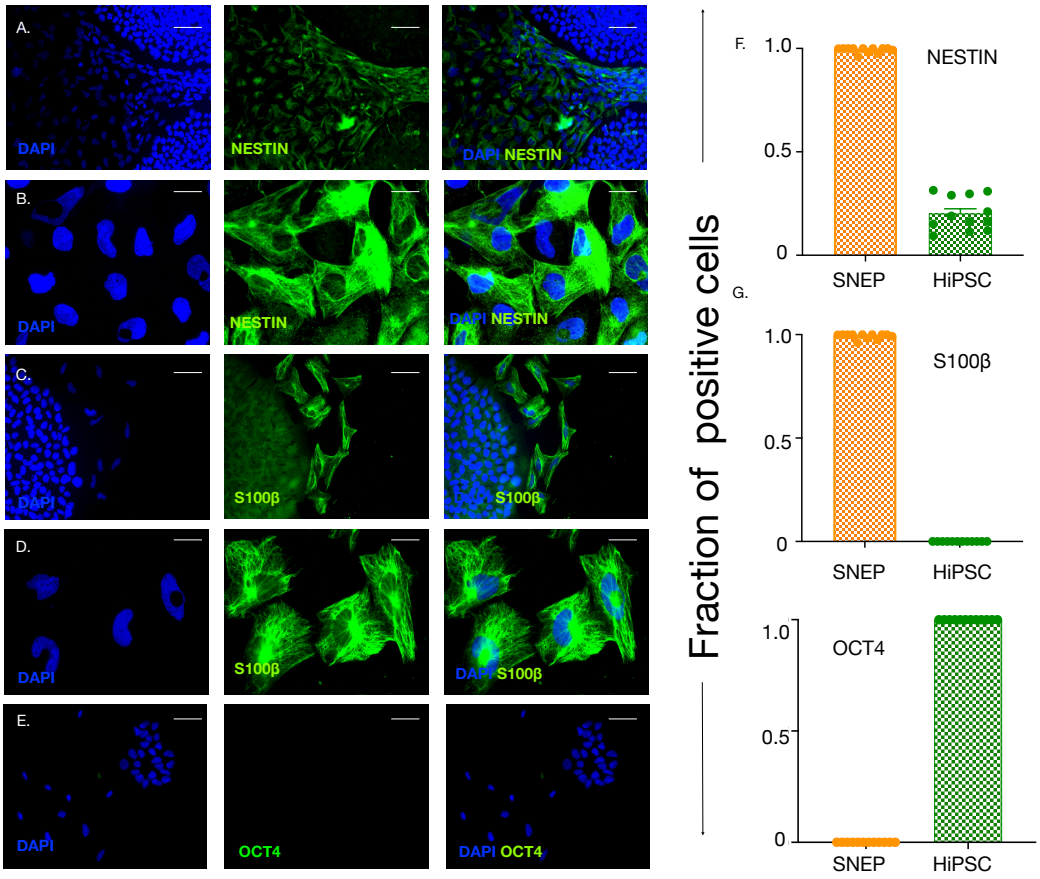

Figure 4.18 Characterisation of HiPSC-derived SNEPs by ICC. (A-E) Representative images of fluorescence staining of DAPI nuclei and immunocytochemical analysis of NE markers NESTIN, S100β, and embryological marker OCT4 in HiPSC-derived SNEP. Fraction of NESTIN+ S100β+ and OCT4+, cells. All images were taken using Olympus DP-50 fluorescent microscope. AlexaFluor 488 secondary antibody used for visualisation of primary antibody binding. All images are representative of n ≥6 images per experimental group from three independent cultures—scale bar representative of 50μm (A,C,E) and 25μm (B,D) respectively.

4.4.9 TGF-β1/PDGF induces myogenic differentiation of NE progenitor stem cells into smooth muscle cell subtypes.

In order to generate embryologically defined myogenic (VSMC) subtypes, HiPSC-derived SNEPs were cultured in DMEM supplemented with 10% FBS, 1% PS, TGF-β1 (2ng/ml), and PDGF (10ng/ml) for 12 days. Following the myogenic differentiation protocol, phase-contrast analysis revealed a distinct change in cellular morphology from an appearance of small spindle neural-like cells (Figure 4.19 A) to large filamentous cells (Figure 4.19 B). Cells were harvested, and RNA was isolated from each sample. RNA samples were analysed by qRT-PCR to measure the expression of NE markers *NESTIN* and *PAX6* and VSMC markers *CNN1* and *MYH11*. Following myogenic differentiation, a significant increase in CNN1 and MYH11 mRNA levels was observed (Figure 4.19 F, G) concomitant with a decrease in *NESTIN*, *S100β,* and *PAX* levels (Figure 4.19 C, D, E).

The expression of NE markers NESTIN, S100β and VSMC markers CNN1 and MYH11 were determined by ICC as described in section 2.2.6.1. Cells were fixed with 3.7% formaldehyde and stained with primary antibodies NESTIN (1:200), S100β (1:100), CNN1 (1:200), and MYH11(1:50) overnight. To generate a fluorescent signal for staining, fluorophore-Alexa Fluor 488-conjugated secondary antibodies were added, and nuclei were stained with DAPI. Using a fluorescent microscope, these stains were visualised, imaged, and analysed to determine the expression of each protein. IgG controls (secondary antibody probing without primary antibody staining) were used to account for background fluorescence or off-target binding of secondary IgGs. The expression of CNN1 and MYH11 in SNEP-VSMC was significantly increase compared to SNEPs (Figure 4.20 A-C). In contrast, the expression of NESTIN and was significantly decreased in SNEP-VSMC in comparison to SNEPs (Figure 4.20 D, E). Positive cells were counted and compared against the total cell DAPI stain cell count for quantitative analysis and are presented as the fraction of positive cells compared to a negative cell control (Figure 4.20 F-I).

To evaluate the localisation of NESTIN positive expression in SNEP and SNEP-VSMCs and morphometric changes in cell size and shape, single cells FACs analysis was conducted using the Image Stream™. SNEP cells displayed positive expression localised

in the cytoplasm compared to IgG endogenous control (Figure 4.21). In contrast, SNEP-VSMCs showed no indication of NESTIN-positive cells. Furthermore, morphometric analysis of images taken using an internal CCD camera showed increased cell size following differentiation of SNEP to SNEP-VSMCs (Figure 4.22).

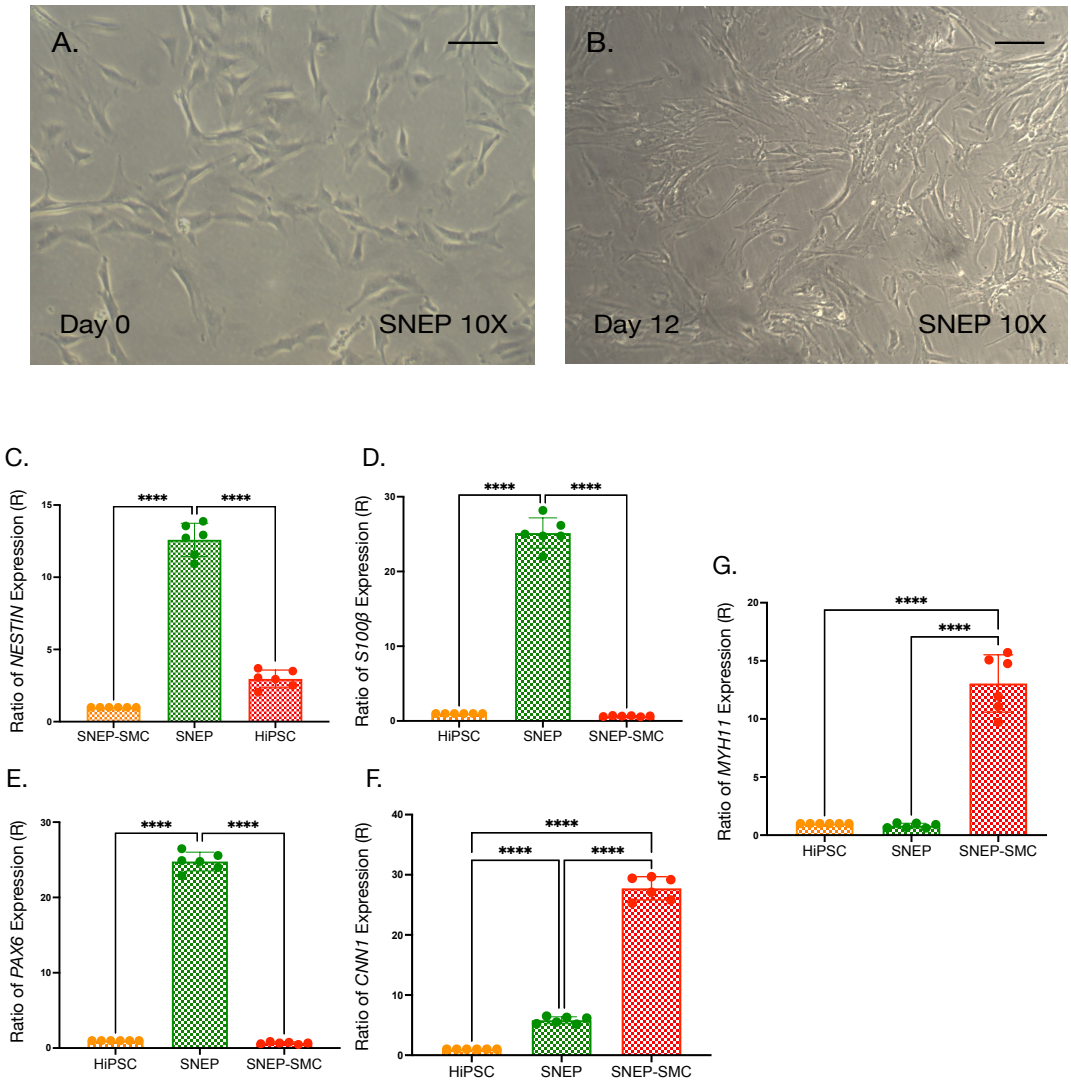

Figure 4.19 Characterisation of TGF-β1/PDGF-mediated myogenic differentiation of SNEPs by qRT-PCR. (A) Phase-contrast images of morphological changes in SNEP following VSMC differentiation at 4X and 10X magnification. Scale bar representative of 20µm. (B, C) Relative mRNA levels NE markers *NESTIN*, *S100β*, *PAX6,* and myogenic markers *CNN1 and MYH11*. Data are expressed as the ratio of mRNA expression close to control and are the mean ± SEM, n = 6, * $p \leq 0.05$ versus HiPSC and * $p \leq 0.05$ versus SNEP-VSMC.

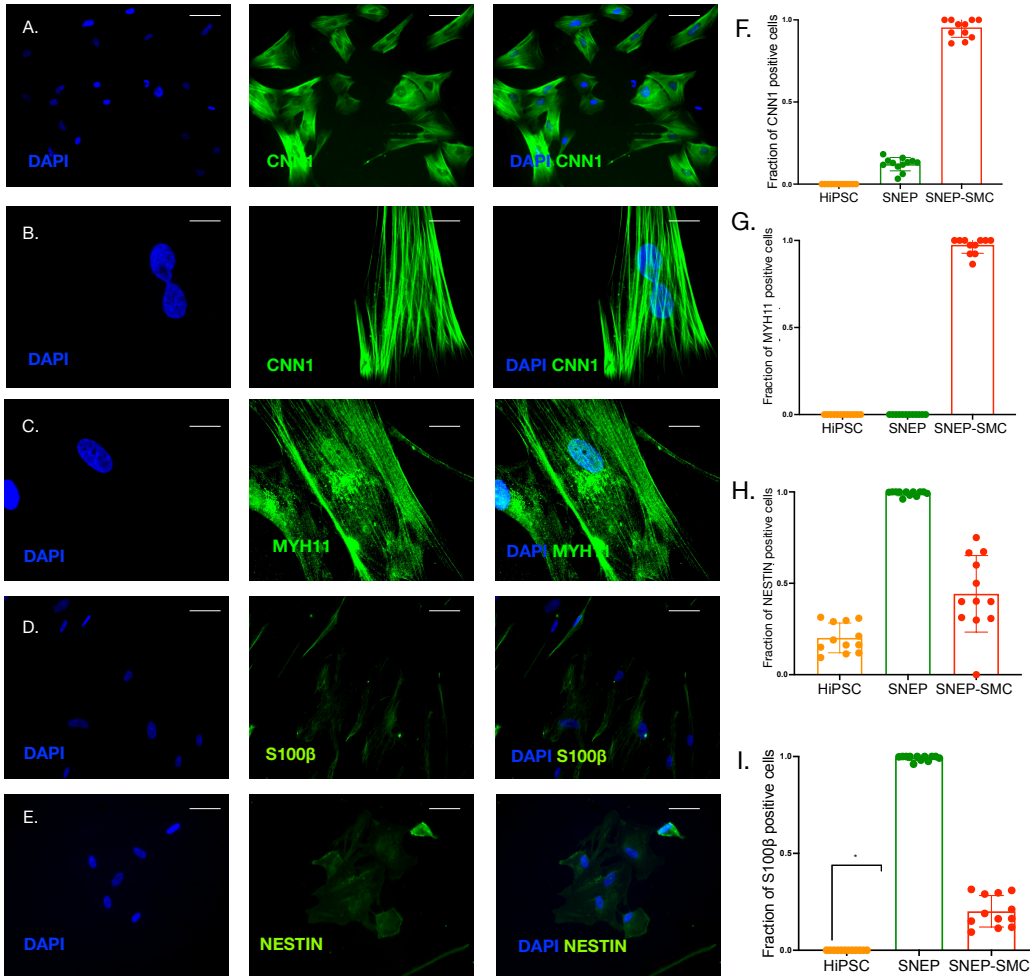

Figure 4.20 Characterisation of TGF-β1/PDGF-mediated myogenic differentiation of SNEPs by ICC. (A-E) Representative images of fluorescence staining of DAPI nuclei and immunocytochemical analysis of the expression of myogenic markers CNN1, MYH11, NE markers S100β , and NESTIN. (F-1) Fraction of $CNN1^{+}$, MYH11+, and S100β+ cells after TGFβ-1/PDGF treatment. All images were taken using Olympus DP-50 fluorescent microscope. AlexaFluor 488 secondary antibody used for visualisation of primary antibody binding. All images are representative of n ≥ 12 images per experimental group from three independent cultures—scale bar representative of 50μm.

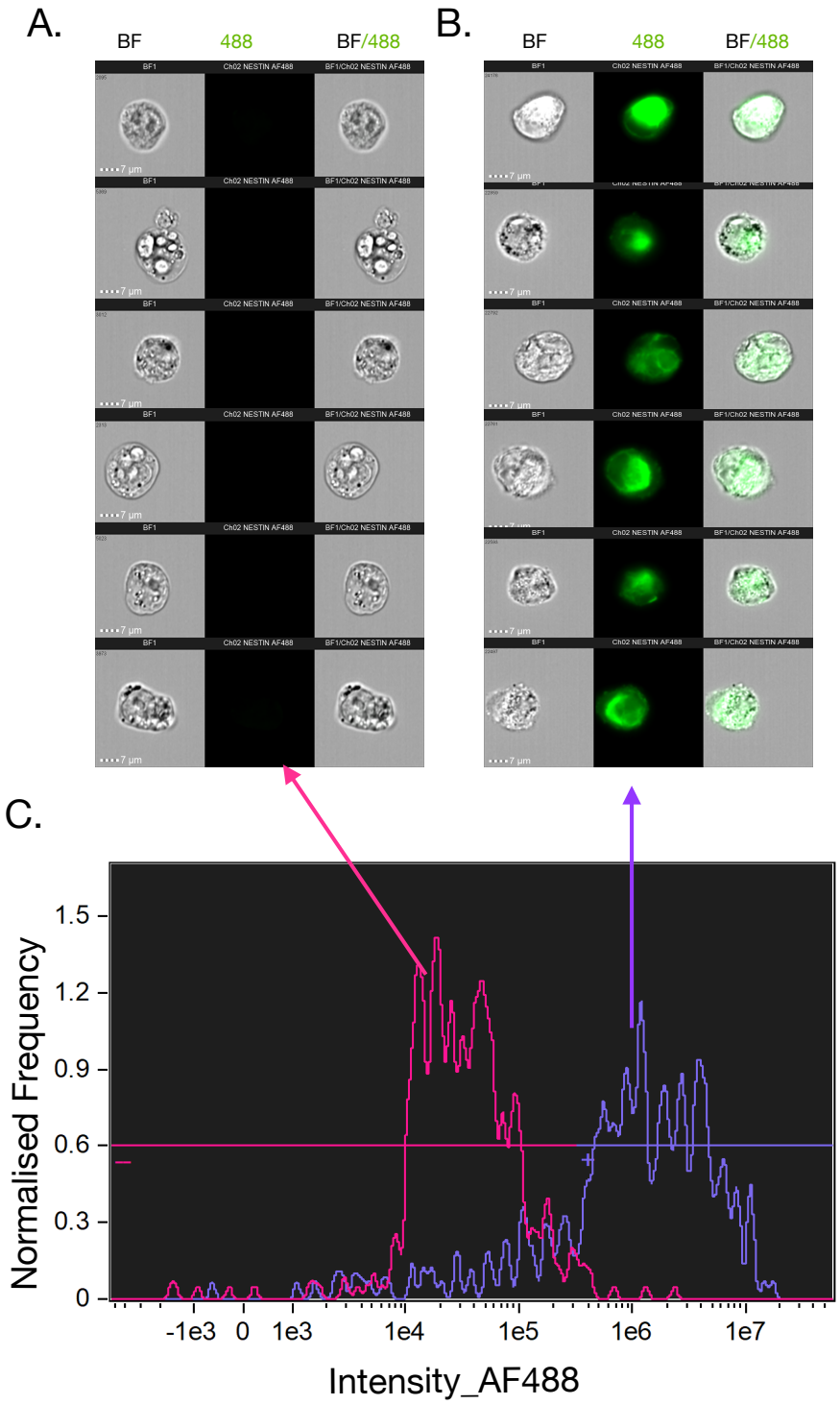

Figure 4.21 Single Cell Flow Cytometry and morphometric analysis of HiPSC-derived SNEPs. (A) Representative images of SNEP-IgG cells using a bright filed CCD camera and 488 detection channel (B) Representative images of Nestin positive SNEP using a bright-field CCD camera and 488 detection channel (C) Histogram representation of IgG and NESTIN positive expression in SNEP IgG (pink) and SNEP-NESTIN (purple) populations. Data analysis was carried out using the ImageStream MKII, n=3.

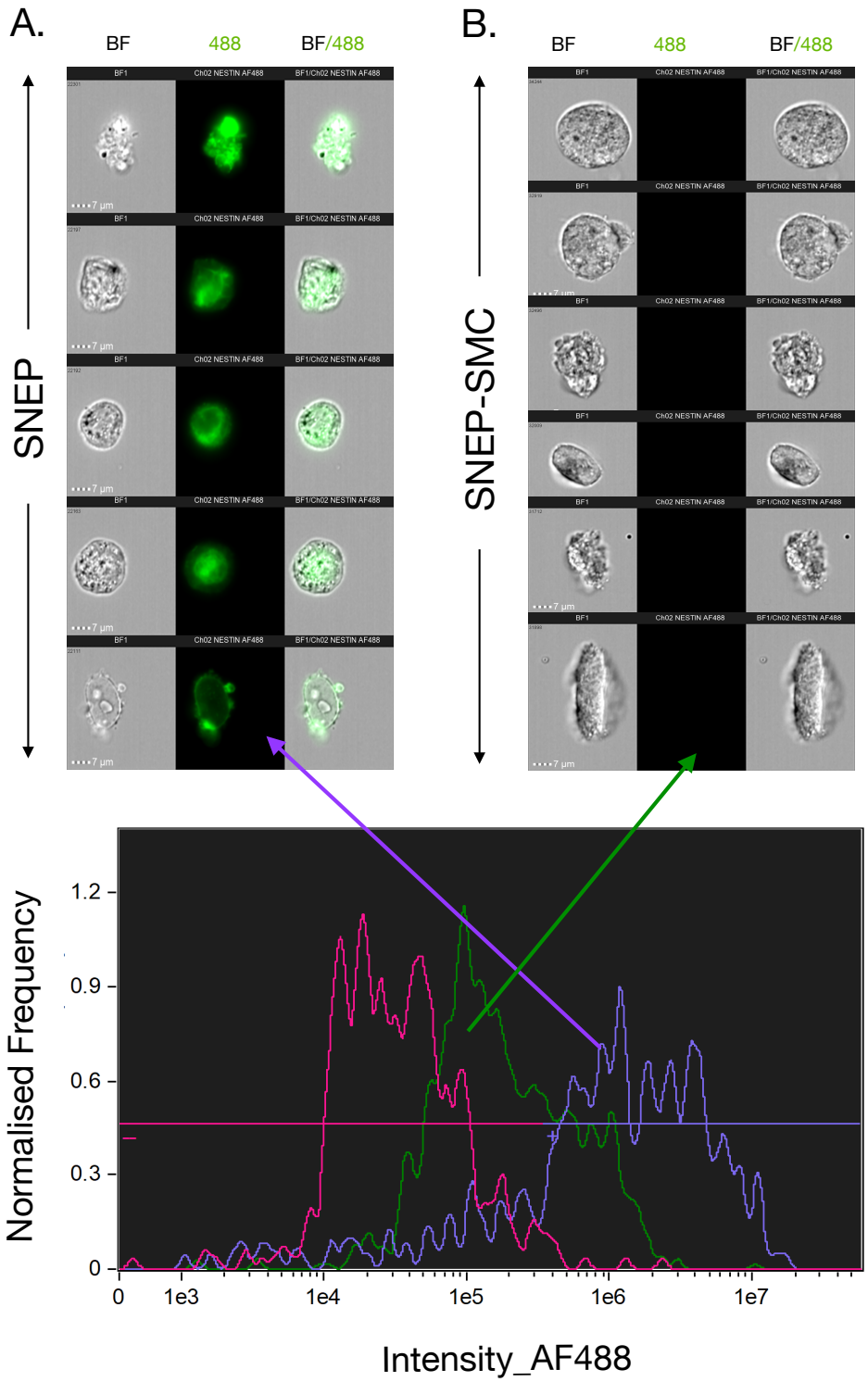

Figure 4.22 Single cell Flow Cytometry and morphometric analysis of HiPSC-derived SNEPs and SNEP-VSMCs. (A) Representative images of SNEP-Nestin cells using a bright filed CCD camera and 488 detection channel (B) Representative images of SNEP-VSMC-Nestin cells using a bright filed CCD camera and 488 detection channel (C) Histogram representation of NESTIN positive expression in SNEP IgG (pink) and SNEP-Neston (purple) and SNEP-VSMC populations. Data analysis was carried out using the ImageStreamX MKII, n=3.

4.4.10 Recombinant Sonic Hh induces myogenic differentiation of SNEP progenitor stem cells into smooth muscle cell subtypes

Having previously shown the role of EV-dependent activation of Hh signalling in rMVSCs in Chapter 3 Section 3.3.7, we sought to validate this finding using our human *in vitro* model. To confirm HiPSC-derived SNEPs were capable of undergoing rSHh-mediated myogenic differentiation, SNEPs were exposed to rSHh (1.0µg/ml) and rSHh + Smo inhibitor, cyclopamine (15mM). Having previously demonstrated TGFβ-1/PDGF mediated SNEP VSMC differentiation, cells were also treated in parallel with TGF-β1 (2ng/ml) and PDGF (10ng/ml) as a positive control for myogenic differentiation.

SNEPS were seeded in 6-well plates at a density of 50,000 cells/well. On day 0, SNEPs were washed using HBSS and treated, rSHh (1.0µg/ml), rSHh/cyclopamine (15mM) and TGF-β1 (2ng/ml) and PDGF (10ng/ml) for 12 d. Following the differentiation protocol, phase-contrast images revealed a distinct change in cellular morphology from small spindle neural-like cells (Figure 4.23 A, C) to large filamentous cells (Figure 4.23 B, D). Cells were harvested, and RNA was isolated from each sample. RNA samples were analysed by qRT-PCR to measure the expression of VSMC markers *CNN1* and *MYH11*. Following VSMC differentiation, a significant increase in CNN1 and MYH11 was observed in rSHh, and TGFβ-1 (2ng/ml), and PDGF treated SNEPs. This response was attenuated in samples treated with rSHh +cyclopamine (Figure 4.23 E, F).

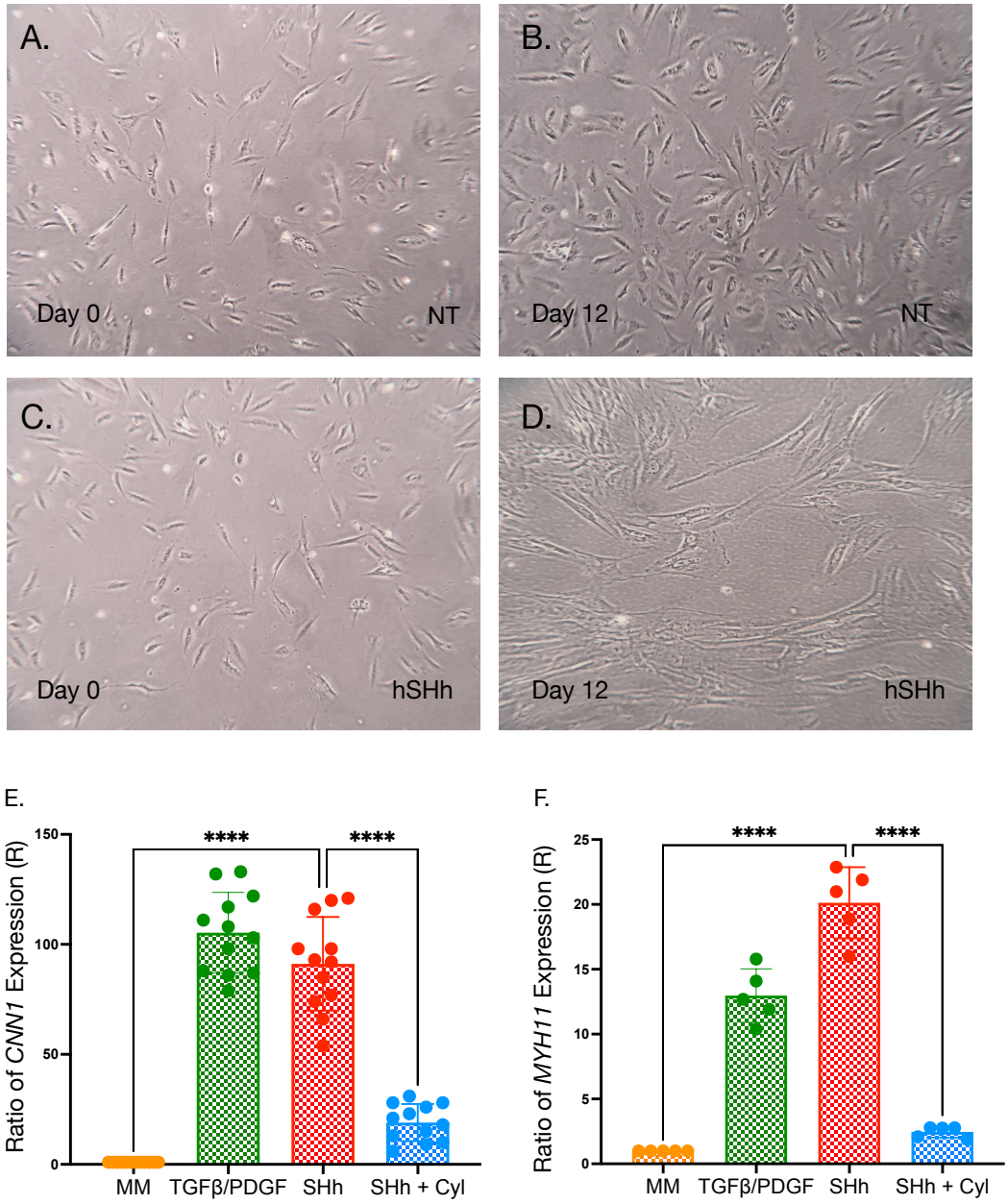

Figure 4.23 Recombinant rSHh stimulation of Hh-mediated myogenic (VSMC) differentiation of SNEPs. (A-D) Phase-contrast images of morphological changes in SNEPs in culture pre-and-post rSHh treatment at 4X and 10X magnification. Scale bar representative of 20µm and 50µm respectively. **(**E, F) Relative levels of CNN1 and MYH11 mRNA expression in SNEPs following rSHh treatment. Data are expressed as the ratio of mRNA expression relative to control and are the mean ± SEM, n = 9, * $p \leq 0.05$ versus MM and * $p \leq 0.05$ versus rSHh + cyclopamine.

4.4.11 Human-induced pluripotent stem cell (HiPSC) differentiation to paraxial (PM) and lateral mesoderm (LM) progenitor stem cells.

Prior to differentiation, HiPSC exhibited clear, distinct colony boundaries. Before differentiation, HiPSC colonies were first allowed to grow to approximately 20% confluency, keeping colony size relatively small (Figure 4.24 A, B), (Figure 4.25 A, B). Paraxial (PM) and lateral mesoderm (LM) differentiation was carried out. Phase-contrast microscopy was performed to monitor changes in cellular morphology during differentiation. Over three days, HiPSC began to lose their defined borders (Figure 4.24 C-D) (Figure 4.25 C-D). Colonies grew larger, giving rise to a mesoderm morphology by day 7 (Figure 4.24 E), (Figure 4.25 E).

Following differentiation, cells were harvested, and RNA was isolated from each sample. RNA samples were analysed by qRT-PCR to measure the relative levels of PM-associated markers *TBX6, PAX1,* and *PAX6* and LM-associated markers *KDR, PAX1,* and *PAX6*. The HiPSC-derived PM progenitor cells had increased expression of *TBX6* and *PAX1* compared to HiPSCs (Figure 2.24 F, G). In contrast, the expression of *PAX6* in PM-progenitors was significantly decreased compared to HiPSC-derived NEPs (Figure 2.24 H). HiPSC-derived LM progenitor cells had increased expression of *KDR* and *PAX1* compared to HiPSCs (Figure 2.25 F, G). In contrast, the expression of *PAX6 in* LM-progenitors was significantly decreased compared to HiPSC-derived NEPs (Figure 2.25 H).

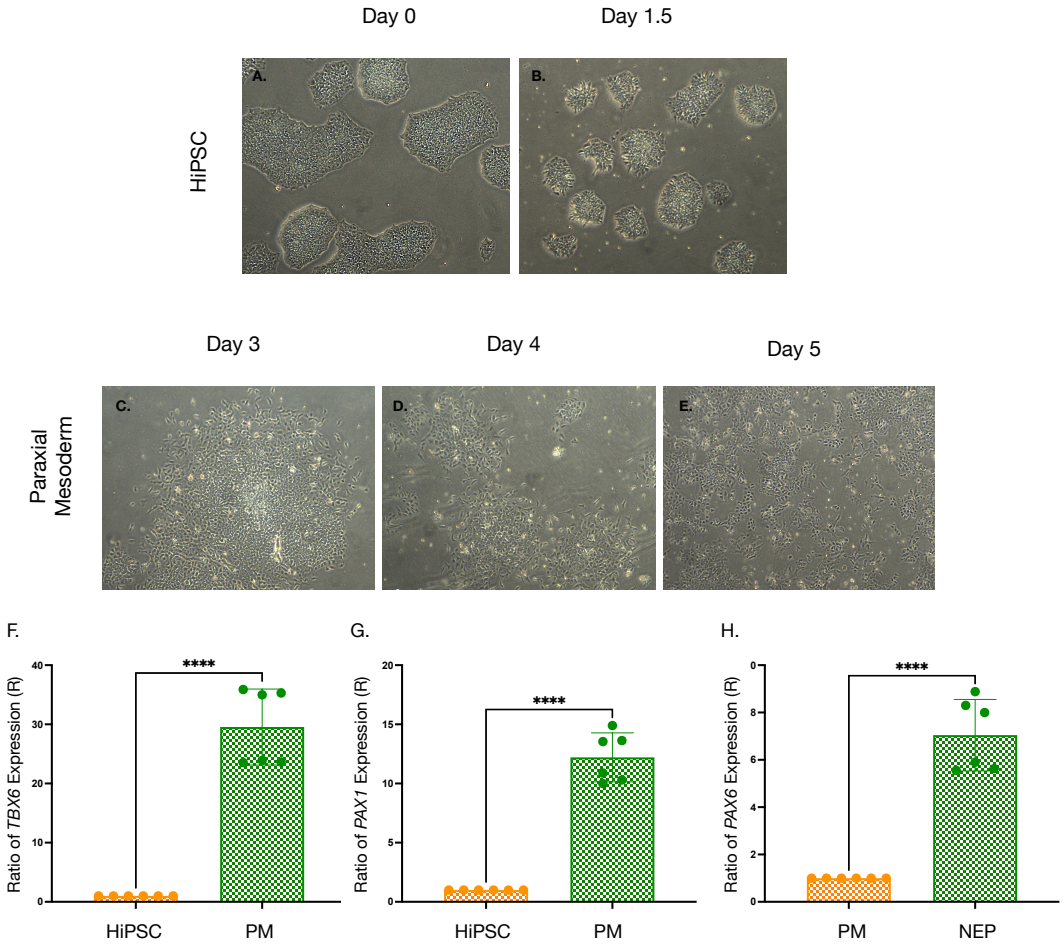

Figure 4.24 Timeline for induction of PM progenitors from HiPSC with chemically defined media. (A) Representative phase-contrast images of typical morphology of HiPSC colony in culture before PM differentiation. (B-E) Induction of PM differentiation after 1.5, 3, 4and 5 d following incubation in CDM supplemented with FGF2 (12 ng ml−1) and SB431542 (10 µM). (F-H) PMs' relative levels of PM markers TBX6, PAX1, and NE marker PAX6 mRNA expression in PMs following differentiation. Data are expressed as the ratio of mRNA expression relative to HPRT and are the mean ± SEM, n = 6, * $p \leq 0.05$ versus HiPSC and * $p \leq 0.05$ PM

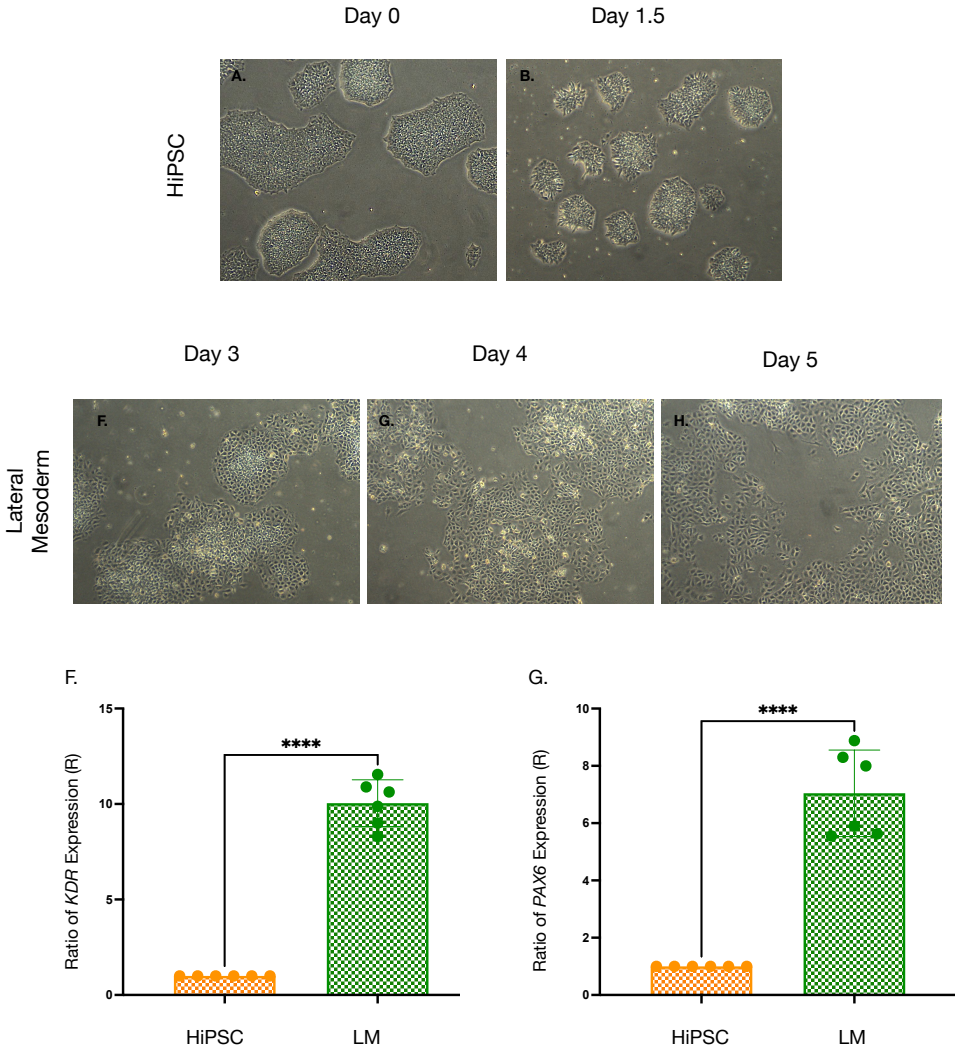

Figure 4.25 Timeline for induction of LM progenitors from HiPSC with chemically defined media. (A) Representative phase-contrast images of typical morphology of HiPSC colony in culture before LM differentiation. (B-E) Induction of LM differentiation after 1.5, 3, 4and 5 d following incubation in CDM supplemented with FGF2 (12 ng ml−1) and SB431542 (10 µM). (F-H) Relative levels of PM markers KDR, PAX1, and NE marker PAX6 mRNA expression in PMs following differentiation. Data are expressed as the ratio of mRNA expression relative to HPRT and are the mean ± SEM, n = 6, * $p \leq 0.05$ versus HiPSC and * $p \leq 0.05$ LM

4.4.12 TGF-β1/PDGF induces myogenic differentiation of PM progenitor stem cells into smooth muscle cell subtypes.

In order to generate embryologically defined myogenic (VSMC) subtypes, HiPSC-derived PM progenitors were cultured in DMEM supplemented with 10% FBS, 1% PS, TGF-β1 (2ng/ml), and PDGF (10ng/ml) for 12 days. A distinct increase in the size of the nucleus and span of the cytoplasm was observed following myogenic of differentiation of PM progenitor stem cells. In addition, the development of continuous myofilaments extending across the cytoplasm was observed in myogenic progeny indicative of the transition of these cells to a defined contractile function. Cells were harvested, and RNA was isolated from each sample. The expression of VSMC markers CNN1 and MYH11 were determined by ICC as described in section 2.2.6.1. Cells were fixed with a 3.7% formaldehyde and stained with primary antibodies CNN1 (1:200) and MYH11(1:50). To generate a fluorescent signal for staining, fluorophore-Alexa Fluor 488-conjugated secondary antibodies were added, and nuclei were stained with DAPI. Using a fluorescent microscope, these stains were visualised, imaged, and analysed to determine the expression of each protein. IgG controls (secondary antibody probing without primary antibody staining) were used to account for background fluorescence or off-target binding of secondary IgGs. Positive cells were counted and compared against the total cell DAPI stain cell count for quantitative analysis and are presented as the fraction of positive cells compared to a negative cell control. The number of CNN1 and MYH11 positive cells increased by ~ 80% in PM-VSMC compared to PMs (Figure 4.26 A-C), (Figure 4.27 A-C).

RNA samples were analysed by qRT-PCR to measure the expression of VSMC markers *CNN1* and *MYH11*. Following myogenic differentiation, a significant increase in CNN1 and MYH11 relative mRNA levels was observed in TGFβ- PDGF treated cells compared to PM and HiPSCs (Figure 4.26 D), (Figure 4.27 D).

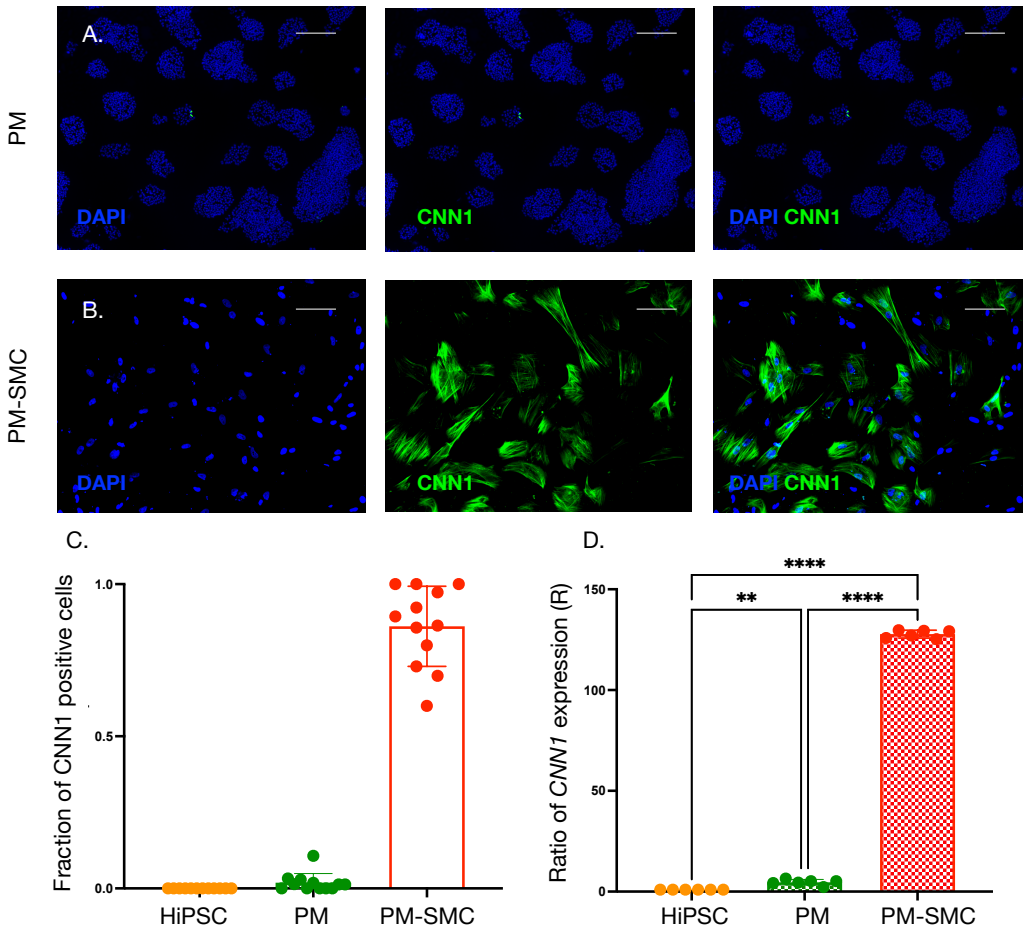

Figure 4.26 Characterisation of TGF-β1/PDGF-mediated myogenic differentiation of PMs by ICC. (A, B) Representative images of fluorescence staining of DAPI nuclei and immunocytochemical analysis of the expression of myogenic marker CNN1, (C) Fraction of $CNN1^{+}$ cells after TGFβ-1/PDGF treatment. All images were taken using Olympus DP-50 fluorescent microscope. AlexaFluor 488 secondary antibody used for visualisation of primary antibody binding. All images are representative of $n \geq 12$ images per experimental group from three independent cultures—scale bar representative of 50μm (D) Relative levels of myogenic marker *CNN1* mRNA expression in PMs following VSMC differentiation. Data are expressed as the ratio of mRNA expression relative to *HPRT* and are the mean ± SEM, n = 6, * $p \leq 0.05$ versus HiPSC and * $p \leq 0.05$ PM.

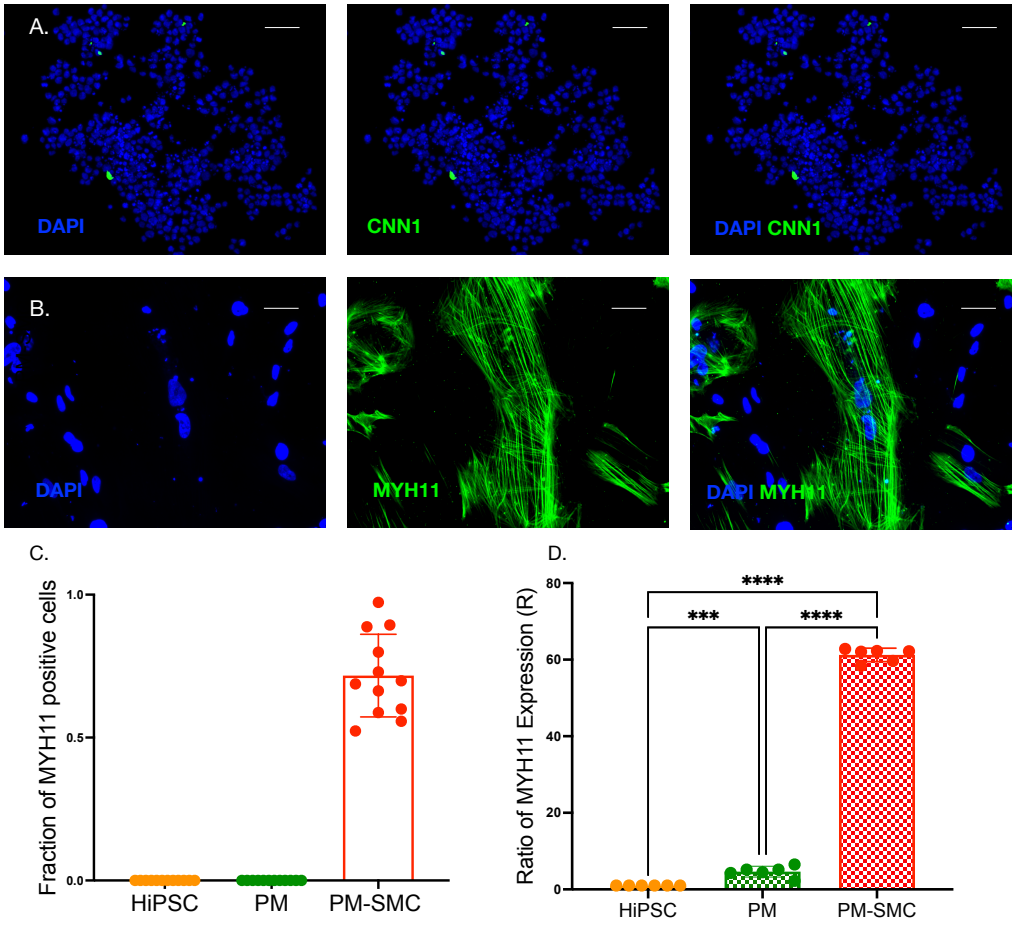

Figure 4.27 Characterisation of TGFβ-1/PDGF-mediated VSMC differentiation of PMs by ICC. (A, B) Representative images of fluorescence staining of DAPI nuclei and immunocytochemical analysis of the expression of myogenic marker MYH11 (C) Fraction of $CNN1^{+}$ cells after TGFβ-1/PDGF treatment. All images were taken using Olympus DP-50 fluorescent microscope. AlexaFluor 488 secondary antibody used for visualisation of primary antibody binding. All images are representative of $n \geq 12$ images per experimental group from three independent cultures—scale bar representative of 50µm (D) Relative levels of myogenic marker *MYH11* mRNA expression in PMs following VSMC differentiation. Data are expressed as the ratio of mRNA expression relative to *HPRT* and are the mean ± SEM, n = 6, * $p \leq 0.05$ versus HiPSC and * $p \leq 0.05$ PM

4.4.13 HiPSC-derived SNEP uptake of endogenous ExoGlow labelled HAEC-derived EVs *in vitro*

To investigate the role of EV facilitation of SHh-dependent myogenic differentiation of HiPSC-SNEPs, confirmatory experiments were carried out to ensure uptake of EVs during HAEC-NG-EV and HAEC-HG-EV treatments. EV uptake assays were performed by incubating endogenous (ExoGlow) and exogenous (Nir-Aza) labelled EVs with HiPSC-derived SNEPs. EVs were isolated using ExoQuick TC. Following isolation, endogenous labelling of isolated EVs has been carried out. ExoGlow labelled EVs were resuspended in SNEP essential eight maintenance media. SNEP cells were seeded onto a 12 well plate at ~1000 cells/well. A dilution of ExoGlow labelled EVs was added to each well (Neat, 1:10, 1:50, 1:100). A control of ExoGlow only was used to ensure positive staining was EV dependent. Cells were imaged using the Celigo Imaging Cytometer at 4 hours and 24 hours using bright field and green (483/32nm) detection channels to determine the optimal time needed to facilitate EV uptake. A heat map was generated indicating fluorescent intensity levels at 4 and 24 hours (Figure 4.28 A). The percentage of ExoGlow^{+} cells after 24-hour incubation was graphed (Figure 4.28 B) was graphed. Fluorescent imaging showed EV uptake after 4 hours and 24 hours with a significant increase in uptake after 24 hours (Figure 4.28 C, D). As expected, the optimal concentration of ExoGlow uptake was incubated with neat isolated EVs (100μg).

Further analysis of SNEP HAEC-EVs was performed by confocal fluorescent microscopy using the Leica TCS SP8 STED microscope. SNEPs were seeded at a density of ~5,000 cells/well onto sterile glass coverslips in a 6-well cell culture plate. ExoGlow labelled HG-EVs (100μg) were incubated for 24 hours to allow optimal EV uptake. Cells were fixed and imaged using the 488 lasers at 20X (Figure 4.29 A), 60X (Figure 4.29 B), and 100X (Figure 4.29 C). The uptake of EVs by HiPSC-SNEPs was confirmed and was located in the cell's cytoplasm with the majority of positive EV staining present around the nucleus. Further, Z-stack imaging enabled visualisation of endocytosed HAEC-ExoGlow-EVs in the cytoplasm with additional membrane staining (Figure 4.29 D, E) indicating that HAEC-EVs can dock to the cell membrane via receptor-ligand binding or be internalised by HiPSC-SNEP.

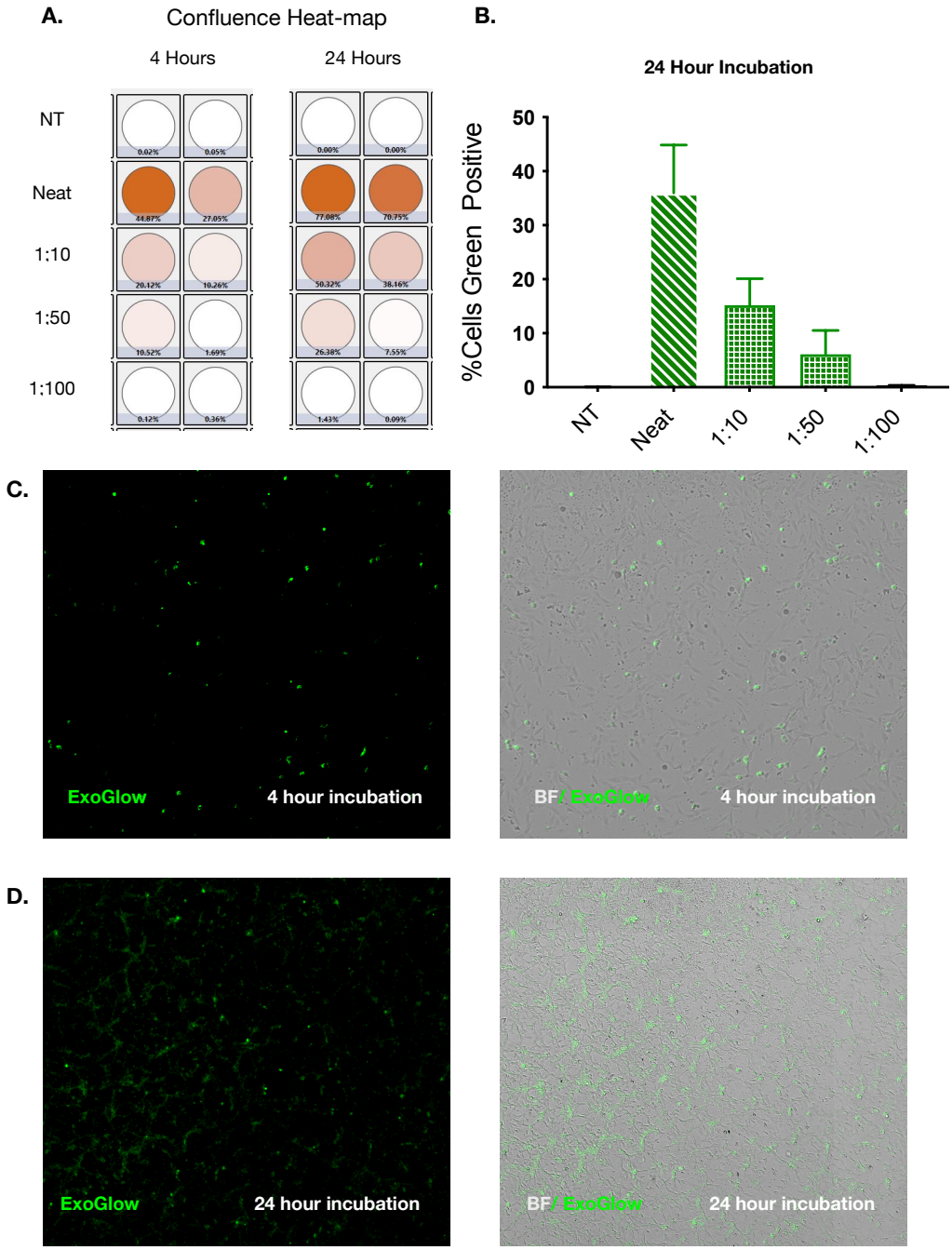

Figure 4.28 HiPSC-derived SNEP uptake of exogenous labelled HG-EVs *in vitro*. Evaluation of SNEP HG-ExoGlow-EV uptake following 24 h incubation. (A) Heatmap representing the percentage of ExoGlow$^+$ cells following incubation over a time course of 4 and 24 h at various HG-EV concentrations. (B) Graphic representation of ExoGlow$^+$ cells using a dilution of ExoGlow labelled HG-EVs. (C,D). Representative images of ExoGlow uptake by SNEPs *in vitro* at 4 hours (C) and 24 hours (D). Scale bar 500µm. Data representative of n=3.

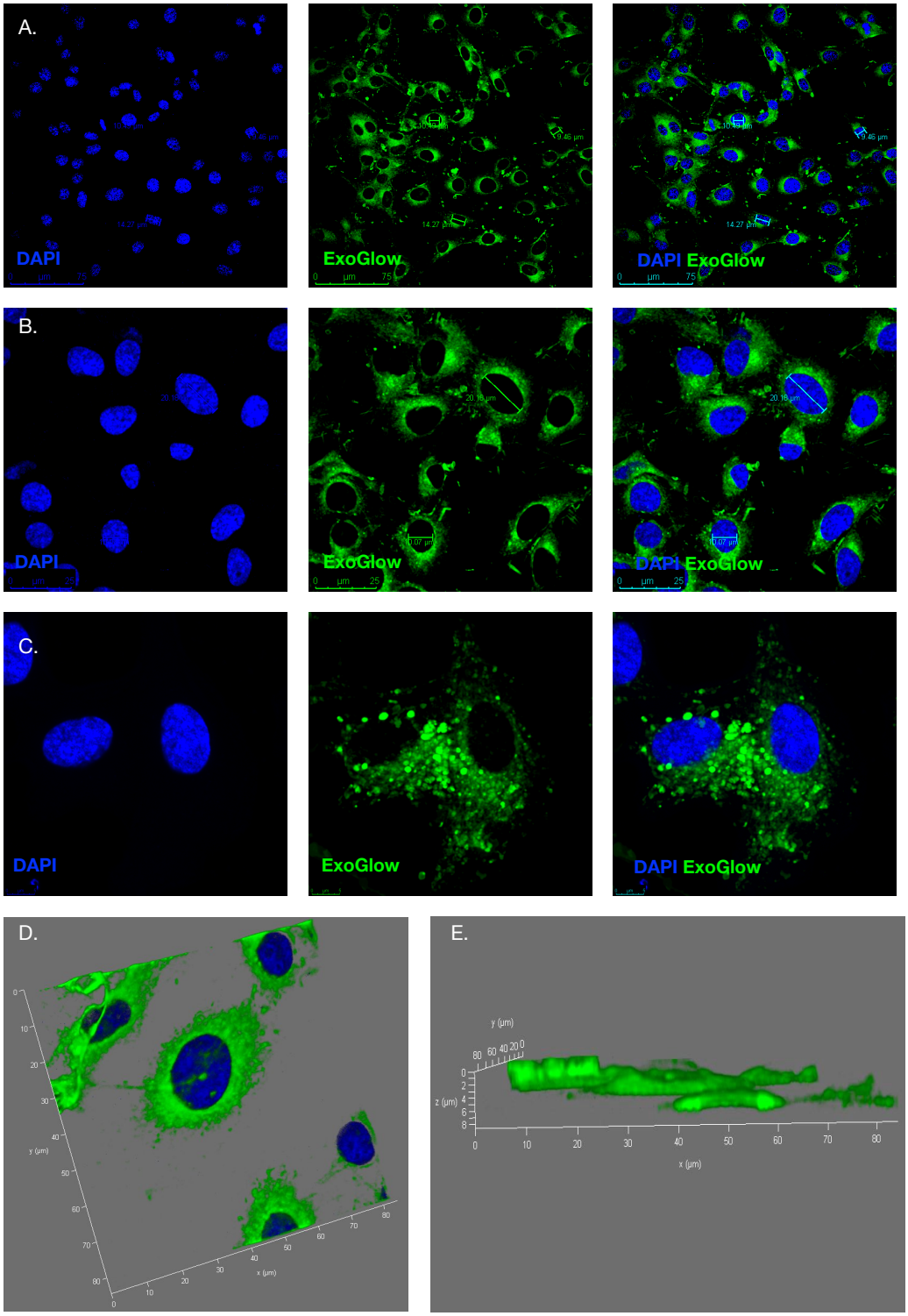

Figure 4.29 HiPSC-derived SNEP uptake of exogenous labelled HG-EVs *in vitro*. (A-C) Representative images of fluorescence staining of DAPI nuclei and fluorescent detection of exogenous labelled HAEC-derived HG-EVs at 20X,60X, and 100X, respectively. (D-E) Z-stack imaging of HAEC-derived HG-EVs after 24 h. All images are representative of n ≥ 12 images per experimental group from three independent cultures—scale bar representative of 75µm, 25µm, and 5µm.

4.4.14 HiPSC-derived SNEP uptake of exogenous Nir-Aza labelled HAEC-derived EVs *in vitro*

SNEP uptake of EVs exogenously labelled during HAEC culture was explored due to the advantageous characteristics of *in vitro* labelling. EV uptake assays were performed by incubating exogenous (Nir-Aza) labelled HG-EV with HiPSC-derived SNEPs. EVs were isolated using ExoQuick. Following isolation, NirAza labelled HG-EVs have resuspended in SNEP Essential 8™ maintenance media. SNEP uptake of NirAza-HAEC-HG-EVs was visualised by confocal fluorescent microscopy using the Leica TCS SP8 STED microscope. SNEPs were seeded at a density of ~5,000 cells/well onto sterile glass coverslips in a 6-well cell culture plate. NirAza labelled HG-EVs were incubated for 24 hours to allow optimal EV uptake. Cells were fixed and imaged using the 642 lasers at 20X (Figure 4.30 A), 60X (Figure 4.30 B), and 100X (Figure 4.30 C). The uptake of EVs by HiPSC-SNEPs was confirmed and localised within the cell's cytoplasm with the majority of positive EV staining present around the nucleus. Further, Z-stack imaging enabled visualisation of endocytosed HAEC-NirAza-EVs in the cytoplasm with additional membrane staining indicating that HAECs can dock to the cell membrane via receptor-ligand binding or be internalised by HiPSC-SNEP (Figure 4.30 D, E)

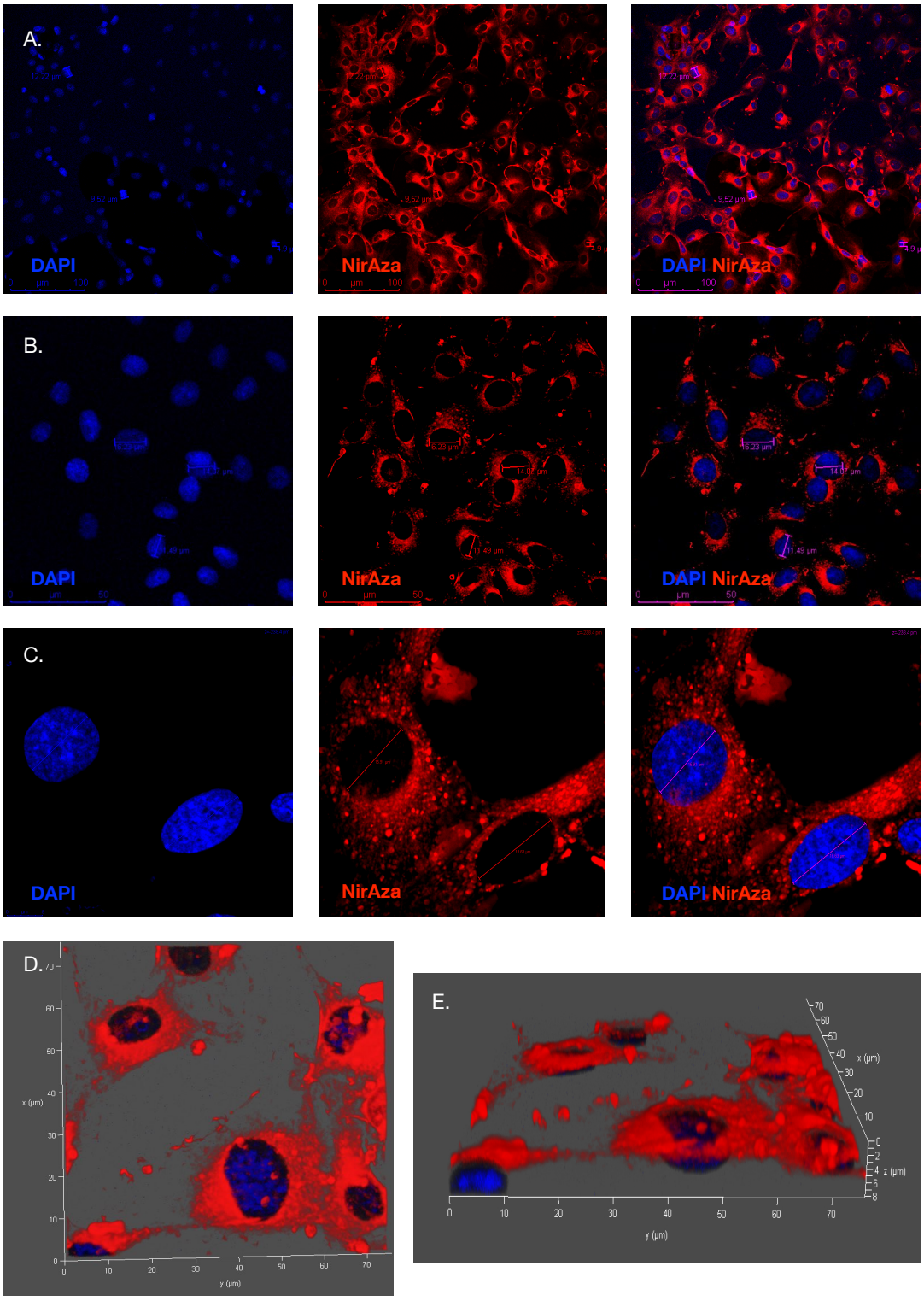

Figure 4.30 HiPSC-derived SNEP uptake of endogenous labelled HG-EVs *in vitro*. (A-C) Representative images of fluorescence staining of DAPI nuclei and fluorescent detection of endogenous labelled HAEC-derived HG-EVs (red) at 20X,60X, and 100X, respectively. (D-E) Z-stack imaging of HAEC-derived HG-EVs after 24 h. All images are representative of n ≥ 12 images per experimental group from three independent cultures—scale bar representative of 75µm, 25µm, and 5µm.

4.4.15 HG-HAEC-EVs induce SHh-dependent myogenic differentiation of HiPSC-derived neurectoderm progenitor cells *in vitro*.

To determine the role of HAEC-EVs in promoting SHh-myogenic differentiation, HiPSC-derived SNEPs were cultured in the absence or presence of EVs purified from normal (NG) and hyperglycaemic (HG) endothelial-derived EVs before the relative mRNA levels of Hh target gene (*GLI1*) and the myogenic differentiation marker gene (*CNN1)* were assessed after 48 hours and 7 days, respectively. The relative levels of *GLI1* mRNA were significantly increased in SNEPs following treatment with HG-EVs compared to NG-EVs and Mannitol (MT-EVs) controls after 48 hrs (Figure 4.31 A). The relative levels of *CNN1* mRNA were also significantly increased in SNEPs treated with HG-EVs compared to NG-EVs and MT-EVs controls, respectively (Figure 4.31 B). In both cases, the direct effect of NG, HG, and MT-treated media on GLI1 and CNN1 mRNA levels in the absence HAECs was not significant (Figure 4.31 A, B).

Further experiments were carried out to verify that HG-EVs activated Hh signalling in SNEPs *in vitro* using two independent Hh signalling inhibitors, cyclopamine and Hh neutralising antibody 5E1. For cyclopamine inhibition of Hh signalling, SNEPs were cultured in 6-well tissue culture plates at a density of ~ 100,000 cells/well. Cells cycling was synchronised by culturing cells in the absence of serum for 24 hours. Following quiescence, SNEPs were washed and treated with 15 mM of cyclopamine in maintenance media for 1 hour. HG-HAEC-derived EVs were added to the SNEP cultures before the cells were harvested after 48 hours for measurement of *GLI1* transcript. A reduction of *GLI1* expression was observed following cyclopamine-dependant inhibition of the Hh signalling pathway (Figure 4.32 A). Positive controls were run in parallel by treating SNEPs with 1.0μg/ml of recombinant SHh in the absence or presence of 15mM cyclopamine.

Hh inhibition was also carried out using a Hh neutralising antibody 5E1. SNEP cells were prepared as above, before the neutralising antibody 5E1 was added to SNEP cultures for 1 hour at a concentration of 1μg/ml. Following antibody incubation, HG-HAEC-derived EVs were added to the SNEP culture. SENPs were harvested after 48 hours for measurement of *Gli1* transcript. A reduction of *GLI1* mRNA expression was observed following 5E1-dependent inhibition of the Hh signalling pathway (Figure 4.32 B).

Positive controls were run in parallel by treating SNEPs with 1.0μg/ml of recombinant SHh in the absence or presence of 5E1.

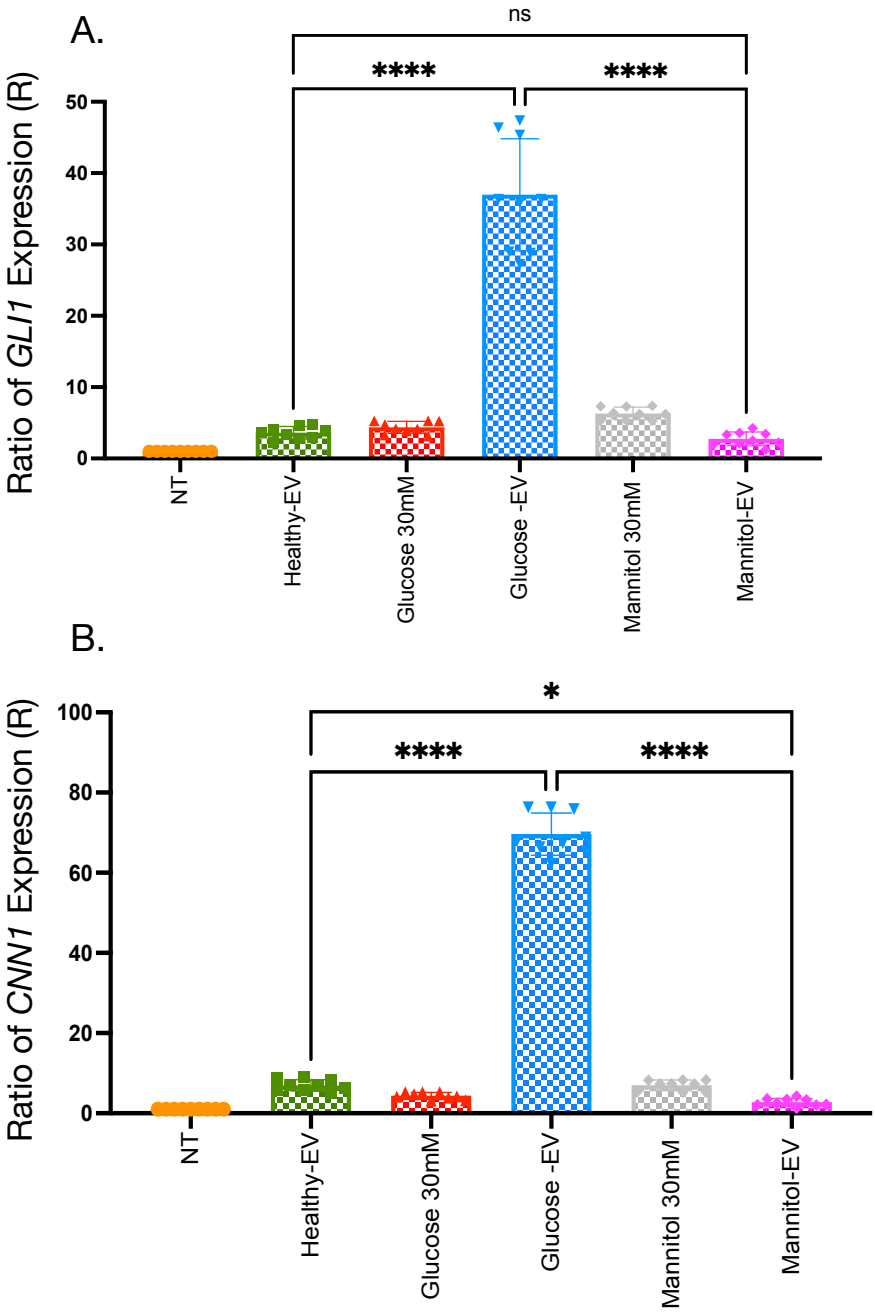

Figure 4.31 HAEC-HG-EVs stimulate Hh target genes in S100β⁺ SNEPs. (A) Relative of *GLI1* and *CNN1* mRNA expression in SNEPs following HAEC-HG-EVs. Data are expressed as the ratio of mRNA expression relative to control healthy EVs and are the mean ± SEM, n = 9, * $p \leq 0.05$ versus glucose-EV and * $p \leq 0.05$ versus mannitol-EVs.

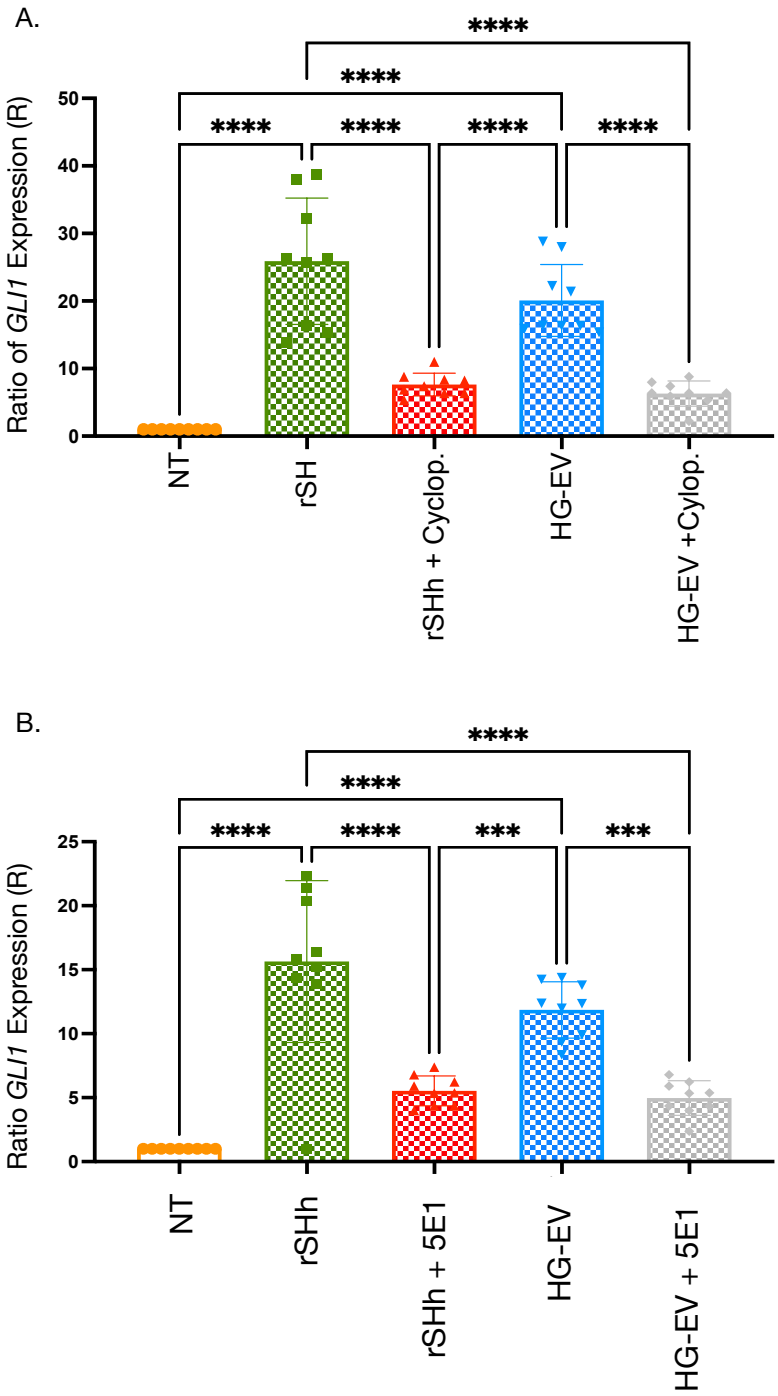

Figure 4.32 Inhibition of EV-mediated SHh response in SNEPS. (A) The relative expression of *GLI1* mRNA levels by qRT-PCR in SNEPs treated for 48 h with Hh signalling inhibitor cyclopamine. (B) The relative expression of *GLI1* mRNA levels by qRT-PCR in SNEPs treated for 48 h with Hh neutralising antibody 5E1. Data are presented as the ratio of *Gli1* expression relative to the negative control sample NT and positive control sample rSHh. Error bars based on SEM. Data representative of n=3 , * $p < 0.05$.

4.4.16 HG-HAEC-EVs induces proliferation of HiPSC-derived neurectoderm progenitor cells, SNEPs, *in vitro*.

Following vascular injury, resident vascular stem cells undergo myogenic differentiation and proliferation, resulting in an increase in the medial and intimal layer of the artery and a subsequent decrease in the luminal (Yuan *et al.*, 2017). To determine the effect of HG-HAEC-EVs on the proliferation profile of SNEPs *in vitro.* SNEPs were seeded at a concentration of ~500 cells/well in a 48-well plate. NG-, HG-, and MT- HAEC-derived EVs were isolated from conditioned media and 100μg of EVs added to each well in the absence or presence of cyclopamine (15mM). Bright-field images were taken at various time points (day 0 – 3). A confluence overlay was applied during each time point using the Celigo imaging platform (Figure 4.33 A). The percentage confluence per well was recorded every 24 hours for three consecutive days. Percentage confluence was recorded on a percentage confluence map and heat map, respectively (Figure 4.33 B). Following three days of incubation, the increase in cell number was graphed. A significant increase in cell proliferation was noticed in HG-HAEC -EV treated samples in comparison to NG-HAEC-EVs and Mannitol-HAEC-EVs (Figure 4.33 C). Moreover, the increase in SNEP proliferation was blocked using Hh signalling pathway inhibitor, cyclopamine (Figure 4.33 D).

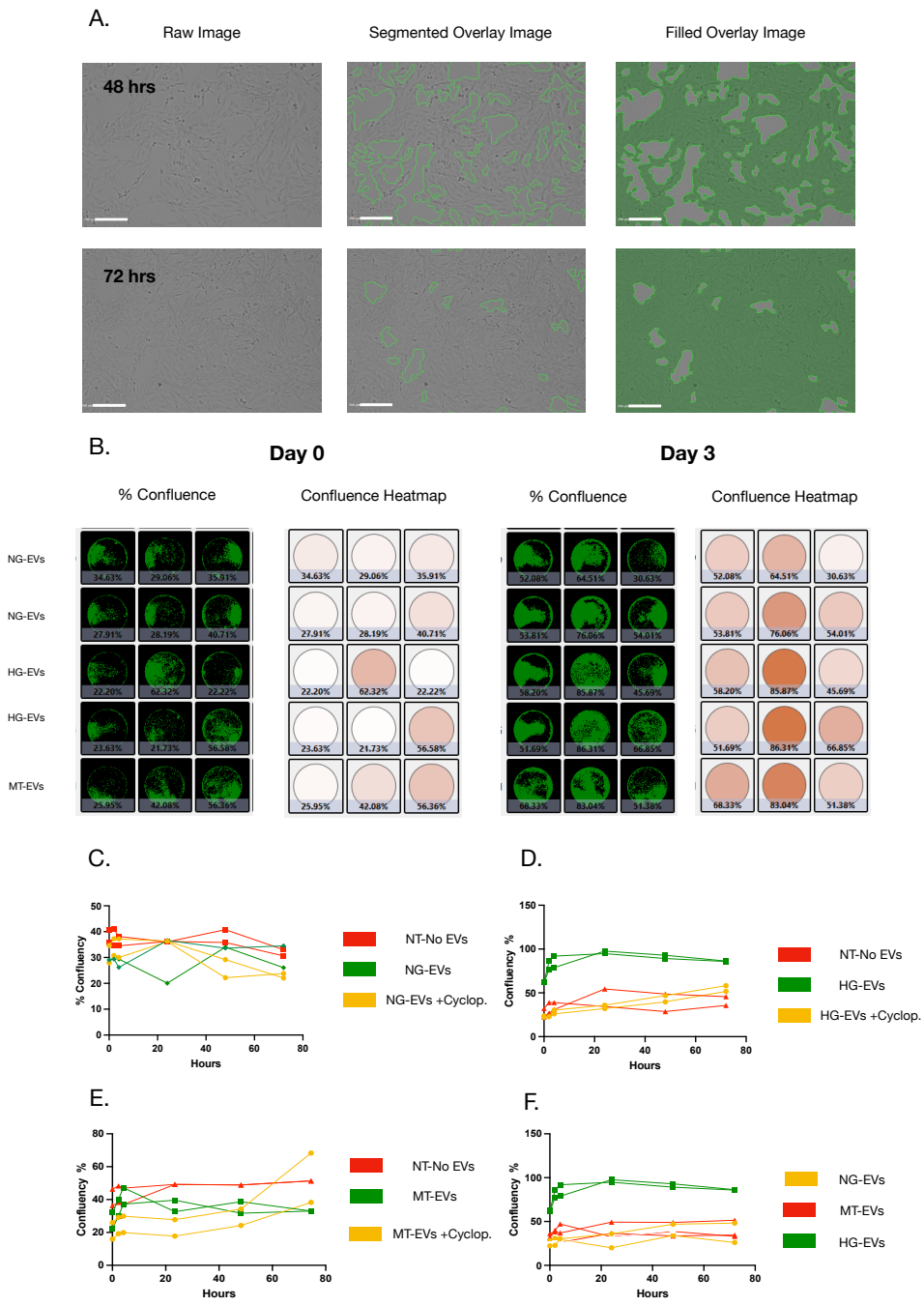

Figure 4.33 HAEC-HG-EVs promote proliferation of SNEPs. (A) Confluence overlay determining an increase in proliferating cells over a period of 48 and 72 h (B) Graphic depiction of percentage confluence per well represented as a % confluence mask and heat map respectively. (C) Comparison of the confluence of SNEPs following exposure to maintenance media (red), NG-EVs (green) and NG-EVs + Cyclopamine (yellow) from 0 – 72 hrs. (D) Comparison of the confluence of SNEPs following exposure to maintenance media (red), HG-EVs (green) and HG-EVs + Cyclopamine (yellow) from 0 – 72 hrs. (E) Comparison of the confluence of SNEPs following exposure to maintenance media (red), MT-EVs (green) and MT-EVs + Cyclopamine (yellow) from 0 – 72 hrs.(F) Comparison of the confluence of SNEPs following exposure to MT-EVs (red), NG-EVs (yellow) and HG-EVs (green) from 0 – 72 hrs.

4.5 Summary

- HAEC displays distinct endothelial cobblestone morphology in culture. ICC and transcriptional analysis confirmed the expression of endothelial-associated markers/genes CD31 and eNOS.
- HG-treated HAECs increases intracellular ROS production via increasing levels of O_2^- production accompanied by elevated *NOX4* and *NOS3* gene expression levels.
- HAECs secrete NG-EVs and HG-EVs with discrete differences in size, and expression of EV-associated proteins *in vitro*.
- HG-EVs can be labelled exogenously and endogenously using ExoGlow and NirAza dyes, respectively.
- HiPSCs express distinct embryological markers NANOG and OCT4.
- HiPSC can be used to generate NE, paraxial (PM) and lateral mesoderm (LM) embryologically defined progenitor stem cells by chemical means. Spontaneous generation of NE progenitors (SNEPs) was confirmed using non-chemical means.
- HiPSC-derived NE, PM, and LM progenitors undergo myogenic differentiation in response to TGF-β1/PDGF treatment
- Recombinant SHh induces myogenic differentiation of HiPSC-derived SNEPS
- HiPSC-derived SNEP endocytoses HG-EVs
- HG-HAEC-derived EVs induce SHh-dependent myogenic differentiation of SNEPs.
- Inhibitors of the Hh signalling pathway cyclopamine and 5E1 block myogenic differentiation of HiPSC-SNEPs following rSHh treatment or exposure to HG-EVs
- HG-HAEC-EVs induces proliferation of HiPSC-derived SNEPs *in vitro,* an effect attenuated following treatment with Hh inhibitor, cyclopamine.

4.6 Discussion

When studying the aetiology and pathophysiological of any human disease with a view to diagnostic and/or therapeutic discovery, the primary critical component is the requirement of a physiologically relevant experimental model of disease. To date, due to practical and ethical concerns, animal modelling, most frequently through the use of rodents (mice and rats), has been key to understanding the development and manifestation of various diseases. More often, the translation of discoveries made in animal models to human trial fails due to genetic, molecular, and physiological reasons (Leenaars *et al.*, 2019). Human tissues have been proposed to alleviate the problems associated with the translation of animal models in human trials. However, studies using human tissues also pose some challenges, including lengthy ethical applications, access to fresh disease samples on an ongoing basis, inability to study subclinical disease as samples are invariably obtained following post-mortem (Kim, 2015).

The use of iPSCs for *in vitro* disease modelling has emerged as an alternative cell source to tissue isolation with superior advantages compared to its predecessors by providing (i) a complicated genetic signature of human tissue and (ii) unlimited resource for identifying the mechanism underlying disease pathogenesis enabling the discovery of sub-clinical biomarkers.

HiPSCs have been extensively used to model the role of VSMCs in the development of vascular diseases (G. H. Liu *et al.*, 2011; Granata *et al.*, 2017). Of interest, HiPSCs are emerging as a useful tool for modelling the development of atherosclerosis through the investigation of embryonic origin on disease susceptibility and the source of VSMC-like cells found in arterial lesions (Liang and Du, 2014; Bargehr *et al.*, 2016). Furthermore, the generation of embryologically defined HiPSC-derived progenitor SCs provides a platform to study the role of EC-STEM CELL communication during pathogenesis of atherosclerosis.

HiPSCs have been deployed to study various aspects of the development of atherosclerosis including the use of ‘disease in a dish’ models for screening the efficacy of novel therapeutic therapies (Davaapil, Shetty and Sinha, 2020; Mallone *et al.*, 2020) as well as isolation of iPSCs for genetic screening of patients considered to have a predisposition to the development of CVD (Davis *et al.*, 2012; Itzhaki *et al.*, 2012; Sun

et al., 2012; Lan *et al.*, 2013). However, the use of HiPSCs has not been reported to investigate cell-cell communication between resident vascular cells during pathogenesis of disease. Furthermore very little research has been carried out using HiPSC models to elicit the role of EV-mediated initiation of discrete molecular changes indicative of sub-clinical atherosclerosis. Data presented in Chapter 3 provided compelling evidence that EVs derived from hyperglycaemic RAECs promoted Hh target gene expression in murine S100β resident vascular stem cells *in vitro.* This finding highlights the potential role of sub clinical detection of Hh from circulating EVs as an early diagnostic biomarker of atherosclerosis as attenuation of Hh signalling in murine models of arteriosclerotic disease results in mitigation of IMT and lesion formation (Redmond *et al.*, 2013; Aravani *et al.*, 2019; Liu *et al.*, 2020; Di Luca *et al.*, 2021). One major limitation of these findings is the model in which they are discovered. In order to determine the true clinical relevance, the detection of Hh^{+} EVs in biological fluids is paramount. Therefore, it was important to determine whether our findings in murine models could be recapitulated using HiPSCs to further validate the importance of endothelial derived EVs harbouring Hh ligands in response to hyperglycaemic conditions to promote a change in S100β vascular stem *in vitro.*

By using HiPSC derived progenitor stem cells *in vitro,* it is now possible to study the transfer of potential pathogenic biological messages from various cell types within the vascular wall, including but not limited to intimal endothelial cell-medial/adventitial stem cell, endothelial cell to medial vascular smooth muscle cells and vascular smooth muscle cell-medial/adventitial stem cell crosstalk. In recent years, circulating EVs have been interrogated as possible surrogate biomarkers for disease through their potential as cell-cell communicators between the aforementioned cells within the vascular wall (Gaceb, Martinez and Andriantsitohaina, 2014). In this study, a HiPSC-derived *in vitro* model was developed to delineate the role of endothelial derived EV transport of the morphogen, SHh during myogenic differentiation of S100β-stem cells in response to hyperglycaemia, typical of their role in response to vascular injury in rodent models. Generation of embryologically defined HiPSC stem cell progenitors and subsequent myogenic differentiation expands our current understanding of vascular pathology and represents an important therapeutic platform for developing early biomarkers for the detection of subclinical atherosclerosis.

Dysfunction of the endothelium at lesion-prone areas of the arterial wall marks the earliest detectable change during the development of atherosclerotic lesions (Stary, 2000; Virmani *et al.*, 2000). Although many systemic factors such as hypercholesterolemia, hyper homocysteinemia, and hyperglycaemia increase the probability of atherosclerotic development, a common denominator of these is represented by an increase in ROS production (Taniyama and Griendling, 2003; Stocker and John F. Keaney, 2004). The presence of excess NOX-derived ROS from studies using various *in vitro* models of hyperglycaemia has been previously reported (Zhang *et al.*, 2008; Taye *et al.*, 2010; Chen *et al.*, 2013). However, relative roles of particular NOX isoforms remain to be determined. For this reason the role of distinct NOX isoforms during activation of EC dysfunction in response to hyperglycemic conditions was determined by detecting differences in biochemical properties. Using both qualitative DHE staining, and quantitative NBT uptake, a significant increase in O2-, a biproduct of specific NOX isoforms NOX1 and NOX2 (Takac *et al.*, 2011) was demonstrated in HAECs

Although the role of NOX4 is often considered protective rather than detrimental to endothelial function, we, along with others, have shown an increase in the expression of NOX4 mRNA levels in HAEC when exposed to hyperglycemic conditions compared to normal conditions *in vitro*. This response is likely due to hyperglycaemic induced NF-KB activation resulting in enhanced interactions of NF-KB/p65 and the NOX4 promoter, a process reported during vascular complications associated with T2D (Williams *et al.*, 2012; Antonopoulos *et al.*, 2015). A consequence associated with elevated NOX-derived EC ROS production is the mediation of eNOS uncoupling. Uncoupling of eNOS is present in T2D, although the relationship between activation of specific NOX isoforms is not clear (Thum *et al.*, 2007). To investigate the effect of NOX-mediated ROS production, levels of eNOS mRNA were measured following HAEC exposure to hyperglycemic conditions for 48 h. An increase in eNOS mRNA levels were demonstrated concordant with previous *in vitro* and *in vivo* studies (Ding *et al.*, 2007; Zhang *et al.*, 2008; Adela *et al.*, 2015).

A cascade of pathological events is initiated due to ED, including an increase in EC permeability and recruitment of circulating monocytes, resulting in macrophage infiltration, and increased levels of lipoproteins. Due to the nature of EC location, ECs are the primary responder to circulating CVD risk factors; however, how the information

is transferred from ECs to resident vascular (Williams *et al.*, 2012)(Quagliaro *et al.*, 2003) cell populations remains unclear. Exposure of vascular ECs to glucose levels above 10 mmol/L (*in vitro* or *in vivo*) is regarded as hyperglycemic conditioning (Popov, 2010). HAEC exposure to hyperglycemic conditions triggers a number of EC modifications including pro-inflammatory, pro-adhesive phenotypic changes (Ido, Carling and Ruderman, 2002; Rajapakse *et al.*, 2009) as well as changes in EC migratory and proliferation properties (McGinn *et al.*, 2003). Furthermore, hyperglycemia has been identified as an independent risk factor for early plaque development (McGill *et al.*, 2001; Järvisalo *et al.*, 2002). Although the role of hyperglycemia in sub clinical development of atherosclerosis is evident, little research has focused on discrete changes in the secretome of ECs derived from normal versus hyperglycemic conditions. The EC secretome, defined as a collection of factors consisting of transmembrane proteins and other biological components secreted by cells into the extracellular space (Berezin, 2017), from serum samples of patients with diabetes, heart failure and atherosclerosis have been shown to be defective in maintaining vascular homeostasis (Lu *et al.*, 2013; Helmke and Vietinghoff, 2016) . Therefore, detection of discrete changes in the secreted profile of ECs represents a platform for the discovery of sub-clinical biomarkers for early detection of atherosclerosis.

Originally considered as cellular was products, the secretion of EVs have been proven to mediate the transfer of functional molecules to target cells serving as mediators of cell-to-cell crosstalk (Becker *et al.*, 2016; Maas, Breakefield and Weaver, 2017; Laulagnier *et al.*, 2018; Laurenzana *et al.*, 2018; Bartel *et al.*, 2020) Moreover, the content of EV encapsulated cargo has previously been reported to indicate cellular health at any given time, making them the ideal candidate for detection of early diagnostic biomarkers for subclinical disease (Yáñez-Mó *et al.*, 2015; Perakis *et al.*, 2017). Changes in EV cargo secreted from ECs in response to hypoxia (de Jong *et al.*, 2012), shear stress (Burghoff and Schrader, 2011) and hypercholesterolemia (Yuan *et al.*, 2020) have been demonstrated. However the main focus of this research has mainly been the initiation of inflammatory processes with a significant gap in our knowledge surrounding the effect of EVs as a driver for discrete molecular changes in stem cells that may control their proliferation and myogenic differentiation during sub-clinical atherosclerosis.

For this reason, the primary aim of this study using HAECs exposed to hyperglycaemic conditions was to generate a cohort of pathological associated EVs for subsequent interrogation as diagnostic biomarkers, in particular SHh, a known mediator of myogenic differentiation of resident vascular stem cells that contribute to subclinical atherosclerosis. To this end, HAECs were cultured in normal and hyperglycemic conditions for a period of 48 h. Following harvest of conditioned medias EVs were isolated using a commercially available PEG precipitation method due to advantageous characteristics, including simplistic isolation protocols and speed. This method utilises a decrease in the solubility of compounds in solutions of super hydrophilic polymers resulting in the isolation of EV fractions. DLS technology was used to determine the size of isolated EVs with a population characterised between 20-60nm for EVs derived from normal conditions and 30-80nm for EVs derived from hyperglycemic conditions. Interestingly a much more homogenous population of EVs were isolated from HAECs in both normal and hyperglycemic conditions in comparison to RAECs derived from similar conditioning. Characterisation of RAEC derived EVs from hyperglycemic conditions suggested isolation of a larger population of EVs classically referred to as microvesicles, which are known to be heterogenous in size (Théry *et al.*, 2018). In comparison, characterisation of EVs from HAECS exposed to normal and hyperglycemic conditions revealed a smaller population of EVs referred to as exosomes which represent a more homogenous population (Willms *et al.*, 2016). However, further characterisation of the biogenesis pathway in which isolated HAEC derived EVs are produced will be required. It is important to note PEG has been previously applied to isolate proteins, nucleic acids, viruses, and other small particles (Yamamoto *et al.*, 1970). Therefore, to overcome this limitation, isolated HAEC-EVs derived from normal and hyperglycemic conditions were characterised based on a suite of techniques to ensure intact isolation of vesicular bodies including FeSEM, DLS, nanoFACs, and dot blot antibody array in line with the minimal information for studies of EVs (MISEV) (Théry *et al.*, 2018).

According to proteomic results gathered in EV databases, ExoCarta and EVpedia, EVs have a defined protein signature (Simpson, Kalra and Mathivanan, 2012; Kim *et al.*, 2013). EVs have been described as highly enriched for tetraspanin, including CD81, CD63, and CD9. Using nanoFACs antibody staining for these markers, HAEC derived EVs were positive for expression of CD81 and CD63 with minimal expression of CD9.Furthermore, antibody dot-blot array distinguished the expression of EV biogenesis

ESCRT proteins ALIX and TSG101, EV-purity marker GM130, and other associated EV proteins including FL0T1, ICAM, EpCAM, and ANXA5. The proteomic profile of EVs changes depending on the cell of origin and the health status of the cell. Although similar expression of tetraspanin proteins CD63 and CD81 were observed, an increase in the expression of proteins normally enriched in EVs including TSG101, ANAXA5 was observed with a notable decrease in EV-associated protein ALIX, a protein reported to play a role in the secretion of smaller EVs (Willms *et al.*, 2018). Taking these findings together, it is clear that EVs secreted in response to a pathologic hyperglycaemic stimulus express differential levels of EV-associated proteins in comparison to EVs derived under normal conditions.

Having shown the secretion, isolation and characterisation of HAEC EVs derived from normal and hyperglycemic conditions, a reporter stem cell model was generated using HiPSCs to determine their functional effects on stem cell proliferation and myogenic differentiation. A hallmark of atherosclerosis is the formation of neointima due to the proliferation and migration of resident vascular cells. Despite extensive research, the origin of neointimal VSMC-like cells remains controversial (Nguyen *et al.*, 2013). It was generally accepted that VSMC switches from a contractile phenotype to a plastic phenotype in response to vascular injury resulting in increased proliferation, the release of pro-inflammatory cytokines and growth factors (Campbell and Campbell, 2012). Although independent studies have proposed the progeny within lesions are derived from various origins, including differentiated medial VSMCs (Campbell and Campbell, 2012; Chappell *et al.*, 2016; Dobnikar *et al.*, 2018), ECs (Cooley *et al.*, 2014; Yuan *et al.*, 2017) and/or resident vascular stem cells (Tang, Wang, Yuan, *et al.*, 2012; KRamann *et al.*, 2016; Yuan *et al.*, 2017; Tang *et al.*, 2020). Of interest in this study is a population of S100β^{+} resident stem cells in the media, termed MVSCs, which have been shown to migrate and differentiate to become neointimal VSMC-like cells (Tang, Wang, Yuan, *et al.*, 2012; Yuan *et al.*, 2017). Our research group have reported similar results using indelibly marked S100β^{+} cells to demonstrate a significant number of neointimal cells are derived from a small parent population of S100β stem cells in the media (Di Luca *et al.*, 2021; Molony *et al.*, 2021).

Generating VSMCs from HiPSCs *in vitro* has been extensively demonstrated through directed differentiation using a cocktail of fibroblast growth factor 2, platelet-derived

growth factor (PDGF), and TGF-β1 (Dash *et al.*, 2015; Yang *et al.*, 2016). However, one of the major concerns for subsequent disease modelling or therapeutic transplant is confirming the absolute specificity of the resulting differentiated cells. It has been established that VSMCs arise from multiple origins during embryonic development, including mesoderm lineages, the neural crest, and the secondary heart field (Majesky and W., 2007; G. Wang *et al.*, 2015). Such embryonic origin is increasingly linked to site-specific susceptibility of vascular diseases, including atherosclerosis and aortic aneurysm (Cheung *et al.*, 2012; Sinha, Iyer and Granata, 2014). Therefore, the specific lineage that VSMCs are derived from must be carefully considered. Neuroectoderm lineage was chosen as it is associated with areas of high risk for atherosclerotic lesion formation (Redheuil *et al.*, 2010). Although the main focus of this study was the development of intermediate NE progenitor stem cells and subsequent generation of embryologically defined VSMCs, we report the generation of origin-specific vascular VSMCs from HiPSCs through intermediate lineages, NE, lateral plate mesoderm, and PM through the use of chemically defined protocols (Yang *et al.*, 2016). Interestingly, a study conducted by Ying et al. in 2003 reported that chemical induction of ESCs using various signalling activators and inhibitors was not necessary for ESCs to commit efficiently to a neural fate. They demonstrated that neural fates emerge in the absence of serum or added growth factors concluding that NE appears to be the default differentiation pathway for ESCs when pluripotency factors are absent (Ying *et al.*, 2003).

We determined whether this process was also valid for NE differentiation of HiPSCs. HiPSC-SNEP were generated in the absence of serum and characterised for NE markers; Nestin, predominantly expressed during early developmental stages in neural and muscle stem/progenitor cells (Sejersen and Lendahl, 1993), calcium-binding protein S100B and NE lineage specification protein PAX6 (Zhang *et al.*, 2010). To ensure our SNEPs were a pure NE population, we investigated the expression of mesoderm lineage marker PAX1 and myogenic markers CNN1 and MYH11. SNEPs did not express PAX1, CNN1, or MYH11 when interrogated by qRT-PCR and ICC, respectively. In most *in vitro* methods, the distinction between NE and mesoderm is based solely on the expression of marker genes. However, this may be concerning as a number of genes are shared between the embryonic lineages and are not lineage-specific. To overcome this limitation, one approach may be to follow epigenetic changes during differentiation of HiPSC to defined lineages facilitating improved differentiation of HiPSCs towards specific stem/progenitor

and VSMC subtypes (Cypris *et al.*, 2019; Efrat, 2021). As pathologic observations in human vessels confirm that early transitional lesions are enriched with VSMC-like cells, we confirm the ability of HiPSC-derived SNEP undergo myogenic differentiation in response to TGF-β1/PDGF. NE lineage-specific SNEPs treated with TGF-β1 and PDGF for 12 d proceeded down a myogenic lineage characterised by morphometric changes displaying contractile filaments, increased expression of VSMC markers CNN1 and MYH11, and a decrease in expression of NE associated markers, NESTIN and S100β. This *in vitro* model offers an ideal platform to study the functional effect of HG-EV on myogenic differentiation of lineage-specific NE-derived intermediate stem/progenitors cells mimicking a process reported *in vitro* in response to vascular injury (Di Luca *et al.*, 2021).

The molecular mechanisms by which resident vascular stem cells differentiate into VSMC-like cells are multifactorial. A number of pathways are reported to play a role, including TGF-β1 and VEGF pathways (G. Wang *et al.*, 2015). A large body of evidence now suggests a role for Hh signalling during the pathogenesis of atherosclerosis as it recapitulates during the onset of vascular disease. This came to light following the implication of HHIPL1 at the chromosome 14q32 CAD locus during several genome wide association studies (GWAS) (Schunkert *et al.*, 2011; Harst and Verweij, 2018). Similarly Hh signalling has also been shown to play a pivotal role in maintenance of adult progenitor/stem cells, tissue repair and atherosclerosis (Dutzmann, Koch, Weisheit, Sonnenschein, Korte, Haertlé, Thum, Bauersachs, Sedding and J.-M. M. Daniel, 2017; Aravani *et al.*, 2019; Di Luca *et al.*, 2021). Hh has been identified through increased lipid uptake by macrophages in murine atherosclerotic models, while HHIP1 deletion reduces atherosclerotic plaque formation (Beckers *et al.*, 2007; Aravani *et al.*, 2019). Furthermore, SHh signalling and EGF-like domain-containing two and signal peptide CUB domains are overexpressed in injured arteries (Morrow *et al.*, 2009; Ali *et al.*, 2013; Dutzmann, Koch, Weisheit, Sonnenschein, Korte, Haertlé, Thum, Bauersachs, Sedding and J. M. Daniel, 2017). The role of Hh in controlling stem cell differentiation during VSMC migration in response to vessel injury remains a strong possible source of neointimal cells during vessel remodelling. Adventitial $Sca1^+$ cells that co-localise with SHh and Ptch1 significantly contribute to intimal thickening *in vivo* (Tsai *et al.*, 2012; Shikatani *et al.*, 2016; Dutzmann, Koch, Weisheit, Sonnenschein, Korte, Haertlé, Thum, Bauersachs, Sedding and J. M. Daniel, 2017) while Hh inhibition with cyclopamine or

local perivascular depletion of Ptch1 attenuates intimal thickening following iatrogenic flow restriction *in vivo* (Redmond *et al.*, 2013; Fitzpatrick *et al.*, 2017).

In this context, the next objective of this study was to narrow our investigation to determine the potential of HAEC EVs derived from hyperglycemic and normal conditioning to activate Hh signalling and myogenic differentiation in our HiPSC-derived NE stem cells, a response mimicked by direct treatment of cells with recombinant SHh. Extensive studies have been carried out to determine mechanisms of morphogen release into the extracellular space (Panáková *et al.*, 2005; Liégeois *et al.*, 2006; Eugster *et al.*, 2007; Dierker, Dreier, *et al.*, 2009; Callejo *et al.*, 2011). Evidence for EV-mediated Hh release comes from the study of genes involved in endocytosis and biogenesis of MVBs which reduce the Hh gradient and target gene activation in Drosophila models (Callejo *et al.*, 2011; Bischoff *et al.*, 2013). Although little is known about the secretion of Hh in vertebrates a study carried out by Vyas et al. identified the secretion of SHh in EV secreted from human HEK cells in culture furthermore they demonstrate that packaging of SHh along with other signalling proteins such as integrins on EVs modulate target gene expression (Vyas *et al.*, 2014)

In order to investigate the role of Hh as a potential biomarker for the detection of sub-clinical atherosclerosis initial studies were carried using the direct treatment of recombinant SHh on HiPSC-derived SNEPS. Herein, we provide evidence that HiPSC-derived S100β SNEPs undergo growth and myogenic differentiation to VSMC-like cells *in vitro* in response to recombinant rSHh. However, it is worth noting that the use of recombinant SHh as a comparison to EV-SHh is not cholesterol modified; therefore, differences in the functionality of rSHh on SNEPS compared to the release of active mature SHh may not be comparable. Nevertheless, following treatment with recombinant SHh, expression of Hh target gene GLI1 and myogenic marker CNN1 were significantly upregulated after 48 h and 7 d respectively in SNEPs. This is supported by previously reported data demonstrating that increases in Hh signalling regulate VSMCs proliferation and migration *in vitro* in CAD patients (Aravani *et al.*, 2019). Furthermore, adventitial $Sca1^{+}$ cells co-localize with SHh and Ptch1 and significantly contribute to intimal thickening *in vivo* (Passman *et al.*, 2008; Tsai *et al.*, 2012; Shikatani *et al.*, 2016; Dutzmann, Koch, Weisheit, Sonnenschein, Korte, Haertlé, Thum, Bauersachs, Sedding and J. M. Daniel, 2017; Di Luca *et al.*, 2021)

Given the pivotal role of EVs during cell-cell communication, the role of EV-mediated transport of SHh to control resident vascular S100β+ NE progenitor stem cells and whether they direct SNEPs to undergo proliferation and myogenic differentiation *in vitro* was evaluated. Imaging and tracking EVs can be challenging due to their small nature. In order to determine HiPSC-derived S100β SNEP uptake of HAEC EVs derived from normal and hyperglycemic cells EVs were fluorescently labelled enabling visualisation of their uptake individual cells, as their biodistribution in target cells SNEPs (Dehghani and Gaborski, 2020). Firstly, to assess the uptake of HAEC EVs isolated from hyperglycemic conditions, exogenous fluorescent labelling of HG-EVs was achieved using ExoGlow™ and detected using the Amnis Cell Stream flow cytometer. HAEC derived EV isolates demonstrated the expression ExoGlow™ (green). Commercially designed for specific labelling of EVs, inadvertent labelling of non-EV contaminants is often present in isolated EV samples that may give false-positive results. To ensure that ExoGlow labelling was EV specific, samples were incubated with TritonX-100 detergent to permeabilise EV membrane resulting in a decrease in fluorescently tagged EVs.

Although exogenous labelling of HAEC-derived EVs was successfully demonstrated, several limitations pertain including loss of EV integrity due to surface modifications, contamination with conjugation reagents, physical damage during labelling steps as well as a maximum conc. of EV proteins (100µg) in a given preparation which may have an effect on the initiation of signalling pathways in reporter cell line, SNEPs. Therefore, an alternative approach was taken for endogenous labelling of HG-EVs using Nir-Aza, an amphiphilic probe. The use of the Nir-Aza probe for EV labelling has been previously reported as an ideal candidate for endogenous EV labelling (Monopoli *et al.*, 2018). Incubation of NIR-AZA probe resulted in non-specific cell internalization leading to intracellular EV labelling in HAECs exposed to normal and hyperglycemic conditions. Following isolation HAECs derived EVs isolated from normal and hyperglycaemic conditions were detected using the Amnis Cell Stream flow cytometer. Although both ExoGlow and NirAza dyes showed successful labelling of RAEC-derived HG-EVs a difference in the detection of EV^+ events was demonstrate, this was due to the method by which EVs are labelled as ExoGlow™ labelling can only be conducted on EV preparations up to 100µg whereas NirAza labels any EV secreted from its host cell.

How EV encapsulated morphogens interact with their target receptors is unknown, nor is it clear whether EVs need to be endocytosed to trigger signalling. However, the possibility of activation through both endocytosis and receptor-ligand docking is strong since SNEP uptake of NirAza-HG-EVs in the cytoplasm of SNEPs was concentrated around the nucleus of the cell with significant membrane-bound staining, either plasma or nuclear, also evident using confocal microscopy. Having shown the uptake of HAEC HG-EVs by SNEP, further functional studies were carried out to address EV-dependent transfer of SHh specifically. Although the packaging of Hh morphogens into EVs for secretion in producing cells is not fully understood, EVs containing Hh have been identified in conditioned media from cultured inset cells (Guduric-Fuchs *et al.*, 2012; Beckett *et al.*, 2013; Gradilla *et al.*, 2014; Matusek *et al.*, 2014; Vyas *et al.*, 2014; Parchure *et al.*, 2015). SHh activation of Hh signalling following SNEP-uptake was clearly evident since SNEPs increased their expression of the Hh target gene, *GLI1* following exposure to HAEC-HG-EVs. In order to determine whether the increase in *GLI1* is hedgehog specific, two alternative mechanisms of Hh signalling inhibition were assessed; attenuation of GLI1 following (i) chemical inhibition of Hh signalling through exposure of HiPSC-derived NE SNEPs with cyclopamine, targeting Smo binding and attenuation of downstream signalling and activation of target Hh genes (ii) biological inhibition of Hh signalling through HiPSC-derived NE SNEP pre-treatment with monoclonal antibody 5E1 that recognises mammalian hedgehog ligands and prevents Hh signalling transduction via the Patched receptor (Cousins *et al.*, 2020). Although the main objective of this study was to determine the feasibility of EV-encapsuled Hh as a diagnostic biomarker of sub-clinical atherosclerosis, this finding also highlights the potential role of 5E1 as a potential therapeutic to inhibit the cascade of pathological events occurring as a result of the activation of the Hh signalling pathway as many studies have shown the role of EVs as a therapeutic in the era of personalised medicine as they can be isolated from a given patient, engineer to contain effect biological therapeutics i.e. 5E1 and readministered as a therapeutic treatment (Mentkowski *et al.*, 2018; R. G. Rogers *et al.*, 2020; Ma *et al.*, 2021; Witwer, 2021). Although Hh target genes were upregulated in HiPSC-derived stem cells in response to HAEC-derived EVs from hyperglycaemic conditions, it could not be assumed that this would result in myogenic differentiation. Therefore the expression of early differentiation marker CNN1 was measured after a 7 d treatment. Confirmation of an upregulation in CNN1 expression was demonstrated in

SNEPs following exposure to hyperglycaemic endothelial derived EVs, a response blocked by both by cyclopamine and 5E1.

A hallmark of sub-clinical atherosclerosis is proliferation and migration of a resident vascular cell resulting in the formation of an increased intima. Further studies evaluating HiPSC-derived SNEP confluency following HAEC-derived EV exposure demonstrated an increase in cell confluency in response to HG-EVs in comparison to NG and MT-EVs and HG-EVs with cyclopamine. Novel findings presented in this study demonstrated for the first time that (i) HAECs exposed to hyperglycaemic conditions secrete EVs that differ in morphological characteristics and EV-related proteins in comparison to HAECs exposed to normal conditions (ii) HiPSC-derived NE-SNEPs actively engage with HAEC derived EVs through internalisation of HiPSC-derived NE SNEPs, (iii) Exposure of HAECs to hyperglycaemic conditions resulted in an increase in SHh expression *in vitro (iv)* HAEC-derived EVs under hyperglycaemic conditions increase Hh signalling, growth and myogenic differentiation of HiPSC-derived NE SNEPs highlighting the potential application of SHh-EV detection as an early diagnostic biomarker for sub-clinical atherosclerosis.

Although a putative role of EV mediated intracellular communication via EC and stem cells is evident from these data, it is worth noting that EV cell-cell communication may also exist amongst various other resident vascular cell populations, including medial SMCs, adventitial progenitors and ECs themselves. This intrinsic intracellular communication pathway is present in both intimal lesions of developing plaques and in advanced plaques suggesting a role of EV participation in both initial and final stages of plaque formation in humans (Leroyer *et al.*, 2007; Bobryshev, Killingsworth and Orekhov, 2013; Perrotta and Aquila, 2016). Therefore, these data may offer a unique platform for the identification of novel diagnostic EV-biomarkers for subclinical detection of CVD.

Chapter 5:

Label-free photonic analysis of HiPSC-derived progenitor stem cells and their myogenic progeny in vascular lesions using supervised machine learning.

5.1 Introduction

Currently, the most frequently studied biomarkers for sub-clinical atherosclerotic disease are circulating biomarkers due to their abundance in bodily fluids, high specificity, high sensitivity, and ease of accessibility, some of which include C-reactive protein (CRP) for the detection of arterial inflammatory conditions (Landry *et al.*, 2017; Ries *et al.*, 2021), cardiac troponin I and T for the detection of acute myocardial infarction AMI, (Apple and Collinson, 2012), B-type natriuretic peptides (BNP AND NT-proBNP) for detection of AMI (Di Angelantonio *et al.*, 2009) and D-dimer for detection of thrombosis, ischemic heart disease and cardiovascular mortality (Tokita *et al.*, 2009). Due to the complexity of both sub-clinical and clinical atherosclerosis development, various diagnostic platforms, including imaging techniques in conjunction with circulating biomarkers, have been deployed to detect CVD, including CA, MRI, ECG, and more commonly, sonographic measurement of cIMT. A hallmark of subclinical atherosclerosis is the accumulation of VSMC-like cells leading to lesion formation, the origin of which has been extensively debated (Bennett, Sinha and Owens, 2016). Lineage tracing and scRNA-seq have revolutionised the analysis of vascular phenotypes in murine models, however these techniques are not as easily performed in human model systems due to the inaccessibility of sub-clinical biopsy samples for scRNA-seq analysis and impracticalities of lineage tracing, with the exception of one study which utilised gender dependent chromosomal X,Y tracking in bone marrow recipients with atherosclerotic disease (Caplice *et al.*, 2003). Therefore, the development of alternative platforms to detect discrete changes in cellular composition of healthy and diseased vessels is necessary for identification of sub-clinical atherosclerosis in human models.

A limitation of the current imaging techniques is the inability to detect plaques prior to their formation, ruling out their application for early detection of sub-clinical atherosclerosis. The use of light as a diagnostic tool has become an increasingly popular as it can be used to characterise biological samples identifying discrete changes indicative of disease (Yun and Kwok, 2017; Molony *et al.*, 2021). The interaction of light with matter, such as tissue, results in the scattering and absorption of light. Interruption of the path of light results in a scattering event which can be recorded and mapped. This characteristic can be used to determine discrete changes in healthy versus disease tissues and cells represented by a change in light scattering profiles. On the other hand, when

light is absorbed by a sample, the energy from the photons changes to vibrational or electronic energy and can result in inelastic scattering or accoustomechanical waves which can be recorded to yield physical, biochemical and molecular information about a sample (Yun and Kwok, 2017).

Two novel label-free technology platforms deployed as diagnostic tools to interrogate discrete cell populations and cellular changes in early 'transitional' atherosclerotic lesions are the vibrational spectroscopy and single cell photonics (Qavi *et al.*, 2009; Cheng and Xie, 2015). Vibrational spectroscopy is a subset of spectroscopy that analyses vibrations within a given material, in this case, a cell, providing a unique spectroscopic output reading that acts as a 'fingerprint' for detection in complex systems such as arterial neointimal formation. FTIR and Raman spectroscopy are two complementary vibrational spectroscopy techniques that can play a significant role in the clinical treatment of disease. FTIR and Raman have previously been used to investigate the components of atherosclerotic plaques and have provided a detailed characterisation of lipid content components of diseased tissues (Lattermann *et al.*, 2013). The spectrum of vibrational energies can be utilised to characterise a molecular structure or changes to it due to environmental cues, including circulating risk factors associated with CVD such as elevated glucose, homocysteine, or cholesterol or in response to the external environment, including hemodynamic factors.

In addition to the use of vibrational spectroscopy, single cell photonics has emerged as a diagnostic and prognostic tool due to advantageous factors, including high sensitivity, low limits of detection, and most importantly for clinical ease of use, non-invasive analysis (Qavi *et al.*, 2009). LiPhos is one such tool that incorporates microfluidics with single cell photonics to reveal light scattering, absorbance and auto-fluorescent emissions from cells that are closely associated with metabolism and protein structural changes under normal and pathological conditions (Ranjit *et al.*, 2015; Habibalahi *et al.*, 2020). In order to measure label-free single-cell photonic emissions *ex vivo,* the use of LoaD platforms has been established (Molony *et al.*, 2021). This allows single-cell detection of photonic emissions across five broadband light wavelengths (between 465 -670nm), enabling the detection of discrete changes in healthy and diseased samples *ex vivo*.

It is clear that alternative diagnostic tools such as FTIR, Raman, and LiPhos have the potential to further our understanding of the development of sub-clinical atherosclerosis through the detection of discrete changes in the composition of the vessel wall. Complementary machine learning tools based primarily on artificial neural network geometries have also been developed as a predictive method to obtain real-time decision-making systems to analyse spectroscopic data (Pradhan *et al.*, 2020). The analysis of tissues and cells using vibrational spectroscopy and photonics results in the generation of large datasets. Principal component analysis (PCA), a dimensionality-reduction method that is often used to reduce the dimensionality of large data sets, by transforming a large set of variables into a smaller one focusing on the greatest variation between groups across datasets. Positive loadings indicate a variable and a principal component are positively correlated: an increase in one results in an increase in the other. Negative loadings indicate a negative correlation. Large (either positive or negative) loadings indicate that a variable has a strong effect on that principal component. (Ling *et al.*, 2002). While PCA identifies differences between the data sets, Linear Discriminant Analysis (LDA) maximises the separability between groups across datasets for the purpose of classification grouping similar spectral sets. In summary PCA performs a feature reduction of the data and LDA classifies the data into one of two or more classes (Crow *et al.*, 2005; Perfecto-Avalos *et al.*, 2019). Similar to LDA an alternative tool known as multi-layer perceptron analysis (MLP) can be used to classify large data sets by artificial neural network (ANN) analysis. ANNs are algorithms which are loosely modelled on the neuronal structure observed in the mammalian cortex and are arranged with a number of input neurons, which represent the information taken from each of the features in the dataset which are then feed into any number of hidden layers before passing to an output layer in which the final decision is presented.

In this Chapter, the combination of vibrational spectroscopy and single cell photonics with supervised machine learning tools, PCA, LDA and multilayer perceptron (MLP) neural network analyses was harnessed to discriminate human S100β vascular stem/progenitor cells from their myogenic progeny *in vitro.* Furthermore, photonic interrogation of single cells from healthy and diseased arteriosclerotic human vessels was then used to determine the presence of S100β progenitors and their myogenic progeny within vascular lesions in an effort to predict the origin of VSMC-like cells during neointimal formation using supervised machine learning.

5.2 Objectives

The main objectives of this chapter were.

(i) To validate the use of vibrational spectroscopy (FTIR and Raman) to discriminate
HiPSC, HiPSC-derived embryologically defined progenitor stem cells (NE and PM) and their respective myogenic progeny

(ii) To interrogate normal, aged and diseased arteriosclerotic (without plaque) and atherosclerotic lesions (with plaque) Raman datasets for the presence of HiPSC-derived progenitor stem cells and/or their myogenic progeny using supervised machine learning in an effort to determine the origin of VSMC-like cells in vascular lesions.

(iii) To validate the use single cell autofluorescence photonic emissions to discriminate HiPSC, HiPSC-derived embryologically defined progenitor stem cells (NE and PM) and their respective myogenic progeny

(iv) To interrogate single cell autofluorescence photonic emissions from diseased arteriosclerotic (without plaque) and atherosclerotic lesions (with plaque) for the presence of HiPSC-derived progenitor stem cells and/or their myogenic progeny using supervised machine learning in an effort to determine the origin of VSMC-like cells in vascular lesions.

5.3 Strategy

The main aim of this chapter was to interrogate vascular cell phenotypes of distinct embryological origin, indicative of sub-clinical atherosclerosis, and discriminate them using a combination of vibrational spectroscopy (FTIR, Raman) and single cell autofluorescence photonic emissions (AF). Furthermore, to determine if the spectral datasets representing distinct cellular phenotypes could be detected within diseased atherosclerotic and arteriosclerotic tissues thereby validating their clinical application for early detection of sub-clinical atherosclerosis.

Firstly, a HiPSC *in vitro* cell culture model (previously characterised in Chapter 4), including HiPSC-derived NE and PM SCs and their myogenic progeny, were used to generate distinct FTIR and Raman spectral datasets to determine their application in

discrimination of undifferentiated HiPSCs from their progenitor stem cells and furthermore from their respective myogenic progeny. In order to do so, HiPSCs, HiPSC-derived progenitor stem cell populations (NEPs, SNEPs, NPCs and PMs) and their respective myogenic progeny were prepared for spectral processing as described in Section 2.2.9. FTIR and Raman spectra of the cytoplasm, were recorded for each population. Spectral datasets were then baseline corrected and subjected to cosmic ray and MIE scattering removal using the extended multiplicative signal correction algorithm. Datasets were then smoothed using Savitzky-Golay filter (k = 3; w = 7) to reduce noise. Dimensionality reduction was achieved through a Multiclass Fisher's Linear Discriminant Analysis (Multiclass FLDA) pre-processing filter, as previously described using WEKA machine learning tool kit, version 3.8.4 (Gunaratne *et al.*, 2019; Pradhan *et al.*, 2020) and further analysed by PCA and LDA and MLP using the multivariate statistical package, PAST4 and WEKA machine learning tool respectively (Section 2.2.11). Secondly, published Raman spectral datasets from normal, aged, arteriosclerotic (without plaque) and atherosclerotic (with plaque) tissues were acquired. Interpolation was carried out (as described in Section 2.2.9.1) to facilitate training of LDA and MLP algorithms before determining (i) if Raman spectral datasets could be used to discriminate normal vessels from diseased vessels (ii) if the Raman spectral datasets of normal or diseased vessels had any spectral similarities to HiPSC-derived cells or stem cell-derived VSMCs.

Having shown the application of Raman to discriminate HiPSCs and their derived progeny, as well as discrimination of normal versus diseased tissues, a novel LoaD platform was used to discriminate to measure label-free single-cell AF photonic emissions across five broadband wavelengths (λ465, λ530, λ565, λ630 and λ670 nm with a bandwidth of 20 nm) HiPSCs, HiPSC-derived NE progenitor stem cell populations (NEPs, SNEP and NPCs) and their respective myogenic progeny. Cells were loaded onto the biochip microfluidic device allowing for V-cup capture (Section 2.2.10.1). Following capture, single-cell photonic readings across five wavelengths were recorded and processed for analysis (Section 2.2.11). In order to determine the application of AF to discriminate normal versus diseased vessels, single cell isolation of cadaveric tissues from normal, atherosclerotic (with plaque) and arteriosclerotic (without plaque) was carried out *ex vivo*. Cells were loaded onto the biochip microfluidic device allowing for V-cup capture Following capture, single-cell photonic readings across five wavelengths

were recorded and processed for analysis . AF datasets of HiPSC-derived NE SCs and their myogenic progeny were interrogated to determine if these spectral datasets could be used to discriminate whether they had any spectral similarities to atherosclerotic or arteriosclerotic spectra.

5.4 Results

5.4.1 FTIR and Raman spectroscopy discriminates HiPSC, and HiPSC derived embryologically defined progenitor stem cells *in vitro*

Detection of sub-clinical atherosclerosis via early detection of 'transitional' adaptive lesion formation is paramount to facilitate early primordial treatment preventing CVD pathogenesis. A hallmark of sub-clinical atherosclerosis is the formation of a neointima made up of VSMC-like cells, the origin of which remains controversial. It is now accepted that the embryological origin, NE versus mesoderm, of VSMCs influences disease localisation and progression (Bargehr *et al.*, 2016). Vibrational spectroscopy techniques have emerged as novel techniques to detect discrete changes in extracellular and intracellular constituents of cells. Using HiPSC to generate embryologically defined NE and PM progenitor stem cells, Raman and FTIR spectroscopy were deployed to discriminate HiPSC-derived progeny *in vitro* based on these biomolecular changes.

HiPSC-derived progenitor stem cells were seeded on calcium fluoride slides for confocal imaging followed by FTIR and Raman spectroscopy. The raw spectra were recorded, processed, and the mean spectrum are presented. Confocal imaging was performed in parallel to allow tracking of the morphological changes associated with differentiation of HiPSCs to intermediate progenitors (NE and PM). Confocal imaging revealed a distinct change in cellular morphologies following their differentiation to intermediate progenitors. HiPSCs *in vitro* grow as dense, defined colonies where all cells within the colony have a homogenous, ovoid shape, with a size of ~ 20 μm in length (Figure 5.1 A, B). Following chemical induced differentiation of HiPSCs to NE and PM intermediate progenitors, the cells detach from the colony and grow as single cells *in vitro*. NE progenitors grow as neural-like cells with defined lamellipodia (Figure 5.1 C-D). In contrast, PM progenitors are oval in shape (Figure 5.1 F).

Having confirmed the morphological changes associated with HiPSC differentiation to NE and PM intermediate progenitors, FTIR spectra were generated for the cytoplasm of each progenitor subtype over a wavenumber range of 1000-1800cm^{-1}. Using WEKA machine learning tool kit, FLDA was carried out to perform a dimensionality-reduction of the large FTIR data set into small sets of variables whilst retaining all information.

PCA carried out using the multivariate statistical package PAST4 was used to focus on the greatest variation between HiPSCs and HiPSC-derived NE (NEP, SNEP, NPC) and PM progeny. The order of the PCs denoted their importance in the dataset, whereby PC1 described the highest amount of variation. A scatter plot of specimens along the first two canonical axes was produced to show maximal and second to maximal separation between all groups. The axes represent linear combinations of the original variables as in PCA, and eigenvalues indicate amount of variation explained by these axes. When only two groups are analysed, a histogram is plotted. The data were classified by assigning each point to the group that gives minimal Mahalanobis distance to the group mean. The Mahalanobis distance was calculated from the pooled within-group covariance matrix, giving a linear discriminant classifier. The given and estimated group assignments was listed for each point. In addition, group assignment were cross-validated by a leave-one-outcross-validation (jack-knifing) procedure. Using PCA 2-way multivariate statistical analysis variation between HiPSC and HiPSC-derived NE and PM progenitor stem cells, a significant separation was observed using PCA scatter (Figure 5.2 A-D). Although clear separation based on PCA of FTIR datasets was demonstrated between HiPSC and HiPSC-derived progeny, direct comparison of spectra from HiPSC-derived NE and PM progenitor stem cells exhibited some similarities (Figure 5.2 E). Using the multivariate statistical package, PAST4, further LDA of spectra from HiPSC and HiPSC-derived NE and PM progenitor stem cells was used to demonstrate the maximum separability between groups across the data set. LDA analysis presented as a histogram revealed that the FTIR profile of HiPSC and HiPSC-derived NE and PM progenitors could be easily separated from each other (Figure 5.3 A-D). Furthermore analysis of HiPSC-derived progeny only showed a distinct separation of HiPSC-derived NE progenitors from PM progeny (Figure 5.3 E), with little differences revealed in HiPSC-derived NE progeny only (Figure 5.3 F).

Raman spectra were generated for each progenitor subtype over a wavenumber of 400-1800 cm^{-1}. Raw data sets were pre-processed for background correction, and smoothing correction was applied. As above, PCA carried out using the multivariate statistical package PAST4 to focus on the greatest variation between HiPSCs and HiPSC-derived NE (NEP, SNEP, NPC) and PM progeny. Using PCA 2-way multivariate statistical analysis variation between HiPSC and HiPSC-derived NE and PM progenitor stem cells a significant separation presented using PCA scatter plots was demonstrated (Figure 5.4 A-D). Although clear separation based on PCA of Raman datasets was demonstrated between HiPSC and HiPSC-derived progeny direct comparison of HiPSC-derived NE and PM progenitor stem cells showed some similarities (Figure 5.4 E). Further LDA using the multivariate statistical package, PAST4 of HiPSC and HiPSC-derived NE and PM progenitor stem cells was used to demonstrate the maximum separability between groups across the data set. LDA analysis presented as a histogram, using the multivariate statistical package PAST4, revealed that the Raman profile of HiPSC and HiPSC-derived NE and PM progenitors could be easily separated from each other (Figure 5.5 A-D). Furthermore analysis of HiPSC-derived progeny only demonstrated no significant separation of HiPSC-derived NE and PM progenitors (Figure 5.3 E).

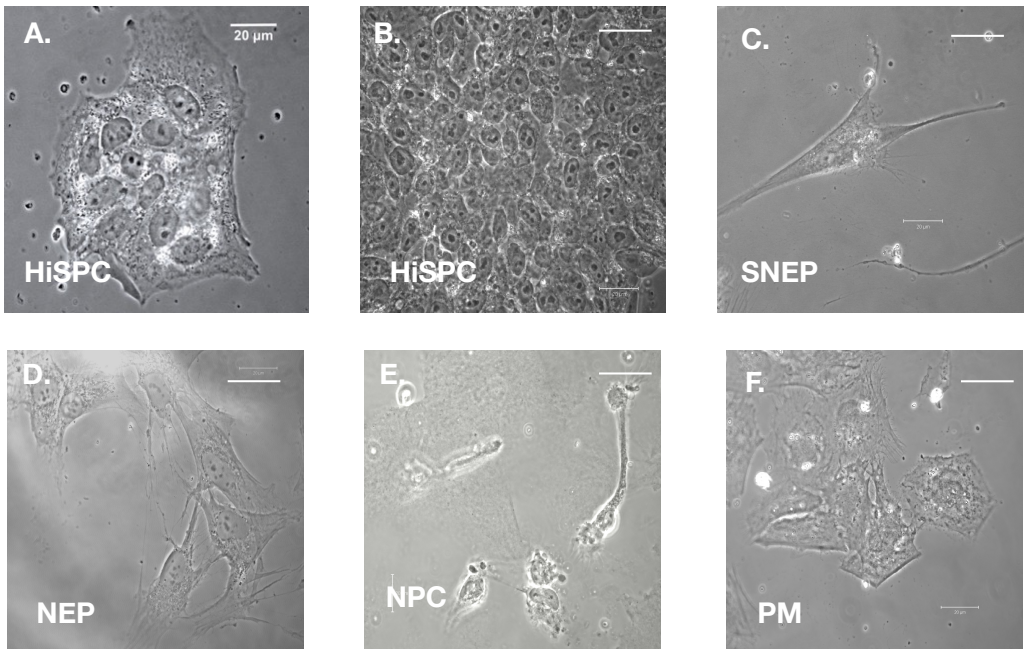

Figure 5.1 Confocal imagining of HiPSC and HiPSC-derived NE and PM progenitor stem cells. (A) Representative confocal images of HiPSC colonies prior to differentiation (A, B), HiPSC-derived NE progenitor stem cells, and (C-E) HiPSC-derived PM progenitor stem cells (F) —scale bar representative of 20µm.

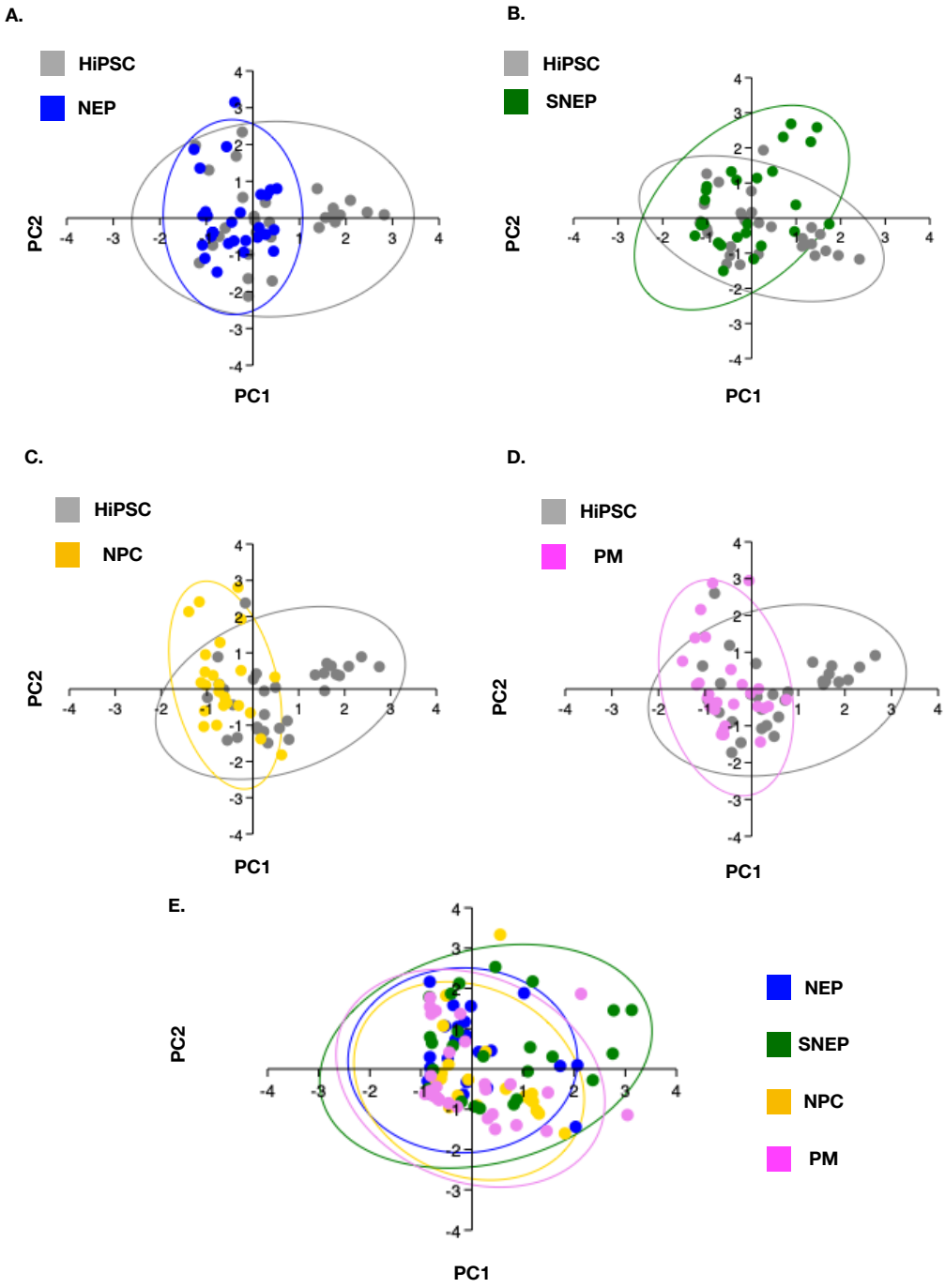

Figure 5.2. PCA loading plots of FTIR spectra for the cytoplasm of HiPSC and HiPSC-derived NE and PM progenitor stem cells. A 2-way scatter plot of the first two principal components after PCA of HiPSC compared to NEP (A), SNEP (B), NPC (C), and PM (D) in *vitro*. (E) A 2-way scatter plot of the first two principal components after PCA of HiPSC-derived NE and PM progeny. Data are representative of 30 cells across 1000-1800 cm^{-1} wavelengths.

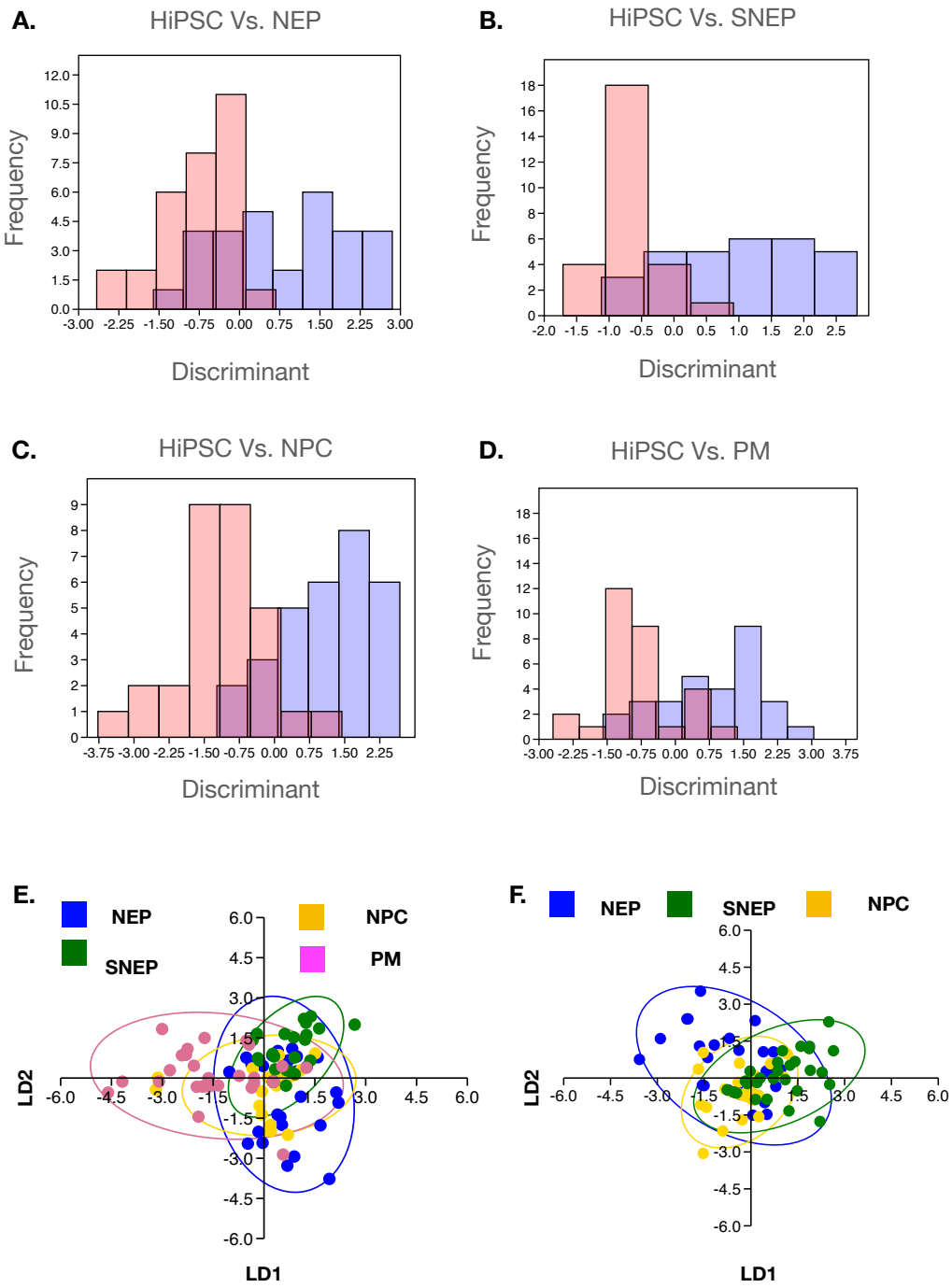

Figure 5.3 LDA loading plots of FTIR spectra for the cytoplasm of HiPSC and HiPSC-derived NE and PM progenitor stem cells. A histogram (discriminant vs. frequency) of HiPSC compared to NEP (A), SNEP (B), NPC (C), and PM (D) *in vitro*. A 2-way scatter plot of the first two components after LDA of HiPSC-derived NE and PM progeny (E) and HiPSC-derived NE progeny only (F). Data are representative of 30 cells across 1000-1800 cm^{-1} wavelengths.

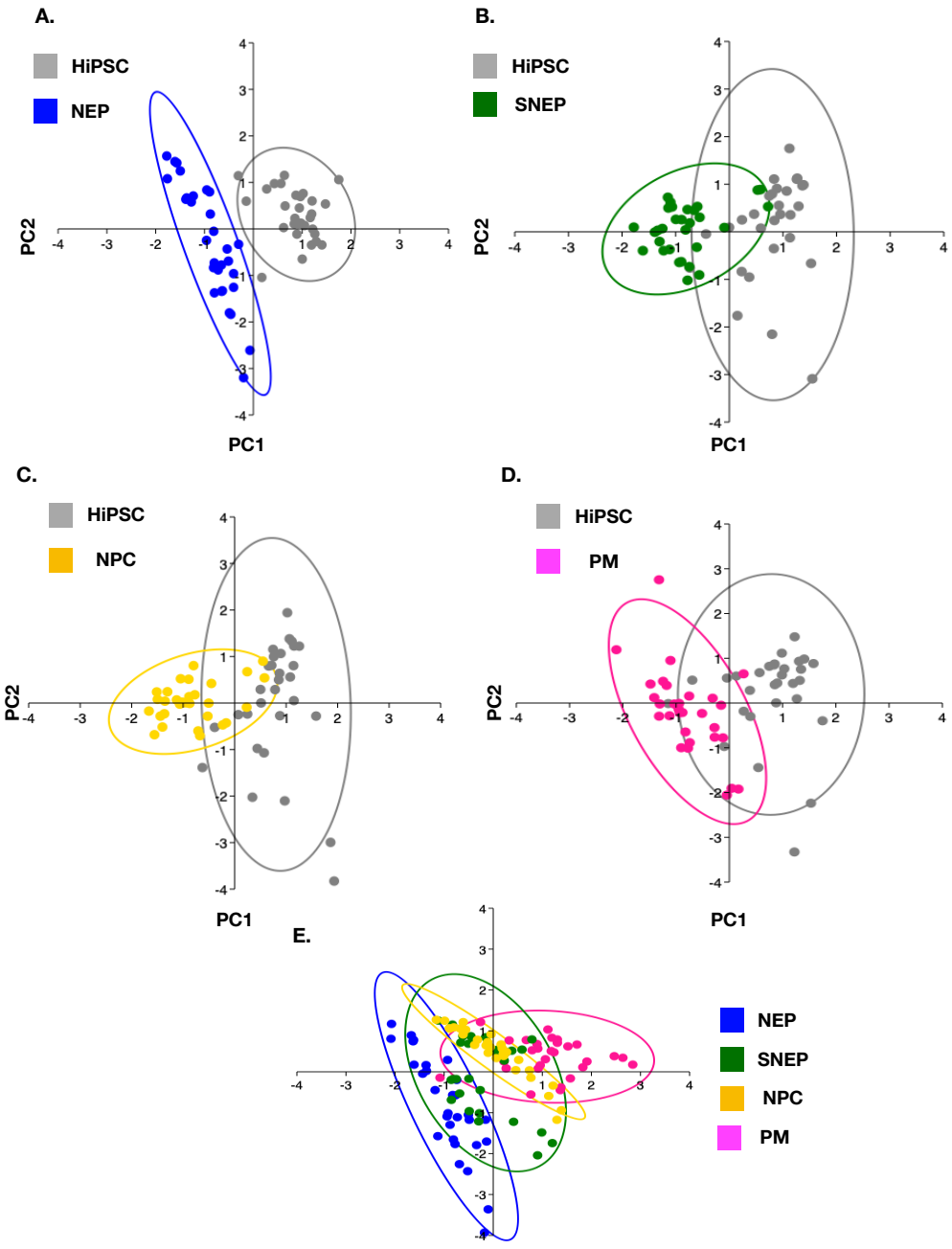

Figure 5.4 PCA loading plots of Raman spectra for the cytoplasm of HiPSC and HiPSC-derived NE and PM progenitor stem cells. A 2-way scatter plot of the first two principal components after PCA of HiPSC compared to NEP (A), SNEP (B), NPC (C), and PM (D) *in vitro*. (E) A 2-way scatter plot of the first two principal components after PCA of HiPSC-derived NE and PM progeny. Data are representative of 30 cells across 400-1000 cm^{-1} wavelengths.

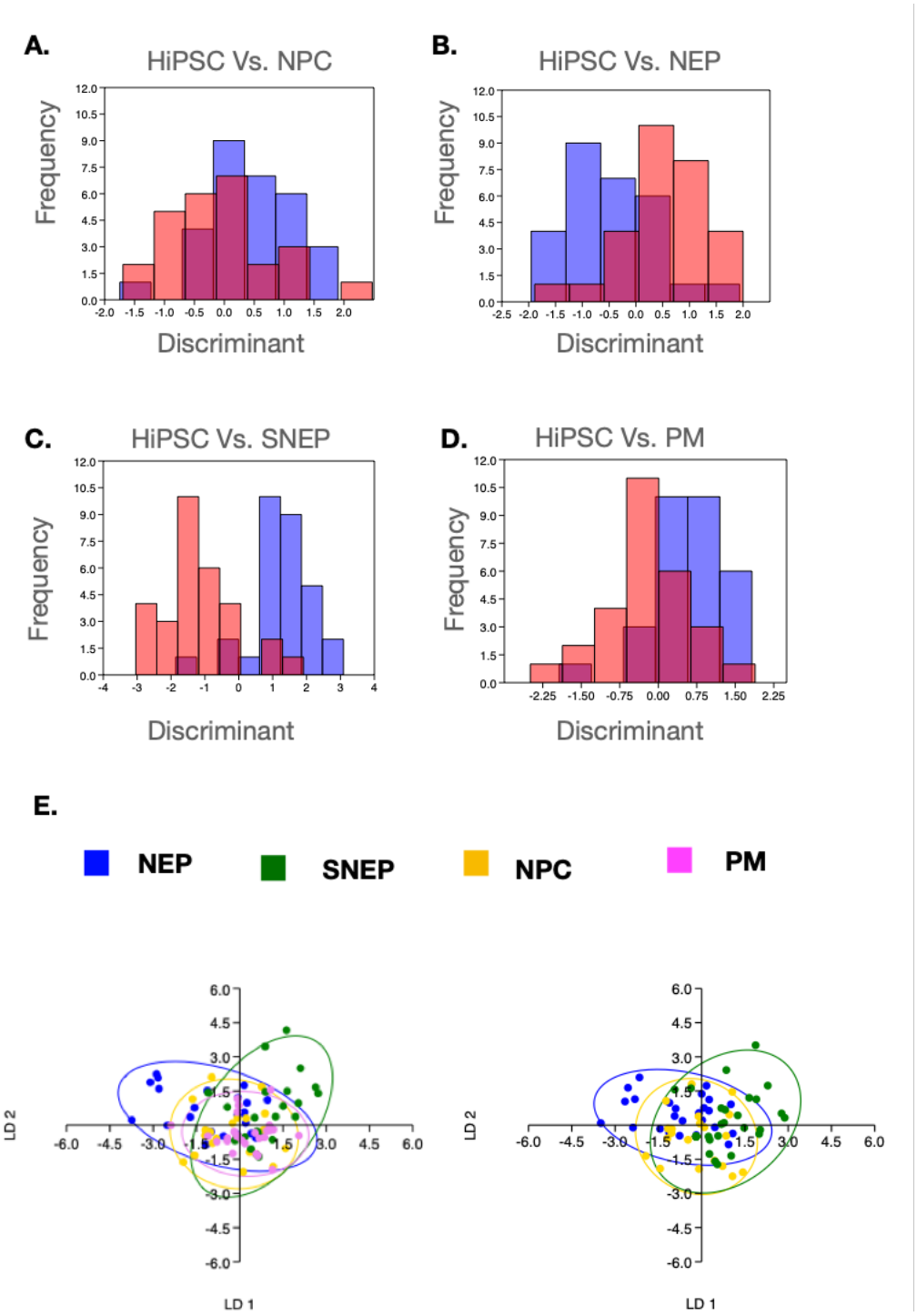

Figure 5.5 LDA loading plots of Raman spectra for the cytoplasm of HiPSC and HiPSC-derived NE and PM progenitor stem cells. A histogram (discriminant vs. frequency) of HiPSC compared to NPC (A), NEP (B), SNEP (C), and PM (D) *in vitro*. A 2-way scatter plot of the first two components after LDA of HiPSC-derived NE and PM progeny and HiPSC-derived NE progeny only (E). Data are representative of 30 cells across 400-1000 cm^{-1} wavelengths.

5.4.2 FTIR and Raman spectroscopy discriminates HiPSC-derived progenitor stem cells from their myogenic progeny subtypes *in vitro*.

The risk of arteriosclerotic disease may depend, in part, on the embryological origin of VSMC progenitors with VSMC of NE origin (ascending) exhibiting a higher risk compared to their PM counterparts (descending) within aortic regions (Cheung *et al.*, 2012; Di Luca *et al.*, 2021). To determine the feasibility of utilising FTIR and Raman as discriminators of distinct embryological vascular progenitor and their myogenic progeny phenotypes *in vitro*, we generated HiPSC-derived NE and PM progenitors and their respective myogenic progeny phenotypes before they were interrogated by FTIR and Raman spectroscopy.

Parallel confocal imaging facilitated tracking of morphological changes to compliment the spectral analysis of discrete changes intracellular components during differentiation. Confocal imaging revealed a distinct change in cellular morphologies following myogenic differentiation.. A distinct increase in the size of the nucleus and span of the cytoplasm was observed following myogenic of differentiation of NE and PM progenitor stem cells. In addition, the development of continuous myofilaments extending across the cytoplasm was observed in myogenic progeny from both NE and LM progenitors, indicative of the transition of these cells to a defined contractile function (Figure 5.6 A-C).

Similar to the analyses carried out in Section 5.4.3 PCA was carried to focus on the greatest variation between HiPSC-derived NE and PM progenitors (SNEP, NPC, PM) and their myogenic progeny (SNEP-SMC, NPC-SMCM PM-SMC). Using PCA 2-way multivariate statistical analysis variation between HiPSC-derived NE and PM progenitor stem cells and their myogenic progeny a significant separation presented using PCA scatter plots was demonstrated (Figure 5.7 A-C). Although clear separation based on PCA of FTIR datasets was demonstrated between HiPSC-derived NE and PM and their myogenic progeny direct comparison of HiPSC-derived NE and PM SMCs showed some similarities, with NPC-SMCs demonstrating the greatest difference (Figure 5.7 E). Further LDA using the multivariate statistical package, PAST4 of HiPSC-derived NE and PM progenitors and their myogenic progeny was used to demonstrate the maximum

separability between groups across the data set. LDA analysis presented as a histogram, using the multivariate statistical package PAST4, revealed that the FTIR profile of HiPSC-derived NE and PM progenitors and their myogenic progeny could be easily separated from each other (Figure 5.8 A-C). Similar to PCA of FTIR datasets HiPSC-derived NE and PM SMCs showed some similarities, with NPC-SMCs demonstrating the greatest difference (Figure 5.8 E)

Raman spectra were generated for each HiPSC-derived NE and PM SMC subtype over a wavenumber of 400-1800 cm^{-1}. Raw data sets were pre-processed for background correction, and smoothing correction was applied. As above, PCA carried out using the multivariate statistical package PAST4 was used to focus on the greatest variation between HiPSC-derived NE and PM progenitors (SNEP, NPC, PM) and their myogenic progeny (SNEP-SMC, NPC-SMCM PM-SMC). Using PCA 2-way multivariate statistical analysis variation between HiPSC-derived NE and PM progenitor stem cells and their SMC progeny a significant separation presented using PCA scatter plots was demonstrated (Figure 5.9 A-C).

Although clear separation based on PCA of Raman datasets was demonstrated between HiPSC and HiPSC-derived progeny, direct comparison of HiPSC-derived NE and PM SMCs revealed some similarities between PM-SMC and NPC-SMC with the greatest difference represented by SNEP-SMCs (Figure 5.9 D). Further LDA using the multivariate statistical package, PAST4 of HiPSC-derived NE and PM progenitor SMCs was used to demonstrate the maximum separability between groups across the data set. LDA analysis presented as a histogram, using the multivariate statistical package PAST4, revealed that the Raman profile of HiPSC-derived NE and PM progenitors and their myogenic progeny could be easily separated from each other (Figure 5.10 A-C). Furthermore analysis of HiPSC-derived NE and PM SMCs only demonstrated similarities between SNEP-SMCs and PM-SMCs (Figure 5.10 E).

Having shown the ability of FTIR and Raman to successfully separate HiPSC from their NE and PM progenitor stem cells and further separation of HiPSC-derived NE and PM stem cells from their myogenic progeny using the multivariate statistical package, PAST4, an alternative machine learning tool, WEKA was used to validate the maximum separability of HiPSC, HiPSC-derived stem cells and HiPSC stem cell-derived SMCs.

The data set was loaded and pre-processed using the FLDA filter to achieve dimensionality reduction, it was the processed using the “Classify” panel with the implementation of for LDA. Cross validation confirmed that optimized neural networks can identify all cell types with high performance, based only on their Raman spectral profile and resulted in an F-score of 1.00. The cells were also trained on a 66 % split before the remainder was tested and the F score remained at 1.00 this was presented as a confusion matrix (Figure 5.11 A). Each HiPSC-derived cell population (i.e. NEP, SNEP, NPC, PM, NPC-SMC, SNEP-SMC, PM-SMC) was then supplied as an unknown. Interrogation of the trained LDA set revealed the spectral profile of cells generated from HiPSCs pr HiPSC-derived progenitor stem cells could be easily separated from each other with accuracies of 93%, 100%, 80%, 97%, 80%, 77%, 84%, and 73% for HiPSC, NEP, NPC, SNEP, PM, NPC-VSMC, PMV-SMC, and SNEP-VSMC respectively on a cross-validated leave-one-out basis (Figure 5.11 B).

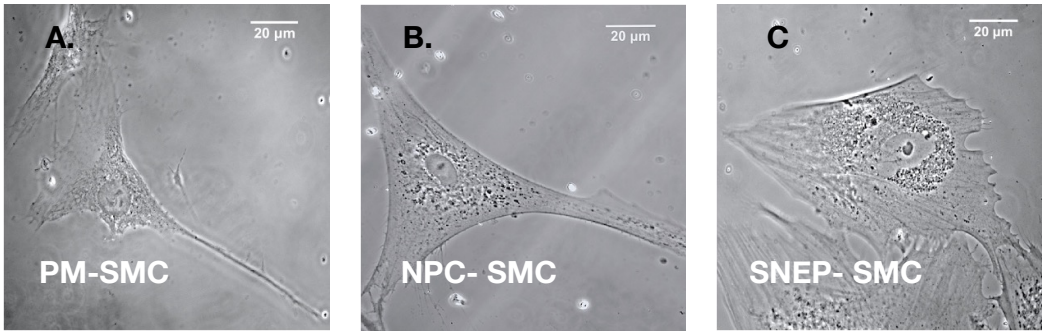

Figure 5.6 Confocal imagining and FTIR spectral analysis of HiPSC-derived PM-VSMC, NEP-VSMC, and SNEP-VSMC. (A) Representative confocal images of HiPSC-derived PM to VSMC differentiation, (B) HiPSC-derived NE to SMC differentiation (C) HiPSC-derived-SNEP to SMC differentiation —scale bar representative of 20µm.

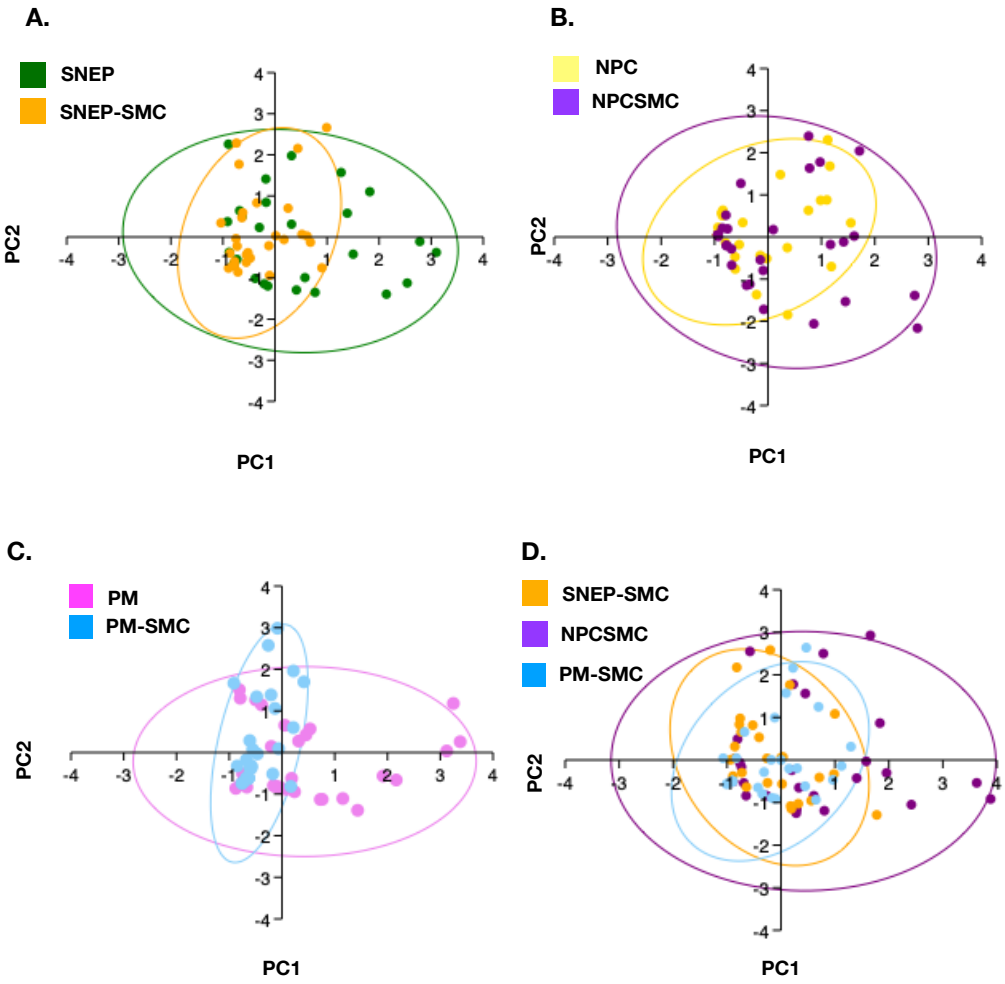

Figure 5.7 PCA loading plots of cytoplasm FTIR spectra for HiPSC-derived NE and PM and their respective myogenic progeny. A 2-way scatter plot of the first two principal components after PCA of HiPSC-NE and PM compared to SMC subtypes (A) SNEP vs. SNEP-SMC (B), NPC vs. NPC-VSMC and (C) PM vs. PM-VSMC *in vitro*. (D) A 2-way scatter plot of the first two principal components after PCA of HiPSC-derived NE and PM derived SMCs. Data are representative of 30 cells across 1000-1800 cm^{-1} wavelengths.

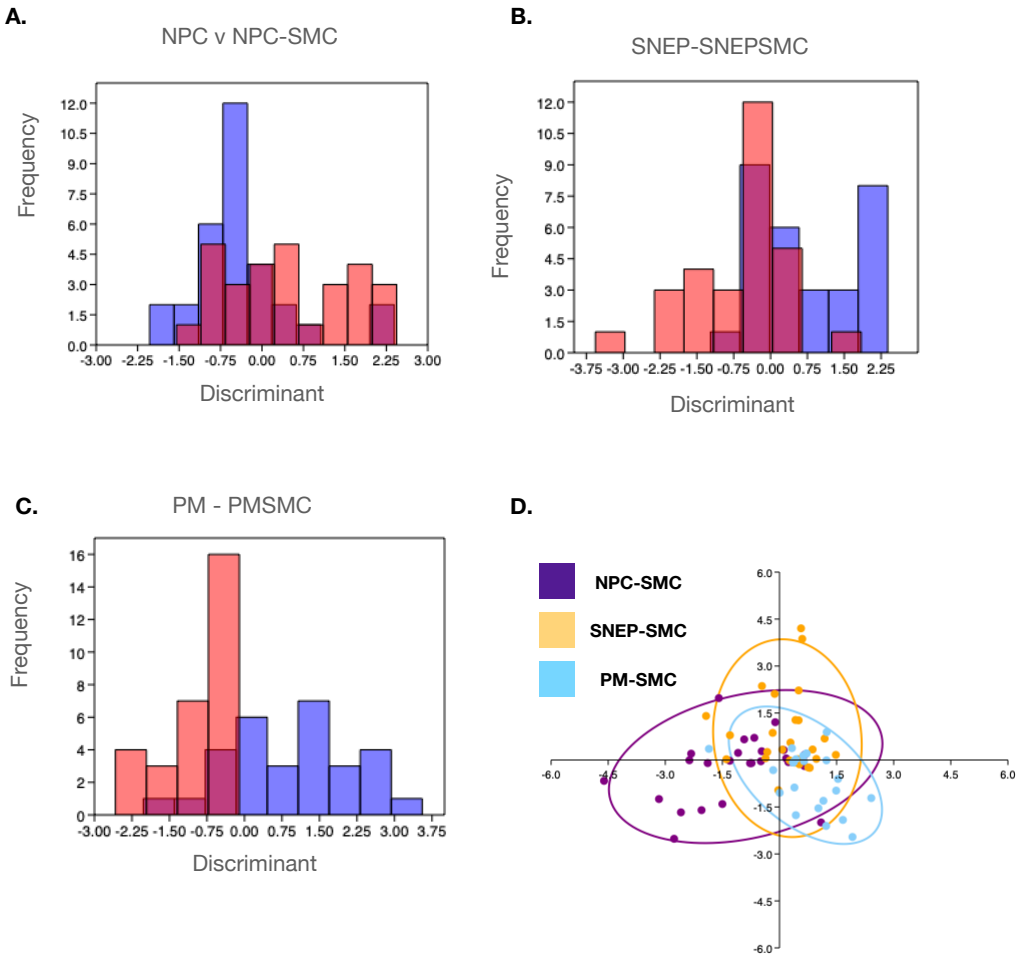

Figure 5.8 LDA loading plots of cytoplasm FTIR spectra for HiPSC-derived NE and PM and their respective myogenic progeny. A 2-way scatter plot of the first two principal components after PCA of HiPSC-NE and PM compared to SMC subtypes (A) SNEP vs. SNEP-SMC (B), NPC vs. NPC-VSMC and (C) PM vs. PM-VSMC *in vitro*. (D) A 2-way scatter plot of the first two principal components after PCA of HiPSC-derived NE and PM derived SMCs. Data are representative of 30 cells across 1000-1800 cm^{-1} wavelengths.

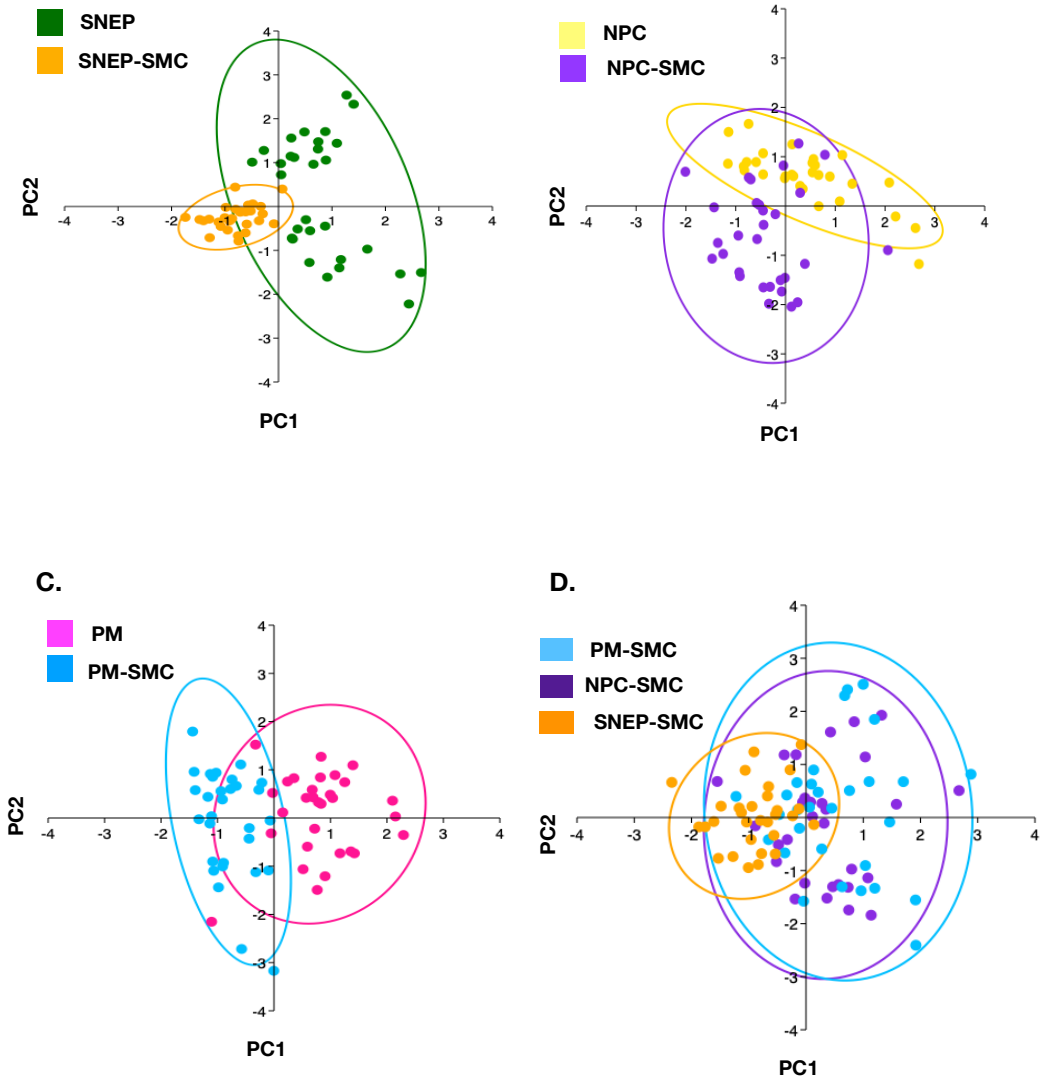

Figure 5.9 PCA loading plots of cytoplasm Raman spectra for HiPSC-derived NE and PM and their respective myogenic progeny. A 2-way scatter plot of the first two principal components after PCA of HiPSC-NE and PM compared to SMC subtypes (A) SNEP vs. SNEP-SMC (B), NPC vs. NPC-VSMC and (C) PM vs. PM-VSMC *in vitro*. (D) A 2-way scatter plot of the first two principal components after PCA of HiPSC-derived NE and PM derived SMCs. Data are representative of 30 cells across 400-1000 cm^{-1} wavelengths.

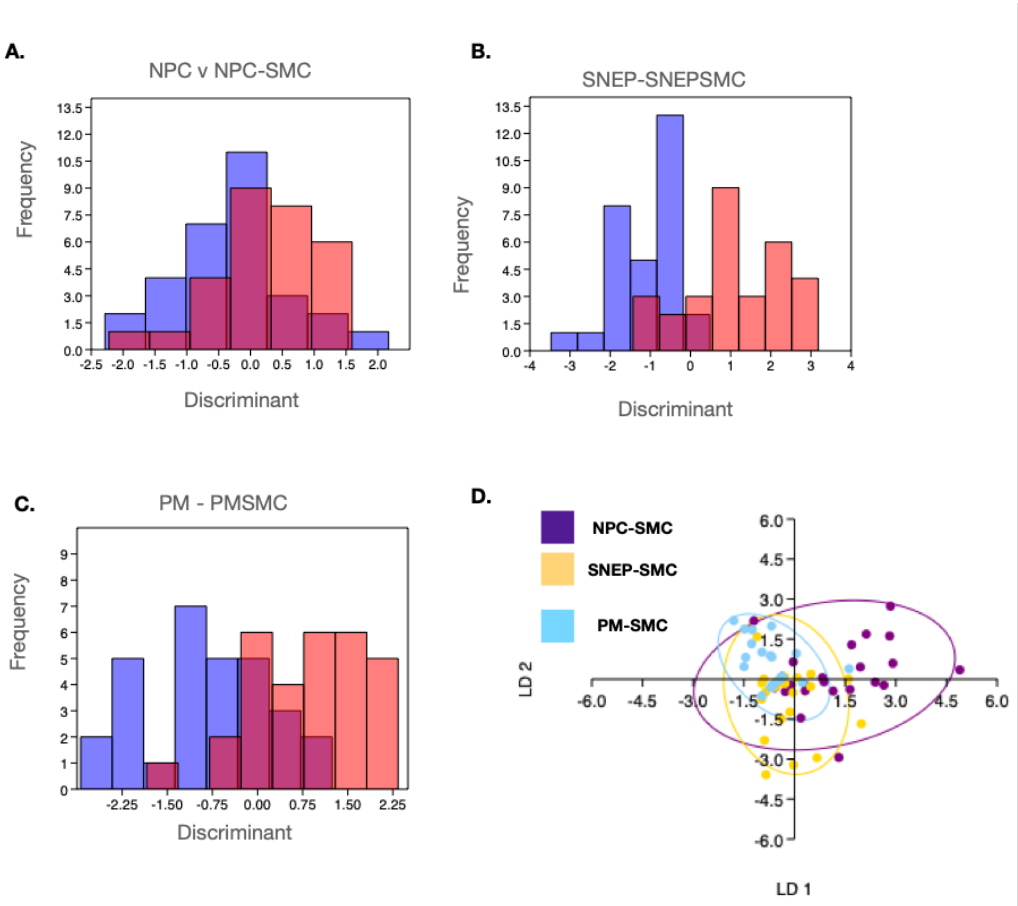

Figure 5.10 LDA loading plots of cytoplasm FTIR spectra for HiPSC-derived NE and PM and their respective myogenic progeny. A 2-way scatter plot of the first two principal components after LDA of HiPSC-NE and PM compared to SMC subtypes (A) NPC vs. NPC-SMC (B), SNEP vs. SNEP-SMC and (C) PM vs. PM-SMC *in vitro*. (D) A 2-way scatter plot of the first two principal components after PCA of HiPSC-derived NE and PM derived SMCs. Data are representative of 30 cells across 400-1000 cm^{-1} wavelengths.

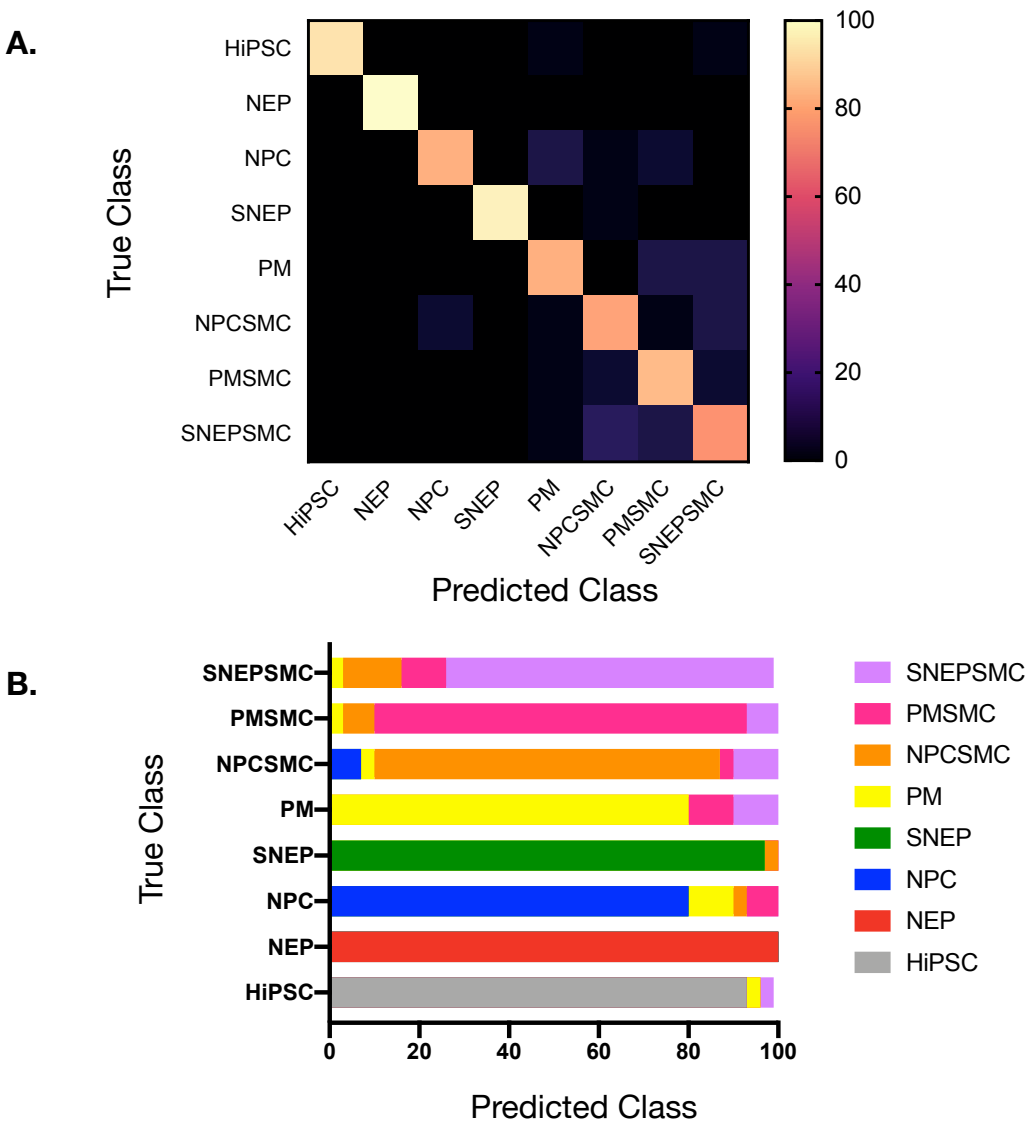

Figure 5.11 LDA of cytoplasmic Raman spectra from HiPSC derived NE and PM progenitor stem cells and their respective myogenic progeny. Confusion matrix of true class and predicted class following a leave-one-out cross-validation procedure by the LDA classifier. Data representative 240 cells across eight cell lines.

5.4.3 FTIR and Raman spectroscopy discriminates healthy human vessels from aged and atherosclerotic vessels

A hallmark of CVD is subclinical atherosclerosis is intimal thickening and arterial remodelling of the vessel wall. Arterial remodelling was categorised into three main categories; atherosclerosis, primary calcification, and fibromuscular IMT, making up most cases (Fishbein and Fishbein, 2009). Having demonstrated the ability of Raman spectroscopy to discriminate between intermediate progenitors of embryologically defined origins and their respective myogenic progeny, Raman spectral datasets from healthy and diseased human tissue datasets were interrogated for the presence of these cellular phenotypes. In order to do so, previously published healthy, aged, arteriosclerotic and atherosclerotic human Raman spectral datasets were first interpolated to match spectral wavelengths from intermediate progenitors and their respective myogenic progeny before they were interrogated for similarities using supervised machine learning.

In order to determine the greatest variation between the aforementioned disease states, PCA was carried out. The order of the PCs denoted their importance in the dataset, whereby PC1 described the highest amount of variation. A scatter plot of specimens along the first two canonical axes was produced to show maximal and second to maximal separation between all groups. The axes represent linear combinations of the original variables as in PCA, and eigenvalues indicate amount of variation explained by these axes. When only two groups are analysed, a histogram is plotted. The data were classified by assigning each point to the group that gives minimal Mahalanobis distance to the group mean. The Mahalanobis distance was calculated from the pooled within-group covariance matrix, giving a linear discriminant classifier. The given and estimated group assignments was listed for each point. In addition, group assignment were cross-validated by a leave-one-outcross-validation (jack-knifing) procedure. Using PCA 2-way multivariate statistical analysis variation between normal vs. aged, atherosclerosis and arteriosclerosis a significant separation presented using PCA scatter plots was demonstrated (Figure 5.12 A-C).

Furthermore, a clear separation was demonstrated between normal, atherosclerosis and arteriosclerosis with the aged cohort dispersed across all three (Figure 5.12 D). LDA revealed the spectral profile of tissues could be easily separated from each other with

accuracy of 88%, 66%, 79%, and 78% for normal, aged arteriosclerosis and atherosclerosis, respectively, on a cross-validated leave-one-out basis (Figure 5.9).

LDA using the machine learning tool, WEKA was used to validate the maximum separability of normal, aged, atherosclerotic and arteriosclerotic datasets. The data set was loaded and pre-processed using the FLDA filter to achieve dimensionality reduction, it was the processed using the "Classify" panel with the implementation of for LDA. Cross validation confirmed that optimized neural networks can identify all cell types with high performance, based only on their Raman spectral profile and resulted in an F-score of 0.86. The cells were also trained on a 66 % split before the remainder was tested and the F score dropped to at 0.81. Each disease state was then supplied as an unknown. Interrogation of the trained LDA set revealed the spectral profile of cells generated from HiPSCs pr HiPSC-derived progenitor stem cells could be easily separated from each other with accuracies of 88%, 66%, 79%, and 78% for normal, aged arteriosclerosis and atherosclerosis, respectively, on a cross-validated leave-one-out basis (Figure 5.13).

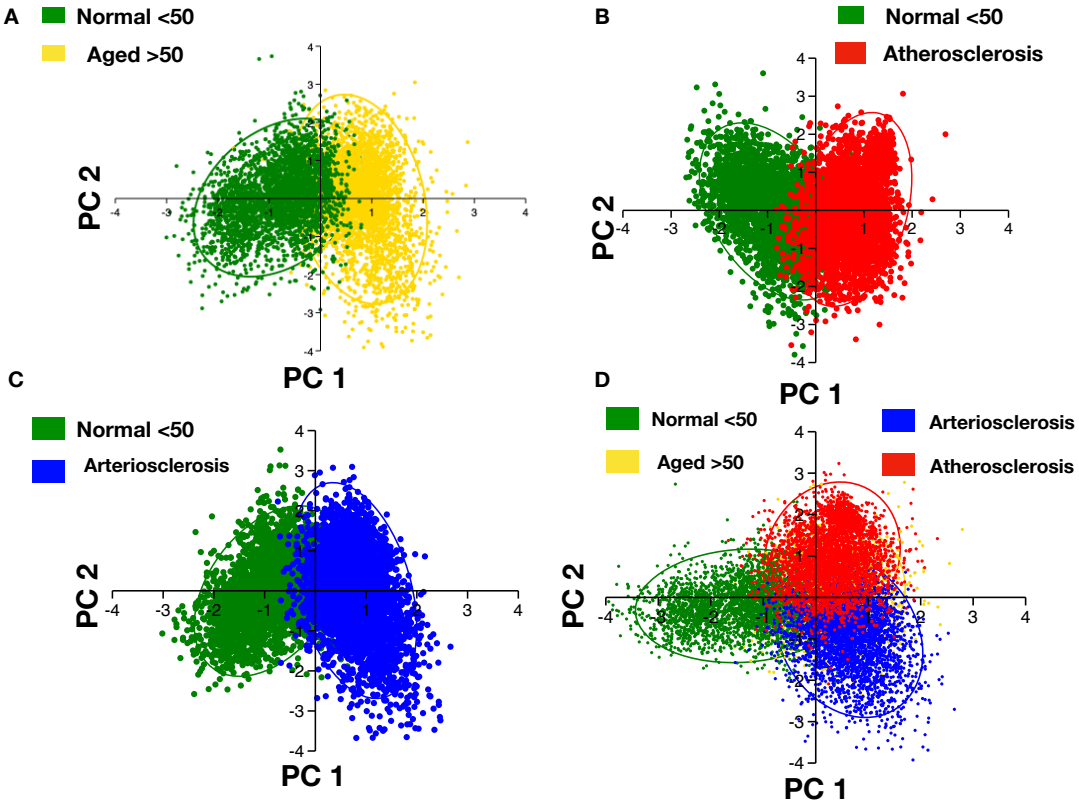

Figure 5.12 PCA loading plots of Raman spectra from healthy and diseased human aortic tissue. 2 and 3-way scatter plot of the first two principal components after PCA of human healthy aortic tissue versus (A) aged, (B) atherosclerosis, (C) arteriosclerosis and (D) aged versus atherosclerosis and arteriosclerosis.

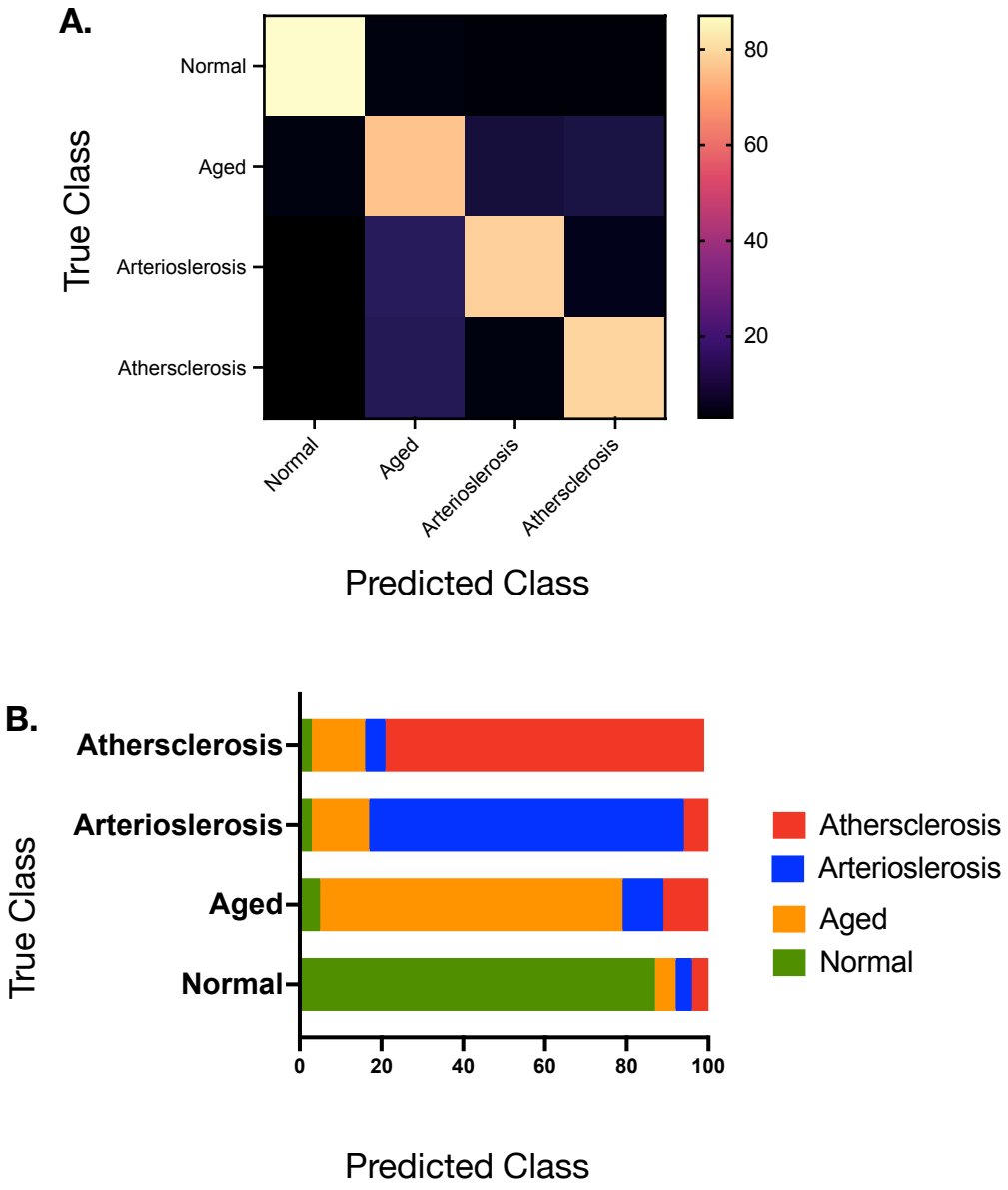

Figure 5.13 LDA of Raman spectra from healthy and diseased human aortic tissue. Confusion matrix of true class and predicted class following a leave-one-out cross-validation procedure by the LDA classifier.

5.4.4 Supervised Machine Learning of Raman spectral datasets from human aortic healthy and diseased tissue to interrogate for the presence of HiPSC-derived progenitor stem cells and/or their myogenic progeny

MLP artificial neural network analysis was deployed to train the algorithm and classify healthy human aortic vessels from aged, arteriosclerotic and atherosclerotic vessels using their Raman spectral profiles before HiPSC-derived NE and PM and their respective myogenic progeny were interrogated using thus supervised machine learning procedure. We optimized several experimental conditions to train the network, including the number of wavelengths for input data, number of hidden layers, momentum, and learning rate. The final classification model had an F-score of 0.787, recall of 0.788 and a precision score of 0.787. Cross-validation confirmed that the optimized neural network could identify tissue types with high performance, based only on their Raman spectra, and resulted in an F-score of 0.769 (Figure 5.14). The tissues were also trained on a 66% split. This trained network was subsequently used to interrogate spectral datasets of cells isolated from HiPSC-derived NE, PM, and their respective myogenic progeny *in vitro.*

Classification of HiPSC-derived NE and PM progenitor stem cells based on the MLP artificial neural network analysis of Raman spectra from normal, aged, arteriosclerotic and atherosclerotic vessels was as follows;

(i) SNEPs: characterised as 46% similar to cells in a normal vessel and 54% similar to cells in an aged vessel with no similarities identified in aged and atherosclerotic vessels (Figure 5.15 A).

(ii) NPCs: characterised as 93% similar to cells in normal vessels, 4% similar to cells in aged vessels and 4% similarity to cells in arteriosclerotic vessels with no similarities to cells found atherosclerotic vessels (Figure 5.15 B).

(iii) PMs: characterised as having 100% similarity to cells in normal vessels (Figure 5.15 C)

(iv) SNEP-SMCs: characterised as having 100% similarity to cells found in arteriosclerotic vessels with no similarity detected in normal, aged and atherosclerotic vessels (Figure 5.15 D)

(v) NPC-SMCs:. Characterised as having 40% similarity to cells in arteriosclerotic vessels and 60% similarity to cells in aged vessels with no similarities in normal or atherosclerotic vessels (Figure 5.15 E)

(vi) PM-VSMCs: Characterised as having 60% similarity to cells in normal vessels, 40% similarity to cells in aged vessels and 7% similarity to cells found in arteriosclerotic vessels (Figure 5.15 F).

Thus, supervised machine learning using MLPs neural network analysis successfully identified each cell type in human aortic tissue training sets with a high degree of accuracy (>70%) and confirmed that a significant number of NE-derived VSMCs are present in arteriosclerotic lesions in comparison to normal, aged and atherosclerotic vessels (Figure 5.16).

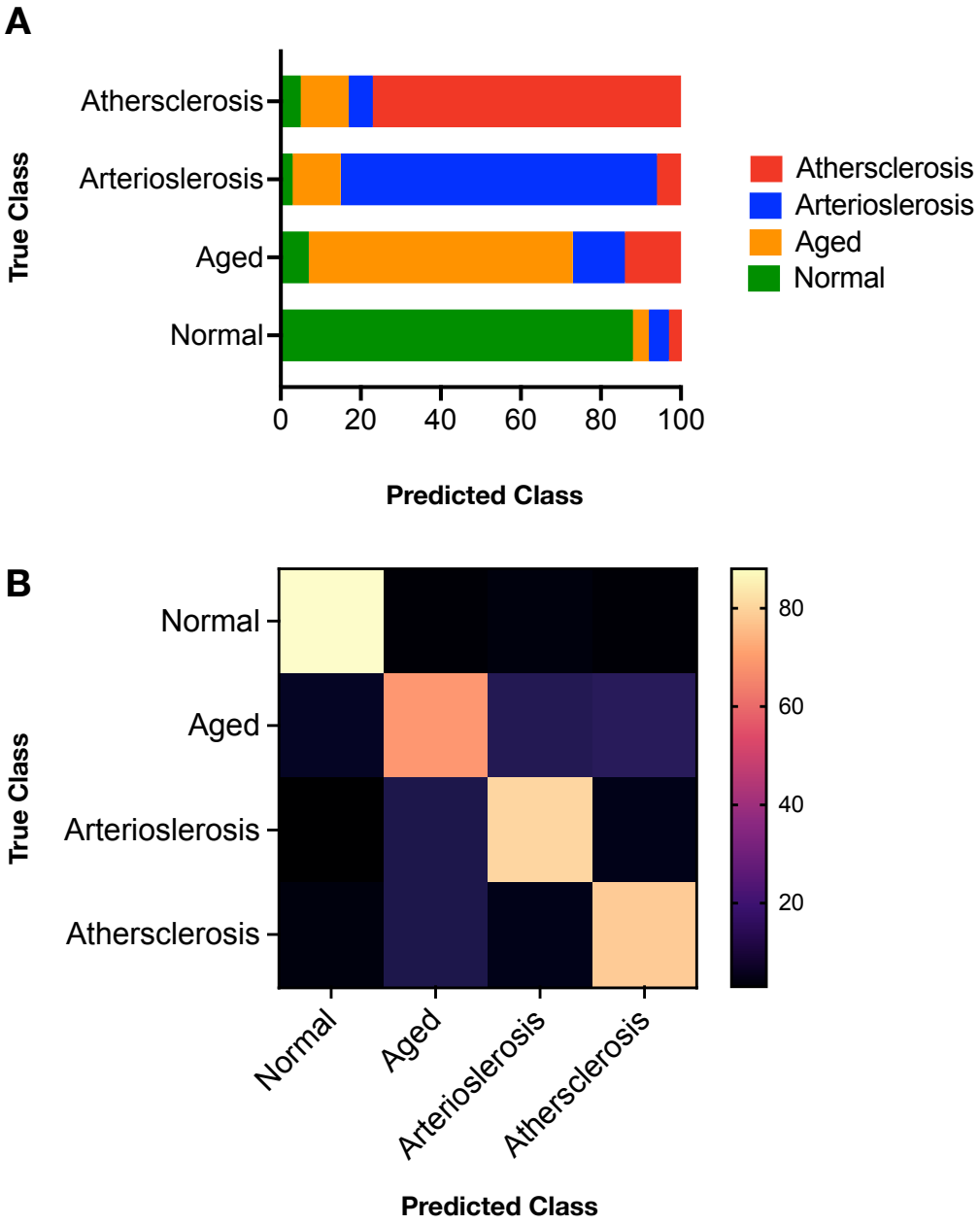

Figure 5.14 MLP neural network analysis of Raman spectra from healthy and diseased human aortic tissue Confusion matrix of true class and predicted class following training with (i) normal, (ii) aged (iii) arteriosclerosis, and (iv) atherosclerotic aortic tissue Raman datasets using MLP neural network analysis.

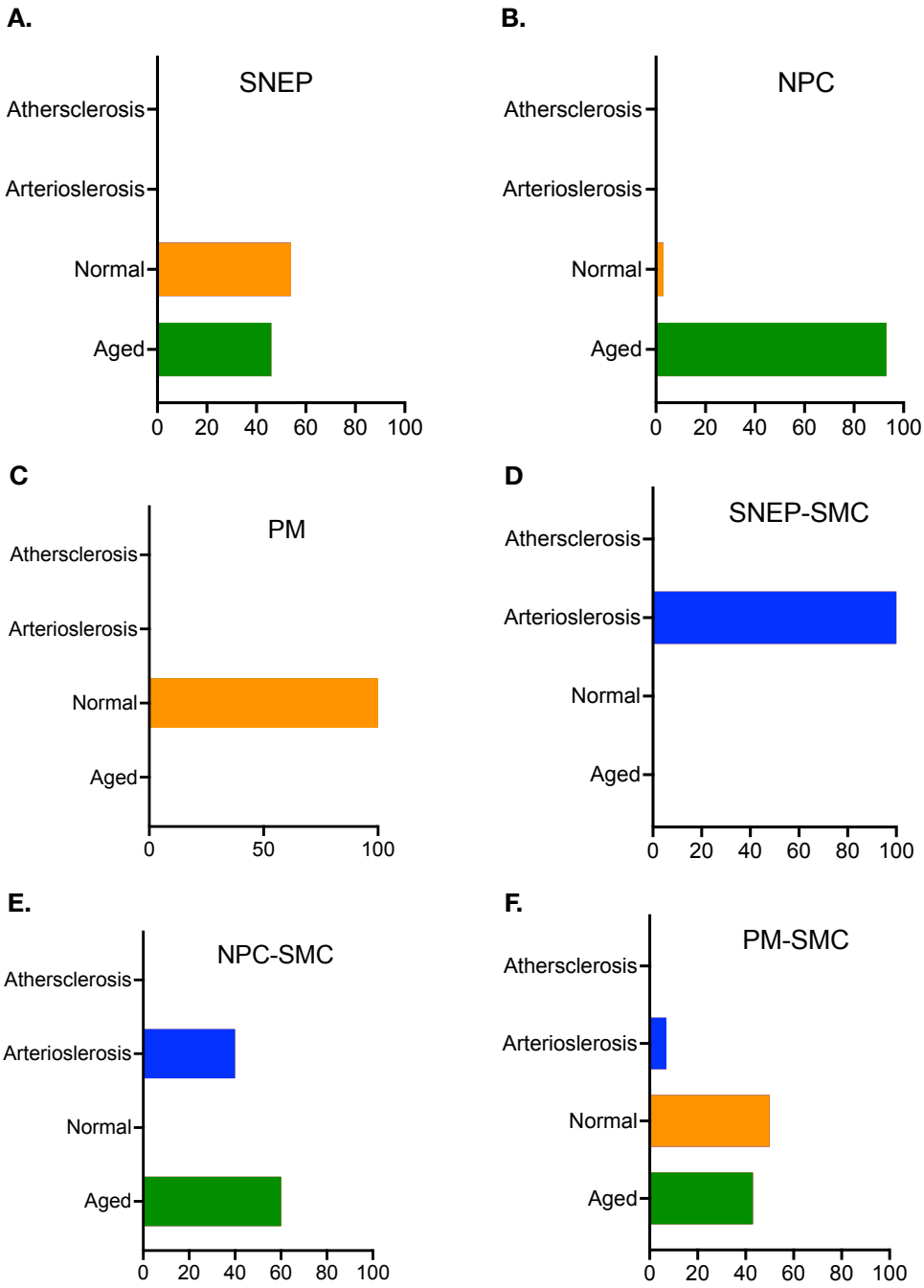

Figure 5.15 Detection of HiPSC-derived NE and PM progenitors and their respective myogenic progeny in healthy and diseased human aortic tissue following MLP analysis of Raman spectral datasets. Percentage of HiPSC-derived NE and PM progenitors and their respective myogenic progeny in normal, aged, arteriosclerotic and atherosclerotic aortic vessels classified using MLP neural network analysis.

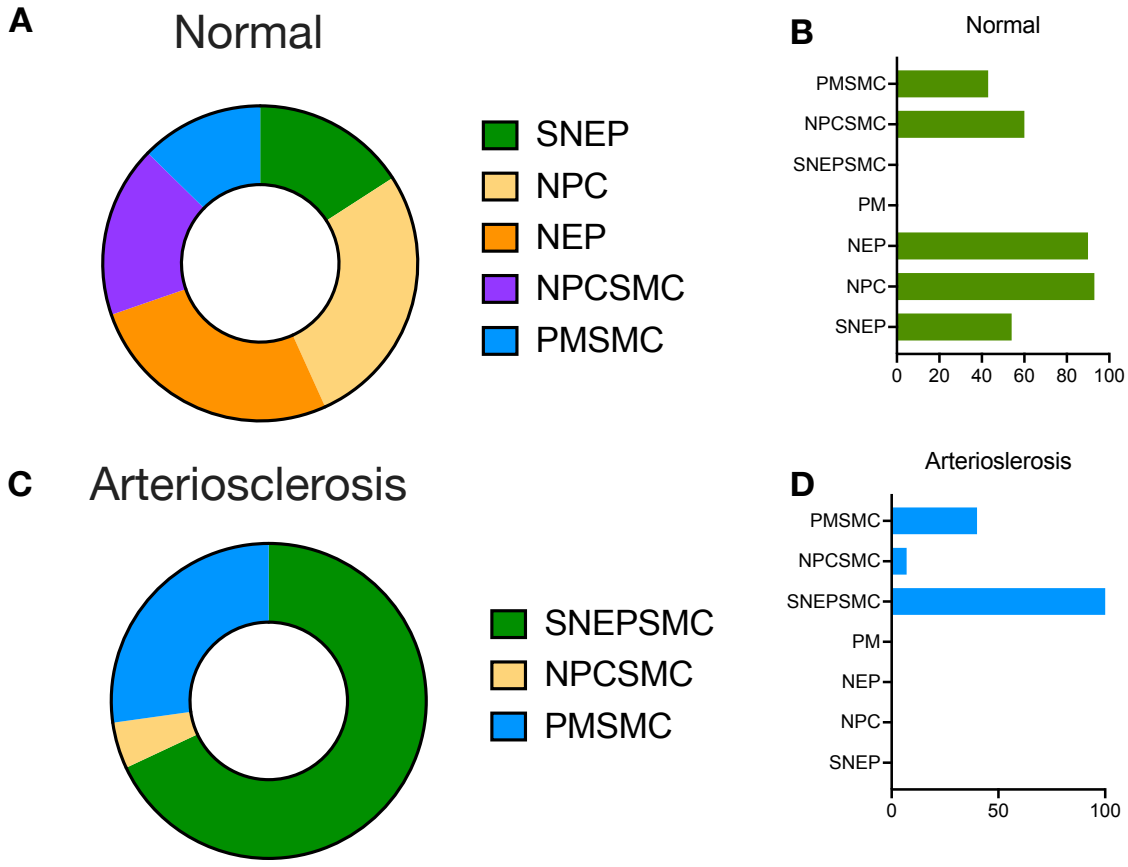

Figure 5.16 MLP neural network analysis identifies HiPSC-derived S100β/Nestin myogenic progeny in arteriosclerotic human vessels. Graphic representation of the percentage of cells in normal and arteriosclerotic vessels using MLP neural network analysis.

5.4.5 Single Cell Photonics of HiPSC-derived NE progenitor stem cells and their respective myogenic progeny

Having demonstrated the ability of FTIR and Raman spectroscopy to successfully discriminate HiPSC-derived progenitor stem cells from their myogenic progeny, we sought to determine whether this could be replicated using a single-cell autofluorescence photonics platform, LiPhos. Firstly, HiPSCs and NE progenitor stem cells were generated and prepared for LiPhos single-cell photonic analysis as describe in Section 2.2.3.2, 2.2.3.3. A limitation of HiPSC-derived progeny is the optimisation of cell culture conditions. As the culture conditions of HiPSC-derived PMs has not yet been optimised generation of PMs for sufficient cell numbers for LiPhos analysis was not carried out. However, HiPSCs were differentiated to PMs and straight to PM-SMCs for LiPhos analysis.

Single-cell photonic profiles of individual cells were measured following capture on V-cups using a centrifugal Lab-on-a-Disc (LoaD) platform, as previously described (King *et al.*, 2019; Molony *et al.*, 2021) and visualised by phase-contrast microscopy on each V-cup (Figure 5.17 A,C,E). The Log10 AF emissions of 50 cells were recorded across five broadband light wavelengths (λ465, λ530, λ565, λ630 and λ670 with a bandwidth of 20 nm) (Figure 5.17) and corrected as fold increase over background for further analysis. The photonic intensity of single cells from HiPSC-derived NEPs showed a significant increase at wavelength λ465 in comparison to HiPSC (Figure 5.17 D), where-as HiPSC-derived SNEPs and NPCs showed a significant decrease at the λ465 wavelength (Figure 5.17 B, F).

Subsequent analysis determined whether undifferentiated HiPSC-derived NE progenitor stem cells could be discriminated from their myogenic progeny following stimulation with media supplemented TGF-β1/PDGF for 12 days. Myogenic differentiation was confirmed by immunohistochemical analysis of cells before and after treatment (Chapter 3 Section 4.4.7, 4.4.9). Single-cells were visualised by phase-contrast microscopy following V-cup capture before their photonic profiles were compared (Figure 5.18 A, C). There was a significant increase in the photonic intensity of SNEP-VSMCs at λ465, λ530, λ630 and λ670 nm (Figure 5.18 B) and at λ530 and λ630nm in NEP-VSMCs (Figure 5.18 D), when compared to their undifferentiated NE controls. Although the analysis of HiPSC-derived PM could not be achieved due to the lack of standardised

culture of HiPSC-derived PMs, HiPSCs were generated and immediately differentiated to a myogenic lineage using TGF-β1/PDGF for 12 days. PM-SMCs were used as a comparison cell for HiPSC-derived NE SMC subtypes to determine differences if any differences in AF photons could be determined. There was a significant increase in the photonic intensity of NEP-VSMCs at λ465, λ530 wavelengths in comparison to PM-SMCs., (Figure 5.19 A) Similarly a significant increase in the photonic intensity at λ465, λ530 wavelengths in comparison to PM-SMCs (Figure 5.19 B).

The spectral data was pre-processed using WEKA machine learning tool kit. FLDA was carried out to perform a dimensionality-reduction of the large Raman data set into small sets of variables whilst retaining all information. PCA carried out using the multivariate statistical package PAST4 was used to focus on the greatest variation between HiPSCs and HiPSC-derived NE (NEP, SNEP) progenitor stem cells and their SMC progeny (NEP-SMC, SNEP-SMC). Using PCA 2-way multivariate statistical analysis variation between HiPSC and HiPSC-derived NE progenitor stem cells a significant separation presented using PCA scatter plots was demonstrated (Figure 5.20 A,C). Similarly, a distinct separation of HiPSC-derived NE progenitor stem cells and their myogenic progeny was demonstrated (Figure 5.21 A,C).

Further LDA using the multivariate statistical package, PAST4 of HiPSC and HiPSC-derived NE progenitor stem cells and their SMC progeny was used to demonstrate the maximum separability between groups across the data set. LDA analysis presented as a histogram, using the multivariate statistical package PAST4, revealed that the Raman profile of HiPSC-derived NE progenitors could be easily separated from each other (Figure 5.20 B,C). Furthermore HiPSC-derived NE progenitor stem cells could be separated from their myogenic progeny (Figure 5.21 B,D).To further classify HiPSC-derived NE progenitor stem cells and their myogenic progeny MLP artificial neural network analysis was deployed. We optimized several experimental conditions to train the network, including the number of wavelengths for input data, number of hidden layers, momentum, and learning rate. The final classification model had an F-score of 0.780, a recall of 0.783, and a precision score of 0.794. Cross-validation confirmed that optimized neural networks could identify tissue types with high performance, based only on their AF emissions, and resulted in an F-score of 0.799 (Figure 5.22).

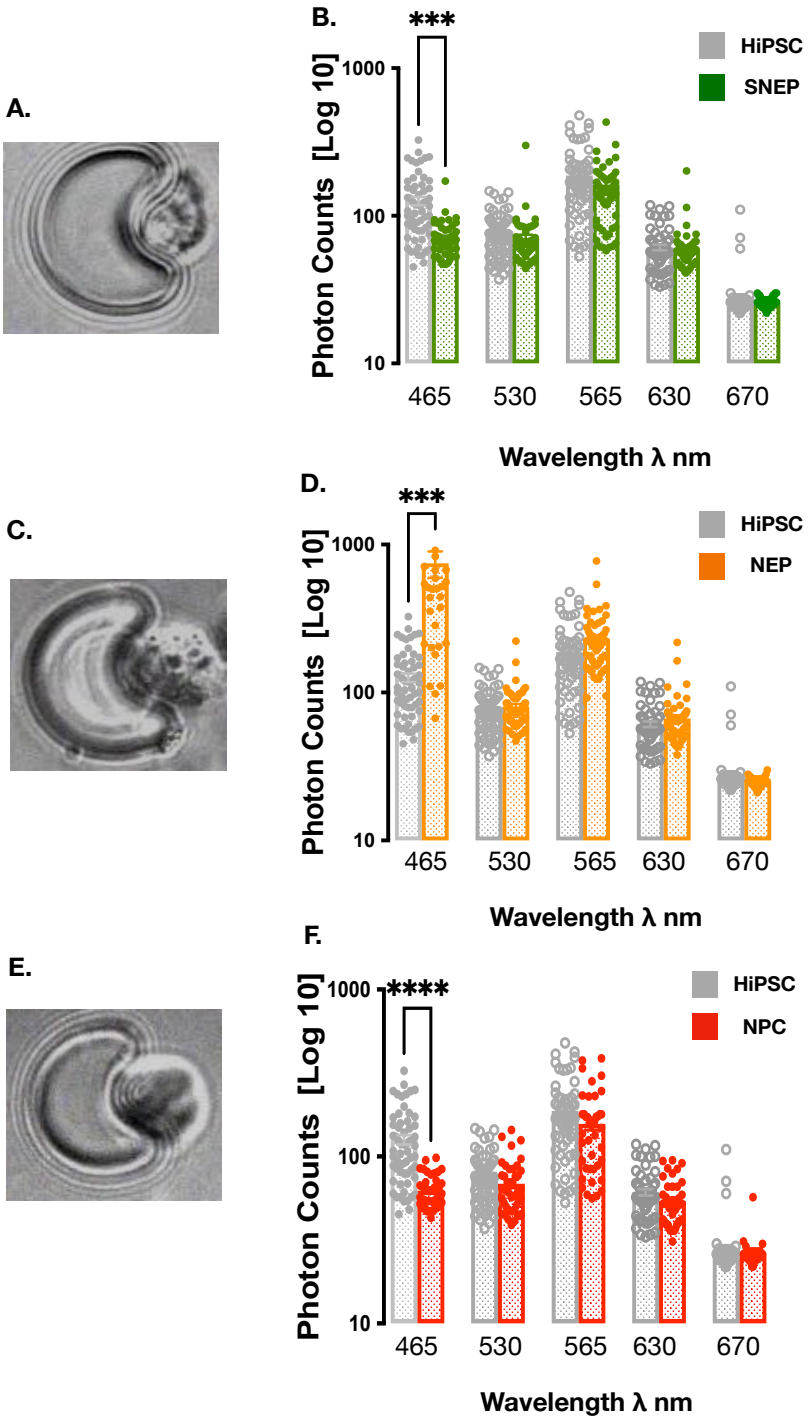

Figure 5.17 Single cell photonics of HiPSCs and their NE progenitor stem cell intermediates (SNEP, NEP and NPC). (A, C, E) Visualisation of HiPSC-derived NE progenitor stem cells on each V-cup in the LoaD platform. (B, D, F) Single-cell auto-fluorescence photon emissions across five broadband light wavelengths (λ465, λ530, λ565, λ630 and λ670 nm with a bandwidth of 20 nm) from HiPSC and HiPSC derived NE progenitor stem cell (SNEP, NEP and NPCs). Data are the mean ± SEM of Log10 photons, $p \leq 0.05$ vs. HiPSC.

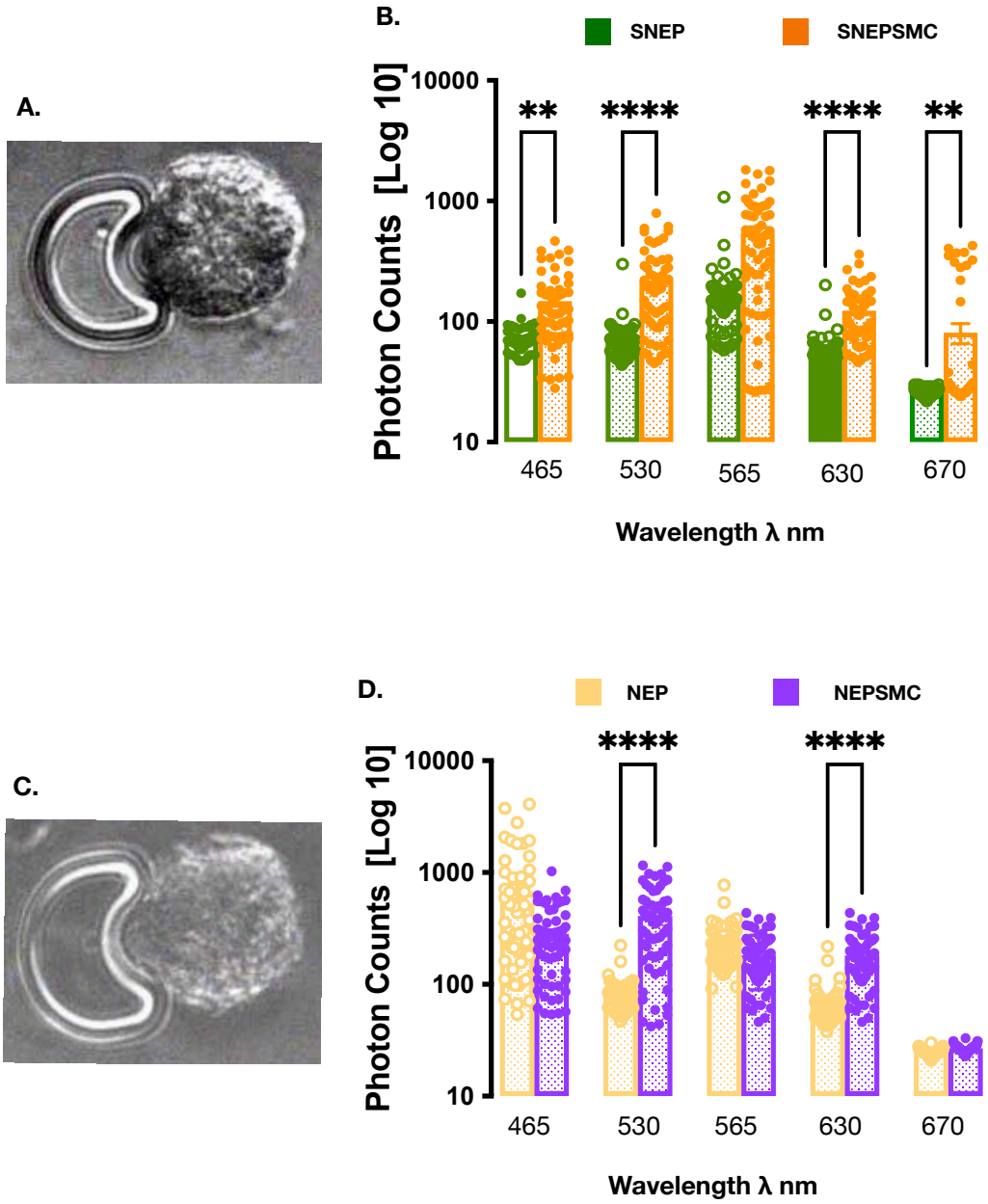

Figure 5.18 Single cell photonics of NE progenitor stem cell intermediates (SNEP, NEP and NPC) and their respective myogenic progeny. (A, C,) Visualisation of NE-derived VSMCs on each V-cup in the LoaD platform. (B, D,) Single-cell auto-fluorescence photon emissions across five broadband light wavelengths (λ465, λ530, λ565, λ630 and λ670 nm with a bandwidth of 20 nm) from HiPSC-derived NE progenitor stem cells and derived VSMC. Data are the mean ± SEM of Log10 photons, $p \leq 0.05$ vs. SNEP, $p \leq 0.05$ vs. NEP.

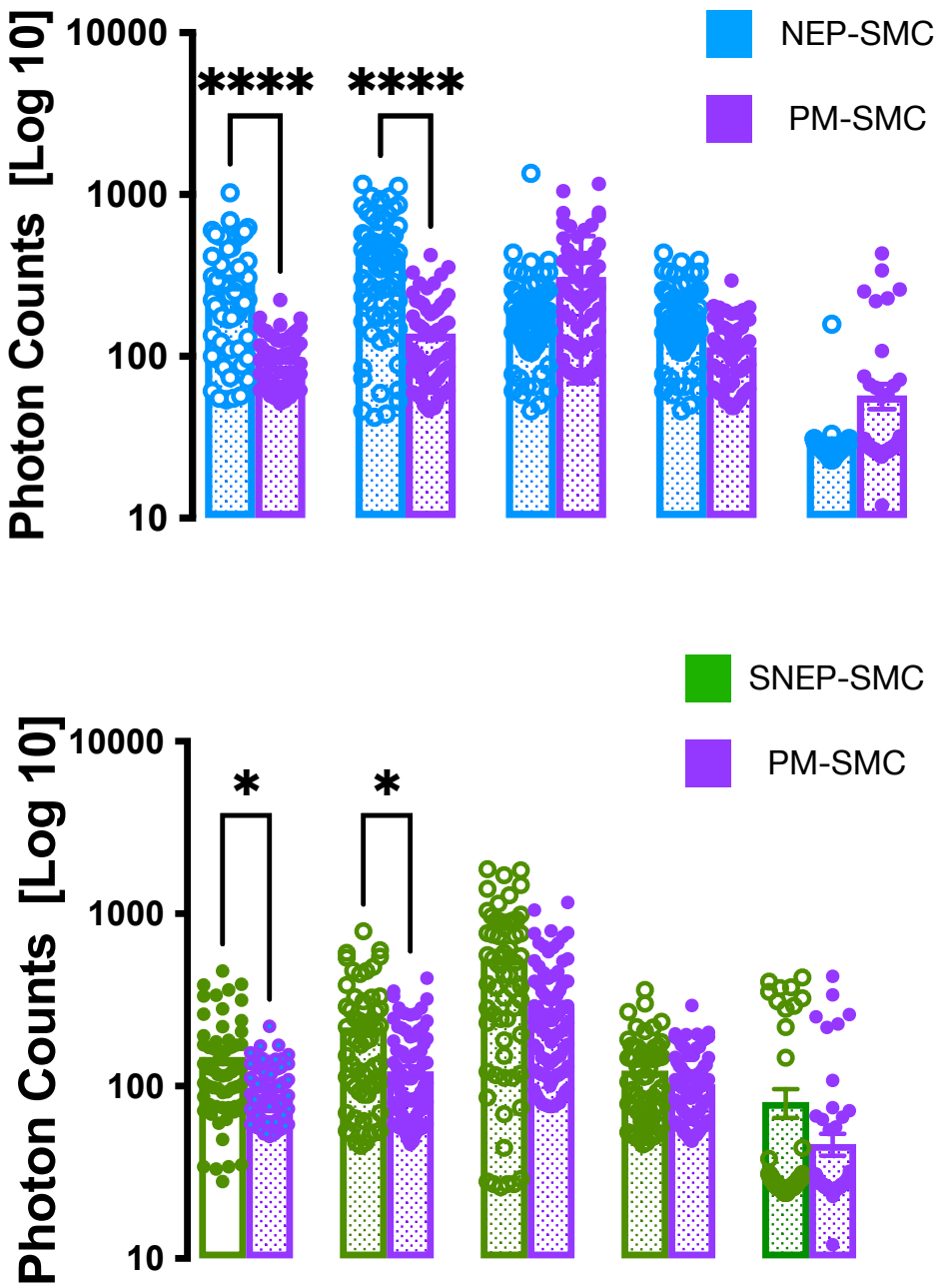

Figure 5.19 Single cell photonics of NE and PM progenitor stem cell derived myogenic progeny. Single-cell auto-fluorescence photon emissions across five broadband light wavelengths (λ465, λ530, λ565, λ630 and λ670 nm with a bandwidth of 20 nm) from NE and PM derived VSMC. Data are the mean ± SEM of Log10 photons, p≤0.05 vs. NEP-SMC, p≤0.05 vs. SNEPSMC.

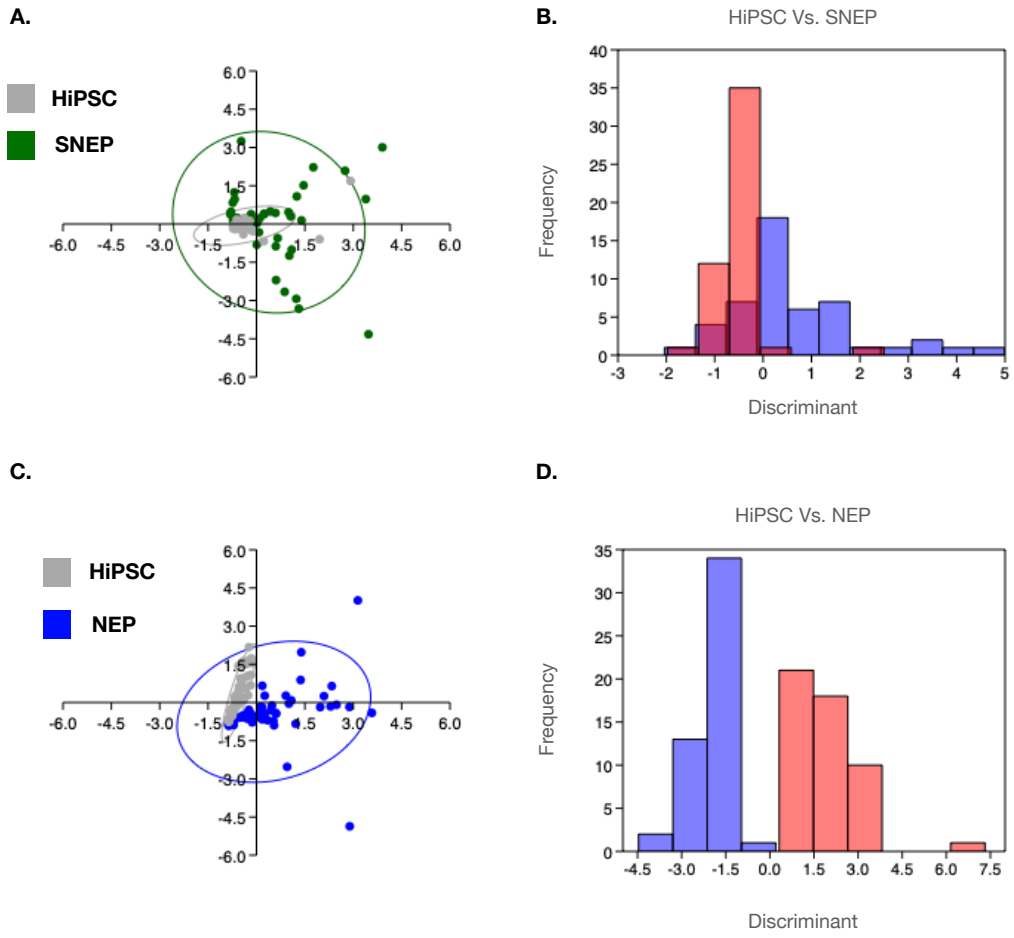

Figure 5.20 PCA and LDA of AF spectra for HiPSCs vs. HiPSC-derived NE progenitor cells. A 2-way scatter plot of the first two principal components after PCA of HiPSCs compared to SNEP (A) and NEP *in vitro*. A 2-way scatter plot of the first two principal components after LDA of HiPSCs compared to SNEPs (B) and NEPs (D). Data are representative of 30 cells across 400-1000 cm^{-1} wavelengths.

.

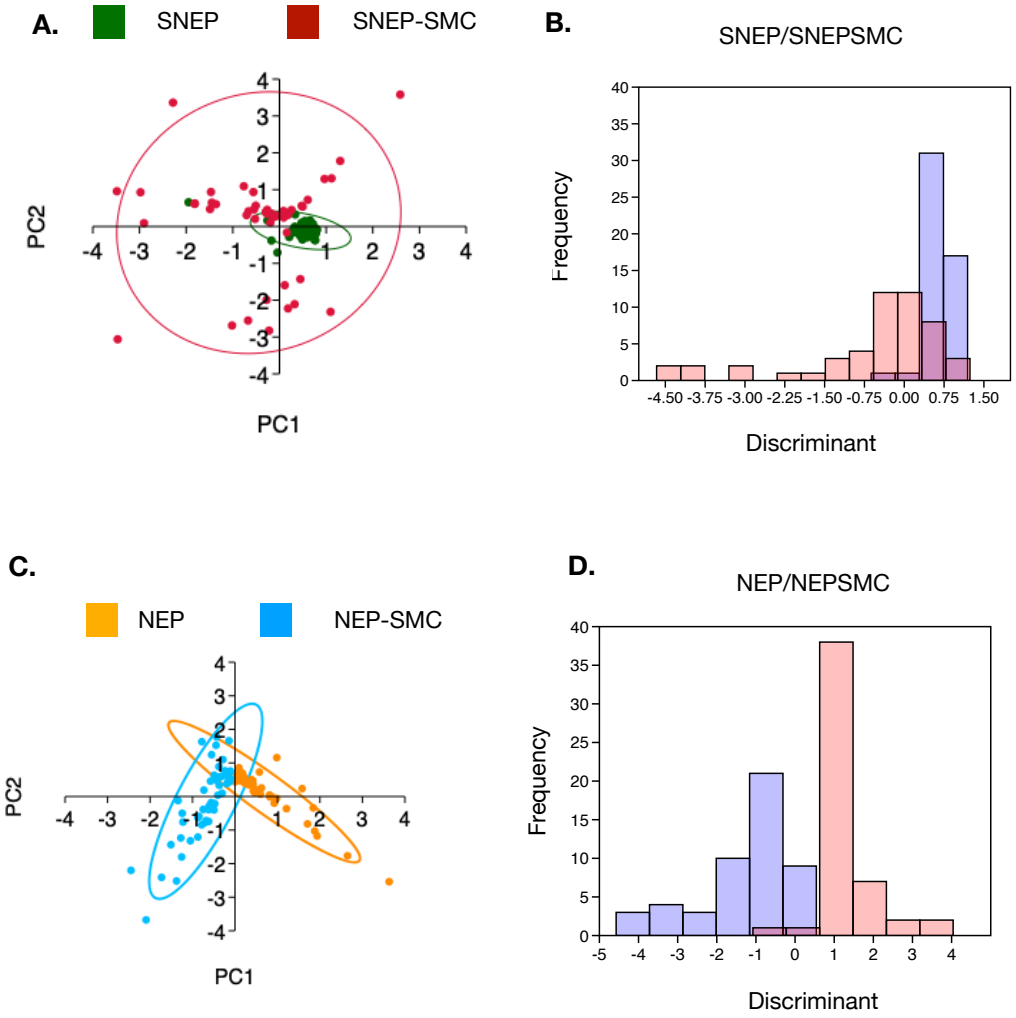

Figure 5.21 PCA and LDA of AF spectra for HiPSC-derived NE progenitor cells versus NE-derived SMCs. A 2-way scatter plot of the first two principal components after PCA of SNEP compared SNEP-SMCs (A) and NEP compared to NEP-SMCs (C) *in vitro*. A 2-way scatter plot of the first two principal components after LDA of SNEPs compared to SNEP-SMCs (B) and NEPs compared to NEP-SMCs (D). Data are representative of 30 cells across 400-1000 cm^{-1} wavelengths.

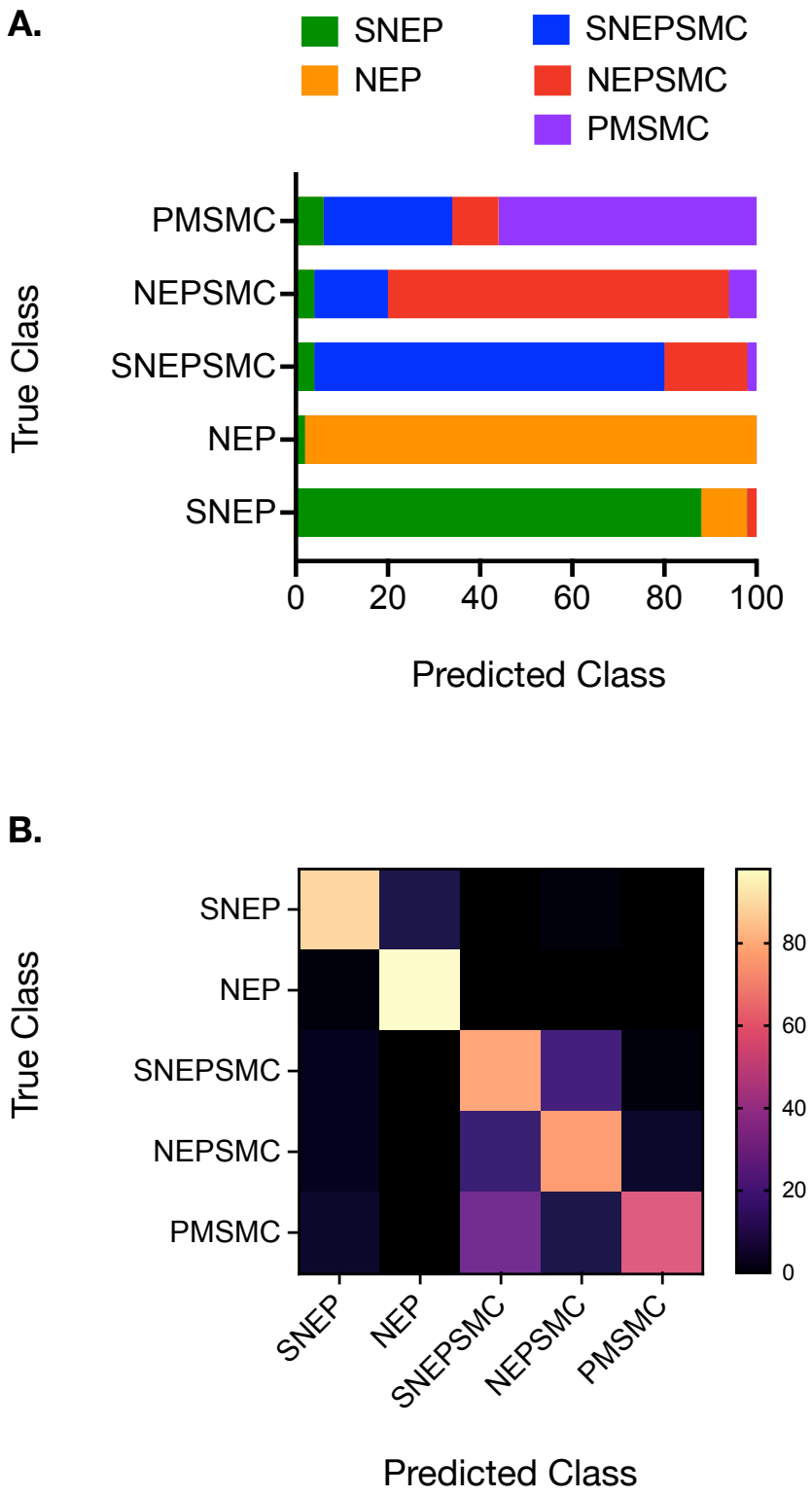

Figure 5.22 MLP neural network analysis of AF spectra from HiPSC-derived NE progenitors and SMC subtypes. Confusion matrix of true class and predicted class following training with human datasets.

5.4.6 Single Cell Photonics of human atherosclerotic (ATH) and arteriosclerotic (ART) cells *ex vivo.*

In order to assess the contribution of HiPSC-derived NE progenitors and/or their myogenic progeny to the overall heterogeneous phenotype of human atherosclerotic and arteriosclerotic lesions single cells derived from cadaveric human atherosclerotic (no plaque) and arteriosclerotic vessels (with plaque) were isolated (Figure 5.23 A, C). Single-cell photonic profiles of individual cells were measured following capture on V-cups using a centrifugal Lab-on-a-Disc (LoaD) platform, as previously described (King *et al.*, 2019; Molony *et al.*, 2021) and visualised by phase-contrast microscopy on each V-cup (Figure 5.23 B,D). The Log10 AF emissions of 50 cells were recorded across five broadband light wavelengths (λ465, λ530, λ565, λ630 and λ670 with a bandwidth of 20 nm) and corrected as fold increase over background for further analysis (Figure 5.23 E). The photonic intensity of single cells derived from ATH showed a significant increase at wavelength all five wavelengths in comparison to ART (Figure 5.23 E).

The spectral data was then pre-processed using WEKA machine learning tool kit. FLDA was carried out to perform a dimensionality-reduction of the large Raman data set into small sets of variables whilst retaining all information. PCA carried out using the multivariate statistical package PAST4 was used to focus on the greatest variation between single-ells isolated from ATH and ART lesions. Using PCA 2-way multivariate statistical analysis variation between ATH and ART a significant separation presented using PCA scatter plots was demonstrated (Figure 5.24 A).

Further LDA using the multivariate statistical package, PAST4 of cells isolated from ATH and ART lesions was used to demonstrate the maximum separability between the two disease groups. LDA analysis presented as a histogram, using the multivariate statistical package PAST4, revealed that the AF profile of ATH and ART could be easily separated from each other (Figure 5.24 B).

LDA using the machine learning tool, WEKA was used to validate the maximum separability of single cells isolated from ATH and ART lesions. The data set was loaded and pre-processed using the FLDA filter to achieve dimensionality reduction, it was the processed using the “Classify” panel with the implementation of for LDA. Cross validation confirmed that optimized neural networks can identify all cell types with high

performance, based only on their AF profile and resulted in an F-score of 0.80.. The cells were also trained on a 66 % split before the remainder was tested and the F score dropped to at 0.78. Each disease state was then supplied as an unknown. Interrogation of the trained LDA set revealed the spectral profile of cells generated from ATH and ART lesions could be easily separated from each other with accuracies of 94% of the ATH cells were classified as similar to each other, with only a small proportion of cells classified as similar to cells from ART vessels. In contrast, 66% of ART cells were classified as similar to each other, with 33% classed as similar to ATH (Figure 5.24 C,D).

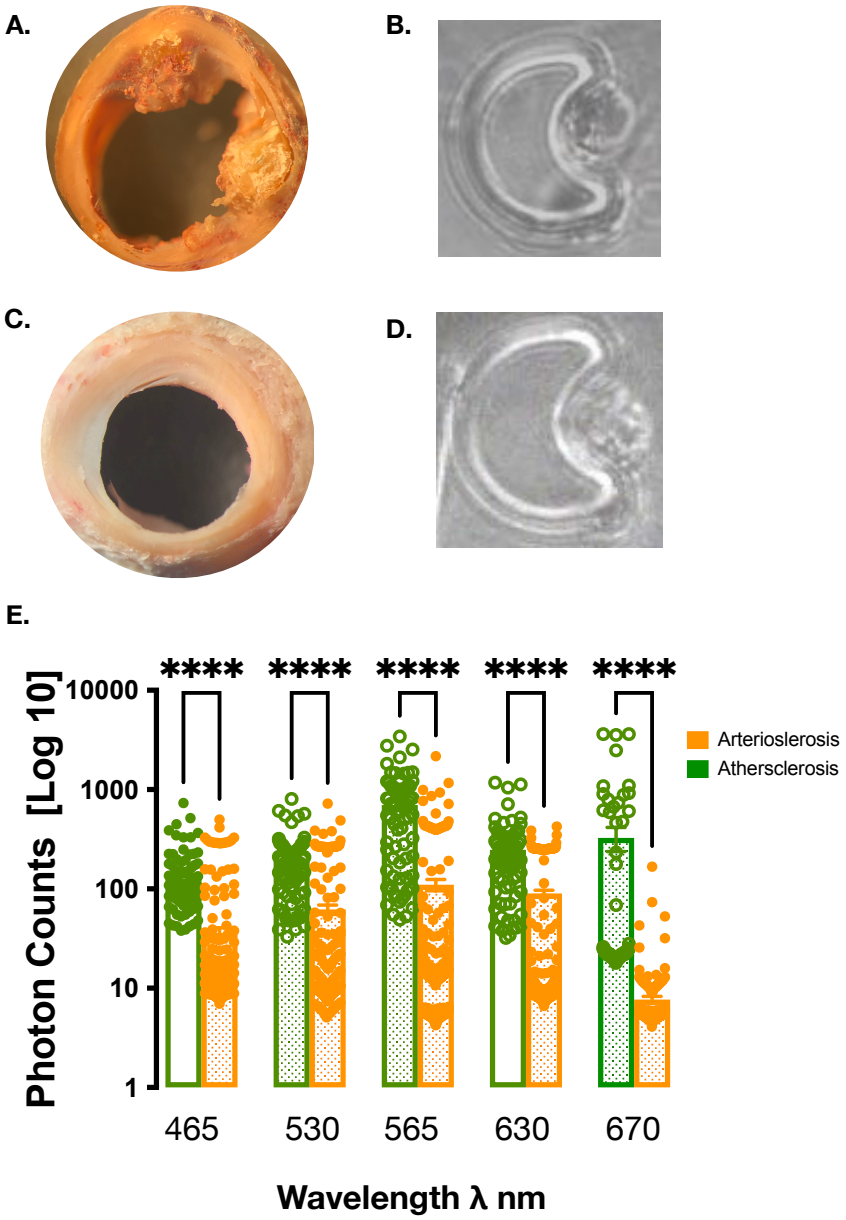

Figure 5.23 Single cell photonics of atherosclerotic (ATH) and arteriosclerotic (ART) lesion cells *ex vivo*. (A, C) Graphic representation of human atherosclerotic and arteriosclerotic cadaveric vessels prior to single-cell digestion. (B, D) Visualisation of atherosclerotic and arteriosclerotic isolated medial cells on each V-cup in the LoaD platform. (E) Single-cell auto-fluorescence photon emissions across five broadband light wavelengths (λ465, λ530, λ565, λ630 and λ670 nm with a bandwidth of 20 nm) from atherosclerotic and arteriosclerotic medial VSMCs. Data are the mean ± SEM of Log10 photons, $p \leq 0.05$ vs. ART.

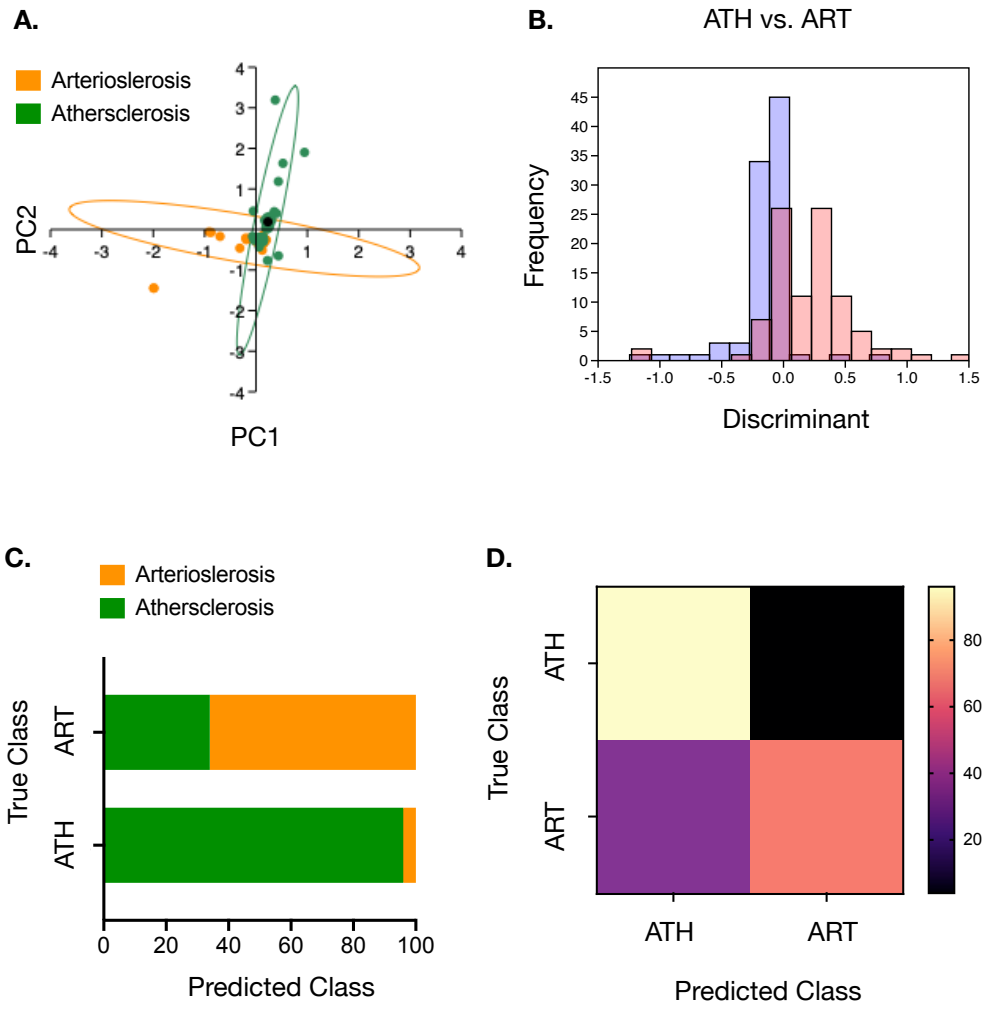

Figure 5.24 PCA and LDA of AF spectra from single cells isolated from atherosclerotic (ATH) and arteriosclerotic (ART) lesions. (A) A 2-way scatter plot of the first two principal components after PCA of single cells isolated from ATH and ART lesions *ex vivo* (B) A 2-way scatter plot of the first two principal components after LDA of single cells isolated from ATH and ART lesions *ex vivo*. (C) LDA of single cells isolated from ATH and ART lesions using WEKA software. Confusion matrix of true class and predicted class following a leave-one-out cross-validation by the LDA classifier.

5.4.7 Supervised Machine Learning of single cell photonic data from human aortic diseased tissue to interrogate for the presence of HiPSC-derived progenitor stem cells and/or their myogenic progeny

MLP artificial neural network analysis was deployed to train the algorithm using AF profiles of HiPSC-derived NE progenitor stem cells (NEP and SNEP), NE-derived SMC progeny (NEPSMC and SNEPSMC) and PM-derived SMC progeny (PM-SMC) before interrogation with ATH and ART AF signatures. To train the network, we optimized several experimental conditions, including the number of wavelengths for input data and the number of hidden layers. The final classification model had an F-score of 0.794, a recall of 0.795, and a precision score of 0.803 (Figure 5.25 A, B). Cross-validation confirmed that optimized neural networks could identify all cell types based only on their singe cell autofluorescence emissions and resulted in an F-score of 0.634. The cells were also trained on a 66% split before the remainder was tested, and the F score dropped to 0.647. This trained data set was subsequently used to interrogate spectral datasets of cells isolated from ATH and ART vessels *ex vivo*.

Classification of ATH and ART cells based on the MLP artificial neural network analysis of AF spectra from HiPSC-derived NE progenitor stem cells, NE-derived SMCs and PM-SMCs characterised single cells isolated from ATH (Figure 5.26 A,B) and ART (Figure 5.26 C,D) vessels *ex vivo* as follows;

(i) Single cells isolated from ATH vessels were characterised as having;
   a. 79% similarity to SNEP-SMCs
   b. 15% similarity to NEP-SMCs
   c. 5% similarity to PM-SMCs
   d. 1% similarity to SNEPs

(ii) Single cells isolated from ART vessels were characterised as having;
   a. 62% similarity to SNEP-SMC
   b. 18% similarity to PM-SMC
   c. 14% similarity to NEP-SMC
   d. 6% similarity to NEP
   e. 2% similarity to SNEP

Thus, supervised machine learning using MLPs neural network analysis of HiPSC-derived stem cell and SMC progeny as a training data set confirmed that a significant number of NE-derived VSMCs are present in ATH and ART vessels.

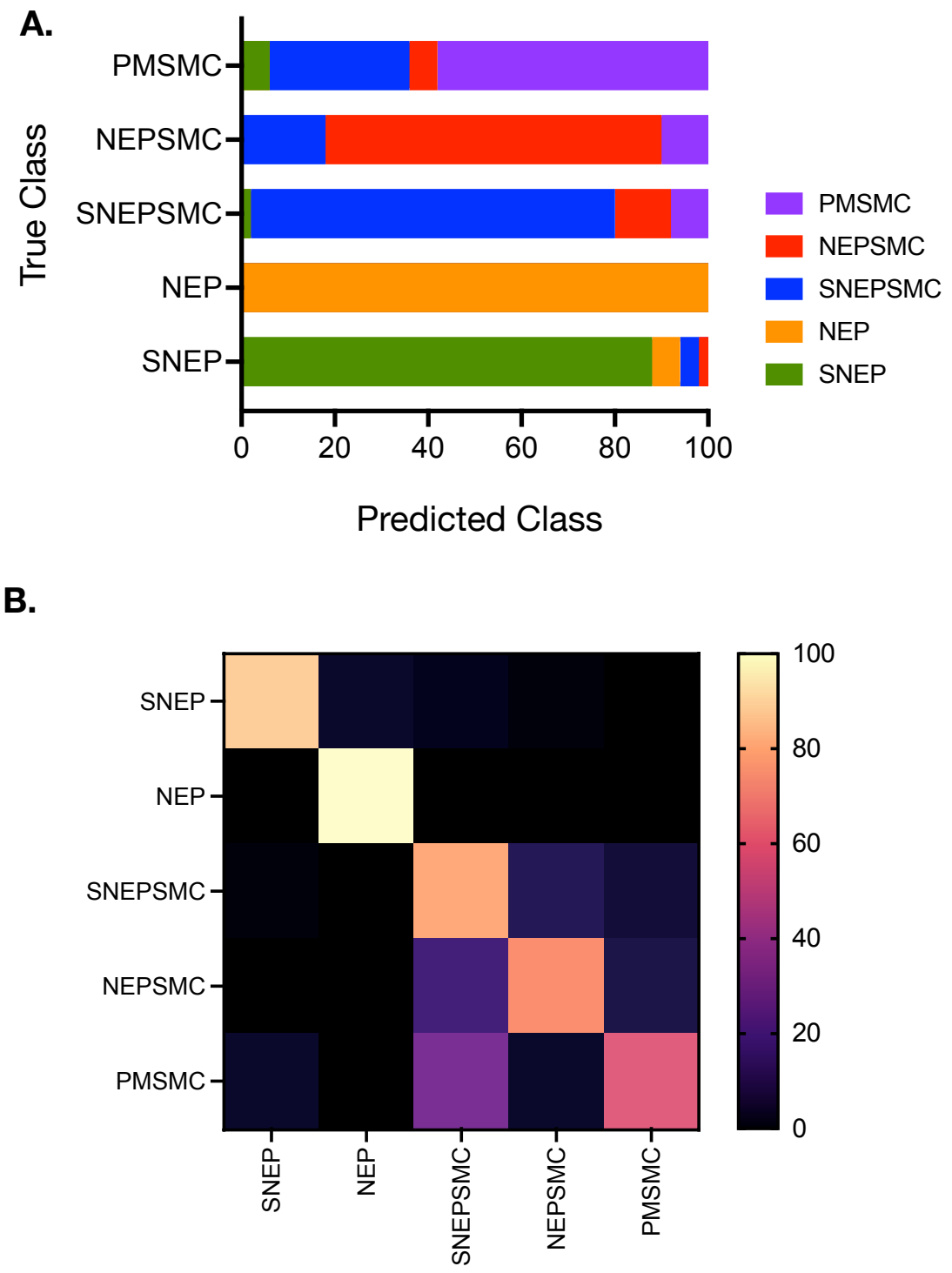

Figure 5.25 MLP neural network algorithm of single-cell AF photonics. Confusion matrix of true class and predicted class following training with (i) SNEP, (ii) NEP (iii) SNEPVSMC, (iv) NEPVSMC, and (v) PMVSMC scPH across five wavelengths using MLP neural network analysis.

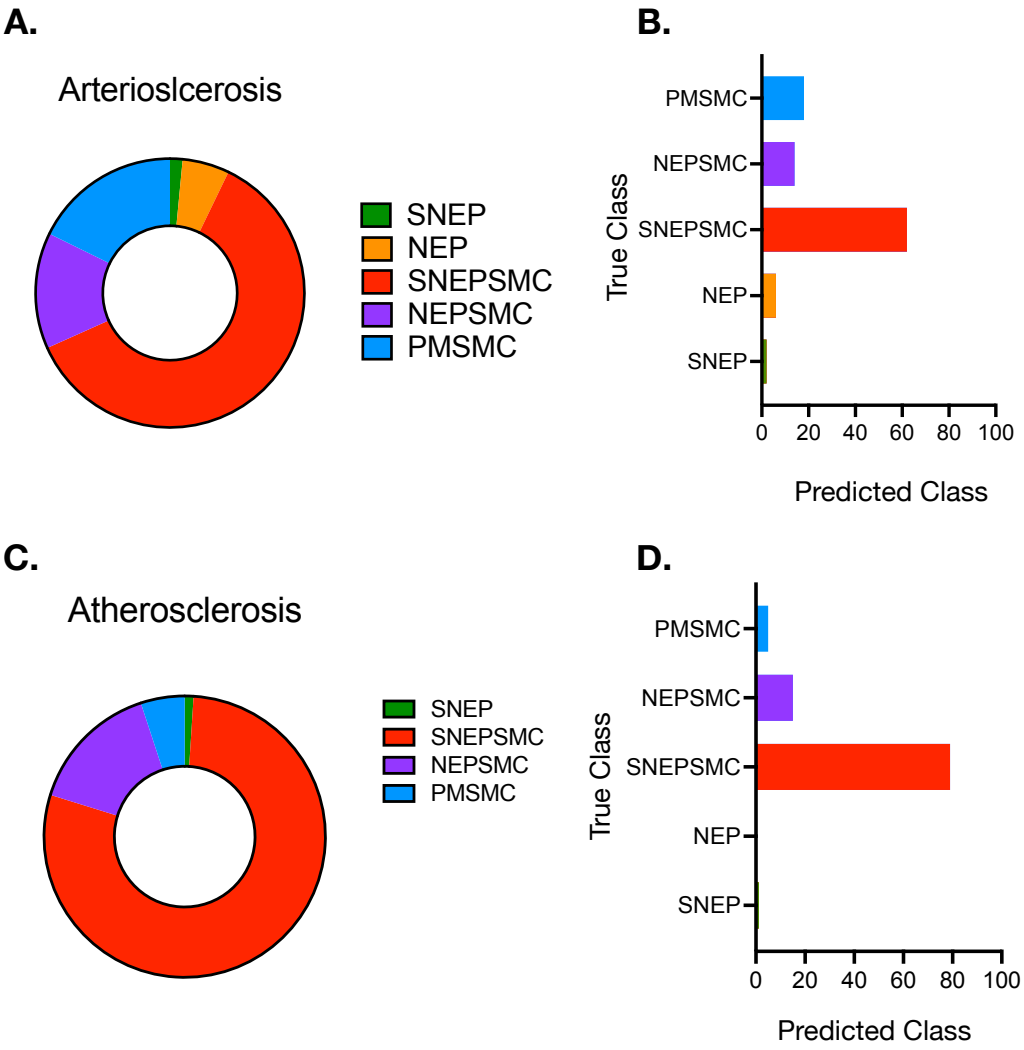

Figure 5.26 MLP neural network analysis identifies HiPSC-derived NE and PM intermediate progenitors and their myogenic subtypes in atherosclerotic and arteriosclerotic human vessels. Graphic representation of the percentage of cells in atherosclerotic and arteriosclerotic vessels using MLP neural network analysis.

5.5 Summary

- PCA and LDA of FTIR and Raman vibrational spectra datasets discriminates HiPSCs from HiPSC-derived NE and PM progenitor stem cells.
- PCA and LDA of FTIR and Raman vibrational spectra datasets discriminates HiPSC-derived NE and PM progenitor stem cells from their myogenic progeny.
- LDA enabled quantification of discrimination of undifferentiated HiPSC-derived NE and PM stem cells from both their myogenic progeny.
- PCA and LDA of Raman vibrational spectra datasets discriminates healthy (<50), aged (>50), atherosclerotic and arteriosclerotic tissues.
- NE stem cell-derived SMCs shared the greatest spectral similarity with arteriosclerotic tissues following cross validation.
- PCA and LDA of single-cell autofluorescence photonic emissions discriminates HiPSCs from HiPSC-derived NE progenitor stem cells.
- NE stem cell-derived SMCs shared the greatest spectral similarity with arteriosclerotic and atherosclerotic tissues following MLP analysis.
- Label-free discrimination *in situ* may facilitate interrogation of these important phenotypes during vascular disease progression

5.6 Discussion

A variety of diagnostic tools have been developed to detect remodelling of the arterial wall indicative of atherosclerosis, including coronary angiography, intravascular ultrasound, magnetic resonance imaging, and ECG. Currently, cIMT is regarded as one of the primary surrogate indices of atherosclerosis (Papageorgiou *et al.*, 2016). However, in some AMI patients, interrogation by angiography reveals no significant lesions within surveyed coronary beds. It is widely accepted that the initial step in the pathogenesis of atherosclerosis is a change in arterial cell composition. A hallmark of subclinical atherosclerosis is the accumulation of VSMC-like cells leading to neointimal thickening and lesion formation. The origin of neointimal cells has been extensively debated over the past decade. While medial SMCs have been purported to contribute to the majority of VSMC-like cells in vascular lesions, the involvement of resident vascular stem cells, in particular resident S100β^{+} stem cells has recently emerged (Di Luca *et al.*, 2021; Molony *et al.*, 2021). The emergence of vibrational spectroscopy and single cell photonics as a diagnostic tool for the detection of sub-clinical atherosclerosis holds promise due to the ability to detect discrete changes in the cellular composition of neointimal VSMC-like cells and discriminate heterogeneous cell populations (Molony *et al.*, 2018, 2021). However, much of this work has been reported using animal models. Herein, this study evaluated the application of single-cell vibrational spectroscopy and photonics as a tool to discriminate HiPSC-derived vascular cell phenotypes *in vitro* before the presence of HiPSC-derived stem cell and their myogenic progeny within vascular lesions was assessed *ex vivo* using supervised machine learning tools.

The use of HiPSCs for *in-vitro* disease modelling is highly appealing as it offers an unlimited source of defined disease-relevant cells (Soldner and Jaenisch, 2012). Although previous studies have demonstrated SMC differentiation of HiPSCs through direct differentiation (Cheung and Sinha, 2011) the generation of vSMCs from defined embryological origins was demonstrated in this study through the use of NE and PM intermediate progenitor stem cells. Following the generation and characterisation of NE and PM progenitor stem cells (Chapter 3, Section 4.4.6, 4.4.8, 4.4.11) TGF-ß1 was used to generate embryologically defined SMCs through the activation of the heteromeric complex of two serine threonine kinase receptors (TßII and ALK5) resulting in a phosphorylation-depended activation of Smad 2 and 3 subsequently complex with Smad

4 and translocate to the nucleus where they stimulate myogenetic gene expression (Massagué, Seoane and Wotton, 2005). Myogenic differentiation of NE and PM-derived SMCs was shown by an increased expression of transcript for SMC differentiation markers (CNN1 and MYH11) and decrease in NE markers (NESTIN and S100ß) and PM markers (PAX1) concomitant with a significant increase in the number of CNN1 and MYH11+ positive cells (Chapter 3, Sections 4.4.7, 4.4.9, 4.4.12). Furthermore distinct changes in cellular morphology of HiPSCs, HiPSC-derived progenitor stem cells and their respective SMC progeny was evaluated using confocal imaging. *In vitro,* NE and PM progenitor cells gradually detached from HiPSC colonies developing extensive lamellipodia, a characteristic fundamental to cell motility and filamentous like prolongations, in search of contact with other cells (Bkaily *et al.*, 1997). A stark difference was observed during myogenic differentiation of intermediate progenitors as SMCs exhibit a less elongated neural like morphology with an increase in the nucleus and cytoplasmic area and the development of myofilaments, a typical hallmark of vascular SMCs (Wilson, 2011).

Previous studies have utilised FTIR to discriminate healthy versus diseased cells with the majority of research conducted in cancer cell lines. FTIR and spectral imaging carried out in conjunction with conventional H&E staining accurately assembles a clustered graph mimicking the histological pattern of axillary lymph nodes and metastatic breast cancer tissues (Caine *et al.*, 2012). Similarly, the application of FTIR as a diagnostic tool has been demonstrated by the ability to distinguish between epithelial, myoepithelial and stomal tissues in benign or cancerous tumours (Walsh *et al.*, 2012). More recently FTIR spectral features of atherosclerotic plaques has been addressed in a bid to determine the biochemical markers of mechanical stiffness during the developmental of atherosclerosis (Wrobel *et al.*, 2015). Analysis of FTIR spectral profiles has also been deployed to address changes in the composition of the vessel wall during development of atherosclerosis the first of which was demonstrated using rabbit aortic tissue (Colley *et al.*, 2004). Since then, FTIR has been performed on healthy versus diseased aortic tissues to evaluate the diagnostic potential of the technique (Bonnier *et al.*, 2008). In addition to the detection of spectral differences between healthy versus diseased aortic tissues FTIR has also been deployed as a diagnostic tool to investigate the role of stem cells in contributing to vascular remodelling. Interrogation of de-differentiated SMCs, undifferentiated bone-marrow MSCs, and their myogenic progeny revealed significant

differences in their respective spectral signatures highlighting the ability of FTIR as an accurate means of detecting specific alteration in cellular profiles (Molony *et al.*, 2018). A major limitation of this study was the use of rodent derived bm-MSCs for the generation of SMCs. Therefore this study sought to overcome this limitation using HiPSC cell culture models to address the application of FTIR in conjunction with multivariant machine learning tools to detect distinct difference between (i) HiPSC and derived NE and PM progeny and (ii) HiPSC-derived NE and PM SMCs. Having demonstrated successful generation of HiPSC intermediate NE and PM progenitors and their subsequent myogenic differentiation *in vitro* , HiPSC-derived progenitor stem cells and their myogenic progeny were interrogated by FTIR to investigated if each population can be clearly distinguished from one another.

Raw FTIR spectral data sets from HiPSCs and HiPSC-derived progeny were analysed using multivariate statistical packages PAST4 and WEKA. Firstly, PCA of HiPSC and HiPSC-derived NE and PM progenitor stem cells revealed a distinct separation between HiPSCs and HiPSC-derived NE (NEP, SNEP, NPC) and PM progeny. The order of the PCs denoted their importance in the dataset, whereby PC1 described the highest amount of variation. A scatter plot of specimens along the first two canonical axes showed maximal and second to maximal separation between all groups. The axes represented linear combinations of the original variables as in PCA, and eigenvalues indicated the amount of variation explained by these axes. Using PCA 2-way multivariate statistical analysis variation between HiPSC and HiPSC-derived NE and PM progenitor stem cells a significant separation was presented using PCA scatter plots. Although clear separation based on PCA of FTIR datasets was demonstrated between HiPSC and HiPSC-derived progeny direct comparison of HiPSC-derived NE and PM progenitor stem cells showed some similarities. This is not surprising as morphological analysis of both NE and PM progenitors should morphological similarities therefore spectral similarities could be attributed to their abundance of stem cell-associated characteristics. LDA of HiPSC-derived NE and PM progenitor stem cells was used to demonstrate the maximum separability between groups across the data set. LDA, presented as a histogram, revealed that the FTIR profile of HiPSC and HiPSC-derived NE and PM progenitors could be easily separated from each other. Furthermore, analysis of NE and PM progeny in the absence of HiPSCs showed a distinct separation.

Although the discrimination of embryonically defined stem cells using FTIR can be useful for the detection of discrete niches of stem cells that may reside in atheroprone versus atheroresistant areas of the vessel the true sub-clinical diagnostic potential lies in the ability to detect the presence of NE-derived SMCs during early stages of neointimal formation. Following FTIR of HiPSC-derived NE and PM SMC progeny PCA demonstrated the ability to separate HiPSC-derived NE and PM progenitors (SNEP, NPC, PM) from their myogenic progeny (SNEP-SMC, NPC-SMCM PM-SMC). Using a PCA 2-way multivariate statistical analysis variation between HiPSC-derived NE and PM progenitor stem cells and their myogenic progeny showed a significant separation presented using PCA scatter plots with NE and PM-derived SMCs clustering away from the cell in which they were derived. Although clear separation based on PCA of FTIR datasets was demonstrated between HiPSC-derived NE and PM and their myogenic progeny direct comparison of HiPSC-derived NE and PM SMCs showed some similarities, with NPC-SMCs demonstrating the greatest difference. Maximum separability between HiPSC-derived stem cells and their myogenic progeny was evaluated using LDA which revealed that the FTIR profile of HiPSC-derived NE and PM progenitors and their myogenic progeny could be easily separated from each other. Although previous studies have focused on spectral differences, mainly differences in spectral peaks, between human embryonic stem cells and their differentiated progeny (Pijanka *et al.*, 2010; Tanthanuch *et al.*, 2010) this study focuses on the ability to separate stem cells and their derived progeny using a combination of FTIR and machine learning tools reducing the time spent on analysis of complex FTIR graphs presenting it as a more applicable tool for sub-clinical disease detection.

While FTIR analysis of HiPSCs and their respective stem cell and SMC progeny facilitated initial screening and discrimination of stem cells versus their SMC progeny, Raman spectroscopy of the cytoplasm of individual cells revealed distinct separation of each cell type *in vitro*. In contrast to FTIR analysis of whole cells Raman spectra were generated from the cytoplasm of individual HiPSCs and HiPSC-derived NE and PM progeny as differences within the cytoplasm are more pronounced as stem cells begin to differentiate down a myogenic lineage (Vazão *et al.*, 2011). PCA of Raman spectroscopic data demonstrated that HiPSCs and their derived stem cell NE and PM cells could be

clearly separated according to the first principal component (PC1). Moreover a 4-way multivariate statistical analysis revealed that HiPSC-derived NE and PM progeny could be clearly discriminated from HiPSCs. Similar findings were reported following TGF-1-dependant myogenic differentiation of HiPSC-derived stem cells as NE and PM-derived SMCs could be clearly separated. LDA of all HiPSC-derived cell lines enabled quantification of this discrimination with the sensitivity and specificity value determined for all cell populations based on a leave-one-out- cross validation. Cross validation confirmed that optimized neural networks can identify all cell types with high performance, based only on their Raman spectral profile Interrogation of the trained LDA set revealed the spectral profile of cells generated from HiPSCs pr HiPSC-derived progenitor stem cells could be easily separated from each other with accuracies of <70%.

In order to truly determine differences in biochemical properties associated with HiPSC-derived stem cell and SMC differentiation further analysis of spectral shifts in these cell populations would provide reliable estimates of changes in *in situ* protein, nucleic acid and lipid content. A limitation of the findings reported is the use of a heterogeneous population of cells in culture, the use of a clonogenic cell may improve separation accuracies as it would give rise to a more homogenous population suited as an improved population for clinical validation. In addition, *ex vivo* analysis of human tissues is a favoured over the use of cells in culture as changes in cells composition can be easily affected by the media in which they are maintained (Kennedy, Mooney, *et al.*, 2014). Vibrational spectroscopy techniques for *ex vivo* analysis of various tissues associated with vascular disease including endothelial dysfunction, atherosclerotic plaque and vessel remodelling has been reported (Buschman *et al.*, 2001; Marzec *et al.*, 2015). Therefore, this study investigated the use of Raman to separate previously published spectral datasets from healthy (<50 year olds) and diseased human tissues (aged, atherosclerotic and arteriosclerotic). To determine the greatest variation between the aforementioned disease states, PCA using PAST4 was carried out. Firstly, using PCA 2-way multivariate statistical analysis variation plot between normal vs. aged, atherosclerosis and arteriosclerosis a significant separation was presented. Secondly, using a 3-way multivariate statistical analysis variation plot a clear separation was observed between aged, atherosclerosis and arteriosclerosis spectral datasets. LDA using the machine learning tool, WEKA was used to validate the maximum separability of normal, aged,

atherosclerotic and arteriosclerotic datasets. Cross validation confirmed that optimized neural networks can identify all cell types with high performance, based only on their Raman spectral profile and resulted in an F-score of 0.86. Each disease state was then supplied as an unknown. Interrogation of the trained LDA set revealed the spectral profile of cells generated from HiPSCs pr HiPSC-derived progenitor stem cells could be easily separated from each other with accuracies of 88%, 66%, 79%, and 78% for normal, aged arteriosclerosis and atherosclerosis, respectively, on a cross-validated leave-one-out basis. Although the ideal diagnostic scenario would sperate each disease state with 100% accuracy inaccuracies may be due to spectral peaks from various constituents of the vessel wall including the elastic lamina as the dataset generated was not cell specific rather across a cross-section of aortic tissue samples.

The use of vibrational spectroscopy was successfully applied to detect changes in spectral signatures of HiPSC-derived stem cells versus their myogenic progeny *in vitro* and healthy, aged, atherosclerotic and arteriosclerotic vessels *ex vivo*. The initial step in the development of arteriosclerosis disease is IMT and neointimal formation therefore this study sought to interrogate the Raman spectral datasets from healthy, aged, atherosclerotic and arteriosclerotic using the spectral profiles of HiPSC-derived stem cells and their SMC progeny using MLP artificial neural network analysis. The algorithm was trained using 66% of the tissue data sets. This trained network was subsequently used to interrogate spectral datasets of cells isolated from HiPSC-derived NE, PM, and their respective myogenic progeny *in vitro.* Interrogation of these early atherosclerotic vessels *in situ* using vibrational spectroscopy could successfully detect the presence of stem-cell derived SMC progeny. This finding supports the use of Raman spectroscopy in particular as a diagnostic potential for sub-clinical atherosclerotic development due to the ability to detect stem cell-derived SMC progeny in arterial vessels. In order to translate this platform for use in a clinical setting the development of a Raman optical probe, similar to that used during brain surgery (Jermyn *et al.*, 2015), would be a necessity.

Having demonstrated the application of FTIR and Raman in discriminating HiPSC-derived stem cell and VSMC progeny, the next objective of this chapter was to investigate the application of single-cell AF to generate similar findings. The application of label-free autofluorescence readings has been underutilised as a diagnostic tool for sub-clinical

disease. The use of light to assess changes in cellular phenotypes has been reported to identify ocular disease or degradation (Fleckenstein, Schmitz-Valckenberg and Holz, 2010). Other clinical applications includes the analysis of skin AF spectra for detection of advanced glycation end products and collagen identified as novel risk factors of chronic kidney disease and CVD (Noordzij *et al.*, 2012; Den Dekker *et al.*, 2013). As with many diagnostic platforms, the use of AF to detect changes in normal versus disease states has been investigated for detection and monitoring of various cancers (Wang *et al.*, 2017; Yuan *et al.*, 2019). Although light as a diagnostic and prognostic tool has several advantages including high sensitivity, non-invasive measurement and low limits of detection the combination of AF and microfluidics photonics enables real time, measurements of relevant analytes in small sample volumes (Sheikh, Lighthouse and Greif, 2014). The use of novel LoaD platforms has demonstrated many attractive qualities for cellular analysis and disease diagnostics (Yun and Kwok, 2017). Microfluidic V-cup capture design and auto-fluorescence readings makes it possible to analyse cell populations within minutes. In this context, using optical multi-parameter interrogation of single cells on this novel LoaD platform in conjunction with multivariant machine learning tools we clearly demonstrate that single cell photonics across five wavelengths is of sufficient coverage to discriminate HiPSC-derived NE progenitor stem cells from their myogenic progeny. Moreover, photonic AF datasets can classify carotid medial SMCs from atherosclerotic and arteriosclerotic vessels *ex vivo* with shared spectral similarities to HiPSC NE-derived SMCs.

Single-cell photonic measurements of HiPSC and HiPSC-derived NE progenitor stem cells across five AF wavelengths were recorded following V-cup capture. The photonic intensity of each stem cell progenitor cell line was compared to that of HiPSCs. Both SNEP and NPCs demonstrated lowered photonic intensities at each wavelength when compared to HiPSCs. In contrast NEPs demonstrated an increase in intensity at λ 465nm + 20nm suggesting that there are biochemical differences between NE-derived stem cell populations. In contrast, the photonic intensity of both NEP and SNEP cells at λ530 and λ603nm + 20nm significantly increased following myogenic differentiation.

The risk of vascular disease may depend on the embryological origin of VSMCs, with VMSCs of NE origin exhibiting a higher risk to their paraxial mesodermal counterpart. Although previous studies comparing undifferentiated bone marrow-derived

mesenchymal stem cells and C3H/10T1/2 MSCs before and after TGF-B1 induced myogenic differentiation *in vitro* have reported an increase in AF at λ465, λ530, λ565, and λ630nm after 7d (Molony *et al.*, 2021) using scPH of NE-derived VSMC populations, we demonstrated distinct differences in photonic intensity at λ465, λ530 after 12 d. These differences may be due to a difference in the length of TGF-b1 treatments or alternatively may be due to differences in embryological origins as bone-marrow derived MSCs are considered good models of SMC differentiation from mesoderm precursors *in vitro* (Boström *et al.*, 2000; Miwa and Era, 2018), In order to determine if this is true further AF analysis of HiPSC-derived PM progenitor stem cells would be needed. Although the direct comparison of AF profiles HiPSC-derived PM and PM-SMCs could not be carried out due to the uncertainty of PM maintenance *in vitro* AF emissions of NE-derived SMCs were significantly increased at 465 and 530 wavenumbers in comparison PM-derived SMCs. Furthermore multivariant analysis using PCA and LDA of single-cell photonic data demonstrated the ability to discriminate HiPSC, NE and PM-derived progenitors and their respective myogenic progeny. This data suggest that single-cell photonic profiles *in vitro* are of sufficient specificity and overall quality for LDA algorithms to discriminate various HiPSC-derived cell types. This shift in intensities at differing auto fluorescent emissions along with the ability to separate NE and PM-derived SMCs by PCA and LDA demonstrates that single cell photonics can be used not only as a label-free photonic platform to discriminate embryologically defined progenitors and their respective myogenic progeny but also to further define embryologically defined myogenic progeny of NE and PM origin, which can be utilised to determine disease-prone areas of the aortic vessel *in vivo*.

Although FTIR, Raman and single cell LiPhos photonics discriminated HiPSC-derived progenitors from their respective myogenic progeny *in vitro,* further experiments were carried out using label-free single cell photonics from atherosclerotic and arteriosclerotic vessels *ex vivo* were interrogated and compared to HiPSC-derived NE progenitor stem cells and their respective myogenic progeny across five broadband light wavelengths. An increase in photonic intensity of single cells from the atherosclerotic vessel *ex vivo* was significantly enhanced across all five wavelengths when compared to single cells from arteriosclerotic vessels. Similarly, PCA and LDA revealed that the photonic profile of cells isolated from atherosclerotic and arteriosclerotic vessels could be easily separated from each other across the five wavelengths. Confusion matrices revealed that 94% of

the atherosclerotic cells were classified as similar to each other. In contrast, 66% of arteriosclerotic cells were classified as similar to each other, with 33% classed as similar to atherosclerotic on a cross-validation leave-one-out-basis suggesting a greater level of cellular heterogeneity exists in single cells isolated from arteriosclerotic vessels as opposed to atherosclerotic vessels. This level of heterogeneity may indicates the existence of specific subsets of medial SMCs within arteriosclerotic lesions therefore further analysis was performed to determine if the photonic profile of atherosclerotic and arteriosclerotic was similar to SMCs derived from NE or PM origins.

Multi-layered neural networks that mimic human neural circuit structure have recently been utilised to classify highly non-linear datasets, proving an ideal candidate for label-free cell subtypes, including HiPSC, generated ECs, lymphocyte cells, and hematopoietic cells (Godinez *et al.*, 2017; Pradhan *et al.*, 2020). Using a pre-trained MLP neural network the classification of HiPSC-derived progenitors and their myogenic progeny was facilitated based on AF emissions alone. Interrogation of this pre-trained MLP artificial neural network using single cells isolated from atherosclerotic and arteriosclerotic lesions further predicted similarities between HiPSC-derived NE progenitor stem cells and their myogenic progeny and single-cells isolated from atherosclerotic and arteriosclerotic vessels These findings identified strong similarities between HiPSC-derived NE SMCs and single cells isolated from atherosclerotic and arteriosclerotic vessels with 76% (62% SNEP-SMC, 15% NEP-SMC) of arteriosclerotic cells classified as NE-derived SMCs and 94% (79% SNEP-SMC, 15% NEP-SMC) of atherosclerotic cells classified as NE-derived SMCs. This finding is not surprising as the tissue sections from which cells were isolated had originated from the carotid bifurcation, an area classified as atheroprone with intimal cells derived from the neural crest (Majesky and W., 2007). In consonance with our findings using MLP of Raman vibrational spectra, we identified a small population of NE-derived stem cells <10% in atherosclerotic and arteriosclerotic photonic datasets with the majority of cells classified as NE derived SNEP-SMCs. Our findings confirm previously reported lineage tracing data that mapped NE S100β+ stem cells and myogenic progeny to vascular lesions (Yuan *et al.*, 2017; Tang *et al.*, 2020; Di Luca *et al.*, 2021). One limitation of this study is the use of cell models *in vitro* to effectively model vSMCs in diseased lesions *in situ*. Although embryologically defined HiPSC-derived stem cell

populations were generated, further cloning of NE and PM populations would ensure a more homogenous population for further clinical testing.

In conclusion, we have demonstrated that vibrational spectroscopy and single cell photonics present as novel diagnostic platforms to facilitate the detection of disease-relevant spectral signatures that reflect cell status, i.e., undifferentiated versus differentiated healthy versus diseased. The detection of changes in cellular status in resident vascular cells may have an important predictive value for the identification of early 'transitional' lesions in subclinical atherosclerosis. These diagnostic platforms can be readily translated to a clinical setting as the data generated is based on vibrational spectroscopy, a technique already utilised for detection of various cancers (Eikje, Aizawa and Ozaki, 2005) and detection of broadband light using *in situ* endoscopic analysis (Pahlevaninezhad *et al.*, 2016). Using a combination of these techniques, this study adds a dimension to the current approach in the stratification of early vascular lesions whereby imaging and photonic signatures are combined to assess lesion progression, thereby enabling more information about the disease before primary prevention interventions are prescribed combating the pathogenesis of CVD progression.

Chapter 6:

General Discussion

CVD remains the lead cause of death worldwide (Virani *et al.*, 2020). To combat the ever-rising prevalence of CVDs, the emphasis on subclinical detection and treatment before clinical manifestation is vital (Hobbs, 2004). Atherosclerosis, a chronic inflammatory disease of the arterial wall, is responsible for various CVDs, including pulmonary hypertension, arteriosclerosis, myocardial infarction (MI) and stroke (Ross, 1999). Unlike most communicable diseases, atherosclerosis is often referred to as a silent killer as patients may remain asymptomatic until the late stages of well-advanced atherosclerotic lesions. Due to the multifactorial complexity of the development of atherosclerosis, various invasive and non-invasive techniques have been developed to measure atherosclerosis and, more recently, sub-clinical atherosclerosis, including non-invasive techniques such as MRI, ultrasonography, as well invasive techniques such as coronary angiography and intravascular ultrasound (Kohsaka and Makaryus, 2008; Celeng *et al.*, 2016). The main focus of such diagnostic platform is to identify physical risk factors such as luminal diameter or stenosis, vessel wall thickness and plaque volume and composition (Toth, 2008; Papageorgiou *et al.*, 2016; Gatto and Prati, 2020). However, a limitation of such platforms is the inability to identify discrete phenotypic changes within the cellular composition of the arterial wall indicative of early sub-clinical atherosclerosis and the accumulation of vSMC-like cells driving neointimal formation.

Subclinical atherosclerosis defines the initiation and progression of early atherosclerotic plaques (Singh *et al.*, 2018). The diagnosis of sub-clinical atherosclerosis is of fundamental importance as it allows the prompt implementation of primary prevention therapeutic measures. A hallmark of subclinical atherosclerosis is the accumulation of vSMC-like cells leading to IMT and the formation of lesions embedded in atheroprone areas of the arterial wall (Bennett, Sinha and Owens, 2016). Central to this process is the development of PIT, the first truly progressive lesion responsible for the rise in the appearance of advanced atherosclerotic plaques (Kolodgie *et al.*, 2007). Although it is widely accepted that the development of a neointima within arterial vessels is due to the migration and proliferation of vSMC-like cells, identifying the origin and molecular mechanisms by which these cells arise is paramount to discovering practical diagnostic tools that can be deployed as general routine surveillance of the vasculature. In recent years, the previously accepted model of medial vSMC de-differentiation/modulation and phenotypic switching to vSMC-like cells within the developing neointima (Owens, Kumar and Wamhoff, 2004) has been challenged by various studies that report a role for

resident medial and /or adventitial vascular stem cells (Tang, Wang, Yuan, *et al.*, 2012; Majesky *et al.*, 2017; Tang *et al.*, 2020; Di Luca *et al.*, 2021; Molony *et al.*, 2021), circulating bone marrow-derived stem cells (Sata, 2003), and/or transition of endothelial cells to mesenchymal stem cells as the primary mode of neointima formation (Cooley *et al.*, 2014). However, the most compelling evidence to date using lineage tracing studies, scRNA-Seq, and single-cell photonics is the discovery of a rare population of (i) differentiated MYH11 medial Sca1+ stem cells (Chappell *et al.*, 2016; Dobnikar *et al.*, 2018) and (ii) resident adventitial and medial S100β+ progenitors stem cells, that undergo myogenic differentiation and migration to the site of injury (Di Luca *et al.*, 2021; Molony *et al.*, 2021)

In order to discover effective detection platforms for subclinical atherosclerosis, a greater understanding of the molecular mechanisms by which these stem cell populations may undergo myogenic differentiation to SMC-like cells is needed. One such pathway that plays a pivotal role in maintaining adult progenitor/stem cells in tissue repair after injury is the Hh signalling pathway (Petrova and Joyner, 2014). GWAS studies in CAD patients have identified increased Hh signalling and vSMC-like proliferation and migration *in vitro* (Schunkert *et al.*, 2011; Aravani *et al.*, 2019). Hh signalling has also been reported to control myogenic differentiation and accumulation of S100β/Sca1^{+} stem cell derived VMSC-like progeny within vascular lesions (Di Luca *et al.*, 2021). Although it is clear that Hh plays a significant role in the pathogenesis of atherosclerosis, the mechanism(s) responsible for activation is(are) less understood. The emerging role of EV facilitation of intercellular communication has attracted huge interest in the potential application of EVs as diagnostic tools in CVD due to their stability and abundance in biological fluids (de Freitas *et al.*, 2021).

Taking into account recent findings and the overall need to continuously improve on the plethora of diagnostic techniques deployed for detection of subclinical atherosclerosis, this study aimed to develop novel strategies that interrogate and discriminate resident vascular stem cell populations and their myogenic progeny by detecting discrete changes at a molecular level in the cellular composition of the arterial wall. To achieve this, two methods for early disease detection were assessed; namely (i) development of a murine and human *in vitro* cell model to investigate the role of endothelial HG-EV mediated transport of SHh morphogen and uptake by a resident NE Nestin/ S100β^{+} progenitor stem

cell within atheroprone regions of arterial vessels (ii) development of a human *in vitro* model to detect vascular cellular phenotypes of distinct embryological origin indicative of sub-clinical atherosclerosis and discriminate them from each other using single-cell photonic analysis using FTIR, Raman and autofluorescence spectra (AF) to predict their presence in human lesions. By taking this approach, this study identified (i) a potential initiator of subclinical atherosclerosis via interrogation of the endothelial cell-derived EVs from dysfunctional ECs for the presence of key modulators of resident vascular stem cell fate and the generation of SMC-like cells, (ii) a resident vascular stem cell that facilitates endothelial derived EV uptake via interrogation of cells in lesions using single cell photonics and vibrational spectroscopy to determine the presence of one of the origins of SMC-like cells in vascular lesions.

6.1 EC-derived HG-EVs facilitate the transport of SHh initiating vSMC differentiation of resident S100β + vascular stem cells *in vitro*.

Although many studies have focused on the role of EV-encapsulated miRNA for prognosis and diagnosis of various CVDs, little is known about the presence of EV associated proteins as activators of pathologic conditions (Navickas *et al.*, 2016; Wendt *et al.*, 2018; Zhou *et al.*, 2018). One of a multitude of pathways recapitulated during vSMC differentiation and neointimal formation is the Hh signalling pathway. Previous studies have identified an abundance of dual labelled Hh-responsive S100β^{+} stem cells derived from a non-SMC parent population in response to iatrogenic flow restriction *in vivo* (Di Luca *et al.*, 2021) whilst studies have also reported the role of S100β^{+} resident vascular stem cells in arterial remodelling following vessel ligation (Tang, Wang, Yuan, *et al.*, 2012; Cao *et al.*, 2017). In addition, the presence of Gli marked cells in vascular lesions following cell fate mapping has been reported indicating the presence of Hh responsive cells within these lesions (KRamann *et al.*, 2015, 2016).

EC dysfunction marks the initiation of a cascade of events of primary importance to the pathogenesis of the vascular disease (Anderson *et al.*, 1995) (Kinlay and Ganz, 1997). Under physiological conditions, vascular ECs secrete low concentrations of EVs. Upon induction of ED, the concentration of EVs significantly increases (Vicencio *et al.*, 2015; Dougherty *et al.*, 2020). Using a diabetic *in vitro* model, we report an increase in EC-derived EVs following acute exposure to HG conditions, a hallmark of diabetes.

Hyperglycaemia induces an increase in oxidative stress by producing intracellular ROS resulting in endothelial dysfunction and accelerated atherosclerosis. Various studies have reported deleterious effects of the endothelium in response to hyperglycaemic conditions, including reduced NO production (Ding *et al.*, 2000; Du *et al.*, 2001), enhanced NF-κB activation (Hamuro *et al.*, 2002), an increase in EC apoptosis (Sheu *et al.*, 2005; Su *et al.*, 2018). This response has also been shown for EVs secreted from ECs exposed to hyperglycaemic conditions. Using *in vitro* cell culture models, EC exposure to hyperglycaemic conditions effectively enhances EC-EV generation and secretion (Burger *et al.*, 2017). Furthermore, differences in both protein and RNA content of EVs secreted from ECs in response to cellular stress stimuli including hypoxic and hyperglycemic conditions has been shown (de Jong *et al.*, 2012). Proteomic analysis of EC-EVs derived from normal and hyperglycaemic conditions have identified differential expression of proteins highlighting differences in vesicular cargo in response to pathologic stimuli. Similarly, EC-derived EVs cultured under high glucose conditions induced endothelial dysfunction, vascular inflammation and prompted atherosclerosis *in vivo* (Burger *et al.*, 2017).

Although these studies identified key pathologic effects and proteomic changes in the vesicular cargo between healthy and hyperglycaemic conditions, the direct identification of key EV-encapsulated modulators of vascular pathogenies is unknown. Having developed well-characterised, robust *in vitro* cell models, the role of EV-mediated EC-stem cell communication was investigated. EV proteins have been associated with CVD risk factors, with changes in vesicular cargo reported in response to smoking and obesity (Kranendonk *et al.*, 2014; Benedikter *et al.*, 2019). Data from this study provided compelling evidence of a distinct change in EVs secreted under physiological and pathological conditions, represented not only by an increase in secreted EVs but also an increase in SHh target genes in S100β^{+} progenitor stem cells when treated with EC-derived HG-EVs, a response blocked by SHh signalling pathway inhibitors cyclopamine and 5E1. In addition, we report an increase in the expression of SHh in ECs exposed to hyperglycemia which it tempting to speculate results in an increase in SHh encapsulated in EVs however further characterisation of HG-EVs to determine the exact levels of SHh would be necessary.

An increase in myogenic differentiation genes CNN1 and MYH11 in S100β$^+$ progenitor stem cells was demonstrated, suggesting that EC-derived EVs generated in response to pathologic stimuli mediate SHh-dependent vSMC differentiation of S100β+ progenitor stem cells *in vitro* as Hh inhibition demonstrate attenuation of EC-derived HG-EV mediated myogenic differentiation. The role of EC-derived HG-EV mediated transport of SHh from ECs to S100β$^+$ NE progenitor stem cells is novel and highlights a diagnostic biomarker responsible for initiating vSMC differentiation and neointimal migration formation. While Hh signalling has been previously implicated in the pathogenesis of atherosclerosis through modulation of differentiated SMC phenotypes (Aravani *et al.*, 2019), studies have also reported an association with hyperglycemic induced activation of Hh signalling in human ECs resulting in endothelial autophagy, a catabolic process in which a cell digest its own components via the lysosomal machinery, a process associated with the pathogenesis of diabetes (Ravikumar *et al.*, 2010). Moreover, inhibition of this Hh signalling cascade via administration of Metformin alleviated hyperglycemia-induced endothelial dysfunction, resulting in its use as a frontline treatment for diabetes and more recently associated as a therapeutic treatment for prevention and improved prognosis of various cancers including pancreatic, gastric and breast cancer (FAN *et al.*, 2015; Song *et al.*, 2017; Niu *et al.*, 2019).

One of the main limitations to these findings was the use of *in vitro* murine models to discover human biomarkers. Although the use of animal models of atherosclerosis has played an essential role to improve the understanding of the molecular mechanisms involved during the pathogenesis of atherosclerosis (Emini Veseli *et al.*, 2017), significant limitations when modelling human disease exist, including disparities in vessel size and composition, the main being the presence of a thickened intimal layer in humans from birth, as well as differences in biochemical activity and fundamental differences in genomic organisation (Barré-Sinoussi and Montagutelli, 2015).To overcome these limitations, an *in vitro* HiPSC model was developed to validate previous findings of EC HG-EV-dependent upregulation of vSMC differentiation of resident S100β+ stem cells. Patient-derived HiPSCs provide an unlimited supply of cells that can be differentiated into the disease-relevant cell harbouring the genetic variation contributing to such a condition (Soldner and Jaenisch, 2012). Additionally, recreating the human pathophysiological conditions in a culture dish eliminates the cross-species discrepancies in animal models. HiPSCs have been extensively used to model the role of

vSMCs in the development of vascular diseases, for example, the neointimal hyperplasia and atherosclerosis associated with Hutchison-Gilford Progeria Syndrome resulting in the identification of premature senescence markers related to the vascular aging of the disease (G. H. Liu *et al.*, 2011). Similarly, HiPSC-derived vSMC models have also been used to investigate the pathogenesis of aortic aneurysms in Marfan syndrome patients and provide insight into novel therapeutic targets (Granata *et al.*, 2017). HiPSCs are also a useful tool for modelling the cardiovascular of atherosclerosis (Liang and Du, 2014; Bargehr *et al.*, 2016). This study presents a novel method of vascular disease modelling using HiPSC-derived stem cells and embryologically defined vSMC progeny to investigate the influence of EC-derived HG-EV on stem cell to vSMC differentiation *in vitro*.

The embryological origin of vSMC has previously been associated with influencing atherosclerosis progression (Cheung *et al.*, 2012). Previous studies have shown HiPSC to vSMC differentiation through an intermediate progenitor stem cell or direct SMC differentiation (Cheung and Sinha, 2011). NE-derived stem cells have been associated with atheroprone areas of the vasculature; for this reason, we demonstrate in detail the derivation of origin-specific NE, PM, and LM progenitor stem cells and furthermore demonstrate their myogenic differentiation capabilities providing a platform to generate an ideal source of isogenic stem cells and vSMCs to study intercellular communication mediated by EC-derived EVs. Developing vSMCs from HiPSC has been extensively demonstrated through directed differentiation using a cocktail of molecules, including fibroblast growth factor 2 (FGF2), platelet-derived growth factor (PDGF-BB), and transforming growth factor-β (TGF-β) (Dash *et al.*, 2015; Yang *et al.*, 2016; Ji *et al.*, 2017). However, one of the major concerns for subsequent disease modelling or the therapeutic potential is confirming the absolute specificity of the resulting differentiated vSMCs. As discussed, the heterogeneity of SMC origin and the association with disease susceptibility requires careful consideration for the derivation of HiPSC vSMC for disease modelling or clinical approaches. For example, whether it is desired to model vSMCs from the aortic arch or descending aorta, neuroectoderm, or paraxial mesoderm specific lineages, respectively, must be guaranteed to confirm correct and accurate modelling (Majesky and W., 2007; Wasteson *et al.*, 2008). To determine the certainty of HiPSC-derived NE progenitor cells, previously published protocols using chemically defined media supplemented with FGF2 and SC431542 were followed (Cheung *et al.*,

2014) and characterised for distinct NE markers PAX6, NESTIN, and S100β. Following confirmation of the generation of a distinct NE progenitor, the first demonstration of activation of Hh signalling of HiPSC-derived NE progenitor stem cells *in vitro* is presented.

Research carried out by our group along with others have shown the role of Hh signalling during vascular pathogenesis (Di Luca *et al*., 2021). Local inhibition of the Hh receptor, pathched-1, attenuates subclinical atherosclerotic disease in murine models (Redmond *et al*., 2013). Furthermore HHIP-LIGWAS studies have shown an association of Hh SNPs with coronary artery disease (Schunkert *et al*., 2011). Taking these findings on board our study identifies one of the possible pathways by which Hh signalling in S100β+ NE progenitor stem cells is activated. Furthermore, EV-encapsulated SHh may prove advantageous over current diagnostic circulating markers, which peak for limited periods during or after disease due to the natural protection of the vesicular membrane (Boukouris and Mathivanan, 2015).

The investigation of EVs as diagnostic biomarkers offers exciting promise not only for biomarker discovery but also for therapeutic and drug delivery for CVD treatment (Vlassov *et al.*, 2012). As such, EV research has expanded rapidly; however, several limitations associated with EV isolation and interrogation, both *in vitro* and *in vivo*, are continuously questioned. Although efforts have been made to standardise EV experimental requirements, including minimal information for studies for studies of EVs guidelines published by the International Society for Extracellular Vesicle (Théry *et al.*, 2018), studies compliant with these guidelines are often incomparable (Kennedy, Russell and Riley, 2020). One of the main limitations faced from the onset of our EV studies was the choice of precipitation method. Numerous methodologies exist to isolate EVs, including ultracentrifugation, size exclusion chromatography, ultrafiltration, immunoaffinity, and microfluidics. Isolation of pure EV pellets is of utmost importance when choosing an isolation method with significant potential for precipitation of non-EV material, including cellular proteins and lipids, to contaminate EV isolates. Although strict guidelines must be adhered to for the generation and characterisation of EVs for therapeutic interventions including the necessity for oversight of relevant national regulatory entities the process for the application of EVs as a diagnostic tool is less rigorous (Théry *et al.*, 2018; Börger *et al.*, 2020). The choice of EV isolation method used

for this study was influenced by the availability of equipment, amount of starting material, and downstream applications (Furi, Momen-Heravi and Szabo, 2017). To confirm the isolation of pure EV fractions, numerous EV detection methods were deployed in this study, including FeSEM, DLS, NTA, NanoFACs, and fluorescent labelling and tracking of isolated EVs. The isolation of membrane-bound vesicles ranging from 30nm-180nm in size was confirmed. Furthermore, expression of CD31, indicating EC origin, and associated EV proteins, including tetraspanin proteins CD63, CD8, TSG101, and HSP confirmed their phenotype. Although a variety of EV characterisation techniques were deployed to establish the isolation of EC-derived EVs it is important to address the possibility of the precipitation of soluble Hh ligands as a contaminant during EV preparation. In order to truly determine the presence of Hh on the membrane of EC-derived EVs further analysis using the Amnis ImageStream would be favourable. This imaging flow cytometry platform allows multi-parametric analyses of EVs at the single vesicle level therefore co-staining of EC-derived EVs using associated known EV makers (e.g. CD81, CD63) and anti-Hh antibody would not only enable the detection of SHh+ EVs but also provide insights into the localisation of SHh on the vesicular membrane (Tertel and Giebel, 2020).

Another general limitation encountered when investigating EV content is the nature of EV heterogeneity. Although cells release large numbers of EVs into their extracellular environment, which exert diverse biological effects on recipient cells, heterogeneity of biophysical characteristics and composition remains challenging for the reproducibility of experimental outcomes. One important consideration that EV studies have to consider is making direct functional comparisons between populations correctly. In this study, direct comparisons of EC-derived NG, HG, and MT-EVs were evaluated to ensure a significant increase in Hh target genes was only detected following the release of EVs from dysfunctional (hyperglycaemic) ECs. Although EV isolations *in vitro* present proof of principle, the translation of EVs from cell culture systems to bodily fluids proves difficult due to a low yield of EV fractions resulting in the necessity of bulk EV productions. Although the data provide compelling evidence for the role of elevated EV-SHh as a diagnostic marker for subclinical atherosclerosis *in vitro* further research is needed to determine the detection of elevated levels of SHh-EVs in CVD patients.

Due to the abundance of large proteins found in blood plasma the detection of vesicular proteins is challenging. Therefore, for routine monitoring of bodily fluids as part of subclinical detection of atherosclerosis, further research is needed to develop a point of care EV diagnostic tool. Performing liquid biopsies is a potentially minimally-invasive route to elucidating underlying functional disturbances; however, the prospect of exploiting EVs as diagnostic biomarkers of CVD is intrinsically dependent on the efficiency at which they can be acquired for analysis. Tailored microfluidic-based devices favour the adaption of vesicular analysis for diagnostic platforms and provide significantly reduced processing times. These devices—some of which incorporate automated pre-treatment—can efficiently enrich EVs from whole blood, perform lysis and supply a nucleic acid, protein, and lipid-rich extract for subsequent analysis (Figure 6.1). The significance of EVs and the cargo they harbour remain in their infancy. Yet, it is anticipated that greater detail will be revealed regarding their role in CVD and how best to interpret their fluctuating presence during disease progression. Ultimately, their clinical value for predicting CVD will be defined by a combination of diagnostic developments, therapeutic strategies, and the ease at which they can be reliably and consistently isolated from samples .

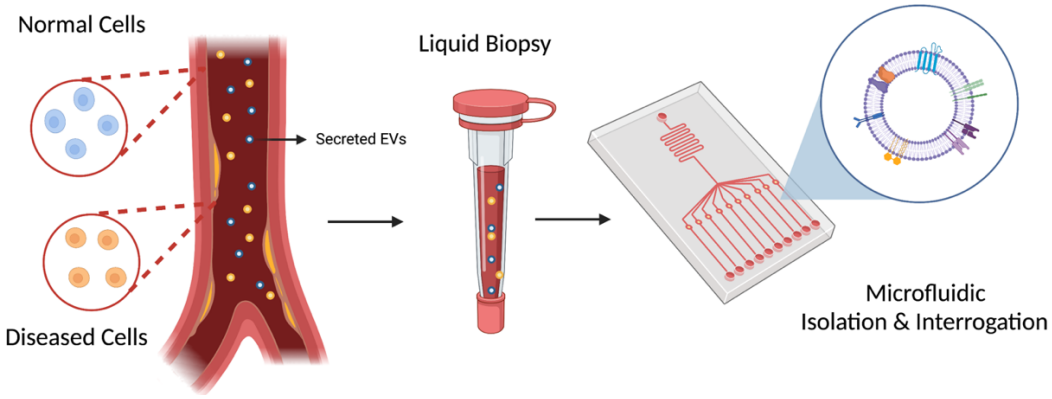

Figure 6.1 Circulating EVs as diagnostic biomarkers for subclinical detection of atherosclerosis. Resident vascular cells secrete EVs containing distinct differences in their cargo when exposed to pathologic stimuli making EVs an ideal candidate detection of disease. Detection of EVs for clinical diagnostic proves challenging therefore further studies into the application of a microfluidic disc for isolation and interrogation is essential.

6.2 Disease-relevant label-free single-cell photonic signatures identify S100β NE progenitor stem cell-derived vSMCs in vascular lesions.

Having investigated the role of circulating biomarkers derived from EC-EVs, the second aim of this study was to assess the application of single-cell vibrational spectroscopy and autofluorescence as a diagnostic tool to study vascular physiology and pathology via non-invasive detection of discrete changes in arterial cell composition. Using defined differentiation protocols, we present data that demonstrates the ability of single photonics using AF, Raman and FTIR spectra to discriminate vascular phenotypes within vascular lesions using supervised machine learning tools based on training algorithms generated from HiPSC- derived stem cells and their myogenic progeny.

Vibrational spectroscopy has shown great promise as a diagnostic tool for detecting discrete changes in cellular compositional makeup due to detecting marginal changes in protein, lipid, and cytoskeletal content of a cell. Although many studies to date have focused on the detection and discrimination of various cancers via the detection of changes in vibrational spectral profiles of tumours (Koljenović *et al.*, 2002; Gniadecka *et al.*, 2004; Haka *et al.*, 2005), the application of FTIR and Raman has emerged as a valuable tool for detection of various neurodegenerative diseases (Devitt *et al.*, 2018) and more recently infectious diseases such as Severe Acute Respiratory Syndrome Coronavirus 2 (SARS-CoV-2) (Carlomagno *et al.*, 2021). Although some work has been carried out investigating the application of Raman as a diagnostic tool for detection of atherosclerosis using mouse *in vivo* and human *ex vivo* models (Krafft *et al.*, 2009; Lattermann *et al.*, 2013; Kiselev *et al.*, 2016), there are still several limitations associated with clinical translation including the time-consuming processing of raw spectral data (Smith, Wright and Ashton, 2016) and differences in the thickness of aortic vessels resulting in longer acquisition times and the accessibility of tissues (Byrne *et al.*, 2016; Smith, Wright and Ashton, 2016).

To overcome this limitation machine learning tools have rapidly grown aiding the prediction, detection and classification of many diseases such as cancers, neurodegenerative diseases, diabetes and CVD (Dwivedi, 2018; Muhammad, Algehyne and Usman, 2020; Murali *et al.*, 2020; Myszczynska *et al.*, 2020). Although the use of label-free detection platforms have proven successful for detection of disease, large bio photonic datasets are often difficult to interpret. For this reason, machine learning tools

have been developed to reduce large numbers of measurements into lower-dimensional outputs. Statistical pattern recognition methods based primarily on artificial neural network geometries, referred to as deep learning, are employed to obtain real-time decision-making systems for that analysis of biphotonic data, in particular, spectroscopic data including spectral data pre-processing and spectral classification (Pradhan *et al.*, 2020). Not only has machine learning enabled the application of label-fee diagnostics for disease detection it has also been applied for analysis of liquid biopsies through the use the use of analysis tools such as support vectors, decision trees and random forests enabling the identification of changes in the profile of circulating biomarkers in diseases such as pre-eclampsia, tuberculosis, Alzheimer disease and many cancers through (Kenny *et al.*, 2005; Cazzoli *et al.*, 2013; Best *et al.*, 2015; Lugli *et al.*, 2015).

Herein, using HiPSC-derived cell model *in vitro*, the feasibility of multivariant analysis of both vibrational spectroscopic analysis and single-cell photonics was addressed as a powerful discriminator of changes in cell phenotypes, NE-derived stem cells, and their myogenic progeny, as an early diagnostic biomarker of stem cell-vSMC differentiation migration during the initial development of PIT. Furthermore, using both Raman vibrational spectra and single-cell photonics, the presence of S100β-NE stem cell-derived vSMCs in vascular lesions was confirmed by the use of multivariant analysis and supervised machine learning tools. This finding supports previously published studies which have identified a population of NE-derived S100β/ $Sca1^{+}$ cells, derived from a non-SMC S100β parent populations through the use single-cell photonics and cell fate mapping using S100ß CreERT2 mice, following injury and IHC analysis of vascular lesions (Di Luca *et al.*, 2021; Molony *et al.*, 2021).

In this study, we determine the greatest variation and further discrimination of HiPSC and derived stem cell and SMC progeny through PC and LDA analysis respectively. Embryologically defined HiPSC-derived NE and PM stem cells were separated from both the parent HiPSC and from each other. Further discrimination was achieved after the generation of NE-VMSC and PM-VMSCs. This is not surprising as fate-mapping studies have previously reported the existence of a mosaic of VMSCs arising from distinct developmental origins populated in defined areas of the vessel wall (Debakey and Glaeser, 2000; Majesky and W., 2007; Ruddy *et al.*, 2008). These findings highlight the use of vibrational spectra to determine atheroprone areas by detecting NE-vSMC rich

regions of the vasculature that can be routinely measured for IMT using existing diagnostic techniques such as ultrasonography. Although the use of HiPSC-derived stem cell progenitors and the generation of vSMC as a disease model allows for the unlimited generation of embryologically defined vSMCs, several limitations exist. Vascular SMCs generated from parent medial SMCs are typically maintained in serum-containing conditions, which, over time, have been reported to undergo phenotypic switching from a quiescent non-dividing contractile phenotype to a proliferative dedifferentiated phenotype losing the expression of vSMC associated markers CNN1 and MYH11 while gaining the expressing stem cell associated markers Sox10, Sox17 and S100β suggesting the presence of a contaminant stem cell population *in vitro* (Owens, Kumar and Wamhoff, 2004; Kennedy, Mooney, *et al.*, 2014). To eliminate this, NE and PMs were freshly differentiated from HiPSCs for Raman, FTIR, and photonic analysis. Following a day 10 vSMC differentiation protocol, vSMCs were characterised and fixed for spectral acquisition. The population of VMSCs acquired showed 100% expression of vSMC associated markers CNN1 and MYH11 with no expression of stem cell-associated markers representing a terminally differentiated vSMC with embryological specificity.

Although discrimination of embryologically defined vSMCs using FTIR, Raman, and single-cell photonic *in vitro* offers an insight into the identification of atheroprone areas in the vasculature, the true diagnostic value lies in the detection of vibrational spectra and single-cell photonics of stem cell-derived vSMC progeny within vascular lesions *ex vivo.* Our analysis facilitated the classification of arterial cells from normal and healthy cohorts using MLP artificial network analysis of (i) previously published Raman datasets from atherosclerotic, arteriosclerosis, aged, and healthy aortic tissue and (ii) single-cell photonics of isolated atherosclerotic and arteriosclerotic cells *ex vivo*. Using this MLP neural network of Raman diseased tissue spectra, we successfully detected HiPSC-derived NE stem cell-cells in normal and aged cohorts with minimal NE or PM-SMCs. However, a significant increase in NE-derived vSMCs was detected in arteriosclerotic tissue datasets. This finding was further supported using the MLP pre-trained neural network of a similar panel of embryologically defined HiPSC-derived stem cells and their myogenic progeny. Upon interrogating single cells isolated from atherosclerotic and arteriosclerotic vessels across five wavelengths for their auto fluorescent spectral profiles, a predominance of S100β NE-derived vSMCS in both arteriosclerosis and atherosclerotic disease tissues was revealed.

Collectively, these findings support previous lineage-tracing and scRNA-seq data that provide compelling evidence for a role of myogenic differentiation of resident adventitial/medial S100β-NE-derived stem cells during the initiation of neointimal formation (Torsney, Hu and Xu, 2005; Tang, Wang, Yuan, *et al.*, 2012; Roostalu *et al.*, 2018; Di Luca *et al.*, 2021; Molony *et al.*, 2021). Although several studies have evaluated changes in autofluorescence signals in response to the differentiation of stem cells to various lineages *in vitro* in general (Rice, Kaplan and Georgakoudi, 2007; Squirrell *et al.*, 2012; Thimm *et al.*, 2015), there is significant oversight and a lack of information about the use of autofluorescence signatures to discriminate stem cells from their myogenic progeny *in vitro* and *in vivo* during PIT development. Although somewhat more advanced, numerous studies have identified and collated Raman signatures of vascular smooth muscle cells and associated extracellular matrix proteins, collagen, and elastin which could serve as early spectral biomarkers for non-atherosclerotic stenotic progression (Lopes *et al.*, 2011; Peres *et al.*, 2011; Marzec *et al.*, 2015). Findings reported in this study can add an extra dimension to current diagnostic methods currently used to detect atherosclerosis due to the feasibility of *in situ* early lesional interrogation to discriminate the presence of stem-cell-derived vSMC in the neointima indicative of vascular pathogenesis. A limitation of the current reported findings is the analysis of cells and tissues *ex vivo*. For diagnostic purposes, the development of a small device capable of *in vivo* analysis is essential. The application of Raman spectroscopy probes has already proved successful in many clinical settings and has previously been deployed intra-operative guidance of brain surgery and endoscopic gastrointestinal procedures (Jermyn *et al.*, 2015; J. Wang *et al.*, 2015). Furthermore, recent advances have been made toward the development of a smart Raman needle with the capability to measure molecular tissue samples both *in vivo* and *ex vivo* (Day and Stone, 2013). These recent advancements are promising for developing a suitable device for routine *in vivo* monitoring of discrete changes in arterial cellular phenotypes that indicate early lesional pathogenesis, enabling primary prevention treatment (Figure 6.2).

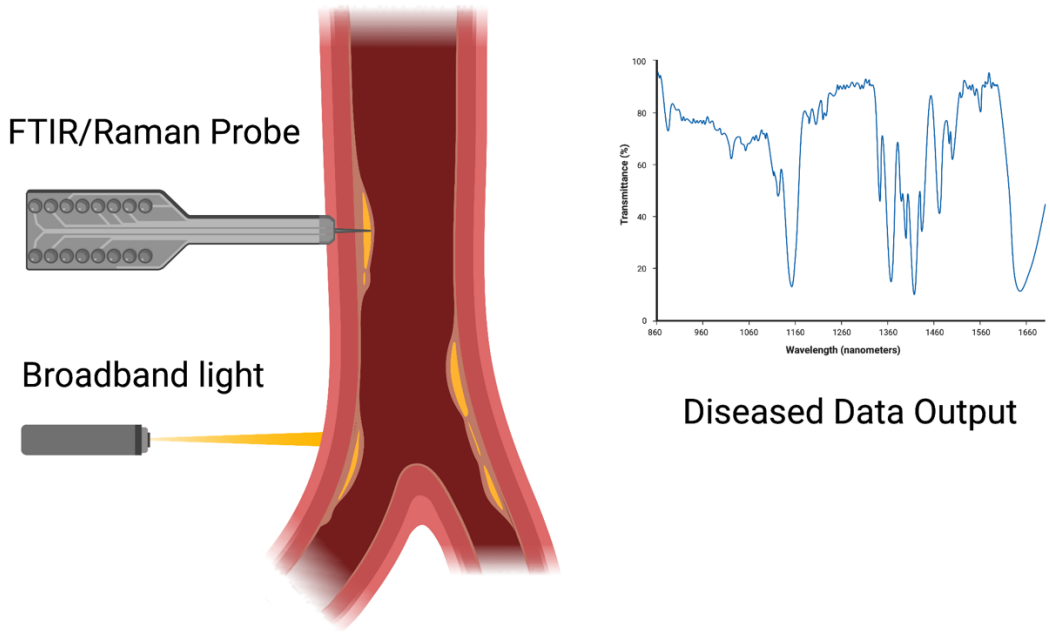

Figure 6.2 FTIR, Raman and single-cell autofluorescence emissions signatures as diagnostic biomarkers for subclinical detection of atherosclerosis. Vibrational spectroscopy has shown great promise as a diagnostic tool for detecting discrete changes in cellular compositional makeup due to the ability to detect marginal changes in protein, lipid, and cytoskeletal content of a cell. Using a Raman/autofluorescence emissions probe routine analysis of the arterial wall *in vivo* can detect discrete changes in cellular composition indicative of sub clinical atherosclerosis.

6.3 Future Work

Using three novel diagnostic platforms, FTIR, Raman and single-cell autofluorescence emissions platforms to interrogate HiPSC-derived undifferentiated NE and PM stem cells and their myogenic progeny, in addition to discrimination of normal and diseased cells and detection of stem cell and VSMC-like cells in diseased lesions, the data in this thesis presents a clinically translatable strategy to specifically detect discrete molecular changes in resident vascular lesions by combination of imaging and photonics signatures. Recent studies have reported the application of Raman spectroscopy in additions to machine learning tools to diagnosis and classify healthy versus tumour tissue. The use of a molecular Raman probe to characterise all major cellular components in combination with PCA and LDA has successfully distinguished cancerous from healthy breast tissue using 16 bands gathered from the fingerprint region (Zúñiga *et al.*, 2019; Kothari *et al.*, 2021).

In order to translate the findings in this research to a clinical setting further *ex vivo* and *in vivo* studies would be required. The data presented in this study represents preliminary *ex vivo* findings of the ability to distinguish healthy versus diseased tissues using Raman spectroscopy from a total of 15 patients per disease state including aged, atherosclerotic and arteriosclerotic lesions. Furthermore *in vivo* analysis has demonstrated the ability to detect distinct changes in resident vascular cells. In order to validate the data presented in this study these findings would need to be tested in patients identified with arteriosclerotic or atherosclerotic lesions *in vivo*. Adaptation of current Raman probes used in clinical environments could be trialled for use in the detection of vascular lesions however there are some limitations regarding the depth at which light can travel through tissue sections which may prove a limiting factor in pursuit of non-invasive detection of early vascular lesions. An alternative approach to facilitate clinical detection of early changes in cellular phenotypes within the vasculature indicative of sub-clinical atherosclerosis would be the use of a Raman probe in conjunction with current catheter technologies which can be threaded up through the artery to the site of vascular damage for real-time measurement of resident cell phenotype changes at atheroprone areas of the vasculature indicative of disease.

While evidence from this study identifies the role of EC-derived HG-EV mediated transport of Hh to resident S100β $^{+}$ NE stem cells resulting in myogenic differentiation and proliferation *in vitro*, further investigation is needed to identify the mechanism by which this occurs to establish a possible means of inhibition. Although we show upregulation of Hh target genes and subsequent myogenic differentiation is Hh dependent on cyclopamine and 5E1 inhibition *in vitro*, further research to determine the full proteomic profile of HG-EVs would be beneficial to identify the presence of co-factors necessary for Hh packaging and secretion. Due to the multifactorial nature of CVDs the best suited strategy to detect discrete changes in the composition of the vasculature is the identification of a panel of biomarkers. Mass spectroscopy is a fundamental technique for the identification and characterisation of protein content of EVs. Several standard proteomic approaches have been used in the proteomic analysis of EVs including, two-dimensional gel electrophoresis, LC-MS/MS and MALDA-TOF/TOF MS. Recent studies have applied these techniques to profile proteomic content secreted from resident vascular cells including cardiomyocytes (Malik *et al.*, 2013), cardiac fibroblasts (Cosme *et al.*, 2017), endothelial cells (Sheldon *et al.*, 2010; de Jong *et al.*, 2012) and smooth

muscle cells (Kapustin *et al.*, 2015; Qiu *et al.*, 2018). In many cases these studies report upregulation of >200 proteins in diseased versus healthy cells. Therefore, further characterisation of the full proteomic profile of EC-derived HG-EVs in comparison to NG and MT EVs would provide greater evidence to the extent of proteomic changes in EV content in response to EC injury.

The use of serological biomarkers have gained momentum in the search for subclinical detection of disease. The discovery of serological biomarkers proves favourable as they require minimum invasion, are cost effective and therefore can be incorporated into routine screening for subclinical detection of disease. Crucially, incorporating EV measurements within diagnostic assessments in clinical settings will depend upon the development of fitting devices to enable rapid and/or high-throughput analysis, potentially demanding adapted processing procedures. Although the detection of Hh in serum samples from CVD patients was not addressed in this study, previous studies have reported successful detection of SHh in serum samples from cancer patients (Noman *et al.*, 2017). In addition to this, elevated levels of SHh proteins have also been associated with fibrotic and vascular manifestation in systemic sclerosis, however the possibility of this being EV-bound was not investigated. In order to translate the findings presented in this study to a clinical setting isolation of EVs from serum samples of healthy patients and patients at risk of or who have had a cardiovascular event would be necessary to determine the presence the levels of circulating SHh^+ EVs.

Detection of EV-SHh requires EV isolation prior to interrogation. A major challenge facing EV profiling in clinical settings is the identification of a standard technique to isolate intact EVs from bodily fluids with high reproducibility and purity. Although this study demonstrates the use of EV enriched preparations on human stem cells the choice of isolation method used has been reported to yield a high recovery of extracellular material with low specificity therefore a further purification step would prove beneficial in determining if the functional effect of high glucose derived EVs on stem cells is in fact EV-dependent. One such purification technique that could be applied in future studies is the use of differential ultracentrifugation using intermediate time/speed with or without wash, tangential flow filtration, and membrane affinity columns. However, conventional EV isolation processes can take over 12 hours to perform and are often reported to produce low recovery rates and result in an impure extract (Patel *et al.*, 2019). Several

factors such as the rotor type, *g*-force and the centrifugation times also affect the purity and yield of EVs, thus compromising centrifugation as a recognised standard for clinical exosome isolation (Cvjetkovic, Lötvall and Lässer, 2014). Future studies using centrifugal microfluidic lab-on-a-disc (LoaD) platforms would be best suited for plasma extraction as previous studies have reported on-disc filtration to extract EVs from separated plasma (Sunkara *et al.*, 2019) as well as isolation of EV subgroups of distinct size (Meng *et al.*, 2021).

Although the findings in this study highlight the role of endothelial-derived EVs in stem cell to smooth muscle cell differentiation, a hallmark of subclinical atherosclerosis the development of a Point of Care (POC) would be best suited for clinical application of EV detection. Hospitals and clinics rely heavily on central laboratories to analyse patient samples and deliver accurate and timely results. This common operational model places the vast majority of blood/sample analysis responsibility on the central laboratory, irrespective of the relative exigency of the test. However, the layout of this model, in which sample transport and handling contribute to delays, is unfavourable for streamlining the triage process and ensuring critical needs are fulfilled. By contrast, point-of-care-testing (POCT) involves conducting a diagnostic test in a patient's proximity and incorporates the use of a compact device to facilitate rapid biomarker measurement. Unlike central laboratories in which a variety of sophisticated instruments and measurement equipment are routinely utilised, a point-of-care (POC) platform is generally robust, with the capacity to perform measurements in a range of test environments and without the need for highly specialised training. The development of compact and user-friendly platforms that can accommodate POC EV analysis. Importantly, some processes are naturally more suited to POCT and are somewhat unrestricted by technological limitations. These are key factors to contemplate when assessing the feasibility of exosome measurement for POCT as current isolation processes and measurement techniques may be inherently unsuited for POCT. In order to translate the findings from this study to a clinical setting the development of centrifugal microfluidic lab-on-a-disc (LoaD) platforms would be necessary for plasma extraction from whole blood incorporating on-disc filtration to extract EVs from separated plasma prior to measurement of SHh levels as an early diagnostic indicator of the potential of stem cell to VSMC differentiation indicative of sub-clinical atherosclerosis.

Although this study demonstrates two potential diagnostic tools to identify surrogate markers of subclinical atherosclerosis by targeting EVs from dysfunctional endothelial cells in addition to interrogation of lesional cells for discrete photonic and vibrational spectroscopic fingerprints, future studies investigating the combination of the photonic/vibrational spectroscopic signatures of healthy versus diseased associated EVs could be explored. Current routine techniques used to characterise EVs such as NTA and DLS have shown successful discrimination of EV concentrations based on the exploitation of light therefore the use of Raman as a discriminator of healthy versus diseased EVs is promising (Tucher *et al.*, 2018; Tian *et al.*, 2021). Recent studies have investigated the detection of distinct changes in EV cargo in response to pathologic stimuli using surface-enhance Raman spectroscopy which allows an increase in the sensitivity of measurements by a plasmonic interaction between analytes and nanostructured surfaces (Chalapathi *et al.*, 2020; Shin, Seo and Choi, 2020; Zhang *et al.*, 2020). The ability to assess the accumulation of stem cell-derived progeny using label free platforms *in situ* or the detection of EVs secreted from these progeny during disease progression may further facilitate interrogation of these phenotypes by their discrete spectroscopic signatures using liquid biopsies and microfluidic platforms.

6.4 Conclusion

The overall aim of this study was to develop novel strategies that interrogate and discriminate disease relevant cell populations and detect the key signalling molecules within endothelial-derived EVs that dictate their fate. Specifically, single-cell photonic analysis of broadband light, Raman and FTIR spectral datasets from normal vSMCs and lesional cells from human vessels *ex vivo* in addition to HiPSC progenitors and their myogenic progeny *in vitro* were analysed using supervised machine learning as novel diagnostic platforms for early detection of vascular phenotypes within lesions. Moreover, the characteristics and effects of endothelial-derived EVs on these resident vascular stem cell fate following hyperglycaemic-induced endothelial dysfunction were assessed using rat and HiPSC models *in vitro* as a potential surrogate marker for early lesion formation.

The cumulative data in this study provides novel insights into the role of EC-EV mediated transport of key signalling molecules responsible for differentiation and proliferation of resident NE S100β^+ stem cell to vSMC migrating to the intimal layer resulting in

neointimal formation. Highlighting the importance of the exploitation of EC-derived EV cargo as a diagnostic marker for sub-clinical detection of atherosclerosis. Furthermore, significant data has been presented to demonstrate the feasibility of photonic techniques FTIR, Raman and autofluorescence emissions signatures of single-cells to discriminate undifferentiated stem cells from their myogenic progeny in vitro, healthy versus lesional cells *ex vivo* and finally interrogation of lesional cells to identify discrete changes in cell phenotypes indicative of early signs of atherosclerosis.

Bibliography

Abdel-Haq, H. (2019) 'Blood exosomes as a tool for monitoring treatment efficacy and progression of neurodegenerative diseases', *Neural Regeneration Research*. doi: 10.4103/1673-5374.243709.

Abels, E. R. and Breakefield, X. O. (2016) 'Introduction to Extracellular Vesicles: Biogenesis, RNA Cargo Selection, Content, Release, and Uptake', *Cellular and Molecular Neurobiology*. doi: 10.1007/s10571-016-0366-z.

Abid Hussein, M. N. *et al.* (2005) 'Cell-derived microparticles contain caspase 3 in vitro and in vivo', *Journal of Thrombosis and Haemostasis*. doi: 10.1111/j.1538-7836.2005.01240.x.

Adela, R. *et al.* (2015) 'Hyperglycaemia Enhances Nitric Oxide Production in Diabetes: A Study from South Indian Patients', *PLOS ONE*. Public Library of Science, 10(4), p. e0125270. doi: 10.1371/JOURNAL.PONE.0125270.

AgouTii, A. *et al.* (2007) 'Sonic hedgehog carried by microparticles corrects endothelial injury through nitric oxide release', *The FASEB Journal*. Wiley, 21(11), pp. 2735–2741. doi: 10.1096/fj.07-8079com.

Aijaz, S., Balda, M. S. and Matter, K. (2006) 'Tight Junctions: Molecular Architecture and Function', *International Review of Cytology*, 248, pp. 261–298.

Aikawa, E. (2016) 'Extracellular vesicles in cardiovascular disease: focus on vascular calcification', *The Journal of Physiology*, 594(11), pp. 2877–2880. doi: 10.1113/JP272112.

Ali, H. *et al.* (2013) 'Localization and characterization of a novel secreted protein, SCUBE2, in the development and progression of atherosclerosis', *Kobe Journal of Medical Sciences*, 59(4).

Andersen, P. *et al.* (2012) 'Non-canonical Notch signaling: Emerging role and mechanism', *Trends in Cell Biology*. Trends Cell Biol, pp. 257–265. doi: 10.1016/j.tcb.2012.02.003.

Anderson, T. J. *et al.* (1995) 'Systemic nature of endothelial dysfunction in atherosclerosis', *The American Journal of Cardiology*. Am J Cardiol, 75(6 SUPPL. 1), pp. 71B-74B. doi: 10.1016/0002-9149(95)80017-M.

Anderson, T. J. (1999) 'Assessment and treatment of endothelial dysfunction in humans', *Journal of the American College of Cardiology*. Elsevier Inc., 34(3), pp. 631–638. doi: 10.1016/S0735-1097(99)00259-4.

Andrews, A. M. and Rizzo, V. (2016) 'Microparticle-induced activation of the vascular

endothelium requires caveolin-1/caveolae', *PLoS ONE*. Public Library of Science, 11(2), p. e0149272. doi: 10.1371/journal.pone.0149272.

Di Angelantonio, E. *et al.* (2009) 'B-type natriuretic peptides and cardiovascular risk: Systematic review and meta-analysis of 40 prospective studies', *Circulation*. Circulation, 120(22), pp. 2177–2187. doi: 10.1161/CIRCULATIONAHA.109.884866.

Antonopoulos, A. S. *et al.* (2015) 'Adiponectin as a Link Between Type 2 Diabetes and Vascular NADPH Oxidase Activity in the Human Arterial Wall: The Regulatory Role of Perivascular Adipose Tissue', *Diabetes*. American Diabetes Association, 64(6), pp. 2207–2219. doi: 10.2337/DB14-1011.

Apple, F. S. and Collinson, P. O. (2012) 'Analytical characteristics of high-sensitivity cardiac troponin assays', *Clinical Chemistry*. American Association for Clinical Chemistry Inc., pp. 54–61. doi: 10.1373/clinchem.2011.165795.

Arandjelovic, S. and Ravichandran, K. S. (2015) 'Phagocytosis of apoptotic cells in homeostasis', *Nature Immunology*. doi: 10.1038/ni.3253.

Aravani, D. *et al.* (2019) 'HHIPL1, a Gene at the 14q32 Coronary Artery Disease Locus, Positively Regulates Hedgehog Signaling and Promotes Atherosclerosis', *Circulation*. Lippincott Williams and Wilkins, 140(6), pp. 500–513. doi: 10.1161/CIRCULATIONAHA.119.041059.

Askevold, E. T. *et al.* (2014) 'The cardiokine secreted Frizzled-related protein 3, a modulator of Wnt signalling, in clinical and experimental heart failure', *Journal of Internal Medicine*. Blackwell Publishing Ltd, 275(6), pp. 621–630. doi: 10.1111/joim.12175.

Atai, N. A. *et al.* (2013) 'Heparin blocks transfer of extracellular vesicles between donor and recipient cells', *Journal of Neuro-Oncology*. doi: 10.1007/s11060-013-1235-y.

Babst, M. (2011) 'MVB vesicle formation: ESCRT-dependent, ESCRT-independent and everything in between', *Current Opinion in Cell Biology*. doi: 10.1016/j.ceb.2011.04.008.

Bacakova, L. *et al.* (2018) 'The Role of Vascular Smooth Muscle Cells in the Physiology and Pathophysiology of Blood Vessels'. IntechOpen. doi: 10.5772/INTECHOPEN.77115.

Bache, K. G. *et al.* (2003) 'Hrs regulates multivesicular body formation via ESCRT recruitment to endosomes', *Journal of Cell Biology*. doi: 10.1083/jcb.200302131.

Badimon, L. *et al.* (2016) 'Role of platelet-derived microvesicles as crosstalk mediators in atherothrombosis and future pharmacology targets: A link between inflammation, atherosclerosis, and thrombosis', *Frontiers in Pharmacology*. doi:

10.3389/fphar.2016.00293.

Baietti, M. F. *et al.* (2012) 'Syndecan-syntenin-ALIX regulates the biogenesis of exosomes', *Nature Cell Biology*. doi: 10.1038/ncb2502.

Bang, C. and Thum, T. (2012) 'Exosomes: New players in cell-cell communication', *International Journal of Biochemistry and Cell Biology*, pp. 2060–2064. doi: 10.1016/j.biocel.2012.08.007.

Bank, A. J. *et al.* (1996) 'Contribution of collagen, elastin, and smooth muscle to in vivo human brachial artery wall stress and elastic modulus', *Circulation*. Lippincott Williams and Wilkins, 94(12), pp. 3263–3270. doi: 10.1161/01.CIR.94.12.3263.

Bank, I. E. M. *et al.* (2015) 'The diagnostic and prognostic potential of plasma extracellular vesicles for cardiovascular disease.', *Expert review of molecular diagnostics*, 15(12), pp. 1577–1588.

Bargehr, J. *et al.* (2016) 'Embryological Origin of Human Smooth Muscle Cells Influences Their Ability to Support Endothelial Network Formation', *STEM CELLS Translational Medicine*. Wiley, 5(7), pp. 946–959. doi: 10.5966/sctm.2015-0282.

Barré-Sinoussi, F. and Montagutelli, X. (2015) 'Animal models are essential to biological research: Issues and perspectives', *Future Science OA*. Future Medicine Ltd. doi: 10.4155/fso.15.63.

Barrès, C. *et al.* (2010) 'Galectin-5 is bound onto the surface of rat reticulocyte exosomes and modulates vesicle uptake by macrophages', *Blood*. doi: 10.1182/blood-2009-07-231449.

Barrett, H. E. *et al.* (2015) 'Characterising human atherosclerotic carotid plaque tissue composition and morphology using combined spectroscopic and imaging modalities', *Biomedical engineering online*. Biomed Eng Online, 14(Suppl 1), p. S5. doi: 10.1186/1475-925X-14-S1-S5.

Bartel, S. *et al.* (2020) 'Extracellular Vesicles as Mediators of Cellular Cross Talk in the Lung Microenvironment', *Frontiers in Medicine*. Frontiers, 7, p. 326. doi: 10.3389/fmed.2020.00326.

Bassan, P. *et al.* (2009) 'Reflection contributions to the dispersion artefact in FTIR spectra of single biological cells', *Analyst*. Analyst, 134(6), pp. 1171–1175. doi: 10.1039/b821349f.

Becker, A. *et al.* (2016) 'Extracellular Vesicles in Cancer: Cell-to-Cell Mediators of Metastasis', *Cancer Cell*. Cell Press, pp. 836–848. doi: 10.1016/j.ccell.2016.10.009.

Beckers, L. *et al.* (2007) 'Disruption of hedgehog signalling in ApoE-/- mice reduces plasma lipid levels, but increases atherosclerosis due to enhanced lipid uptake by macrophages', *Journal of Pathology*. J Pathol, 212(4), pp. 420–428. doi:

10.1002/path.2193.

Beckett, K. *et al.* (2013) 'Drosophila S2 cells secrete wingless on exosome-like vesicles but the wingless gradient forms independently of exosomes', *Traffic*. John Wiley & Sons, Ltd, 14(1), pp. 82–96. doi: 10.1111/tra.12016.

Beckler, M. D. *et al.* (2013) 'Proteomic analysis of exosomes from mutant KRAS colon cancer cells identifies intercellular transfer of mutant KRAS', *Molecular and Cellular Proteomics*. Mol Cell Proteomics, 12(2), pp. 343–355. doi: 10.1074/mcp.M112.022806.

Bellin, G. *et al.* (2019) 'Exosome in Cardiovascular Diseases: A Complex World Full of Hope.', *Cells*. MDPI AG, 8(2), p. 166. doi: 10.3390/cells8020166.

Benedetto, A. *et al.* (2006) 'A Novel Exosome-Mediated Apical Secretion Pathway Involving the V0-sector of the V-ATPase in C. elegans Epidermal Cells', *European Worm Meeting*.

Benedikter, B. J. *et al.* (2019) 'Proteomic analysis reveals procoagulant properties of cigarette smoke-induced extracellular vesicles', *Journal of Extracellular Vesicles*. J Extracell Vesicles, 8(1). doi: 10.1080/20013078.2019.1585163.

Bennett, M. R., Sinha, S. and Owens, G. K. (2016) 'Vascular Smooth Muscle Cells in Atherosclerosis', *Circulation research*, 118(4), pp. 692–702.

Berezin, A. E. (2017) 'Endothelial Repair and Endothelial Cell-Derived Secretome', *Insights in Biology and Medicine*. Heighten Science Publications Corporation, 1(1), pp. 001–008. doi: 10.29328/journal.hjbm.1001001.

Bernal-Mizrachi, L. *et al.* (2003) 'High levels of circulating endothelial microparticles in patients with acute coronary syndromes', *American Heart Journal*. doi: 10.1016/S0002-8703(03)00103-0.

Best, M. G. *et al.* (2015) 'RNA-Seq of Tumor-Educated Platelets Enables Blood-Based Pan-Cancer, Multiclass, and Molecular Pathway Cancer Diagnostics', *Cancer Cell*. Cell Press, 28(5), pp. 666–676.

Bischoff, M. *et al.* (2013) 'Cytonemes are required for the establishment of a normal Hedgehog morphogen gradient in Drosophila epithelia', *Nature Cell Biology*. Nat Cell Biol, 15(11), pp. 1269–1281. doi: 10.1038/ncb2856.

Bishop, N. and Woodman, P. (2001) 'TSG101/Mammalian VPS23 and Mammalian VPS28 Interact Directly and Are Recruited to VPS4-induced Endosomes', *Journal of Biological Chemistry*. American Society for Biochemistry and Molecular Biology, 276(15), pp. 11735–11742. doi: 10.1074/JBC.M009863200.

Bkaily, G. *et al.* (1997) 'The use of confocal microscopy in the investigation of cell

structure and function in the heart, vascular endothelium and smooth muscle cells', *Molecular and Cellular Biochemistry*. Springer, 172(1–2), pp. 171–194. doi: 10.1023/A:1006840228104.

Blanc, L. and Vidal, M. (2018) 'New insights into the function of Rab GTPases in the context of exosomal secretion', *Small GTPases*. doi: 10.1080/21541248.2016.1264352.

Bobik, A. (2006) 'Transforming growth factor-βs and vascular disorders', *Arteriosclerosis, Thrombosis, and Vascular Biology*. Lippincott Williams & Wilkins, pp. 1712–1720. doi: 10.1161/01.ATV.0000225287.20034.2c.

Bobrie, A. *et al.* (2011) 'Exosome Secretion: Molecular Mechanisms and Roles in Immune Responses', *Traffic*. doi: 10.1111/j.1600-0854.2011.01225.x.

Bobrie, A. *et al.* (2012) 'Diverse subpopulations of vesicles secreted by different intracellular mechanisms are present in exosome preparations obtained by differential ultracentrifugation', *Journal of Extracellular Vesicles*. doi: 10.3402/jev.v1i0.18397.

Bobryshev, Y. V., Killingsworth, M. C. and Orekhov, A. N. (2013) 'Increased Shedding of Microvesicles from Intimal Smooth Muscle Cells in Athero-Prone Areas of the Human Aorta: Implications for Understanding of the Predisease Stage', *Pathobiology*. Karger Publishers, 80(1), pp. 24–31. doi: 10.1159/000339430.

Bonifacino, J. S. and Glick, B. S. (2004) 'The mechanisms of vesicle budding and fusion.', *Cell*. doi: 10.1016/S0092-8674(03)01079-1.

Bonnier, F. *et al.* (2008) 'Detection of pathological aortic tissues by infrared multispectral imaging and chemometrics', *Analyst*. Analyst, 133(6), pp. 784–790. doi: 10.1039/b717164a.

Börger, V. *et al.* (2020) 'International Society for Extracellular Vesicles and International Society for Cell and Gene Therapy statement on extracellular vesicles from mesenchymal stromal cells and other cells: considerations for potential therapeutic agents to suppress coronavirus disease-19', *Cytotherapy*. Elsevier, 22(9), pp. 482–485. doi: 10.1016/J.JCYT.2020.05.002.

Le Borgne, R. (2006) 'Regulation of Notch signalling by endocytosis and endosomal sorting', *Current Opinion in Cell Biology*. doi: 10.1016/j.ceb.2006.02.011.

Le Borgne, R. and Schweisguth, F. (2003) 'Notch signaling: Endocytosis makes Delta signal better', *Current Biology*. doi: 10.1016/S0960-9822(03)00199-4.

Bornfeldt, K. E. (2016) 'Does Elevated Glucose Promote Atherosclerosis? Pros and Cons', *Circulation Research*. Lippincott Williams and Wilkins, pp. 190–193. doi: 10.1161/CIRCRESAHA.116.308873.

Boström, K. *et al.* (2000) 'HOXB7 overexpression promotes differentiation of C3H10T1/2 cells to smooth muscle cells', *Journal of Cellular Biochemistry*, 78(2), pp.

210–221. doi: 10.1002/(SICI)1097-4644(20000801)78:2<210::AID-JCB4>3.0.CO;2-Z.

Boukouris, S. and Mathivanan, S. (2015) 'Exosomes in bodily fluids are a highly stable resource of disease biomarkers', *Proteomics - Clinical Applications*. Proteomics Clin Appl, pp. 358–367. doi: 10.1002/prca.201400114.

Boulanger, C. M. *et al.* (2017) 'Extracellular vesicles in coronary artery disease', *Nature Reviews Cardiology*. Nature Publishing Group, 14(5), pp. 259–272. doi: 10.1038/nrcardio.2017.7.

Brandes, R. P., Takac, I. and Schröder, K. (2011) 'No Superoxide—No Stress?', *Arteriosclerosis, Thrombosis, and Vascular Biology*. Lippincott Williams & WilkinsHagerstown, MD, 31(6), pp. 1255–1257. doi: 10.1161/ATVBAHA.111.226894.

Bray, S. J. (2006) 'Notch signalling: a simple pathway becomes complex', *Nature Reviews Molecular Cell Biology*, 7(9), pp. 678–689.

Brennan, K. *et al.* (2020) 'A comparison of methods for the isolation and separation of extracellular vesicles from protein and lipid particles in human serum', *Scientific Reports*. Nature Publishing Group, 10(1), pp. 1–13. doi: 10.1038/s41598-020-57497-7.

Brenner, A. W., Su, G. H. and Momen-Heravi, F. (2019) 'Isolation of extracellular vesicles for cancer diagnosis and functional studies', in *Methods in Molecular Biology*. Methods Mol Biol, pp. 229–237. doi: 10.1007/978-1-4939-8879-2_21.

Briscoe, J. and Thérond, P. P. (2013) 'The mechanisms of Hedgehog signalling and its roles in development and disease', *Nature Reviews Molecular Cell Biology*. Nature Publishing Group, pp. 418–431. doi: 10.1038/nrm3598.

Bueno-Betí, C. *et al.* (2019) 'Microparticles harbouring Sonic hedgehog morphogen improve the vasculogenesis capacity of endothelial progenitor cells derived from myocardial infarction patients', *Cardiovascular Research*. Oxford University Press, 115(2), pp. 409–418. doi: 10.1093/cvr/cvy189.

Burger, D. *et al.* (2017) 'High glucose increases the formation and pro-oxidative activity of endothelial microparticles', *Diabetologia*. Springer Verlag, 60(9), pp. 1791–1800. doi: 10.1007/s00125-017-4331-2.

Burger, R. *et al.* (2012) 'Array-based capture, distribution, counting and multiplexed assaying of beads on a centrifugal microfluidic platform', *Lab on a Chip*. The Royal Society of Chemistry, 12(7), pp. 1289–1295. doi: 10.1039/c2lc21170j.

Burghoff, S. and Schrader, J. (2011) 'Secretome of human endothelial cells under shear stress', *Journal of Proteome Research*. American Chemical Society, 10(3), pp. 1160–1169. doi: 10.1021/pr100937a.

Buschman, H. P. *et al.* (2001) 'Raman microspectroscopy of human coronary

atherosclerosis: Biochemical assessment of cellular and extracellular morphologic structures in situ', *Cardiovascular Pathology*. Cardiovasc Pathol, 10(2), pp. 69–82. doi: 10.1016/S1054-8807(01)00064-3.

Buschow, S. I. *et al.* (2009) 'MHC II In dendritic cells is targeted to lysosomes or t cell-induced exosomes via distinct multivesicular body pathways', *Traffic*. doi: 10.1111/j.1600-0854.2009.00963.x.

Butler, H. J. *et al.* (2016) 'Using Raman spectroscopy to characterize biological materials', *Nature Protocols*. Nature Publishing Group, 11(4), pp. 664–687. doi: 10.1038/nprot.2016.036.

Buzas, E. I. *et al.* (2014) 'Emerging role of extracellular vesicles in inflammatory diseases', *Nature Reviews Rheumatology*. Nat Rev Rheumatol, pp. 356–364. doi: 10.1038/nrrheum.2014.19.

Byrne, H. J. *et al.* (2016) 'Spectral pre and post processing for infrared and Raman spectroscopy of biological tissues and cells', *Chemical Society Reviews*. The Royal Society of Chemistry, pp. 1865–1878. doi: 10.1039/c5cs00440c.

C, Beyer *et al.* (2018) 'Elevated serum levels of sonic hedgehog are associated with fibrotic and vascular manifestations in systemic sclerosis', *Annals of the rheumatic diseases*. Ann Rheum Dis, 77(4), pp. 626–628. doi: 10.1136/ANNRHEUMDIS-2016-210834.

Caine, S. *et al.* (2012) 'The application of Fourier transform infrared microspectroscopy for the study of diseased central nervous system tissue', *NeuroImage*. Neuroimage, pp. 3624–3640. doi: 10.1016/j.neuroimage.2011.11.033.

Callejo, A. *et al.* (2011) 'Dispatched mediates Hedgehog basolateral release to form the long-range morphogenetic gradient in the Drosophila wing disk epithelium', *Proceedings of the National Academy of Sciences of the United States of America*. National Academy of Sciences, 108(31), pp. 12591–12598. doi: 10.1073/pnas.1106881108.

Campbell, J. H. and Campbell, G. R. (2012) 'Smooth muscle phenotypic modulation-a personal experience', *Arteriosclerosis, Thrombosis, and Vascular Biology*. Lippincott Williams & Wilkins Hagerstown, MD, 32(8), pp. 1784–1789. doi: 10.1161/ATVBAHA.111.243212.

Cao, T. *et al.* (2017) 'S100B promotes injury-induced vascular remodeling through modulating smooth muscle phenotype', *Biochimica et Biophysica Acta - Molecular Basis of Disease*. Biochim Biophys Acta Mol Basis Dis, 1863(11), pp. 2772–2782. doi: 10.1016/j.bbadis.2017.07.002.

Caplice, N. M. *et al.* (2003) 'Smooth muscle cells in human coronary atherosclerosis can originate from cells administered at marrow transplantation', *Proceedings of the National Academy of Sciences of the United States of America*. National Academy of Sciences, 100(8), pp. 4754–4759. doi: 10.1073/pnas.0730743100.

Carlomagno, C. *et al.* (2021) 'COVID-19 salivary Raman fingerprint: innovative approach for the detection of current and past SARS-CoV-2 infections', *Scientific Reports*. Nature Publishing Group, 11(1), pp. 1–13. doi: 10.1038/s41598-021-84565-3.

Carmen Martínez, M. *et al.* (2006) 'Transfer of differentiation signal by membrane microvesicles harboring hedgehog morphogens', *Blood*. Blood, 108(9), pp. 3012–3020. doi: 10.1182/blood-2006-04-019109.

Cazzoli, R. *et al.* (2013) 'microRNAs Derived from Circulating Exosomes as Noninvasive Biomarkers for Screening and Diagnosing Lung Cancer', *Journal of Thoracic Oncology*. Elsevier, 8(9), pp. 1156–1162. doi: 10.1097/JTO.0B013E318299AC32.

Celeng, C. *et al.* (2016) 'Non-invasive and invasive imaging of vulnerable coronary plaque', *Trends in Cardiovascular Medicine*. Elsevier, 26(6), pp. 538–547. doi: 10.1016/J.TCM.2016.03.005.

Chalapathi, D. *et al.* (2020) 'Surface-Enhanced Raman Spectroscopy as a Tool for Distinguishing Extracellular Vesicles under Autophagic Conditions: A Marker for Disease Diagnostics', *Journal of Physical Chemistry B*. J Phys Chem B, 124(48), pp. 10952–10960. doi: 10.1021/acs.jpcb.0c06910.

Chamley-Campbell, J., Campbell, G. R. and Ross, R. (1979) 'The smooth muscle cell in culture', *Physiological Reviews*. Physiol Rev, pp. 1–61. doi: 10.1152/physrev.1979.59.1.1.

Chappell, J. *et al.* (2016) 'Extensive Proliferation of a Subset of Differentiated, yet Plastic, Medial Vascular Smooth Muscle Cells Contributes to Neointimal Formation in Mouse Injury and Atherosclerosis Models', *Circulation Research*. Lippincott Williams and Wilkins, 119(12), pp. 1313–1323. doi: 10.1161/CIRCRESAHA.116.309799.

Chen, F. *et al.* (2013) 'Resveratrol protects vascular endothelial cells from high glucose-induced apoptosis through inhibition of nadph oxidase activation-driven oxidative stress', *CNS Neuroscience and Therapeutics*. CNS Neurosci Ther, 19(9), pp. 675–681. doi: 10.1111/cns.12131.

Chen, P. Y. *et al.* (2019) 'Endothelial TGF-β signalling drives vascular inflammation and atherosclerosis', *Nature Metabolism*. Nature Research, 1(9), pp. 912–926. doi: 10.1038/s42255-019-0102-3.

Chen, Q. *et al.* (2016) 'Different populations of Wnt-containing vesicles are individually released from polarized epithelial cells', *Scientific Reports*. doi: 10.1038/srep35562.

Cheng, J. X. and Xie, X. S. (2015) 'Vibrational spectroscopic imaging of living systems: An emerging platform for biology and medicine', *Science*. American Association for the Advancement of Science, 350(6264). doi: 10.1126/science.aaa8870.

Cherepanova, O. A. *et al.* (2016) 'Activation of the pluripotency factor OCT4 in smooth muscle cells is atheroprotective', *Nature Medicine*. doi: 10.1038/nm.4109.

Cheung, C. *et al.* (2012) 'Generation of human vascular smooth muscle subtypes provides insight into embryological origing-dependent disease susceptibility', *Nature Biotechnology*. doi: 10.1038/nbt.2107.

Cheung, C. *et al.* (2014) 'Directed differentiation of embryonic origin-specific vascular smooth muscle subtypes from human pluripotent stem cells', *Nature Protocols*. doi: 10.1038/nprot.2014.059.

Cheung, C. and Sinha, S. (2011) 'Human embryonic stem cell-derived vascular smooth muscle cells in therapeutic neovascularisation', *Journal of Molecular and Cellular Cardiology*. J Mol Cell Cardiol, pp. 651–664. doi: 10.1016/j.yjmcc.2011.07.014.

Chironi, G. *et al.* (2006) 'Circulating leukocyte-derived microparticles predict subclinical atherosclerosis burden in asymptomatic subjects', *Arteriosclerosis, Thrombosis, and Vascular Biology*. doi: 10.1161/01.ATV.0000249639.36915.04.

Cho, Hyun Ju *et al.* (2013) 'Vascular Calcifying Progenitor Cells Possess Bidirectional Differentiation Potentials', *PLoS Biology*. doi: 10.1371/journal.pbio.1001534.

Choi, K. *et al.* (1998) 'A common precursor for hematopoietic and endothelial cells.', *Development (Cambridge, England)*, 125(4), pp. 725–32. Available at: http://www.ncbi.nlm.nih.gov/pubmed/9435292.

Chorro, F. J., Such-Belenguer, L. and López-Merino, V. (2009) 'Animal Models of Cardiovascular Disease', *Revista Española de Cardiología (English Edition)*. Elsevier, 62(1), pp. 69–84. doi: 10.1016/s1885-5857(09)71516-6.

Choudhry, Z. *et al.* (2014) 'Sonic hedgehog signalling pathway: A complex network', *Annals of Neurosciences*. doi: 10.5214/ans.0972.7531.210109.

Christ, L. *et al.* (2017) 'Cellular Functions and Molecular Mechanisms of the ESCRT Membrane-Scission Machinery', *Trends in Biochemical Sciences*. doi: 10.1016/j.tibs.2016.08.016.

Christianson, H. C. *et al.* (2013) 'Cancer cell exosomes depend on cell-surface heparan sulfate proteoglycans for their internalization and functional activity', *Proceedings of the National Academy of Sciences*. doi: 10.1073/pnas.1304266110.

Chuang, P. T. and McMahon, A. P. (1999) 'Vertebrate hedgehog signalling modulated by induction of a hedgehog- binding protein', *Nature*. Nature, 397(6720), pp. 617–621.

doi: 10.1038/17611.

Churchman, A. T. and Siow, R. C. M. (2009) ‘Isolation, Culture and Characterisation of Vascular Smooth Muscle Cells’, in *Angiogenesis Protocols*. Totowa, NJ: Humana Press, pp. 127–138.

Colley, C. S. *et al.* (2004) ‘Spectroscopic imaging of arteries and atherosclerotic plaques’, *Biopolymers*. John Wiley & Sons, Ltd, 74(4), pp. 328–335. doi: 10.1002/bip.20069.

Colombo, M. *et al.* (2013) ‘Analysis of ESCRT functions in exosome biogenesis, composition and secretion highlights the heterogeneity of extracellular vesicles.’, *Journal of cell science*. doi: 10.1242/jcs.128868.

Colombo, M., Raposo, G. and Théry, C. (2014) ‘Biogenesis, Secretion, and Intercellular Interactions of Exosomes and Other Extracellular Vesicles’, *Annual Review of Cell and Developmental Biology*. doi: 10.1146/annurev-cellbio-101512-122326.

Del Conde, I. *et al.* (2005) ‘Tissue-factor-bearing microvesicles arise from lipid rafts and fuse with activated platelets to initiate coagulation’, *Blood*. doi: 10.1182/blood-2004-03-1095.

Conn, P. M. (2013) *Animal Models for the Study of Human Disease*, *Animal Models for the Study of Human Disease*. doi: 10.1016/C2011-0-05225-0.

Cooley, B. C. *et al.* (2014) ‘TGF-β signaling mediates endothelial-to-mesenchymal transition (EndMT) during vein graft remodeling’, *Science Translational Medicine*, 6(227), p. 227ra34. doi: 10.1126/scitranslmed.3006927.

Cosme, J. *et al.* (2017) ‘Hypoxia-Induced Changes in the Fibroblast Secretome, Exosome, and Whole-Cell Proteome Using Cultured, Cardiac-Derived Cells Isolated from Neonatal Mice’, *Journal of Proteome Research*. J Proteome Res, 16(8), pp. 2836–2847. doi: 10.1021/acs.jproteome.7b00144.

Cousins, F. L. *et al.* (2020) ‘The effects of hedgehog ligand neutralising antibody 5E1 in a mouse model of endometriosis’, *BMC Research Notes*. BioMed Central, 13(1), pp. 1–6. doi: 10.1186/s13104-020-05299-5.

Croce, A. C. *et al.* (2018) ‘Autofluorescence-based optical biopsy: An effective diagnostic tool in hepatology’, *Liver International*. Blackwell Publishing Ltd, pp. 1160–1174. doi: 10.1111/liv.13753.

Crow, P. *et al.* (2005) ‘The use of Raman spectroscopy to differentiate between different prostatic adenocarcinoma cell lines’, *British Journal of Cancer*. Nature Publishing Group, 92(12), pp. 2166–2170. doi: 10.1038/sj.bjc.6602638.

Curaj, A. *et al.* (2018) ‘Molecular Ultrasound Imaging of Junctional Adhesion Molecule A Depicts Acute Alterations in Blood Flow and Early Endothelial Dysregulation’,

Arteriosclerosis, Thrombosis, and Vascular Biology. Lippincott Williams and Wilkins, 38(1), pp. 40–48. doi: 10.1161/ATVBAHA.117.309503.

Cvjetkovic, A., Lötvall, J. and Lässer, C. (2014) 'The influence of rotor type and centrifugation time on the yield and purity of extracellular vesicles', *Journal of Extracellular Vesicles*. Co-Action Publishing, 3(1). doi: 10.3402/jev.v3.23111.

Cypris, O. *et al.* (2019) 'Tracking of epigenetic changes during hematopoietic differentiation of induced pluripotent stem cells', *Clinical Epigenetics*. BioMed Central, 11(1). doi: 10.1186/S13148-019-0617-1.

D'Angelo, G. *et al.* (2015) 'Endocytosis of hedgehog through dispatched regulates long-range signaling', *Developmental Cell*. Cell Press, 32(3), pp. 290–303. doi: 10.1016/j.devcel.2014.12.004.

D'Souza, B., Meloty-Kapella, L. and Weinmaster, G. (2010) 'Canonical and Non-Canonical Notch Ligands', *Current Topics in Developmental Biology*. Academic Press, 92(C), pp. 73–129. doi: 10.1016/S0070-2153(10)92003-6.

Dash, B. C. C. *et al.* (2015) *Induced pluripotent stem cell-derived vascular smooth muscle cells: Methods and application*, *Biochemical Journal*. doi: 10.1042/BJ20141078.

Davaapil, H., Shetty, D. K. and Sinha, S. (2020) 'Aortic "Disease-in-a-Dish": Mechanistic Insights and Drug Development Using iPSC-Based Disease Modeling', *Frontiers in Cell and Developmental Biology*. Frontiers, p. 1232. doi: 10.3389/fcell.2020.550504.

Davis, R. P. *et al.* (2012) 'Cardiomyocytes derived from pluripotent stem cells recapitulate electrophysiological characteristics of an overlap syndrome of cardiac sodium channel disease', *Circulation*. Circulation, 125(25), pp. 3079–3091. doi: 10.1161/CIRCULATIONAHA.111.066092.

Day, J. C. C. and Stone, N. (2013) 'A subcutaneous Raman needle probe', *Applied Spectroscopy*. Appl Spectrosc, 67(3), pp. 349–354. doi: 10.1366/12-06651.

Debakey, M. E. and Glaeser, D. H. (2000) 'Patterns of atherosclerosis: Effect of risk factors on recurrence and survival - Analysis of 11,890 cases with more than 25-year follow-up', *American Journal of Cardiology*. Elsevier, 85(9), pp. 1045–1053. doi: 10.1016/S0002-9149(00)00694-9.

Dehghani, M. and Gaborski, T. R. (2020) 'Fluorescent labeling of extracellular vesicles', in *Methods in Enzymology*. Academic Press, pp. 15–42. doi: 10.1016/bs.mie.2020.09.002.

Den Dekker, M. A. M. *et al.* (2013) 'Skin autofluorescence, a non-invasive marker for AGE accumulation, is associated with the degree of atherosclerosis', *PLoS ONE*. Public Library of Science, 8(12), p. e83084. doi: 10.1371/journal.pone.0083084.

Denzer, K. *et al.* (2000) 'Follicular Dendritic Cells Carry MHC Class II-Expressing Microvesicles at Their Surface', *The Journal of Immunology*. doi: 10.4049/jimmunol.165.3.1259.

Van Deun, J. *et al.* (2014) 'The impact of disparate isolation methods for extracellular vesicles on downstream RNA profiling', *Journal of Extracellular Vesicles*. Taylor & Francis, 3(1). doi: 10.3402/jev.v3.24858.

Devitt, G. *et al.* (2018) 'Raman Spectroscopy: An Emerging Tool in Neurodegenerative Disease Research and Diagnosis', *ACS Chemical Neuroscience*. ACS Chem Neurosci, 9(3), pp. 404–420. doi: 10.1021/acschemneuro.7b00413.

Dierker, T., Dreier, R., *et al.* (2009) 'Heparan Sulfate-modulated, Metalloprotease-mediated Sonic Hedgehog Release from Producing Cells', *The Journal of Biological Chemistry*. American Society for Biochemistry and Molecular Biology, 284(12), p. 8013. doi: 10.1074/JBC.M806838200.

Dignat-George, F. and Boulanger, C. M. (2011) 'The many faces of endothelial microparticles', *Arteriosclerosis, Thrombosis, and Vascular Biology*. Arterioscler Thromb Vasc Biol, 31(1), pp. 27–33. doi: 10.1161/ATVBAHA.110.218123.

Dimassi, S. *et al.* (2016) 'Role of eNOS- and NOX-containing microparticles in endothelial dysfunction in patients with obesity', *Obesity*. Blackwell Publishing Inc., 24(6), pp. 1305–1312. doi: 10.1002/oby.21508.

Ding, H. *et al.* (2007) 'Oxidative stress and increased eNOS and NADPH oxidase expression in mouse microvessel endothelial cells', *Journal of Cellular Physiology*. J Cell Physiol, 212(3), pp. 682–689. doi: 10.1002/jcp.21063.

Ding, Y. *et al.* (2000) 'Effects of stimulated hyperglycemia, insulin, and glucagon on endothelial nitric oxide synthase expression', *American Journal of Physiology - Endocrinology and Metabolism*. American Physiological Society, 279(1 42-1). doi: 10.1152/ajpendo.2000.279.1.e11.

Dobnikar, L. *et al.* (2018) 'Disease-relevant transcriptional signatures identified in individual smooth muscle cells from healthy mouse vessels', *Nature Communications*. Nature Publishing Group, 9(1), pp. 1–17. doi: 10.1038/s41467-018-06891-x.

Dong, L. *et al.* (2015) 'Comparison of plaque characteristics in narrowings with ST-elevation myocardial infarction (STEMI), non-STEMI/unstable angina pectoris and stable coronary artery disease (from the ADAPT-DES IVUS Substudy).', *The American journal of cardiology*. Am J Cardiol, 115(7), pp. 860–6. doi: 10.1016/j.amjcard.2015.01.008.

Dougherty, J. A. *et al.* (2020) 'Human Cardiac Progenitor Cells Enhance Exosome Release and Promote Angiogenesis Under Physoxia', *Frontiers in Cell and Developmental Biology*. Frontiers Media SA, 8. doi: 10.3389/fcell.2020.0530.

Drummond, G. R. and Sobey, C. G. (2014) 'Endothelial NADPH oxidases: which NOX to target in vascular disease?', *Trends in Endocrinology & Metabolism*, 25(9), pp. 452–463.

Du, X. L. *et al.* (2001) 'Hyperglycemia inhibits endothelial nitric oxide synthase activity by posttranslational modification at the Akt site', *Journal of Clinical Investigation*. The American Society for Clinical Investigation, 108(9), pp. 1341–1348. doi: 10.1172/JCI11235.

Durgin, B. G. *et al.* (2017) 'Smooth muscle cell-specific deletion of col15α1 unexpectedly leads to impaired development of advanced atherosclerotic lesions', *American Journal of Physiology - Heart and Circulatory Physiology*. American Physiological Society, 312(5), pp. H943–H958. doi: 10.1152/ajpheart.00029.2017.

During, A. (2000) 'Mechanisms of angiogenesis and arteriogenesis', *Nature Medicine*, 6(3), pp. 389–395.

Dutzmann, J., Koch, A., Weisheit, S., Sonnenschein, K., Korte, L., Haertlé, M., Thum, T., Bauersachs, J., Sedding, D. G. and Daniel, J. M. (2017) 'Sonic hedgehog-dependent activation of adventitial fibroblasts promotes neointima formation', *Cardiovascular Research*. Oxford University Press, 113(13), pp. 1653–1663. doi: 10.1093/cvr/cvx158.

Dwivedi, A. K. (2018) 'Performance evaluation of different machine learning techniques for prediction of heart disease', *Neural Computing and Applications*. Springer, 29(10), pp. 685–693. doi: 10.1007/s00521-016-2604-1.

Echelard, Y. *et al.* (1993) 'Sonic hedgehog, a member of a family of putative signaling molecules, is implicated in the regulation of CNS polarity', *Cell*. doi: 10.1016/0092-8674(93)90627-3.

Edgar, J. R., Eden, E. R. and Futter, C. E. (2014) 'Hrs- and CD63-Dependent Competing Mechanisms Make Different Sized Endosomal Intraluminal Vesicles', *Traffic*. doi: 10.1111/tra.12139.

Ediriweera, D. S. *et al.* (2018) 'Increase in premature mortality due to non-communicable diseases in Sri Lanka during the first decade of the twenty-first century', *BMC Public Health*, 18(1), p. 584.

Efrat, S. (2021) 'Epigenetic Memory: Lessons From iPS Cells Derived From Human β Cells', *Frontiers in Endocrinology*. Frontiers, 11, p. 1063. doi: 10.3389/FENDO.2020.614234.

Egido, J. *et al.* (2011) 'Animal models of cardiovascular diseases', *Journal of Biomedicine and Biotechnology*. J Biomed Biotechnol. doi: 10.1155/2011/497841.

Eikje, N. S., Aizawa, K. and Ozaki, Y. (2005) 'Vibrational spectroscopy for molecular characterisation and diagnosis of benign, premalignant and malignant skin tumours', *Biotechnology Annual Review*. Biotechnol Annu Rev, pp. 191–225.doi: 10.1016/S1387-2656(05)11006-0.

Emini Veseli, B. *et al.* (2017) 'Animal models of atherosclerosis', *European Journal of Pharmacology*. Elsevier, 816, pp. 3–13. doi: 10.1016/J.EJPHAR.2017.05.010.

Ender, F. *et al.* (2020) 'Detection and quantification of extracellular vesicles via FACS: Membrane labeling matters!', *International Journal of Molecular Sciences*, 21(1). doi: 10.3390/ijms21010291.

Escola, J. M. *et al.* (1998) 'Selective enrichment of tetraspan proteins on the internal vesicles of multivesicular endosomes and on exosomes secreted by human B-lymphocytes', *Journal of Biological Chemistry*. doi: 10.1074/jbc.273.32.20121.

Eugster, C. *et al.* (2007) 'Lipoprotein-Heparan Sulfate Interactions in the Hh Pathway', *Developmental Cell*. Dev Cell, 13(1), pp. 57–71. doi: 10.1016/j.devcel.2007.04.019.

Evans, M. J. and Kaufman, M. H. (1981) 'Establishment in culture of pluripotential cells from mouse embryos', *Nature*. Nature Publishing Group, 292(5819), pp. 154–156. doi: 10.1038/292154a0.

Ezan, J. *et al.* (2004) 'FrzA/sFRP-1, a secreted antagonist of the Wnt-Frizzled pathway, controls vascular cell proliferation in vitro and in vivo', *Cardiovascular Research*. Cardiovasc Res, 63(4), pp. 731–738. doi: 10.1016/j.cardiores.2004.05.006.

Fader, C. M. *et al.* (2009) 'TI-VAMP/VAMP7 and VAMP3/cellubrevin: two v-SNARE proteins involved in specific steps of the autophagy/multivesicular body pathways', *Biochimica et Biophysica Acta (BBA) - Molecular Cell Research*, 1793(12), pp. 1901–1916. doi: 10.1016/j.bbamcr.2009.09.011.

FAN, C. *et al.* (2015) 'Metformin exerts anticancer effects through the inhibition of the Sonic hedgehog signaling pathway in breast cancer', *International Journal of Molecular Medicine*. Spandidos Publications, 36(1), p. 204. doi: 10.3892/IJMM.2015.2217.

Farese, R. V. *et al.* (1996) 'Phenotypic analysis of mice expressing exclusively apolipoprotein B48 or apolipoprotein B100', *Proceedings of the National Academy of Sciences of the United States of America*. Proc Natl Acad Sci U S A, 93(13), pp. 6393–6398. doi: 10.1073/pnas.93.13.6393.

Fast, L. A. *et al.* (2017) 'Tetraspanins in infections by human cytomegalo- and

papillomaviruses', *Biochemical Society Transactions*. doi: 10.1042/bst20160295.

Fauré, J. *et al.* (2006) 'Exosomes are released by cultured cortical neurones', *Molecular and Cellular Neuroscience*. doi: 10.1016/j.mcn.2005.12.003.

Feng, D. *et al.* (2010) 'Cellular internalization of exosomes occurs through phagocytosis', *Traffic*. doi: 10.1111/j.1600-0854.2010.01041.x.

Fernandez-Borja, M. *et al.* (1999) 'Multivesicular body morphogenesis requires phosphatidylinositol 3-kinase activity', *Current Biology*. doi: 10.1016/S0960-9822(99)80048-7.

Fillinger, M. F. *et al.* (1997) 'Coculture of endothelial cells and smooth muscle cells in bilayer and conditioned media models', *Journal of Surgical Research*. J Surg Res, 67(2), pp. 169–178. doi: 10.1006/jsre.1996.4978.

Finkel, T. (2011) 'Signal transduction by reactive oxygen species', *The Journal of Cell Biology*, 194(1), pp. 7–15.

Fishbein, G. A. and Fishbein, M. C. (2009) 'Arteriosclerosis: Rethinking the current classification', *Archives of Pathology and Laboratory Medicine*, pp. 1309–1316. doi: 10.1043/1543-2165-133.8.1309.

Fitzner, D. *et al.* (2011) 'Selective transfer of exosomes from oligodendrocytes to microglia by macropinocytosis', *Journal of Cell Science*. doi: 10.1242/jcs.074088.

Fitzpatrick, E. *et al.* (2017) 'Alcohol Reduces Arterial Remodeling by Inhibiting Sonic Hedgehog-Stimulated Stem Cell Antigen-1 Positive Progenitor Stem Cell Expansion', *Alcoholism: Clinical and Experimental Research*. Blackwell Publishing Ltd, 41(12), pp. 2051–2065. doi: 10.1111/acer.13499.

Flaumenhaft, R. *et al.* (2009) 'Megakaryocyte-derived microparticles: direct visualization and distinction from platelet-derived microparticles', *Blood*. doi: 10.1182/blood-2008-06-163832.

Fleckenstein, M., Schmitz-Valckenberg, S. and Holz, F. G. (2010) 'Fundus Autofluorescence Imaging in Clinical Use.', *Review of Ophthalmology*, 17(8), pp. 64–68. Available at: https://www.reviewofophthalmology.com/article/fundus-autofluorescence-imaging-in-clinical-use (Accessed: 27 August 2021).

Förstermann, U. (2010) 'Nitric oxide and oxidative stress in vascular disease', *Pflugers Archiv European Journal of Physiology*. doi: 10.1007/s00424-010-0808-2.

Frank, E. *et al.* (2004) 'Data mining in bioinformatics using Weka', *Bioinformatics*. Oxford Academic, 20(15), pp. 2479–2481. doi: 10.1093/bioinformatics/bth261.

Freeman, D. W. *et al.* (2018) 'Altered extracellular vesicle concentration, cargo, and function in diabetes', *Diabetes*. American Diabetes Association Inc., 67(11), pp. 2377–2388. doi: 10.2337/db17-1308.

de Freitas, R. C. C. *et al.* (2021) 'Circulating extracellular vesicles as biomarkers and drug delivery vehicles in cardiovascular diseases', *Biomolecules*, 11(3), pp. 1–20. doi: 10.3390/biom11030388.

Frühbeis, C., Fröhlich, D. and Krämer-Albers, E. M. (2012) 'Emerging roles of exosomes in neuron-glia communication', *Frontiers in Physiology*. doi: 10.3389/fphys.2012.00119.

Fujita, Y. *et al.* (2015) 'Extracellular vesicles in lung microenvironment and pathogenesis', *Trends in Molecular Medicine*. Elsevier Ltd, pp. 533–542. doi: 10.1016/j.molmed.2015.07.004.

Furi, I., Momen-Heravi, F. and Szabo, G. (2017) 'Extracellular vesicle isolation: present and future', *Annals of Translational Medicine*. AME Publications, 5(12), p. 263. doi: 10.21037/ATM.2017.03.95.

Fuster, J. J. *et al.* (2012) 'Animal models of atherosclerosis', in *Progress in Molecular Biology and Translational Science*. Prog Mol Biol Transl Sci, pp. 1–23. doi: 10.1016/B978-0-12-394596-9.00001-9.

Gaceb, A., Martinez, M. C. and Andriantsitohaina, R. (2014) 'Extracellular vesicles: New players in cardiovascular diseases', *The International Journal of Biochemistry & Cell Biology*. Pergamon, 50(1), pp. 24–28. doi: 10.1016/J.BIOCEL.2014.01.018.

Galkina, E. *et al.* (2006) 'Lymphocyte recruitment into the aortic wall before and during development of atherosclerosis is partially L-selectin dependent', *The Journal of Experimental Medicine*, 203(5), pp. 1273–1282.

Gardiner, C. *et al.* (2016) 'Techniques used for the isolation and characterization of extracellular vesicles: Results of a worldwide survey', *Journal of Extracellular Vesicles*. J Extracell Vesicles, 5(1). doi: 10.3402/jev.v5.32945.

Gatto, L. and Prati, F. (2020) 'Subclinical atherosclerosis: How and when to treat it?', *European Heart Journal, Supplement*. Oxford Academic, 22(Supplement_E), pp. E87–E90. doi: 10.1093/EURHEARTJ/SUAA068.

Ghantous, C. M. *et al.* (2020) 'Advances in cardiovascular biomarker discovery', *Biomedicines*, 8(12), pp. 1–19. doi: 10.3390/biomedicines8120552.

Gniadecka, M. *et al.* (2004) 'Melanoma Diagnosis by Raman Spectroscopy and Neural Networks: Structure Alterations in Proteins and Lipids in Intact Cancer Tissue', *Journal of Investigative Dermatology*. Elsevier, 122(2), pp. 443–449. doi: 10.1046/j.0022-

202X.2004.22208.x.

Godinez, W. J. *et al.* (2017) 'A multi-scale convolutional neural network for phenotyping high-content cellular images', *Bioinformatics*. Bioinformatics, 33(13), pp. 2010–2019. doi: 10.1093/bioinformatics/btx069.

Gomez, D. *et al.* (2013) 'Detection of histone modifications at specific gene loci in single cells in histological sections', *Nature Methods*, 10(2), pp. 171–177. doi: 10.1038/nmeth.2332.

Gomez, D. and Owens, G. K. (2012) 'Smooth muscle cell phenotypic switching in atherosclerosis', *Cardiovascular Research*, 95(2), pp. 156–164. doi: 10.1093/cvr/cvs115.

Gomez, D., Swiatlowska, P. and Owens, G. K. (2015) 'Epigenetic Control of Smooth Muscle Cell Identity and Lineage Memory', *Arteriosclerosis, Thrombosis, and Vascular Biology*. NIH Public Access, 35(12), pp. 2508–2516. doi: 10.1161/ATVBAHA.115.305044.

Gonzalez-Calero, L., Martin-Lorenzo, M. and Alvarez-Llamas, G. (2014) 'Exosomes: A potential key target in cardio-renal syndrome', *Frontiers in Immunology*. doi: 10.3389/fimmu.2014.00465.

Goodenough, D. A. (1996) 'Connexins, Connexons, and Intercellular Communication', *Annual Review of Biochemistry*, 65(1), pp. 475–502. doi: 10.1146/annurev.biochem.65.1.475.

Gordon, C. *et al.* (2011) 'Circulating endothelial microparticles as a measure of early lung destruction in cigarette smokers', *American Journal of Respiratory and Critical Care Medicine*. Am J Respir Crit Care Med, 184(2), pp. 224–232. doi: 10.1164/rccm.201012-2061OC.

Gordon, W. R., Arnett, K. L. and Blacklow, S. C. (2008) 'The molecular logic of Notch signaling--a structural and biochemical perspective.', *Journal of cell science*, 121(Pt 19), pp. 3109–19. doi: 10.1242/jcs.035683.

Gradilla, A. C. *et al.* (2014) 'Exosomes as Hedgehog carriers in cytoneme-mediated transport and secretion', *Nature Communications*. doi: 10.1038/ncomms6649.

Granata, A. *et al.* (2017) 'An iPSC-derived vascular model of Marfan syndrome identifies key mediators of smooth muscle cell death', *Nature Genetics*. doi: 10.1038/ng.3723.

Gridley, T. (2010) *Notch signaling in the vasculature*, *Current Topics in Developmental Biology*. doi: 10.1016/S0070-2153(10)92009-7.

Gross, J. C. *et al.* (2012) 'Active Wnt proteins are secreted on exosomes', *Nature Cell Biology*. Nat Cell Biol, 14(10), pp. 1036–1045. doi: 10.1038/ncb2574.

Grundy, S. M. *et al.* (1999) 'Diabetes and cardiovascular disease: A statement for healthcare professionals from the american heart association', *Circulation*. Lippincott Williams and Wilkins, pp. 1134–1146. doi: 10.1161/01.CIR.100.10.1134.

Guduric-Fuchs, J. *et al.* (2012) 'Selective extracellular vesicle-mediated export of an overlapping set of microRNAs from multiple cell types', *BMC Genomics*. doi: 10.1186/1471-2164-13-357.

Gunaratne, R. *et al.* (2019) 'Machine learning classification of human joint tissue from diffuse reflectance spectroscopy data', *Biomedical Optics Express*. Optical Society of America, 10(8), p. 3889. doi: 10.1364/boe.10.003889.

Gupta, M. K. *et al.* (2015) 'Oligoproline-derived nanocarrier for dual stimuli-responsive gene delivery', *Journal of Materials Chemistry B*. Royal Society of Chemistry, 3(36), pp. 7271–7280. doi: 10.1039/c5tb00988j.

Guruharsha, K. G., Kankel, M. W. and Artavanis-Tsakonas, S. (2012) *The Notch signalling system: Recent insights into the complexity of a conserved pathway*, *Nature Reviews Genetics*. Nat Rev Genet. doi: 10.1038/nrg3272.

Ha, D., Yang, N. and Nadithe, V. (2016) 'Exosomes as therapeutic drug carriers and delivery vehicles across biological membranes: current perspectives and future challenges', *Acta Pharmaceutica Sinica B*. doi: 10.1016/j.apsb.2016.02.001.

Habibalahi, A. *et al.* (2020) 'Non-invasive real-time imaging of reactive oxygen species (ROS) using auto-fluorescence multispectral imaging technique: A novel tool for redox biology', *Redox Biology*. Elsevier, 34, p. 101561. doi: 10.1016/J.REDOX.2020.101561.

Haery, C., Sachar, R. and Ellis, S. G. (2004) 'Drug-eluting stents: the beginning of the end of restenosis?', *Cleveland Clinic journal of medicine*, 71(10), pp. 815–24. Available at: http://www.ncbi.nlm.nih.gov/pubmed/15529487 (Accessed: 14 June 2019).

Hagensen, M. K. *et al.* (2019) 'Increased retention of LDL from type 1 diabetic patients in atherosclerosis-prone areas of the murine arterial wall', *Atherosclerosis*. Elsevier Ireland Ltd, 286, pp. 156–162. doi: 10.1016/j.atherosclerosis.2019.02.027.

Haka, A. S. *et al.* (2005) 'Diagnosing breast cancer by using Raman spectroscopy', *Proceedings of the National Academy of Sciences of the United States of America*. National Academy of Sciences, 102(35), pp. 12371–12376. doi: 10.1073/pnas.0501390102.

Halloran, B. G. *et al.* (1997) 'Macrophage products inhibit human aortic smooth muscle cell proliferation and alter 1α(I) procollagen expression', in *Annals of Vascular Surgery*. Ann Vasc Surg, pp. 80–84. doi: 10.1007/s100169900014.

Hamuro, M. *et al.* (2002) 'High glucose induced nuclear factor kappa B mediated inhibition of endothelial cell migration', *Atherosclerosis*. Atherosclerosis, 162(2), pp. 277–287. doi: 10.1016/S0021-9150(01)00719-5.

Hannafon, B. N. and Ding, W. Q. (2013) 'Intercellular communication by exosome-derived microRNAs in cancer', *International Journal of Molecular Sciences*. doi: 10.3390/ijms140714240.

Hao, H., Gabbiani, G. and Bochaton-Piallat, M. L. (2003) 'Arterial smooth muscle cell heterogeneity: Implications for atherosclerosis and restenosis development', *Arteriosclerosis, Thrombosis, and Vascular Biology*. Arterioscler Thromb Vasc Biol, pp. 1510–1520. doi: 10.1161/01.ATV.0000090130.85752.ED.

Harding, C. and Stahl, P. (1983) 'Transferrin recycling in reticulocytes: pH and iron are important determinants of ligand binding and processing', *Biochemical and Biophysical Research Communications*. doi: 10.1016/0006-291X(83)91776-X.

Harst, P. van der and Verweij, N. (2018) 'Identification of 64 Novel Genetic Loci Provides an Expanded View on the Genetic Architecture of Coronary Artery Disease', *Circulation Research*. Wolters Kluwer Health, 122(3), p. 433. doi: 10.1161/CIRCRESAHA.117.312086.

Heiss, C. *et al.* (2008) 'Brief Secondhand Smoke Exposure Depresses Endothelial Progenitor Cells Activity and Endothelial Function. Sustained Vascular Injury and Blunted Nitric Oxide Production', *Journal of the American College of Cardiology*. J Am Coll Cardiol, 51(18), pp. 1760–1771. doi: 10.1016/j.jacc.2008.01.040.

Helmke, A. and Vietinghoff, S. von (2016) 'Extracellular vesicles as mediators of vascular inflammation in kidney disease', *World Journal of Nephrology*. World J Nephrol, 5(2), p. 125. doi: 10.5527/wjn.v5.i2.125.

Hergenreider, E. *et al.* (2012) 'Atheroprotective communication between endothelial cells and smooth muscle cells through miRNAs', *Nature Cell Biology*. doi: 10.1038/ncb2441.

Higashi, Y. *et al.* (2009) 'Endothelial function and oxidative stress in cardiovascular diseases.', *Circulation journal : official journal of the Japanese Circulation Society*, 73(3), pp. 411–8. Available at: http://www.ncbi.nlm.nih.gov/pubmed/19194043.

High, F. A. *et al.* (2007) 'An essential role for Notch in neural crest during cardiovascular development and smooth muscle differentiation', *Journal of Clinical Investigation*. American Society for Clinical Investigation, 117(2), pp. 353–363. doi: 10.1172/JCI30070.

Hobbs, R. (2004) 'Cardiovascular disease: Different strategies for primary and

secondary prevention?', *Heart*, 90(10), pp. 1217–1223. doi: 10.1136/hrt.2003.027680.

Holford, J. M. (2009) *Biological Science*, *Bmj*. doi: 10.1136/bmj.1.4928.1462.

Hoofnagle, M. H. *et al.* (2006) 'Origin of Neointimal Smooth Muscle', *Arteriosclerosis, Thrombosis, and Vascular Biology*. Lippincott Williams & Wilkins, 26(12), pp. 2579–2581. doi: 10.1161/01.ATV.0000249623.79871.bc.

Hooper, C. *et al.* (2012) 'Wnt3a induces exosome secretion from primary cultured rat microglia', *BMC Neuroscience*. doi: 10.1186/1471-2202-13-144.

Hooper, J. E. and Scott, M. P. (2005) 'Communicating with hedgehogs', *Nature Reviews Molecular Cell Biology*. doi: 10.1038/nrm1622.

Hoshino, D. *et al.* (2013) 'Exosome secretion is enhanced by invadopodia and drives invasive behavior', *Cell Reports*. doi: 10.1016/j.celrep.2013.10.050.

Howitt, J. and Hill, A. F. (2016) 'Exosomes in the pathology of neurodegenerative diseases', *Journal of Biological Chemistry*. doi: 10.1074/jbc.R116.757955.

Hsu, C. *et al.* (2010) 'Regulation of exosome secretion by Rab35 and its GTPase-activating proteins TBC1D10A-C', *Journal of Cell Biology*. doi: 10.1083/jcb.200911018.

Hu, Y. *et al.* (2004) 'Abundant progenitor cells in the adventitia contribute to atherosclerosis of vein grafts in ApoE-deficient mice', *Journal of Clinical Investigation*. doi: 10.1172/JCI19628.

Hughes, C. *et al.* (2010) 'SR-FTIR spectroscopy of renal epithelial carcinoma side population cells displaying stem cell-like characteristics', in *Analyst*. The Royal Society of Chemistry, pp. 3133–3141. doi: 10.1039/c0an00574f.

Ido, Y., Carling, D. and Ruderman, N. (2002) 'Hyperglycemia-induced apoptosis in human umbilical vein endothelial cells: Inhibition by the AMP-activated protein kinase activation', *Diabetes*. American Diabetes Association, 51(1), pp. 159–167. doi: 10.2337/diabetes.51.1.159.

Ikari, Y. *et al.* (1999) 'Neonatal intima formation in the human coronary artery', *Arteriosclerosis, Thrombosis, and Vascular Biology*. Lippincott Williams and Wilkins, 19(9), pp. 2036–2040. doi: 10.1161/01.ATV.19.9.2036.

International Diabetes Federation (2019) *International Diabetes Federation. Diabetes Atlas, 9th ed. Int DiabFed 2019.*

Ishibashi, S. *et al.* (1993) 'Hypercholesterolemia in low density lipoprotein receptor

knockout mice and its reversal by adenovirus-mediated gene delivery', *Journal of Clinical Investigation*. American Society for Clinical Investigation, 92(2), pp. 883–893. doi: 10.1172/JCI116663.

Iso, T., Kedes, L. and Hamamori, Y. (2003) 'HES and HERP families: Multiple effectors of the Notch signaling pathway', *Journal of Cellular Physiology*, 194(3), pp. 237–255. doi: 10.1002/jcp.10208.

Itzhaki, I. *et al.* (2012) 'Modeling of catecholaminergic polymorphic ventricular tachycardia with patient-specific human-induced pluripotent stem cells', *Journal of the American College of Cardiology*. J Am Coll Cardiol, 60(11), pp. 990–1000. doi: 10.1016/j.jacc.2012.02.066.

Jahn, R. and Scheller, R. H. (2006) 'SNAREs - Engines for membrane fusion', *Nature Reviews Molecular Cell Biology*. doi: 10.1038/nrm2002.

Jain, R. K. (2003) 'Molecular regulation of vessel maturation', *Nature medicine*, 9(6), pp. 685–693.

Jansen, F. *et al.* (2013) 'High glucose condition increases NADPH oxidase activity in endothelial microparticles that promote vascular inflammation', *Cardiovascular Research*. Oxford Academic, 98(1), pp. 94–106. doi: 10.1093/cvr/cvt013.

Jansen, F., Nickenig, G. and Werner, N. (2017) 'Extracellular Vesicles in Cardiovascular Disease: Potential Applications in Diagnosis, Prognosis, and Epidemiology', *Circ Res*. doi: 10.1161/CIRCRESAHA.117.310752.

Järvisalo, M. J. *et al.* (2002) 'Carotid artery intima-media thickness in children with type 1 diabetes', *Diabetes*. American Diabetes Association, 51(2), pp. 493–498. doi: 10.2337/diabetes.51.2.493.

Jermyn, M. *et al.* (2015) 'Intraoperative brain cancer detection with Raman spectroscopy in humans', *Science Translational Medicine*. Sci Transl Med, 7(274). doi: 10.1126/scitranslmed.aaa2384.

Ji, H. *et al.* (2017) 'Application of induced pluripotent stem cells to model smooth muscle cell function in vascular diseases', *Current Opinion in Biomedical Engineering*, 1, pp. 38–44. doi: 10.1016/j.cobme.2017.02.005.

Jiang, X. *et al.* (2000) 'Fate of the mammalian cardiac neural crest.', *Development*, 127(8), pp. 1607–1616.

Johnstone, R. M. *et al.* (1987) 'Vesicle formation during reticulocyte maturation. Association of plasma membrane activities with released vesicles (exosomes).', *Journal of Biological Chemistry*.

de Jong, O. G. *et al.* (2012) 'Cellular stress conditions are reflected in the protein and RNA content of endothelial cell-derived exosomes', *Journal of Extracellular Vesicles*. Wiley-Blackwell, 1(1). doi: 10.3402/jev.v1i0.18396.

Kajimoto, T. *et al.* (2013) 'Ongoing activation of sphingosine 1-phosphate receptors mediates maturation of exosomal multivesicular endosomes', *Nature Communications*. doi: 10.1038/ncomms3712.

Kalra, H. *et al.* (2012) 'Vesiclepedia: A Compendium for Extracellular Vesicles with Continuous Community Annotation', *PLoS Biology*. doi: 10.1371/journal.pbio.1001450.

Kapustin, A. N. *et al.* (2015) 'Vascular smooth muscle cell calcification is mediated by regulated exosome secretion', *Circulation Research*. Lippincott Williams & Wilkins Hagerstown, MD, 116(8), pp. 1312–1323. doi: 10.1161/CIRCRESAHA.116.305012.

Kapustin, A. N. *et al.* (2017) 'Prothrombin Loading of Vascular Smooth Muscle Cell-Derived Exosomes Regulates Coagulation and Calcification', *Arteriosclerosis, Thrombosis, and Vascular Biology*. doi: 10.1161/ATVBAHA.116.308886.

Kapustin, A. N. and Shanahan, C. M. (2016) 'Emerging roles for vascular smooth muscle cell exosomes in calcification and coagulation', *Journal of Physiology*. doi: 10.1113/JP271340.

Katzmann, D. J., Babst, M. and Emr, S. D. (2001) 'Ubiquitin-dependent sorting into the multivesicular body pathway requires the function of a conserved endosomal protein sorting complex, ESCRT-I', *Cell*. doi: 10.1016/S0092-8674(01)00434-2.

Keller, S. *et al.* (2007) 'CD24 is a marker of exosomes secreted into urine and amniotic fluid', *Kidney International*. doi: 10.1038/sj.ki.5002486.

Kennedy, E., Mooney, C. J., *et al.* (2014) 'Adult vascular smooth muscle cells in culture express neural stem cell markers typical of resident multipotent vascular stem cells', *Cell and Tissue Research*. NIH Public Access, 358(1), pp. 203–216. doi: 10.1007/s00441-014-1937-2.

Kennedy, E., Hakimjavadi, R., *et al.* (2014) 'Embryonic rat vascular smooth muscle cells revisited - A model for neonatal, neointimal SMC or differentiated vascular stem cells?', *Vascular Cell*. Vasc Cell, 6(1), pp. 1–13. doi: 10.1186/2045-824X-6-6.

Kennedy, T. L., Russell, A. J. and Riley, P. (2020) 'Experimental limitations of extracellular vesicle-based therapies for the treatment of myocardial infarction', *Trends in Cardiovascular Medicine*. doi: 10.1016/j.tcm.2020.08.003.

Kenny, L. C. *et al.* (2005) 'Novel biomarkers for pre-eclampsia detected using metabolomics and machine learning', *Metabolomics*. Springer, 1(3), pp. 227–234. doi: 10.1007/s11306-005-0003-1.

Kerr, J. F. R., Wyllie, A. H. and Currie, A. R. (1972) 'Apoptosis: A basic biological phenomenon with wide-ranging implications in tissue kinetics', *British Journal of Cancer*. doi: 10.1038/bjc.1972.33.

Kim, C. (2015) 'iPSC technology-Powerful hand for disease modeling and therapeuticscreen', *BMB Reports*. Korean Society for Biochemistry and Molecular Biology, 48(5), p. 256. doi: 10.5483/BMBREP.2015.48.5.100.

Kim, D.-K. K. *et al.* (2013) 'EVpedia: An integrated database of high-throughput data for systemic analyses of extracellular vesicles', *Journal of Extracellular Vesicles*. Taylor & Francis, 2(1). doi: 10.3402/jev.v2i0.20384.

King, D. *et al.* (2019) 'Label-Free Multi Parameter Optical Interrogation of Endothelial Activation in Single Cells using a Lab on a Disc Platform', *Scientific Reports*, 9(1). doi: 10.1038/s41598-019-40612-8.

Kinlay, S. and Ganz, P. (1997) 'Role of endothelial dysfunction in coronary artery disease and implications for therapy', in *American Journal of Cardiology*. Elsevier Inc. doi: 10.1016/S0002-9149(97)00793-5.

Kiselev, R. *et al.* (2016) 'Design and first applications of a flexible Raman micro-spectroscopic system for biological imaging', *Biomedical Spectroscopy and Imaging*. IOS Press, 5(2), pp. 115–127. doi: 10.3233/bsi-160141.

Kishore, R., Garikipati, V. N. S. and Gumpert, A. (2016) 'Tiny Shuttles for Information Transfer: Exosomes in Cardiac Health and Disease', *Journal of Cardiovascular Translational Research*. doi: 10.1007/s12265-016-9682-4.

Klinkert, K. and Echard, A. (2016) 'Rab35 GTPase: A Central Regulator of Phosphoinositides and F-actin in Endocytic Recycling and Beyond', *Traffic*. doi: 10.1111/tra.12422.

Koga, H. *et al.* (2005) 'Elevated levels of VE-cadherin-positive endothelial microparticles in patients with type 2 diabetes mellitus and coronary artery disease', *Journal of the American College of Cardiology*. J Am Coll Cardiol, 45(10), pp. 1622–1630. doi: 10.1016/j.jacc.2005.02.047.

Kohsaka, S. and Makaryus, A. N. (2008) 'Coronary Angiography Using Noninvasive Imaging Techniques of Cardiac CT and MRI', *Current Cardiology Reviews*. Bentham Science Publishers, 4(4), p. 323. doi: 10.2174/157340308786349444.

Koles, K. *et al.* (2012) 'Mechanism of Evenness Interrupted (Evi)-Exosome Release at Synaptic Boutons', *Journal of Biological Chemistry*, 287(20), pp. 16820–16834. doi: 10.1074/jbc.M112.342667.

Koljenović, S. *et al.* (2002) ‘Discriminating vital tumor from necrotic tissue in human glioblastoma tissue samples by Raman spectroscopy’, *Laboratory Investigation*. Nature Publishing Group, 82(10), pp. 1265–1277. doi: 10.1097/01.LAB.0000032545.96931.B8.

Kolodgie, F. D. *et al.* (2007) ‘Is pathologic intimal thickening the key to understanding early plaque progression in human atherosclerotic disease?’, *Arteriosclerosis, Thrombosis, and Vascular Biology*. Lippincott Williams & Wilkins, pp. 986–989. doi: 10.1161/ATVBAHA.0000258865.44774.41.

Kong, J. *et al.* (2018) ‘Exosomes of endothelial progenitor cells inhibit neointima formation after carotid artery injury’, *Journal of Surgical Research*. Elsevier, 232, pp. 398–407. doi: 10.1016/j.jss.2018.06.066.

Konstantinov, I. E. and Jankovic, G. M. (2013) ‘Alexander I. Ignatowski: A pioneer in the study of atherosclerosis’, *Texas Heart Institute Journal*. Texas Heart Institute, 40(3), pp. 247–249. Available at: /pmc/articles/PMC3709240/ (Accessed: 8 August 2021).

Korin, N. *et al.* (2012) ‘Shear-activated nanotherapeutics for drug targeting to obstructed blood vessels’, *Science*. Science, 337(6095), pp. 738–742. doi: 10.1126/science.1217815.

Kornberg, T. B. and Roy, S. (2014) ‘Cytonemes as specialized signaling filopodia’, *Development (Cambridge)*. Development, 141(4), pp. 729–736. doi: 10.1242/dev.086223.

Korshunov, V. A. and Berk, B. C. (2003) ‘Flow-Induced Vascular Remodeling in the Mouse: A Model for Carotid Intima-Media Thickening’, *Arteriosclerosis, Thrombosis, and Vascular Biology*, 23(12), pp. 2185–2191. doi: 10.1161/01.ATV.0000103120.06092.14.

Kothari, R. *et al.* (2021) ‘Raman spectroscopy and artificial intelligence to predict the Bayesian probability of breast cancer’, *Scientific Reports 2021 11:1*. Nature Publishing Group, 11(1), pp. 1–17. doi: 10.1038/s41598-021-85758-6.

Kowal, J. *et al.* (2016) ‘Proteomic comparison defines novel markers to characterize heterogeneous populations of extracellular vesicle subtypes’, *Proceedings of the National Academy of Sciences*. doi: 10.1073/pnas.1521230113.

Kowal, J., Tkach, M. and Théry, C. (2014) ‘Biogenesis and secretion of exosomes’, *Current Opinion in Cell Biology*. doi: 10.1016/j.ceb.2014.05.004.

Krafft, C. *et al.* (2009) ‘Disease recognition by infrared and Raman spectroscopy’, *Journal of Biophotonics*. J Biophotonics, pp. 13–28. doi: 10.1002/jbio.200810024.

KRamann, R. *et al.* (2015) ‘Perivascular Gli1+ progenitors are key contributors to

injury-induced organ fibrosis', *Cell stem cell*. NIH Public Access, 16(1), p. 51. doi: 10.1016/J.STEM.2014.11.004.

KRamann, R. *et al.* (2016) 'Adventitial MSC-like Cells Are Progenitors of Vascular Smooth Muscle Cells and Drive Vascular Calcification in Chronic Kidney Disease', *Cell Stem Cell*. Cell Stem Cell, 19(5), pp. 628–642. doi: 10.1016/j.stem.2016.08.001.

Krämer-Albers, E. M. *et al.* (2007) 'Oligodendrocytes secrete exosomes containing major myelin and stress-protective proteins: Trophic support for axons?', *Proteomics - Clinical Applications*. doi: 10.1002/prca.200700522.

Kranendonk, M. E. *et al.* (2014) 'Extracellular vesicle markers in relation to obesity and metabolic complications in patients with manifest cardiovascular disease', *Cardiovascular Diabetology*. BioMed Central, 13(1), pp. 1–11. doi: 10.1186/1475-2840-13-37.

Kumar, A. and Lindner, V. (1997) 'Remodeling with neointima formation in the mouse carotid artery after cessation of blood flow', *Arteriosclerosis, Thrombosis, and Vascular Biology*. Arterioscler Thromb Vasc Biol, 17(10), pp. 2238–2244. doi: 10.1161/01.ATV.17.10.2238.

Kurpinski, K. *et al.* (2010) 'Transforming growth factor-β and notch signaling mediate stem cell differentiation into smooth muscle cells', *Stem cells (Dayton, Ohio)*, 28(4), pp. 734–742. doi: 10.1002/stem.319.

Kuwabara, Y. *et al.* (2011) 'Increased microRNA-1 and microRNA-133a levels in serum of patients with cardiovascular disease indicate myocardial damage', *Circulation: Cardiovascular Genetics*. doi: 10.1161/CIRCGENETICS.110.958975.

Laakso, M. (1999) 'Hyperglycemia and cardiovascular disease in type 2 diabetes', *Diabetes*. Diabetes, pp. 937–942. doi: 10.2337/diabetes.48.5.937.

Laird, D. W. (2010) 'The gap junction proteome and its relationship to disease', *Trends in Cell Biology*, 20(2), pp. 92–101.

Lambeth, J. D., Kawahara, T. and Diebold, B. (2007) 'Regulation of Nox and Duox enzymatic activity and expression', *Free Radical Biology and Medicine*, 43(3), pp. 319–331. doi: 10.1016/j.freeradbiomed.2007.03.028.

Lan, F. *et al.* (2013) 'Abnormal calcium handling properties underlie familial hypertrophic cardiomyopathy pathology in patient-specific induced pluripotent stem cells', *Cell Stem Cell*. Cell Stem Cell, 12(1), pp. 101–113. doi: 10.1016/j.stem.2012.10.010.

Lan, T.-H., Huang, X.-Q. and Tan, H.-M. (2013) 'Vascular fibrosis in atherosclerosis.', *Cardiovascular pathology : the official journal of the Society for Cardiovascular Pathology*. Cardiovasc Pathol, 22(5), pp. 401–7. doi: 10.1016/j.carpath.2013.01.003.

Landry, A. *et al.* (2017) 'Causes and outcomes of markedly elevated C-reactive protein levels', *Canadian Family Physician*. College of Family Physicians of Canada, 63(6), pp. e316–e323. Available at: /pmc/articles/PMC5471098/ (Accessed: 25 May 2021).

Langille, B. L. (1996) 'Arterial remodeling: relation to hemodynamics', *Canadian Journal of Physiology and Pharmacology*, 74(7), pp. 834–841.

Lässer, C. *et al.* (2016) 'Exosomes in the nose induce immune cell trafficking and harbour an altered protein cargo in chronic airway inflammation', *Journal of Translational Medicine*. doi: 10.1186/s12967-016-0927-4.

Lattermann, A. *et al.* (2013) 'Characterization of atherosclerotic plaque depositions by Raman and FTIR imaging', *Journal of Biophotonics*. John Wiley & Sons, Ltd, 6(1), pp. 110–121. doi: 10.1002/JBIO.201200146.

Laulagnier, K. *et al.* (2018) 'Amyloid precursor protein products concentrate in a subset of exosomes specifically endocytosed by neurons', *Cellular and Molecular Life Sciences*. doi: 10.1007/s00018-017-2664-0.

Laurenzana, I. *et al.* (2018) 'Extracellular Vesicles: A New Prospective in Crosstalk between Microenvironment and Stem Cells in Hematological Malignancies', *Stem Cells International*. Hindawi Limited. doi: 10.1155/2018/9863194.

Lawson, C. *et al.* (2016) 'Microvesicles and exosomes: New players in metabolic and cardiovascular disease', *Journal of Endocrinology*. doi: 10.1530/JOE-15-0201.

Lazar, I. *et al.* (2015) 'Proteome characterization of melanoma exosomes reveals a specific signature for metastatic cell lines', *Pigment Cell and Melanoma Research*. Pigment Cell Melanoma Res, 28(4), pp. 464–475. doi: 10.1111/pcmr.12380.

Leenaars, C. H. C. *et al.* (2019) 'Animal to human translation: A systematic scoping review of reported concordance rates', *Journal of Translational Medicine*. BioMed Central, pp. 1–22. doi: 10.1186/s12967-019-1976-2.

Leroyer, A. S. *et al.* (2007) 'Cellular Origins and Thrombogenic Activity of Microparticles Isolated From Human Atherosclerotic Plaques', *Journal of the American College of Cardiology*. Elsevier, 49(7), pp. 772–777. doi: 10.1016/J.JACC.2006.10.053.

Lespagnol, A. *et al.* (2008) 'Exosome secretion, including the DNA damage-induced p53-dependent secretory pathway, is severely compromised in TSAP6/Steap3-null mice', *Cell Death & Differentiation*, 15(11), pp. 1723–1733. doi: 10.1038/cdd.2008.104.

Leszczynska, A. *et al.* (2018) 'Exosomes from normal and diabetic human corneolimbal keratocytes differentially regulate migration, proliferation and marker expression of limbal epithelial cells', *Scientific Reports*. Nature Publishing Group, 8(1), pp. 1–13. doi:

10.1038/s41598-018-33169-5.

Li, F. *et al.* (2010) 'Sonic hedgehog signaling induces vascular smooth muscle cell proliferation via induction of the G1 cyclin-retinoblastoma axis', *Arteriosclerosis, Thrombosis, and Vascular Biology*. Lippincott Williams & Wilkins, 30(9), pp. 1787–1794. doi: 10.1161/ATVBAHA.110.208520.

Li, J. M. and Shah, A. M. (2004) 'Endothelial cell superoxide generation: Regulation and relevance for cardiovascular pathophysiology', *American Journal of Physiology - Regulatory Integrative and Comparative Physiology*. American Physiological Society, pp. 1014–1030. doi: 10.1152/ajpregu.00124.2004.

Li, S. *et al.* (2016) 'Cell-Derived Microparticles in Patients with Type 2 Diabetes Mellitus: A Systematic Review and Meta-Analysis', *Cellular Physiology and Biochemistry*. S. Karger AG, pp. 2439–2450. doi: 10.1159/000452512.

Li, Y. *et al.* (2012) 'Deficiency in the NADPH oxidase 4 predisposes towards diet-induced obesity', *International Journal of Obesity*. Int J Obes (Lond), 36(12), pp. 1503–1513. doi: 10.1038/ijo.2011.279.

Li, Y. *et al.* (2013) 'Comparing the diagnostic values of circulating microRNAs and cardiac troponin T in patients with acute myocardial infarction', *Clinics*. doi: 10.6061/clinics/2013(01)oa12.

Liang, B. *et al.* (2013) 'Characterization and proteomic analysis of ovarian cancer-derived exosomes', *Journal of Proteomics*. J Proteomics, 80, pp. 171–182. doi: 10.1016/j.jprot.2012.12.029.

Liang, P. and Du, J. (2014) 'Human induced pluripotent stem cell for modeling cardiovascular diseases', *Regenerative Medicine Research*. EDP Sciences, 2(1), p. 4. doi: 10.1186/2050-490x-2-4.

Libby, P. (2000) 'Changing concepts of atherogenesis', in *Journal of Internal Medicine*. J Intern Med, pp. 349–358. doi: 10.1046/j.1365-2796.2000.00654.x.

Liégeois, S. *et al.* (2006) 'The V0-ATPase mediates apical secretion of exosomes containing Hedgehog-related proteins in Caenorhabditis elegans', *Journal of Cell Biology*. J Cell Biol, 173(6), pp. 949–961. doi: 10.1083/jcb.200511072.

Lin, Y. *et al.* (2001) 'Hyperglycemia-induced Production of Acute Phase Reactants in Adipose Tissue', *Journal of Biological Chemistry*. Elsevier, 276(45), pp. 42077–42083. doi: 10.1074/jbc.M107101200.

Lindner, V., Fingerle, J. and Reidy, M. A. (1993) 'Mouse model of arterial injury', *Circulation Research*. Circ Res, 73(5), pp. 792–796. doi: 10.1161/01.RES.73.5.792.

Ling, J. *et al.* (2002) 'Direct Raman imaging techniques for study of the subcellular

distribution of a drug', *Applied Optics*. Appl Opt, 41(28), p. 6006. doi: 10.1364/ao.41.006006.

Liu, G. H. *et al.* (2011) 'Recapitulation of premature ageing with iPSCs from Hutchinson-Gilford progeria syndrome', *Nature*. doi: 10.1038/nature09879.

Liu, H. *et al.* (2014) 'Circulating endothelial microparticles involved in lung function decline in a rat exposed in cigarette smoke maybe from apoptotic pulmonary capillary endothelial cells', *Journal of Thoracic Disease*. Pioneer Bioscience Publishing, 6(6), pp. 649–655. doi: 10.3978/j.issn.2072-1439.2014.06.26.

Liu, W. *et al.* (2011) 'Differential effects of daily-moderate versus weekend-binge alcohol consumption on atherosclerotic plaque development in mice', *Atherosclerosis*. ccc-ccc, 219(2), pp. 448–454. doi: 10.1016/j.atherosclerosis.2011.08.034.

Liu, W. *et al.* (2020) 'Moderate Alcohol Consumption Targets S100β+ Vascular Stem Cells and Attenuates Injury-Induced Neointimal Hyperplasia', *Alcoholism: Clinical and Experimental Research*. Alcohol Clin Exp Res, 44(9), pp. 1734–1746. doi: 10.1111/acer.14415.

Liu, Y. *et al.* (2017) 'Endothelial microparticles activate endothelial cells to facilitate the inflammatory response', *Molecular Medicine Reports*. Spandidos Publications, 15(3), pp. 1291–1296. doi: 10.3892/mmr.2017.6113.

Lobb, R. J. *et al.* (2015) 'Optimized exosome isolation protocol for cell culture supernatant and human plasma', *Journal of Extracellular Vesicles*. Taylor & Francis, 4(1). doi: 10.3402/jev.v4.27031.

Lopes, R. M. *et al.* (2011) 'Diagnostic model based on Raman spectra of normal, hyperplasia and prostate adenocarcinoma tissues in vitro', *Spectroscopy*, 25(2), pp. 89–102. doi: 10.3233/SPE-2011-0494.

Lorenz, M. W. *et al.* (2007) 'Prediction of clinical cardiovascular events with carotid intima-media thickness: A systematic review and meta-analysis', *Circulation*. Circulation, 115(4), pp. 459–467. doi: 10.1161/CIRCULATIONAHA.106.628875.

Louvi, A. and Artavanis-Tsakonas, S. (2012) 'Notch and disease: A growing field', *Seminars in Cell and Developmental Biology*. doi: 10.1016/j.semcdb.2012.02.005.

Loyer, X. *et al.* (2018) 'Intra-cardiac release of extracellular vesicles shapes inflammation following myocardial infarction short communication', *Circulation Research*. Lippincott Williams and Wilkins, 123(1), pp. 100–106. doi: 10.1161/CIRCRESAHA.117.311326.

Lu, Y. *et al.* (2013) 'Endothelial microparticles exert differential effects on functions of Th1 in patients with acute coronary syndrome', *International Journal of Cardiology*. Int J Cardiol, 168(6), pp. 5396–5404. doi: 10.1016/j.ijcard.2013.08.050.

Luca, M. Di *et al.* (2018) 'Characterisation of resident multipotent vascular stem cells (MVSCS) from susceptible and non-susceptible arteriosclerotic regions of the mouse aorta', *Heart*. BMJ Publishing Group Ltd and British Cardiovascular Society, 104(Suppl 4), pp. A10–A10. doi: 10.1136/heartjnl-2018-scf.25.

Di Luca, M. *et al.* (2021) 'The Calcium Binding Protein S100β Marks Hedgehog-Responsive Perivascular Stem Cells That Contribute to Intimal Thickening Following Iatrogenic Flow Restriction', *npj Regenerative Medicine*. Nature Publishing Group, 6(10), pp. 2059–2071. doi: 10.2139/ssrn.3599853.

Lugli, G. *et al.* (2015) 'Plasma exosomal miRNAs in persons with and without Alzheimer disease: Altered expression and prospects for biomarkers', *PLoS ONE*. Public Library of Science, 10(10), p. e0139233. doi: 10.1371/journal.pone.0139233.

Ma, Y. *et al.* (2021) 'Extracellular Vesicles: An Emerging Nanoplatform for Cancer Therapy', *Frontiers in Oncology*. Frontiers, p. 3340. doi: 10.3389/fonc.2020.606906.

Maalouf, R. M. *et al.* (2012) 'Nox4-derived reactive oxygen species mediate cardiomyocyte injury in early type 1 diabetes', *American Journal of Physiology - Cell Physiology*. American Physiological Society, 302(3), p. C597. doi: 10.1152/ajpcell.00331.2011.

Maas, S. L. N., Breakefield, X. O. and Weaver, A. M. (2017) 'Extracellular Vesicles: Unique Intercellular Delivery Vehicles', *Trends in Cell Biology*. Elsevier Ltd, pp. 172–188. doi: 10.1016/j.tcb.2016.11.003.

MacGrogan, D., Luxán, G. and de la Pompa, J. L. (2014) 'Genetic and functional genomics approaches targeting the Notch pathway in cardiac development and congenital heart disease.', *Briefings in functional genomics*. Brief Funct Genomics, pp. 15–27. doi: 10.1093/bfgp/elt036.

Machida, T. *et al.* (2015) 'MicroRNAs in salivary exosome as potential biomarkers of aging', *International Journal of Molecular Sciences*. doi: 10.3390/ijms160921294.

Madison, M. N., Jones, P. H. and Okeoma, C. M. (2015) 'Exosomes in human semen restrict HIV-1 transmission by vaginal cells and block intravaginal replication of LP-BM5 murine AIDS virus complex', *Virology*. doi: 10.1016/j.virol.2015.03.040.

Majesky, M. W. *et al.* (2017) 'Differentiated Smooth Muscle Cells Generate a Subpopulation of Resident Vascular Progenitor Cells in the Adventitia Regulated by Klf4.', *Circulation research*. NIH Public Access, 120(2), pp. 296–311. doi: 10.1161/CIRCRESAHA.116.309322.

Majesky, M. W. W. and W., M. M. (2007) *Developmental basis of vascular smooth*

muscle diversity, *Arteriosclerosis, Thrombosis, and Vascular Biology*. Arterioscler Thromb Vasc Biol. doi: 10.1161/ATVBAHA.107.141069.

Malik, Z. A. *et al.* (2013) 'Cardiac myocyte exosomes: Stability, HSP60, and proteomics', *American Journal of Physiology - Heart and Circulatory Physiology*. Am J Physiol Heart Circ Physiol, 304(7). doi: 10.1152/ajpheart.00835.2012.

Mallat, Z. *et al.* (1999) 'Shed membrane microparticles with procoagulant potential in human atherosclerotic plaques: A role for apoptosis in plaque thrombogenicity', *Circulation*. doi: 10.1161/01.CIR.99.3.348.

Mallat, Z. *et al.* (2000) 'Elevated levels of shed membrane microparticles with procoagulant potential in the peripheral circulating blood of patients with acute coronary syndromes', *Circulation*. doi: 10.1161/01.CIR.101.8.841.

Mallone, A. *et al.* (2020) 'Human induced pluripotent stem cell-derived arteries as personalized models of atherosclerosis on-a-chip', *bioRxiv*, p. 2020.11.27.401034. doi: 10.1101/2020.11.27.401034.

Marigo, V. and Tabin, C. J. (1996) 'Regulation of patched by Sonic hedgehog in the developing neural tube', *Proceedings of the National Academy of Sciences of the United States of America*. National Academy of Sciences, 93(18), pp. 9346–9351. doi: 10.1073/pnas.93.18.9346.

Marzec, K. M. *et al.* (2015) 'Vascular diseases investigated ex vivo by using Raman, FT-IR and complementary methods', *Pharmacological Reports*. Pharmacol Rep, pp. 744–750. doi: 10.1016/j.pharep.2015.05.001.

Massagué, J., Seoane, J. and Wotton, D. (2005) 'Smad transcription factors', *Genes and Development*. Genes Dev, pp. 2783–2810. doi: 10.1101/gad.1350705.

Mastoridis, S. *et al.* (2018) 'Multiparametric analysis of circulating exosomes and other small extracellular vesicles by advanced imaging flow cytometry', *Frontiers in Immunology*. Frontiers Media SA, 9(JUL), p. 1583. doi: 10.3389/fimmu.2018.01583.

Masyuk, A. I., Masyuk, T. V. and Larusso, N. F. (2013) 'Exosomes in the pathogenesis, diagnostics and therapeutics of liver diseases', *Journal of Hepatology*. doi: 10.1016/j.jhep.2013.03.028.

Mathivanan, S. and Simpson, R. J. (2009) 'ExoCarta: A compendium of exosomal proteins and RNA', *Proteomics*. doi: 10.1002/pmic.200900351.

Matsumoto, J. *et al.* (2018) 'The Transport Mechanism of Extracellular Vesicles at the Blood-Brain Barrier', *Current Pharmaceutical Design*. doi: 10.2174/1381612823666170913164738.

Matsumoto, S. *et al.* (2013) 'Circulating p53-responsive MicroRNAs are predictive indicators of heart failure after acute myocardial infarction', *Circulation Research*. doi: 10.1161/CIRCRESAHA.113.301209.

Matusek, T. *et al.* (2014) 'The ESCRT machinery regulates the secretion and long-range activity of Hedgehog', *Nature*. Nature Publishing Group, 516(729), pp. 99–103. doi: 10.1038/nature13847.

McGill, H. C. *et al.* (2001) 'Effects of nonlipid risk factors on atherosclerosis in youth with a favorable lipoprotein profile', *Circulation*. Circulation, 103(11), pp. 1546–1550. doi: 10.1161/01.CIR.103.11.1546.

McGinn, S. *et al.* (2003) 'High glucose-mediated effects on endothelial cell proliferation occur via p38 MAP kinase', *American Journal of Physiology - Endocrinology and Metabolism*. Am J Physiol Endocrinol Metab, 285(4 48-4). doi: 10.1152/ajpendo.00572.2002.

McGough, I. J. and Vincent, J.-P. (2016) 'Exosomes in developmental signalling', *Development*. doi: 10.1242/dev.126516.

Meister, M. *et al.* (2017) 'Regulation of cargo transfer between ESCRT-0 and ESCRT-I complexes by flotillin-1 during endosomal sorting of ubiquitinated cargo', *Oncogenesis*. doi: 10.1038/oncsis.2017.47.

Meldolesi, J. (2018) 'Exosomes and Ectosomes in Intercellular Communication', *Current Biology*. doi: 10.1016/j.cub.2018.01.059.

Meng, W. and Takeichi, M. (2009) 'Adherens Junction: Molecular Architecture and Regulation', *Cold Spring Harbor Perspectives in Biology*, 1(6), p. a002899.

Meng, Y. *et al.* (2021) 'Microfluidics for extracellular vesicle separation and mimetic synthesis: Recent advances and future perspectives', *Chemical Engineering Journal*. Elsevier, 404, p. 126110. doi: 10.1016/J.CEJ.2020.126110.

Mentkowski, K. I. *et al.* (2018) 'Therapeutic Potential of Engineered Extracellular Vesicles', *AAPS Journal*. AAPS J. doi: 10.1208/s12248-018-0211-z.

Messenger, S. W. *et al.* (2018) 'A Ca2+-stimulated exosome release pathway in cancer cells is regulated by Munc13-4.', *The Journal of cell biology*. Rockefeller University Press, 217(8), pp. 2877–2890. doi: 10.1083/jcb.201710132.

Meuwese, M. C. *et al.* (2007) 'Serum Myeloperoxidase Levels Are Associated With the Future Risk of Coronary Artery Disease in Apparently Healthy Individuals. The EPIC-Norfolk Prospective Population Study', *Journal of the American College of Cardiology*. J Am Coll Cardiol, 50(2), pp. 159–165. doi: 10.1016/j.jacc.2007.03.033.

Meza, C. A. *et al.* (2019) 'Endothelial dysfunction: Is there a hyperglycemia-induced

imbalance of NOX and NOS?', *International Journal of Molecular Sciences*. MDPI AG, p. 3775. doi: 10.3390/ijms20153775.

Michael, M. Z., Gleadle, J. M. and King, H. W. (2012) 'Hypoxic enhancement of exosome release by breast cancer cells', *BMC Cancer*. doi: 10.1186/1471-2407-12-421.

Miwa, H. and Era, T. (2018) 'Tracing the destiny of mesenchymal stem cells from embryo to adult bone marrow and white adipose tissue via pdgfrα expression', *Development (Cambridge)*. Development, 145(2). doi: 10.1242/dev.155879.

Molony, C. *et al.* (2018) 'Label-free discrimination analysis of de-differentiated vascular smooth muscle cells, mesenchymal stem cells and their vascular and osteogenic progeny using vibrational spectroscopy', *Biochimica et Biophysica Acta - Molecular Cell Research*. doi: 10.1016/j.bbamcr.2017.11.006.

Molony, C. *et al.* (2021) 'Disease-Relevant Single Cell Photonic Signatures Identify S100β Stem Cells and their Myogenic Progeny in Vascular Lesions', *Stem Cell Reviews and Reports*. Springer, pp. 1–28. doi: 10.1007/s12015-021-10125-x.

Monici, M. (2005) 'Cell and tissue autofluorescence research and diagnostic applications', *Biotechnology Annual Review*. Biotechnol Annu Rev, pp. 227–256. doi: 10.1016/S1387-2656(05)11007-2.

Monopoli, M. P. *et al.* (2018) 'Endogenous exosome labelling with an amphiphilic NIR-fluorescent probe', *Chemical Communications*. The Royal Society of Chemistry, 54(52), pp. 7219–7222. doi: 10.1039/C8CC02135J.

Del Monte, G. *et al.* (2011) 'Differential notch signaling in the epicardium is required for cardiac inflow development and coronary vessel morphogenesis', *Circulation Research*. Circ Res, 108(7), pp. 824–836. doi: 10.1161/CIRCRESAHA.110.229062.

Montecalvo, A. *et al.* (2012) 'Mechanism of transfer of functional microRNAs between mouse dendritic cells via exosomes', *Blood*. doi: 10.1182/blood-2011-02-338004.

Mooney, C. J. *et al.* (2015) 'Hedgehog and Resident Vascular Stem Cell Fate', *Stem Cells International*, 2015, pp. 1–16. doi: 10.1155/2015/468428.

Morales-Kastresana, A. *et al.* (2017) 'Labeling extracellular vesicles for nanoscale flow cytometry', *Scientific Reports*. Nature Publishing Group, 7(1), pp. 1–10. doi: 10.1038/s41598-017-01731-2.

Morelli, A. E. *et al.* (2004) 'Endocytosis, intracellular sorting, and processing of exosomes by dendritic cells', *Blood*. doi: 10.1182/blood-2004-03-0824.

Morrow, D., Sweeney, C., *et al.* (2005) 'Cyclic Strain Inhibits Notch Receptor Signaling in Vascular Smooth Muscle Cells In Vitro', *Circulation research*, 96(5), pp.

567–575.

Morrow, D., Scheller, A., *et al.* (2005) ‘Notch-mediated CBF-1/RBP-Jκ-dependent regulation of human vascular smooth muscle cell phenotype in vitro’, *American Journal of Physiology - Cell Physiology*. Am J Physiol Cell Physiol, 289(5 58-5), pp. C1188--C1196. doi: 10.1152/ajpcell.00198.2005.

Morrow, D. *et al.* (2007) ‘Cyclic strain regulates the Notch/CBF-1 signaling pathway in endothelial cells: Role in angiogenic activity’, *Arteriosclerosis, Thrombosis, and Vascular Biology*. doi: 10.1161/ATVBAHA.107.142778.

Morrow, D. *et al.* (2009) ‘Sonic Hedgehog induces Notch target gene expression in vascular smooth muscle cells via VEGF-A.’, *Arteriosclerosis, thrombosis, and vascular biology*, 29(7), pp. 1112–1118. doi: 10.1161/ATVBAHA.109.186890.

Muhammad, L. J., Algehyne, E. A. and Usman, S. S. (2020) ‘Predictive Supervised Machine Learning Models for Diabetes Mellitus’, *SN Computer Science*. Nature Publishing Group, 1(5), p. 240. doi: 10.1007/s42979-020-00250-8.

Murali, N. *et al.* (2020) ‘Supervised Machine Learning in Oncology: A Clinician’s Guide’, *Digestive Disease Interventions*. NIH Public Access, 04(01), pp. 073–081. doi: 10.1055/s-0040-1705097.

Muralidharan-Chari, V. *et al.* (2010) ‘Microvesicles: mediators of extracellular communication during cancer progression’, *Journal of Cell Science*. doi: 10.1242/jcs.064386.

Myszczynska, M. A. *et al.* (2020) ‘Applications of machine learning to diagnosis and treatment of neurodegenerative diseases’, *Nature Reviews Neurology*. Nature Publishing Group, pp. 440–456. doi: 10.1038/s41582-020-0377-8.

Nakagawa, K. and Nakashima, Y. (2018) ‘Pathologic intimal thickening in human atherosclerosis is formed by extracellular accumulation of plasma-derived lipids and dispersion of intimal smooth muscle cells’, *Atherosclerosis*. Elsevier Ireland Ltd, 274, pp. 235–242. doi: 10.1016/j.atherosclerosis.2018.03.039.

Nakajima, Y. *et al.* (2000) ‘Mechanisms involved in valvuloseptal endocardial cushion formation in early cardiogenesis: Roles of transforming growth factor (TGF)-β and bone morphogenetic protein (BMP)’, *Anatomical Record*, pp. 119–127. doi: 10.1002/(SICI)1097-0185(20000201)258:2<119::AID-AR1>3.0.CO;2-U.

Nakashima, Y., Wight, T. N. and Sueishi, K. (2008) ‘Early atherosclerosis in humans: Role of diffuse intimal thickening and extracellular matrix proteoglycans’, *Cardiovascular Research*. Cardiovasc Res, pp. 14–23. doi: 10.1093/cvr/cvn099.

Nam, D. *et al.* (2009) 'Partial carotid ligation is a model of acutely induced disturbed flow, leading to rapid endothelial dysfunction and atherosclerosis', 297(4), pp. H1535–H1543. doi: 10.1152/ajpheart.00510.2009.

Nanbo, A. *et al.* (2013) 'Exosomes Derived from Epstein-Barr Virus-Infected Cells Are Internalized via Caveola-Dependent Endocytosis and Promote Phenotypic Modulation in Target Cells', *Journal of Virology*. doi: 10.1128/jvi.01310-13.

Narayanan, A. S. *et al.* (1976) 'The smooth muscle cell: III. Elastin synthesis in arterial smooth muscle cell culture.', *Journal of Cell Biology*. The Rockefeller University Press, 68(3), pp. 411–419. doi: 10.1083/jcb.68.3.411.

Naseri, Z. *et al.* (2018) 'Exosome-mediated delivery of functionally active miRNA-142-3p inhibitor reduces tumorigenicity of breast cancer in vitro and in vivo', *International Journal of Nanomedicine*. Int J Nanomedicine, 13, pp. 7727–7747. doi: 10.2147/IJN.S182384.

Navickas, R. *et al.* (2016) 'Identifying circulating microRNAs as biomarkers of cardiovascular disease: A systematic review', *Cardiovascular Research*. Cardiovasc Res, 111(4), pp. 322–337. doi: 10.1093/cvr/cvw174.

Ndrepepa, G. *et al.* (2008) 'Myeloperoxidase level in patients with stable coronary artery disease and acute coronary syndromes', *European Journal of Clinical Investigation*. Eur J Clin Invest, 38(2), pp. 90–96. doi: 10.1111/j.1365-2362.2007.01908.x.

Newman, A. A. *et al.* (2018) 'Irradiation abolishes smooth muscle investment into vascular lesions in specific vascular beds', *JCI insight*. NLM (Medline), 3(15). doi: 10.1172/jci.insight.121017.

Nguyen, A. T. *et al.* (2013) 'Smooth Muscle Cell Plasticity', *Circulation research*, 112(1), pp. 17–22.

Nie, D. M. *et al.* (2016) 'Endothelial microparticles carrying hedgehog-interacting protein induce continuous endothelial damage in the pathogenesis of acute graft-versus-host disease', *American Journal of Physiology - Cell Physiology*. American Physiological Society, 310(10), pp. C821–C835. doi: 10.1152/ajpcell.00372.2015.

Niu, C. *et al.* (2019) 'Metformin alleviates hyperglycemia-induced endothelial impairment by downregulating autophagy via the Hedgehog pathway', *Autophagy*. Taylor & Francis, 15(5), p. 843. doi: 10.1080/15548627.2019.1569913.

Noman, A. S. *et al.* (2017) 'Serum sonic hedgehog (SHH) and interleukin-(IL-6) as dual prognostic biomarkers in progressive metastatic breast cancer', *Scientific Reports*. Nature Publishing Group, 7(1). doi: 10.1038/S41598-017-01268-4.

Noordzij, M. J. *et al.* (2012) 'Skin autofluorescence is increased in patients with carotid artery stenosis and peripheral artery disease', *International Journal of Cardiovascular Imaging*. Int J Cardiovasc Imaging, 28(2), pp. 431–438. doi: 10.1007/s10554-011-9805-6.

Nozaki, T. *et al.* (2009) 'Significance of a Multiple Biomarkers Strategy Including Endothelial Dysfunction to Improve Risk Stratification for Cardiovascular Events in Patients at High Risk for Coronary Heart Disease', *Journal of the American College of Cardiology*. doi: 10.1016/j.jacc.2009.05.022.

Ono, R. *et al.* (2019) 'Exosome-mediated horizontal gene transfer occurs in double-strand break repair during genome editing', *Communications Biology*. Nature Publishing Group, 2(1), pp. 1–8. doi: 10.1038/s42003-019-0300-2.

Osteikoetxea, X. *et al.* (2015) 'Differential detergent sensitivity of extracellular vesicle subpopulations', *Organic and Biomolecular Chemistry*, 13(38), pp. 9775–9782. doi: 10.1039/c5ob01451d.

Ostrowski, M. *et al.* (2010) 'Rab27a and Rab27b control different steps of the exosome secretion pathway', *Nature Cell Biology*. doi: 10.1038/ncb2000.

Otero-Cacho, A. *et al.* (2018) 'Determination of hemodynamic risk for vascular disease in planar artery bifurcations', *Scientific Reports*. Nature Publishing Group, 8(1), pp. 1–7. doi: 10.1038/s41598-018-21126-1.

Owens, G. K. (1995) 'Regulation of differentiation of vascular smooth muscle cells', *Physiological Reviews*, 75(3), pp. 487–517.

Owens, G. K., Kumar, M. S. and Wamhoff, B. R. (2004) 'Molecular regulation of vascular smooth muscle cell differentiation in development and disease', *Physiological Reviews*. Physiol Rev, pp. 767–801. doi: 10.1152/physrev.00041.2003.

Pahlevaninezhad, H. *et al.* (2016) 'Endoscopic high-resolution autofluorescence imaging and OCT of pulmonary vascular networks', *Optics Letters*. Optical Society of America, 41(14), p. 3209. doi: 10.1364/ol.41.003209.

Palis, J., McGrath, K. E. and Kingsley, P. D. (1995) 'Initiation of hematopoiesis and vasculogenesis in murine yolk sac explants.', *Blood*, 86(1), pp. 156–63. Available at: http://www.ncbi.nlm.nih.gov/pubmed/7795222.

Palm, W. *et al.* (2013) 'Secretion and Signaling Activities of Lipoprotein-Associated Hedgehog and Non-Sterol-Modified Hedgehog in Flies and Mammals', *PLoS Biology*. Public Library of Science, 11(3), p. e1001505. doi: 10.1371/journal.pbio.1001505.

Pan, B. T. *et al.* (1985) 'Electron microscopic evidence for externalization of the transferrin receptor in vesicular form in sheep reticulocytes', *Journal of Cell Biology*. doi: 10.1083/jcb.101.3.942.

Pan, B. T. and Johnstone, R. M. (1983) 'Fate of the transferrin receptor during maturation of sheep reticulocytes in vitro: Selective externalization of the receptor', *Cell*. doi: 10.1016/0092-8674(83)90040-5.

Panáková, D. *et al.* (2005) 'Lipoprotein particles are required for Hedgehog and Wingless signalling', *Nature*. Nature, 435(7038), pp. 58–65. doi: 10.1038/nature03504.

Pang, L. *et al.* (2014) 'TGF-β1/Smad signaling, MMP-14, and MSC markers in arterial injury: Discovery of the molecular basis of restenosis', *International Journal of Clinical and Experimental Pathology*. E-Century Publishing Corporation, 7(6), pp. 2915–2924. Available at: www.ijcep.com/ (Accessed: 24 May 2021).

Papageorgiou, N. *et al.* (2016) 'Imaging Subclinical Atherosclerosis: Where Do We Stand?', *Current Cardiology Reviews*. Bentham Science Publishers, 13(1), pp. 47–55. doi: 10.2174/1573403x12666160803095855.

Parchure, A. *et al.* (2015) 'Oligomerization and endocytosis of Hedgehog is necessary for its efficient exovesicular secretion', *Molecular Biology of the Cell*. American Society for Cell Biology, 26(25), pp. 4700–4717. doi: 10.1091/mbc.E15-09-0671.

Passman, J. N. *et al.* (2008) 'A sonic hedgehog signaling domain in the arterial adventitia supports resident Sca1+ smooth muscle progenitor cells', *Proceedings of the National Academy of Sciences*. National Academy of Sciences, 105(27), pp. 9349–9354. doi: 10.1073/pnas.0711382105.

Patel, G. K. *et al.* (2019) 'Comparative analysis of exosome isolation methods using culture supernatant for optimum yield, purity and downstream applications', *Scientific Reports 2019 9:1*. Nature Publishing Group, 9(1), pp. 1–10. doi: 10.1038/s41598-019-41800-2.

Pearson, J. (1996) 'Endothelial cell control of vascular homeostasis', *Blood Coagulation & Fibrinolysis*, 7(7), p. 726.

Pence, I. and Mahadevan-Jansen, A. (2016) 'Clinical instrumentation and applications of Raman spectroscopy', *Chemical Society Reviews*. Royal Society of Chemistry, pp. 1958–1979. doi: 10.1039/c5cs00581g.

Pepinsky, R. B. *et al.* (1998) 'Identification of a palmitic acid-modified form of human Sonic hedgehog', *Journal of Biological Chemistry*. J Biol Chem, 273(22), pp. 14037–14045. doi: 10.1074/jbc.273.22.14037.

Perakis, S. *et al.* (2017) 'Emerging concepts in liquid biopsies', *BMC Medicine 2017 15:1*. BioMed Central, 15(1), pp. 1–12. doi: 10.1186/S12916-017-0840-6.

Peres, M. B. *et al.* (2011) 'Classification model based on Raman spectra of selected morphological and biochemical tissue constituents for identification of atherosclerosis in human coronary arteries', *Lasers in Medical Science*. Lasers Med Sci, 26(5), pp. 645–655. doi: 10.1007/s10103-011-0908-z.

Perfecto-Avalos, Y. *et al.* (2019) 'Discriminant analysis and machine learning approach for evaluating and improving the performance of immunohistochemical algorithms for COO classification of DLBCL', *Journal of Translational Medicine*. BioMed Central, 17(1), pp. 1–12. doi: 10.1186/s12967-019-1951-y.

Perrotta, I. and Aquila, S. (2016) 'Exosomes in human atherosclerosis: An ultrastructural analysis study', *Ultrastructural Pathology*. Ultrastruct Pathol, 40(2), pp. 101–106. doi: 10.3109/01913123.2016.1154912.

Peters, P. J. *et al.* (1989) 'Molecules relevant for T cell-target cell interaction are present in cytolytic granules of human T lymphocytes', *European Journal of Immunology*. doi: 10.1002/eji.1830190819.

Petrova, R. and Joyner, A. L. (2014) 'Roles for Hedgehog signaling in adult organ homeostasis and repair', *Development (Cambridge)*. doi: 10.1242/dev.083691.

Pfeffer, S. R. (2001) 'Rab GTPases: Specifying and deciphering organelle identity and function', *Trends in Cell Biology*. doi: 10.1016/S0962-8924(01)02147-X.

Pfeffer, S. R. (2007) 'Unsolved Mysteries in Membrane Traffic', *Annual Review of Biochemistry*. doi: 10.1146/annurev.biochem.76.061705.130002.

Pijanka, J. K. *et al.* (2010) 'Vibrational spectroscopy differentiates between multipotent and pluripotent stem cells', in *Analyst*. Analyst, pp. 3126–3132. doi: 10.1039/c0an00525h.

Pluskota, E. *et al.* (2008) 'Expression, activation, and function of integrin (mac-1) on neutrophil-derived microparticles', *Blood*. doi: 10.1182/blood-2007-12-127183.

Pocognoni, C. A., Berberián, M. V. and Mayorga, L. S. (2015) 'ESCRT (Endosomal Sorting Complex Required for Transport) Machinery Is Essential for Acrosomal Exocytosis in Human Sperm1', *Biology of Reproduction*. doi: 10.1095/biolreprod.115.132001.

Podbilewicz, B. (2014) 'Virus and Cell Fusion Mechanisms', *Annual Review of Cell and Developmental Biology*. doi: 10.1146/annurev-cellbio-101512-122422.

van der Pol, E. *et al.* (2012) 'Classification, Functions, and Clinical Relevance of Extracellular Vesicles', *Pharmacological Reviews*. doi: 10.1124/pr.112.005983.

van der Pol, E. *et al.* (2014) 'Particle size distribution of exosomes and microvesicles determined by transmission electron microscopy, flow cytometry, nanoparticle tracking analysis, and resistive pulse sensing', *Journal of Thrombosis and Haemostasis*. J Thromb Haemost, 12(7), pp. 1182–1192. doi: 10.1111/jth.12602.

Van Der Pol, E. *et al.* (2010) 'Optical and non-optical methods for detection and characterization of microparticles and exosomes', *Journal of Thrombosis and Haemostasis*. J Thromb Haemost, pp. 2596–2607. doi: 10.1111/j.1538-7836.2010.04074.x.

Polizio, A. H. *et al.* (2011) 'Heterotrimeric G i proteins link hedgehog signaling to activation of Rho small GTPases to promote fibroblast migration', *Journal of Biological Chemistry*. doi: 10.1074/jbc.M110.197111.

Pols, M. S. and Klumperman, J. (2009) 'Trafficking and function of the tetraspanin CD63', *Experimental Cell Research*. doi: 10.1016/j.yexcr.2008.09.020.

Popov, D. (2010) 'Endothelial cell dysfunction in hyperglycemia: Phenotypic change, intracellular signaling modification, ultrastructural alteration, and potential clinical outcomes', *International Journal of Diabetes Mellitus*. No longer published by Elsevier, pp. 189–195. doi: 10.1016/j.ijdm.2010.09.002.

Porter, J. A. *et al.* (1996) 'Hedgehog patterning activity: Role of a lipophilic modification mediated by the carboxy-terminal autoprocessing domain', *Cell*. Elsevier B.V., 86(1), pp. 21–34. doi: 10.1016/S0092-8674(00)80074-4.

Potente, M. and Mäkinen, T. (2017) 'Vascular heterogeneity and specialization in development and disease', *Nature Reviews Molecular Cell Biology*. Nature Publishing Group, pp. 477–494. doi: 10.1038/nrm.2017.36.

Potts, J. D. and Runyan, R. B. (1989) 'Epithelial-mesenchymal cell transformation in the embryonic heart can be mediated, in part, by transforming growth factor beta.', *Developmental biology*, 134(2), pp. 392–401. Available at: http://www.ncbi.nlm.nih.gov/pubmed/2744239 (Accessed: 24 June 2019).

Poursaleh, A. *et al.* (2019) 'Isolation of intimal endothelial cells from the human thoracic aorta: Study protocol', *Medical Journal of the Islamic Republic of Iran*. Iran University of Medical Sciences, 33(1), p. 51. doi: 10.34171/mjiri.33.51.

Pradhan, P. *et al.* (2020) 'Deep learning a boon for biophotonics?', *Journal of Biophotonics*. John Wiley & Sons, Ltd, 13(6), p. e201960186. doi: 10.1002/JBIO.201960186.

Psaltis, P. J. *et al.* (2012) 'Identification of a monocyte-predisposed hierarchy of hematopoietic progenitor cells in the adventitia of postnatal murine aorta', *Circulation*.

doi: 10.1161/CIRCULATIONAHA.111.059360.

Pugsley, M. K. and Tabrizchi, R. (2000) 'The vascular system: An overview of structure and function', *Journal of Pharmacological and Toxicological Methods*, 44(2), pp. 333–340. doi: 10.1016/S1056-8719(00)00125-8.

Qavi, A. J. *et al.* (2009) 'Label-Free Technologies for Quantitative Multiparameter Biological Analysis', *Analytical and bioanalytical chemistry*. NIH Public Access, 394(1), p. 121. doi: 10.1007/S00216-009-2637-8.

Qian, S. *et al.* (2021) 'Remnant Cholesterol and Common Carotid Artery Intima-Media Thickness in Patients With Ischemic Stroke', *Circulation: Cardiovascular Imaging*. Ovid Technologies (Wolters Kluwer Health). doi: 10.1161/circimaging.120.010953.

Qin, W. *et al.* (2016) 'Exosomes in human breast milk promote EMT', *Clinical Cancer Research*. doi: 10.1158/1078-0432.CCR-16-0135.

Qiu, H. *et al.* (2018) 'Proteomic Profiling Exosomes from Vascular Smooth Muscle Cell', *Proteomics - Clinical Applications*. Proteomics Clin Appl, 12(5). doi: 10.1002/prca.201700097.

Quagliaro, L. *et al.* (2003) 'Intermittent High Glucose Enhances Apoptosis Related to Oxidative Stress in Human Umbilical Vein Endothelial Cells: The Role of Protein Kinase C and NAD(P)H-Oxidase Activation', *Diabetes*. Diabetes, 52(11), pp. 2795–2804. doi: 10.2337/diabetes.52.11.2795.

Raiborg, C. and Stenmark, H. (2009) 'The ESCRT machinery in endosomal sorting of ubiquitylated membrane proteins.', *Nature*. doi: 10.1038/nature07961.

Rajapakse, A. G. *et al.* (2009) 'The hexosamine biosynthesis inhibitor azaserine prevents endothelial inflammation and dysfunction under hyperglycemic condition through antioxidant effects', *American Journal of Physiology - Heart and Circulatory Physiology*. Am J Physiol Heart Circ Physiol, 296(3). doi: 10.1152/ajpheart.00756.2008.

Ranjit, S. *et al.* (2015) 'Imaging Fibrosis and Separating Collagens using Second Harmonic Generation and Phasor Approach to Fluorescence Lifetime Imaging', 5(1), pp. 1–10. Available at: https://pubmed.ncbi.nlm.nih.gov/26293987/ (Accessed: 13 July 2021).

Raposo, G. *et al.* (1996) 'B lymphocytes secrete antigen-presenting vesicles', *Journal of Experimental Medicine*. doi: 10.1084/jem.183.3.1161.

Raposo, G. and Stoorvogel, W. (2013) 'Extracellular vesicles: Exosomes, microvesicles, and friends', *Journal of Cell Biology*. doi: 10.1083/jcb.201211138.

Ravikumar, B. *et al.* (2010) 'Regulation of mammalian autophagy in physiology and pathophysiology', *Physiological Reviews*. Physiol Rev, pp. 1383–1435. doi:

10.1152/physrev.00030.2009.

Razi, M. (2006) 'Distinct Roles for Tsg101 and Hrs in Multivesicular Body Formation and Inward Vesiculation', *Molecular Biology of the Cell*. doi: 10.1091/mbc.e05-11-1054.

Record, M. *et al.* (2011) 'Exosomes as intercellular signalosomes and pharmacological effectors', *Biochemical Pharmacology*. doi: 10.1016/j.bcp.2011.02.011.

Record, M. (2013) 'Exosomal lipids in cell-cell communication', in *Emerging Concepts of Tumor Exosome-Mediated Cell-Cell Communication*. doi: 10.1007/978-1-4614-3697-3_3.

Redheuil, A. *et al.* (2010) 'Reduced ascending aortic strain and distensibility: Earliest manifestations of vascular aging in humans', *Hypertension*. Lippincott Williams & Wilkins, 55(2), pp. 319–326. doi: 10.1161/HYPERTENSIONAHA.109.141275.

Redmond, E. M. *et al.* (2013) 'Inhibition of patched-1 prevents injury-induced neointimal hyperplasia', *Arteriosclerosis, Thrombosis, and Vascular Biology*. Lippincott Williams & WilkinsHagerstown, MD, 33(8), pp. 1960–1964. doi: 10.1161/ATVBAHA.113.301843.

Reinert, R. B. *et al.* (2012) 'Tamoxifen-induced cre-loxp recombination is prolonged in pancreatic islets of adult mice', *PLoS ONE*. Edited by K. Maedler. PLoS One, 7(3), p. e33529. doi: 10.1371/journal.pone.0033529.

Rensen, S. S. M., Doevendans, P. A. F. M. and Van Eys, G. J. J. M. (2007) 'Regulation and characteristics of vascular smooth muscle cell phenotypic diversity', *Netherlands Heart Journal*. Bohn Stafleu van Loghum, pp. 100–108. doi: 10.1007/BF03085963.

Revenfeld, A. L. S. *et al.* (2014) 'Diagnostic and prognostic potential of extracellular vesicles in peripheral blood', *Clinical Therapeutics*. Elsevier, pp. 830–846. doi: 10.1016/j.clinthera.2014.05.008.

Rezende, F. *et al.* (2018) 'The NADPH organizers NoxO1 and p47phox are both mediators of diabetes-induced vascular dysfunction in mice', *Redox Biology*. Elsevier B.V., 15, pp. 12–21. doi: 10.1016/j.redox.2017.11.014.

Ribeiro-Rodrigues, T. M. *et al.* (2017) 'Exosomes secreted by cardiomyocytes subjected to ischaemia promote cardiac angiogenesis', *Cardiovascular Research*. Oxford University Press, 113(11), pp. 1338–1350. doi: 10.1093/cvr/cvx118.

Rice, W. L., Kaplan, D. L. and Georgakoudi, I. (2007) 'Quantitative biomarkers of stem cell differentiation based on intrinsic two-photon excited fluorescence', *Journal of Biomedical Optics*. International Society for Optics and Photonics, 12(6), p. 060504. doi: 10.1117/1.2823019.

Ridger, V. C. *et al.* (2017) 'Microvesicles in vascular homeostasis and diseases',

Thrombosis and Haemostasis. doi: 10.1160/th16-12-0943.

Ries, W. *et al.* (2021) 'C-Reactive Protein Apheresis as Anti-inflammatory Therapy in Acute Myocardial Infarction: Results of the CAMI-1 Study', *Frontiers in Cardiovascular Medicine*. Frontiers Media SA, 8. doi: 10.3389/fcvm.2021.591714.

Al Rifai, M. *et al.* (2018) 'The prevalence and correlates of subclinical atherosclerosis among adults with low-density lipoprotein cholesterol', *Atherosclerosis*. Atherosclerosis, 274, pp. 61–66. doi: 10.1016/j.atherosclerosis.2018.04.021.

Riha, G. M. *et al.* (2005) 'Roles of hemodynamic forces in vascular cell differentiation', *Annals of Biomedical Engineering*, 33(6), pp. 772–779. doi: 10.1007/s10439-005-3310-9.

Robbins, P. D., Dorronsoro, A. and Booker, C. N. (2016) 'Regulation of chronic inflammatory and immune processes by extracellular vesicles', *Journal of Clinical Investigation*. J Clin Invest, pp. 1173–1180. doi: 10.1172/JCI81131.

Robbins, P. D. and Morelli, A. E. (2014) 'Regulation of immune responses by extracellular vesicles', *Nature Reviews Immunology 2014 14:3*. Nature Publishing Group, 14(3), pp. 195–208. doi: 10.1038/nri3622.

Rogers, M. A. *et al.* (2020) Annexin A1-dependent tethering promotes extracellular vesicle aggregation revealed with single-extracellular vesicle analysis, *Sci. Adv*. Available at: http://advances.sciencemag.org/ (Accessed: 28 May 2021).

Rogers, R. G. *et al.* (2020) 'Extracellular Vesicles as Therapeutic Agents for Cardiac Fibrosis', *Frontiers in Physiology*. Frontiers, p. 479. doi: 10.3389/fphys.2020.00479.

Roostalu, U. *et al.* (2018) 'Distinct cellular mechanisms underlie smooth muscle turnover in vascular development and repair', *Circulation Research*. Lippincott Williams and Wilkins, 122(2), pp. 267–281. doi: 10.1161/CIRCRESAHA.117.312111.

Ross, R. (1999) 'Atherosclerosis An Inflammatory Disease', *The New England journal of medicine*, 340(2), pp. 115–126.

Ross, R. and Glomset, J. A. (1973) 'Atherosclerosis and the arterial smooth muscle cell', *Science*. American Association for the Advancement of Science, pp. 1332–1339. doi: 10.1126/science.180.4093.1332.

Ruddy, J. M. *et al.* (2008) 'Regional heterogeneity within the aorta: Relevance to aneurysm disease', *Journal of Thoracic and Cardiovascular Surgery*. J Thorac Cardiovasc Surg, 136(5), pp. 1123–1130. doi: 10.1016/j.jtcvs.2008.06.027.

Sada, K. *et al.* (2016) 'Hyperglycemia induces cellular hypoxia through production of mitochondrial ROS followed by suppression of aquaporin-1', *PLoS ONE*. doi: 10.1371/journal.pone.0158619.

Sáez, T. *et al.* (2019) 'Exosomes derived from monocytes and from endothelial cells mediate monocyte and endothelial cell activation under high D-glucose conditions', *Immunobiology*. doi: 10.1016/j.imbio.2019.02.004.

Sainz, J. *et al.* (2006) 'Isolation of "Side Population" Progenitor Cells From Healthy Arteries of Adult Mice', *Arteriosclerosis, Thrombosis, and Vascular Biology*. Lippincott Williams & Wilkins, 26(2), pp. 281–286. doi: 10.1161/01.ATV.0000197793.83391.91

Sakamoto, A. *et al.* (2018) *Pathologic intimal thickening: Are we any closer to understand early transitional plaques that lead to symptomatic disease?*, *Atherosclerosis*. Atherosclerosis. doi: 10.1016/j.atherosclerosis.2018.04.033.

Sanan, D. A. *et al.* (1998) 'Low density lipoprotein receptor-negative mice expressing human apolipoprotein B-100 develop complex atherosclerotic lesions on a chow diet: No accentuation by apolipoprotein(a)', *Proceedings of the National Academy of Sciences of the United States of America*. National Academy of Sciences, 95(8), pp. 4544–4549. doi: 10.1073/pnas.95.8.4544.

Sanders, T. A., Llagostera, E. and Barna, M. (2013) 'Specialized filopodia direct long-range transport of SHH during vertebrate tissue patterning', *Nature*. Nature Publishing Group, 497(7451), pp. 628–632. doi: 10.1038/nature12157.

Sandoo, A. *et al.* (2010) 'The Endothelium and Its Role in Regulating Vascular Tone', *The Open Cardiovascular Medicine Journal*, 4(1), pp. 302–312.

Santos, A. *et al.* (2015) 'Cardiovascular imaging: What have we learned from animal models?', *Frontiers in Pharmacology*. Frontiers, p. 227. doi: 10.3389/fphar.2015.00227.

Sartore, S. *et al.* (2001) 'Contribution of Adventitial Fibroblasts to Neointima Formation and Vascular Remodeling', *Circulation Research*. Lippincott Williams & Wilkins, 89(12), pp. 1111–1121. doi: 10.1161/hh2401.100844.

Sata, M. *et al.* (2000) 'A mouse model of vascular injury that induces rapid onset of medial cell apoptosis followed by reproducible neointimal hyperplasia', *Journal of Molecular and Cellular Cardiology*. J Mol Cell Cardiol, 32(11), pp. 2097–2104. doi: 10.1006/jmcc.2000.1238.

Sata, M. (2003) 'Circulating Vascular Progenitor Cells Contribute to Vascular Repair, Remodeling, and Lesion Formation', *Trends in Cardiovascular Medicine*. Elsevier, 13(6), pp. 249–253. doi: 10.1016/S1050-1738(03)00106-3.

Sato, M. *et al.* (2008) 'Rab11 is required for synchronous secretion of chondroitin proteoglycans after fertilization in Caenorhabditis elegans', *Journal of Cell Science*. doi: 10.1242/jcs.034678.

Savina, A. *et al.* (2003) ‘Exosome release is regulated by a calcium-dependent mechanism in K562 cells’, *Journal of Biological Chemistry*. doi: 10.1074/jbc.M301642200.

Savina, A., Vidal, M. and Colombo, M. I. (2002) ‘The exosome pathway in K562 cells is regulated by Rab11.’, *Journal of cell science*.

Schiele, T. M. (2005) ‘Current understanding of coronary in-stent restenosis: Pathophysiology, clinical presentation, diagnostic work-up, and management’, *Zeitschrift fur Kardiologie*, pp. 772–790. doi: 10.1007/s00392-005-0299-x.

Schneeberger, E. E. and Lynch, R. D. (2004) ‘The tight junction: a multifunctional complex’, *American Journal of Physiology-Cell Physiology*, 286(6), pp. C1213--C1228.

Schunkert, H. *et al.* (2011) ‘Large-scale association analysis identifies 13 new susceptibility loci for coronary artery disease’, *Nature Genetics 2011 43:4*. Nature Publishing Group, 43(4), pp. 333–338. doi: 10.1038/ng.784.

Schwartz, S. M., DeBlois, D. and O’Brien, E. R. M. (1995) *The intima: Soil for atherosclerosis and restenosis*, *Circulation Research*. Lippincott Williams & Wilkins. doi: 10.1161/01.RES.77.3.445.

Sejersen, T. and Lendahl, U. (1993) ‘Transient expression of the intermediate filament nestin during skeletal muscle development’, *Journal of Cell Science*, 106(4), pp. 1291–1300. doi: 10.1242/jcs.106.4.1291.

Shankman, Laura S. *et al.* (2015) ‘KLF4-dependent phenotypic modulation of smooth muscle cells has a key role in atherosclerotic plaque pathogenesis’, *Nature Medicine*. doi: 10.1038/nm.3866.

Sheikh, A. Q., Lighthouse, J. K. and Greif, D. M. (2014) ‘Recapitulation of developing artery muscularization in pulmonary hypertension’, *Cell Reports*. Cell Rep, 6(5), pp. 809–817. doi: 10.1016/j.celrep.2014.01.042.

Sheldon, H. *et al.* (2010) ‘New mechanism for Notch signaling to endothelium at a distance by delta-like 4 incorporation into exosomes’, *Blood*. American Society of Hematology, 116(13), pp. 2385–2394. doi: 10.1182/blood-2009-08-239228.

Shen, L. *et al.* (2011) ‘Tight Junction Pore and Leak Pathways: A Dynamic Duo’, *Annual Review of Physiology*, 73(1), pp. 283–309. doi: 10.1146/annurev-physiol-012110-142150.

Sheu, M. L. *et al.* (2005) ‘High glucose induces human endothelial cell apoptosis through a phosphoinositide 3-kinase-regulated cyclooxygenase-2 pathway’, *Arteriosclerosis, Thrombosis, and Vascular Biology*. Lippincott Williams & Wilkins, 25(3), pp. 539–545. doi: 10.1161/01.ATV.0000155462.24263.e4.

Shi, Y. and Vanhoutte, P. M. (2017) ‘Macro- and microvascular endothelial dysfunction

in diabetes', *Journal of Diabetes*. John Wiley and Sons Inc., pp. 434–449. doi: 10.1111/1753-0407.12521.

Shields, S. B. *et al.* (2009) 'ESCRT ubiquitin-binding domains function cooperatively during MVB cargo sorting', *Journal of Cell Biology*. doi: 10.1083/jcb.200811130.

Shikatani, E. A. *et al.* (2016) 'C-Myb Regulates Proliferation and Differentiation of Adventitial Sca1+ Vascular Smooth Muscle Cell Progenitors by Transactivation of Myocardin', *Arteriosclerosis, Thrombosis, and Vascular Biology*. Lippincott Williams and Wilkins, 36(7), pp. 1367–1376. doi: 10.1161/ATVBAHA.115.307116.

Shimizu, K. *et al.* (2001) 'Host bone-marrow cells are a source of donor intimal smooth- muscle–like cells in murine aortic transplant arteriopathy', *Nature Medicine*. Nature Publishing Group, 7(6), pp. 738–741. doi: 10.1038/89121.

Shin, H., Seo, D. and Choi, Y. (2020) 'Extracellular Vesicle Identification Using Label-Free Surface-Enhanced Raman Spectroscopy: Detection and Signal Analysis Strategies', *Molecules (Basel, Switzerland)*. Multidisciplinary Digital Publishing Institute (MDPI). doi: 10.3390/molecules25215209.

Shin, M., Nagai, H. and Sheng, G. (2009) 'Notch mediates Wnt and BMP signals in the early separation of smooth muscle progenitors and blood/endothelial common progenitors', *Development*. Development, 136(4), pp. 595–603. doi: 10.1242/dev.026906.

Shioi, A. *et al.* (2002) 'Induction of bone-type alkaline phosphatase in human vascular smooth muscle cells: Roles of tumor necrosis factor-α and oncostatin M derived from macrophages', *Circulation Research*. Circ Res, 91(1), pp. 9–16. doi: 10.1161/01.RES.0000026421.61398.F2.

Simons, M. and Raposo, G. (2009) 'Exosomes - vesicular carriers for intercellular communication', *Current Opinion in Cell Biology*. Curr Opin Cell Biol, pp. 575–581. doi: 10.1016/j.ceb.2009.03.007.

Simpson, R. J. *et al.* (2009) 'Exosomes: Proteomic insights and diagnostic potential', *Expert Review of Proteomics*. doi: 10.1586/epr.09.17.

Simpson, R. J., Kalra, H. and Mathivanan, S. (2012) 'ExoCarta as a resource for exosomal research', *Journal of Extracellular Vesicles*. Wiley-Blackwell, 1(1). doi: 10.3402/JEV.V1I0.18374.

Simsek, S. *et al.* (2010) 'Endothelial dysfunction, inflammation, and apoptosis in diabetes mellitus', *Mediators of Inflammation*, 2010. doi: 10.1155/2010/792393.

Singh, S. S. *et al.* (2018) 'Subclinical atherosclerosis, cardiovascular health, and disease

risk: Is there a case for the Cardiovascular Health Index in the primary prevention population?', *BMC Public Health*, 18(1), p. 429. doi: 10.1186/s12889-018-5263-6.

Sinha, S. *et al.* (2016) 'Cortactin promotes exosome secretion by controlling branched actin dynamics', *Journal of Cell Biology*. doi: 10.1083/jcb.201601025.

Sinha, S., Iyer, D. and Granata, A. (2014) 'Embryonic origins of human vascular smooth muscle cells: Implications for in vitro modeling and clinical application', *Cellular and Molecular Life Sciences*. Birkhauser Verlag AG, pp. 2271–2288. doi: 10.1007/s00018-013-1554-3.

Skonieczna, M. *et al.* (2017) 'NADPH Oxidases (NOX): Insights into Selected Functions and Mechanisms of Action in Cancer and Stem Cells', *Oxidative Medicine and Cellular Longevity*, 2017(8411), pp. 9420515–9420539. doi: 10.1155/2017/9420539.

Sluijter, J. P. G. *et al.* (2014) 'Microvesicles and exosomes for intracardiac communication', *Cardiovascular Research*. doi: 10.1093/cvr/cvu022.

Sluijter, J. P. G. *et al.* (2018) 'Extracellular vesicles in diagnostics and therapy of the ischaemic heart: Position Paper from the Working Group on Cellular Biology of the Heart of the European Society of Cardiology', *Cardiovascular Research*. Oxford University Press, pp. 19–34. doi: 10.1093/cvr/cvx211.

Smith, R., Wright, K. L. and Ashton, L. (2016) 'Raman spectroscopy: An evolving technique for live cell studies', *Analyst*. The Royal Society of Chemistry, pp. 3590–3600. doi: 10.1039/c6an00152a.

Soldner, F. and Jaenisch, R. (2012) 'iPSC Disease Modeling', *Science*, 338(6111), pp. 1155–1156. doi: 10.1126/science.1227682.

Soleti, R. *et al.* (2009) 'Microparticles harboring Sonic Hedgehog promote angiogenesis through the upregulation of adhesion proteins and proangiogenic factors', *Carcinogenesis*. Oxford Academic, 30(4), pp. 580–588. doi: 10.1093/carcin/bgp030.

Song, Z. *et al.* (2017) 'Metformin suppresses the expression of Sonic hedgehog in gastric cancer cells', 15(4), pp. 1909–1915. doi: 10.3892/MMR.2017.6205.

Soung, Y. H. *et al.* (2017) 'Exosomes in cancer diagnostics', *Cancers*. doi: 10.3390/cancers9010008.

Squirrell, J. M. *et al.* (2012) 'Endogenous Fluorescence Signatures in Living Pluripotent Stem Cells Change with Loss of Potency', *PLoS ONE*. Public Library of Science, 7(8), p. e43708. doi: 10.1371/journal.pone.0043708.

Srivastava, P. (2002) 'Interaction of heat shock proteins with peptides and antigen presenting cells: chaperoning of the innate and adaptive immune responses.', *Annual*

review of immunology. doi: 10.1146/annurev.immunol.20.100301.064801.

Stary, H. C. (2000) 'Natural History and Histological Classification of Atherosclerotic Lesions', *Arteriosclerosis, Thrombosis, and Vascular Biology*. Lippincott Williams & Wilkins, 20(5), pp. 1177–1178. doi: 10.1161/01.ATV.20.5.1177.

Stenmark, H. (2009) 'Rab GTPases as coordinators of vesicle traffic', *Nature Reviews Molecular Cell Biology*. doi: 10.1038/nrm2728.

Stocker, R. and John F. Keaney, J. (2004) 'Role of Oxidative Modifications in Atherosclerosis', *https://doi.org/10.1152/physrev.00047.2003*. American Physiological Society, 84(4), pp. 1381–1478. doi: 10.1152/PHYSREV.00047.2003.

Street, J. M. *et al.* (2017) 'Urine Exosomes: An Emerging Trove of Biomarkers', in *Advances in Clinical Chemistry*. doi: 10.1016/bs.acc.2016.07.003.

Stuffers, S. *et al.* (2009) 'Multivesicular endosome biogenesis in the absence of ESCRTs', *Traffic*. doi: 10.1111/j.1600-0854.2009.00920.x.

Su, J. *et al.* (2018) 'Improvement of vascular dysfunction by argirein through inhibiting endothelial cell apoptosis associated with ET-1/Nox4 signal pathway in diabetic rats', *Scientific Reports*. Nature Publishing Group, 8(1), p. 12620. doi: 10.1038/s41598-018-30386-w.

Sukumar, P. *et al.* (2013) 'Nox2 NADPH oxidase has a critical role in insulin resistance-related endothelial cell dysfunction', *Diabetes*. Diabetes, 62(6), pp. 2130–2134. doi: 10.2337/db12-1294.

Sun, N. *et al.* (2012) 'Patient-specific induced pluripotent stem cells as a model for familial dilated cardiomyopathy', *Science Translational Medicine*. Sci Transl Med, 4(130). doi: 10.1126/scitranslmed.3003552.

Sunkara, V. *et al.* (2019) 'Fully automated, label-free isolation of extracellular vesicles from whole blood for cancer diagnosis and monitoring', *Theranostics*, 9(7), pp. 1851–1863. doi: 10.7150/thno.32438.

Svensson, K. J. *et al.* (2013) 'Exosome Uptake Depends on ERK1/2-Heat Shock Protein 27 Signaling and Lipid Raft-mediated Endocytosis Negatively Regulated by Caveolin-1', *Journal of Biological Chemistry*, 288(24), pp. 17713–17724. doi: 10.1074/jbc.M112.445403.

Takac, I. *et al.* (2011) 'The E-loop is involved in hydrogen peroxide formation by the NADPH oxidase Nox4', *Journal of Biological Chemistry*. American Society for Biochemistry and Molecular Biology, 286(15), pp. 13304–13313. doi: 10.1074/jbc.M110.192138.

Takahashi, K. *et al.* (2007) 'Induction of Pluripotent Stem Cells from Adult Human Fibroblasts by Defined Factors', *Cell*. Cell, 131(5), pp. 861–872. doi:

10.1016/j.cell.2007.11.019.

Takahashi, K. and Yamanaka, S. (2006) 'Induction of Pluripotent Stem Cells from Mouse Embryonic and Adult Fibroblast Cultures by Defined Factors', *Cell*. Cell, 126(4), pp. 663–676. doi: 10.1016/j.cell.2006.07.024.

Takahashi, S. *et al.* (2012) 'Rab11 regulates exocytosis of recycling vesicles at the plasma membrane', *Journal of Cell Science*. doi: 10.1242/jcs.102913.

Takasugi, M. (2018) 'Emerging roles of extracellular vesicles in cellular senescence and aging', *Aging Cell*. Blackwell Publishing Ltd. doi: 10.1111/acel.12734.

Takayama, T. *et al.* (2015) 'A murine model of arterial restenosis: Technical aspects of femoral wire injury', *Journal of Visualized Experiments*. J Vis Exp, 2015(97). doi: 10.3791/52561.

Tamai, K. *et al.* (2010) 'Exosome secretion of dendritic cells is regulated by Hrs, an ESCRT-0 protein', *Biochemical and Biophysical Research Communications*. doi: 10.1016/j.bbrc.2010.07.083.

Tan, E., Asada, H. H. and Ge, R. (2018) 'Extracellular vesicle-carried Jagged-1 inhibits HUVEC sprouting in a 3D microenvironment', *Angiogenesis*. Springer Netherlands, 21(3), pp. 571–580. doi: 10.1007/s10456-018-9609-6.

Tang, J. *et al.* (2020) 'Arterial Sca1+ Vascular Stem Cells Generate De Novo Smooth Muscle for Artery Repair and Regeneration', *Cell Stem Cell*. Cell Press, 26(1), pp. 81-96.e4. doi: 10.1016/j.stem.2019.11.010.

Tang, N. *et al.* (2016) 'Monocyte exosomes induce adhesion molecules and cytokines via activation of NF-κB in endothelial cells', *FASEB Journal*. doi: 10.1096/fj.201600368RR.

Tang, Z., Wang, A., Yuan, F., *et al.* (2012) 'Differentiation of multipotent vascular stem cells contributes to vascular diseases', *Nature Communications*. Nature Publishing Group, 3(1), pp. 1–13. doi: 10.1038/ncomms1867.

Tang, Z., Wang, A., Wang, D., *et al.* (2012) 'Smooth Muscle Cells: To Be or Not To Be?', *Circulation Research*, 112(1), pp. 23–26. doi: 10.1161/circresaha.112.281055.

Taniyama, Y. and Griendling, K. K. (2003) 'Reactive Oxygen Species in the Vasculature', *Hypertension*. Lippincott Williams & Wilkins, 42(6), pp. 1075–1081. doi: 10.1161/01.HYP.0000100443.09293.4F.

Tanthanuch, W. *et al.* (2010) 'Neural differentiation of mouse embryonic stem cells studied by FTIR spectroscopy', *Journal of Molecular Structure*, 967(1–3), pp. 189–195. doi: 10.1016/j.molstruc.2010.01.007.

Tauro, B. J. *et al.* (2013) 'Two Distinct Populations of Exosomes Are Released from LIM1863 Colon Carcinoma Cell-derived Organoids', *Molecular & Cellular Proteomics*. doi: 10.1074/mcp.m112.021303.

Taye, A. *et al.* (2010) 'Effect of apocynin on NADPH oxidase-mediated oxidative stress-LOX-1-eNOS pathway in human endothelial cells exposed to high glucose', *European Journal of Pharmacology*, 627(1–3), pp. 42–48. Available at: https://pubmed.ncbi.nlm.nih.gov/19878672/ (Accessed: 23 May 2021).

Tertel, T. and Giebel, B. (2020) 'Amnis ImageStream - Analysis of individual extracellular vesicles by imaging flow cytometry', *Cytotherapy*. Elsevier, 22(5), p. S55. doi: 10.1016/J.JCYT.2020.03.075.

van Tetering, G. and Vooijs, M. (2011) 'Proteolytic cleavage of Notch: "HIT and RUN".', *Current molecular medicine*, 11(4), pp. 255–69.

Théry, C. *et al.* (1999) 'Molecular characterization of dendritic cell-derived exosomes: Selective accumulation of the heat shock protein hsc73', *Journal of Cell Biology*. doi: 10.1083/jcb.147.3.599.

Théry, C. *et al.* (2001) 'Proteomic Analysis of Dendritic Cell-Derived Exosomes: A Secreted Subcellular Compartment Distinct from Apoptotic Vesicles', *The Journal of Immunology*. doi: 10.4049/jimmunol.166.12.7309.

Théry, C. *et al.* (2018) 'Minimal information for studies of extracellular vesicles 2018 (MISEV2018): a position statement of the International Society for Extracellular Vesicles and update of the MISEV2014 guidelines', *https://doi.org/10.1080/20013078.2018.1535750*. Taylor & Francis, 7(1). doi: 10.1080/20013078.2018.1535750.

Théry, C., Zitvogel, L. and Amigorena, S. (2002) 'Exosomes: Composition, biogenesis and function', *Nature Reviews Immunology*. doi: 10.1038/nri855.

Thimm, T. N. *et al.* (2015) 'Endogenous Optical Signals Reveal Changes of Elastin and Collagen Organization during Differentiation of Mouse Embryonic Stem Cells', *Tissue Engineering - Part C: Methods*. Mary Ann Liebert, Inc., 21(10), pp. 995–1004. doi: 10.1089/ten.tec.2014.0699.

Thormodsson, F. R. and Olafsson, I. H. (2005) 'Isolation and culturing of human vascular smooth muscle cells', in *Methods in Molecular Biology*. Methods Mol Biol, pp. 197–210. doi: 10.1385/1-59259-874-9:197.

Thum, T. *et al.* (2007) 'Endothelial Nitric Oxide Synthase Uncoupling Impairs Endothelial Progenitor Cell Mobilization and Function in Diabetes', *Diabetes*. American Diabetes Association, 56(3), pp. 666–674. doi: 10.2337/DB06-0699.

Tian, F. *et al.* (2021) 'Protein analysis of extracellular vesicles to monitor and predict therapeutic response in metastatic breast cancer', *Nature Communications 2021 12:1*. Nature Publishing Group, 12(1), pp. 1–13. doi: 10.1038/s41467-021-22913-7.

Tieu, B. C. *et al.* (no date) 'An adventitial IL-6/MCP1 amplification loop accelerates macrophage-mediated vascular inflammation leading to aortic dissection in mice', *Am Soc Clin Investig*.

Timmis, A. *et al.* (2018) 'European Society of Cardiology: Cardiovascular Disease Statistics 2017', *European Heart Journal*, 39(7), pp. 508–579. doi: 10.1093/eurheartj/ehx628.

Tintut, Y. *et al.* (2002) 'Monocyte/macrophage regulation of vascular calcification in vitro', *Circulation*. Circulation, 105(5), pp. 650–655. doi: 10.1161/hc0502.102969.

Tintut, Y. *et al.* (2003) 'Multilineage Potential of Cells From the Artery Wall', *Circulation*. Lippincott Williams & Wilkins, 108(20), pp. 2505–2510. doi: 10.1161/01.CIR.0000096485.64373.C5.

Tiwari, S. (2014) 'Oxidative Stress and Antioxidant Defense in Cells', *Global Journal For Research Analysis*, 3(8), pp. 11–14. doi: 10.15373/22778160/august2014/4.

Tokita, Y. *et al.* (2009) 'Utility of rapid D-dimer measurement for screening of acute cardiovascular disease in the emergency setting', *Journal of Cardiology*. J Cardiol, 53(3), pp. 334–340. doi: 10.1016/j.jjcc.2008.12.001.

Torsney, E., Hu, Y. and Xu, Q. (2005) 'Adventitial progenitor cells contribute to arteriosclerosis', *Trends in Cardiovascular Medicine*. Elsevier Inc., pp. 64–68. doi: 10.1016/j.tcm.2005.02.003.

Toschi, E. *et al.* (2002) 'Effect of acute hyperglycemia on insulin secretion in humans', in *Diabetes*. American Diabetes Association Inc., pp. S130–S133. doi: 10.2337/diabetes.51.2007.s130.

Toth, P. P. (2008) 'Subclinical atherosclerosis: What it is, what it means and what we can do about it', *International Journal of Clinical Practice*. John Wiley & Sons, Ltd, pp. 1246–1254. doi: 10.1111/j.1742-1241.2008.01804.x.

Townsend, N. M. *et al.* (2012) *European cardiovascular disease statistics 2012*. Available at: www.ehnheart.org (Accessed: 6 August 2021).

Trajkovic, K. *et al.* (2008) 'Ceramide triggers budding of exosome vesicles into multivesicular endosomes', *Science*. doi: 10.1126/science.1153124.

Tsai, T. N. *et al.* (2012) 'Contribution of stem cells to neointimal formation of decellularized vessel grafts in a novel mouse model', *American Journal of Pathology*.

Am J Pathol, 181(1), pp. 362–373. doi: 10.1016/j.ajpath.2012.03.021.

Tucher, C. *et al.* (2018) 'Extracellular Vesicle Subtypes Released From Activated or Apoptotic T-Lymphocytes Carry a Specific and Stimulus-Dependent Protein Cargo', *Frontiers in Immunology*. Frontiers Media SA, 9(MAR), p. 534. doi: 10.3389/FIMMU.2018.00534.

Ueba, T. *et al.* (2010) 'Plasma Level of Platelet-Derived Microparticles Is Associated with Coronary Heart Disease Risk Score in Healthy Men', *Journal of Atherosclerosis and Thrombosis*. doi: 10.5551/jat.2964.

Valadi, H. *et al.* (2007) 'Exosome-mediated transfer of mRNAs and microRNAs is a novel mechanism of genetic exchange between cells.', *Nature cell biology*, 9(6), pp. 654–9. doi: 10.1038/ncb1596.

Varga, Z. *et al.* (2014) 'Towards traceable size determination of extracellular vesicles', *Journal of Extracellular Vesicles*. Wiley-Blackwell, 3(1), pp. 1–10. doi: 10.3402/jev.v3.23298.

Vasan, R. S. (2006) 'Biomarkers of cardiovascular disease: Molecular basis and practical considerations', *Circulation*. Lippincott Williams & Wilkins, pp. 2335–2362. doi: 10.1161/CIRCULATIONAHA.104.482570.

Vazão, H. *et al.* (2011) 'Towards the Maturation and Characterization of Smooth Muscle Cells Derived from Human Embryonic Stem Cells', *PLOS ONE*. Public Library of Science, 6(3), p. e17771. doi: 10.1371/JOURNAL.PONE.0017771.

Vella, L. J. *et al.* (2008) 'The role of exosomes in the processing of proteins associated with neurodegenerative diseases', in *European Biophysics Journal*. doi: 10.1007/s00249-007-0246-z.

Verma, M. *et al.* (2015) 'Extracellular vesicles: Potential applications in cancer diagnosis, prognosis, and epidemiology', *BMC Clinical Pathology*. doi: 10.1186/s12907-015-0005-5.

Versari, D. *et al.* (2009) 'Endothelial dysfunction as a target for prevention of cardiovascular disease.', *Diabetes care*. Diabetes Care. doi: 10.2337/dc09-s330.

Vicencio, J. M. *et al.* (2015) 'Plasma exosomes protect the myocardium from ischemia-reperfusion injury', *Journal of the American College of Cardiology*. Elsevier USA, 65(15), pp. 1525–1536. doi: 10.1016/j.jacc.2015.02.026.

Vidal, M. *et al.* (1989) 'Asymmetric distribution of phospholipids in the membrane of vesicles released during in vitro maturation of guinea pig reticulocytes: Evidence precluding a role for "aminophospholipid translocase"', *Journal of Cellular Physiology*. doi: 10.1002/jcp.1041400308.

Vijayagopal, P. and Luke Glancy, D. (1996) 'Macrophages stimulate cholesteryl ester accumulation in cocultured smooth muscle cells incubated with lipoprotein-proteoglycan complex', *Arteriosclerosis, Thrombosis, and Vascular Biology*. Arterioscler Thromb Vasc Biol, 16(9), pp. 1112–1121. doi: 10.1161/01.ATV.16.9.1112.

Villarroya-Beltri, C. *et al.* (2014) 'Sorting it out: Regulation of exosome loading', *Seminars in Cancer Biology*. doi: 10.1016/j.semcancer.2014.04.009.

Virani, S. S. *et al.* (2020) 'Heart disease and stroke statistics—2020 update: A report from the American Heart Association', *Circulation*. Lippincott Williams and Wilkins, pp. E139–E596. doi: 10.1161/CIR.0000000000000757.

Virmani, R. *et al.* (2000) 'Lessons From Sudden Coronary Death', *Arteriosclerosis, Thrombosis, and Vascular Biology*. Lippincott Williams & Wilkins, 20(5), pp. 1262–1275. doi: 10.1161/01.ATV.20.5.1262.

Vlassov, A. V. *et al.* (2012) 'Exosomes: Current knowledge of their composition, biological functions, and diagnostic and therapeutic potentials', *Biochimica et Biophysica Acta - General Subjects*. doi: 10.1016/j.bbagen.2012.03.017.

Vyas, N. *et al.* (2014) 'Vertebrate Hedgehog is secreted on two types of extracellular vesicles with different signaling properties', *Scientific Reports*. doi: 10.1038/srep07357.

Waldenström, A. *et al.* (2012) 'Cardiomyocyte microvesicles contain DNA/RNA and convey biological messages to target cells', *PLoS ONE*. doi: 10.1371/journal.pone.0034653.

Walsh, M. J. *et al.* (2012) 'Attenuated total reflectance Fourier-transform infrared spectroscopic imaging for breast histopathology', *Vibrational Spectroscopy*. Vib Spectrosc, 60, pp. 23–28. doi: 10.1016/j.vibspec.2012.01.010.

Wang, A. *et al.* (2011) 'Derivation of Smooth Muscle Cells with Neural Crest Origin from Human Induced Pluripotent Stem Cells', *Cells, Tissues, Organs*, 195(1–2), pp. 5–14. doi: 10.1159/000331412.

Wang, D. *et al.* (2018) 'Adult Stem Cells in Vascular Remodeling', *Theranostics*, 8(3), pp. 815–829.

Wang, D. *et al.* (2019) 'Exosomes from mesenchymal stem cells expressing miR-125b inhibit neointimal hyperplasia via myosin IE', *Journal of Cellular and Molecular Medicine*. J Cell Mol Med, 23(2), pp. 1528–1540. doi: 10.1111/jcmm.14060.

Wang, G. *et al.* (2015) 'Origin and differentiation of vascular smooth muscle cells', *Journal of Physiology*. J Physiol, 593(14), pp. 3013–3030. doi: 10.1113/JP270033.

Wang, G. K. *et al.* (2010) 'Circulating microRNA: A novel potential biomarker for

early diagnosis of acute myocardial infarction in humans', *European Heart Journal*. doi: 10.1093/eurheartj/ehq013.

Wang, J. *et al.* (2015) 'Comparative study of the endoscope-based bevelled and volume fiber-optic Raman probes for optical diagnosis of gastric dysplasia in vivo at endoscopy', *Analytical and Bioanalytical Chemistry*. Anal Bioanal Chem, 407(27). doi: 10.1007/s00216-015-8727-x.

Wang, M. *et al.* (2017) 'Autofluorescence imaging and spectroscopy of human lung cancer', *Applied Sciences (Switzerland)*. Multidisciplinary Digital Publishing Institute, 7(1), p. 32. doi: 10.3390/app7010032.

Wang, X. *et al.* (2006) 'Mouse models of neointimal hyperplasia: Techniques and applications', *Medical Science Monitor*. Available at: https://pubmed.ncbi.nlm.nih.gov/16940942/ (Accessed: 8 August 2021).

Wanjare, M., Agarwal, N. and Gerecht, S. (2015) 'Biomechanical strain induces elastin and collagen production in human pluripotent stem cell-derived vascular smooth muscle cells', *American Journal of Physiology - Cell Physiology*. American Physiological Society, 309(4), pp. C271–C281. doi: 10.1152/ajpcell.00366.2014.

Wasteson, P. *et al.* (2008) 'Developmental origin of smooth muscle cells in the descending aorta in mice', *Development*, 135(10), pp. 1823–1832. doi: 10.1242/dev.020958.

Wendt, S. *et al.* (2018) 'Evaluation of the cardioprotective potential of extracellular vesicles – a systematic review and meta-analysis', *Scientific Reports*. Nature Publishing Group, 8(1), pp. 1–14. doi: 10.1038/s41598-018-33862-5.

Wiese, C., Heisig, J. and Gessler, M. (2010) 'Hey bHLH factors in cardiovascular development', in *Pediatric Cardiology*. doi: 10.1007/s00246-009-9609-9.

Wilkins E, Wilson L, Wickramasinghe K, Bhatnagar P, Leal J, Luengo-Fernandez R, Burns R, Rayner M, T. N. (2018) *European Cardiovascular Disease Statistics 2017 edition*. Available at: www.ehnheart.org (Accessed: 6 August 2021).

Williams, C. R. *et al.* (2012) 'Rosiglitazone attenuates NF-κB-mediated Nox4 upregulation in hyperglycemia-activated endothelial cells', *American Journal of Physiology - Cell Physiology*. Am J Physiol Cell Physiol, 303(2). doi: 10.1152/ajpcell.00227.2011.

Williams, S. B. *et al.* (1998) 'Acute hyperglycemia attenuates endothelium-dependent vasodilation in humans in vivo', *Circulation*. Lippincott Williams and Wilkins, 97(17), pp. 1695–1701. doi: 10.1161/01.CIR.97.17.1695.

Willms, E. *et al.* (2016) 'Cells release subpopulations of exosomes with distinct molecular and biological properties', *Scientific Reports*. Nature Publishing Group, 6(1),

pp. 1–12. doi: 10.1038/srep22519.

Willms, E. *et al.* (2018) 'Extracellular vesicle heterogeneity: Subpopulations, isolation techniques, and diverse functions in cancer progression', *Frontiers in Immunology*. Frontiers, p. 738. doi: 10.3389/fimmu.2018.00738.

Wilson, D. (2011) 'Vascular smooth muscle structure and function', in *Mechanisms of Vascular Disease: A Reference Book for Vascular Specialists*. University of Adelaide Press, pp. 13–24. doi: 10.1017/UPO9781922064004.003.

Witwer, K. W. (2021) 'On your MARCKS, get set, deliver: Engineering extracellular vesicles', *Molecular Therapy*. Elsevier, 29(5), pp. 1664–1665. doi: 10.1016/j.ymthe.2021.04.013.

Wolfers, J. *et al.* (2001) 'Tumor-derived exosomes are a source of shared tumor rejection antigens for CTL cross-priming', *Nature Medicine*. doi: 10.1038/85438.

Wollert, T. *et al.* (2009) 'The ESCRT machinery at a glance', *Journal of Cell Science*. doi: 10.1242/jcs.029884.

World Health Organization (2006) *Definition and diagnosis of diabetes mellitus and intermediate hyperglycemia RepoRt of a WHo/IDf ConsultatIon*.

World Health Organization (2018) *WHO - The top 10 causes of death*, *24 Maggio*. Available at: https://www.who.int/news-room/fact-sheets/detail/the-top-10-causes-of-death (Accessed: 6 August 2021).

Wrobel, T. P. *et al.* (2015) 'Effects of Low Carbohydrate High Protein (LCHP) diet on atherosclerotic plaque phenotype in ApoE/LDLR-/- mice: FT-IR and Raman imaging', *Scientific Reports*. Nature Publishing Group, 5(1), pp. 1–9. doi: 10.1038/srep14002.

Xie, C. *et al.* (2011) 'Smooth muscle cell differentiation in vitro: Models and underlying molecular mechanisms', *Arteriosclerosis, Thrombosis, and Vascular Biology*. Arterioscler Thromb Vasc Biol, pp. 1485–1494. doi: 10.1161/ATVBAHA.110.221101.

Xu, M. D. *et al.* (2016) 'Proteomic characteristics of circulating microparticles in patients with newly-diagnosed type 2 diabetes', *American Journal of Translational Research*.

Xuan, W., Khan, M. and Ashraf, M. (2020) 'Extracellular Vesicles From Notch Activated Cardiac Mesenchymal Stem Cells Promote Myocyte Proliferation and Neovasculogenesis', *Frontiers in Cell and Developmental Biology*. Frontiers Media SA, 8. doi: 10.3389/fcell.2020.00011.

Yagi, Y. *et al.* (2017) 'Next-generation sequencing-based small RNA profiling of cerebrospinal fluid exosomes', *Neuroscience Letters*. doi: 10.1016/j.neulet.2016.10.042.

Yakimchuk, K. (2015) 'Exosomes: isolation methods and specific markers', *Materials and Methods*. doi: 10.13070/mm.en.5.1450.

Yamamoto, K. R. *et al.* (1970) 'Rapid bacteriophage sedimentation in the presence of polyethylene glycol and its application to large-scale virus purification', *Virology*. Academic Press, 40(3), pp. 734–744. doi: 10.1016/0042-6822(70)90218-7.

Yamamoto, S. *et al.* (2015) 'Inflammation-induced endothelial cell-derived extracellular vesicles modulate the cellular status of pericytes', *Scientific Reports*. Nature Publishing Group, 5(1), pp. 1–10. doi: 10.1038/srep08505.

Yamanaka, S. (2007) 'Strategies and New Developments in the Generation of Patient-Specific Pluripotent Stem Cells', *Cell Stem Cell*. Cell Stem Cell, pp. 39–49. doi: 10.1016/j.stem.2007.05.012.

Yáñez-Mó, M. *et al.* (2015) 'Biological properties of extracellular vesicles and their physiological functions', *https://doi.org/10.3402/jev.v4.27066*. Taylor & Francis, 4(2015), pp. 1–60. doi: 10.3402/JEV.V4.27066.

Yang, L. *et al.* (2016) 'Differentiation of human induced-pluripotent stem cells into smooth-muscle cells: Two novel protocols', *PLoS ONE*, 11(1), p. e0147155. doi: 10.1371/journal.pone.0147155.

Yin, M., Loyer, X. and Boulanger, C. M. (2015) 'Extracellular vesicles as new pharmacological targets to treat atherosclerosis', *European Journal of Pharmacology*. Elsevier, 763, pp. 90–103. doi: 10.1016/j.ejphar.2015.06.047.

Ying, Q. L. *et al.* (2003) 'Conversion of embryonic stem cells into neuroectodermal precursors in adherent monoculture', *Nature Biotechnology*. doi: 10.1038/nbt780.

Yoo, Y. K. *et al.* (2018) 'Toward exosome-based neuronal diagnostic devices', *Micromachines*. doi: 10.3390/mi9120634.

Youn, J. Y., Gao, L. and Cai, H. (2012) 'The p47 phox- and NADPH oxidase organiser 1 (NOXO1)-dependent activation of NADPH oxidase 1 (NOX1) mediates endothelial nitric oxide synthase (eNOS) uncoupling and endothelial dysfunction in a streptozotocin-induced murine model of diabetes', *Diabetologia*. Diabetologia, 55(7), pp. 2069–2079. doi: 10.1007/s00125-012-2557-6.

Youn, S. W. *et al.* (2019) 'Modification of cardiac progenitor cell-derived exosomes by miR-322 provides protection against myocardial infarction through nox2-dependent angiogenesis', *Antioxidants*. Multidisciplinary Digital Publishing Institute (MDPI), 8(1). doi: 10.3390/antiox8010018.

Yu, X., Harris, S. L. and Levine, A. J. (2006) 'The regulation of exosome secretion: A novel function of the p53 protein', *Cancer Research*. doi: 10.1158/0008-5472.CAN-05-4579.

Yuan, F. *et al.* (2017) 'Contribution of vascular cells to neointimal formation', *PLoS ONE*, 12(1), pp. e0168914--11. doi: 10.1371/journal.pone.0168914.

Yuan, S. Y. and Rigor, R. R. (2011) 'Regulation of Endothelial Barrier Function', *Colloquium Series on Integrated Systems Physiology: From Molecule to Function*, 3(1), pp. 1–146. doi: 10.4199/c00025ed1v01y201101isp013.

Yuan, X. *et al.* (2020) 'Reversal of Endothelial Extracellular Vesicle-Induced Smooth Muscle Phenotype Transition by Hypercholesterolemia Stimulation: Role of NLRP3 Inflammasome Activation', *Frontiers in Cell and Developmental Biology*. Frontiers, 8, p. 1671. doi: 10.3389/fcell.2020.597423.

Yuan, Y. *et al.* (2019) 'Autofluorescence of NADH is a new biomarker for sorting and characterizing cancer stem cells in human glioma', *Stem Cell Research and Therapy*. BioMed Central, 10(1), pp. 1–13. doi: 10.1186/s13287-019-1467-7.

Yuana, Y., Sturk, A. and Nieuwland, R. (2013) 'Extracellular vesicles in physiological and pathological conditions', *Blood Reviews*. doi: 10.1016/j.blre.2012.12.002.

Yun, S. H. and Kwok, S. J. J. (2017) 'Light in diagnosis, therapy and surgery', *Nature Biomedical Engineering*. Nature Publishing Group, pp. 1–16. doi: 10.1038/s41551-016-0008.

Zhang, H. *et al.* (2020) 'Raman Spectroscopy characterization extracellular vesicles from bovine placenta and peripheral blood mononuclear cells', *PLoS ONE*. Public Library of Science, 15(7), p. e0235214. doi: 10.1371/journal.pone.0235214.

Zhang, J. C. *et al.* (1999) 'Stimulation of tissue factor expression in human microvascular and macrovascular endothelial cells by cultured vascular smooth muscle cells in vitro', *Journal of Vascular Research*. J Vasc Res, 36(2), pp. 126–132. doi: 10.1159/000025635.

Zhang, M. *et al.* (2013) 'NADPH oxidases in heart failure: Poachers or gamekeepers?', *Antioxidants and Redox Signaling*. Antioxid Redox Signal, pp. 1024–1041. doi: 10.1089/ars.2012.4550.

Zhang, Q. *et al.* (2008) 'Paradoxical Activation of Endothelial Nitric Oxide Synthase by NADPH Oxidase', *Arteriosclerosis, Thrombosis, and Vascular Biology*. Lippincott Williams & Wilkins, 28(9), pp. 1627–1633. doi: 10.1161/ATVBAHA.108.168278.

Zhang, X. *et al.* (2010) 'Pax6 is a human neuroectoderm cell fate determinant', *Cell*

stem cell. NIH Public Access, 7(1), p. 90. doi: 10.1016/J.STEM.2010.04.017.

Zhang, Y. *et al.* (2021) 'The effect of extracellular vesicles on the regulation of mitochondria under hypoxia', *Cell Death and Disease*. Nature Publishing Group, pp. 1–14. doi: 10.1038/s41419-021-03640-9.

Zhao, L. *et al.* (2017) 'Exosomes Derived from Human Pulmonary Artery Endothelial Cells Shift the Balance between Proliferation and Apoptosis of Smooth Muscle Cells', *Cardiology (Switzerland)*. Karger Publishers, 137(1), pp. 43–53. doi: 10.1159/000453544.

Zhou, S. S. *et al.* (2018) 'MiRNAS in cardiovascular diseases: Potential biomarkers, therapeutic targets and challenges review-article', *Acta Pharmacologica Sinica*. Acta Pharmacol Sin, pp. 1073–1084. doi: 10.1038/aps.2018.30.

Zhou, Y. *et al.* (2014) 'Trend of telomerase activity change during human iPSC self-renewal and differentiation revealed by a quartz crystal microbalance based assay', *Scientific Reports*, 4. doi: 10.1038/srep06978.

Zhou, Z. W. *et al.* (2012) 'Mechanism of reversal of high glucose-induced endothelial nitric oxide synthase uncoupling by tanshinone IIA in human endothelial cell line EA.hy926', *European Journal of Pharmacology*. Eur J Pharmacol, 697(1–3), pp. 97–105. doi: 10.1016/j.ejphar.2012.09.051.

Zhu, X. *et al.* (2017) 'Comprehensive toxicity and immunogenicity studies reveal minimal effects in mice following sustained dosing of extracellular vesicles derived from HEK293T cells', *Journal of Extracellular Vesicles*. doi: 10.1080/20013078.2017.1324730.

Zimmet, P., Alberti, K. G. M. M. and Shaw, J. (2001) 'Global and societal implications of the diabetes epidemic', *Nature*. Nature Publishing Group, pp. 782–787. doi: 10.1038/414782a.

Zitvogel, L. *et al.* (1998) 'Eradication of established murine tumors using a novel cell-free vaccine: Dendritic cell-derived exosomes', *Nature Medicine*. doi: 10.1038/nm0598-594.

Zúñiga, W. C. *et al.* (2019) 'Raman Spectroscopy for Rapid Evaluation of Surgical Margins during Breast Cancer Lumpectomy', *Scientific Reports 2019 9:1*. Nature Publishing Group, 9(1), pp. 1–16. doi: 10.1038/s41598-019-51112-0.

Zwaal, R. F. and Schroit, A. J. (1997) 'Pathophysiologic implications of membrane phospholipid asymmetry in blood cells.', *Blood*.

Appendices

Appendix A

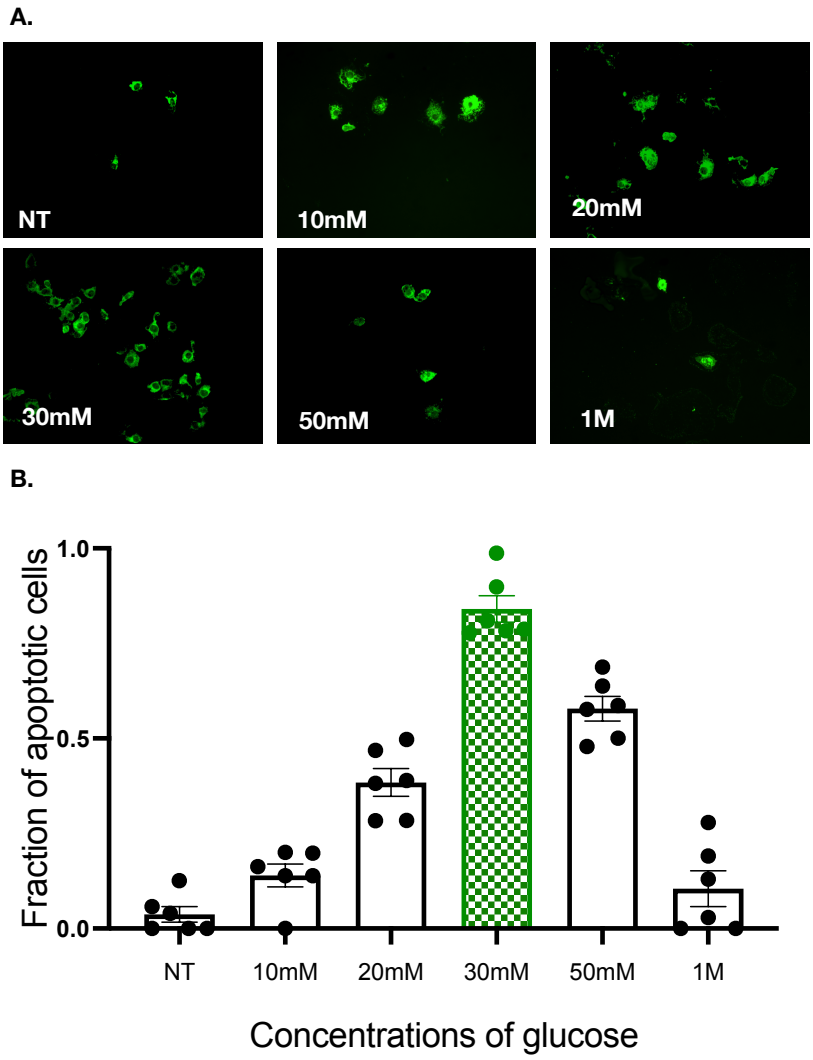

Supplementary Figure 1. Hyperglycaemic conditions (HG) induce rat aortic endothelial dysfunction by fluorescent microscopy analysis of Annexin V-FITC. (A) Fluorescence staining of Annexin V-FITC in rat aortic endothelial cells treated with various glucose concentrations (0mM – 1M). (B) The fraction of Annexin V-FITC^{+} cells per glucose treatment. All images are representative of n ≥ 6 images per experimental group from two independent cultures. Scale bar representative of 50µm. Data representative of n≥6 images per experimental group from two independent cultures. Error bars based on SEM.